EXPLORING THE POTENTIAL OF PARTICLE RADIOTHERAPY: HELIUM, NEUTRONS, CARBON, AND OTHER HEAVY IONS

EDITED BY: Daniel Michael Trifiletti, Stephanie E. Combs and Timothy Dean Malouff

PUBLISHED IN: Frontiers in Oncology

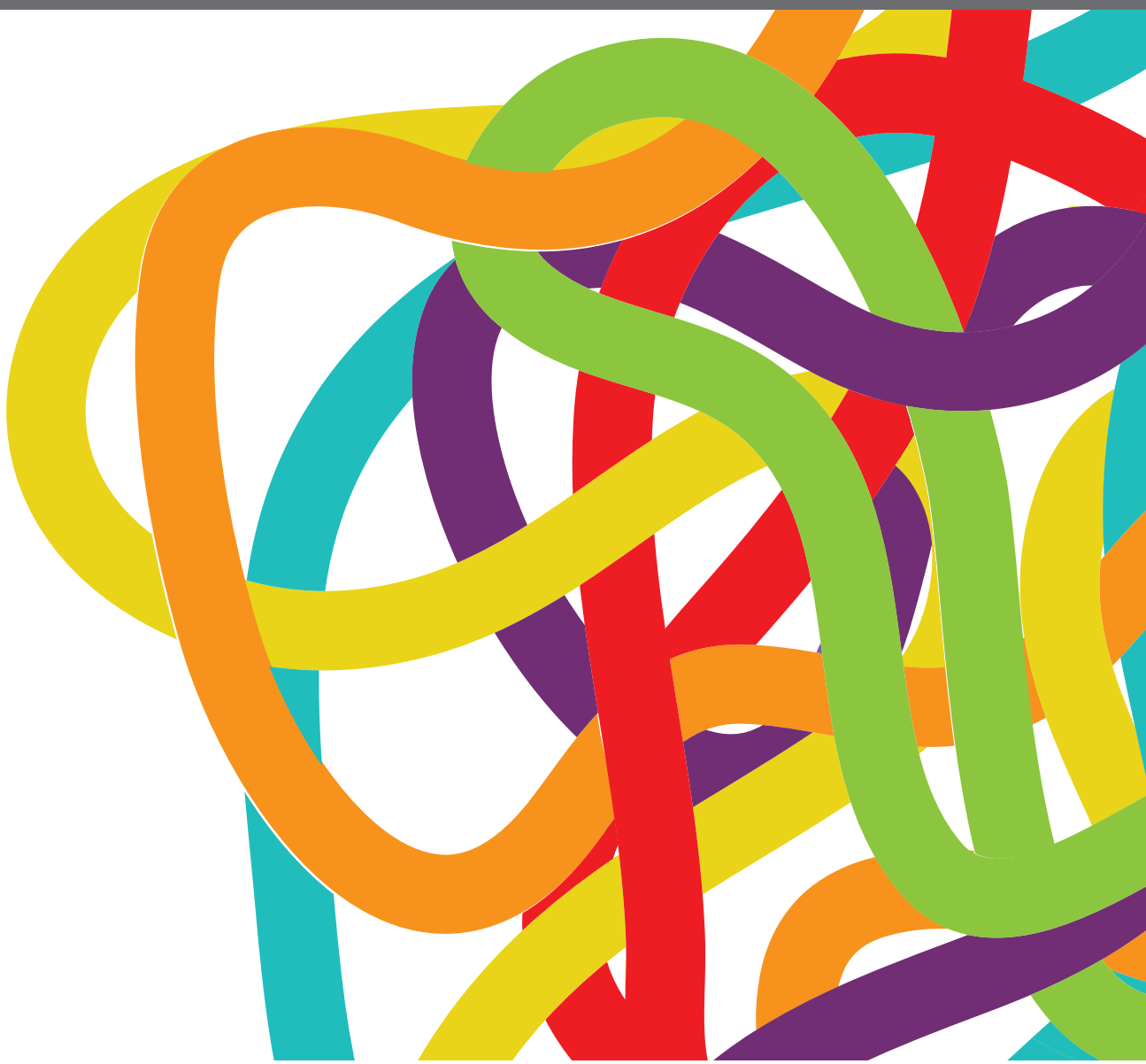

frontiers Research Topics

Frontiers eBook Copyright Statement

The copyright in the text of individual articles in this eBook is the property of their respective authors or their respective institutions or funders. The copyright in graphics and images within each article may be subject to copyright of other parties. In both cases this is subject to a license granted to Frontiers.

The compilation of articles constituting this eBook is the property of Frontiers.

Each article within this eBook, and the eBook itself, are published under the most recent version of the Creative Commons CC-BY licence. The version current at the date of publication of this eBook is CC-BY 4.0. If the CC-BY licence is updated, the licence granted by Frontiers is automatically updated to the new version.

When exercising any right under the CC-BY licence, Frontiers must be attributed as the original publisher of the article or eBook, as applicable.

Authors have the responsibility of ensuring that any graphics or other materials which are the property of others may be included in the CC-BY licence, but this should be checked before relying on the CC-BY licence to reproduce those materials. Any copyright notices relating to those materials must be complied with.

Copyright and source acknowledgement notices may not be removed and must be displayed in any copy, derivative work or partial copy which includes the elements in question.

All copyright, and all rights therein, are protected by national and international copyright laws. The above represents a summary only. For further information please read Frontiers' Conditions for Website Use and Copyright Statement, and the applicable CC-BY licence.

ISSN 1664-8714
ISBN 978-2-88971-387-5
DOI 10.3389/978-2-88971-387-5

About Frontiers

Frontiers is more than just an open-access publisher of scholarly articles: it is a pioneering approach to the world of academia, radically improving the way scholarly research is managed. The grand vision of Frontiers is a world where all people have an equal opportunity to seek, share and generate knowledge. Frontiers provides immediate and permanent online open access to all its publications, but this alone is not enough to realize our grand goals.

Frontiers Journal Series

The Frontiers Journal Series is a multi-tier and interdisciplinary set of open-access, online journals, promising a paradigm shift from the current review, selection and dissemination processes in academic publishing. All Frontiers journals are driven by researchers for researchers; therefore, they constitute a service to the scholarly community. At the same time, the Frontiers Journal Series operates on a revolutionary invention, the tiered publishing system, initially addressing specific communities of scholars, and gradually climbing up to broader public understanding, thus serving the interests of the lay society, too.

Dedication to Quality

Each Frontiers article is a landmark of the highest quality, thanks to genuinely collaborative interactions between authors and review editors, who include some of the world's best academicians. Research must be certified by peers before entering a stream of knowledge that may eventually reach the public - and shape society; therefore, Frontiers only applies the most rigorous and unbiased reviews.
Frontiers revolutionizes research publishing by freely delivering the most outstanding research, evaluated with no bias from both the academic and social point of view. By applying the most advanced information technologies, Frontiers is catapulting scholarly publishing into a new generation.

What are Frontiers Research Topics?

Frontiers Research Topics are very popular trademarks of the Frontiers Journals Series: they are collections of at least ten articles, all centered on a particular subject. With their unique mix of varied contributions from Original Research to Review Articles, Frontiers Research Topics unify the most influential researchers, the latest key findings and historical advances in a hot research area! Find out more on how to host your own Frontiers Research Topic or contribute to one as an author by contacting the Frontiers Editorial Office: frontiersin.org/about/contact

EXPLORING THE POTENTIAL OF PARTICLE RADIOTHERAPY: HELIUM, NEUTRONS, CARBON, AND OTHER HEAVY IONS

Topic Editors:
Daniel Michael Trifiletti, Mayo Clinic Florida, United States
Stephanie E. Combs, Technical University of Munich, Germany
Timothy Dean Malouff, Mayo Clinic Florida, United States

Citation: Trifiletti, D. M., Combs, S. E., Malouff, T. D., eds. (2021). Exploring the Potential of Particle Radiotherapy: Helium, Neutrons, Carbon, and Other Heavy Ions. Lausanne: Frontiers Media SA. doi: 10.3389/978-2-88971-387-5

Table of Contents

frontiers in Oncology

EDITORIAL
published: 29 July 2021
doi: 10.3389/fonc.2021.740974

Editorial: Exploring the Potential of Particle Radiotherapy: Helium, Neutrons, Carbon, and Other Heavy Ions

Timothy D. Malouff[1]*, *Stephanie E. Combs*[2] and *Daniel M. Trifiletti*[1]

[1] Department of Radiation Oncology, Mayo Clinic Florida, Jacksonville, FL, United States, [2] Department of Radiation Oncology, Technical University of Munich, Munich, Germany

Keywords: particle, carbon, helium, neutron, heavy ions, radiation

Editorial on the Research Topic

Exploring the Potential of Particle Radiotherapy: Helium, Neutrons, Carbon, and Other Heavy Ions

OVERVIEW

Radiation therapy is a cornerstone modality in the treatment of malignant diseases. Since the inception of the field over a century ago, clinicians and researchers have focused on improving the therapeutic ratio of radiation therapy, therefore minimizing toxicities while maximizing tumor control. The use of particle therapy to improve the therapeutic ratio can be traced to 1946, when Dr. Robert Wilson first proposed the use of accelerated protons and heavy ions for oncological treatments in a landmark paper (1). Today, clinicians and researchers are investigating the use of a variety of different ions for therapeutic use, including protons, carbon ions, fast neutrons, boron neutron capture, and multi-ion therapy (2). Each of the heavy ions have unique radiobiological and physical properties that must be taken into consideration, although they all share some common features, such as a high linear energy transfer (LET) and relative biological effectiveness (RBE). These properties theoretically make heavy ions more potent at causing DNA damage and hopefully improving tumor control (3, 4)

Our topic accepted a total of 17 articles from 48 authors, demonstrating the emergence and importance of particle therapy in providing the best care for patients. Our topic can be divided into the following topics:

PROTON AND CARBON IONS

Much of our clinical experience with particle therapy involves proton therapy, which is widely used in the US and throughout the world, followed by carbon ion radiotherapy, with centers treating throughout Europe, Asia, and a planned center in the US (5–9). Carbon ion radiotherapy, which is the focus of our Research Topic, takes advantage of the Bragg peak, a sharp lateral penumbra, high LET, and high RBE to maximize cell kill while minimizing normal tissue irradiated (3). Clinical studies have suggested safety and efficacy of carbon ions in the treatment of a variety of malignancies (2).

Our topic includes three excellent clinical reviews describing the clinical experience of particle therapy for skull base sarcomas (Yang et al.), adenoid cystic carcinoma of the nasal cavity and sinuses (Hu et al.), and meningiomas (Li et al.). Additionally, studies by Huang et al. and Yang et al. demonstrate

OPEN ACCESS

Edited and reviewed by:
Timothy James Kinsella, Warren Alpert Medical School of Brown University, United States

***Correspondence:**
Timothy D. Malouff
malouff.timothy@mayo.edu

Specialty section:
This article was submitted to Radiation Oncology, a section of the journal Frontiers in Oncology

Received: *14 July 2021*
Accepted: *16 July 2021*
Published: *29 July 2021*

Citation:
Malouff TD, Combs SE and Trifiletti DM (2021) Editorial: Exploring the Potential of Particle Radiotherapy: Helium, Neutrons, Carbon, and Other Heavy Ions. Front. Oncol. 11:740974. doi: 10.3389/fonc.2021.740974

molecular mechanisms for the bystander effect and abscopal effect, an area of excitement and a potential niche for heavy ion therapies. Furthermore, Sun et al. and Toppi et al. report on methods to evaluate dose distribution following carbon ion radiotherapy.

FAST NEUTRON THERAPY

Although not commonly used, fast neutron therapy is another area of interest, as neutrons have a high have a high LET and RBE despite not exhibiting a Bragg peak (10). Jones authored a comprehensive review on the clinical radiobiology of fast neutron therapy, as well as the historical and future concerns of implementing neutron therapy.

BORON NEUTRON CAPTURE THERAPY

Although first proposed in 1936, boron neutron capture therapy (BNCT) has experienced a resurgence in interest (11). BNCT is based on the principle of irradiating nonradioactive boron-10 with neutrons, leading to the production of a lithium-7 and an alpha particle. The alpha particle is a form of high LET radiation that deposits energy over the distance of about the diameter of one cell, therefore selectively targeting tumor cells while avoiding normal tissue toxicity. This technique has largely been limited due to the limited selectiveness of the boron compounds (11–13). The review by Malouff et al. describes the clinical experience and future directions of BNCT.

MULTI-ION THERAPY

Although much of our clinical experience is based on individual particles used alone, there is a resurgence of interest in combining the use of multiple ions to take advantage of the unique characteristics of each ion. For instance, helium, neon, silicon, nitrogen, and argon were all studied at the Lawrence Berkeley National Laboratory in the 1970s (14). In the review by Ebner et al., the authors describe the initial work, as well as the challenges associated, with combining these ions in a single treatment to best distribute high LET regions in tumors while minimizing high LET regions in normal tissues or areas of subclinical disease.

CONCLUSION

Overall, particle therapy represents an area of excitement in radiation oncology, as is evidenced by the excellent articles listed above. We hope that our Research Topic promotes discussion, identifies gaps in knowledge, and inspires future generations to continue investigating the therapeutic use of heavy ions.

AUTHOR CONTRIBUTIONS

All authors contributed to the article and approved the submitted version.

REFERENCES

1. Wilson RR. Radiological Use of Fast Protons. *Radiology* (1946) 47(5):487–91. doi: 10.1148/47.5.487
2. Malouff TD, Mahajan A, Krishnan S, Beltran C, Seneviratne DS, Trifiletti DM. Carbon Ion Therapy: A Modern Review of an Emerging Technology. *Front Oncol* (2020) 10:82. doi: 10.3389/fonc.2020.00082
3. Mohamad O, Sishc BJ, Saha J, Pompos A, Rahimi A, Story MD, et al. Carbon Ion Radiotherapy: A Review of Clinical Experiences and Preclinical Research, With an Emphasis on DNA Damage/Repair. *Cancers (Basel)* (2017) 9:(6). doi: 10.3390/cancers9060066
4. Saager M, Peschke P, Brons S, Debus J, Karger CP. Determination of the Proton RBE in the Rat Spinal Cord: Is There an Increase Towards the End of the Spread-Out Bragg Peak? *Radiother Oncol* (2018) 128(1):115–20. doi: 10.1016/j.radonc.2018.03.002
5. Rackwitz T, Debus J. Clinical Applications of Proton and Carbon Ion Therapy. *Semin Oncol* (2019) 46(3):226–32. doi: 10.1053/j.seminoncol.2019.07.005
6. Lazar AA, Schulte R, Faddegon B, Blakely EA, Roach M3rd. Clinical Trials Involving Carbon-Ion Radiation Therapy and the Path Forward. *Cancer* (2018) 124(23):4467–76. doi: 10.1002/cncr.31662
7. Particle Therapy Co-Operative Group. *Particle Therapy Facilities in Clinical Operation* (2020). Available at: https://www.ptcog.ch/index.php/facilities-in-operation (Accessed June 2020).
8. Particle Therapy Co-Operative Group. *Particle Therapy Facilties Under Construction* (2020). Available at: https://www.ptcog.ch/index.php/facilities-under-construction (Accessed June 2020).
9. Particle Therapy Co-Operative Group. *Particle Therapy Facilities in a Planning Stage* (2020). Available at: https://www.ptcog.ch/index.php/facilities-in-planning-stage (Accessed June 2020).
10. Hill MA. The Variation in Biological Effectiveness of X-Rays and Gamma Rays With Energy. *Radiat Prot Dosimetry* (2004) 112(4):471–81. doi: 10.1093/rpd/nch091
11. Nedunchezhian K, Aswath N, Thiruppathy M, Thirugnanamurthy S. Boron Neutron Capture Therapy - A Literature Review. *J Clin Diagn Res* (2016) 10 (12):Ze01–ze04. doi: 10.7860/jcdr/2016/19890.9024
12. Sauerwein W, Wittig A, Moss R, Nakagawa K. *Neutron Capture Therapy: Principles and Applications*. Edition 1. Heidelberg New York Dordrecht London: Springer (2012) 1–16.
13. Barth RF, Zhang Z, Liu T. A Realistic Appraisal of Boron Neutron Capture Therapy as a Cancer Treatment Modality. *Cancer Commun (Lond)* (2018) 38 (1):36. doi: 10.1186/s40880-018-0280-5
14. Castro JR, Quivey JM, Lyman JT, Chen GT, Phillips TL, Tobias CA. Radiotherapy With Heavy Charged Particles at Lawrence Berkeley Laboratory. *J Can Assoc Radiol* (1980) 31(1):30–4.

Conflict of Interest: The authors declare that the research was conducted in the absence of any commercial or financial relationships that could be construed as a potential conflict of interest.

Publisher's Note: All claims expressed in this article are solely those of the authors and do not necessarily represent those of their affiliated organizations, or those of the publisher, the editors and the reviewers. Any product that may be evaluated in this article, or claim that may be made by its manufacturer, is not guaranteed or endorsed by the publisher.

Copyright © 2021 Malouff, Combs and Trifiletti. This is an open-access article distributed under the terms of the Creative Commons Attribution License (CC BY). The use, distribution or reproduction in other forums is permitted, provided the original author(s) and the copyright owner(s) are credited and that the original publication in this journal is cited, in accordance with accepted academic practice. No use, distribution or reproduction is permitted which does not comply with these terms.

frontiers in Oncology

ORIGINAL RESEARCH
published: 28 July 2020
doi: 10.3389/fonc.2020.01264

Impact of Inter-fractional Anatomical Changes on Dose Distributions in Passive Carbon-Ion Radiotherapy for Prostate Cancer: Comparison of Vertical and Horizontal Fields

Ayaka Yokoyama[1], Yoshiki Kubota[2], Hidemasa Kawamura[2], Yuhei Miyasaka[2], Nobuteru Kubo[2], Hiro Sato[2], Satoshi Abe[1], Kazuhisa Tsuda[1], Takayuki Sutou[1], Tatsuya Ohno[2] and Takashi Nakano[2]*

[1] Department of Radiology, Gunma University Hospital, Maebashi, Japan, [2] Gunma University Heavy Ion Medical Center, Maebashi, Japan

OPEN ACCESS

Edited by:
Stephanie E. Combs, Technical University of Munich, Germany

Reviewed by:
Timothy Dean Malouff, Mayo Clinic Florida, United States
Young Kwok, University of Maryland Medical Center, United States

***Correspondence:**
Yoshiki Kubota
y_kubota@gunma-u.ac.jp

Specialty section:
This article was submitted to Radiation Oncology, a section of the journal Frontiers in Oncology

Received: 27 February 2020
Accepted: 18 June 2020
Published: 28 July 2020

Citation:
Yokoyama A, Kubota Y, Kawamura H, Miyasaka Y, Kubo N, Sato H, Abe S, Tsuda K, Sutou T, Ohno T and Nakano T (2020) Impact of Inter-fractional Anatomical Changes on Dose Distributions in Passive Carbon-Ion Radiotherapy for Prostate Cancer: Comparison of Vertical and Horizontal Fields. Front. Oncol. 10:1264. doi: 10.3389/fonc.2020.01264

Purpose: We quantified the inter-fractional changes associated with passive carbon-ion radiotherapy using vertical and horizontal beam fields for prostate cancer.

Methods: In total, 118 treatment-room computed tomography (TRCT) image sets were acquired from 10 patients. Vertical (anterior–posterior) and horizontal (left–right) fields were generated on the planning target volume identified by treatment planning CT. The dose distribution for each field was recalculated on each TRCT image set at the bone-matching position and evaluated using the dose–volume parameters for the prostate and rectum V95 values. To confirm adequate margins, we generated vertical and horizontal fields with 0-, 2-, 4-, and 6-mm isotropic margins from the prostate and recalculated the dose distributions on all TRCT image sets. Sigmoid functions were fitted to a plot of acceptable ratios (that is, when prostate V95 $>$ 98%) vs. the isotropic margin size to identify the margin at which this ratio was achieved in 95% of patients with a vertical or horizontal field.

Results: The prostate V95 values (mean $\pm$ standard deviation) were 99.89 $\pm$ 0.62% and 99.99 $\pm$ 0.00% with vertical and horizontal fields, respectively; this difference was not statistically significant ($p = 0.067$). The rectum V95 values were 1.93 $\pm$ 1.25 and 1.88 $\pm$ 0.96 ml with vertical and horizontal fields, respectively; the difference was not statistically significant ($p = 0.432$). The estimated adequate margins were 2.2 and 3.0 mm for vertical and horizontal fields, respectively.

Conclusions: Although there is no significant difference, horizontal fields offer higher reproducibility for prostate dosing than vertical fields in our clinical setting, and 3.0 mm was found to be an adequate margin for inter-fractional changes.

Keywords: carbon-ion radiotherapy, prostate cancer, patient positioning, inter-fractional anatomical change, adequate margin

INTRODUCTION

Prostate cancer is the second most common cancer in males according to the International Agency for Research on Cancer (1). The outcomes of radiotherapy are equal or better than those of surgery (2). One type of radiotherapy, carbon-ion radiotherapy (CIRT), reportedly reduces the risk of acute and late toxicities with outcomes that are equal or better than those of conformal radiotherapy and intensity-modulated radiation therapy (3–7).

Carbon-ion beams provide sharper dose distributions than photon beams because they benefit from the Blagg peak and a sharp lateral penumbra (8, 9). However, carbon-ion beams are sensitive to changes in the target position or water-equivalent path length (WEL) to the target, which may result in changes in dose distributions (10–14). The reproducibility of dose distributions for inter-fractional anatomical changes is very important to ensure safe treatment of patients; however, few reports have focused on this topic in the context CIRT for prostate cancer.

In our previous study, we evaluated the influence of the beam field angle during setup the range uncertainty on the rectal and target doses in CIRT for prostate cancer (15). Our results showed that the prostate and rectal dose deviations did not vary significantly with the field angle. However, while the setup uncertainty was considered in this study, inter-fractional anatomical changes in the prostate, bladder, and/or rectum were not. To improve the safety of CIRT, it is necessary to evaluate the influence of such anatomical changes on the dose distribution. Additionally, whether a vertical or horizontal field is more robust against inter-fractional changes remains unclear. Further, because a vertical field must be used instead of a horizontal field in certain cases, such as when the patient has a metal hip implant, it is important to evaluate the robustness of a vertical field against inter-fractional changes. Hence, in this study, we evaluated the robustness of horizontal and vertical fields against inter-fractional anatomical changes using daily computed tomography (CT) images acquired in a treatment room.

MATERIALS AND METHODS

Patient

This prospective study included 10 consecutive patients with prostate cancer who had agreed to participate in this study and had been treated with 12 fractions of passive-irradiation CIRT at Gunma University Heavy Ion Medical Center from June 2017 to March 2018. The patients' characteristics are detailed in **Table 1**. This study was conducted in accordance with the Declaration of Helsinki and approved by the institutional review board at Gunma University Hospital (1564). The study was registered at the University Hospital Medical Information Network Clinical Trials Registry (UMIN-CTR trial number: 000029495). All patients provided written informed consent to participate in this study and their data were anonymized.

TABLE 1 | Patient characteristics.

Patient Number	Age	Prostate Volume (ml)	Rectal Volume (ml)	Bladder Volume (ml)
P1	67	17.2	48.5	322.5
P2	72	18.7	70.5	192.8
P3	59	22.0	68.9	198.5
P4	76	17.4	38.7	214.2
P5	73	23.4	44.6	139.1
P6	76	20.6	48.0	146.3
P7	66	15.0	31.7	155.4
P8	70	18.5	39.8	113.3
P9	60	32.8	35.5	89.7
P10	78	19.2	61.1	105.2
Median	71	18.95	46.3	150.85

The prostate, rectal, and bladder volumes were measured from the treatment planning CT.

CT Image Acquisition and Actual Treatment

Twelve CT data sets were acquired on each day of treatment to investigate the effects of tumor movement and inter-fractional changes on the dose decided in the treatment planning stage. All patients were immobilized in the supine position by a shell fitter (Kuraray, Tokyo, Japan) to depress the abdomen and prevent body movement. A MoldCare cushion (Alcare, Tokyo, Japan) was used to provide trunk support while the patient was irradiated and CT images were acquired. CT images for treatment planning (PlanCT) were acquired on a scanner (Aquilion LB®, Self-Propelled; Canon Medical Systems, Otawara, Tochigi, Japan) in a simulation room.

Each patient retained his urine for 20 min before entering the irradiation room. The patient was positioned with the aid of orthogonal X-ray imaging (16, 17). If gas or feces was observed inside or close to the target on the X-ray images, a degassing or enema procedure was performed. This radiotherapy irradiation procedure was performed on each of the 12 separate days. After the radiotherapy, one set of CT images was acquired using a treatment-room CT (TRCT) system of the same type as in the simulation room (18). TRCT image sets were obtained from each patient in the same position as used for irradiation and with the same tube voltage, tube current, field of view, and slice thickness settings used for the PlanCT.

Treatment Planning

In this study, we used a CIRT system (19) with a heavy ion irradiation device (Mitsubishi Electric, Tokyo, Japan) with passive irradiation (20) and a treatment planning system (TPS) (XiO-N, Mitsubishi Electric). The passive irradiation field was generated using a scatterer and wobbling, and the field was collimated to the outside of the planning target volume (PTV) using a multi-leaf collimator. A pencil-beam algorithm was used to calculate the dose distributions (21, 22). The relative biological effectiveness (RBE) was included in the absorbed dose using a spread-out Bragg peak concept (23), and the clinical dose was defined as Gy (RBE). The PTV1 for the prostate cancer treatment for each patient was determined after adding 8-mm anterior and lateral margins, 6-mm cranial and caudal margins, and a 5-mm posterior margin to the prostate as well as 3-mm lateral margins, 5-mm cranial and caudal margins, and a 5-mm

posterior margin to the proximal seminal vesicle. The PTV2 was created by subtracting 6 mm from the circumscribed position of the PTV1 in the cranial and caudal directions and subtracting the circumscribed region of the rectum in the posterior direction of PTV1 from the PTV1. The CIRT plan was generated such that the percentages of PTV1 and PTV2 receiving >95% of the prescribed dose (V95) were >95%. Irradiation was applied with fields from the left and right sides. Two of the fields were applied in four fractions, and the other two were applied in two fractions, which results in an initial field of 8 fractions to PTV1 and a boost field of 4 fractions to PTV2; thus, there was a total of 12 fractions. Each fraction was 4.3 Gy (RBE), and the total dose was therefore $4.3 \times 12 = 51.6$ Gy (RBE).

Data Analysis

The inter-fractional prostate displacements were measured from bone-matching positions to prostate-matching positions between the PlanCT and subsequent TRCT images for each patient ($n = 118$; 2 CT sets were not acquired because of a CT system failure) using commercial software (MIM Maestro®; MIM Software, Cleveland, OH, USA). The registration was based on the translation in three directions (left–right (LR), anterior–posterior (AP), and superior–inferior (SI), each defined as + and – values) because CT images cannot be rotated for dose calculation with the XiO-N system. Prostate contours were generated on all TRCT images by the rigid image registration method based on the PlanCT, and the rectum and bladder were manually delineated on all TRCT images. After generation and delineation, an oncologist and medical physicist checked the contours. Additionally, deviations from the volumes on the PlanCT to those measured on each TRCT were calculated. The WELs in the AP direction were then measured from the patient's body surface to the isocenter of the beam's direction plane, and the correlation between the prostate displacements and the WEL deviations in the AP direction was evaluated.

Initial and boost fields on horizontal and vertical (LR and AP directions, respectively) were generated and used for evaluation. Examples of the dose distributions associated with vertical and horizontal fields are shown in **Figure 1**. The daily dose distributions for the initial and boost fields in the vertical and horizontal directions were recalculated on all TRCT sets at the bone-matching position. The dose–volume parameters of the prostate V95, rectum V95, V50, and V10 were also evaluated. For the rectal volume evaluation, the rectal wall was considered to be 3 mm thick, as described previously (24, 25). Additionally, the correlation between the prostate displacement and the dose–volume parameters of the prostate V95 and those between the rectal volume deviation and the deviations in the dose–volume parameters of the rectum V95, V50, and V10 were evaluated.

To estimate the appropriate margins in CIRT for prostate cancer to ensure robustness against inter-fractional anatomical changes, vertical and horizontal fields were generated on the PlanCT with 0-, 2-, 4-, and 6-mm isotropic margins to the prostate. The dose distributions were then recalculated for all TRCT images at the bone-matching position. Sigmoid functions were fitted to the plot of the acceptance ratio vs. the isotropic margin size to identify the margin that enables 95% of the examined patients to achieve an acceptable condition (prostate V95 > 98%) for each field in the vertical and horizontal directions.

Statistics

All dose–volume parameters for vertical and horizontal fields, as well as the prostate displacements and WEL deviations in the AP direction, were compared using *t*-tests; $p = 0.05$ was considered statistically significant.

RESULTS

The measured prostate displacements and rectal and bladder volume variations are shown in **Figure 2**. The mean ± standard deviation of the prostate displacement for all patients were 0.08 ± 0.50, 0.46 ± 1.32, and −0.12 ± 1.87 mm in the LR, SI, and AP directions, respectively, and those for the rectal and bladder volume deviations were −1.07 ± 9.37 and 2.55 ± 95.36 ml, respectively. The correlation between prostate displacement and WEL deviation in the AP direction is shown in **Figure 3**. The mean ± standard deviation of the prostate displacement and WEL deviation were −0.13 ± 1.88 and 0.82 ± 2.04 mm, respectively; the mean difference was not statistically significant.

The dose–volume parameters on PlanCT and TRCT are shown in **Table 2**. There were no statistically significant differences between the daily prostate V95 with initial fields in the vertical and horizontal directions. For the boost field, however, the prostate V95 was significantly lower in the vertical than horizontal direction.

The correlations between prostate displacement and prostate V95 and between rectal volume deviation and rectal dose volume are shown in **Figure 4**. The correlations of prostate displacement with bladder volume deviation and rectal volume deviation in the AP direction are shown in **Figure 5**. The prostate and rectal dose volume and acceptance ratio graphs are shown in **Figure 6**. Based on these data, adequate margins in the vertical field and horizontal field for an acceptance ratio of 95% were determined to be 2.2 and 3.0 mm, respectively.

DISCUSSION

Our results showed that the average inter-fractional prostate displacement was 0.46 ± 1.32 mm in the SI direction and −0.12 ± 1.87 mm in the AP direction. Our measured displacements were similar to those measured from in-room CT (26) using a flat-type shell similar to that used in this study. However, these displacements were smaller than those measured under cone-beam CT (27, 28) or megavoltage CT (29) with different shell types or without the shell. It was hypothesized that the patient immobilization induced by pressing with a flat shell may also suppress prostate displacement.

Table 2 shows that the prostate coverage was better with the horizontal field than with the vertical field. The difference was statistically significant for the boost fields because they do not have a margin in the posterior direction from the prostate, which results in less consistent coverage than with the initial fields, which have a large margin. There are two possible reasons for

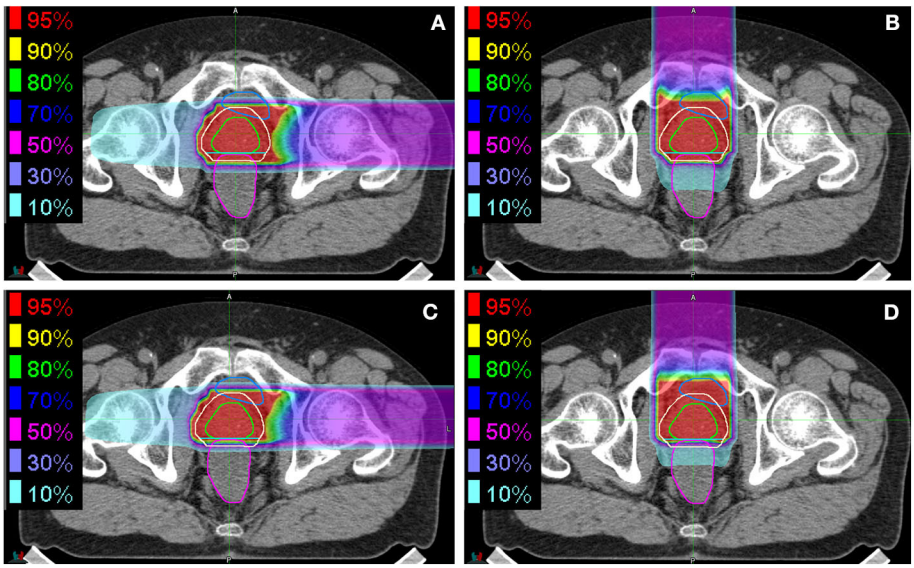

FIGURE 1 | Examples of dose distributions for **(A,B)** initial fields and **(C,D)** boost fields from **(A,C)** the horizontal direction and **(B,D)** the vertical direction. The green, almond, cyan, blue, and magenta lines delineate the prostate, PTV1, PTV2, bladder, and rectum, respectively.

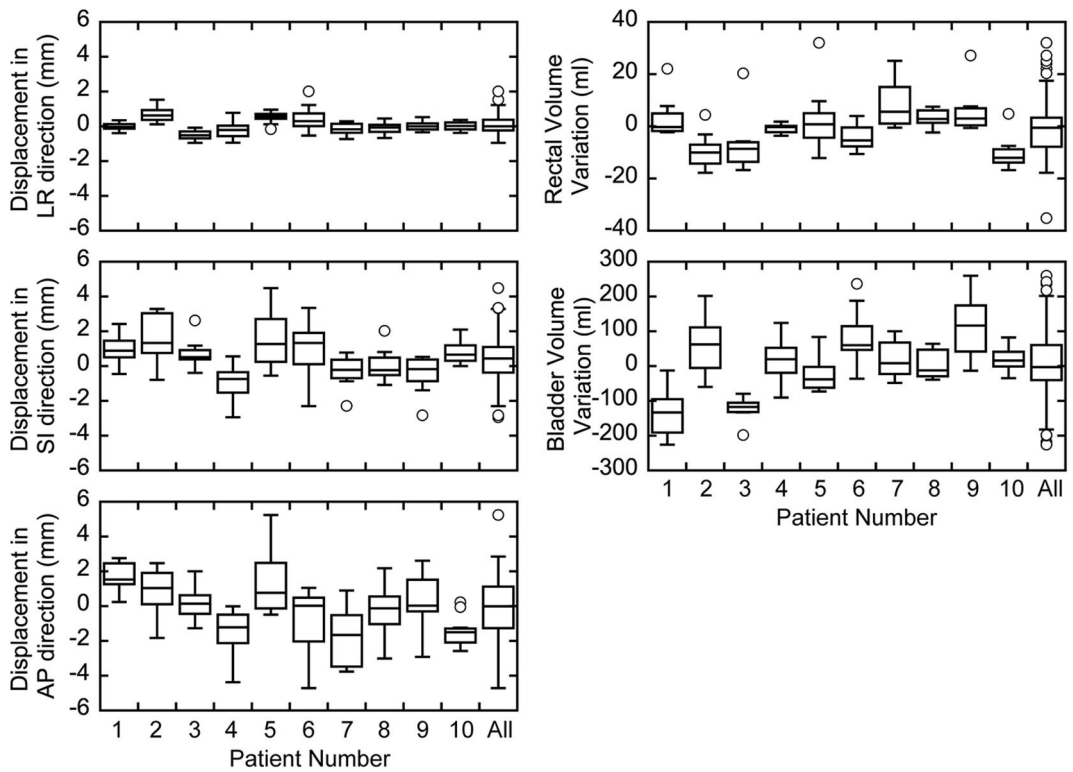

FIGURE 2 | Box plots of prostate displacements and inter-fractional variations in the rectal and bladder volumes for each patient.

the target coverage with the vertical field being worse than that with the horizontal field. The first is that the coverage of the vertical field in the treatment planning is slightly worse than that of the horizontal field. Because the dose calculation in XiO-N is a forward calculation, the 95% isodose line does not perfectly match the PTV. This effect is mostly observed along the beam axis rather than in the lateral direction perpendicular to the beam and results in worse coverage on the posterior side of the prostate

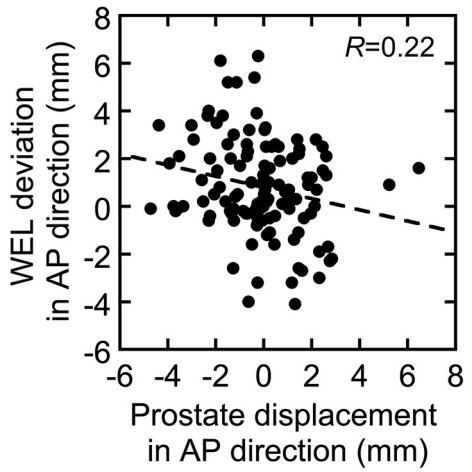

FIGURE 3 | Correlation between prostate displacement and water-equivalent path length (WEL) deviation in the AP direction. The dotted line shows linear fitting to the data.

with the vertical field than with the horizontal field. The second possible explanation is that the prostate displacements in the AP direction are slightly larger than the WEL changes in the AP direction, as illustrated in **Figure 3**, although the difference was not statistically significant. The prostate displacements in the AP direction affect the dose distribution in the vertical field, while the WEL deviations in the AP direction influence the dose distribution in the horizontal field. Thus, it is possible that the vertical field is more strongly affected by inter-fractional WEL deviations than is the horizontal field by the prostate displacements, which results in worse target coverage with the vertical field. Hence, if target coverage is a priority, the use of a vertical boost field may not be ideal.

There was no significant difference in the rectal wall dose between the rectum V95 values associated with the initial and boost fields. However, the vertical fields resulted in significantly lower rectum V50 values and significantly higher V10 values than the horizontal fields. It was assumed that the distal fall off in the vertical field was steeper than the lateral penumbra in the horizontal field, which explains why a significant difference was observed in the rectum V50 but not in the V95. Additionally, the difference in the rectum V10 values was attributed to the fact that the dose on the distal tail in the vertical field was higher than that on the lateral tail in the horizontal field. While these results capture inter-fractional anatomical changes, similar tendencies were observed in our previous study considering setup uncertainties and beam range uncertainties (15). Therefore, it can be concluded that a vertical field is more effective for reducing the rectal middle dose, while a horizontal field is more effective for reducing the rectal low dose.

Figure 4 shows that the correlation coefficients between the inter-fractional prostate displacement and prostate coverage were high in the SI and AP directions but low in the LR direction. Furthermore, the correlations of the prostate displacement with the deviations in the bladder volume and rectal volume were low ($R = 0.25$ and 0.34), as shown in **Figure 5**. This finding indicates that it is difficult to control the prostate displacement only by managing the inter-fractional bladder volume, rectal gas, and presence of feces in the rectum. However, monitoring the bladder volume and rectal gas and feces may effectively prevent changes in the bladder and rectal volumes as shown in this study because the TRCT images were acquired after these steps were taken; hence, such management techniques may be necessary to ensure patient safety. Because vertical fields are more sensitive to prostate displacements (because the fitting curve is steeper than in the horizontal field), and because the correlation coefficients between the rectal volume deviation and rectal wall dose volume ranged from medium to high, it can be inferred that managing the rectal gas or feces is important to control the rectal dose. In particular, because the ratio of the increase in the rectal dose to the increase in the rectal volume is higher with a vertical than horizontal field, more care must be taken when using a vertical field.

Figure 6 shows that vertical fields need smaller margins than horizontal fields. When generating the treatment planning beam, we use a spread-out Bragg peak size of 5 mm for a horizontal field and 10 mm for a vertical field in our facility. Therefore, an extra dose is delivered upstream of the target to ensure the target dose in each directional field. Because the inter-fractional prostate displacements tend to be larger in the AP than LR direction, as shown in **Figure 2**, it is assumed that vertical field, that extra dose is delivered in anterior direction, provide greater target coverage than the horizontal field when the margin is small. In practice, horizontal fields provide greater target coverage when the margin is sufficient (4 mm). Therefore, the challenge in delivering an extra dose is a situation specific to our facility; however, the same problem would occur at other facilities that use passive irradiation. Thus, 3-mm margins would be required for both vertical and horizontal fields.

The scope of this study is limited to the effects of inter-fractional changes because the TRCT images were acquired only one time after each irradiation. However, there may be more intra-fractional changes during the treatment. Although previous studies have indicated that the intra-fractional changes are smaller than the inter-fractional changes (28–30), it is necessary to consider both changes when determining the appropriate margins. Assuming that the intra-fractional change is equivalent to the inter-fractional change, a margin of $3 \times \sqrt{2} = 4.2$ mm would be required to ensure patient safety.

Furthermore, this study focused on single beams. If using a combination of vertical and horizontal fields, the lower rectal dose would increase more than when using only a horizontal field; however, the dose distributions can be expected to be more robust because the uncertainty of each field is distributed. Additionally, this study considered only the daily dose distribution. Because accumulating dose distributions are effective for predicting treatment outcomes and toxicities (31), we plan to evaluate the cumulative dose distributions in a future study. However, care should be taken because the use of a deformable image registration method to calculate the accumulated dose may produce some errors (32).

TABLE 2 | Dose volume of prostate and rectum.

			Initial			Boost		
			Vertical	Horizontal	*p*-value	Vertical	Horizontal	*p*-value
Plan	Prostate	V95 (%)	100 ± 0	100 ± 0	–	99.89 ± 0.07	99.99 ± 0.02	0.002
	Rectum	V95 (ml)	2.03 ± 0.48	1.93 ± 0.38	0.097	0.01 ± 0.02	0.03 ± 0.04	0.188
		V50 (ml)	3.10 ± 0.64	3.64 ± 0.70	<0.001	1.06 ± 0.23	1.90 ± 0.40	<0.001
		V10 (ml)	9.42 ± 1.79	5.11 ± 0.90	<0.001	6.08 ± 0.94	3.26 ± 0.67	<0.001
Daily	Prostate	V95 (%)	99.89 ± 0.62	100.00 ± 0.00	0.067	95.95 ± 5.81	97.88 ± 3.87	<0.001
	Rectum	V95 (ml)	1.93 ± 1.25	1.88 ± 0.96	0.432	0.37 ± 0.69	0.43 ± 0.65	0.145
		V50 (ml)	3.09 ± 1.63	3.57 ± 1.14	<0.001	1.19 ± 1.28	1.83 ± 0.98	<0.001
		V10 (ml)	9.43 ± 2.16	5.04 ± 1.37	<0.001	6.06 ± 1.99	3.22 ± 1.11	<0.001
Deviation	Prostate	V95 (%)	−0.11 ± 0.62	0.00 ± 0.00	0.067	−4.06 ± 5.83	−2.12 ± 3.88	<0.001
	Rectum	V95 (ml)	−0.10 ± 1.22	−0.05 ± 1.00	0.349	0.36 ± 0.69	0.40 ± 0.66	0.317
		V50 (ml)	−0.01 ± 1.60	−0.07 ± 1.14	0.402	0.14 ± 1.30	−0.07 ± 1.00	0.005
		V10 (ml)	0.03 ± 1.80	−0.07 ± 1.34	0.258	−0.01 ± 1.67	−0.03 ± 1.17	0.881

The Plan values show the mean ± standard deviation for each of 10 patients, the Daily values show the mean ± standard deviation of the 118 images from irradiation days, and the Deviation values show the mean ± standard deviations of the differences between the Plan and Daily values. Initial shows the fields to the PTV1, and Boost shows the field to the PTV2. Vx, volume receiving greater than x% of the prescription dose.

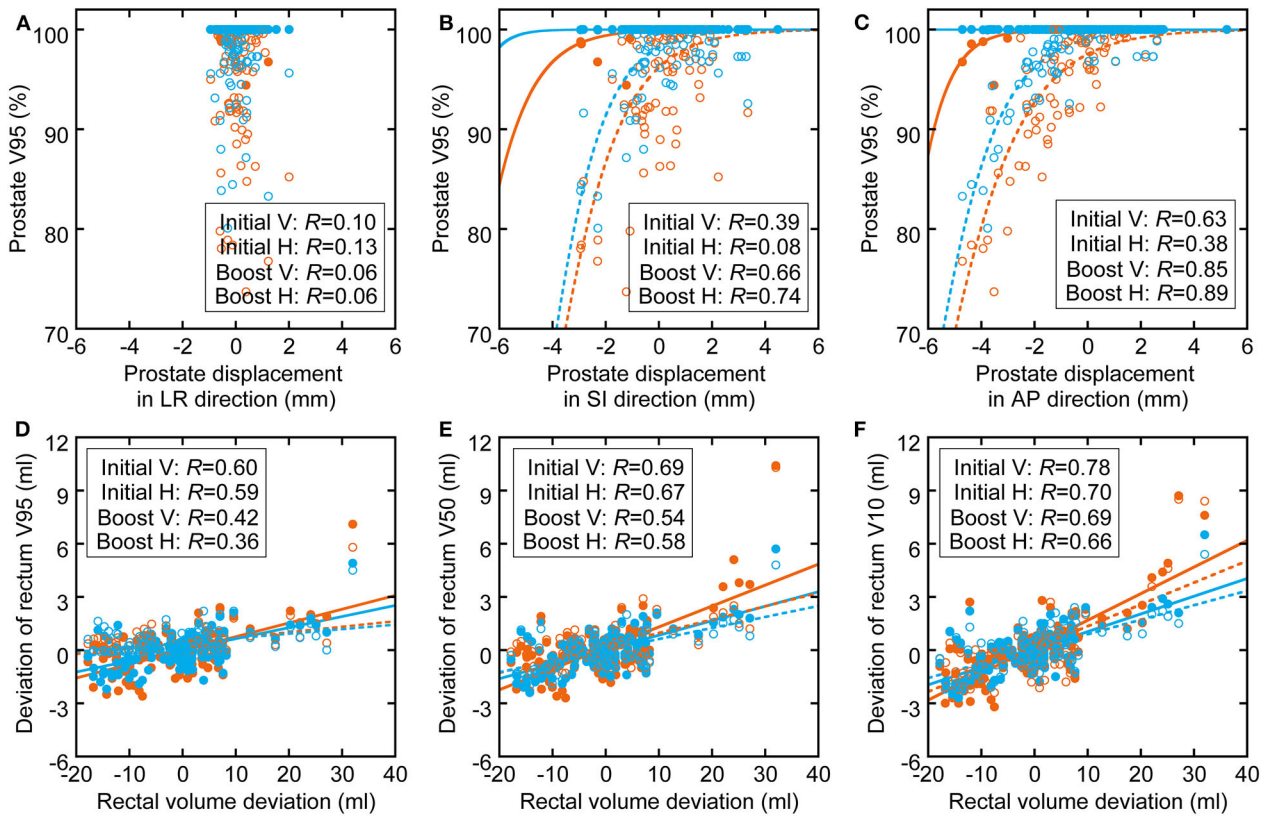

FIGURE 4 | Correlation between **(A–C)** prostate displacement and prostate dose volume deviation (sigmoid fitting) and between **(D–F)** rectal volume deviation and rectal dose volume deviation (linear fitting). The orange circles and lines show the parameters of vertical fields, and the light blue circles and lines show the parameters of horizontal fields. The filled circles and solid lines show initial fields, and the hollow circles and dotted lines show boost fields.

Another limitation of this study was that although 118 TRCT images were acquired, the number of patients in the sample set was low (10 patients). Therefore, further analyses with more patient data are necessary. Additionally, our evaluation did not include the seminal vesicle volume. Because the dose coverage would decrease because of inter-fractional movements

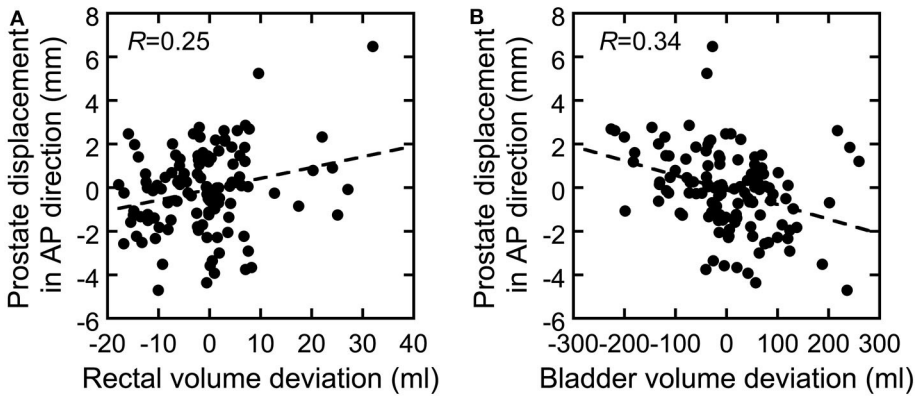

FIGURE 5 | Correlation between deviations in **(A)** rectal volume and **(B)** bladder volume vs. the prostate displacement in the AP direction.

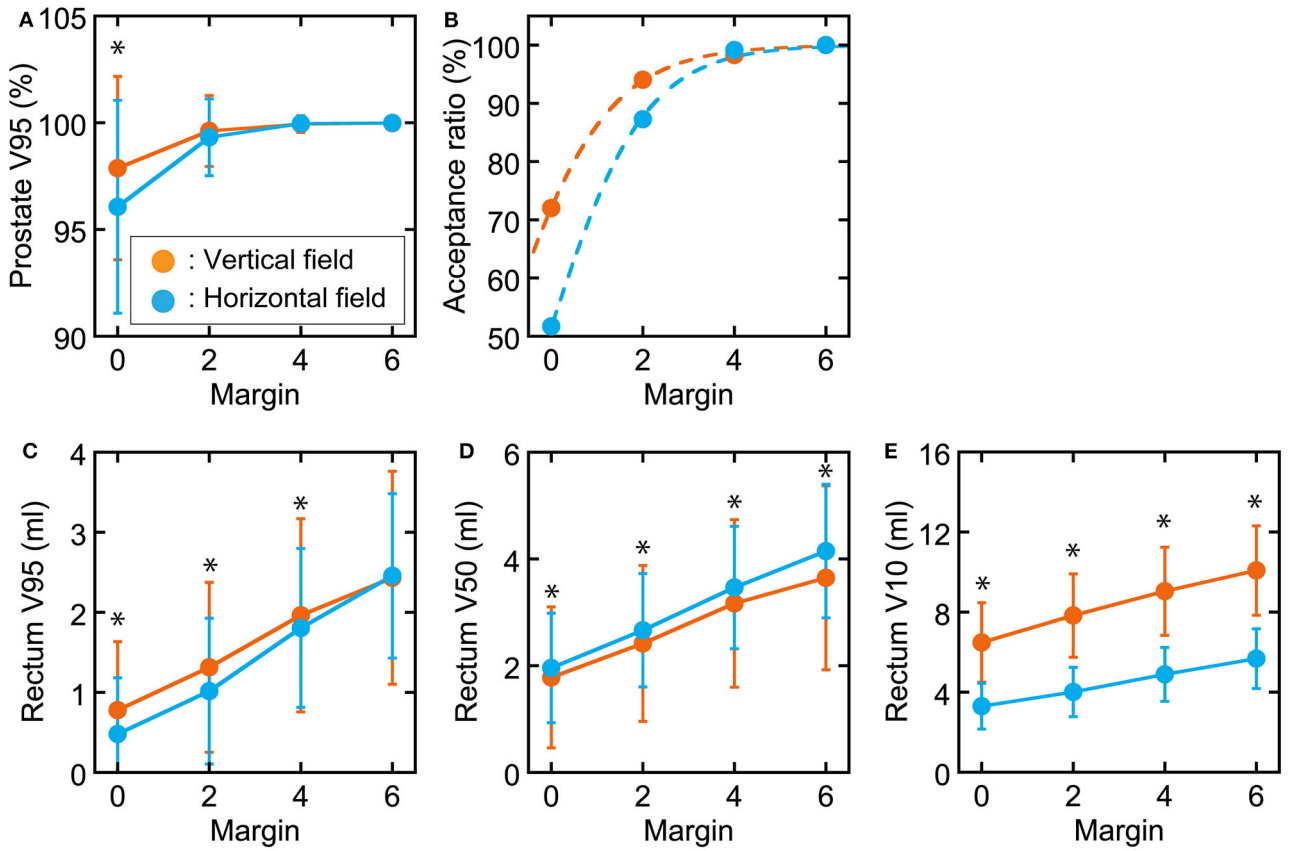

FIGURE 6 | Graphs of prostate and rectum dose–volume parameters and acceptance ratio in each margin. **(A)** Prostate V95. **(B)** Acceptance ratio when prostate V95 > 98% with fitted sigmoid functions. Rectal **(C)** V95, **(D)** V50, and **(E)** V10 values as functions of the margin used. Orange circles show vertical fields, and light blue circles show horizontal fields. *Statistically significant difference.

of the seminal vesicles, further evaluations are needed. Moreover, the prostate contours observed on TRCT were generated by the rigid image registration method from the PlanCT, which may include small errors because of inter-fractional anatomical changes.

CONCLUSION

In this study, we evaluated the robustness of horizontal and vertical fields against inter-fractional anatomical changes using daily CT images acquired in the treatment room during CIRT

for prostate cancer. The results showed that horizontal fields better ensure that the target dose is delivered than vertical fields. Vertical fields are effective for reducing the rectal middle dose, and horizontal fields are effective for reducing the rectal low dose. Finally, a 3-mm margin was found to be sufficient to ensure robustness against inter-fractional changes.

DATA AVAILABILITY STATEMENT

The datasets generated for this study are available on request to the corresponding author.

ETHICS STATEMENT

The studies involving human participants were reviewed and approved by Institutional review board at Gunma University Hospital. The patients/participants provided their written informed consent to participate in this study. Written informed consent was obtained from the individual(s) for the publication of any potentially identifiable images or data included in this article.

AUTHOR CONTRIBUTIONS

AY, YK, and HK designed and directed the analyses. AY, YK, HK, YM, NK, HS, SA, and KT generated a database and performed data collection. AY, YK, and HK participated substantially in the preparation of the manuscript. TS, TO, and TN supervised the project. All authors contributed to the article and approved the submitted version.

ACKNOWLEDGMENTS

The authors thank the radiology technologists, medical doctors, nurses, and medical physicists at Gunma University Heavy Ion Medical Center for their valuable insights. The authors also thank Taku Miyabe and Masashi Ohishi at the Accelerator Engineering Corporation, Chiba, Japan, for technical support. We thank Stephanie Knowlton, PhD and Angela Morben, DVM, ELS, from Edanz Group (https://en-author-services.edanzgroup.com/), for editing a draft of this manuscript.

REFERENCES

1. International Agency for Research on Cancer. *Global Cancer Observatory (GCO)*. Available online at: http://gco.iarc.fr/ (accessed January 20, 2020).
2. Hernandez DJ, Nielsen ME, Han M, Partin AW. Contemporary evaluation of the D'amico risk classification of prostate cancer. *Urology.* (2007) 70:931–5. doi: 10.1016/j.urology.2007.08.055
3. Michalski J, Winter K, Roach M, Markoe A, Sandler HM, Ryu J, et al. Clinical outcome of patients treated with 3D conformal radiation therapy (3D-CRT) for prostate cancer on RTOG 9406. *Int J Radiat Oncol Biol Phys.* (2012) 83:e363–70. doi: 10.1016/j.ijrobp.2011.12.070
4. Cahlon O, Zelefsky MJ, Shippy A, Chan H, Fuks Z, Yamada Y, et al. Ultra-high dose (86.4 Gy) IMRT for localized prostate cancer: toxicity and biochemical outcomes. *Int J Radiat Oncol Biol Phys.* (2008) 71:330–7. doi: 10.1016/j.ijrobp.2007.10.004
5. Sveistrup J, af Rosenschöld PM, Deasy JO, Oh JH, Pommer T, Petersen PM, et al. Improvement in toxicity in high risk prostate cancer patients treated with image-guided intensity-modulated radiotherapy compared to 3D conformal radiotherapy without daily image guidance. *Radiat Oncol.* (2014) 9:44. doi: 10.1186/1748-717X-9-44
6. Nomiya T, Tsuji H, Kawamura H, Ohno T, Toyama S, Shioyama Y, et al. A multi-institutional analysis of prospective studies of carbon ion radiotherapy for prostate cancer: a report from the Japan Carbon ion Radiation Oncology Study Group (J-CROS). *Radiother Oncol.* (2016) 121:288–93. doi: 10.1016/j.radonc.2016.10.009
7. Kawamura H, Kubo N, Sato H, Mizukami T, Katoh H, Ishikawa H, et al. Moderately hypofractionated carbon ion radiotherapy for prostate cancer; a prospective observational study "GUNMA0702". *BMC Cancer.* (2020) 20:75. doi: 10.1186/s12885-020-6570-8
8. Kraft G. Tumor therapy with heavy charged particles. *Prog Part Nucl Phys.* (2000) 45:S473–544. doi: 10.1016/S0146-6410(00)00112-5
9. Ohno T. Particle radiotherapy with carbon ion beams. *EPMA J.* (2013) 4:1–7. doi: 10.1186/1878-5085-4-9
10. Irie D, Saitoh JI, Shirai K, Abe, T, Kubota Y, et al. Verification of dose distribution in carbon ion radiation therapy for stage I lung cancer. *Int J Radiat Oncol Biol Phys.* (2016) 96:1117–23. doi: 10.1016/j.ijrobp.2016.09.002
11. Sakai M, Kubota Y, Saitoh JI, Irie D, Shirai K, Okada R, et al. Robustness of patient positioning for interfractional error in carbon ion radiotherapy for stage I lung cancer: bone matching versus tumor matching. *Radiother Oncol.* (2018) 129:95–100. doi: 10.1016/j.radonc.2017.10.003
12. Abe S, Kubota Y, Shibuya K, Koyama Y, Abe T, Ohno T, et al. Fiducial marker matching versus vertebral body matching: dosimetric impact of patient positioning in carbon ion radiotherapy for primary hepatic cancer. *Phys Med.* (2017) 33:114–20. doi: 10.1016/j.ejmp.2016.12.018
13. Houweling AC, Fukata K, Kubota Y, Shimada H, Rasch CR, Ohno T, et al. The impact of interfractional anatomical changes on the accumulated dose in carbon ion therapy of pancreatic cancer patients. *Radiother Oncol.* (2016) 119:319–25. doi: 10.1016/j.radonc.2016.03.004
14. Kubota Y, Katoh H, Shibuya K, Shiba S, Abe S, Sakai M, et al. Comparison between bone matching and marker matching for evaluation of intra- and inter-fractional changes in accumulated dose of carbon ion radiotherapy for hepatocellular carcinoma. *Radiother Oncol.* (2019) 137:77–82. doi: 10.1016/j.radonc.2019.04.026
15. Kubota Y, Kawamura H, Sakai M, Tsumuraya R, Tashiro M, Yusa K, et al. Changes in rectal dose due to alterations in beam angles for setup uncertainty and range uncertainty in carbon-ion radiotherapy for prostate cancer. *PLoS ONE.* (2016) 11:e0153894. doi: 10.1371/journal.pone.0153894
16. Kubota Y, Tashiro M, Shinohara A, Abe S, Souda S, Okada R, et al. Development of an automatic evaluation method for patient positioning error. *J Appl Clin Med Phys.* (2015) 16:100–11. doi: 10.1120/jacmp.v16i4.5400
17. Kubota Y, Hayashi H, Abe S, Souda S, Okada R, Ishii T, et al. Evaluation of the accuracy and clinical practicality of a calculation system for patient positional displacement in carbon ion radiotherapy at five sites. *J Appl Clin Med Phys.* (2018) 19:144–53. doi: 10.1002/acm2.12261
18. Li Y, Kubota Y, Tashiro M, Ohno T. Value of three-dimensional imaging systems for image-guided carbon ion radiotherapy. *Cancers.* (2019) 11:297. doi: 10.3390/cancers11030297
19. Ohno T, Kanai T, Yamada S, Yusa K, Tashiro M, Shimada H, et al. Carbon ion radiotherapy at the Gunma University heavy ion medical center: new facility set-up. *Cancers.* (2011) 3:4046–60. doi: 10.3390/cancers3044046
20. Renner TR, Chu WT. Wobbler facility for biomedical experiments. *Med Phys.* (1987) 14:825–34. doi: 10.1118/1.596009
21. Kanematsu N, Yonai S, Ishizaki A. The grid-dose-spreading algorithm for dose distribution calculation in heavy charged particle radiotherapy. *Med Phys.* (2008) 35:602–7. doi: 10.1118/1.2829878
22. Kanematsu N. Dose calculation algorithm of fast fine-heterogeneity correction for heavy charged particle radiotherapy. *Phys Med.* (2011) 27:97–102. doi: 10.1016/j.ejmp.2010.05.001
23. Kanai T, Endo M, Minohara S, Miyahara N, Koyama-ito H, Matsufuji N, et al. Biophysical characteristics of HIMAC clinical irradiation system for

heavy-ion radiation therapy. *Int J Radiat Oncol Biol Phys.* (1999) 44:201–10. doi: 10.1016/S0360-3016(98)00544-6
24. Tucker SL, Dong L, Cheung R, Johnson J, Mohan R, Huang EH, et al. Comparison of rectal dose-wall histogram versus dose-volume histogram for modeling the incidence of late rectal bleeding after radiotherapy. *Int J Radiat Oncol Biol Phys.* (2004) 60:1589–601. doi: 10.1016/j.ijrobp.2004.07.712
25. Andrzejewski P, Kuess P, Knäusl B, Pinker K, Georg P, Knoth J, et al. Feasibility of dominant intraprostatic lesion boosting using advanced photon-, proton- or brachytherapy. *Radiother Oncol.* (2015) 117:509–14. doi: 10.1016/j.radonc.2015.07.028
26. Maeda Y, Sato Y, Shibata S, Bou S, Yamamoto K, Tamamura H, et al. Effects of organ motion on proton prostate treatments, as determined from analysis of daily CT imaging for patient positioning. *Med Phys.* (2018) 45:1844–56. doi: 10.1002/mp.12869
27. Palombarini M, Mengoli S, Fantazzini P, Cadioli C, Degli Esposti C, Frezza GP. Analysis of inter-fraction setup errors and organ motion by daily kilovoltage cone beam computed tomography in intensity modulated radiotherapy of prostate cancer. *Radiat Oncol.* (2012) 7:56. doi: 10.1186/1748-717X-7-56
28. Tanyi JA, He T, Summers PA, Mburu RG, Kato CM, Rhodes SM, et al. Assessment of planning target volume margins for intensity-modulated radiotherapy of the prostate gland: role of daily inter- and intrafraction motion. *Int J Radiat Oncol Biol Phys.* (2010) 78:1579–85. doi: 10.1016/j.ijrobp.2010.02.001
29. Wust P, Joswig M, Graf R, Böhmer D, Beck M, Barelkowski T, et al. Dosimetric implications of inter- and intrafractional prostate positioning errors during tomotherapy: comparison of gold marker-based registrations with native MVCT. *Strahlenther Onkol.* (2017) 193:700–6. doi: 10.1007/s00066-017-1141-x
30. Beltran C, Herman MG, Davis BJ. Planning target margin calculations for prostate radiotherapy based on intrafraction and interfraction motion using four localization methods. *Int J Radiat Oncol Biol Phys.* (2008) 70:289–95. doi: 10.1016/j.ijrobp.2007.08.040
31. Shelley LEA, Scaife JE, Romanchikova M, Harrison K, Forman JR, Bates AM, et al. Delivered dose can be a better predictor of rectal toxicity than planned dose in prostate radiotherapy. *Radiother Oncol.* (2017) 123:466–71. doi: 10.1016/j.radonc.2017.04.008
32. Kubota Y, Okamoto M, Li Y, Shiba S, Okazaki S, Komatsu S, et al. Evaluation of intensity- and contour-based deformable image registration accuracy in pancreatic cancer patients. *Cancers.* (2019) 11:1447. doi: 10.3390/cancers11101447

Conflict of Interest: The authors declare that the research was conducted in the absence of any commercial or financial relationships that could be construed as a potential conflict of interest.

Copyright © 2020 Yokoyama, Kubota, Kawamura, Miyasaka, Kubo, Sato, Abe, Tsuda, Sutou, Ohno and Nakano. This is an open-access article distributed under the terms of the Creative Commons Attribution License (CC BY). The use, distribution or reproduction in other forums is permitted, provided the original author(s) and the copyright owner(s) are credited and that the original publication in this journal is cited, in accordance with accepted academic practice. No use, distribution or reproduction is permitted which does not comply with these terms.

frontiers in Oncology

ORIGINAL RESEARCH
published: 14 August 2020
doi: 10.3389/fonc.2020.01396

Skin Dose Reduction by Layer-Stacking Irradiation in Carbon Ion Radiotherapy for Parotid Tumors

Nobuteru Kubo[1], Yoshiki Kubota[1], Takahiro Oike[1], Hidemasa Kawamura[1], Makoto Sakai[1], Ayaka Imamura[1], Shuichiro Komatsu[1], Yuhei Miyasaka[1], Hiro Sato[1], Atsushi Musha[1], Naoko Okano[1], Katsuyuki Shirai[1,2], Jun-ichi Saitoh[1,3], Kazuaki Chikamatsu[4] and Tatsuya Ohno[1]*

[1] Gunma University Heavy Ion Medical Center, Maebashi, Japan, [2] Department of Radiology, Saitama Medical Center, Jichi Medical University, Omiya-Ku, Japan, [3] Department of Radiation Oncology, Faculty of Medicine, University of Toyama, Toyama, Japan, [4] Department of Otolaryngology-Head and Neck Surgery, Gunma University Graduate School of Medicine, Maebashi, Japan

Background: Layer-stacking irradiation (LSI) results in the accumulation of multiple small spread-out Bragg peaks along the beam direction. Although the superiority of LSI to conventional passive irradiation (CPI) regarding normal tissue sparing is theoretically evident, the clinical benefit of LSI has not been demonstrated. Here, we compared LSI with CPI using the same treatment planning-computed tomography images used for carbon ion radiotherapy (CIRT).

Methods: Twenty-one parotid tumors were analyzed. The clinical target volume (CTV) 1 and CTV2 encompassed the parotid grand and the tumor, respectively. CTV1 and CTV2 received 36 Gy (RBE: relative biological effectiveness) in nine fractions and 64 Gy (RBE) in 16 fractions, respectively, using either LSI or CPI. CTV coverage was assessed by DX%, which is the dose covering at least X% of the target volume. Skin dose was assessed by SX, which is the skin surface area receiving at least X Gy (RBE).

Results: For CTV1 and CTV2, there were no significant differences in D2% between LSI and CPI. D50% and D98% were slightly higher for CPI; however, the absolute difference between the two methods was <3%. S10–S60 (in increments of 10) were significantly lower for LSI than for CPI ($P < 0.001$ for all parameters). LSI was associated with a significant trend toward dose reduction at the skin area irradiated with a higher dose by CPI ($P < 0.001$).

Conclusions: LSI achieved better skin sparing than CPI without sacrificing target volume coverage in parotid tumor patients.

Keywords: carbon ion radiotherapy, head and neck tumors, layer-stacking irradiation, parotid tumors, radiation dermatitis, dose surface-area histogram, skin dose

OPEN ACCESS

Edited by:
Daniel Michael Trifiletti, Mayo Clinic Florida, United States

Reviewed by:
Henry Soo-Min Park, Yale University, United States
Eric Lehrer, Icahn School of Medicine at Mount Sinai, United States

****Correspondence:***
Nobuteru Kubo
kubo0330@gmail.com

Specialty section:
This article was submitted to Radiation Oncology, a section of the journal Frontiers in Oncology

Received: *17 January 2020*
Accepted: *02 July 2020*
Published: *14 August 2020*

Citation:
Kubo N, Kubota Y, Oike T, Kawamura H, Sakai M, Imamura A, Komatsu S, Miyasaka Y, Sato H, Musha A, Okano N, Shirai K, Saitoh J, Chikamatsu K and Ohno T (2020) Skin Dose Reduction by Layer-Stacking Irradiation in Carbon Ion Radiotherapy for Parotid Tumors. Front. Oncol. 10:1396. doi: 10.3389/fonc.2020.01396

INTRODUCTION

Carbon ion radiotherapy holds great promise in cancer treatment. Current evidence suggests that carbon ion radiotherapy is more effective for tumor control than standard care (1). In conventional passive irradiation (CPI) with carbon ions, treatment beams are broadened in the lateral direction using a pair of wobbler magnets and a scatterer, and the Bragg peaks are broadened along the

beam direction using a ridge filter to form a spread-out Bragg peak (SOBP) (2). This enables dose distribution that is highly conformal to tumors. However, CPI methods have several shortcomings: i.e., normal tissues located at the entrance of the target receive excessive doses because the SOBP length is fixed by the diameter of the target (**Figure 1A**). This effect becomes greater in bulky tumors irradiated using long-length SOBPs, which increase the risk of toxicity to normal tissues. To overcome this issue, layer-stacking irradiation (LSI) was developed (3). In LSI, a finite number of small SOBPs are accumulated along the beam direction, contributing to dose reduction to normal tissues at the region near the entrance (**Figure 1B**). New carbon ion radiotherapy facilities prefer to adopt the spot-scanning technique, which is another irradiation method aimed at achieving high-dose conformation, However, already existing carbon ion radiotherapy facilities still employ passive beam treatment rooms, which are not adapted for spot-scanning. In Japan, about half of carbon ion radiotherapy facilities have passive beam treatment rooms. Therefore, LSI has the advantage that it can be used as an alternative method in facilities where the installation of scanning beam systems is prohibitive (4–6).

From these perspectives, the usefulness of LSI is theoretically evident, especially for the treatment of superficial tumors. However, the clinical benefit of this method over CPI remains to be demonstrated. To address this issue, we chose parotid tumors as a model in the present analysis. In carbon ion radiotherapy for parotid tumors, sparing of the skin is important because parotid glands are anatomically adjacent to the skin. A study that reported the outcomes of carbon ion radiotherapy for parotid tumors showed that the doses prescribed to the target were compromised in 57% of the patients to avoid exposure of the skin or the brain to high-dose irradiation (7). Another multi-institutional study that reported the outcomes of carbon ion radiotherapy for salivary gland tumors, 84% of which were parotid tumors, showed that the incidence of grade-3 dermatitis was 10% according to Common Terminology Criteria for Adverse Events version 4.0 (8). Based on these data, the present study compared treatment plans created using LSI with those created using CPI in the same set of patients with parotid tumors treated with carbon ion radiotherapy by analyzing target volume coverage and skin doses.

MATERIALS AND METHODS

Patient Characteristics

Between October 2010 and March 2019, 21 consecutive patients with parotid tumors were treated with carbon ion radiotherapy at Gunma University Heavy Ion Medical Center (GHMC). **Table 1** shows patient and tumor characteristics.

Treatment Planning

Computed tomography images used for treatment planning were acquired at 2-mm slice thickness. The voxel dimensions of all

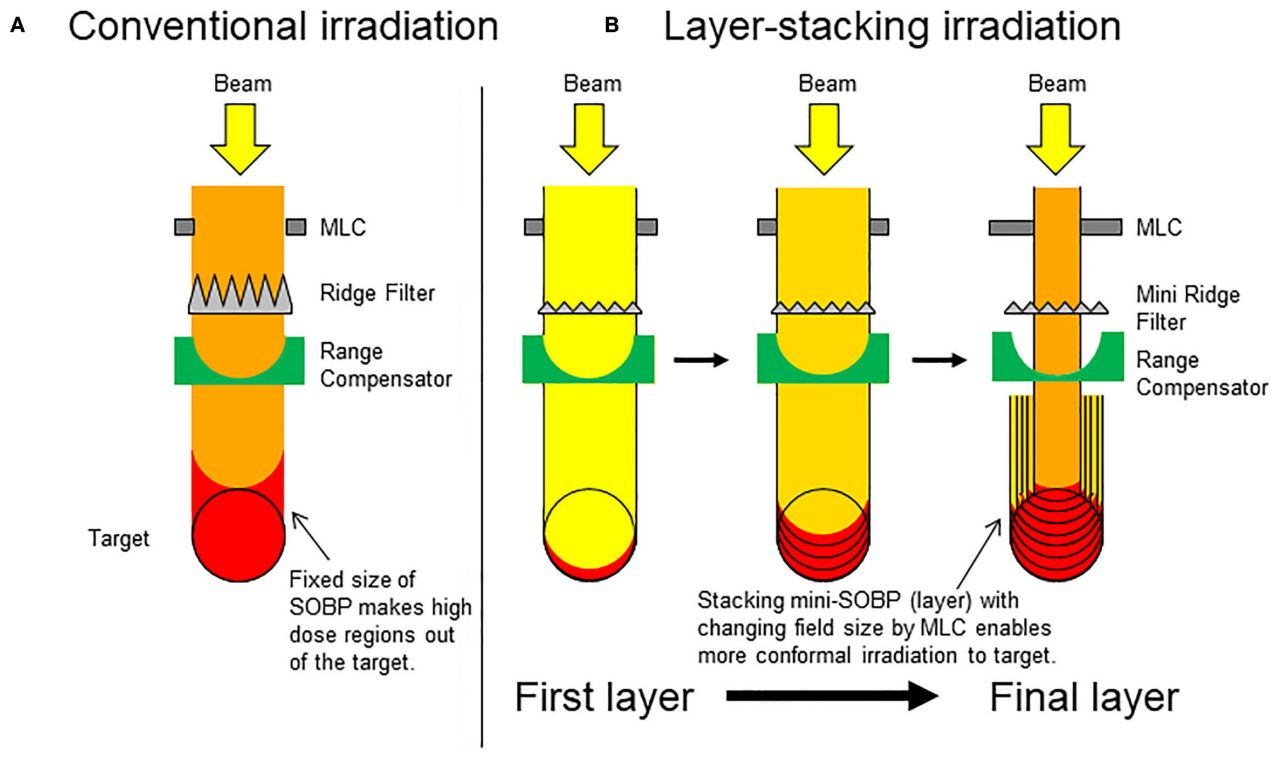

FIGURE 1 | Schematic presentation of conventional passive irradiation and layer-stacking irradiation. **(A)** Conventional passive irradiation; **(B)** layer-stacking irradiation.

CT images were ∼0.88 × 0.88 × 2.0 mm. Treatment plans were generated using XiO-N systems (Elekta, Stockholm, Sweden). Target volumes used in clinical practice were used in this study as follows: clinical target volume (CTV) 1 generally encompassed the whole anatomical site of the tumor origin (i.e., parotid grand), whereas CTV2 encompassed the tumor.

In the treatment planning for carbon ion radiotherapy, the unit Gy (RBE, relative biological effectiveness) is used to describe the prescribed dose (9). Thirty-six Gy (RBE) in nine fractions and 64 Gy (RBE) in 16 fractions were prescribed to CTV1 and CTV2, respectively.

Treatment plans using CPI were generated as described previously (10). The SOBP size used for CPI varied by 5 and 10 mm for horizontal and vertical beams, respectively.

In LSI, 5-mm SOBPs were stacked in the beam direction in steps of 2.5 mm using the range shifter, and the shape of multi leaf collimator (MLC) was changed at every step after 12 steps (i.e., 30 mm). The SOBP size varied by 2.5 mm. The initial shapes used for LSI were those used for conventional irradiation.

The same planning settings were used for CPI and LSI (e.g., the settings for proximal and distal margins to the targets, beam energy, and the number and direction of the beams), and the SOBP size was determined based on the target and proximal and distal margins.

Plan Evaluation

Correlation analysis of carbon ion doses with CTVs or with the skin was performed using MIM Maestro (version 6.8.7., MIM Software Inc., Cleveland, OH, USA). D2%, D50%, D98%, and the homogeneity index (HI) were used as the endpoints for CTV coverage. DX% indicates the dose that covers at least X% of a given target volume. HI is calculated using the following equation: HI = (D2% – D98%)/D50% (11).

The skin volume was defined as the region within 0.02 cm under the skin surface (12). Skin surface area (cm^2) was defined as the skin volume divided by 0.02. SX was used as the endpoint for dose-skin surface area analysis, where SX indicates the skin surface area irradiated with at least X Gy (RBE).

Statistics

Differences in the values between two groups were examined using Wilcoxon rank-sum test. The trend in skin dose reduction by LSI for S10 through S60 was examined using the Jonckheere-Terpstra test. A $P < 0.05$ was considered statistically significant. All statistical analyses were performed using SPSS (version 25; SPSS Inc., Chicago, IL, USA).

RESULTS

Comparison of Target Volume Coverage

First, we compared target volume coverage between CPI and LSI in the same set of 21 parotid tumors (**Table 2**).

For CTV1, there were no significant differences in D2% between the two methods. D50% and D98% were significantly higher for CPI. However, the absolute differences between the two methods were small (within 2 and 3% for D50% and D98%, respectively). HI was significantly and slightly higher for LSI.

TABLE 1 | Patient and tumor characteristics.

Variable	*n* (%)
Age	
Median (range)	62 (42–87)
Gender	
Male	11 (52)
Female	10 (48)
Histology	
Adenoid cystic carcinoma	5 (24)
Adenocarcinoma	4 (19)
Mucoepidermoid carcinoma	3 (14)
Epithelial-myoepithelial carcinoma	3 (14)
Salivary duct carcinoma	3 (14)
Acinic cell carcinoma	1 (5)
Synovial sarcoma	1 (5)
Carcinoma	1 (5)
T stage	
T1	1 (5)
T2	2 (10)
T3	3 (14)
T4a	9 (43)
T4b	6 (29)
***N* stage**	
0	18 (86)
1	1 (5)
2	2 (10)
3	0 (0)
M stage	
0	21 (100)
1	0 (0)
Primary or recurrent tumor	
Primary tumor	15 (71)
Recurrence after surgery	6 (29)
CTV volume (cm^3)	
CTV1 median (range)	83.0 (15.5–253.7)
CTV2 median (range)	62.7 (8.7–189.0)

For CTV2, there were no significant differences in D2% between the two methods. D50% and D98% were significantly higher for CPI. However, the absolute differences between the two methods were small (within 1 and 2% for D50% and D98%, respectively). HI was significantly and slightly higher for LSI.

Taken together, these data indicate that target volume coverage achieved by LSI is comparable to that achieved by CPI.

Comparison of Skin Dose

After confirming that target volume coverage was comparable between the treatment plans created using two methods, we compared the skin doses. Overall, the skin doses were lower for LSI than for CPI throughout the dose range (**Figure 2**). S10, S20, S30, S40, S50, and S60 were significantly lower for LSI than for CPI (**Table 3**). There was a significant trend toward dose reduction associated with LSI at the skin area irradiated

TABLE 2 | Target volume coverage by conventional passive irradiation and layer-stacking irradiation.

Target volume	Index	Conventional (mean ± SD)	Layer-stacking (mean ± SD)	*P*-values	% difference (mean ± SD)
CTV1	D2%	65.0 ± 0.5	64.6 ± 1.3	0.247	1.0 ± 1.9
	D50%	63.2 ± 2.1	62.4 ± 2.0	<0.001	1.2 ± 1.4
	D98%	50.5 ± 7.9	49.7 ± 7.2	0.006	2.6 ± 2.5
	HI	0.23 ± 0.12	0.24 ± 0.11	0.025	NA
CTV2	D2%	65.0 ± 0.5	65.0 ± 0.6	0.506	0.56 ± 0.59
	D50%	64.1 ± 0.5	63.8 ± 0.4	0.002	0.69 ± 0.45
	D98%	61.0 ± 3.1	60.3 ± 2.7	0.002	1.6 ± 1.0
	HI	0.06 ± 0.04	0.07 ± 0.04	<0.001	NA

D2%, D50%, and D98% are shown in Gy (RBE). P-values were assessed by Wilcoxon rank-sum test. The % difference indicates the ratio of absolute difference between DX% for conventional passive irradiation and that for layer-stacking irradiation to DX% for conventional passive irradiation expressed as a percentage. SD, standard deviation; NA, not assessed.

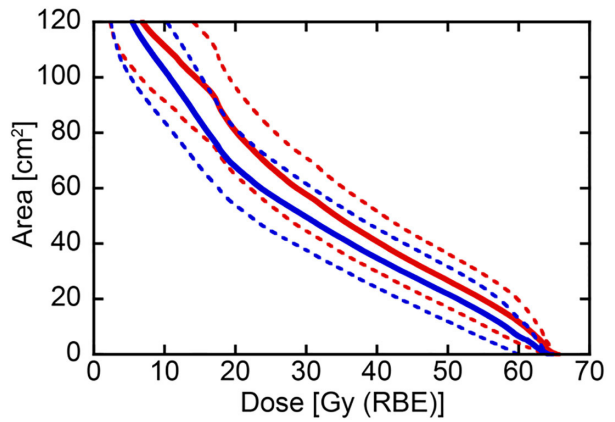

FIGURE 2 | Dose-surface area histogram for the skin comparing conventional passive irradiation and layer-stacking irradiation in the same 21 parotid tumor cases. Solid and dotted lines indicate mean and 95% confidence interval, respectively. Red and blue lines show conventional passive irradiation and layer-stacking irradiation, respectively.

with a higher dose by CPI ($P < 0.001$; **Figures 3**, **4**). Taken together, these data demonstrate that skin sparing by LSI is superior to that of CPI in the treatment of parotid tumors, especially in the high-dose range. **Figure 5** shows that the skin sparing ability of LSI correlated with the distance from CTV2 to the skin.

DISCUSSION

This is the first study comparing LSI with CPI using a cohort of patients treated with carbon ion radiotherapy. The treatment plans were tested in 21 patients with parotid tumors, and the results showed that LSI was superior to CPI regarding skin sparing, especially at the high-dose range, without compromising target volume coverage. The treatment

TABLE 3 | Skin surface dose for conventional passive irradiation and layer-stacking irradiation.

Index	Conventional (mean ± SD)	Layer-stacking (mean ± SD)	*P*-values
S10	111.3 ± 47.3	102.5 ± 44.6	<0.001
S20	80.6 ± 37.9	67.6 ± 33.1	<0.001
S30	57.7 ± 31.5	49.6 ± 28.6	<0.001
S40	40.7 ± 26.1	34.7 ± 25.5	<0.001
S50	26.6 ± 23.2	21.7 ± 23.6	<0.001
S60	11.5 ± 18.5	6.5 ± 15.4	<0.001

P-values were assessed by Wilcoxon rank-sum test. SD, standard deviation.

for head-and-neck non-squamous cell carcinoma has not been standardized, and evidence suggests that carbon ion radiotherapy achieves favorable local control and overall survival in patients with this disease (13–17). Taken together, the present data suggest that carbon ion radiotherapy for head-and-neck non-squamous cell carcinomas can be improved by using LSI.

The dosimetric parameters associated with the risk of skin toxicities after carbon ion radiotherapy have been reported extensively. Takakusagi et al. reported the outcomes of malignant bone and soft tissue tumors treated with carbon ion radiotherapy and showed that grade-2 acute dermatitis increased when S40 exceeded 25 cm^2 (12). In this study, LSI decreased the number of patients in which the S40 exceeded 25 cm^2 by 14% (from 15 patients to 12 patients). Yanagi et al. reported the outcomes of bone and soft tissue sarcomas treated with carbon ion radiotherapy and showed that grade-3 chronic dermatitis increased when S60 exceeded 20 cm^2 (18). In this study, LSI decreased the number of patients in which the S60 exceeded 20 cm^2 by 33% (from 3 patients to 2 patients). The two studies by Takakusagi et al. and Yanagi et al. suggest that the risk of skin toxicities after carbon ion radiotherapy is higher in the high-dose range (i.e., S40–S60). In this study, the skin dose reduction by LSI was greater at the high-dose range. This indicates the potential of LSI for the efficient reduction of skin toxicities associated with carbon ion radiotherapy, which may improve the quality of life of patients. Further study is warranted to investigate whether skin dose reduction by CPI affects clinical outcomes.

However, LSI has several shortcomings. In the LSI systems used in our institution (i.e., GHMC) and in the National Institutes of Radiological Sciences, Japan (2), the initial MLC shape is fixed within a depth of 30 mm (i.e., 12 steps). Therefore, achieving dose distribution conformal to the tumors using LSI is difficult when the tumor diameter is <30 mm. In the present cohort, the LSI-based treatment plan resulted in a slightly higher skin dose than that of the CPI-based treatment plan in a patient with a small tumor whose CTV2 volume was 10.1 cm^3 (as indicated in light blue in the second case from the right in **Figure 3**). In addition, irradiation time is longer for LSI than for CPI. In the present study, the median irradiation times per port for CPI and LSI were 46 and 105 s, respectively. Therefore, the indications for LSI should be carefully determined according to tumor size.

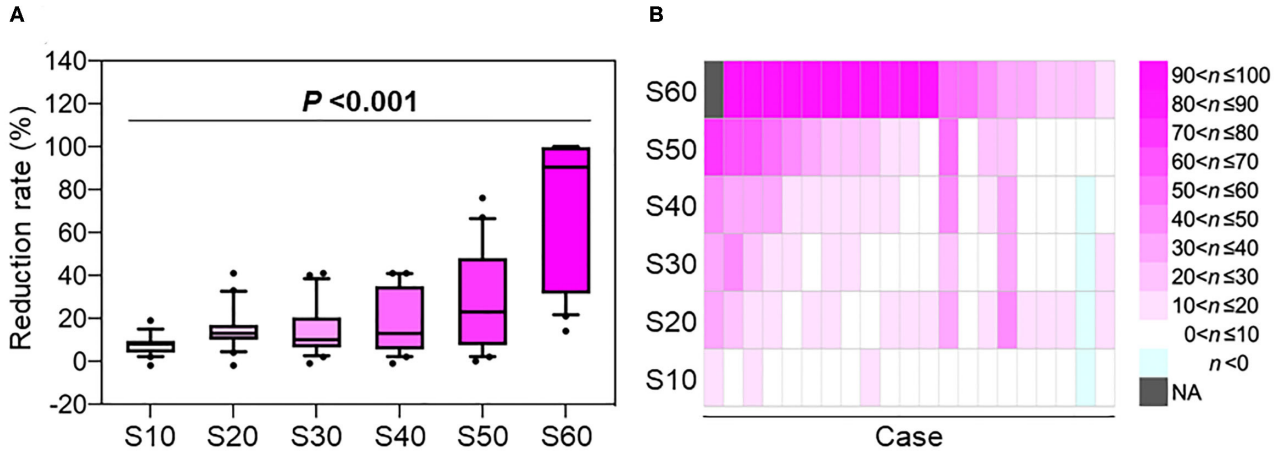

FIGURE 3 | The rate of skin dose reduction in the treatment plans created using layer-stacking irradiation compared with those created by conventional passive irradiation as controls. **(A)** Box whisker plot. Boxes indicate 25th percentile through 75th percentile. Top and bottom whiskers show 10th and 90th percentile, respectively. *P*-value was assessed using the Jonckheere-Terpstra test. **(B)** Heatmap showing the data from an individual subject. *n* indicates the reduction rate expressed as a percentage. NA, not assessed because the control value was zero.

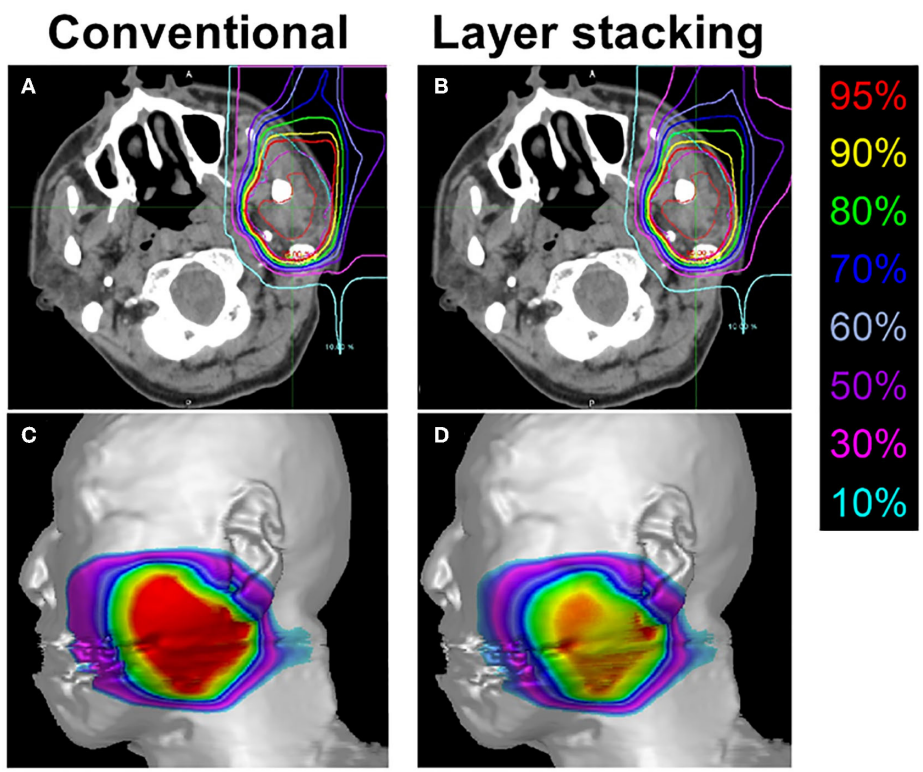

FIGURE 4 | Representative treatment plans created by conventional passive irradiation and layer-stacking irradiation for the same subject. **(A,B)** Dose distribution in axial computed tomography images. Gross tumor volume, clinical target volume (CTV) 1, and CTV2 are indicated in red, cyan, and magenta, respectively; **(C,D)** dose-surface area model for the skin.

The present study had several limitations. First, the skin dose was analyzed in a relatively small number of parotid tumor cases ($n = 21$). Second, the effect of LSI on dose reduction in other organs at risk needs to be investigated in cancers other than parotid tumors. Further studies using larger cohorts would help identify the patients who would most benefit from LSI.

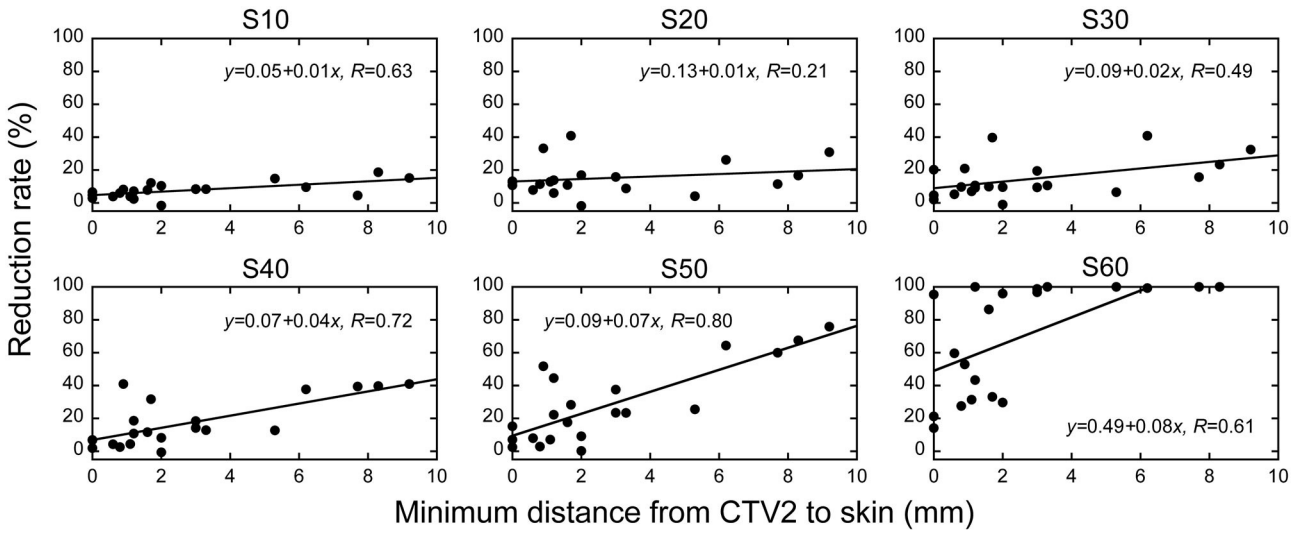

FIGURE 5 | The association between the distance from CTV2 to skin at the axial isocenter sleeve and skin dose reduction rate in layer-stacking irradiation and conventional passive irradiation. The vertical axis shows the reduction in the dose of irradiation the skin receives when layer-stacking irradiation is employed. SX indicates the skin surface area irradiated with at least X Gy (RBE).

In summary, we showed, for the first time, that LSI is superior to CPI regarding skin sparing, especially at the high-dose range, without sacrificing target volume coverage in patients with parotid tumors. Further studies are warranted to determine the benefits of LSI for other cancers and other organs at risk.

DATA AVAILABILITY STATEMENT

The raw data supporting the conclusions of this article will be made available by the authors, without undue reservation, to any qualified researcher.

ETHICS STATEMENT

The studies involving human participants were reviewed and approved by the institutional review board of Gunma University Hospital. Written informed consent for participation was not required for this study in accordance with the national legislation and the institutional requirements.

AUTHOR CONTRIBUTIONS

NK, YK, MS, and TOi designed and directed the analyses. NK, YK, AI, SK, YM, HS, AM, and NO generated a database and performed data collection. NK, YK, and TOi participated substantially in the preparation of the manuscript. HK, KS, JS, KC, and TOh supervised the project. All authors provide approval for publication of the content.

FUNDING

This project was supported by GHMC.

ACKNOWLEDGMENTS

The authors thank the radiology technologists, medical doctors, and medical physicists at GHMC for their valuable insights. The authors also thank Taku Miyabe, Masashi Ohishi, and Ryo Tsumuraya of the Accelerator Engineering Corporation (Chiba, Japan) for technical support.

REFERENCES

1. Schlaff CD, Krauze A, Belard A, O'Connell JJ, Camphausen KA. Bringing the heavy: carbon ion therapy in the radiobiological and clinical context. *Radiat Oncol.* (2014) 9:88. doi: 10.1186/1748-717X-9-88
2. Mori S, Kanematsu N, Asakura H, Sharp GC, Kumagai M, Dobashi S, et al. Four-dimensional lung treatment planning in layer-stacking carbon ion beam treatment: comparison of layer-stacking and conventional ungated/gated irradiation. *Int J Radiat Oncol Biol Phys.* (2011) 80:597–607. doi: 10.1016/j.ijrobp.2010.07.1982
3. Kanematsu N, Endo M, Futami Y, Kanai T, Asakura H, Oka H, et al. Treatment planning for the layer-stacking irradiation system for three-dimensional conformal heavy-ion radiotherapy. *Med Phys.* (2002) 29:2823–9. doi: 10.1118/1.1521938
4. Furukawa T, Inaniwa T, Sato S, Tomitani T, Minohara S, Noda K, et al. Design study of a raster scanning system for moving target irradiation in heavy-ion radiotherapy. *Med Phys.* (2007) 34:1085–97. doi: 10.1118/1.2558213
5. Kanai T, Kanematsu N, Minohara S, Komori M, Torikoshi M, Asakura H, et al. Commissioning of a conformal irradiation system for heavy-ion radiotherapy using a layer-stacking method. *Med Phys.* (2006) 33:2989–97. doi: 10.1118/1.2219771

6. Mori S, Kumagai M, Miki K. Four-dimensional layer-stacking carbon-ion beam dose distribution by use of a lung numeric phantom. *Radiol Phys Technol.* (2015) 8:232–42. doi: 10.1007/s12194-015-0312-7
7. Koto M, Hasegawa A, Takagi R, Ikawa H, Naganawa K, Mizoe J-E, et al. Definitive carbon-ion radiotherapy for locally advanced parotid gland carcinomas. *Head Neck.* (2017) 39:724–9. doi: 10.1002/hed.24671
8. Hayashi K, Koto M, Demizu Y, Saitoh JI, Suefuji H, Okimoto T, et al. A retrospective multicenter study of carbon-ion radiotherapy for major salivary gland carcinomas: subanalysis of J-CROS 1402 HN. *Cancer Sci.* (2018) 109:1576–82. doi: 10.1111/cas.13558
9. Kanai T, Endo M, Minohara S, Miyahara N, Koyama-ito H, Tomura H, et al. Biophysical characteristics of HIMAC clinical irradiation system for heavy-ion radiation therapy. *Int J Radiat Oncol.* (1999) 44:201–10. doi: 10.1016/S0360-3016(98)00544-6
10. Ohno T, Kanai T, Yamada S, Yusa K, Tashiro M, Shimada H, et al. Carbon Ion Radiotherapy at the Gunma University Heavy Ion Medical Center: New Facility Set-up. *Cancers.* (2011) 3:4046–60. doi: 10.3390/cancers3044046
11. International Commission on Radiation Units and Measurements Report 83. Report 83. Prescribing, recording, and reporting photon-beam inten- sity-modulated radiation therapy (IMRT). *J ICRU.* (2010) 10:34–35. doi: 10.1007/s00066-011-0015-x
12. Takakusagi Y, Saitoh J-I, Kiyohara H, Oike T, Noda S-E, Ohno T, et al. Predictive factors of acute skin reactions to carbon ion radiotherapy for the treatment of malignant bone and soft tissue tumors. *Radiat Oncol.* (2017) 12:185. doi: 10.1186/s13014-017-0927-4
13. Sulaiman NS, Demizu Y, Koto M, Saitoh J ichi, Suefuji H, Tsuji H, et al. Multicenter study of carbon-ion radiation therapy for adenoid cystic carcinoma of the head and neck: subanalysis of the Japan Carbon-Ion Radiation Oncology Study Group (J-CROS) Study (1402 HN). *Int J Radiat Oncol Biol Phys.* (2018) 100:639–46. doi: 10.1016/j.ijrobp.2017.11.010
14. Mizoguchi N, Tsuji H, Toyama S, Kamada T, Tsujii H, Nakayama Y, et al. Carbon-ion radiotherapy for locally advanced primary or postoperative recurrent epithelial carcinoma of the lacrimal gland. *Radiother Oncol.* (2015) 114:373–7. doi: 10.1016/j.radonc.2015.01.009
15. Shirai K, Koto M, Demizu Y, Suefuji H, Ohno T, Tsuji H. Multi-institutional retrospective study of mucoepidermoid carcinoma treated with carbon-ion radiotherapy. (2017) 108:1447–51. doi: 10.1111/cas.13270
16. Suefuji H, Koto M, Demizu Y, Saitoh J-I, Shioyama Y, Tsuji H, et al. A Retrospective multicenter study of carbon ion radiotherapy for locally advanced olfactory neuroblastomas. *Anticancer Res.* (2018) 38:1665–70. doi: 10.21873/anticanres.12399
17. Saitoh J ichi, Koto M, Demizu Y, Suefuji H, Ohno T, Tsuji H, et al. A multicenter study of carbon-ion radiation therapy for head and neck adenocarcinoma. *Int J Radiat Oncol Biol Phys.* (2017) 99:442–9. doi: 10.1016/j.ijrobp.2017.04.032
18. Yanagi T, Kamada T, Tsuji H, Imai R, Serizawa I, Tsujii H. Dose-volume histogram and dose-surface histogram analysis for skin reactions to carbon ion radiotherapy for bone and soft tissue sarcoma. *Radiother Oncol.* (2010) 95:60–5. doi: 10.1016/j.radonc.2009.08.041

Conflict of Interest: The authors declare that the research was conducted in the absence of any commercial or financial relationships that could be construed as a potential conflict of interest.

Copyright © 2020 Kubo, Kubota, Oike, Kawamura, Sakai, Imamura, Komatsu, Miyasaka, Sato, Musha, Okano, Shirai, Saitoh, Chikamatsu and Ohno. This is an open-access article distributed under the terms of the Creative Commons Attribution License (CC BY). The use, distribution or reproduction in other forums is permitted, provided the original author(s) and the copyright owner(s) are credited and that the original publication in this journal is cited, in accordance with accepted academic practice. No use, distribution or reproduction is permitted which does not comply with these terms.

frontiers in Oncology

ORIGINAL RESEARCH
published: 19 August 2020
doi: 10.3389/fonc.2020.01610

The Impacts of Different Types of Radiation on the CRT and PDL1 Expression in Tumor Cells Under Normoxia and Hypoxia

Yangle Huang[1,2], Qingting Huang[1,2], Jingfang Zhao[2,3], Yuanli Dong[1,2], Lijia Zhang[2,3], Xumeng Fang[1,2], Pian Sun[1,2], Lin Kong[1,2] and Jiade Jay Lu[1,2]**

[1] Department of Radiation Oncology, Shanghai Proton and Heavy Ion Center, Fudan University Cancer Hospital, Shanghai, China, [2] Shanghai Engineering Research Center of Proton and Heavy Ion Radiation Therapy, Shanghai, China, [3] Department of Medical Physics, Shanghai Proton and Heavy Ion Center, Fudan University Cancer Hospital, Shanghai, China

OPEN ACCESS

Edited by:
Timothy Dean Malouff,
Mayo Clinic Florida, United States

Reviewed by:
Nina Edin,
University of Oslo, Norway
Danushka Seneviratne,
Mayo Clinic Florida, United States

***Correspondence:**
Lin Kong
lin.kong@sphic.org.cn
Jiade Jay Lu
jiade.lu@sphic.org.cn

Specialty section:
This article was submitted to Radiation Oncology, a section of the journal Frontiers in Oncology

Received: *07 May 2020*
Accepted: *24 July 2020*
Published: *19 August 2020*

Citation:
Huang Y, Huang Q, Zhao J, Dong Y, Zhang L, Fang X, Sun P, Kong L and Lu JJ (2020) The Impacts of Different Types of Radiation on the CRT and PDL1 Expression in Tumor Cells Under Normoxia and Hypoxia. Front. Oncol. 10:1610. doi: 10.3389/fonc.2020.01610

Introduction: Hypoxia is a hallmark of cancer that may contribute to an immunosuppressive microenvironment and promote radioresistance. High linear energy transfer (LET) radiation is considered to be able to overcome the negative effects of hypoxia. However, the anti-tumorigenic effects induced by low or high LET radiation have not been fully elucidated. This study aimed to compare the effects of different types of radiation on the immune response, particularly the impact on calreticulin (CRT), and programmed cell death ligand 1 (PDL1) expression.

Methods: Four human tumor cell lines were investigated in this study. Cells in normoxic and hypoxic groups were irradiated with 4Gy (physical dose) photon, proton, and carbon-ion radiation, respectively. The expression of CRT and PDL1 was detected 48 h after irradiation, and the median fluorescence intensities (MFIs) were compared by flow cytometry. Meanwhile, the radiosensitivity of tumor cells in each group was also compared by colony formation assays and flow cytometry.

Results: All types of radiation could significantly inhibit the colony formation of tumor cells under normoxia. However, the efficacy of photon and proton radiation was impaired under hypoxia. Carbon-ion radiation could still inhibit colony formation. The percentage of viable cells after irradiation was higher under hypoxia compared with those under normoxia. The CRT expression under normoxia was significantly increased after radiation. Carbon-ion radiation enhanced CRT expression compared to photon and proton radiation. Conversely, under hypoxia, the CRT expression level was significantly upregulated at baseline (0Gy). Radiation could not increase the expression further. PDL1 expression was also significantly increased by radiation under normoxia in all cell lines except the Ln18 cell line. Carbon-ion radiation induced the most significant increase. Under hypoxia, the PDL1 expression level was also upregulated at baseline and radiation could not increase expression further.

Conclusion: Tumor cells were resistant to photon and proton but sensitive to carbon-ion radiation under hypoxia. Carbon-ion radiation could induce the highest CRT and PDL1 expression under normoxia. However, under hypoxia, radiation could not further enhance the high baseline expression of CRT and PDL1.

Keywords: proton radiation, carbon-ion radiation, normoxia, hypoxia, calreticulin, PDL1

INTRODUCTION

Hypoxia is one of the hallmarks of malignant tumors (1). Tumors under hypoxia are more aggressive than those under normoxia, which is characterized by a higher rate of metastasis and increased resistance to chemo- and radiotherapy (2, 3). Thus, hypoxia is considered an unfavorable prognostic factor for various malignant tumors, especially inoperable head and neck cancers (4). Though many hypoxia-targeting strategies have been investigated in clinical research, they have been ineffective (5). Additionally, hypoxia can contribute to the immune escape of tumor cells via the upregulation of programmed cell death ligand 1 (PDL1) in a hypoxia-inducible factor-1α (HIF-1α)-dependent manner (6). Thus, the anti-tumor effects exerted by the immune system following radiation would be reduced in an immunosuppressive hypoxic environment.

It is widely acknowledged that the cytotoxic effects of radiation are predominantly due to the damage of DNA in cells. DNA damage can be caused by both the direct and indirect effects of radiation. For low linear energy transfer (LET) radiation, like photon, DNA is damaged indirectly via free radicals, while for high LET radiation, like carbon-ion, DNA is ionized, and damaged directly (7). Free radicals react with DNA to form superoxide in the presence of molecular oxygen, which results in DNA damage. The absence of oxygen would therefore decrease DNA damage mediated by radicals (8). However, the direct effect of radiation is independent of oxygen. Thus, the contribution of oxygen is likely different between the low and high LET radiation. Previous studies have shown that the oxygen enhancement ratio (OER) for photon radiation is 2.5–3.5, while for carbon-ion radiation, the OER is closer to 1–1.5 (9). Therefore, carbon-ion radiation is considered able to overcome the unfavorable effect of hypoxia on radiotherapy, at least to some extent.

Carbon-ion and proton radiation are the most advanced techniques used in clinical practice. They have radio-biological and radio-physical advantages over conventional photon radiation. However, the anti-tumor effects induced by proton and carbon-ion radiation have not been fully elucidated. Increased translocation of calreticulin (CRT) to the surface of cell membrane occurs when cells undergo immunogenic cell death, and ecto-CRT has been shown to play an important role in adaptive immune response (10). We previously compared the impact of photon, proton, and carbon-ion radiation on CRT expression in normoxic conditions (11). The impacts of different types of radiation on CRT and PDL1 expression under hypoxia are still poorly understood. Thus, our aim was to compare the effects of photon, proton, and carbon-ion radiation on the expression of CRT and PDL1 under normoxia and hypoxia. This study provided important information and improved our understanding of the anti-tumorigenic responses induced by radiotherapy, especially proton and carbon-ion radiation.

MATERIALS AND METHODS

Cell Lines and Culture Conditions

Four human tumor cell lines were investigated in this study. These included tongue squamous carcinoma cell lines Tca8113 and Cal27, and the glioma cell lines Ln229 and Ln18. All cells were cultured in DMEM medium containing 10% fetal bovine serum (FBS) supplemented with 1% streptomycin and penicillin. Tumor cells in the normoxic group were cultured in an incubator at 37°C containing 5% CO_2 and 21% O_2, while cells in the hypoxic group were cultured in a hypoxic chamber at 37°C containing 5% CO_2 and 0.5% O_2.

Irradiation

Exponentially growing tumor cells were irradiated with photon, proton, or carbon-ion radiation as previously described (11). The LET value of photon, proton, and carbon-ion radiation was 2.00, 1.98, and 29.14 keV/μm, respectively. The irradiation doses mentioned are physical doses. Cells in the normoxic group were exposed to radiation directly. While cells in the hypoxic group were placed in a hypoxic culture bag (AnaeroPack, Mitsubishi Gas Chemical Company) in advance, to ensure that tumor cells were in hypoxic condition during the radiation. After irradiation, cells from all the groups, including the mock-irradiated control group (0Gy), were washed twice with phosphate buffer saline (PBS), and the culture medium was replaced. Cells were then immediately cultured in normoxic or hypoxic condition as mentioned above.

Colony Formation Assay

After irradiation with 4Gy of photon, proton, or carbon-ion radiation, the tumor cells in both the normoxic and hypoxic groups were immediately trypsinized and evenly seeded (5000 cells per well) in six-well plates. Three independent experiments were performed for each group. Cells were then cultured in normoxic or hypoxic conditions to form colonies. Colonies were fixed with methanol and stained with crystal violet after 7 days. Images of each group were captured by a colony counting machine (GelCount, Oxford Optronix Ltd.). Only those containing more than 50 cell colonies were counted. The survival fraction (SF) of tumor cells was calculated as follows: colony formation rate in the irradiating group/colony formation rate in the control group.

Flow Cytometry Analysis of Live and Dead Cells

Tumor cells were cultured for 48 h following irradiation with different types of radiation under normoxia or hypoxia. Tumor cells in each group, including the control group (0Gy), were washed with PBS and harvested using trypsin solution without EDTA. Cells were double stained with PE/Annexin V and 7-Amino-Actinomycin (7AAD; Apoptosis detection kit, BD Pharmingen, 559763) according to the manufacturer's instructions. Samples of each group were examined by flow cytometry (CytoFLEX S, Beckman Coulter), and the results were analyzed by CytoExpert software (version 2.3, Beckman Coulter).

Flow Cytometry Analysis of CRT and PDL1 Expression

Tumor cells were harvested 48 h after irradiation. Each sample was incubated in blocking buffer (PBS containing 5% FBS) for 15 min, followed by washing with cold PBS. Tumor cells were then incubated with P-phycoerythrin (PE) conjugated anti-CRT (PE-CRT, Abcam, and ab83220) or anti-PDL1 (PE-PDL1, CST, and 71391) monoclonal antibodies, respectively. The fluorescence intensity of CRT and PDL1 in each group was detected on a flow cytometer (CytoFLEX S, Beckman Coulter). Flow cytometry results were analyzed by FlowJo (version 10.0.7, Three Star, Inc). The median fluorescence intensity (MFI) was compared between irradiated groups and the non-irradiated group (control group). The fold change of MFI was used to compare the expression of CRT and PDL1 among different groups.

Statistical Analysis

Statistical analysis was conducted by GraphPad Prism (version 7.0, GraphPad Software). Unpaired Student's t test was used to test the significant difference between two independent samples. Two-way ANOVA was used to test the significant difference between two independent groups. P value < 0.05 was considered statistically significant.

RESULTS

Comparison of the Inhibitory Effects on Colony Formation by Photon, Proton, and Carbon-Ion Radiation Under Normoxia and Hypoxia

Four tumor cell lines were irradiated with 4Gy (physical dose) photon, proton, or carbon-ion radiation under normoxic or hypoxic conditions. Cells were trypsinized immediately after irradiation and cultured in six-well plates (5000 cells/well). Mock-irradiated groups (0Gy) under normoxia and hypoxia were cultured like controls. After culture for 7–11 days, cells were fixed and stained with crystal violet. The SF and the representative images of colony formation for each group are shown in **Figure 1**. The SF of each cell line under normoxia or hypoxia following different types of radiation is shown in **Table 1**.

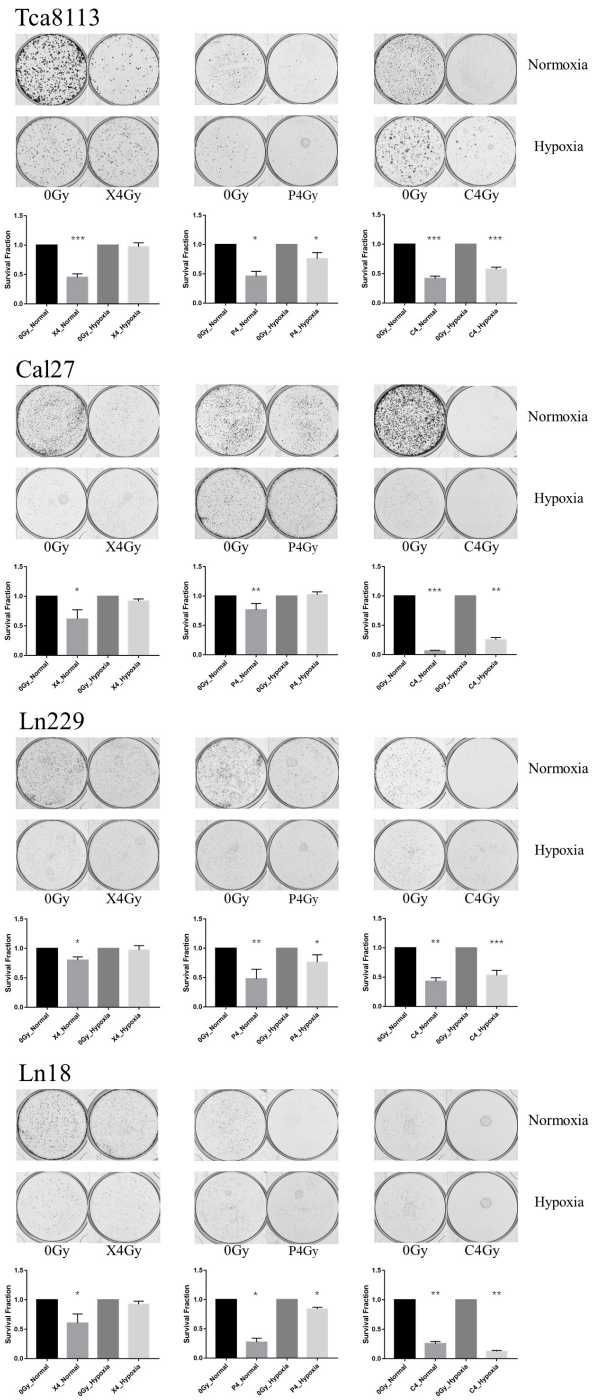

FIGURE 1 | Comparison of the inhibitory effects on colony formation by the three types of radiation under normoxia and hypoxia. Tumor cells were irradiated with 4Gy (physical dose) photon, proton, or carbon-ion radiation under normoxia or hypoxia conditions. Survival fraction (SF) was calculated as: colony formation rate in the irradiated group/colony formation rate in the control group. The representative images of colony formation for each tumor cell group are shown in the upper panels. The histograms indicate the SF of tumor cells exposed to different types of radiation under normoxic and hypoxic conditions. Results are presented as mean ± s.d. Statistical significance of each irradiated group relative to the corresponding control group (0Gy) was indicated by asterisks. *$p < 0.05$, **$p < 0.01$, and ***$p < 0.001$.

TABLE 1 | The survival fraction of tumor cells following irradiation under normoxia and hypoxia.

Tumor cell	Normoxia group	SF	95% CI	Hypoxia group	SF	95% CI
Tca8113	X4	0.45	0.30–0.60	X4	0.97	0.80–1.14
Tca8113	P4	0.46	0.25–0.67	P4	0.76	0.50–1.02
Tca8113	C4	0.42	0.32–0.52	C4	0.58	0.49–0.66
Cal27	X4	0.62	0.23–1.00	X4	0.91	0.83–1.01
Cal27	P4	0.76	0.50–1.04	P4	1.02	0.90–1.15
Cal27	C4	0.06	0.04–0.09	C4	0.25	0.16–0.35
Ln229	X4	0.80	0.66–0.90	X4	0.97	0.79–1.16
Ln229	P4	0.48	0.07–0.89	P4	0.76	0.45–1.08
Ln229	C4	0.43	0.28–0.58	C4	0.53	0.31–0.75
Ln18	X4	0.60	0.22–0.99	X4	0.93	0.80–1.05
Ln18	P4	0.27	0.10–0.44	P4	0.84	0.77–0.91
Ln18	C4	0.26	0.17–0.34	C4	0.12	0.08–0.16

SF, survival fraction.

TABLE 2 | The percentage of viable tumor cells in each group 48 h after irradiation under normoxia and hypoxia.

Tumor cell	Normoxia group	Survival (%)	95% CI	Hypoxia group	Survival (%)	95% CI
Tca8113	0Gy	98.39	97.96–98.81	0Gy	97.61	95.43–99.79
Tca8113	X4	91.34	89.91–92.77	X4	96.57	94.34–98.80
Tca8113	P4	90.38	88.75–92.01	P4	94.22	92.34–96.10
Tca8113	C4	84.81	83.19–86.44	C4	90.63	90.22–91.05
Cal27	0Gy	99.29	98.86–99.71	0Gy	97.64	96.35–98.93
Cal27	X4	91.37	91.06–91.68	X4	94.82	93.33–96.32
Cal27	P4	87.78	86.38–89.17	P4	92.06	90.38–93.74
Cal27	C4	86.31	85.49–87.13	C4	90.52	90.03–91.00
Ln229	0Gy	97.04	96.53–97.54	0Gy	94.80	94.17–95.43
Ln229	X4	91.37	89.66–93.08	X4	91.84	90.05–93.63
Ln229	P4	91.34	90.82–91.85	P4	92.78	92.39–93.17
Ln229	C4	85.99	84.95–87.02	C4	90.02	89.59–90.45
Ln18	0Gy	98.7	98.08–99.31	0Gy	98.06	97.69–98.44
Ln18	X4	92.33	91.05–93.61	X4	97.00	96.43–97.58
Ln18	P4	92.39	90.38–94.41	P4	96.29	95.53–97.05
Ln18	C4	80.17	79.51–80.83	C4	92.05	90.45–93.65

According to the results above, photon, proton, and carbon-ion radiation could all inhibit colony formation of tumor cells under normoxia. However, the SF of the photon and proton radiation groups under hypoxia was not significantly reduced. Conversely, carbon-ion radiation significantly reduced the SF in hypoxic conditions. These results suggested that the ability of photon and proton radiation to inhibit tumor cell colony formation was weakened under hypoxia, while carbon-ion radiation still possessed solid inhibitory effects under hypoxia. Therefore, carbon-ion radiation was less affected by hypoxia when compared to photon and proton irradiation.

Comparison Between the Percentage of Viable and Dead Tumor Cells After Photon, Proton, and Carbon-Ion Radiation Under Normoxia and Hypoxia

In order to compare the percentage of viable and dead tumor cells 48 h after exposure to different types of radiation under normoxia and hypoxia, we treated tumor cells with 4Gy physical dose photon, proton, and carbon-ion radiation under normoxic and hypoxic conditions. Irradiated cell groups, in addition to mock-irradiated control groups (0Gy), were cultured under the same oxygen conditions for 48 h. Next, we used Annexin V/7-AAD to detect viable and dead cells by flow cytometry. Cells that were Annexin V-negative and 7-AAD-negative (AV-/7AAD-) were considered viable. The percent viability of tumor cells in each group are shown in **Table 2**. Annexin V-positive and 7-AAD-negative (AV+/7AAD-) cells were considered to be in early apoptosis, while Annexin V and 7-AAD positivity (AV+/7AAD+) suggested that cells were in late apoptosis or dead. Representative flow cytometry images for each group and the percentages of viable and dead cells are shown in **Figure 2**.

The percentage of viable tumor cells was all increased under hypoxia in comparison to normoxia following irradiation with photon, proton, or carbon-ion radiation, which suggests that tumor cells were more resistant to radiation in hypoxic conditions. Carbon-ion radiation was capable of inducing more

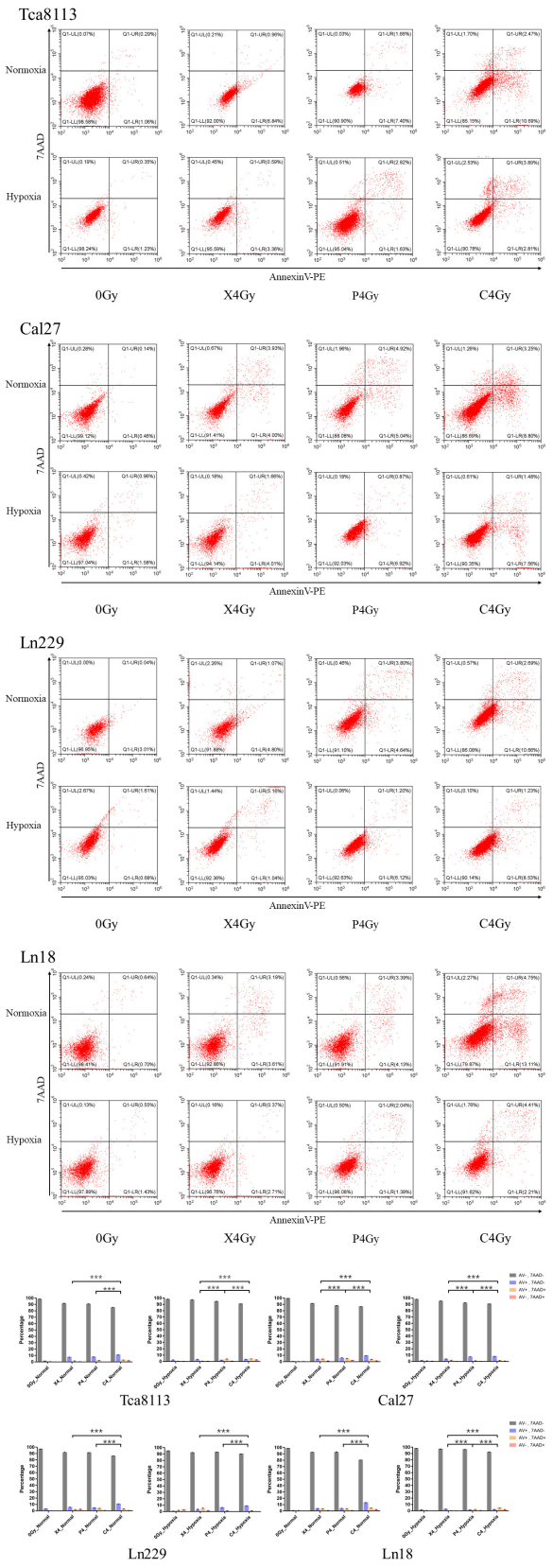

FIGURE 2 | Continued

FIGURE 2 | Comparison between the percentage of viable and dead cells under normoxia and hypoxia. Tumor cells in normoxic and hypoxic conditions were exposed to 4Gy physical dose photon, proton, or carbon-ion radiation. Cell survival was detected 48 h after irradiation using the Annexin V/7-AAD double staining kit. Representative flow cytometry images for each group are shown in the scatter plots. Statistical analysis of the cell survival and death percentages for each group are shown in the histograms. Each experiment was repeated at least three times. ***$p < 0.001$.

cell death compared with photon or proton radiation at the same physical dose while cells were hypoxic.

Comparison of Tumor Cell CRT Expression Under Normoxia and Hypoxia in Each Group

Next, we compared the changes in expression of CRT on the tumor cell membrane 48 h after irradiation with 4Gy physical dose photon (X4), proton (P4), or carbon-ion (C4) radiation compared to the control group (0Gy) under normoxia and hypoxia. The MFI of CRT staining was detected by flow cytometry for each group. Representative flow cytometry images and statistical significance are demonstrated in **Figure 3**.

The fold change of CRT expression in each irradiation group compared to the control group under normoxia and hypoxia are listed in **Table 3**.

When comparing the CRT expression between normoxic and hypoxic cells at baseline (0Gy, control groups), all the tumor cells in the hypoxic groups expressed more CRT than the normoxic groups. As demonstrated in **Figure 4**, the CRT expression under hypoxia increased by 2.21-fold (95% CI: 1.33–3.09), 4.27-fold (95% CI: 3.90–4.63), 1.63-fold (95% CI: 1.58–1.68), and 1.18-fold (95% CI: 1.10–1.26) for Tca8113, Cal27, Ln229, and Ln18 cell lines, respectively.

These results indicated that photon, proton, and carbon-ion radiation could all significantly increase the expression of CRT on tumor cells in normoxic conditions. Carbon-ion radiation could induce more CRT expression compared to photon and proton radiation at the same physical dose. Alternatively, the CRT expression on tumor cells was upregulated at baseline (0Gy) in hypoxic conditions. In these hypoxic conditions, photon, proton, or carbon-ion radiation could not further increase CRT expression. In some radiation groups, CRT expression was decreased after radiation.

Comparison of PDL1 Expression in Tumor Cells Under Normoxia and Hypoxia Following Irradiation

We compared the changes in PDL1 expression on tumor cell membranes 48 h after exposure to 4Gy physical dose photon (X4), proton (P4), or carbon-ion (C4) radiation under normoxia or hypoxia. The MFI of PDL1 was also detected by flow cytometry in each group. Representative flow cytometry images and statistical significance are demonstrated in **Figure 5**.

The fold change of PDL1 expression in each irradiation group compared to the control group under normoxia and hypoxia are listed in **Table 4**.

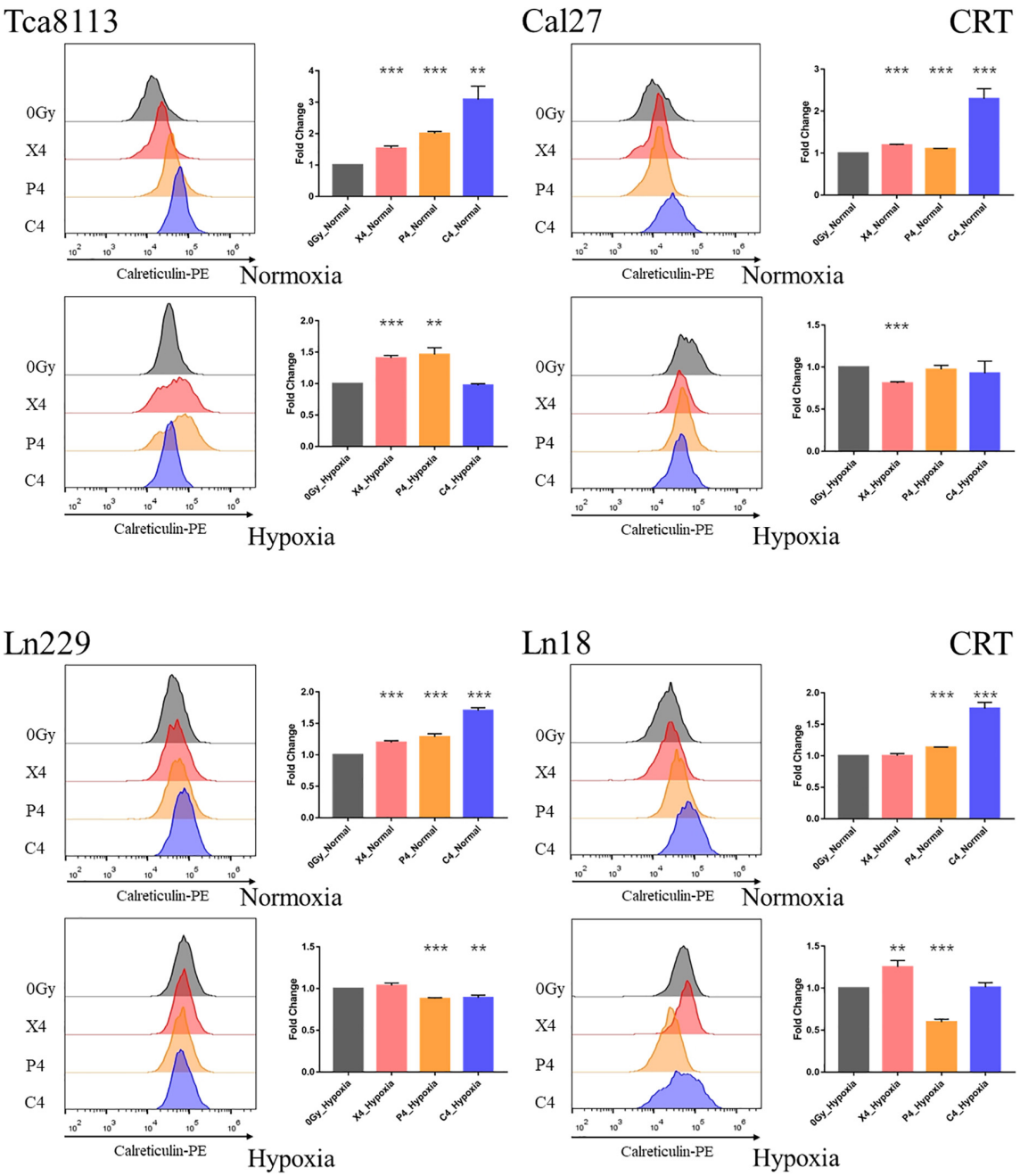

FIGURE 3 | Comparison of CRT expression under normoxia and hypoxia. Tumor cells were exposed to 4Gy physical dose photon, proton, or carbon-ion radiation. The expression level of CRT on the tumor cell surface was detected by flow cytometry 48 h after irradiation. Representative flow cytometry images for each group are shown in the half-offset histograms. The horizontal axis represents the fluorescence intensity of CRT-PE, and the vertical axis represents the number of cells. The fold change of the median fluorescence intensity (MFI) for each group relative to the control group (0Gy) is shown in the bar charts. Results are presented as mean ± s.d. Each experiment was repeated at least three times. Statistical significance of each irradiated group relative to the control group (0Gy) was indicated by asterisks. $^{**}p < 0.01$, and $^{***}p < 0.001$.

The baseline PDL1 expression (0Gy, control group) of all tumor cell lines in hypoxic conditions was upregulated in comparison to those in the normoxic group. As shown in **Figure 6**, the PDL1 expression under hypoxia increased by 2.64-fold (95% CI: 2.04–3.25), 1.36-fold (95% CI: 0.84–1.89), 1.50-fold (95% CI: 1.03–1.98), and 1.28-fold (95% CI: 0.53–2.04) for Tca8113, Cal27, Ln229, and Ln18 cell lines, respectively.

These results indicated that all types of radiation could increase the expression of PDL1 in all tumor cell lines except the Ln18 cell line under normoxic conditions,

TABLE 3 | The changes in CRT expression for each irradiation group under normoxia and hypoxia.

Irradiating group (normoxia)	Fold change	95% CI	Irradiating group (hypoxia)	Fold change	95% CI
Tca8113_X4	1.53	1.35–1.71	Tca8113_X4	1.41	1.30–1.51
Tca8113_P4	2.00	1.84–2.17	Tca8113_P4	1.46	1.19–1.74
Tca8113_C4	3.09	2.02–4.15	Tca8113_C4	0.97	0.91–1.04
Cal27_X4	1.19	1.13–1.25	Cal27_X4	0.81	0.76–0.85
Cal27_P4	1.11	1.08–1.13	Cal27_P4	0.97	0.86–1.09
Cal27_C4	2.30	1.70–2.90	Cal27_C4	0.93	0.56–1.29
Ln229_X4	1.20	1.12–1.27	Ln229_X4	1.03	0.95–1.12
Ln229_P4	1.29	1.16–1.41	Ln229_P4	0.88	0.86–0.90
Ln229_C4	1.70	1.58–1.82	Ln229_C4	0.89	0.81–0.97
Ln18_X4	1.00	0.92–1.08	Ln18_X4	1.26	1.08–1.15
Ln18_P4	1.13	1.12–1.15	Ln18_P4	0.60	0.52–0.67
Ln18_C4	1.75	0.90–1.86	Ln18_C4	1.01	0.88–1.14

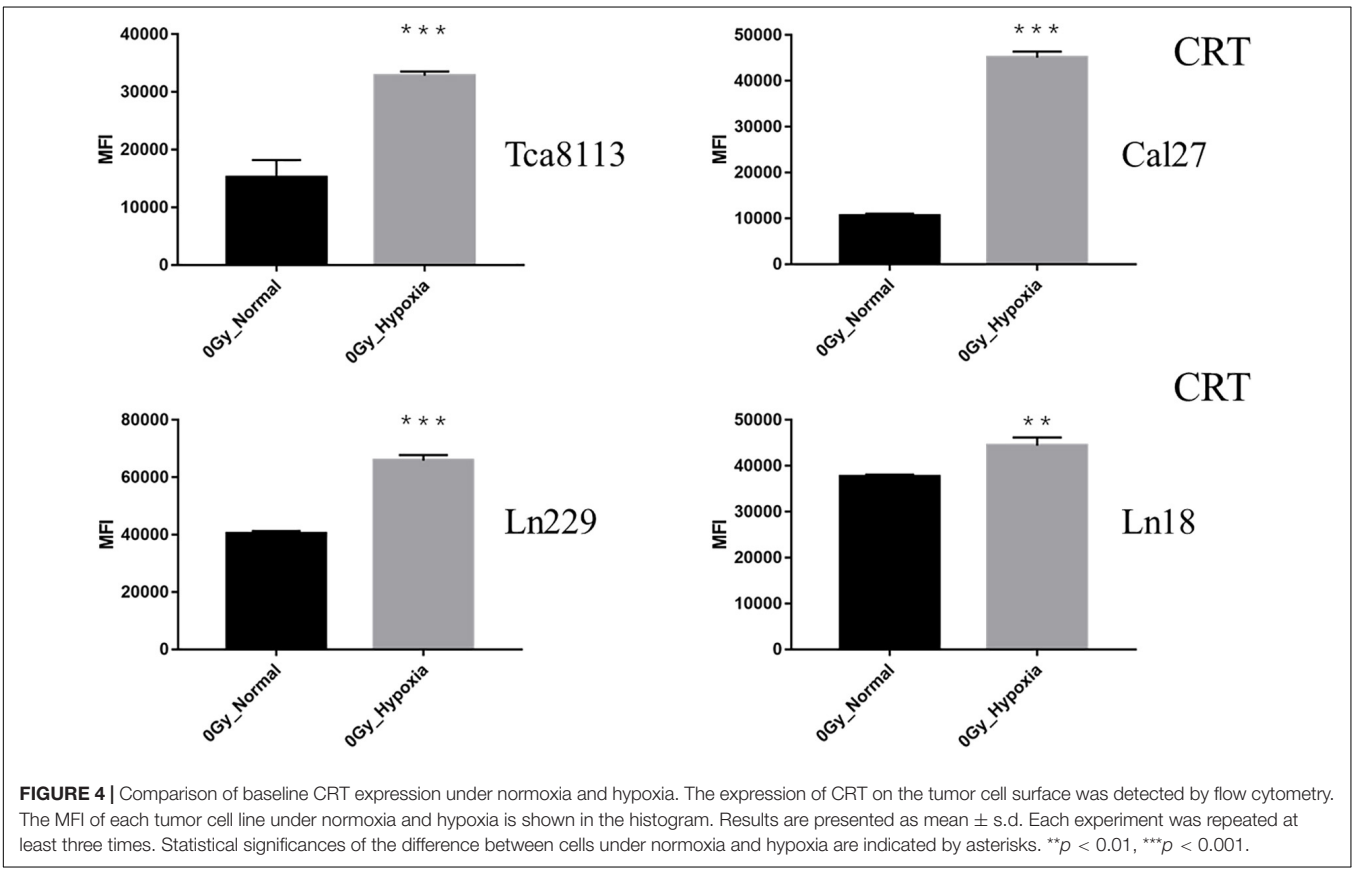

FIGURE 4 | Comparison of baseline CRT expression under normoxia and hypoxia. The expression of CRT on the tumor cell surface was detected by flow cytometry. The MFI of each tumor cell line under normoxia and hypoxia is shown in the histogram. Results are presented as mean ± s.d. Each experiment was repeated at least three times. Statistical significances of the difference between cells under normoxia and hypoxia are indicated by asterisks. $^{**}p < 0.01$, $^{***}p < 0.001$.

while under hypoxic conditions, the expression of PDL1 on tumor cells was upregulated at baseline (0Gy). Under these conditions, photon, proton, or carbon-ion radiation could not further increase PDL1 expression. Carbon-ion radiation could increase PDL1 expression more effectively than photon or proton radiation at the same physical dose under normoxia, but not under hypoxia. In some tumor cell lines, like Cal27 and Ln229, PDL1 expression may even be downregulated after exposure to carbon-ion radiation.

DISCUSSION

Oxygen plays an important role in the tumor response to radiotherapy, and the oxygenation profile of tumors tends to be very heterogeneous. Some tumors are well oxygenated while others are hypoxic (2). Even in different regions of a tumor, the oxygen concentration can be quite different (12). Thus, there can be normoxic and hypoxic regions within the tumor mass, and the extent of hypoxia varies. However, even a small amount of oxygen can be significant. When the oxygen concentration

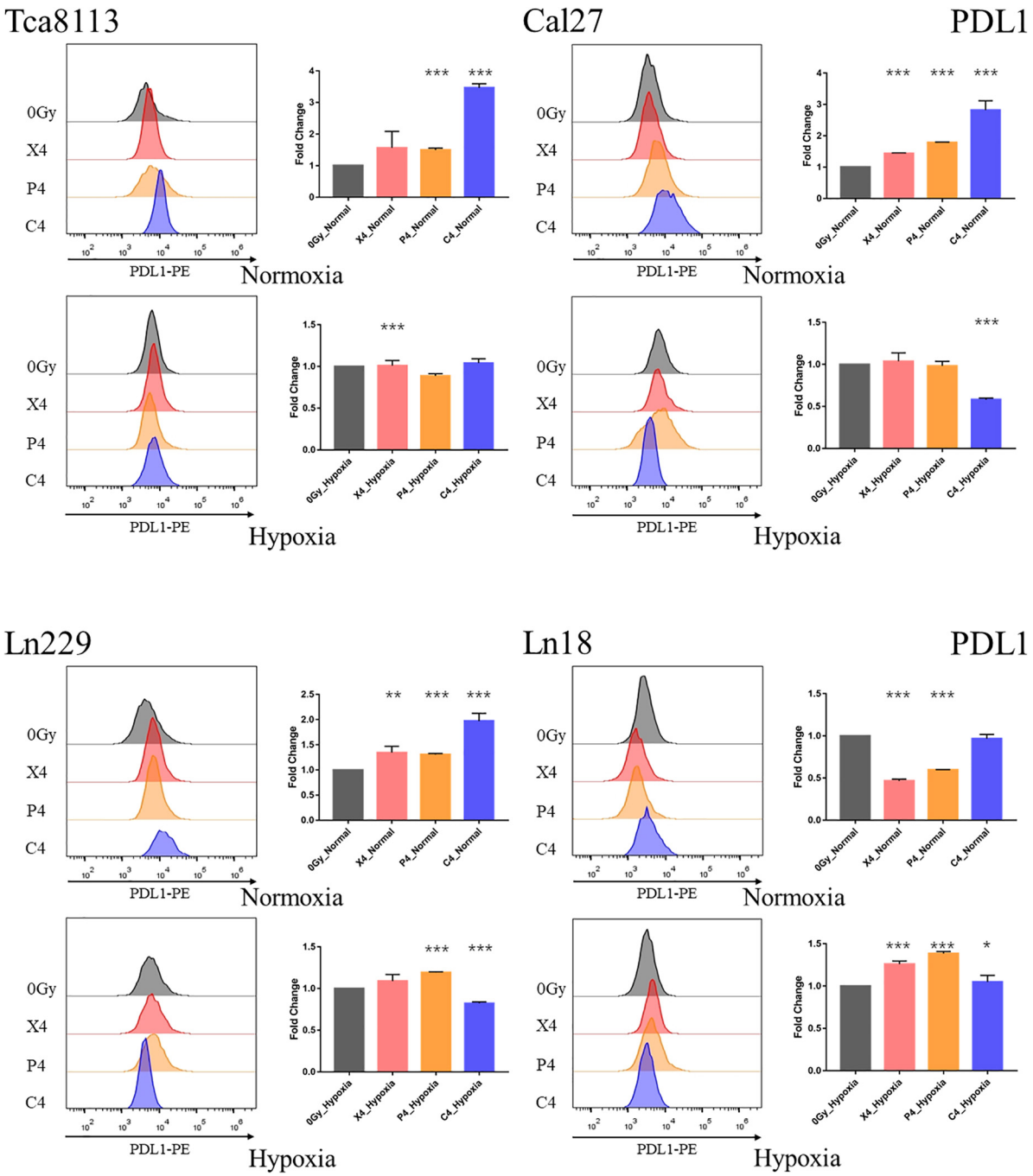

FIGURE 5 | Comparison of PDL1 expression under normoxia and hypoxia. Tumor cells were exposed to 4Gy physical dose photon, proton, or carbon-ion radiation. The expression level of PDL1 on the tumor cell surface was detected by flow cytometry 48 h after irradiation. Representative flow cytometry images of each group are shown in the half-offset histograms. The horizontal axis represents the fluorescence intensity of PDL1-PE, and the vertical axis represents the number of cells. The fold change of the MFI for each group relative to the control group (0Gy) is shown in the bar charts. Results are presented as mean ± s.d. Each experiment was repeated at least three times. Statistical significance of each irradiated group relative to the control group (0Gy) was indicated by asterisks. $^{*}p < 0.05$, $^{**}p < 0.01$, and $^{***}p < 0.001$.

reaches 2%, the dose–response curve of the cell to radiation is no different from that observed in normoxic conditions. When the oxygen concentration is about 0.5%, the radiosensitivity of the cell is about half that in well-oxygenated conditions (7). Therefore, in this study, we used 0.5% oxygen concentrations to simulate the hypoxic environment in tumors. The normoxic group was exposed to around 21% oxygen. Here, we compared the expression of anti-tumor immunity-related molecules, CRT

TABLE 4 | The changes in PDL1 expression for each irradiation group under normoxia and hypoxia.

Irradiating group (normoxia)	Fold change	95% CI	Irradiating group (hypoxia)	Fold change	95% CI
Tca8113_X4	1.57	0.74–2.40	Tca8113_X4	1.01	0.95–1.08
Tca8113_P4	1.50	1.34–1.65	Tca8113_P4	0.89	0.84–0.93
Tca8113_C4	3.47	3.16–3.78	Tca8113_C4	1.04	0.98–1.11
Cal27_X4	1.44	1.41–1.48	Cal27_X4	1.04	0.93–1.14
Cal27_P4	1.79	1.77–1.80	Cal27_P4	0.98	0.85–1.12
Cal27_C4	2.82	2.45–3.19	Cal27_C4	0.58	0.55–0.61
Ln229_X4	1.35	1.22–1.48	Ln229_X4	1.09	1.01–1.17
Ln229_P4	1.31	1.26–1.36	Ln229_P4	1.19	1.18–1.21
Ln229_C4	1.97	1.60–2.38	Ln229_C4	0.82	0.78–0.87
Ln18_X4	0.47	0.42–0.52	Ln18_X4	1.26	1.17–1.35
Ln18_P4	0.60	0.59–0.61	Ln18_P4	1.39	1.36–1.41
Ln18_C4	0.97	0.84–1.09	Ln18_C4	1.05	0.95–1.15

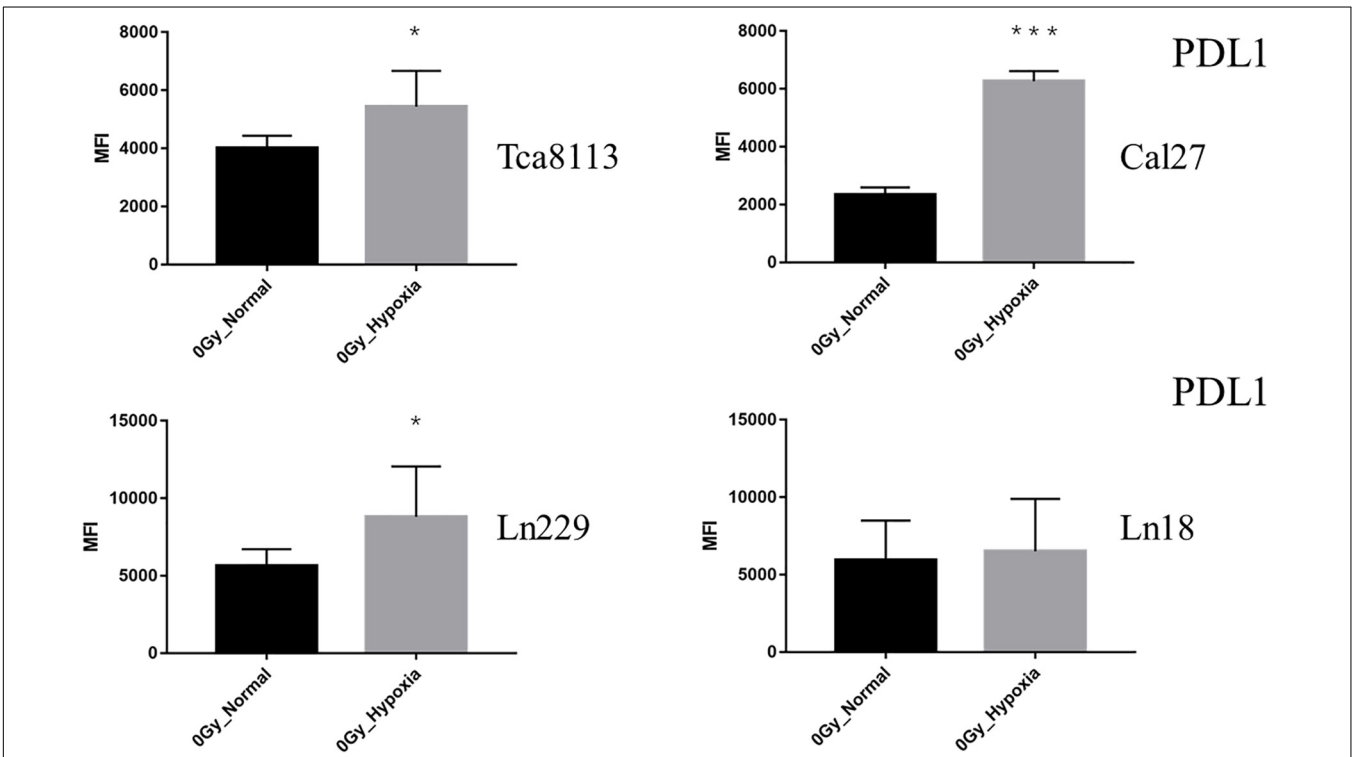

FIGURE 6 | Comparison of baseline PDL1 expression under normoxia and hypoxia. The expression of PDL1 on the tumor cell surface was detected by flow cytometry. The MFI of each tumor cell line under normoxia and hypoxia is shown in the histogram. Results are presented as mean ± s.d. Each experiment was repeated at least three times. Statistical significance of the difference between cells under normoxia and hypoxia are indicated by asterisks. *$p < 0.05$, ***$p < 0.001$.

and PDL1, in response to different types of radiation in normoxic and hypoxic conditions.

The first section of this study compared the radioresistance of tumor cells in normoxic and hypoxic conditions to photon, proton, or carbon-ion radiation exposure. Colony formation assays and analysis of apoptosis indicated that tumor cells were significantly resistant to photon and proton radiation, although carbon-ion radiation still displayed effective cytotoxic effects toward tumor cells under hypoxia. In comparison to low LET radiation, like photon and proton, the cytotoxic effect of high LET radiation, like carbon ion, was less affected by hypoxic conditions. These results were consistent with previous studies concerning the OER of photon, proton, and carbon-ion radiation (9). As the OER value of carbon-ion radiation is lower than that of photon and proton radiation (1–1.5 vs. 2–3), the biological effects of carbon-ion radiation were not greatly affected by the oxygenation conditions. In addition to the difference in ionization effects (direct effect vs. indirect effect), different types of radiation can also produce different effects on the expression of radioresistance-related genes, like HIF1α. Worn et al. demonstrated that photon radiation could significantly upregulate HIF1α expression, while carbon-ion radiation did

not induce increased HIF1α expression (13). HIF1α, as an important transcription factor, is involved in the expression of a series of downstream genes, such as vascular endothelial growth factor (VEGF). Thus, inhibiting HIF1α expression could significantly enhance the radiosensitivity of tumor cells (14, 15). In hypoxic conditions, there may be a synergistic effect between radiation and hypoxia on inducing HIF1α expression. Thus, the discrepant impacts on HIF1α upregulation by different types of radiation might partly affect the cytotoxic efficacy of radiotherapy, especially under hypoxia.

Photon, proton, and carbon-ion radiation could increase the expression of CRT in all four tumor cell lines in normoxic conditions. Consistent with our previous study, carbon-ion radiation could increase CRT expression compared with photon and proton radiation at the same physical dose (4Gy) (11). These results indicated that carbon-ion radiation might be able to enhance immunogenic cell death and enhance anti-tumorigenic responses compared with photon and proton radiation. When under hypoxic conditions, we found that the baseline (0Gy, group) CRT expression levels in the four tumor cell lines were significantly increased compared with those under normoxia. The expression level was upregulated by 2.21- to 4.27-fold for tongue squamous carcinoma cell lines, and by 1.18- to 1.63-fold for glioma cell lines (all $p < 0.05$). This upregulation of CRT expression might result from endoplasmic reticulum stress (ER stress) induced by hypoxia (16). When under the pressure of ER stress, large amounts of CRT (which is originally located in the endoplasmic reticulum cavity) would translocate to the surface of the cell membrane. Radiation can also induce ER stress mediated by reactive oxygen species (ROS) (17). Based on this study, CRT expression was not further increased by radiation compared with the control group in hypoxic conditions. Even carbon-ion radiation could not further increase the expression of CRT expression under hypoxic conditions. This phenomenon suggested that there might be an overlapping effect between CRT expression during hypoxia and radiation, which were both mediated by ER stress. The pressure of hypoxia induced abundant CRT translocation to the surface of the cell membrane and therefore radiation could not increase this further.

Previous studies have revealed that radiation could upregulate PDL1 expression (18, 19). The impact of radiation on PDL1 expression was thought to be related to DNA double-strand breaks (DSB) and the process of DNA damage repair (DDR) (20). Inhibiting key pathways within DDR, such as BRCA2 and Ku70/80, could result in a significant increase in PDL1 expression. We showed that all types of radiation could increase the expression of PDL1 under normoxia but carbon-ion radiation was the most effective. These results might be explained by the fact that carbon-ion radiation is capable of inducing more DSBs at the same physical dose (21, 22). However, for glioma cell line LN18, the expression level of PDL1 was downregulated to some extent, rather than upregulated after exposure to radiation. This suggested that PDL1 expression induced by irradiation may have cell specificity. Different tumors, even different subtypes, might have distinct PDL1 expression patterns in response to radiation, because of the discrepancy between radiosensitivity and DDR capacity. While under hypoxia, we observed that the baseline PDL1 expression was increased compared to groups under normoxia. Barsoum et al. reported that hypoxia could increase PDL1 expression in tumor cells through the HIF1α pathway, which resulted in the immune escape of tumors (6). Our current research showed that PDL1 expression was not further upregulated after exposure to radiation in hypoxic condition. In some irradiation groups, the expression levels of PDL1 were even downregulated compared with the control group. This could be because tumor cells exhibited radiation resistance under hypoxia. As such, the extent of DNA damage caused by radiation was reduced. As discussed previously, DDR was related to PDL1 expression, which may reflect the observed results. Additionally, the DDR process of tumor cells will also be altered under hypoxia (23–25). In some hypoxic tumor cells, the expression of homologous recombination repair (HRR) pathway-related genes, such as RAD51 and BCRA1, will be downregulated (26, 27), while the expression of non-homologous end-joining (NHEJ) pathway-related genes, such as ATM and DNA-PKcs, will be upregulated (28, 29). Regulation of DDR-related gene expression will also affect the radiosensitivity of tumor cells (30). Furthermore, for low and high LET radiation, the importance of distinct DDR pathways, like HRR and NHEJ, in response to DNA damage might be different. This might be another reason that the expression of PDL1 was different after exposure to photon, proton, or carbon-ion radiation under hypoxia.

In conclusion, this study compared the impacts of different types of radiation on CRT and PDL1 expression under normoxia and hypoxia. We found that carbon-ion radiation could increase CRT and PDL1 expression compared with photon and proton radiation in normoxic conditions. However, under hypoxia, the baseline expression levels of CRT and PDL1 were upregulated. Under these conditions, radiation could not further increase CRT and PDL1 expression. However, the underlying mechanisms regulating expression of these proteins have not been fully elucidated. In order to explore a therapeutic strategy that can overcome the immunosuppressive environment of hypoxia and enhance radiation-induced anti-tumorigenic responses, further studies are warranted, especially for the effective combination of immunotherapy and modern radiotherapy techniques, like proton and carbon-ion radiation.

DATA AVAILABILITY STATEMENT

The original contributions presented in the study are included in the article/**Supplementary Material**, further inquiries can be directed to the corresponding author/s.

AUTHOR CONTRIBUTIONS

JL and LK: conception and design, and administrative support. JZ, YH, and LZ: provision of study materials. YH, YD, QH, XF, and PS: collection and assembly of data. YH and YD: data analysis and interpretation. YH, LK, and JL: manuscript writing. All authors: final approval of manuscript.

FUNDING

This work was supported by the National Key Research and Development Program of China (Project No. 2018YFC0115700), the Program of Shanghai Academic/Technology Research Leader (Project Nos. 19XD1432900 and 18XD1423000), and the Science and Technology Commission of Shanghai Municipality (Project No. 19JC1414800).

ACKNOWLEDGMENTS

We deeply appreciate Bilikere S. Dwarakanath (Department of Research and Development, Shanghai Proton and Heavy Ion Center, Shanghai, China), Yun Sun (Department of Research and Development, Shanghai Proton and Heavy Ion Center, Shanghai, China), and Michael F. Moyes (Department of Medical Physics, Shanghai Proton and Heavy Ion Center, Shanghai, China) for their kind help.

SUPPLEMENTARY MATERIAL

The Supplementary Material for this article can be found online at: https://www.frontiersin.org/articles/10.3389/fonc.2020.01610/full#supplementary-material

REFERENCES

1. Vaupel P, Mayer A. Hypoxia in tumors: pathogenesis-related classification, characterization of hypoxia subtypes, and associated biological and clinical implications. *Adv Exp Med Biol*. (2014) 812:19–24. doi: 10.1007/978-1-4939-0620-8_3
2. Hill RP, Bristow RG, Fyles A, Koritzinsky M, Milosevic M, Wouters BG. Hypoxia and predicting radiation response. *Semin Radiat Oncol*. (2015) 25:260–72. doi: 10.1016/j.semradonc.2015.05.004
3. Baumann R, Depping R, Delaperriere M, Dunst J. Targeting hypoxia to overcome radiation resistance in head & neck cancers: real challenge or clinical fairytale? *Expert Rev Anticancer Ther*. (2016) 16:751–8. doi: 10.1080/14737140.2016.1192467
4. Nordsmark M, Bentzen SM, Rudat V, Brizel D, Lartigau E, Stadler P, et al. Prognostic value of tumor oxygenation in 397 head and neck tumors after primary radiation therapy. An international multi-center study. *Radiother Oncol*. (2005) 77:18–24. doi: 10.1016/j.radonc.2005.06.038
5. Horsman MR, Overgaard J. The impact of hypoxia and its modification of the outcome of radiotherapy. *J Radiat Res*. (2016) 57:i90–8. doi: 10.1093/jrr/rrw007
6. Barsoum IB, Smallwood CA, Siemens DR, Graham CH. A mechanism of hypoxia-mediated escape from adaptive immunity in cancer cells. *Cancer Res*. (2014) 74:665–74. doi: 10.1158/0008-5472.CAN-13-0992
7. Hall EJ, Giaccia AJ. *Radiobiology for the Radiologist*. 7th ed. Philadelphia, PA: Lippincott Williams & Wilkins. (2012).
8. Kappler M, Taubert H, Eckert AW. Oxygen sensing, homeostasis, and disease. *N Engl J Med*. (2011) 365:1845–6; author reply 1846. doi: 10.1056/NEJMc1110602
9. Held KD, Kawamura H, Kaminuma T, Paz AES, Yoshida Y, Liu Q, et al. Effects of charged particles on human tumor cells. *Front Oncol*. (2016) 6:23. doi: 10.3389/fonc.2016.00023
10. Kepp O, Senovilla L, Vitale I, Vacchelli E, Adjemian S, Agostinis P, et al. Consensus guidelines for the detection of immunogenic cell death. *Oncoimmunology*. (2014) 3:e955691. doi: 10.4161/21624011.2014.955691
11. Huang Y, Dong Y, Zhao J, Zhang L, Kong L, Lu JJ. Comparison of the effects of photon, proton and carbon-ion radiation on the ecto-calreticulin exposure in various tumor cell lines. *Ann Transl Med*. (2019) 7:542. doi: 10.21037/atm.2019.09.128
12. Chan N, Koch CJ, Bristow RG. Tumor hypoxia as a modifier of DNA strand break and cross-link repair. *Curr Mol Med*. (2009) 9:401–10. doi: 10.2174/156652409788167050
13. Wozny AS, Lauret A, Battiston-Montagne P, Guy JB, Beuve M, Cunha M, et al. Differential pattern of HIF-1α expression in HNSCC cancer stem cells after carbon ion or photon irradiation: one molecular explanation of the oxygen effect. *Br J Cancer*. (2017) 116:1340–9. doi: 10.1038/bjc.2017.100
14. Zhao J, Du F, Luo Y, Shen G, Zheng F, Xu B. The emerging role of hypoxia-inducible factor-2 involved in chemo/radioresistance in solid tumors. *Cancer Treat Rev*. (2015) 41:623–33. doi: 10.1016/j.ctrv.2015.05.004
15. Balamurugan K. HIF-1 at the crossroads of hypoxia, inflammation, and cancer. *Int J Cancer*. (2016) 138:1058–66. doi: 10.1002/ijc.29519
16. Bi M, Naczki C, Koritzinsky M, Fels D, Blais J, Hu N, et al. ER stress-regulated translation increases tolerance to extreme hypoxia and promotes tumor growth. *EMBO J*. (2005) 24:3470–81. doi: 10.1038/sj.emboj.7600777
17. Cubillos-Ruiz JR, Bettigole SE, Glimcher LH. Tumorigenic and immunosuppressive effects of endoplasmic reticulum stress in cancer. *Cell*. (2017) 168:692–706. doi: 10.1016/j.cell.2016.12.004
18. Dovedi SJ, Adlard AL, Lipowska-Bhalla G, McKenna C, Jones S, Cheadle EJ, et al. Acquired resistance to fractionated radiotherapy can be overcome by concurrent PD-L1 blockade. *Cancer Res*. (2014) 74:5458–68. doi: 10.1158/0008-5472.CAN-14-1258
19. Te Wu C, Chen WC, Chang YH, Lin WY, Chen MF. The role of PD-L1 in the radiation response and clinical outcome for bladder cancer. *Sci Rep*. (2016) 6:1–9. doi: 10.1038/srep19740
20. Sato H, Niimi A, Yasuhara T, Permata TBM, Hagiwara Y, Isono M, et al. DNA double-strand break repair pathway regulates PD-L1 expression in cancer cells. *Nat Commun*. (2017) 8:1751. doi: 10.1038/s41467-017-01883-9
21. Jiang G-L. Particle therapy for cancers: a new weapon in radiation therapy. *Front Med*. (2012) 6:165–72. doi: 10.1007/s11684-012-0196-4
22. Bao C, Sun Y, Dong Y, Le Z, Lin L-C, Kong L, et al. The relative biological effectiveness of proton and carbon ion beams in photon-sensitive and resistant nasopharyngeal cancer cells. *Transl Cancer Res*. (2018) 7:170–9. doi: 10.21037/tcr.2018.01.25
23. Cartwright IM, Su C, Haskins JS, Salinas VA, Sunada S, Yu H, et al. DNA repair deficient chinese hamster ovary cells exhibiting differential sensitivity to charged particle radiation under aerobic and hypoxic conditions. *Int J Mol Sci*. (2018) 19:2228. doi: 10.3390/ijms19082228
24. Hauth F, Toulany M, Zips D, Menegakis A. Cell-line dependent effects of hypoxia prior to irradiation in squamous cell carcinoma lines. *Clin Transl Radiat Oncol*. (2017) 5:12–9. doi: 10.1016/j.ctro.2017.06.001
25. Chan N, Koritzinsky M, Zhao H, Bindra R, Glazer PM, Powell S, et al. Chronic hypoxia decreases synthesis of homologous recombination proteins to offset chemoresistance and radioresistance. *Cancer Res*. (2008) 68:605–14. doi: 10.1158/0008-5472.CAN-07-5472
26. Kumareswaran R, Ludkovski O, Meng A, Sykes J, Pintilie M, Bristow RG. Chronic hypoxia compromises repair of DNA double-strand breaks to drive genetic instability. *J Cell Sci*. (2012) 125:189–99. doi: 10.1242/jcs.092262
27. Bindra RS, Gibson SL, Meng A, Westermark U, Jasin M, Pierce AJ, et al. Hypoxia-induced down-regulation of BRCA1 expression by E2Fs. *Cancer Res*. (2005) 65:11597–604. doi: 10.1158/0008-5472.CAN-05-2119

28. Bencokova Z, Kaufmann MR, Pires IM, Lecane PS, Giaccia AJ, Hammond EM. ATM activation and signaling under hypoxic conditions. *Mol Cell Biol*. (2009) 29:526–37. doi: 10.1128/mcb.01301-08
29. Um JH, Kang CD, Bae JH, Shin GG, Kim DW, Kim DW, et al. Association of DNA-dependent protein kinase with hypoxia inducible factor-1 and its implication in resistance to anticancer drugs in hypoxic tumor cells. *Exp Mol Med*. (2004) 36:233–42. doi: 10.1038/emm.2004.32
30. Sprong D, Janssen HL, Vens C, Begg AC. Resistance of hypoxic cells to ionizing radiation is influenced by homologous recombination status. *Int J Radiat Oncol Biol Phys*. (2006) 64:562–72. doi: 10.1016/j.ijrobp.2005.09.031

Conflict of Interest: The authors declare that the research was conducted in the absence of any commercial or financial relationships that could be construed as a potential conflict of interest.

Copyright © 2020 Huang, Huang, Zhao, Dong, Zhang, Fang, Sun, Kong and Lu. This is an open-access article distributed under the terms of the Creative Commons Attribution License (CC BY). The use, distribution or reproduction in other forums is permitted, provided the original author(s) and the copyright owner(s) are credited and that the original publication in this journal is cited, in accordance with accepted academic practice. No use, distribution or reproduction is permitted which does not comply with these terms.

frontiers in Oncology

ORIGINAL RESEARCH
published: 04 September 2020
doi: 10.3389/fonc.2020.01691

Influence of α-Particle Radiation on Intercellular Communication Networks of Tunneling Nanotubes in U87 Glioblastoma Cells

Nicole Matejka and Judith Reindl*

Institut für Angewandte Physik und Messtechnik, Fakultaet für Luft- und Raumfahrttechnik, Universitaet der Bundeswehr Muenchen, Neubiberg, Germany

Cellular communication plays a crucial role in the coordination and organization of cancer cells. Especially processes such as uncontrolled cell growth, invasion, and therapy resistance (development), which are features of very malignant tumors like glioblastomas, are supported by an efficient cell-to-cell communication in the tumor environment. One powerful way for cells to communicate are tunneling nanotubes (TNTs). These tiny membrane tunnels interconnect cells over long distances and serve as highways for information exchange between distant cells. Here, we study the response of cellular communication via TNTs in U87 glioblastoma cells to homogeneous irradiation with α-particles as a stress factor. We describe the development of TNT networks in certain time steps after irradiation using confocal live-cell imaging and suggest an evaluation method to characterize these communication networks. Our results show that irradiated cells establish their network faster and have more cell-to-cell connections with high TNT content than sham-irradiated controls within the first 24 h. These findings suggest that there is an additional trigger upon radiation damage which results in fast and intensive network formation by TNTs as a radiation damage response mechanism.

Keywords: cellular communication, tunneling nanotubes, high-LET, cancer, bystander effect, glioblastoma

OPEN ACCESS

Edited by:
Daniel Michael Trifiletti, Mayo Clinic, United States

Reviewed by:
Virgínea De Araújo Farias, Mayo Clinic, United States
Henry Jeison Ruiz-Garcia, Mayo Clinic, United States

****Correspondence:***
Nicole Matejka
Nicole.matejka@unibw.de

Specialty section:
This article was submitted to Radiation Oncology, a section of the journal Frontiers in Oncology

Received: *20 May 2020*
Accepted: *29 July 2020*
Published: *04 September 2020*

Citation:
Matejka N and Reindl J (2020) Influence of α-Particle Radiation on Intercellular Communication Networks of Tunneling Nanotubes in U87 Glioblastoma Cells. Front. Oncol. 10:1691. doi: 10.3389/fonc.2020.01691

INTRODUCTION

Glioblastomas are one of the most common and most aggressive brain tumors, which are characterized by their high invasiveness and recurrence. Despite multimodal treatment, patients have a median survival of no more than 15 months and show a five-year survival rate below 10% (1–3). This poor prognosis is a result of the aggressive nature of glioblastomas composed of genomic instability, uncontrolled cellular proliferation, intratumoral heterogeneity, resistance to apoptosis, and high diffuse infiltration rates into the surrounding tissue (4–7). Due to these features, glioblastomas exhibit a considerably high chemo- and radioresistance, and despite extensive research on glioblastoma treatment, the responsible mechanisms for the aggressive nature are poorly understood or even unknown.

Radiotherapy is, besides surgery and chemotherapy, mostly in combination with one or even both, the treatment of choice for glioblastoma for ∼50% of all treated tumors worldwide (8, 9).

Abbreviations: DSB, DNA double strand break; TNT, tunneling nanotube.

The aim of radiotherapy is to specifically exploit the harmful effects of radiation in order to stop the proliferation of tumor cells but to protect healthy tissue as much as possible at the same time. For this purpose, it is indispensable to comprehend how radiation affects tissues and organisms and to understand the principle mechanisms occurring in cells upon radiative exposure. From a molecular biological point of view, ionizing radiation affects cellular life by depositing energy in cells, which causes breakages of chemical bonds. Therefore, proteins, lipids, genetic material, as well as other cellular components can be damaged by radiation. A critical damage for the survival of cells is the DNA double strand break (DSB), in which the DNA, the carrier of the genomic information, is completely severed (10). An erroneous repair of this type of damage can lead to cell death or mutation and consequent tumor formation. However, in cellular networks such as tissues, not only DNA damage in the single cells but also intracellular signal transduction as well as cell-to-cell communication play key roles in the damage response. It has been observed that irradiated cells send signals to neighboring cells, thus influencing the cellular survival of these cells, too. This communication can lead to so-called non-targeted effects such as the bystander effect, in which non-irradiated cells show biological radiation response due to signal-transfer from neighboring, irradiated cells (11, 12). In contrast, it was also reported that healthy cells can transport organelles, proteins, or signals to damaged cells in order to support repair and cell survival (13–16). In both cases, cell-to-cell communication directly influences the biological effects to the tissue and therefore to the organism caused by radiative stress. The underlying mechanism as well as the question of to what extend cellular communication affects the cell survival and genetic alterations after irradiation remain obscure (17). During evolution, cells developed several approaches to communicate. In 2004, a new kind of intercellular communication was reported and termed tunneling nanotubes (TNTs) (18). TNTs are thin membrane channels with a diameter in the nanometer range that directly connect cells over long distances up to 100 μm (19). They facilitate the direct cell-to-cell transfer of several cargoes such as organelles, viruses, and signals (20). Membranous connections between cells are not only found *in vitro*; such communication networks also occur *in vivo* (16, 21, 22). It was shown that especially in glioblastomas, membrane tunnels can form complex communication networks which have several biological functions and are responsible for enhancing tumor progression, radio- as well as chemoresistance (23). Furthermore, TNTs are more frequently found under a wide range of stress conditions including hypoxia (24, 25), serum starvation (22), infection (26), inflammation (21, 27), toxic treatment (28), UV- (15), and X-ray- (16), and particle-irradiation (29). Thus, it is strongly suspected that TNTs are highly linked to stress response and are triggered by stress alarm signals. For these reasons, cellular communication along these versatile, flexible membrane bridges might be a promising target for cancer treatment, especially for highly migratory and invasive tumors like glioblastomas which have a poor prognosis. A better understanding of the direct cellular response to radiation via TNTs might help to improve radiation therapies. New therapy approaches can be developed which influence the transfer of signals or the network itself. These drugs may be able to amplify the cell killing effect in the tumor environment. Also rescue of damaged healthy tissue can be a target of this kind of new therapy approaches.

Here, we study the response of TNT communication networks in glioblastoma cells on radiative stress induced by α-particle radiation. In this context, two essential questions are addressed: whether TNT communication networks are indeed influenced by particle radiation and if cellular communication is enhanced due to radiation exposure. Furthermore, we were interested in characterizing the complexity and strength of the cellular network formed by TNTs. We therefore developed an analysis method for TNT networks *in vitro* for a quantitative analysis of cellular communication via TNTs. Here, the TNT network is analyzed by addressing parameters regarding cell-to-cell connectivity and TNT density within one connection. Cells are classified into *isolated* cells, which are not involved in the network, and *connected* cells, which contribute to the network. Cell-to-cell connections are subdivided into *simple* and *complex* connections with respect to the number of TNTs they consist of in order to dissolve the strictness of the individual connections. With this method, it is possible to comprehend direct cellular communication response to radiation and to gain insight into the influence of cell-to-cell communication on the survival of cells and their behavior upon radiation.

MATERIALS AND METHODS

Cell Culture and Irradiation

The human U87 (ATCC, HTB-14) glioblastoma cell line was kindly provided by the Institute for Radiation Medicine (Helmholtz Zentrum München GmbH, 85764 Neuherberg, Germany) and cultured in DMEM, high glucose medium (Sigma-Aldrich) supplemented with 10% FCS and 1% Penicillin/Streptavidin at a temperature of 37°C (100% humidity, 5% CO_2). One day before irradiation, cells were seeded on round, high precision glass coverslips with 25 mm in diameter and a precise thickness of 170 ± 5 μm (Marienfeld, 150,000 cells/well). The cells were irradiated by α-particles using an Americium-241 source with an activity of 0.37 GBq, resulting in a dose rate of 0.12 Gy/min. The irradiator was built and calibrated by Roos and Kellerer (30) and ensures a homogenous dose distribution. We did further calibration using CR39 nuclear track detectors to precisely get the dose rate of 0.12 Gy/min (7). The functionality is ensured by measurements using dosimeters during the whole irradiation period. When reaching the cell layer, the α-particles have a reduced energy of 1.4 MeV which corresponds to a LET of 200 keV/μm. The cells were irradiated for 10 minutes resulting in a final dose of 1.2 Gy. This was the maximum possible dose for irradiation. Cells needed to be irradiated without medium coverage, and at 10 min the layer was reduced to zero (see **Supplementary Figure 1**). If cells would be kept longer, they would dry out and cell death would occur. The used dose is comparable to the dose of 1.3 Gy, which was used in a previous study, where cell survival and invasion of glioblastoma was studied using α-particle radiation (7). After irradiation, the cells

were further cultured in fresh medium at 37°C, 100% humidity, and 5% CO_2 until evaluation. The experiment was conducted 3–4 times with one sample each. At 72 h for the sham-irradiated control, only two samples worked.

Plasma Membrane Staining and Live-Cell Confocal Imaging

After post-irradiation incubation of 1, 6, 24, and 72 h, the cells were labeled with a 1.5X CellMask Orange plasma membrane stain solution (Thermo Fisher Scientific) for 10 min at 37°C, 100% humidity, and 5% CO_2, resulting in a stable, homogeneous fluorescence labeling of the plasma membrane in living cells.

For live-cell confocal imaging, a custom-made live-cell imaging container and a confocal microscope (Leica TCS SP8 3X) were used. Sample, microscope stage, and microscope were kept at a constant temperature of 37°C by a climate chamber. The excitation laser wavelength for CellMask Orange was 554 nm, with a detection range of 567–635 nm. Laser power for the excitation laser was in the range of 5 mW. In order to record a large area with best resolution, mosaic images were acquired using a 100× oil objective (Leica HCX PL APO 100x/1.4 Oil), resulting in a lateral resolution of 250 nm and an axial resolution of about 600 nm. Per sample, 100 partial images with an overlap of 20% were acquired and collected together to create one final merged image. This image has a size of about 670 μm × 670 μm. Each final merged image contains between 30 and 200 cells per sample. All samples were acquired in z-stacks with a step size of 400 nm and a pixel size of 40 nm. Live-cell imaging was preferred to cell fixation in order to avoid TNT breakage and distortion (18). The cells were scanned bidirectionally and with a scanning speed of 600 Hz to ensure a fast image acquisition, which reduces movement artifacts and stressing of the cells caused by long light exposures. Additionally, the complete image acquisition duration was kept under 1 h to ensure as few network changes as possible during image capture.

Statistical Analysis

For resolving significant differences, the two-sample t-test (GraphPad QuickCalcs) was used and a p-value of ≤ 0.05 was considered statistically significant.

RESULTS

To our experience, TNTs can be formed at any time in a cell culture. However, the amount of TNTs or rather the cell-to-cell connectivity established by TNTs can vary and depends on the current stress level of the cells. One aim of this pilot study was to design a network analysis method, which enables researchers to trace the development of a TNT communication network in living cells. We applied this method on α-particle irradiated cells. Irradiation was performed using 1.2 Gy, which was the highest dose possible with this imaging setup and is comparable to the dose used in previous studies on the reaction of glioblastoma to α-particle radiation (7).

Network Analysis Method

The analysis method can be followed in **Figure 1**: In the first step of the evaluation, each cell was located and marked by a black dot in a transparent copy of the respective sample (**Figure 1A**). Here, the original picture is faded in the background and the cells are visible as bright structures. In the second step, the TNT connections between the cells were tracked and the determined number of connections was drawn as a color-coded line in the respective transparent copy (**Figures 1B,C**). TNTs were counted by hand while scrolling through the image and looking at each cell separately. For evaluation, it was distinguished whether the cells were connected by 1–2 or more than 2 tubes. Connections containing 1 or 2 tubes are referred to as *simple* connections, whereas those consisting of 3 or more tubes are referred to as *complex* connections (**Figure 1B**). The underlying idea of the differentiation of connections according to the tube density is that the exchange of signals and cargoes is enhanced when more tubes are available for the transport (31, 32). Thus, it reveals the strength of the individual connection. A partition into more than two subgroups, e.g., each TNT number alone, was not recommended because connections containing exactly 2, 3, of 4 tubes were rarely present (see **Figure 1C** and **Supplementary Table 1**) independent of treatment and time. Furthermore, at a TNT number of 5 or higher, the individual TNTs inside the connections can be so close together that they are not distinguishable anymore and, therefore, not countable. Thus, a classification of connections into two (*simple* and *complex*) instead of more subgroups was used for a quantitative evaluation. Maximum projections of a very dense tube connection and a single tube connection are shown in **Figures 1D,E**, respectively. These are the corresponding enlargements of the selections marked by red frames in **Figures 1B,C**.

With this method, the connection frequency per cell, subdivided into the corresponding tube density within the connection, can be determined. This is done by counting the respective colored lines. Additionally, one can identify how dense the cells are connected among each other. This cell-to-cell connectivity can be studied by counting the connected lines at each dot, in other words, by counting the number of cells to which the currently viewed cell is connected. With these measured variables it is possible to make qualitative and quantitative statements of the cellular communication systems composed of TNTs.

The TNT networks were evaluated at several times in order to comprehend possible communication stages during the recovery phase after irradiation. Finally, the irradiated samples were compared to sham-irradiated controls as reference to establish the impact of radiation on TNTs.

Temporal Development of Cell-to-Cell Connectivity

A cell is considered a connected cell if it has at least one connection. With growing time, the fraction of connected cells increases significantly in both groups, irradiated and non-irradiated samples (**Figure 2**). At 1 h after irradiation, both groups have the same quantity of connected cells (44% ± 9% in

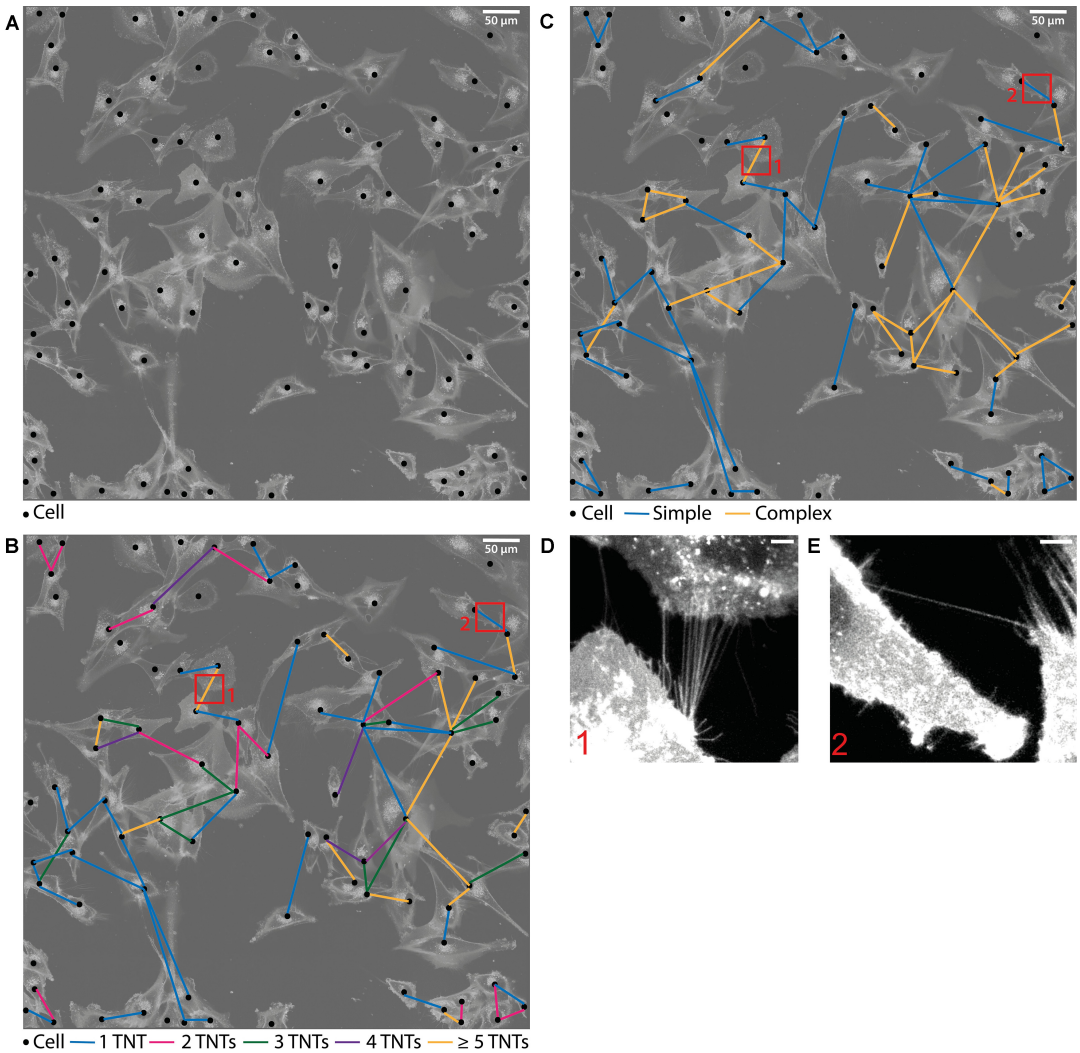

FIGURE 1 | Evaluation method of the TNT network. **(A)** Drawn picture of one sample. The original image is transparent in the background where the cells are visible as white structures. Each cell is marked as a black dot. **(B,C)** TNT connections between the cells are drawn as colored lines. The colors represent the different tube density per connection. Connections containing 1–2 TNTs are referred to as simple connections whereas connections consisting of more than 2 TNTs are referred to as complex connections. The enlargements correspond to the respective selection indicated with red frames, showing a dense tube connection **(D)** and a single tube connection **(E)**. These two images are maximum projections of the corresponding confocal z-stacks. Scale bars: **(A–C)** 50 µm, **(D,E)** 5 µm.

irradiated and 42% ± 5% in sham-irradiated cell populations). After the total observation time of 72 h, the fraction of connected cells increases to values of (84 ± 2)% in irradiated cell populations and (88 ± 2)% in sham-irradiated controls. However, it is also recognizable that this development happens with different speeds in the respective cell populations. Irradiated cell populations increase their fraction of interconnected cells faster than sham-irradiated control populations. Six hours after irradiation, a significant difference ($p < 0.05$) between the fractions of interconnected cells of irradiated (79 ± 5%) and sham-irradiated controls (61 ± 5%) is visible. Irradiated cell populations show almost twice as many connected cells (79 ± 5%) compared to 1 h after irradiation (44 ± 9%). After this jump within the first 6 h after irradiation, this value does not change much during the remaining observation time, staying at a fraction of about 85% of all cells that are connected to at least one other cell. In contrast, the fraction of connected cells in sham-irradiated controls seems to grow more continuously and not volatile. After 24 h, the difference between irradiated and sham-irradiated cells is not significant anymore. After 72 h, the connectivity of both groups equaled completely to the level of about 85% connected cells.

When considering this development, we asked ourselves whether different cell densities play a role in the characteristic of the TNT network. In **Figure 3A** the average cell densities for both groups at the four incubation times are shown. In contrast to the temporal development of the cell-to-cell connectivity (**Figure 2**), there is no noticeable steady growth of the cell density over time. The average cell densities for sham and irradiated samples at one time-point are comparable, except for 24 h. Here, the cell density of the irradiated samples is much higher than that of

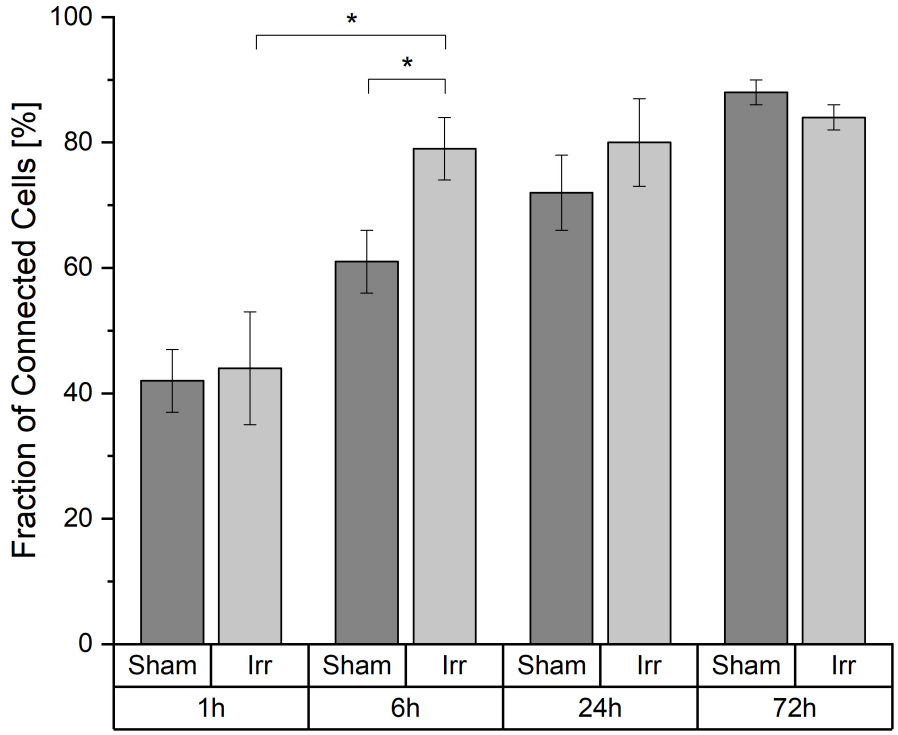

FIGURE 2 | Temporal development of the cell-to-cell connectivity. Mean values ± SEM are shown. A p-value ≤ 0.05 is indicated by *.

the sham-irradiated controls. For a detailed analysis, we directly looked at the single samples. For comparison, the cell density for each sample for 1 h is shown in **Figure 3B** and for 24 h in **Figure 3C**. The 6 and 72 h are shown in **Supplementary Figure 2**. One hour after (sham-) irradiation, the sham-irradiated controls all have a similar cell density, whereas the irradiated samples have two low and two high cell densities. However, in the two samples with a higher cell density no trend toward a higher cell-to-cell connectivity is visible, as one sample has a low fraction and one a high fraction of connected cells. For 24 h the effect that the cell density does not play a specific role in the cell-to-cell connectivity is even more pronounced. Here, all samples show similar fractions of connected cells independent of irradiation status and cell density. Overall, the cell densities of the individual samples differ from one another, but there is no concrete correlation between cell density and fraction of connected cells identifiable. Samples with a higher cell density do not show a significant rise of the cell-to-cell connectivity. Only with growing time the fraction of connected cells steadily increases, traceable in **Figure 2** and when comparing the fraction of connected cells at 1 h (**Figure 3B**) and 24 h (**Figure 3C**), where the cell-to-cell connectivity grows from 43 to 81%, respectively.

Temporal Development of Complexity of the Connections

In **Figure 4**, the temporal development of the distribution between the two kinds of connection, *simple* and *complex*, for irradiated and sham-irradiated samples is shown. The frequencies are normalized to the overall number of connections found in the respective sample. Regardless of time and treatment, there are always more *simple* than *complex* connections. However, the exact distribution of the different connection types is neither independent of time nor treatment. Up to 6 h after (sham-) irradiation, the partitioning of the connections is the same for irradiated and sham-treated samples. Thereby, an average frequency of 0.66 ± 0.01 for *simple* connections and 0.34 ± 0.01 for *complex* connections was observed. However, at an incubation period of 24 h, there are significant differences regarding the proportion of simple and complex connections: Non-irradiated cells exhibit much more *simple* connections than irradiated cells ($p < 0.05$). Consequently, more *complex* connections are found in the irradiated samples than in the control samples. After three days, the proportions for irradiated and sham samples converge again. In the irradiated cell populations, the proportion of *complex* connections with more than two TNTs and therefore network strength increases significantly from 1 to 24 h after irradiation, remaining at this level for the next two days until the end of incubation. In sham-irradiated samples, the complexity of connections is largely constant over the first 24 h and then increases significantly in the following 48 h.

Temporal Development of the Fraction of Highly Connected Cells

When considering the temporal development of the fraction of cells which are at least connected to two or more cells and

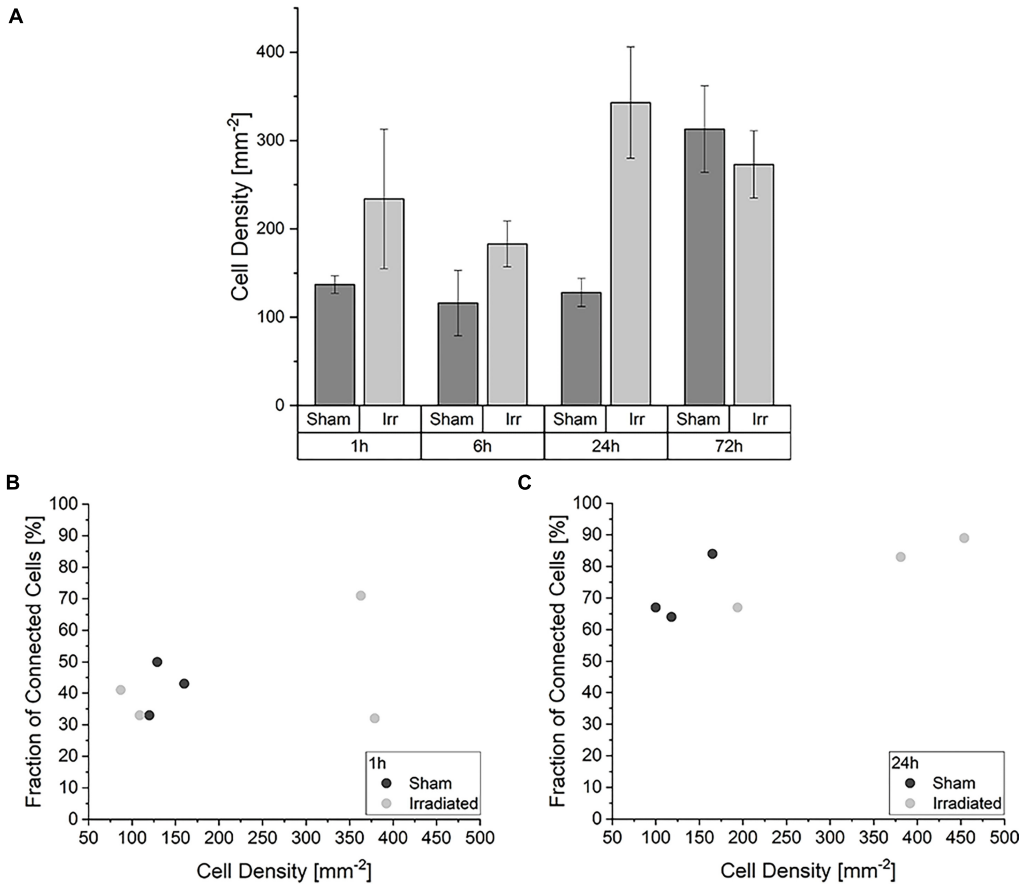

FIGURE 3 | Impact of the cell density in the development of the TNT network. **(A)** Average cell densities of sham- and irradiated samples at different incubation times. Mean values ± SEM are shown. Analysis of the fraction of connected cells within irradiated and sham-irradiated samples in dependence of the cell density for the times 1 h **(B)** and 24 h **(C)**. Each dot represents one sample.

thus highly connected into the network, a lower connectivity is recognizable for sham-irradiated controls compared to irradiated samples only at 24 h after (sham-) irradiation (**Figure 5**). In 1 and 6 h after (sham-) irradiation, irradiated and sham-irradiated samples exhibit nearly the same proportion of highly connected cells. This behavior changes at an incubation time of 24 h. At this time, the amount of highly connected cells increases further in irradiated cell populations to a value of 48 ± 16%, whereas untreated cell populations seem to exhibit a small decrease of this cell fraction to 24 ± 12%. This difference vanishes again after 72 h, where the fractions of highly connected cells align with each other, reaching values of 54 ± 5% and 57 ± 2% in irradiated and sham-irradiated cells, respectively. During the complete observation time, the number of highly connected cells increases in both groups, sham- and irradiated.

DISCUSSION

The presented data show that both irradiated and non-irradiated cells expand and upgrade their communication network during growth, visible by more *complex* connections, i.e., higher number of TNTs per connection, and higher cell-to-cell connectivity, i.e., more cells connected to at least one other cell as well as more cells connected to several other cells, 72 h after (sham-)irradiation. However, irradiated cells establish their TNT communication network faster than sham-irradiated cells. The fraction of cells that are connected to at least one other cell and thus involved in the network jumps to a higher level in irradiated samples than in sham controls between 1 and 6 h after irradiation. Sham-irradiated cell populations show a more continuous network growth and the same connectivity of about 85% that irradiated samples show at 6 h are only reached after about 24 h.

These findings suggest that there are different triggers inducing the TNT formation in irradiated and non-irradiated cells. It seems that in irradiated cells, the TNT formation and the development of the cellular communication network is accelerated by an additional mechanism, which is not active in the sham-irradiated cell populations. With this faster development of their TNT communication network, irradiated cells may be able to deal with the radiative stress and to trigger survival mechanisms.

TNT formation can be realized by cell dislodgement after cell-to-cell contact or by filopodia growth (33). We have

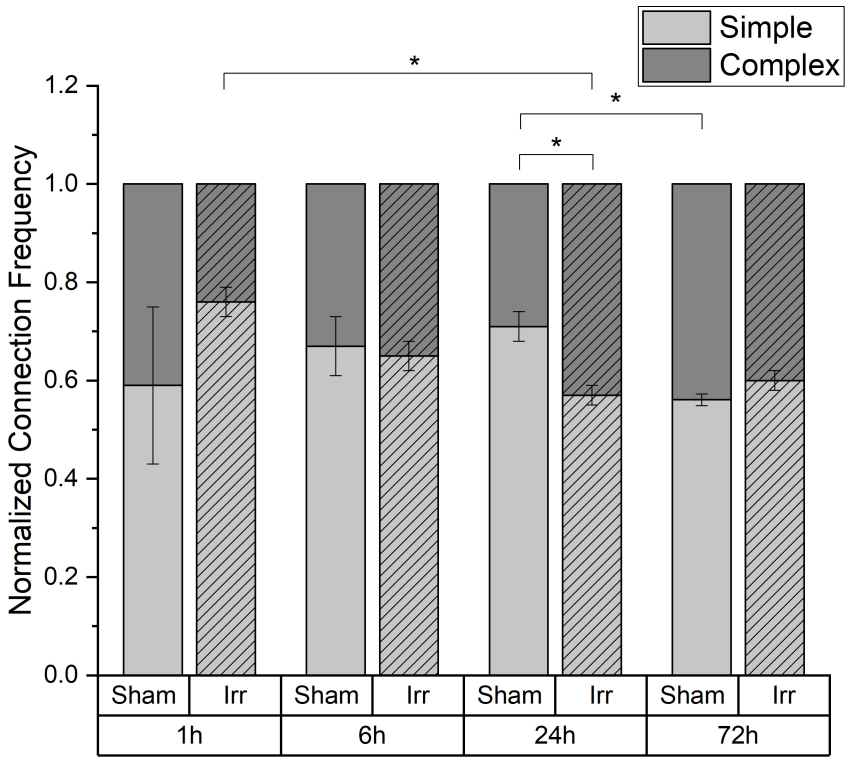

FIGURE 4 | Temporal development of the proportion of simple and complex connections in irradiated and sham-irradiated cell populations. Those frequencies are normalized to the total number of found connections. Mean values ± SEM are shown. A p-value ≤ 0.05 is indicated by *.

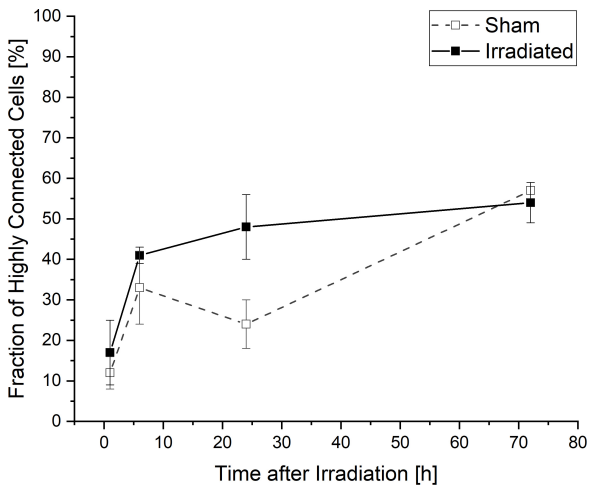

FIGURE 5 | Temporal development of highly connected cells which are interconnected to two or more cells. Mean values ± SEM are shown.

observed and recorded that TNT formation in U87 cells occurs via cell dislodgement (**Supplementary Figure 3**), but this does not exclude that TNT formation can additionally be realized by filopodia growth in U87 cells. It might be possible that selective TNT formation is realized by filopodia growth and the usual communication network is established by cell dislodgement after cell division or encountering of cells. Therefore, it could be possible that the communication network in cells is enhanced upon irradiation and an additional mechanism causes an increased triggering of TNT formation by filopodia growth. This would explain the immediate rise of the fraction of interconnected cells within 6 h in irradiated cell populations. The release of stress signals into the medium, originating from the irradiated, stressed cells, could induce filopodia growth and lead to an orientated TNT formation.

After this immediate jump, the networking cell fraction of about 85% does not change further in irradiated cell populations during the complete observation period of up to 72 h, suggesting that after 6 h the additional triggering of TNT formation is attenuated or a saturation regarding the development of the TNT network has been reached.

In almost all cellular communication networks there are cells that are interconnected with several cells, i.e., more than one other cell. This portion of cells can be considered as an indicator of the complexity of a communication network. Here, more highly connected cells tend to be present in irradiated samples than in controls after 24 h. Additionally, there are significantly more *complex* connections found in irradiated cells than in sham-irradiated controls at this point of time. After the expansion of the TNT network within the first 6 h by involving as many cells as possible, the focus is now on condensing and strengthening their network. By contrast, the sham-irradiated samples build

their network more slowly and are non-complex, mostly by the formation of *simple* tube connections to one other cell.

After three days, irradiated and sham-irradiated samples have aligned themselves and exhibit the same values regarding fraction of connected cells, average and distribution of the number of connections per cell (**Supplementary Figure 4** and **Supplementary Table 1**), as well as proportion of *simple* and *complex* connections. This suggests that the additional triggering of TNT formation in irradiated cells has been stopped and the network is not further expanded and strengthened by the irradiated cells at a certain point. This might be due to a saturation in the establishment of the TNT network or because irradiated cells are no longer able to further expand their communication network. Furthermore, the fact that most repair processes (about 88% γ-H2AX fluorescence decay) are finished 48 h after high-LET irradiation (34) can lead to a stop of oriented TNT formation. Additionally, remaining TNT connections to apoptotic cells, which cannot be rescued, might become detached to isolate these irrecoverable cells, similar to the model proposed by Rustom (35). Consequently, it would be interesting to evaluate incubation times longer than three days, to figure out if the controls are further able to expand and strengthen their network and thus will pass the irradiated cells. If this is true, it would demonstrate that cells are hampered in their communication via TNTs by irradiation.

Overall, the aim of this small sample pilot study was to determine whether there are any differences in cell communication by TNTs between irradiated and non-irradiated cells. The findings demonstrate that the communication network via TNTs is influenced by irradiation and its establishment is accelerated. Irradiated cells build up and condense their communication network faster than non-irradiated cells within the first 24 h. However, after this period the controls catch up and are equal again within 72 h after (sham-) irradiation.

With our analysis method for investigating TNT networks, it is possible to follow and draw quantitative conclusions about the cellular communication along these tiny tunnels. In the literature, scientists often count each individual TNT and define parameters like the "TNT index," which gives the number of TNT per cell (36, 37). However, when considering glioblastoma cells such as U87 cells, which can have very dense cell-to-cell connections consisting of many indistinguishable TNTs, counting of each individual TNT is sometimes even impossible. Additionally, it has been reported that a higher number of TNTs between two cells leads to an amplification of electrical signals (31, 32). Thus, one can assume that a cell-to-cell connection with a higher TNT density is probably more efficient for exchanging many cargoes in a short period than a connection by only a few TNTs. In this context, we think that a differentiation between cell-to-cell connections with a high or low TNT density is more appropriate than counting each individual TNT.

A major challenge in investigating the response of cellular communication via TNTs to stress occurs due to the fluctuations of cell density. Since TNTs can be formed after direct cell-to-cell contact, one could imagine that more TNTs can be found in denser cell populations than in non-confluent. In this study, U87 cells were cultivated for 72 h, leading to a higher cell density due to growth compared to the cell density directly after irradiation. Also seeding of the cells causes unpredictable, inhomogeneous gaps between the individual cells as the U87 cell line used in this study does not grow in homogeneous monolayers but tends to cluster in bulks. Thus, in one sample there can be areas with a very high cell density and areas with a very low cell density. To exclude a bias coming from selection of distinct locations, the imaged positions were randomly chosen. Consequently, very high local differences in the cell density can occur. However, the temporal development of connected cells (see **Figures 2**, **3**) reveals that the cell-to-cell connectivity increases, although the cell density does not change significantly. Therefore, we assume that the cell density has only a subordinate role in the TNT establishment. Nevertheless, it would be beneficial to have similar cell-to-cell distances when studying the role of TNTs in stress conditions.

CONCLUSION

In this work, we introduced a method to examine TNT networks *in vitro* in a quantitative and qualitative manner with the aim to obtain a better understanding of cellular communication networks. Furthermore, we figured out that the cellular communication via TNTs is influenced by radiation in U87 glioblastoma cells. This could mean that there may be an additional mechanism which causes the irradiated cells to form TNTs faster and more frequently than normal. It might be that irradiated cells release signal molecules into the medium which can lead to an increased TNT formation by filopodia growth. Additionally, our results show that irradiated U87 cell populations have more *complex* connections consisting of several TNTs as compared to non-irradiated cell populations after 24 h. This could signify that the irradiated cells strengthen their TNT network more intensively than non-treated cells. This probably indicates an increased communication via TNTs with the idea that the more TNTs, the more cargoes can be transferred at the same time. However, this hypothesis remains to be proven. After 72 h of incubation, our results suggest that the most features of the TNT network are the same again for both irradiated and non-irradiated samples.

For obtaining an even better understanding of how cellular communication via TNTs is involved or activated after exposure to radiation, it is necessary to perform live-cell imaging videos of TNT formations in irradiated and non-irradiated cells. Here, cell-tracking of single cells would be beneficial. It is also important to find out whether cell dislodgement or division leads to the formation of one single TNT or to several densely packed TNTs. Furthermore, it is essential to identify the transferred cargoes along the TNTs, since this would provide a better understanding of the interfering mechanisms of cell-to-cell communication and would be the evidence that there is indeed an exchange of information via TNTs after irradiation.

Overall, intercellular communication via TNTs seems to play an important role in the response of glioblastoma cells to radiation. A better understanding of the mechanisms and the biological functions behind these communication networks

could help to improve the treatment of these aggressive tumors in the future.

DATA AVAILABILITY STATEMENT

All datasets presented in this study are included in the article/**Supplementary Material**.

AUTHOR CONTRIBUTIONS

NM designed the study, performed the experiment and analysis, discussed the data, and wrote the manuscript. JR gave the idea and designed the study, discussed the data, and wrote the manuscript. Both authors contributed to the article and approved the submitted version.

FUNDING

The authors are funded by EU project RADIATE and DFG Cluster of Excellence: Munich-Centre for Advanced Photonics.

ACKNOWLEDGMENTS

We thank Dr. Stefanie Girst for her critical proofreading and Prof. Dr. Thomas Schmid for providing U-87 MG cells.

SUPPLEMENTARY MATERIAL

The Supplementary Material for this article can be found online at: https://www.frontiersin.org/articles/10.3389/fonc.2020.01691/full#supplementary-material

REFERENCES

1. Krex D, Klink B, Hartmann C, von Deimling A, Pietsch T, Simon M, et al. Long-term survival with glioblastoma multiforme. *Brain.* (2007) 130:2596–606. doi: 10.1093/brain/awm204
2. Babu R, Komisarow JM, Agarwal VJ, Rahimpour S, Iyer A, Britt D, et al. Glioblastoma in the elderly: the effect of aggressive and modern therapies on survival. *J Neurosurg.* (2016) 124:998–1007. doi: 10.3171/2015.4.JNS142200
3. Demuth T, Berens ME. Molecular mechanisms of glioma cell migration and invasion. *J Neurooncol.* (2004) 70:217–28. doi: 10.1007/s11060-004-2751-6
4. Hanahan D, Weinberg RA. Hallmarks of cancer: the next generation. *Cell.* (2011) 144:646–74. doi: 10.1016/j.cell.2011.02.013
5. Wank M, Schilling D, Schmid TE, Meyer B, Gempt J, Barz M, et al. Human glioma migration and infiltration properties as a target for personalized radiation medicine. *Cancers (Basel).* (2018) 10:456. doi: 10.3390/cancers10110456
6. Venkatesh VS, Lou E. Tunneling nanotubes: a bridge for heterogeneity in glioblastoma and a new therapeutic target? *Cancer Rep.* (2019) 2:e1185. doi: 10.1002/cnr2.1185
7. Wank M, Schilling D, Reindl J, Meyer B, Gempt J, Motov S, et al. Evaluation of radiation-related invasion in primary patient-derived glioma cells and validation with established cell lines: impact of different radiation qualities with differing LET. *J Neurooncol.* (2018) 139:583–90. doi: 10.1007/s11060-018-2923-4
8. Baskar R, Lee KA, Yeo R, Yeoh K-W. Cancer and radiation therapy: current advances and future directions. *Int J Med Sci.* (2012) 9:193–9. doi: 10.7150/ijms.3635
9. Delaney G, Jacob S, Featherstone C, Barton M. The role of radiotherapy in cancer treatment. *Cancer.* (2005) 104:1129–37. doi: 10.1002/cncr.21324
10. Khanna KK, Jackson SP. DNA double-strand breaks: signaling, repair and the cancer connection. *Nat Genet.* (2001) 27:247–54. doi: 10.1038/85798
11. Desouky O, Ding N, Zhou G. Targeted and non-targeted effects of ionizing radiation. *J Radiat Res Appl Sci.* (2015) 8:247–54. doi: 10.1016/j.jrras.2015.03.003
12. Prise KM, O'Sullivan JM. Radiation-induced bystander signalling in cancer therapy. *Nat Rev Cancer.* (2009) 9:351–60. doi: 10.1038/nrc2603
13. Rodriguez A-M, Nakhle J, Griessinger E, Vignais M-L. Intercellular mitochondria trafficking highlighting the dual role of mesenchymal stem cells as both sensors and rescuers of tissue injury. *Cell Cycle.* (2018) 17:712–21. doi: 10.1080/15384101.2018.1445906
14. Torralba D, Baixauli F, Sánchez-Madrid F. Mitochondria know no boundaries: mechanisms and functions of intercellular mitochondrial transfer. *Front Cell Dev Biol.* (2016) 4:107. doi: 10.3389/fcell.2016.00107
15. Wang X, Gerdes H-H. Transfer of mitochondria via tunneling nanotubes rescues apoptotic PC12 cells. *Cell Death Differ.* (2015) 22:1181–91. doi: 10.1038/cdd.2014.211
16. Osswald M, Jung E, Sahm F, Solecki G, Venkataramani V, Blaes J, et al. Brain tumour cells interconnect to a functional and resistant network. *Nature.* (2015) 528:93–8. doi: 10.1038/nature16071
17. Matejka N, Reindl J. Perspectives of cellular communication through tunneling nanotubes in cancer cells and the connection to radiation effects. *Radiat Oncol.* (2019) 14:1–11. doi: 10.1186/s13014-019-1416-8
18. Rustom A, Saffrich R, Markovic I, Walther P, Gerdes H-H. Nanotubular highways for intercellular organelle transport. *Science.* (2004) 303:1007–10. doi: 10.1126/science.1093133
19. Sowinski S, Jolly C, Berninghausen O, Purbhoo MA, Chauveau A, Köhler K, et al. Membrane nanotubes physically connect T cells over long distances presenting a novel route for HIV-1 transmission. *Nat Cell Biol.* (2008) 10:211–9. doi: 10.1038/ncb1682
20. Ariazi J, Benowitz A, De Biasi V, Den Boer ML, Cherqui S, Cui H, et al. Tunneling nanotubes and gap junctions-their role in long-range intercellular communication during development, health, and disease conditions. *Front Mol Neurosci.* (2017) 10:333. doi: 10.3389/fnmol.2017.00333
21. Chinnery HR, Pearlman E, McMenamin PG. Cutting edge: membrane nanotubes in vivo: a feature of MHC class II+ cells in the mouse cornea. *J Immunol.* (2008) 180:5779–83. doi: 10.4049/jimmunol.180.9.5779
22. Lou E, Fujisawa S, Morozov A, Barlas A, Romin Y, Dogan Y, et al. Tunneling nanotubes provide a unique conduit for intercellular transfer of cellular contents in human malignant pleural mesothelioma. *PLoS One.* (2012) 7:e33093. doi: 10.1371/journal.pone.0033093
23. Osswald M, Jung E, Wick W, Winkler F. Tunneling nanotube—like structures in brain tumors. *Cancer Rep.* (2019) 2:1. doi: 10.1002/cnr2.1181
24. Desir S, Dickson EL, Vogel RI, Thayanithy V, Wong P, Teoh D, et al. Tunneling nanotube formation is stimulated by hypoxia in ovarian cancer cells. *Oncotarget.* (2016) 7:43150–61. doi: 10.18632/oncotarget.9504
25. Zhu D, Tan KS, Zhang X, Sun AY, Sun GY, Lee JC-M. Hydrogen peroxide alters membrane and cytoskeleton properties and increases intercellular connections in astrocytes. *J Cell Sci.* (2005) 118:3695–703. doi: 10.1242/jcs.02507
26. Eugenin EA, Gaskill PJ, Berman JW. Tunneling nanotubes (TNT) are induced by HIV-infection of macrophages: a potential mechanism for intercellular HIV trafficking. *Cell Immunol.* (2009) 254:142–8. doi: 10.1016/j.cellimm.2008.08.005
27. Ranzinger J, Rustom A, Abel M, Leyh J, Kihm L, Witkowski M, et al. Nanotube action between human mesothelial cells reveals novel aspects of inflammatory responses. *PLoS One.* (2011) 6:e29537. doi: 10.1371/journal.pone.0029537
28. Kabaso D, Lokar M, Kralj-Iglič V, Veranič P, Iglič A. Temperature and cholera toxin B are factors that influence formation of membrane nanotubes in RT4 and T24 urothelial cancer cell lines. *Int J Nanomed.* (2011) 6:495–509. doi: 10.2147/IJN.S16982

29. Reindl J, Shevtsov M, Dollinger G, Stangl S, Multhoff G. Membrane Hsp70-supported cell-to-cell connections via tunneling nanotubes revealed by live-cell STED nanoscopy. *Cell Stress Chaperones.* (2019) 24:213–21. doi: 10.1007/s12192-018-00958-w
30. Roos H, Kellerer AM. Design criteria and performance parameters of an alpha irradiation device for cell studies. *Phys Med Biol.* (1989) 34:1823–32. doi: 10.1088/0031-9155/34/12/006
31. Wang X, Gerdes H-H. Long-distance electrical coupling via tunneling nanotubes. *Biochim Biophys Acta.* (2012) 1818:2082–6. doi: 10.1016/j.bbamem.2011.09.002
32. Wang X, Veruki ML, Bukoreshtliev NV, Hartveit E, Gerdes H-H. Animal cells connected by nanotubes can be electrically coupled through interposed gap-junction channels. *Proc Natl Acad Sci USA.* (2010) 107:17194–9. doi: 10.1073/pnas.1006785107
33. Abounit S, Zurzolo C. Wiring through tunneling nanotubes–from electrical signals to organelle transfer. *J Cell Sci.* (2012) 125:1089–98. doi: 10.1242/jcs.083279
34. Schmid TE, Dollinger G, Beisker W, Hable V, Greubel C, Auer S, et al. Differences in the kinetics of gamma-H2AX fluorescence decay after exposure to low and high LET radiation. *Int J Radiat Biol.* (2010) 86:682–91. doi: 10.3109/09553001003734543
35. Rustom A. The missing link: does tunnelling nanotube-based supercellularity provide a new understanding of chronic and lifestyle diseases? *Open Biol.* (2016) 6:160057. doi: 10.1098/rsob.160057
36. Lou E, Zhai E, Sarkari A, Desir S, Wong P, Iizuka Y, et al. Cellular and molecular networking within the ecosystem of cancer cell communication via tunneling nanotubes. *Front Cell Dev Biol.* (2018) 6:95. doi: 10.3389/fcell.2018.00095
37. Ady JW, Desir S, Thayanithy V, Vogel RI, Moreira AL, Downey RJ, et al. Intercellular communication in malignant pleural mesothelioma: properties of tunneling nanotubes. *Front Physiol.* (2014) 5:400. doi: 10.3389/fphys.2014.00400

Conflict of Interest: The authors declare that the research was conducted in the absence of any commercial or financial relationships that could be construed as a potential conflict of interest.

Copyright © 2020 Matejka and Reindl. This is an open-access article distributed under the terms of the Creative Commons Attribution License (CC BY). The use, distribution or reproduction in other forums is permitted, provided the original author(s) and the copyright owner(s) are credited and that the original publication in this journal is cited, in accordance with accepted academic practice. No use, distribution or reproduction is permitted which does not comply with these terms.

frontiers in Oncology

REVIEW
published: 15 September 2020
doi: 10.3389/fonc.2020.01537

Clinical Radiobiology of Fast Neutron Therapy: What Was Learnt?

Bleddyn Jones [1,2,3]*

[1] Gray Laboratory, Department of Oncology, University of Oxford, Oxford, United Kingdom, [2] Green Templeton College, University of Oxford, Oxford, United Kingdom, [3] University College Department of Medical Physics & Biomedical Engineering, London, United Kingdom

Neutron therapy was developed from neutron radiobiology experiments, and had identified a higher cell kill per unit dose and an accompanying reduction in oxygen dependency. But experts such as Hal Gray were sceptical about clinical applications, for good reasons. Gray knew that the increase in relative biological effectiveness (RBE) with dose fall-off could produce marked clinical limitations. After many years of research, this treatment did not produce the expected gains in tumour control relative to normal tissue toxicity, as predicted by Gray. More detailed reasons for this are discussed in this paper. Neutrons do not have Bragg peaks and so did not selectively spare many tissues from radiation exposure; the constant neutron RBE tumour prescription values did not represent the probable higher RBE values in late-reacting tissues with low α/β values; the inevitable increase in RBE as dose falls along a beam would also contribute to greater toxicity than in a similar megavoltage photon beam. Some tissues such as the central nervous system white matter had the highest RBEs partly because of the higher percentage hydrogen content in lipid-containing molecules. All the above factors contributed to disappointing clinical results found in a series of randomised controlled studies at many treatment centres, although at the time they were performed, neutron therapy was in a catch-up phase with photon-based treatments. Their findings are summarised along with their technical aspects and fractionation choices. Better understanding of fast neutron experiments and therapy has been gained through relatively simple mathematical models—using the biological effective dose concept and incorporating the RBEmax and RBEmin parameters (the limits of RBE at low and high dose, respectively—as shown in the **Appendix**). The RBE itself can then vary between these limits according to the dose per fraction used. These approaches provide useful insights into the problems that can occur in proton and ion beam therapy and how they may be optimised. This is because neutron ionisations in living tissues are mainly caused by recoil protons of energy proportional to the neutron energy: these are close to the proton energies that occur close to the Bragg peak region. To some extent, neutron RBE studies contain the highest RBE ranges found within proton and ion beams near Bragg peaks. In retrospect, neutrons were a useful radiobiological tool that has continued to inform the scientific and clinical community about the essential radiobiological principles of all forms of high linear energy transfer therapy. Neutron radiobiology and its implications should be taught on training courses and studied closely by clinicians, physicists, and biologists engaged in particle beam therapies.

Keywords: neutron therapy, radiobiology, radiotherapy, hadron, high LET, RBE

OPEN ACCESS

Edited by:
Timothy Dean Malouff, Mayo Clinic Florida, United States

Reviewed by:
Nobuyuki Kanematsu, National Institutes for Quantum and Radiological Science and Technology, Japan
Pankaj Chaudhary, Queen's University Belfast, United Kingdom

***Correspondence:**
Bleddyn Jones
bleddyn.jones@oncology.ox.ac.uk

Specialty section:
This article was submitted to Radiation Oncology, a section of the journal Frontiers in Oncology

Received: *15 May 2020*
Accepted: *17 July 2020*
Published: *15 September 2020*

Citation:
Jones B (2020) Clinical Radiobiology of Fast Neutron Therapy: What Was Learnt? Front. Oncol. 10:1537. doi: 10.3389/fonc.2020.01537

INTRODUCTION

To understand the motivation for neutron therapy and its research history, readers from different academic backgrounds require a good working knowledge of radiobiology, as well as insights into the historical development of x-ray (or photon)—based radiotherapy. This is important because fast neutron therapy was essentially competing with best practice using x-rays (or photons).

This review focuses on the clinical radiobiology aspects of fast neutron therapy, which considers the interaction between radiobiology discoveries and their applications in treatment, with radiobiological modelling used not only as analytical tool, but also as a guide to clinical practice. It is not meant to be a comprehensive review of treatment results or the quite separate topic of experimental neutron radiobiology.

It is essential to consider the progressive technical development of photon-based treatments (most of which have been beneficial), as well as the present shift to greater use of charged particle therapy and place neutron therapy within these different radiation modalities. Neutrons are hadrons and are sometimes included within the general concept of hadron therapy, which can cause confusion because neutrons have no electrostatic charge. Readers should be aware of the important aspects of dose distribution for neutrons and photons (a progressive attenuation with tissue distance or depth) but that protons and ions have Bragg peaks due not only to their charge but also a velocity reduction along particle tracks. The term *fast neutrons* refers to neutrons that have sufficient energy to cause recoil protons that ionise materials. They should be distinguished from very low energy thermal neutrons found in nuclear reactors.

A Brief Synopsis of External Beam Radiotherapy Development

In order to compare the effectiveness of neutrons with x-rays (photons), the following information must be understood, especially the fact that more sophisticated technical developments in treatment delivery occurred sooner in the case of x-rays than with neutrons. Technical developments were mainly based on the achievement of higher photon energies, which increased the range or tissue depth, while also for megavoltage photons reducing the skin or entry dose before attaining full secondary electronic equilibrium at the maximum dose, followed by pseudoexponential attenuation with increasing tissue depth. Increasing the photon energy to the megavoltage range was also accompanied by more uniform tissue attenuation depending on the electron density rather than the actual atomic composition at lower energies. Improvements in imaging techniques further improved radiotherapy targeting, and it became possible to superimpose radiation depth dose curves in three-dimensional (3-D) space on the relevant scan or even combination of fused scan images.

During the 1950s and 1960s, external radiation beams progressed to the megavoltage energy range by use of 60-cobalt units and later increasing use of electron linear accelerators, which depended on the cavity magnetron principles originally used in radar applications (1).

With such competition, the already existing cyclotron accelerators were only rarely used for clinical neutron applications until a later time. For example, acceleration of protons onto beryllium targets to produce fast neutrons for experimental and clinical studies (2). Megavoltage photon radiation produced improved depth dose curves, enabling deeper seated tumour to be treated and with fewer beams, thus reducing the integral dose compared to when lower voltage beams were used.

Along with the computing advances mentioned previously, during the 1990s it became possible to shape each individual beam in order to match the clinically defined target by introducing variable strips of shielding metal in the accelerator collimation system. This became known as conformal radiotherapy. A UK randomised clinical trial showed that normal tissue side effects were reduced because of the large reduction in normal tissue volume irradiated to a high dose but without a reduction in prostate cancer tumour control with long-term analysis (3). The beam control possibilities improved further by using the multileaf collimator (MLC) to vary the beam intensity along its profile: this became known as intensity-modulated radiotherapy (IMRT), which further improved the degree of dose conformity to the defined target volume. Again, randomised studies of IMRT showed significant improvement of parotid gland function while treating head and neck cancer (4). However, in order to achieve the best available conformity to the target volume, the net effect was to increase the amount of tissue exposed to medium or lower doses, with some potential for causing more subtle later effects such as cancer induction or late vascular effects over subsequent time periods of 5 to 30 years. More recently, developments include robotically controlled small linacs, offering rapid changes in beam direction and intensity modulation of beamlets, which can further improve the conformity index and can be used with more precise body immobilisation techniques and state-of-the-art image guidance techniques (5). These treatments, depending on the dose distributions achieved, can be given in fewer treatments (hypofractionation) or even in a single session (often referred to as radiosurgery) (6).

Over the past two decades, and from a small initial base, there has been an expansion in cyclotron or synchrotron acceleration to deliver protons and light ions for cancer therapy in more than 100 hospitals worldwide (7, 8). These positively charged particles with their Bragg peaks whose tissue depths can be controlled by good energy selection coupled with detailed imaging, so that preferential energy deposition can occur in the selected cancer volume and its immediate surroundings.

Figure 1 shows the relative time frames of x-rays–based and neutron therapy along with its associated radiobiology.

Biological Effects

The above discussion has been concerned with the physical aspects of radiotherapy, but the important biological effects must be considered next. Neutrons have higher biological effects, quantified by the relative biological effectiveness (RBE) concept.

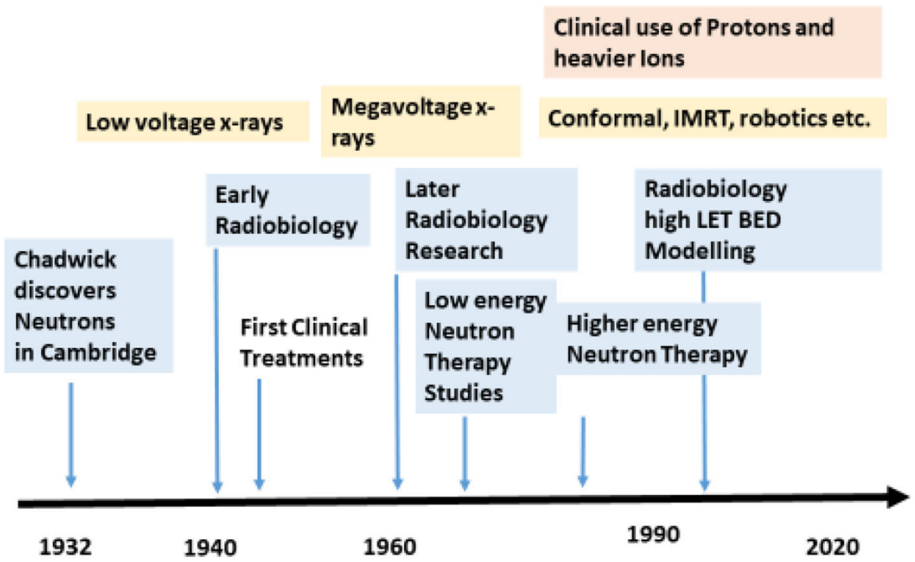

FIGURE 1 | Approximate time frame for neutron research and therapy indicated by blue with x-ray/photon developments in yellow.

RBE is the ratio of the dose of the reference radiation divided by the dose of the neutron radiation for the same biological effect. It follows that the reference radiation dose must be divided by the RBE in order to provide the equivalent (and lower) neutron dose, as shown:

$$\text{RBE} = \frac{\text{Dose (photons)}}{\text{Dose (neutrons)}} \quad (1)$$

$$\text{Dose (neutrons)} = \frac{\text{Dose (photons)}}{\text{RBE}} \quad (2)$$

Research studies showed that the biological effects of photon radiation varied not only with dose but also the dose rate, the degree of dose fractionation (in which the dose can be split in time into different treatment sessions), the chemical environment of the cells (some chemicals protecting and others sensitising radiation by influencing the yield of free radicals), and also the "quality" of the radiation. The latter refers to the linear energy transfer (LET) characteristics of a radiation, which depends not only on the nature of the radiation (e.g., photon or hadron), its energy (lower energies confer higher LET), and the total nuclear electrostatic charge given by the Z number of each element. Photons ionise by means of electronic interactions, forming secondary electrons in matter. Lower energy electrons converted by 10 to 100 keV photons have higher LET and biological effects than those in the megavoltage range (9).

Physical Interactions of Neutrons With Matter

Neutrons do not interact with atomic electrons like photons do, but instead the uncharged fast neutrons efficiently interact with hydrogen nuclei, producing recoil protons that ionise. As well as water, other biological macromolecules containing a relatively high proportion of water hydrogen include lipids and lipoproteins, so that neutrons will deposit more energy in tissues that contain, for example myelin and sphingomyelin in brain and spinal cord white matter, and of course in body fat. Fatty tissue contains long fatty acid chains CH_3-$(CH_2)_N$-COOH, and exists in the connective tissues that surround many organs of the body and through which the vital blood vessels pass. The abdomen contains a large intraperitoneal fat pad called the omentum, which is in intimate contact with the bowel. The KERMA (kinetic energy released per unit mass) in lipid-containing tissues can exceed that in water, which contains a relatively high proportion of hydrogen (11.1% by weight), resulting in increased local dose and bioeffectiveness. Previously published data from a detailed study (10) were combined to show a linear relationship between the percentage of hydrogen (%H) contained in some materials and tissues and KERMA. The increase in KERMA is ∼8.8% per unit increase in the %H as shown in **Figure 2**.

NEUTRON THERAPY AND RADIOBIOLOGY

Some general comments are appropriate at this stage in order to fully appreciate the issues discussed below. Experts tend to be dismissive of the history of fast neutron therapy, because of the disappointing clinical outcomes, and many clinical specialists were afterwards sceptical about using any form of particle therapy emerging from a cyclotron. To understand this topic fully, the radiobiology and therapy have to be taken together, with a later description of advances in the radiobiological understanding, which occurred that followed with time.

Why Study Neutron Therapy and Radiobiology?

It is now vital that lessons learnt from fast neutrons' radiobiology experiments and from the clinical trials are acknowledged

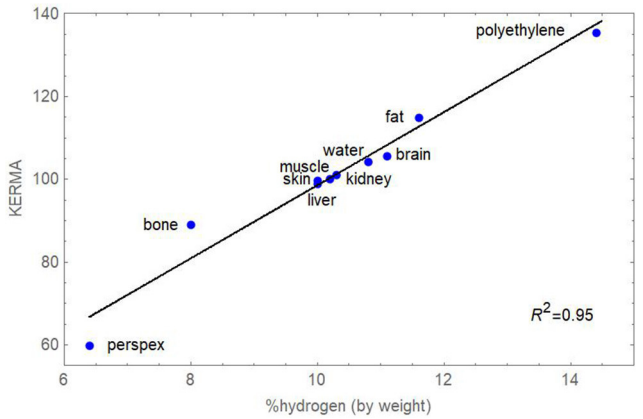

FIGURE 2 | Plot of percentage hydrogen (by weight) and KERMA for a range of materials and tissues exposed to five different fast neutron beams. Standard errors are not shown for individual points since they are small (average 0.78, the largest being 2.1 for bone). Data obtained from Awschalom, Rosenberg & Mravca (10).

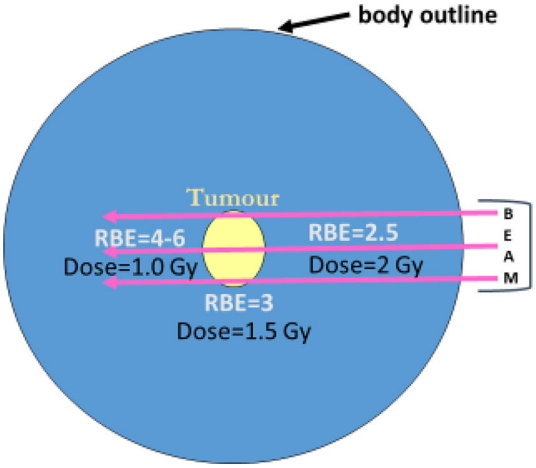

FIGURE 3 | Schematic diagram of external neutron beams passing through a tumour (yellow) with progressive increase in RBE and dose reduction. Prescription of radiation used RBE of 3 at the tumour depth and assumes this to be operative at all other points within a patient, but the RBE is increasing where dose fall-off occurs beyond the tumour target as illustrated.

and that these invaluable data should be part of the essential background required for making progress with other hadrons (protons and ion beam therapy). Ignoring the facts that have emerged may lead to a repetition of disappointing clinical results and eventual reduction of referrals for proton and ion beam therapy. It is vital to understand that most of neutron ionisation occurs from recoil protons, as well as some nuclear fragments, so their radiobiological features, including their RBE values, will be similar to those of a proton beam in the Bragg peak region where the LET and dose increase substantially. This fact has not been sufficiently well-recognised within the proton therapy community until very recently (11, 12), and RBE values in the fast neutron range have been found at the end of spread-out Bragg peaks in the human lung (13). These aspects should be borne in mind when reading the remainder of this review, where it will become apparent that RBE issues cannot be dismissed lightly in any form of particle therapy.

The Historical Case for Neutron Therapy

The medical rationale for fast neutron therapy of cancer was based on initial scientific *in vitro* experimental evidence of more efficient cell killing per unit dose and a reduced dependency on tissue oxygen tension. The history of neutron therapy illustrates the problems that can arise when partial scientific knowledge is used in an attempt to improve the treatment of a complex biological condition such as cancer; it is self-evident that the sterilisation of cancer cells by a radiation technique in an *in vitro* laboratory experiment is more likely to be successful than the elimination of a malignant tumour situated close to essential organs/tissues of the body. For future radiotherapy developments, particularly the use of proton and ion beam therapy, this history is important.

In 1940, Gray et al. (14) had shown that it was possible to achieve the same level of biological effect with a lower dose of neutrons than with γ- or x-rays. This difference was quantified by the RBE. Fast neutron RBE values of 1.5 to 5 were found in a variety of biological systems (bacteria, plants, transplanted animal cancers). The immediate inference was that neutrons would be ideal for cancer therapy, yet the first human treatments in the United States (again in the early 1940s) showed marked toxicity, because the relationship between the exposure dose and RBE had not yet been identified (15). Gray remained sceptical and realised that neutron therapy may not be successful because of the spatial changes in RBE, which would inevitably occur within the human body. He knew that RBE was inversely related to dose, so that dose fall-off with distance along a neutron beam would inevitably be accompanied by higher RBE values in normal tissues beyond any cancer target, as shown in **Figure 3**. His opinion on neutrons had devastating personal consequences for radiobiology and radiotherapy, because he was dismissed from his post as director of radiotherapy physics at the Hammersmith Hospital, although his career was rescued by the philanthropic formation of the Gray laboratory elsewhere in London (16) and is also now remembered by the SI unit of absorbed dose in units of Grays. Gray believed that neutrons were an important tool for research, for the investigation of high LET effects, but should not necessarily be used for treatment. He was eventually proved correct, and the wealth of fast neutron experimental data (much of it performed in the United Kingdom) probably provides the best insights into high LET phenomena, especially that the inverse dose per fraction effect on RBE is especially marked in late-reacting normal tissues when compared with acute-reacting tissues.

Further Experimental Work

Further interest arose because of the discovery that high LET radiations, e.g., fast neutrons, with increased clustering of ionisation events along micrometre distances of their tracks,

are less dependent than are x-rays on the presence of oxygen to produce cell death (oxygen essentially amplifies low-LET ionisations by increasing the yield of reactive free radicals in solution). The previous work of Gray and others had shown that many cancers contained zones of very low oxygen tension, which were considered an important cause of radioresistance. To overcome this problem, high-pressure oxygen (HPO) was used in experimental radiotherapy from the 1960s for several decades. In the United Kingdom, the initial results in animal experimental systems were impressive (17). In clinical practice, HPO had many disadvantages, because patients had to be placed within HPO tanks or chambers, and there was no overall improvement in patient survival, although some tumour types were better controlled (18). An attractive alternative to HPO was the use cyclotrons to accelerate protons—to around 16 to 20 MeV to produce fast neutrons with high LET properties and reduced oxygen dependency for cell killing within cancers. It was argued by the neutron enthusiasts that the use of HPO chambers would be unnecessary if neutron therapy would be used more extensively.

Clinical Research

The research efforts were complicated by there being several generations of technical equipment initially based on static beams, followed later with rotating gantries (19) and finally higher neutron energies in order to match the treatment geometry and depth dose characteristics of clinical megavoltage treatments. This technical evolution occurred at much later times than with photons, so neutron therapy was continually in a catch-up state.

Many developed countries started neutron therapy research programs, often based in single institutions and concentrating on treating rare tumours such as sarcomas. Some encountered severe tissue complications and were discontinued. The usefulness of neutron therapy could not be gauged from the emerging data sets, containing small numbers of patients in each tumour class, so it eventually became necessary to perform randomised studies on more commonly occurring cancers in order to determine the role of fast neutrons in the treatment of cancer.

The UK Medical Research Council Trials

The UK Medical Research Council (with other charitable contributions) funded three important sequential projects to investigate the usefulness of fast neutron therapy (20), from the late 1960s onwards until around 1992. Further work on the radiobiology also continued in parallel.

1. At Hammersmith (University of London), clinical studies were conducted by Dr. Mary Catterall with initial promise using a geometrically limited fixed horizontal beam (21, 22). Despite clear evidence that the neutron RBE was inversely related to dose per fraction in a wide variety of animal tissues, the clinical dose prescriptions used a fixed RBE. There was no 3-D dose computing availability for a more sophisticated approach. Accordingly, the dose plan took no account of the increase in RBE in normal tissues beyond the tumour, where lower doses would inevitably increase the RBE. The treatment schedules used 1.5 Gy three times per week. Promising results were reported for parotid gland and air sinus tumours, and the incidence of complications appeared to be reducing with better dose selection. A randomised trial comparing outcomes with conventional photon-based treatments involved control patients treated with x-rays or cobalt beams at other hospitals without defined protocols so that a wide range of doses, including some that were unsuitable, were used. From that time on, cancer trials were conducted with greater rigor.
2. Arnott and Duncan at Edinburgh Royal Infirmary (University of Edinburgh) used stricter "in-house" randomised trials to compare megavoltage x-rays (with their superior tissue penetration) with relatively poorly penetrating fast neutrons (as in Hammersmith), but for both radiation classes, the beams could be rotated on a gantry. The photon-treated controls were consequently treated with fewer beams per treatment plan, and the neutron treatments contained up to seven fields per plan, thus increasing the integral dose of neutrons. Treatments were supervised by site-specialised cancer experts with good academic supervision. Although in some instances improved local cancer control was achieved, enhanced normal tissue toxicity was also reported. It is interesting to note that the neutron dose per fraction of 0.9 Gy, given five times per week, was lower than that used in Hammersmith, thus inevitably increasing the RBE and its normal tissue consequences.
3. Errington and Warenius at Clatterbridge (University of Liverpool) used an extended fast neutron energy (obtained using 64-MeV protons from a cyclotron) with depth doses equivalent to 5-MeV x-rays in randomised trials, some of which were jointly undertaken with Seattle and Fermilab (USA). The dose per fraction chosen was the same as Hammersmith and treatment delivered 3 days per week to relatively advanced T3 head and neck and pelvic cancers. Compared with the photon treatments, neutron therapy toxicity was not increased, but there was no improvement in tumour control, and rather surprisingly, the metastatic rate appeared to be increased (perhaps due to the intermittent dose fractionation used).

Taken together, all these trials showed that neutrons conferred no clinical advantage, as comprehensively summarised by Duncan (20), which should be consulted for further details and references.

Other Neutron Therapy Studies

In many other countries, relatively low energy neutrons had been tried without recourse to formal trials and with little convincing success, although a small randomised trial reported by Laramore et al. (23) showed benefits for neutrons in the control of unresectable cancers of the parotid gland, which was similar to the findings at Hammersmith. In this trial, it is possible that a higher dose of x-rays with an electron boost in the control arm might have produced the same result. The actual tumour RBE, which was probably higher than that used in the prescription since the adenoid cystic carcinomas used in the trial, was very slow growing, but some tumours may contain a high fatty acid concentration, which could

increase neutron KERMA (24). Relatively superficial air sinus cancers were also thought to be better controlled by neutron therapy, although there was always concern that neutrons were particularly damaging to the underlying brain tissues, where it had been identified previously at Hammersmith that the white matter RBE was around 5 rather than 3, again for reasons already identified above.

Some later neutron therapy research used polyethylene and iron MLCs, which initially started in Seattle (25), and then in Essen and Detroit, where intensity-modulated neutron therapy was introduced (using the MLC), especially for the treatment of prostate cancer (26). However, the inevitable increase in low-dose volume (often referred to in some countries as the low-dose "bath") does raise concerns about integral dose concerns and especially since the Edinburgh group had by 2006 reported a significant increase in radiation-induced sarcomas over a period of 30 years (27), although such a risk could perhaps be discounted in elderly patients. From that time onwards, there has been increasing competition for prostate cancer treatments using brachytherapy, proton therapy, and robotic surgery.

RETROSPECTIVE INSIGHTS

In retrospect, neutron therapy failed to match its original promise for the following physical and radiobiological reasons:

- Routine absorbed dose computations did not include the highly efficient neutron interaction with hydrogen, resulting in higher energy release in hydrogen rich tissues such as brain white matter and fat, which surrounds most important organs and is closely associated with their blood supply.
- Dismissal of the well-established finding of RBE variations in different tissues and its important increase with a falling dose, which mitigates the effect of a reduction in physical dose beyond a cancer.
- The appreciation that RBE also varies with cell proliferation rate, so that slow-growing tumours have higher values. It is the slow-growing stem cells and vascular cells that contribute to the severe normal tissue damage at extended time periods after irradiation.

Some Generic Knowledge

Several generic improvements emerged as a consequence what was found useful in the neutron therapy trials. Nearly all clinical trials in radiotherapy after that time followed the Clatterbridge UK and North American RTOG neutron trials by inclusion of data monitoring committees, as well as rigorous quality assurance (QA) systems for dosimetry, as well as clinical standards. When the detailed QA systems established for neutrons were applied as a result of discussion within the PTCOG (Particle Therapy Co-operative Group), the study coordinated at Loma Linda showed potentially significant discrepancies in some major proton centres and which required correction by up to 7% (28). Furthermore, when the UK Hospital Physicists decided to compare dosimetry standards at all UK radiotherapy centres by using thermoluminescent dosimetry in the same body phantom (29), the Clatterbridge Hospital results were closest to the dosimeter used in the UK National Physical Laboratory. This was a good example of how the discipline of the neutron trials exerted an influence on the conduct of radiotherapy physics in one hospital.

Mathematical Modelling

The early neutron radiobiology was well summarised by Bewley (30) and remains relevant to particle therapy. In 1998, mathematical modelling, which included RBE within biological effective dose (BED) equations, showed that neutrons would only be capable of improving clinical outcomes in the case of the treatment geometry provided by very superficial cancers with little normal tissue coverage (31), exactly the condition for air sinus and parotid tumours. The further extension of BED equations that contain RBE allowances in many radiobiological settings has the potential for guiding clinical practice (32), and the relevant equations are given below and in the **Appendix**. These BED equations used the RBEmax and RBEmin concepts in conjunction with the reference radiation tissue α/β ratio, which are known with greater confidence than the much higher neutron α/β values.

The standard low LET BED equation is

$$\mathrm{BED} = \mathrm{D_L}\left(1 + \frac{d_L}{\left(\frac{\alpha}{\beta}\right)_L}\right), \tag{3}$$

where D symbols refer to total doses and d the dose per fraction given in n treatments (or fractions) with subscripts L and H used to denote high and low LET radiations, respectively, the latter being the reference radiation for RBE estimations.

For high LET radiations, Equation 10 can be modified (31, 33) by inclusion of RBEmax and RBEmin (formal definitions are given in the **Appendix**) where to be

$$\mathrm{BED} = D_H\left(\mathrm{RBEmax} + \frac{\mathrm{RBEmin}^2 d_H}{\left(\frac{\alpha}{\beta}\right)_L}\right) \tag{4}$$

Isoeffect calculations then use the equality:

$$D_L\left(1 + \frac{d_L}{\left(\frac{\alpha}{\beta}\right)_L}\right) = D_H\left(\mathrm{RBEmax} + \frac{\mathrm{RBEmin}^2 d_H}{\left(\frac{\alpha}{\beta}\right)_L}\right) \tag{5}$$

By definition, $D_\mathrm{L} = \mathrm{n_L}.\mathrm{d_L}$, and $D_\mathrm{H} = \mathrm{n_H}.\mathrm{d_H}$, so that any two schedules with the same number of fractions can be either compared or equated for an isoeffect as in Equation 5.

For single doses, Equation 5 is modified to be:

$$d_L\left(1 + \frac{d_L}{\left(\frac{\alpha}{\beta}\right)_L}\right) = d_H\left(\mathrm{RBEmax} + \frac{\mathrm{RBEmin}^2 d_H}{\left(\frac{\alpha}{\beta}\right)_L}\right) \tag{6}$$

Further details on obtaining an RBE at any dose per fraction are given in the **Appendix**.

Important Radiobiological Concepts That Emerged From Fast Neutron Experimental Studies

Radiobiology studies had already shown high neutron RBE values, which varied inversely with dose, reductions in oxygen enhancement ratio (OER), and cell cycle phase dependency, and with greater dose per fraction insensitivity, with similar findings for heavier ions (34). Also, Batterman et al. (35) had shown that human tumour RBE values were related to their volumetric doubling times and which can be related to tumour potential doubling times (**Figure 4**) (36). Extended analysis of the fast neutron experiments at Hammersmith and Clatterbridge continued in more recent times, providing many informative reports and interpreted using the linear-quadratic model of radiation effect as in Carabe-Fernandez et al. (33, 37) and Jones et al. (38), which model the well-recognised inverse dose per fraction and RBE effects (using the RBEmax and RBEmin concepts), in different tissues represented by their characteristic α/β ratios. Acute-reacting tissues, such as oesophageal mucosal reactions, show almost no change in RBE with dose per fraction, but later-reacting tissue effects in skin, lung, and kidney show greater changes in RBE with dose per fraction.

The graphical fits in these articles are informative, as linear-quadratic model theory does predict (**Appendix**) that the RBEmax is inversely related to the α/β ratio (**Figure 5A**), whereas RBEmin is directly proportional to the square root of α/β (**Figure 5B**). By using these relationships, for the most critical low α/β (late-reacting) tissues, the RBE at low dose is highest, but changes to be the lowest RBE at high dose when compared with more rapid proliferating tissues (or tumours) with high α/β ratios that have a "flatter" response, as shown in **Figure 6A**. In these figures, it is important to note that the RBEmax represents the RBE at near-zero dose, forming the intercept of the curves where dose is zero, and that RBEmin is the limiting value at high dose and that always exceeds unity. If RBEmin is not used, the RBE will approach 1 at high dose, whereas in experimental normal tissue systems, RBE asymptotically approaches values of between 1.2 and 1.4 in most instances. However, some data sets do contain a limited number of RBEmin values around 1, which implies little or no increment in β and possible other influences associated with experimental design, biological variation, and the smaller influence of the reference irradiator being low KeV x-rays. RBEmin *in vitro* data can only be obtained from direct estimation of β values; the dose range cannot be as high as *in vivo* studies because of limited surviving colonies in the former.

Figure 6B used lower RBEmax and RBEmin values, iteratively adjusted to match the conventionally used proton RBE of 1.1, for $\alpha/\beta = 10$ Gy [the α/β value of the *in vivo* jejunal crypt assay, which was mostly used to achieve this RBE value in mid-spread out Bragg peak (SOBP) (11)]. By then varying the α/β ratio to represent different tissues/tumours, the dose per fraction effect can be further estimated, although in this case there is no crossing-over of the curves. At 2 Gy per fraction, the curve for $\alpha/\beta = 2$ Gy (normally used of central nervous tissue) provides an RBE estimated of around 1.2, which is very close to that predicted by a different proton model (39).

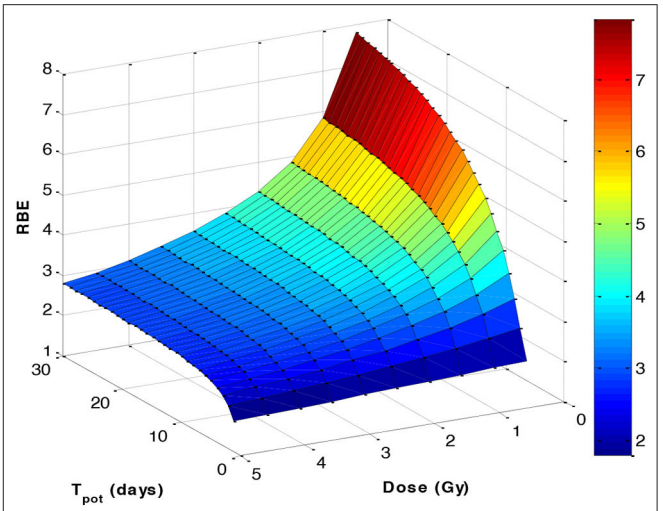

FIGURE 4 | A 3-D plot based on the Batterman data set (35), assuming a 90% cell loss factor to convert the volume doubling time to an estimated potential doubling time (T_{pot}), which is itself inversely related to the α/β ratio by a function $\alpha/\beta = 48.9/T_{pot}$. The RBE was then estimated using the linear-quadratic formulations given in the **Appendix**.

If the overall RBE is controlled by RBEmax and RBEmin and that these parameters are, respectively, inversely and directly related to the reference radiation α/β ratio (details given in **Figure 5** legends and **Appendix**), then a practical clinical RBE cannot be assumed to be only related to RBEmax. Mathematical models that predict RBE from changes in only the α parameter or only from α/β are probably incomplete, because it is necessary to include specific increases in the β parameter with LET, although these are less marked than for the α parameter. Comparisons of models that predict proton RBE values have been made by Paganetti et al. (12) and Warenius et al. (40).

At Clatterbridge Hospital, Warenius and Britten (41) had identified that the respective rank orders of radiosensitivity values for photons and neutrons were different. This is a consequence of the transition of RBE between the limits provided by RBE max and RBEmin (as shown in **Figure 6A**) and other nonlinear effects such as the progressive reduction of RBE increments with increasing intrinsic (photon) radiosensitivity found in cellular experiments (39).

It has also been shown that the LET values produced by the Clatterbridge fast neutrons increases the α-radiosensitivity parameter by a factor of 3.17, but the β parameter increases by $1.59\sqrt{\beta}$ on average (42). The increment in α for the Clatterbridge fast neutron and x-ray comparisons in cell lines are shown in **Figure 7**, where a saturation effect appears to limit the increase in radiosensitivity (39).

Previously, it was widely thought that β did not increase significantly with LET, as evidenced in meticulous experiments

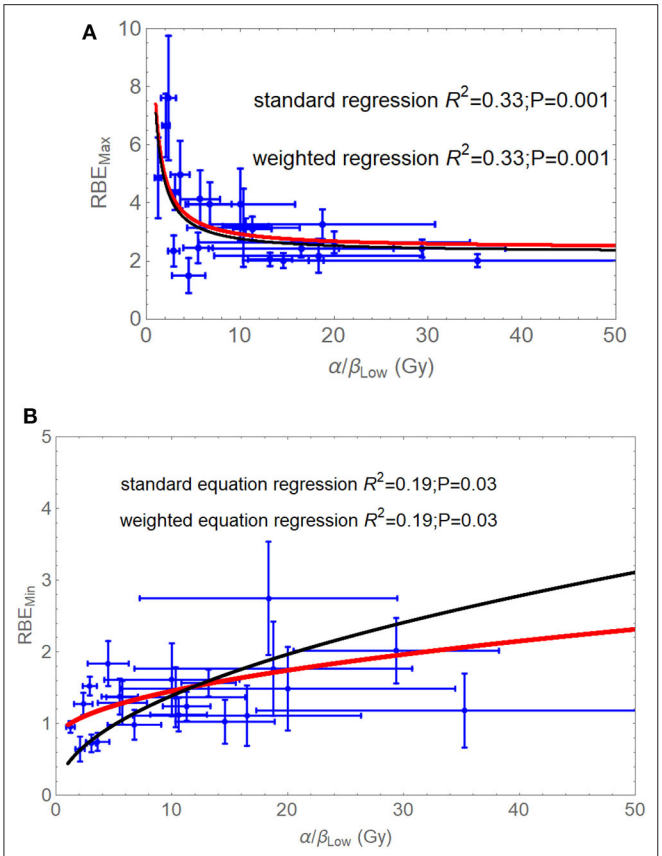

FIGURE 5 | (A,B) Graphical displays of RBE_{max} **(A)** and RBE_{min} **(B)** plotted with respect to the reference low LET α/β ratio, as adapted from Jones et al. (38). Least squares fitting are **(A)** RBEmax = 2.43 + 4.97/$(\alpha/\beta)_L$ (no standard error weighting) and RBEmax = 2.29 + 4.81/$(\alpha/\beta)_L$ (with standard error weighting), **(B)** RBEmin = 0.76 + 0.22$\sqrt{(\alpha/\beta)_L}$ (no standard error weighting), and RBEmin = 0.73 + 0.19$\sqrt{(\alpha/\beta)_L}$ (with standard error weighting). Modified from Jones et al. (38).

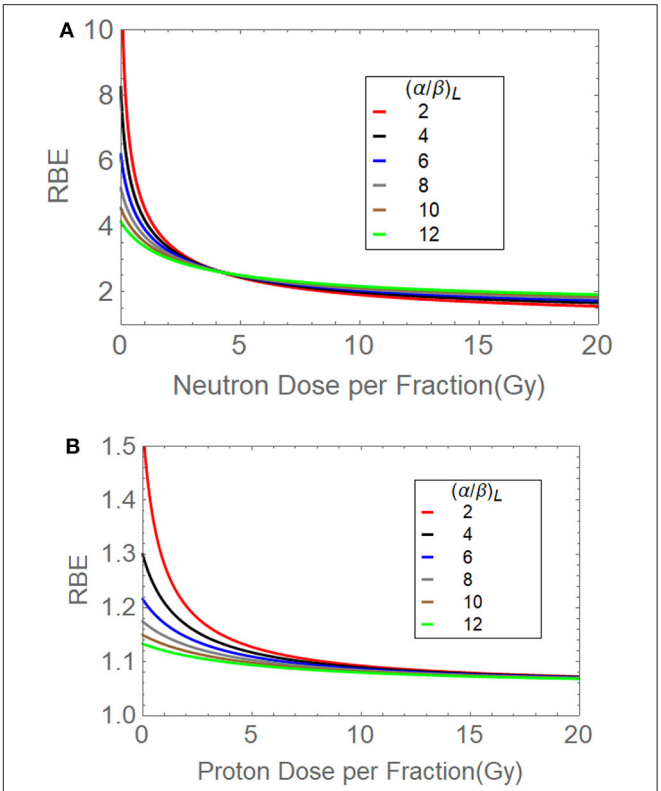

FIGURE 6 | (A,B) The relationships between **(A)** fast neutron dose per fraction and RBE for different α/β ratios, and **(B)** the transformation of the above to provide a near-flat response for α/β of 10 and 12 Gy to simulate proton data by modification of RBEmax and RBEmin. The red curves suggest how brain and spinal cord tissues may behave (α/β = 2 Gy), followed by a gradual change in α/β to faster-growing systems such as many rapidly growing tumour types and acute-reacting normal tissues (α/β = 10 Gy). Modified from Jones et al. (38).

involving only the V-79 cell line by Jones (43), but the Clatterbridge *in vitro* experimental neutron and x-ray data set contained over 20 cell lines, and the increase in β can be seen in **Figures 8**, **9** (39, 42, 44), where the V-79 line is shown as being just above the line that represents no change in the β parameter. Many proton RBE models have used the V-79 cell line without any allowance for an increment in RBE with LET and so could underestimate or even exclude use of RBEmin (12, 39, 40).

Improved BED assessments of not only neutrons but also for other ion beams have included such saturation effects (39, 44).

BORON NEUTRON CAPTURE THERAPY

At present, the only promising development for neutrons is arguably boron neutron capture therapy (BNCT), a complex binary therapy that involves a low-dose exposure to thermal or epithermal neutrons, which are selectively captured by boron-labelled amino acids that avidly enter rapidly growing tumour cells. The reaction creates more intense localised ionisation by generating an α particle and a lithium ion, with tissue ranges of only around 10 μm (about one-cell diameter). The RBE issues within BNCT are further complicated by the dose being dependent on the concentration of the boron-containing compound, which is reflected in a compound biological effectiveness or CBE (45). Some pilot studies have shown promise in highly malignant brain tumours or for recurrent tumours, although in uncontrolled, highly selected patients (46, 47), and the future prospects remain uncertain, although hospital-based accelerators for thermal neutron sources could reduce the inconvenient dependency on a nuclear reactor as a source (48). Further discussion is beyond the scope of this article.

DISCUSSION

The Neutron Aftermath

Following the fast neutron clinical trials, the UK funding authorities decided not to invest in further ambitious radiation projects; and as a result a general decline in UK radiotherapy and radiobiology research followed, although the Clatterbridge cyclotron was successfully adapted for ocular proton therapy.

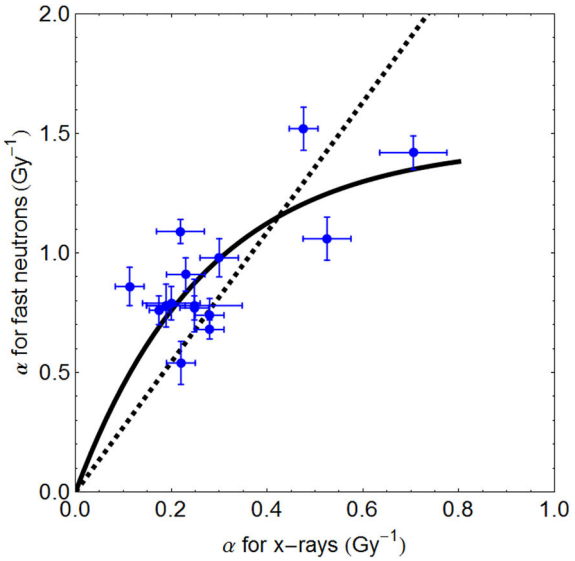

FIGURE 7 | Plots of α radiosensitivity with standard errors for 5-MeV x-rays and 64-MeV neutrons. The fitted curve follow the relationship $\alpha(\text{neutron}) = 5.37/3.68(1-e^{3.68\alpha(-x-ray)})$. The hatched line represents a linear fit, which would inappropriately lead to much higher α_H values.

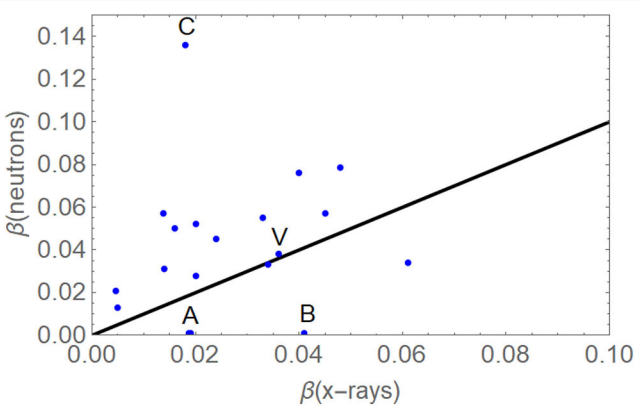

FIGURE 8 | Plots of the β parameter for megavoltage photons and neutrons. Outlying cell lines with β neutrons close to zero (labelled A and B) were excluded because of probable experimental error, and the extremely high value (C) was due to known radiation repair deficiency and was also excluded. The black line will be followed if there is no change in β with increasing LET, but most nonexcluded data points are above that line. The V-79 data point (labelled V) falls just above it. Application of the sign test indicates that the hypothesis that β is the same for neutrons and megavoltage x-rays can be rejected ($p < 0.01$). Adapted from Jones (42), with no error bars for ease of viewing.

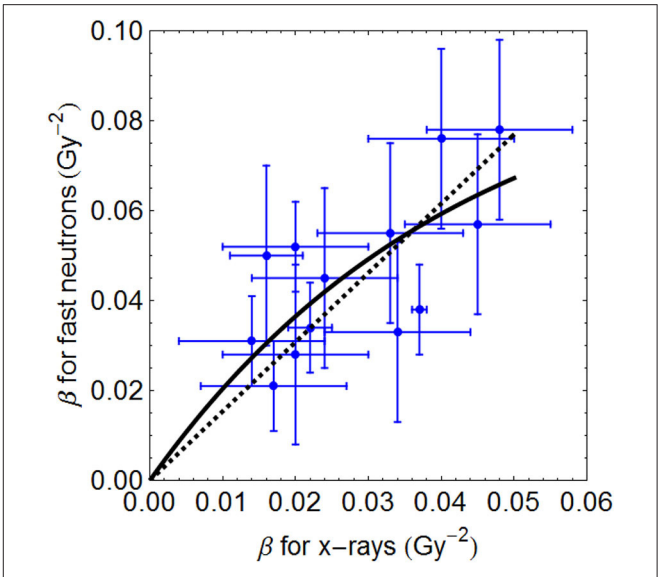

FIGURE 9 | The representative data in **Figure 8**, with error bars and fitted with a linear function and by a saturation curve described by β (neutron) = $2.29/23.57\ (1-e^{-23.57\beta(x-ray)})$. The later fit is preferable because the linear equation will continue to increase beyond acceptable limits.

There emerged a clinical scepticism regarding the use of cyclotrons in radiotherapy and high LET radiations in general. In other countries, more progress was achieved using charged particle therapy (protons or light ions) produced from cyclotrons or the larger synchrotrons. Some of these countries had no prior experience of high-LET radiations in the form of fast neutrons.

In Japan, the government selected proton and carbon ion therapy as a patient-friendly alternative to fast neutrons, but interestingly applied neutron experimental data to link the LET and RBE for treatment prescriptions (49), although not used with a dose-per-fraction effect, and there was effectively no exit dose where further RBE increments could make a significant difference. This approach has been replaced by modifications of the MKM (microdosimetric kinetic model), which originally did not allow for the increments in β with LET (resulting in a high dose RBEmin of 1), but now β effects have been introduced as a consequence of the neutron experience (50). The crossover effects observed in **Figures 4A,B** appear to be consistent with clinical results of reduced side effects with increasing hypofractionation in Japan (51).

A major radiotherapy research question over the next few decades will be whether carbon ions are superior to protons in specific cancers, because of better beam ballistics and dose localisation and/or the apparent greater reduction in the oxygen effect. Suit et al. (52) have pointed out that because even the neutron studies did not show a convincing overall local tumour control improvement, it should not be expected that carbon ions will provide improved efficacy because the oxygen effect dependency is greater for spread-out carbon ion peaks than for fast neutrons (OER ratios of around 1.8–2 compared with 1.6–1.8, respectively).

The process of reoxygenation in tumours during radiotherapy for schedules lasting several weeks may be the reason why hypoxic radioresistance is not especially important with photons and may explain why the control x-ray treatments, as in the Clatterbridge studies, produced results that were at least as good as with neutrons (20). However, the identification of tumours with slow reoxygenation kinetics may yet be important

because use of high LET therapy and dose escalation may then be important.

Improvement of Neutron Bioeffect Prediction

Because fast neutron energies are part of a spectrum, in principle it is possible to predict most of the RBE by considering the recoil proton energies and then applying proton RBE models (12, 39, 40) or more complex predictive models (4, 53). These models vary in terms of the inclusion of biological data and the increase in β with LET, but most appear to give realistic values compared with the incorrect assumption that all protons have an RBE of 1.1, which is an oversimplification even at mid–spread-out Bragg peak (11). Knowledge of neutron RBE continues to be required in medicine and radiation protection and for space travel.

Mixed Neutron and Photon Fields

Research at the Gray Laboratory led by McNally had shown nonlinear effects on cell survival when photon and neutron irradiations were used sequentially, with a short temporal separation, which would not change DNA repair significantly (54). Lower doses of neutrons dominated the effectiveness, but this influence was dependent on the level of surviving fraction. Although Zaider and Rossi (55) proposed a quadrature addition of the β terms, there does not appear to be a satisfactory method for predicting mixed beam effects. The present writer is of the opinion that because the α radiosensitivity will depend on LET in a biphasic way by following the general relationship between LET and RBE, it is suggested that LET-dependent RBE models should be used in such situations, coupled with the neutron LET spectrum. This is a complex problem. German scientists are now exploring mixed field irradiation by use of their local effect model (56). Although neutron beams normally contain γ-rays, measured experimental RBEs will include such mixed field effects.

Neutron Carcinogenesis

The problem of neutron-induced cancers has already been mentioned (27). Further radiobiological details have been reviewed by Trott (57), because neutrons and γ-rays are released from proton and other ion beam interactions in the human body and so can increase with depth along a beam. It is also the case that the RBEmax and RBEmin concepts can be applied to radiation carcinogenesis caused by high LET radiations such as neutrons (58).

Educational Aspects

The history of neutron experimental and clinical studies should be taught to doctors and physicists during their radiotherapy training. This is because the general principles learnt are educationally informing. These topics should be studied in greater detail by those engaged in particle beam therapies. At present, there is a curious lack of emphasis on RBE issues in proton therapy teaching courses, but regulatory bodies should insist on a good background of radiobiological understanding in high LET radiations in order to guide future clinical decision makers. Neutron experimental data sets were not examples of "wasted research," because they have been further analysed 20 to 40 years after their original publication and have some impact on informing radiation modellers of how to improve proton and ion beam therapy. Health policy makers and research funding bodies should also study this overall neutron experience, because it contains many important lessons.

CONCLUSIONS

The following conclusions can be made:

1. It is important that the same fundamental errors that were made with neutrons are not repeated with charged particles. All, rather than some, of the scientific information needs to be included when deciding what may be best to apply in the clinic.
2. As with neutrons, so also with all charged particles, an elevated RBE can be favourable only if the tumour RBE exceeds that of the prescription RBE, but can be a disadvantage when the critical normal tissue RBE exceeds the prescription RBE if accompanied by insufficient normal tissue dose sparing.
3. For any form of radiation therapy, radiobiological testing should be sufficiently comprehensive to identify strengths and weaknesses and include testing in many cell lines and tissues with different radiobiological characteristics and not just a few or one.
4. In retrospect, better radiobiological modelling would have alerted clinicians of at least some of the adverse features and might have prevented the widespread use of fast neutrons, or at least restricted their use to specially defined situations.
5. All new forms of radiotherapy need to be tested in high-quality clinical centres, using the best input from physics, biology, and medicine and use randomised controlled studies wherever possible. These must include rigorous external dosimetry QA and data monitoring committees.
6. The experimental fast neutron database remains important and has implications for proton therapy because neutrons mainly ionise by forming recoil protons.
7. The neutron experimental and clinical experience should be taught to doctors and physicists embarking on careers in radiotherapy and should be studied in greater detail by those engaged in particle beam therapies, as well as health policy decision makers.

AUTHOR CONTRIBUTIONS

The author confirms being the sole contributor of this work and has approved it for publication.

ACKNOWLEDGMENTS

The author was grateful to a large number of scientists and clinicians some of which especially include Roger Dale, Gillies McKenna, John Hopewell, Oliver Scott, Jack Fowler, Mark Hill, Boris Vojnovic, Ken Peach, Claire Timlin, Herman Suit, Peter

O'Neil, Dudley Goodhead, Kevin Prise, Stuart Green, Karen Kirkby, David Colling, Douglas Errington, Andrzej Kacperek, Richard Britten and Hilmar Warenius for stimulating discussions and encouragement. Also for the encouragement provided by the former Cyclotron Trust (UK).

SUPPLEMENTARY MATERIAL

The Supplementary Material for this article can be found online at: https://www.frontiersin.org/articles/10.3389/fonc.2020.01537/full#supplementary-material

REFERENCES

1. Thwaites DI, Tuohy JB. Back to the future: the history and development of the clinical linear accelerator. *Phys Med Biol.* (2006) 51:R343–62. doi: 10.1088/0031-9155/51/13/R20
2. Fowler JF. Chapter 4. Types of radiation and their sources. Medical physics handbooks. In: *Nucelar Particles in Cancer Treatment*. Bristol: Adam Hilger (1981).
3. Dearnaley DP, Jovic G, Syndikus I, Khoo V, Cowan RA, Graham JD, et al. Escalated-dose versus control-dose conformal radiotherapy for prostate cancer: long-term results from the MRC RT01 randomised controlled trial. *Lancet Oncol.* (2014) 15:464–73. doi: 10.1016/S1470-2045(14)70040-3
4. Nutting CM, Morden JP, Harrington KJ, Urbano TG, Bhide SA, Clark C et al. Parotid-sparing intensity modulated versus conventional radiotherapy in head and neck cancer (PARSPORT): a phase 3 multicentre randomised controlled trial. *Lancet Oncol.* (2011) 12:127–36 doi: 10.1016/S1470-2045(10)70290-4
5. Hussein M,Heijmen BJM, Verellen D Nisbet A. Automation in intensity modulated radiotherapy treatment planning-a review of recent innovations. *Br J Radiol.* (2018) 91:20180270. doi: 10.1259/bjr.20180270
6. Yang I, Udawatta M, Prashant GN, Lagman C, Bloch O, Jensen R, et al. Stereotactic radiosurgery for neurosurgical patients: a historical review and current perspectives. *World Neurosurg.* (2019) 122:522–31. doi: 10.1016/j.wneu.2018.10.193
7. Jones B, Rosenberg I. Particle therapy cooperative oncology group (PTCOG40), insitute curie (2004). *Bri J Radiol.* (2005) 78:99–102. doi: 10.1259/bjr/18664944
8. *Particle Therapy Co-Operative Group*. Available online at: https://www.ptcog.ch/index.php/facilities-in-operation
9. Hill MA. The variation in biological effectiveness of X-rays and gamma rays with energy. *Radiat Prot Dosimetry.* (2004) 112:471–81. doi: 10.1093/rpd/nch091
10. Awschalom M, Rosenberg I Mravca A. Kermas for various substances averaged over the energy spectra of fast neutron therapy beams: a study in uncertainties. *Med Phys.* (1983) 10:395–409. doi: 10.1118/1.595390
11. Jones B. Why RBE must be a variable and not a constant in proton therapy. *Brit J Radiol.* (2016) 89:20160116. doi: 10.1259/bjr.20160116
12. Paganetti H, Blakely E, Carabe-Fernandez A, Carlson DJ, Das IJ et al. Report of the AAPM TG-256 on the relative biological effectiveness of proton beams in radiation therapy. *Med Phys.* (2019) 46:e53–78. doi: 10.1002/mp.13390
13. Underwood TSA, Grassberger C, Bass R, MacDonald SM, Meyersohn NM et al. Asymptomatic late-phase radiographic changes among chest-wall patients are associated with a proton RBE exceeding 1.1. *Int J Radiat Oncol Biol Phys.* (2018) 101:809–19. doi: 10.1016/j.ijrobp.2018.03.037
14. Gray LH, Mottram JC, Read J. Some experiments upon the biological effects of fast neutrons. *Br J Radiol.* (1940) 13:371–88. doi: 10.1259/0007-1285-13-155-371
15. Wilson RR. Radiological use of fast protons. *Radiology.* (1946) 47:487–91. doi: 10.1148/47.5.487
16. Jones B Hendry J. Jack Fowler and Oliver Scott. *The British Journal of Radiology*. (2017) 90:20160904. doi: 10.1259/bjr.20160904.o
17. Gray LH, Conger AD, Ebert M, Hornsey S, Scott OCA. The concentration of oxygen dissolved in tissues at the time of irradiation as a factor in radiotherapy. *Brit J Radiology*. (1953) 26:638–48. doi: 10.1259/0007-1285-26-312-638
18. Henk JM, Kunkler PB, Smith CW. Radiotherapy and hyperbaric oxygen in head and neck cancer. Final report of first controlled clinical trial. *Lancet.* (1977) 2:101–3. doi: 10.1016/S0140-6736(77)90116-7
19. Bonnett DE, Blake SW, Shaw JE, Bewley DK. The Clatterbridge high-energy neutron therapy facility: specification and performance. *Br J Radiol.* (1988) 61:38–46. doi: 10.1259/0007-1285-61-721-38
20. Duncan W. An evaluation of the results of neutron therapy trials. *Acta Oncol.* (1994) 33:299–306. doi: 10.3109/02841869409098421
21. Catteral M, Bewley DK. *Fast Neutrons in the Treatment of Cancer*. London: Academic press (1979).
22. Catterall M. The assessment of the results of neutron therapy. *Int J Radiat Oncol Biol Phys.* (1982) 8:1573–80. doi: 10.1016/0360-3016(82)90619-8
23. Laramore GE, Krall JM, Griffin TW, Duncan W, Richter MP, Saroja KR, et al. Neutron versus photon irradiation for un-resectable salivary gland tumors: final report of an RTOG-MRC randomized clinical trial. *Int J Radiat Oncol Biol Phys.* (1993) 27:235–40. doi: 10.1016/0360-3016(93)90233-L
24. Jiang YP, Tang YL, Wang SS, Wu JS, Zhang M, Pang X, et al. PRRX1-induced epithelial-to-mesenchymal transition in salivary adenoid cystic carcinoma activates the metabolic reprogramming of free fatty acids to promote invasion and metastasis. *Cell Prolif.* (2020) 53:e12705. doi: 10.1111/cpr.12705
25. Brahme A, Eenmaa J, Lindbäck S, Montelius A, Wootton P. Neutron beam characteristics from 50 MeV protons on beryllium using a continuously variable multi-leaf collimator. *Radiother Oncol.* (1983) 1:65–76. doi: 10.1016/S0167-8140(83)80008-5
26. Snyder M, Joiner MC, Konski A, Bossenberger T, Burmeister J. Dose escalation in prostate cancer using intensity modulated neutron radiotherapy. *Radiother Oncol.* (2011) 99:201–6. doi: 10.1016/j.radonc.2011.05.019
27. MacDougall RH, Kerr GR, Duncan W. Incidence of sarcoma in patients treated with fast neutrons. *Int J Radiat Oncol Biol Phys.* (2006) 66:842–4. doi: 10.1016/j.ijrobp.2006.05.062
28. Vatnitsky S, Siebers J, Miller D, Moyers M, Schaefer M, Jones D, et al. Proton dosimetry intercomparison. *Radiother Oncol.* (1996) 41:169–77. doi: 10.1016/S0167-8140(96)01800-2
29. Thwaites DI, Williams JR, Aird EG, Klevenhagen SC, Williams PC. A dosimetric intercomparison of megavoltage photon beams in UK radiotherapy centres. *Phys Med Biol.* (1992) 37:445–61. doi: 10.1088/0031-9155/37/2/011
30. Bewley DK. *The Physics and Radiobiology of Fast Neutron Beams*. Bristol UK: Institute of Physics Publishing. (1989).
31. Dale RG, Jones B. The assessment of RBE effects using the concept of biologically effective dose. *Int J Radiat Oncol Biol.* (1998) 43:639–45. doi: 10.1016/S0360-3016(98)00364-2
32. Jones B, Dale RG. The evolution of practical radiobiological modelling. *Br J Radiol.* (2018) 20:20180097. doi: 10.1259/bjr.20180097
33. Carabe-Fernandez A, Dale RG, Jones B. The incorporation of the concept of minimum RBE (RBEmin) into the linear-quadratic model and the potential for improved radiobiological analysis of high-LET treatments. *Int J Radia Biol.* (2007) 83:27–39. doi: 10.1080/09553000601087176
34. Skarsgard LD. Radiobiology with heavy charged particles: a historical review. *Phys Med.* (1998) 14 (Suppl) 1:1–19.
35. Battermann JJ, Breur K, Hart GA, van Peperzeel HA. Observations on pulmonary metastases in patients after single doses and multiple fractions of fast neutrons and cobalt-60 gamma rays. *Eur J Cancer.* (1981) 17:539–48. doi: 10.1016/0014-2964(81)90056-6
36. Jones B. Chapter 2. The essential Radiobiology Background. In: *Practical Radiobiology for Proton Therapy Planning*. Bristol: Institute of Physics Publishing. (2017). p. 29–31. doi: 10.1088/978-0-7503-1338-4

37. Carabe-Fernandez A, Dale RG, Hopewell JW, Jones B, Paganetti H. Fractionation effects in particle radiotherapy: implications for hypo-fractionation regimes. *Phys Med Biol.* (2010) 55:5685–700. doi: 10.1088/0031-9155/55/19/005
38. Jones B, Underwood TC, Carabe-Fernandez A, Dale RG. Further analysis of fast neutron relative biological effects and implications for charged particle therapy. *Br J Radiol.* (2011) 84:S11–8. doi: 10.1259/bjr/67509851
39. Jones B. Towards achieving the full clinical potential of proton therapy by inclusion of LET and RBE models. *Cancers.* (2015) 7:460–80. doi: 10.3390/cancers7010460
40. Warenius HM, Britten RA, Browning PG, Morton IE, Peacock JH. Identification of human in vitro cell lines with greater intrinsic cellular radiosensitivity to 62.5 MeV (p–>Be+) neutrons than 4 MeV photons. *Int J Radiat Oncol Biol Phys.* (1994) 28:913–20 doi: 10.1016/0360-3016(94)90112-0
41. Warenius HM, Britten RA. *In vitro* studies of intrinsic cellular radiosensitivity following 4 MeV photons or 62.5 MeV (p–>Be+) neutrons. Potential implications for high LET therapy. *Acta Oncol.* (1994) 33:241–9. doi: 10.3109/02841869409098414
42. Jones B. The apparent increase in the β-parameter of the linear quadratic model with increased linear energy transfer during particle irradiation. *Brit J Radiology.* (2010) 83:433–6. doi: 10.1259/bjr/68792966
43. Jones B. A simpler energy transfer efficiency model to predict relative biological effect (RBE) for protons and heavier ions. *Front Oncol.* (2015) 5:184. doi: 10.3389/fonc.2015.00184
44. Chapman JD, Blakely EA, Smith KC, Urtasun RC. Radiobiological characterization of the inactivating events produced in mammalian cells by helium and heavy ions. *Int J Radiat Oncol Biol Phys.* (1977) 3:97–102 doi: 10.1016/0360-3016(77)90234-6
45. Hopewell JW, Morris GM, Schwint A, Coderre JA. The radiobiological principles of boron neutron capture therapy: a critical review. *Appl Radiat Isot.* (2011) 69:1756–9. doi: 10.1016/j.apradiso.2011.04.019
46. Kageji T, Nagahiro S, Mizobuchi Y, Matsuzaki K, Nakagawa Y, Kumada H. Boron neutron capture therapy (BNCT) for newly-diagnosed glioblastoma: comparison of clinical results obtained with BNCT and conventional treatment. *J Med Invest.* (2014) 61:254–63. doi: 10.2152/jmi.61.254
47. Lim D, Quah DS, Leech M, Marignol L. Clinical potential of boron neutron capture therapy for locally recurrent inoperable previously irradiated head and neck cancer. *Appl Radiat Isot.* (2015) 106:237–41. doi: 10.1016/j.apradiso.2015.07.044
48. Barth RF, Grecula JC. Boron neutron capture therapy at the crossroads - Where do we go from here? *Appl Radiat Isot.* (2020) 160:109029. doi: 10.1016/j.apradiso.2019.109029
49. Kanai T, Furusawa Y, Fukutsu K, Itsukaichi H, Eguchi-Kasai K, Ohara H. Irradiation of mixed beam and design of spread-out Bragg peak for heavy-ion radiotherapy. *Radiation Research.* (1997) 147:78–85. doi: 10.2307/3579446
50. Chen Y, Li J, Li C, Qiu R, Wu Z. A modified microdosimetric kinetic model for relative biological effectiveness calculation. *Phys Med Biol.* (2017) 63:015008. doi: 10.1088/1361-6560/aa9a68
51. Kamada T, Tsujii H, Blakely EA, Debus J, De Neve W, Durante M, et al. Carbon ion radiotherapy in Japan: an assessment of 20 years of clinical experience. *Lancet Oncol.* (2015) 16:e93–100. doi: 10.1016/S1470-2045(14)70412-7
52. Suit H, DeLaney T, Goldberg S, Paganetti H, Clasie B, Gerweck L et al. Proton vs carbon ion beams in the definitive radiation treatment of cancer patients. *Radiother Oncol.* (2010) 95:3–22. doi: 10.1016/j.radonc.2010.01.015
53. Rørvik E, Fjæra LF, Dahle TJ, Dale JE, Engeseth GM, Stokkevåg CH, et al. Exploration and application of phenomenological RBE models for proton therapy.Phys Med Biol. (2018). 63:185013. doi: 10.1088/1361-6560/aad9db
54. McNally NJ, de Ronde J, Hinchliffe M. The effect of sequential irradiation with X-rays and fast neutrons on the survival of V79 Chinese hamster cells. *Int J Radiat Biol Relat Stud Phys Chem Med.* (1984) 45:301–10. doi: 10.1080/09553008414550441
55. Zaider M, Rossi HH. The synergistic effects of different radiations. *Radiat Res.* (1980) 83:732–9. doi: 10.2307/3575352
56. Pfuhl T Friedrich T, Scholz M. Prediction of cell survival after exposure to mixed radiation fuields with the local effect model. *Radiat Res.* (2020) 193:130–42. doi: 10.1667/RR15456.1
57. Trott KR. Special radiobiological features of second cancer risk after particle radiotherapy. *Phys Med.* (2017) 42:221–7. doi: 10.1016/j.ejmp.2017.05.002
58. Jones B. Modelling carcinogenesis after radiotherapy using poisson statistics: implications for IMRT, protons and ions. *J. Radiol. Prot.* (2009) 29:A143–57. doi: 10.1088/0952-4746/29/2A/S10

Conflict of Interest: The author declares that the research was conducted in the absence of any commercial or financial relationships that could be construed as a potential conflict of interest.

Copyright © 2020 Jones. This is an open-access article distributed under the terms of the Creative Commons Attribution License (CC BY). The use, distribution or reproduction in other forums is permitted, provided the original author(s) and the copyright owner(s) are credited and that the original publication in this journal is cited, in accordance with accepted academic practice. No use, distribution or reproduction is permitted which does not comply with these terms.

frontiers in Oncology

ORIGINAL RESEARCH
published: 16 September 2020
doi: 10.3389/fonc.2020.01368

Particle Beam Radiation Therapy for Skull Base Sarcomas

Jing Yang[1,2], Weixu Hu[1,2], Xiyin Guan[1,2], Jiyi Hu[1,2], Jing Gao[1,2], Xianxin Qiu[1,2], Qingting Huang[1,2], Wenna Zhang[1,2], Lin Kong[1,2,3] and Jiade J. Lu[1,2]**

[1] Department of Radiation Oncology, Shanghai Proton and Heavy Ion Center, Shanghai, China, [2] Shanghai Engineering Research Center of Proton and Heavy Ion Radiation Therapy, Shanghai, China, [3] Department of Radiation Oncology, Shanghai Proton and Heavy Ion Center, Fudan University Shanghai Cancer Hospital, Shanghai, China

Background: To report the clinical experience of carbon-ion and proton radiation therapy for skull base sarcomas.

Methods: An analysis of the retrospective data registry from the Shanghai Proton and Heavy Ion Center for patients with skull base sarcomas was conducted. The 1-/2-year local relapse-free, distant metastasis-free, progression-free, and overall survival (LRFS, DMFS, PFS, OS) rates as well as associated prognostic indicators were analyzed. Radiotherapy-induced acute and late toxicities were summarized.

Results: Between 7/2014 and 5/2019, 62 patients with skull base sarcomas of various subtypes received carbon-ion radiation therapy (53), proton radiation therapy (5), or proton radiation therapy + carbon-ion boost (4). With a median follow-up of 20.4 (range 2.73–91.67) months, the 1-/2-year OS, LRFS, DMFS, and PFS rates were 91.2%/80.2%, 89.2%/80.2%, 86.0%/81.1%, and 75.8%/62.9%, respectively. Grade 3 mucositis and grade 4 hemorrhage were observed in 1 patient for each. Only grade 1 and grade 2 toxicities were observed except for the same patient with grade 4 acute toxicity died of severe hemorrhage (grade 5). Multivariate analyses revealed the lack of prior RT was an independent favorable prognostic factor for OS, PFS, and LRFS, age under 40 was associated with improved OS, early T-disease (T1/2) showed a significant association with better PFS.

Conclusion: With few observed acute and late toxicities, particle beam radiation therapy provided effective tumor control and overall survival for patients with skull base sarcomas.

Keywords: proton beam radiation therapy, carbon-ion beam radiation therapy, sarcoma, skull base, charged particle radiation therapy

OPEN ACCESS

Edited by:
Daniel Michael Trifiletti, Mayo Clinic Florida, United States

Reviewed by:
Chong Zhao, Sun Yat-sen University Cancer Center (SYSUCC), China
Young Kwok, University of Maryland Medical Center, United States

***Correspondence:**
Lin Kong
lin.kong@sphic.org.cn
Jiade J. Lu
jiade.lu@sphic.org.cn

Specialty section:
This article was submitted to Radiation Oncology, a section of the journal Frontiers in Oncology

Received: *10 May 2020*
Accepted: *29 June 2020*
Published: *16 September 2020*

Citation:
Yang J, Hu W, Guan X, Hu J, Gao J, Qiu X, Huang Q, Zhang W, Kong L and Lu JJ (2020) Particle Beam Radiation Therapy for Skull Base Sarcomas. Front. Oncol. 10:1368. doi: 10.3389/fonc.2020.01368

INTRODUCTION

Bone and soft-tissue sarcomas of the base of the skull (SBS) are rare and account for < 1% of all head and neck malignancies (1–5). Surgery is the treatment of choice for SBS regardless of the histology subtypes. However, *en bloc* resection with sufficient surgical margin of skull base tumors is universally challenging due to the complexity of the anatomy. Although adjuvant radiation is commonly recommended, both the anatomical complexity, and radioresistant nature of most histology subtypes of SBS negated the efficacy of photon-based radiation, including the more conformal intensity-modulated radiotherapy (IMRT) technology. As such, despite aggressive multidisciplinary approaches, the prognosis of patients with SBS is poor as compared with patients

with sarcomas in other anatomical regions (6, 7). For SBS patients with unresectable or inoperable disease, prognosis is usually dismal after radiotherapy (8–12).

Accelerated charged particle (e.g., protons, helium, and carbon ion) beams deposit relatively low energy in the path of traveling in the body but distribute most dose just before they stop at the Bragg peak. Such physical feature of particle beams makes it possible to deliver high-dose radiation to the tumor while limiting the dose to the organs at risk (OARs) close to the tumor. Also, heavy-ion (such as carbon ion) beams have higher linear energy transfer and greater relative biological effectiveness (RBE), which range between 2 and 5, depending on the beam energy, tissue and cell types, and fraction dose as compared with photon/proton (13, 14). Both features are critical for the treatment of radioresistant tumors that occur near-critical or sensitive OARs such as SBS. However, evidence supporting the use of particle beam radiation therapy (PBRT) for the management of SBS is scant. This paper reports the clinical results, in terms of disease control, survival, and treatment-associated adverse effects, of a relatively large group of SBS patients treated with PBRT at the Shanghai Proton and Heavy Ion Center (SPHIC) over the past 5 years.

METHODS

This is a retrospective study and was approved by the Institutional Review Board of SPHIC.

Patient Population and Pretreatment Workups

Due to the significant difference of the biological behavior as compared with other histological subtypes of SBS, patients with chordoma of the skull base or cervical spine were not included in this analysis. After this exclusion, a total of 62 consecutive and non-selected patients with skull base bone and soft-tissue sarcoma who received PBRT with definitive intention at the SPHIC between July 2014, when the first SBS patient was treated at SPHIC, and May 2019 were included in this retrospective analysis.

All patients were evaluated according to the standardized pre-radiation workups, including a complete history, and physical examination, imaging studies (contrast-enhanced MRI preferred, but CT allowed if MRI is contraindicated) of the head and neck region, routing lab tests (complete blood count, serum electrolytes, and renal/hepatic function tests), fluorodeoxyglucose positron emission tomography/CT (or thoracic/abdominal CT and bone scan), and EKG. All patients were staged according to the American Joint Committee on Cancer, seventh edition, tumor–nodes–metastases staging system regardless of the time of diagnosis, as differentiation (grades) were not available to some patients diagnosed after January 2018.

Particle Beam Radiation Therapy

All patients were registered and immobilized using AlphaCradle® and customized thermoplastic masks in the supine position. CT scans for PBRT planning were taken at 1.5-mm slice thickness without contrast from the vertex to the inferior margin of clavicular heads. The fusion of MRI taken in treatment position with immobilization mask and planning CT was applied for all patients before target volume delineation.

The gross tumor volume (GTV) was defined as the gross tumor visualized on imaging studies or clinical examination. GTV with a 1–3-mm expansion was treated to the prescribed dose to the tumor. CTV for gross and subclinical disease included an area with risk for subclinical disease as well as the pretreatment tumor bed for patients who received surgery and/or chemotherapy before PBRT. A maximum of a 5-mm margin was typically added to the CTV for the planning target volume (PTV) to mitigate uncertainty about dose distribution and potential setup errors.

PBRT (both proton and carbon-ion therapies [CIRT]) were delivered with pencil beam scanning (PBS) technology, typically consisted of beams from two to three directions. PBRT planning was performed using the Syngo® treatment planning system (version VC11 and 13) (Siemens, Erlangen, Germany). Individual factors such as patient positioning reproducibility and/or beam angles were chosen for optimal dosimetry. At SPHIC, only multi-field optimization was used for planning of PBRT using PBS technology for head and neck cancer patients. A typical treatment plan is displayed in **Figure 1**. The range uncertainty of our IONTRIS particle treatment system is ± 3.5% but could be modified according to the dose constrains of adjacent OARs. Setup accuracy was confirmed daily with orthogonal X-ray using bony landmarks as reference.

Doses of PBRT were measured by Gy (RBE) to account for the RBE differences as compared with photon-based RT. The dose constraints of the OARs were based on the TD5/5 described by Emami et al. (15) except for the optic nerves ($D_{20} < 30$ Gy [RBE]), brain stem ($D_{max} < 45$ Gy [RBE]), spinal cord ($D_{max} < 30$ Gy [RBE]), and temporal lobes ($V_{40} < 7.66$ cc; $V_{50} < 4.66$ cc), which were set using the previous experience from the National Institute of Radiation and Quantum Science of Japan (16). For patients who received salvage re-irradiation, the previous RT plans were obtained, and the doses to the OARs were identified. Recovery from the previous radiation therapy dose was set at 70% regardless of the latent time between the two courses of RT (17).

Systemic Therapy

Chemotherapy and targeted therapy were administered at the discretion of the referring medical oncologists. Due to the substantial differences in the biological behaviors of different histologic subtypes of SBS, various regimens and schedules of systemic therapy were used. However, no patient with chondrosarcoma received systemic therapy. Concurrent systemic therapy was allowed during PBRT.

Follow-Up and Toxicity Evaluation

Patients were evaluated weekly during PBRT for acute toxicities, response to treatment, and the potential need for replanning for PBRT due to substantial anatomical alteration. Weekly verification CT scans were typically performed after the second week of PBRT to assess any changes in anatomy. After the completion of PBRT, all patients were required to be followed up based on the standardized institutional follow-up protocol.

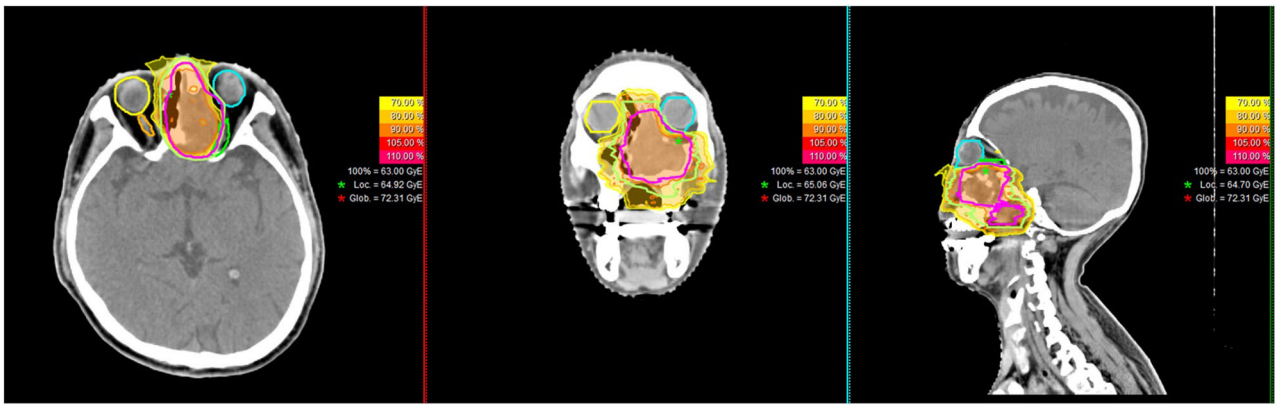

FIGURE 1 | A typical treatment plan of a patient with soft-tissue sarcoma of the skull base.

The first follow-up was set at 4 weeks post-treatment; then, patients were examined every 3 months for the first 2 years, every 6 months up to the fifth year, then annually after that. Non-local or domestic patients unable to follow up in person were followed locally, and results were communicated. The Common Terminology Criteria for Adverse Events (CTC.AE) version 4.03 was used to grade acute (from the start to up to 3 months after the end of PBRT) as well as late adverse effects that occur any time after 3 months after PBRT until last follow-up for this group of patients.

Statistics

The progression-free survival (PFS), locoregional relapse-free survival (LRFS), and distant metastasis-free survival (DMFS) rates were calculated from the start of PBRT, and the overall survival (OS) rates were from the diagnosis using the Kaplan–Meier method. Univariate and multivariate analyses on survivals were performed using the Kaplan–Meier method (with log-rank test) and Cox proportional hazards model. $P < 0.05$ were considered statistically significant. All statistical analyses were performed using SPSS (version 18.0).

RESULTS

Study Population

The diagnosis of all 62 patients with skull base bone or soft-tissue sarcomas (chordoma excluded) were confirmed histologically. No patient presented with distant metastasis at diagnosis. Twenty-eight (18) patients presented with soft-tissue sarcoma, 28 presented with chondrosarcomas, and 6 with osteosarcomas. Thirty-three patients were diagnosed with T3/4 disease and accounted for 53.3% of the cohort. Only 1 patient presented with N1 disease. Seventeen cases had previous photon-based radiation therapy and received salvage CIRT. Among these 17 cases, 12 patients suffered radiation-induced second primary sarcomas. The characteristics of patients and their disease are detailed in **Table 1**.

Particle Beam Radiation Therapy

All patients received PBRT according to the planned schedule. No patients had an unplanned treatment break. Four patients (three with chondrosarcoma and one with rhabdomyosarcoma) treated at the beginning of our clinical services received proton therapy followed by a CIRT boost. Five patients with chondrosarcoma accrued to our phase II randomized trial (proton vs. carbon ion for chondrosarcoma) received intensity-modulated proton therapy only to 64–70 Gy (RBE)/32–35 Fx depending on the dose constraints of the OARs. Fifty-three patients received intensity-modulated CIRT regimens using our dose escalation [54–73.5 Gy [RBE]/18–23 Fxn], randomized trials [70 Gy [RBE] in 20 fractions for chondrosarcomas only], or standard institutional protocol [CIRT to 63 Gy [RBE]/18 fractions to 70 Gy [RBE]/20 fractions depending on the pathology types, tumor volumes, and dose constrains of the OARs].

Disease Control and Patients' Survival

All patients were followed up according to the planned schedule, and the median follow-up time was 20.4 (range 2.73–91.67) months. Eleven patients had deceased. Eleven and 10 events of locoregional recurrence and distant metastasis had occurred, which are detailed later. The 1/2-year overall survival (OS), LRFS, DMFS, and PFS rates for the entire cohort were 91.2/80.2, 89.2/80.2, 86.0/81.1, and 75.8/62.9%, respectively (**Figure 2**).

RT-Naïve Patients

Among the 45 RT-naïve patients in this cohort, 5 deceased at the time of this analysis due to distant metastasis (4 cases) or local recurrence (1 case). Locoregional or distant recurrences occurred in 2 and 6 patients, respectively. One additional patient experienced both local and distant recurrence. The 1/2-year OS, LRFS, DMFS, and PFS rates were 95.3/91.8, 97.6/91.6, 88.4/82.6, and 86.1/74.6%, respectively (**Figure 3**).

Re-irradiation Patients

Seventeen patients received re-irradiation using CIRT only. Six of the 17 patients deceased due to local recurrence (5 cases) or massive hemorrhage (1 case). Locoregional or distant recurrences

TABLE 1 | Characteristics of the 62 patients, their disease, and treatments.

Characteristic	No.	%
Sex		
Male	37	59.7
Female	25	40.3
Age (years)		
Median	38	
Range	14–71	
Histology		
Chondrosarcoma	28	45.2
Rhabdomyosarcoma	8	12.9
Spindle cell sarcoma	6	9.7
Osteosarcoma	6	9.7
Pleomorphic sarcoma	3	4.8
Others 1–2 of each	11	17.7
T-classification		
1	28	45.2
2	1	1.6
3	5	8.1
4	28	45.2
N-classification		
0	61	98.4
1	1	1.6
2	0	0.0
3	0	0.0
Re-irradiation		
Yes	17	27.4
No	45	72.6
Second primary		
Yes	12	19.4
No	50	80.6
Surgery		
R0 + R1	15	24.2
R2 + biopsy + no surgery	47	75.8
Chemotherapy		
Yes	17	27.4
No	45	72.6
PBRT types		
PRT	5	8.1
CIRT	53	85.5
PRT + CIRT	4	6.5
GTV (cm^3)		
Median	47.45	
Range	0–1003.97	

PRT, proton radiotherapy; CIRT, carbon-ion radiotherapy.

occurred in 6 and 1 patients, respectively. Two additional patients had both local and distant recurrence. The 1/2-year OS, LRFS, DMFS, and PFS rates were 68.1/51.1, 63.6/43.6, 79.5/79.5, and 44.4/23.7%, respectively (**Figure 3**).

Adverse Effects

Grade 1/2 oral mucositis and dermatitis of radiation area were the most commonly observed acute adverse effects (17.7/6.5 and 17.7/1.6%, respectively). Grade 3 mucositis was observed in only 1 patient. Another patient with previous radical radiotherapy experienced grade 4 hemorrhage during the treatment and immediately received embolization of the bleeding artery then completed the planned CIRT for radiation-induced second primary pleomorphic sarcoma. The same patient died from hemorrhage (grade 5) at 3.4 months after the completion of PBRT. No other $\geqq$ grade 3 acute radiation-induced toxicity (**Tables 2**, **3**).

Prognostic Factors

Univariate analyses (UVA), including sex, age, status of prior RT (RT-naïve vs. re-RT), pathology (non-chondrosarcoma vs. chondrosarcoma), T-category, surgery status, volume of GTV, PBRT type, and total dose, were compared by log-rank test to demonstrate the differences of the survival probabilities of OS, PFS, LRFS, and DMFS, respectively. The results of UVA are detailed in **Table 4**.

All the factors of UVA were performed in multivariate analyses (MVA) using Cox regression for OS, PFS, and LRFS. Lack of prior RT (i.e., RT-naïve) was statistically associated with robust OS, PFS, and LRFS ($p = 0.020$, 0.010, and < 0.001, respectively) advantages over re-irradiation, with the hazard ratios of 4.66 (1.268–17.120), 3.416 (1.347–8.664), and 11.990 (3.152–45.610), respectively, making it an independent prognostic factor for OS, PFS, and LRFS. Additionally, age under 40 years was associated with improved OS ($p = 0.001$). Early T-disease (T1/2) showed a significant association with better PFS ($p = 0.024$).

DISCUSSION

Bone and soft-tissue SBS are rare. No randomized evidence has validated the optimal management of SBS. The anatomic constraints from adjacent critical OARs pose challenges to both surgical and photon radiation-based approaches. Also, most subtypes of SBS are relatively resistant to photon-based radiotherapy. In theory, disease control would be improved with escalation of radiation dose. Also, the prevailing use of IMRT, which allows for improved dose distributions, may benefit the therapeutic ratio for malignancies of the base of the skull (19–21). Nevertheless, it is debatable whether such improvement in conformality actually translates into improved outcomes for SBS: with conventional radiation, local control rates have been commonly estimated between 50 and 60% (3 years), with or without surgery, highlighting the difficulty of achieving local disease control with radiation alone (7, 22).

SBS seems to be an ideal indication to be managed by PBRT, considering both physical, and biological advantages. Minimal exit dose (after the Bragg's peak) and substantially reduced penumbra over photon techniques, including IMRT, provides sharper dose gradients between target volume(s) and

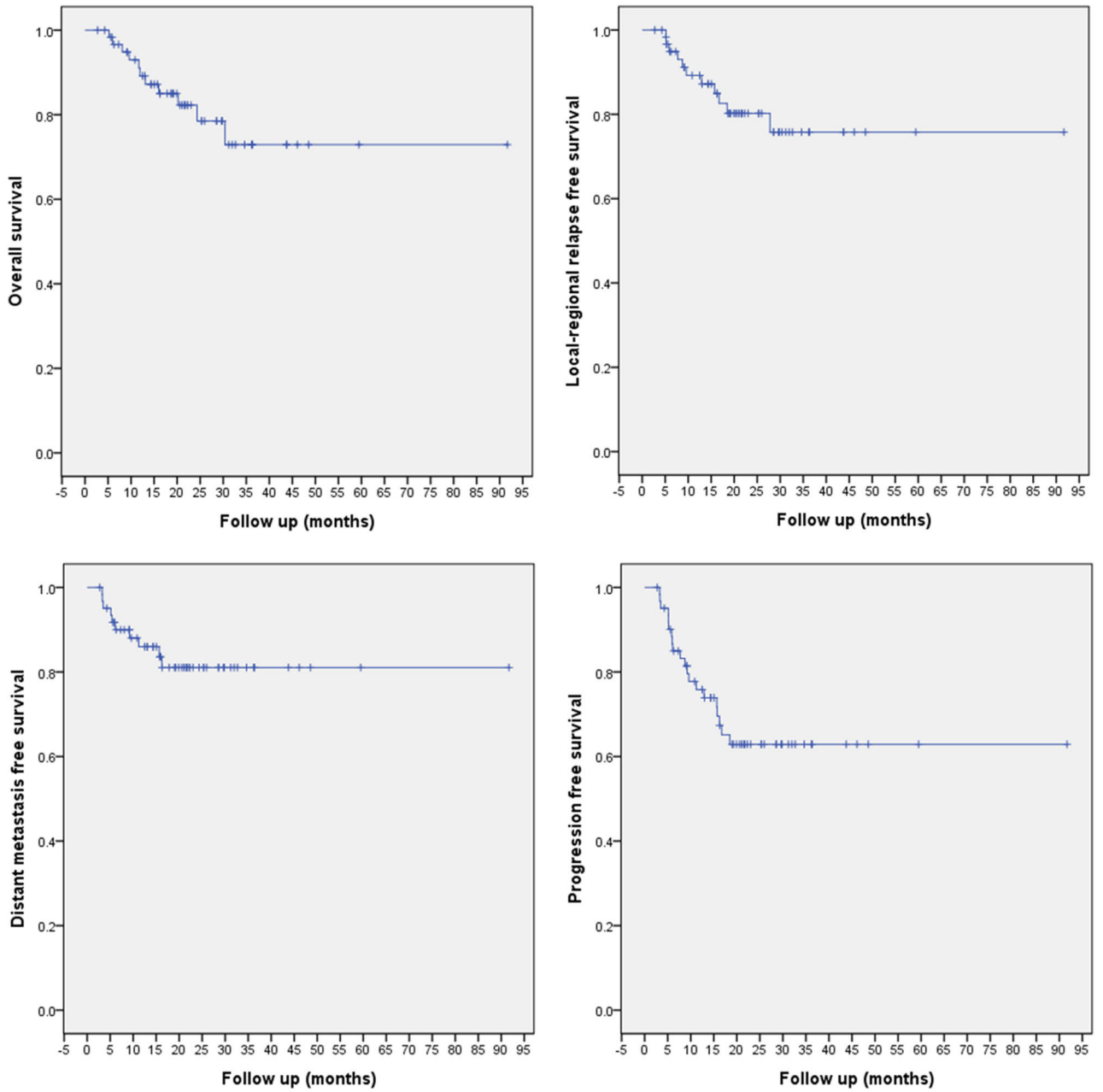

FIGURE 2 | OS, LRFS, DMFS, and PFS of the entire cohort of 62 SBS patients treated with PBRT.

the critical OARs that constrains the radiation doses. Also, particle beams with higher linear energy transfer (e.g., carbon ion) produces significantly higher biological effectiveness as compared with photon beams (23), a clear advantage for radioresistant histologies such as most subtypes of sarcomas. Clinical data from several retrospective studies showed that PBRT could achieve favorable disease control for head and neck sarcomas or base of skull tumors, including chordoma and chondrosarcoma, even in patients with unresected or recurrent diseases (24–29). In our previous studies, PBRT for head and neck sarcomas, including those involving skull base, produced effective tumor controls, and overall survivals in both primary and recurrent patients; the 1/2-year OS and LRFS for the entire cohort were 92.9/90.0 and 88.4/78.9%, respectively (24, 25). For chondrosarcoma of the skull base, PBRT attained more favorable outcomes; results from Heidelberg Ion Beam Therapy Center reported both the 5-year OS, and local controls were over 90% and over 85%, respectively (26, 28). Most of the other papers included substantial cases of chordoma of the cervical spine or skull base, a condition that has a significantly different biological behavior from bone and soft-tissue sarcomas (18, 26, 27).

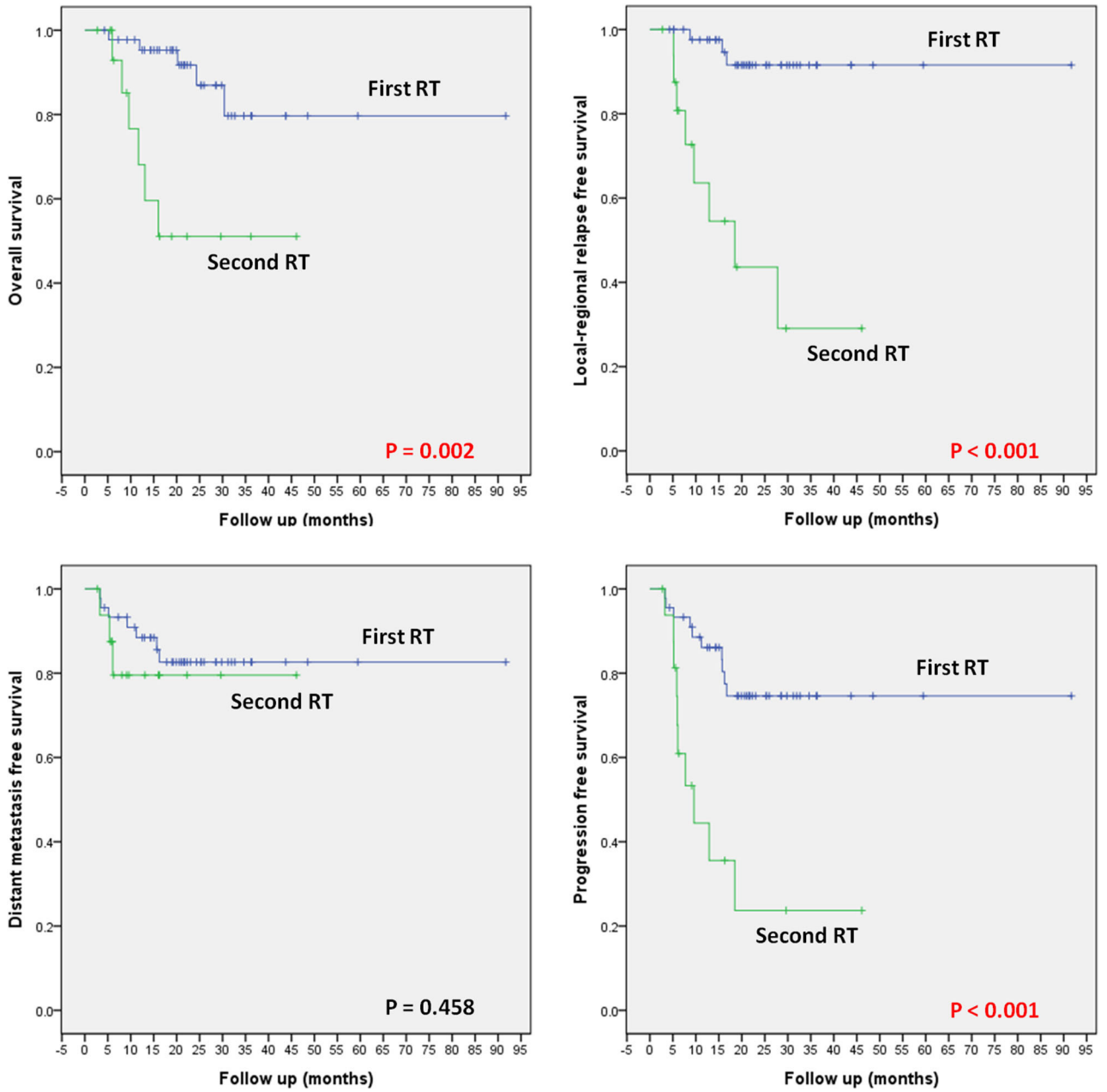

FIGURE 3 | OS, LRFS, DMFS, and PFS according to the status of prior RT (i.e., first-time RT vs. re-irradiation).

Also, PBRT has been successfully used in other malignancies other than sarcomas of the skull base, including those with extensive involvement of the orbits. In a retrospective study of 57 patients with skull base tumors treated with proton therapy or CIRT between 2003 and 2009, a 3-year OS and LPFS rates of 61 and 56% were reported, respectively (30). Results of PBRT for patients with orbital tumors after eye-sparing surgery produced excellent local controls; our center (SPHIC) reported the 2-year OS and LRFS of 100 and 93.3%, respectively, similar to those in MD Anderson Cancer Center of 100 and 100%, respectively (31, 32). However, the literature on the use of PBRT for the treatment of base of skull sarcomas other than chordoma, which are usually more aggressive and challenging conditions that precludes *en bloc* surgical resection due to their anatomical location, is scarce. The 2-year OS and LPFS rates of our patients treated mostly with CIRT were both 80.2%, and those rates of radiation-naïve patients were both > 91.0%. However, direct comparison between the results in terms of survival and disease control of our patient and previous publications may not be meaningful, as

TABLE 2 | Types and frequency of acute toxicities using CTC.AE.

Toxicity	Grade									
	1		2		3		4		5	
	No.	%	No.	%	No.	%	No.	%	No.	%
Mucositis/mucosal necrosis	11	17.7	4	6.5	1	1.6	1	1.6	0	
Skin	11	17.7	1	1.6	0		0		0	
Pain	0		1	1.6	0		0		0	
Tinnitus	1	1.6	0		0		0		0	

PBRT was also well-tolerated in terms of late adverse effects. Only grade 1 and grade 2 toxicities were observed except for the same patient mentioned with grade 4 acute toxicity died of severe hemorrhage (grade 5).

TABLE 3 | Types and frequency of late toxicities using CTC.AE.

Toxicity	Grade									
	1		2		3		4		5	
	No.	%	No.	%	No.	%	No.	%	No.	%
Salivary glands (dry mouth)	2	3.2	5	8.1	0		0		0	
Decreased hearing	3	4.8	2	3.2	0		0		0	
Skin	3	4.8	0		0		0		0	
Headache	3	4.8	0		0		0		0	
Parageusia	2	3.2	0		0		0		0	
Radiation encephalopathy	2	3.2	0		0		0		0	
Decreased vision	0		2	3.2	0		0		0	
Tinnitus	1	1.6	0		0		0		0	
Posterior cranial nerves damage	0		1	1.6	0		0		0	
Diplopia	0		1	1.6	0		0		0	
Ptosis	0		1	1.6	0		0		0	
Hemorrhage	0		0		0		0		1	1.6

pathologies of patients, treatment modalities, and follow-up time differed substantially.

One of the major clinical advantages of PBRT is its favorable profile of treatment-associated toxicity as compared with conventional radiotherapy. In the current cohort, only one patient experienced grade 3 mucositis. Another developed grade 4 mucosal necrosis with bleeding and later died of hemorrhage of the internal carotid artery. Therefore, both the acute and late toxicities observed in our patients were minimal in severity and frequency. Similar findings were observed after PBRT for skull base malignancies using proton therapy and CIRT (30, 33). Overall, historical data showed that moderate to severe (grade 2–5) acute and late toxicities ranged between 10 and 20% for skull base tumors treated with PBRT. With the use of more modern PBRT technology, such as PBS, improved acute, and late toxicities could be further achieved.

Not surprisingly, RT-naïve patients had significantly better OS, PFS, and LRFS ($p = 0.020$, 0.010, and < 0.001, respectively) over re-irradiation. Also, early T-disease (T1/2) showed a significant association with better PFS ($p = 0.024$). These findings were similar to those reported previously for

TABLE 4 | Univariate analyses for survival outcomes of 62 cases by Kaplan–Meier method (log-rank).

Variables	OS	PFS	LRFS	DMFS
Sex (male vs. female)	0.155	0.497	0.477	0.802
Age (< vs. ≥ 40)	*0.004*	0.050	0.052	0.980
Re-irradiation for recurrence or second primary sarcomas (no vs. yes)	*0.002*	*< 0.001*	*< 0.001*	0.458
Pathology (non-chondrosarcoma vs. chondrosarcoma)	0.084	*0.003*	*0.020*	0.170
T-category (T1/2 vs. T3/4)	*0.025*	*0.001*	*0.024*	0.129
Surgery (R0/R1 vs. biopsy/R2)	0.166	*0.061*	0.148	0.217
GTV (< vs. ≥ 47.45 cm^3) median	0.169	*0.011*	*0.041*	0.102
PBRT type (IMPT vs. CIRT vs. IMPT + CIRT)	0.624	0.351	0.338	0.640
Total dose (≤ vs. > 63 Gy) median	0.197	0.099	*0.042*	0.646

OS, overall survival; PFS, progress-free survival; LRFS, local recurrence free survival; DMFS, distant metastasis free survival; PBRT, particle beam radiation therapy. The italic values indicates p > 0.05.

chondrosarcoma or other based on skull tumors treated using PBRT (33). Interestingly, we did not find that the extent of surgery (R0/R1 vs. R2/biopsy) before PBRT improved patients' survival or disease control in MVA, although a trend favoring complete surgery was observed in UVA. However, such findings might be caused by the limited number of R0/R1 patients in our cohort, and many patients who had biopsy were re-irradiated.

Our study also has few important limitations. The foremost is its retrospective nature and the inclusion of a heterogeneous group of patients. However, for a relatively rare condition such as SBS, it will be difficult if not improbable to perform a prospective randomized trial for each histological subtype of the disease. As such, most of the previously published studies provided results of retrospective analyses that included a heterogeneity group of histologic subtypes, and many included chordoma as well. Second, partly due to the heterogeneity in their histological diagnosis, patients' treatment in terms of surgery and chemotherapy varied substantially. Finally, local recurrence of head neck sarcoma usually occurs within the first 2 years after the completion of radiotherapy (7, 25); thus, our follow-up period of 20.4 months provided an acceptable estimation of patients' survival and disease control. Nevertheless, PBRT-induced long-term toxicities, particularly the CNS structures adjacent to the base skull, would require longer follow-up time.

CONCLUSION

Our results showed that PBRT is a promising modality for definitive treatment for patients with base of skull bone and soft-tissue sarcomas, with a high probability of local disease control than historical data and mild to moderate acute and late toxicity. Before, radiotherapy was the most important negative prognosticator of LPFS, PFS, and OS. Also, advanced age and

T-disease were significantly associated with poor OS and PFS, respectively. PBRT has the potential to improve the therapeutic ratio, thereby treatment outcomes. The use of PBRT as a definitive treatment modality in skull base sarcomas is worth further investigation, preferably in a prospective fashion, and validation with longer follow-up.

DATA AVAILABILITY STATEMENT

All datasets presented in this study are included in the article.

ETHICS STATEMENT

This is a retrospective study and was approved by the Institutional Review Board (IRB) of SPHIC.

AUTHOR CONTRIBUTIONS

JL: conception and design. LK: administrative support. JL and LK: provision of study patients. JY, XG, JG, JH, WH, XQ, QH, and WZ: collection and assembly of data. JY: data analysis and interpretation. JL and JY: manuscript writing. All authors: final approval of manuscript.

FUNDING

This work was supported by grants from the Scientific Research projects of the Shanghai Science and Technology Committee (Project No. 19411951000), Shanghai Municipal Commission of Health and Family Planning (Project No. 20174Y0076), and Pudong New Area Science and Technology Development Foundation (Project No. PKJ2018-Y50).

REFERENCES

1. Farhood AI, Hajdu SI, Shiu MH, Strong EW. Soft tissue sarcomas of the head and neck in adults. *Am J Surg*. (1990) 160:365–9. doi: 10.1016/S0002-9610(05)80544-6
2. Eeles RA, Fisher C, A'Hern RP, Robinson M, Rhys-Evans P, Henk JM, et al. Head and neck sarcomas: prognostic factors and implications for treatment. *Br J Cancer*. (1993) 68:201–7. doi: 10.1038/bjc.1993.314
3. Chen SA, Morris CG, Amdur RJ, Werning JW, Villaret DB, Mendenhall WM. Adult head and neck soft tissue sarcomas. *Am J Clin Oncol*. (2005) 28:259–63. doi: 10.1097/01.coc.0000158440.27229.d6
4. Mendenhall WM, Mendenhall CM, Werning JW, Riggs CE, Mendenhall NP. Adult head and neck soft tissue sarcomas. *Head Neck*. (2005) 27:916–22. doi: 10.1002/hed.20249
5. Huber GF, Matthews TW, Dort JC. Soft-tissue sarcomas of the head and neck: a retrospective analysis of the Alberta experience 1974 to 1999. *Laryngoscope*. (2006) 116:780–5. doi: 10.1097/01.MLG.0000206126.48315.85
6. Ballo MT, Zagars GK, Cormier JN, Hunt KK, Feig BW, Patel SR, et al. Interval between surgery and radiotherapy: effect on local control of soft tissue sarcoma. *Int J Radiat Oncol Biol Phys*. (2004) 58:1461–7. doi: 10.1016/j.ijrobp.2003.09.079
7. Gil Z, Patel SG, Singh B, Cantu G, Fliss DM, Kowalski LP, et al. Analysis of prognostic factors in 146 patients with anterior skull base sarcoma: an international collaborative study. *Cancer*. (2007) 110:1033–41. doi: 10.1002/cncr.22882
8. Pisters PW, Harrison LB, Leung DH, Woodruff JM, Casper ES, Brennan MF. Long-term results of a prospective randomized trial of adjuvant brachytherapy in soft tissue sarcoma. *J Clin Oncol*. (1996) 14:859–68. doi: 10.1200/JCO.1996.14.3.859
9. Kassir RR, Rassekh CH, Kinsella JB, Segas J, Carrau RL, Hokanson JA. Osteosarcoma of the head and neck: meta-analysis of nonrandomized studies. *Laryngoscope*. (1997) 107:56–61. doi: 10.1097/00005537-199701000-00013
10. Yang JC, Chang AE, Baker AR, Sindelar WF, Danforth DN, Topalian SL, et al. Randomized prospective study of the benefit of adjuvant radiation therapy in the treatment of soft tissue sarcomas of the extremity. *J Clin Oncol*. (1998) 16:197–203. doi: 10.1200/JCO.1998.16.1.197
11. O'Sullivan B, Davis AM, Turcotte R, Bell R, Catton C, Chabot P, et al. Preoperative versus postoperative radiotherapy in soft-tissue sarcoma of the limbs: a randomised trial. *Lancet*. (2002) 359:2235–41. doi: 10.1016/S0140-6736(02)09292-9
12. Davis AM, O'Sullivan B, Turcotte R, Bell R, Catton C, Chabot P, et al. Late radiation morbidity following randomization to preoperative versus postoperative radiotherapy in extremity soft tissue sarcoma. *Radiother Oncol*. (2005) 75:48–53. doi: 10.1016/j.radonc.2004.12.020
13. Kanai T, Endo M, Minohara S, Miyahara N, Koyama-ito H, Tomura H, et al. Biophysical characteristics of HIMAC clinical irradiation system for heavy-ion radiation therapy. *Int J Radiat Oncol Biol Phys*. (1999) 44:201–10. doi: 10.1016/S0360-3016(98)00544-6
14. Tsujii H KT, Baba M. Clinical advantages of carbon-ion radiotherapy. *New J Phys*. (2008) 10:3–12. doi: 10.1088/1367-2630/10/7/075009
15. Emami B, Lyman J, Brown A, Coia L, Goitein M, Munzenrider JE, et al. Tolerance of normal tissue to therapeutic irradiation. *Int J Radiat Oncol Biol Phys*. (1991) 21:109–22. doi: 10.1016/0360-3016(91)90171-y
16. Koto M. Skull base and upper cervical spine tumors. In: Tsujii HKT, Shirai T, editors. *Carbon-Ion Radiotherapy Principles, Practices, and Treatment Planning*. Heidelberg: Springer (2014). p. 155–61. doi: 10.1007/978-4-431-54457-9_18
17. Nieder C, Milas L, Ang KK. Tissue tolerance to reirradiation. *Semin Radiat Oncol*. (2000) 10:200–9. doi: 10.1053/srao.2000.6593
18. Weber DC, Malyapa R, Albertini F, Bolsi A, Kliebsch U, Walser M, et al. Long term outcomes of patients with skull-base low-grade chondrosarcoma and chordoma patients treated with pencil beam scanning proton therapy. *Radiother Oncol*. (2016) 120:169–74. doi: 10.1016/j.radonc.2016.05.011
19. Liang ZG, Kusumawidjaja G, Kazmi F, Wee JTS, Chua MLK. Intensity-modulated radiotherapy for paranasal sinuses and base of skull tumors. *Oral Oncol*. (2018) 86:61–8. doi: 10.1016/j.oraloncology.2018.09.010
20. Kim JW, Suh CO, Hong CK, Kim EH, Lee IJ, Cho J, et al. Maximum surgical resection and adjuvant intensity-modulated radiotherapy with simultaneous integrated boost for skull base chordoma. *Acta Neurochirurgica*. (2017) 159:1825–34. doi: 10.1007/s00701-016-2909-y
21. Sahgal A, Chan MW, Atenafu EG, Masson-Cote L, Bahl G, Yu E, et al. Image-guided, intensity-modulated radiation therapy (IG-IMRT) for skull base chordoma and chondrosarcoma: preliminary outcomes. *Neuro Oncol*. (2015) 17:889–94. doi: 10.1093/neuonc/nou347
22. Minard-Colin V, Kolb F, Saint-Rose C, Fayard F, Janot F, Rey A, et al. Impact of extensive surgery in multidisciplinary approach of pterygopalatine/infratemporal fossa soft tissue sarcoma. *Pediatr Blood Cancer*. (2013) 60:928–34. doi: 10.1002/pbc.24374
23. Durante M, Orecchia R, Loeffler JS. Charged-particle therapy in cancer: clinical uses and future perspectives. *Nat Rev Clin Oncol*. (2017) 14:483–95. doi: 10.1038/nrclinonc.2017.30
24. Yang J, Gao J, Qiu X, Hu J, Hu W, Wu X, et al. Intensity-modulated proton and carbon-ion radiation therapy in the management of head and neck sarcomas. *Cancer Med*. (2019) 8:4574–86. doi: 10.1002/cam4.2319
25. Yang J, Gao J, Wu X, Hu J, Hu W, Kong L, et al. Salvage carbon ion radiation therapy for locally recurrent or radiation-induced second primary sarcoma of the head and neck. *J Cancer*. (2018) 9:2215–23. doi: 10.7150/jca.24313
26. Uhl M, Mattke M, Welzel T, Oelmann J, Habl G, Jensen AD, et al. High control rate in patients with chondrosarcoma of the skull base after carbon

ion therapy: first report of long-term results. *Cancer*. (2014) 120:1579–85. doi: 10.1002/cncr.28606
27. Demizu Y, Mizumoto M. Proton beam therapy for bone sarcomas of the skull base and spine: a retrospective nationwide multicenter study in Japan. *Cancer Sci.* (2017) 108:972–7. doi: 10.1111/cas.13192
28. Mattke M, Vogt K, Bougatf N, Welzel T, Oelmann-Avendano J, Hauswald H, et al. High control rates of proton- and carbon-ion-beam treatment with intensity-modulated active raster scanning in 101 patients with skull base chondrosarcoma at the Heidelberg Ion Beam Therapy Center. *Cancer*. (2018) 124:2036–44. doi: 10.1002/cncr.31298
29. Guan X, Gao J, Hu J, Hu W, Yang J, Qiu X, et al. The preliminary results of proton and carbon ion therapy for chordoma and chondrosarcoma of the skull base and cervical spine. *Radiat Oncol.* (2019) 14:206. doi: 10.1186/s13014-019-1407-9
30. Morimoto K, Demizu Y, Hashimoto N, Mima M, Terashima K, Fujii O, et al. Particle radiotherapy using protons or carbon ions for unresectable locally advanced head and neck cancers with skull base invasion. *Jpn J Clin Oncol*. (2014) 44:428–34. doi: 10.1093/jjco/hyu010
31. Hu W, Hu J, Gao J, Yang J, Qiu X, Kong L, et al. Outcomes of orbital malignancies treated with eye-sparing surgery and adjuvant particle radiotherapy: a retrospective study. *BMC Cancer*. (2019) 19:776. doi: 10.1186/s12885-019-5964-y
32. Holliday EB, Esmaeli B, Pinckard J, Garden AS, Rosenthal DI, Morrison WH, et al. A multidisciplinary orbit-sparing treatment approach that includes proton therapy for epithelial tumors of the orbit and ocular adnexa. *Int J Radiat Oncol Biol Phys*. (2016) 95:344–52. doi: 10.1016/j.ijrobp.2015.08.008
33. Noel G, Gondi V. Proton therapy for tumors of the base of the skull. *Chin Clin Oncol*. (2016) 5:51. doi: 10.21037/cco.2016.07.05

Conflict of Interest: The authors declare that the research was conducted in the absence of any commercial or financial relationships that could be construed as a potential conflict of interest.

Copyright © 2020 Yang, Hu, Guan, Hu, Gao, Qiu, Huang, Zhang, Kong and Lu. This is an open-access article distributed under the terms of the Creative Commons Attribution License (CC BY). The use, distribution or reproduction in other forums is permitted, provided the original author(s) and the copyright owner(s) are credited and that the original publication in this journal is cited, in accordance with accepted academic practice. No use, distribution or reproduction is permitted which does not comply with these terms.

frontiers in Oncology

ORIGINAL RESEARCH
published: 30 September 2020
doi: 10.3389/fonc.2020.572493

Particle Beam Radiation Therapy for Adenoid Cystic Carcinoma of the Nasal Cavity and Paranasal Sinuses

Weixu Hu[1,2], *Jiyi Hu*[1,2], *Qingting Huang*[1,2], *Jing Gao*[1,2], *Jing Yang*[1,2], *Xianxin Qiu*[1,2], *Lin Kong*[2,3]* and *Jiade J. Lu*[1,2]*

[1] Department of Radiation Oncology, Shanghai Proton and Heavy Ion Center, Shanghai, China, [2] Shanghai Engineering Research Center of Proton and Heavy Ion Radiation Therapy, Shanghai, China, [3] Department of Radiation Oncology, Shanghai Proton and Heavy Ion Center, Fudan University Cancer Hospital, Shanghai, China

OPEN ACCESS

Edited by:
Timothy Dean Malouff,
Mayo Clinic Florida, United States

Reviewed by:
Daniel Ebner,
Brown University, United States
Michael Andrew Samuels,
University of Miami, United States
Jose Angelito Ugalde Hardillo,
Erasmus Medical Center, Netherlands

***Correspondence:**
Lin Kong
lin.kong@sphic.org.cn
Jiade J. Lu
jiade.lu@sphic.org.cn

Specialty section:
This article was submitted to Radiation Oncology, a section of the journal Frontiers in Oncology

Received: 14 June 2020
Accepted: 27 August 2020
Published: 30 September 2020

Citation:
Hu W, Hu J, Huang Q, Gao J, Yang J, Qiu X, Kong L and Lu JJ (2020) Particle Beam Radiation Therapy for Adenoid Cystic Carcinoma of the Nasal Cavity and Paranasal Sinuses. Front. Oncol. 10:572493. doi: 10.3389/fonc.2020.572493

Background: Sinonasal adenoid cystic carcinoma (SNACC) presents a challenge to oncologists due to its complex anatomy and poor prognosis. Although radiation therapy, either definitive or adjuvant to surgery, is an important part of the multidisciplinary management of SNACC, photon-based radiotherapy yielded suboptimal local control. The purpose of this study was to report the clinical results of a large patient cohort treated with particle beam radiation therapy.

Methods: Patients with SNACC that received proton beam therapy (PBT), carbon-ion radiotherapy (CIRT) or a combination of CIRT and PBT between May 2015 and May 2019 were included in the analysis. Three patients were treated with PBT, 17 with CIRT and 18 received PBT and a CIRT boost. Overall survival (OS), progression-free survival (PFS), local control (LC), regional control (RC), and distant metastasis-free (DMF) rates were calculated using the Kaplan-Meier method. Toxicities were reported using the CTCAE (version 4.03).

Results: A total of 38 patients were included in this analysis. Of these patients, 12 had recurrent disease, including 10 whose previous photon-based RT had failed. The most common primary tumor site was the maxillary sinus. Thirty-six patients (94.7%) suffered from locally advanced disease (T3-4). After a median follow-up of 27.2 months, the 3-year OS, PFS, LC, RC, and DMF rates were 96.7, 80.6, 90.0, 100, and 88.7%, respectively. No acute toxicities of grade 3 or above were observed. Two patients experienced grade 3 xerostomia or vision decreased, and one patient died of hemorrhage.

Conclusion: PBT, CIRT or a combination of CIRT and PBT appeared to be a promising treatment option for SNACC and produced satisfactory local control and toxicity profile. Longer follow-up is needed to verify the long-term benefit of particle-beam radiation therapy (PBRT) for patients with SNACC.

Keywords: nasal cavity and paranasal sinuses adenoid cystic carcinoma, radiotherapy, particle-beam radiation therapy, proton beam therapy, carbon-ion radiotherapy

INTRODUCTION

Adenoid cystic carcinoma (ACC) is a rare condition that accounts for 3–5% of all head and neck malignancies (1). ACC is characterized by a slow growth rate but a high probability of local infiltration, perineural spread, and distant metastasis. ACC usually arises in the major salivary glands; however, with 10–25% of ACC cases originating in the nasal cavity and paranasal sinuses, it is responsible for 5–15% of sinonasal malignancies (2). Sinonasal ACC (SNACC) presents a challenge to oncologists due to its complex anatomy and poor prognosis compared with carcinomas that affect the major salivary glands. The 5-year overall survival (OS) rate is approximately 60% for patients with SNACC compared with 90% for all head and neck ACC (3).

Although surgery is the mainstay of treatment for head and neck ACC, the 10-year local control (LC) of surgery alone was only 60%, and even as low as 30% in patients with positive margins (4). For SNACC patients, complete resection within sufficient safety margins is usually not feasible. Therefore, radiation therapy (RT), either definitive or adjuvant to surgery, is an important part of the multidisciplinary management of SNACC. However, ACC is resistant to photon-based RT (5). This is part of the reason why SNACC, a condition that is also not amenable to surgical resection, has a poor prognosis with the 5-year DSS rate being only 37.3% when treated with RT alone (6). It is clear that a more effective local treatment is needed.

Particle-beam radiation therapy (PBRT), which uses protons or heavier ions such as helium or carbon ions, is relevant in the treatment of SNACC. A particle beam deposits low doses of radiation along its travel path through the body, before reaching its target and distributing most of its dose immediately prior to termination at the Bragg peak. The lateral penumbra of particle beams is significantly sharper than that in photon beams. Compared with photon-based intensity-modulated RT (IMRT), this feature of PBRT improves the therapeutic ratio by introducing a sharp dose gradient between the tumor volume of and adjacent to critical organs at risk (OARs). Also, high linear energy transfer (LET) particles, such as carbon ions, have a relative higher biological effectiveness (RBE) of 2–5, depending on beam energy, fraction dose, and the cell and tissue types irradiated, as compared to photons and protons (the prescribed proton doses used RBE value of 1.1) (7, 8). Both features are of especially importance in the management of SNACC for overcoming the condition's anatomical complexity and resistance to conventional RT. However, while there is ample evidence describing the use of PBRT in heterogeneous ACC patient populations, there is minimal specific data available in relation to SNACC.

The purpose of this study was to report the clinical results of a large patient cohort treated with PBRT at the Shanghai Proton and Heavy Ion Center (SPHIC) over the past five years, including local control, survival and adverse events associated with PBRT.

METHODS

Pre-treatment Workups

All newly diagnosed cases were confirmed by pathology. For patients with recurrent disease, pathological and/or radiological diagnoses were required. All patients were evaluated according to the standardized pre-radiation work-ups of the SPHIC for head and neck cancers. This included a complete history and physical examination (H&P); imaging study of the head and neck region (enhanced magnetic resonance imaging [MRI] was preferred, but computerized tomography [CT] with contrast was permitted if MRI was contraindicated or declined by the patient); routine lab tests (full blood count; serum electrolytes; liver and kidney function tests); fluorodeoxyglucose-positron emission tomography/CT (FDG-PET/CT) (or a thoracic/abdominal CT and a whole body bone scan); urine analysis; and an electrocardiogram (EKG). All disease was staged according to the seventh (diagnosed before 1 January, 2018) or eighth (diagnosed after 1 January, 2018) edition of the AJCC (American Joint Committee on Cancer) TNM (tumor, nodes, metastases) staging system. This study was approved by SPHIC's institutional review board (IRB) with a waiver of informed consent.

Particle Beam Radiation Therapy

AlphaCradle® and thermoplastic masks were used to immobilize patients in a supine position. Simulation CT of the head and neck region without intravenous (IV) contrast was performed at a slice thickness of 1.5 mm. Simulation MRI was also carried out, and then MRI-CT fusion was used to delineate the target and OARs. All disease foci discovered on clinical examination or during imaging studies were the gross tumor volumes (GTVs). Three clinical target volumes (CTVs) were delineated: CTV-G or CTV-N covered primary site (GTVp) or positive neck lymph nodes (GTVnd) plus 1–3 mm depend on the surrounding OARs. CTV 1 included the tumor bed (after R1 resection), the pretreatment tumor bed (the tumor region before R2 resection) and high-risk areas for tumor extension; CTV 2 included the ipsilateral or bilateral jugular lymph node region, depending on cervical lymph node status and primary tumor extension Planning target volumes (PTVs) included the CTVs plus a 3–6 mm expansion to account for range uncertainty and setup errors. OARs delineated included the brain, temporal lobes, brainstem, spinal cord, optic nerves and chiasm, lenses, cochleae, parotid glands, and larynx. Doses of intensity-modulated proton or carbon-ion therapy (IMPT or IMCT) were prescribed in Gy (RBE). The RBE value for proton radiotherapy was 1.1 and for carbon-ion radiotherapy was between 2.8 and 3.7 (depending on the depth in the spread-out Bragg peaks). The dose constraints for OARs were based on normal tissue tolerance as described by Emami et al. (9) and the National Institute of Radiation and Quantum Science (QST Hospital) (10). Intensity-modulated proton therapy (IMPT) and intensity-modulated carbon-ion therapy (IMCT) were delivered with pencil-beam scanning (PBS). Multi-field optimization (MFO) with two to three arrangements was used in most treatment plans. The Siemens Syngo treatment planning system (TPS) was used to plan the IMPT and IMCT. CT without IV contrast was performed weekly on all patients to verify the dose distribution.

Systemic Therapy

No patient in this cohort received concurrent systemic therapy, such as chemotherapy or target therapy, during PBRT. Eleven patients received induction chemotherapy or target therapy.

The most commonly used chemotherapy regimens were adriamycin-cyclophosphamide-cisplatin, gemcitabine-cisplatin, or apatinib.

Follow-Up and Toxicity Evaluation

Patients were treated as in-patients and evaluated for acute toxicities daily. Weekly CT scans started from week 2 of PBRT and were used to evaluate response to treatment and any need to re-plan PBRT due to substantial anatomical alterations. Following the completion of treatment, patients were evaluated for adverse effects and disease control according to SPHIC's standardized institutional follow-up protocol. The first follow-up was at four weeks after PBRT completion. The patients were then followed up every three to four months for two years, every six months for three more years, and yearly thereafter.

Each follow-up included a complete H&P, routine lab tests, and imaging studies of the head and neck regions. Other tests, such as PET-CT scans, were also carried out, depending on clinical findings at the time of follow-up. Acute toxicities were defined as those that occurred within 3 months at the initiation of PBRT. Toxicities that occurred after this period until the last follow-up were late toxicities. Both acute and late toxicities was evaluated by the Common Terminology Criteria for Adverse Events (CTCAE) version 4.03.

Statistical Analysis

OS was defined as the duration between diagnosis and death or last follow-up. Local control (LC), regional control (RC), and distant metastasis-free (DMF) were defined as the duration between diagnosis and corresponding failure of control. The LC, RC, DMF, progression-free survival (PFS), and OS rates were calculated using the Kaplan-Meier method performed with SPSS (Version 25.0). Univariate analysis using COX regression model performed with SPSS (Version 25.0). Univariate analysis using competing risk model performed with R statistical software (version3.4.1; R Foundation, Austria).

RESULTS

Patient Characteristics

Forty-one consecutive patients with SNACC were treated at SPHIC between May, 2015, and May, 2019. Three of these patients had distant metastasis (DM) at diagnosis and were excluded. The remaining 38 were included in the analysis. Of these patients, 12 had recurrent disease, including 10 whose previous photon-based RT had failed. The most common primary tumor site was the maxillary sinus. Only two patients presented with T2 disease. The remaining patients suffered from locally advanced disease (T3-4), including one patient with bilateral neck adenopathy. Twenty-nine patients (76.3%) had skull base involvement. Due to extension of the primary tumor, R0 or R1 resections were only achieved in six patients. Thirty-two patients (84.2%) had gross residual tumor before receiving PBRT, and the median GTV volume was 56.8 ml. Eleven patients received induction chemotherapy or target therapy before PBRT. The patients' characteristics are detailed in **Table 1**.

TABLE 1 | Characteristics of patients.

Characteristics	No. (%)
Total	**38 (100%)**
Gender	
Male	18 (47.4%)
Female	20 (52.6%)
Age	
Median(range), years	45 (17–75)
T category	
T1	0
T2	2 (5.3%)
T3	7 (18.4%)
T4	29 (76.3%)
N category	
N0	37 (97.4%)
N2	1 (2.6%)
Tumor location	
Maxillary sinus	30 (78.9%)
Ethmoid sinus	4 (10.5%)
Nasal cavity	4 (10.5%)
Skull base involvement	
Yes	29 (76.3%)
No	9 (23.7%)
Surgery	
Without surgery	4 (10.5%)
With surgery	23 (60.5%)
Biopsy	11 (28.9%)
Gross tumor	
With gross tumor	32 (84.2%)
Without gross tumor	6 (15.8%)
GTV ml, median (range)	56.8 (7.7–183.6)
Re-irradiation	
Irradiation naïve	28 (73.7%)
Re-irradiation	10 (26.3%)
Disease status	
Initial disease	26 (68.4%)
Recurrent disease	12 (31.6%)
Radiation technique	
Proton	3 (7.9%)
CIRT	17 (44.7%)
Proton and CIRT	18 (47.4%)
Median dose to GTV (range), Gy (RBE)	69.5 (56–73.5)
Induction chemotherapy or apatinib therapy	
Yes	11 (28.9%)
No	27 (71.1%)

Particle-Beam Radiotherapy

Three patients were treated with proton beam therapy (PBT), 17 with carbon-ion radiotherapy (CIRT) and 18 received PBT and a CIRT boost.

The patients who had R0 resections received PBT using 56 Gy (RBE) in 28 fractions at the surgical bed and high-risk regions. Of the 4 patients who had R1 resections, 3 received CIRT using

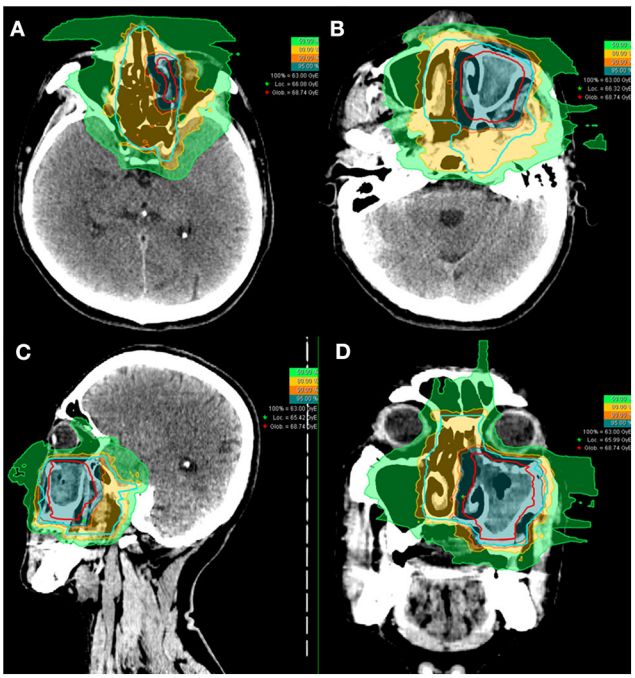

FIGURE 1 | Axial **(A,B)**, sagittal **(C)**, and coronal **(D)** views of a typical intensity-modulated carbon ion radiotherapy treatment plan.

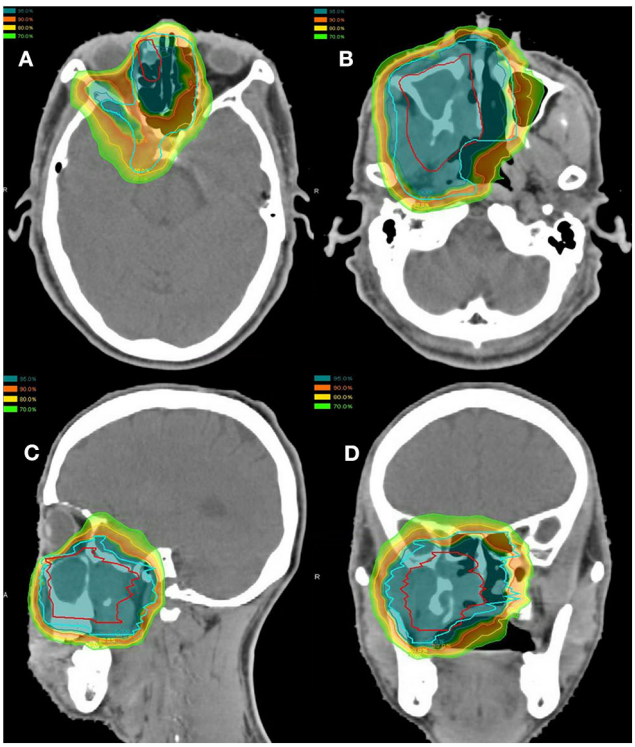

FIGURE 2 | Axial **(A,B)**, sagittal **(C)**, and coronal **(D)** views of a typical intensity-modulated proton and carbon ion-boost radiotherapy treatment plan.

63 Gy (RBE) in 18 fractions to the tumor bed and 54 Gy (RBE) in 18 fractions to the high risk regions using the simultaneous integrated boost technique. The other R1 patient received PBT (56 Gy (RBE)/28 fractions) followed by a CIRT boost (15 Gy (RBE)/5 fractions). Of the patients with gross disease at their initial treatment, 1 received PBT (66 Gy (RBE)/30 fractions), 4 received CIRT (63-70 Gy (RBE) at the gross tumors and 54-60 Gy (RBE) at the high-risk regions in 18-20 fractions), and 17 patients received a combination of PBT (56 Gy (RBE)/28 fractions) and a CIRT boost (15-17.5 Gy (RBE)/5 fractions). Based on cervical lymph node status as well asand the location and extension of the primary tumor, unilateral neck irradiation was performed in nine patients, and bilateral neck irradiation was performed in seven patients.

Of the 10 patients who were re-irradiated, CIRT using 60-66 Gy (RBE) in 20-22 fractions was given to the recurrent tumor and 54-59.4 Gy (RBE) in 20-22 fractions for the high-risk regions. None of the re-irradiated patients received CIRT to the neck. Typical treatment plans for the combination of PBT and CIRT boost or CIRT alone are illustrated in **Figures 1**, **2**.

Disease Control and Survival Outcomes

The cohort's median follow-up was 27.2 months (5–56.6 months). All but one patient were alive at their last follow-up. This patient had received re-irradiation and died from hemorrhage 10 months after the completion of CIRT without evidence of disease progression. Two in-field and one out-field local failure were observed, include two patients who had received CIRT re-irradiation for recurrent disease. Two patients developed DM at 21.5 and 22.8 months after PBRT. No regional failures were observed. The 3-year OS, PFS, LC, RC, and distant metastasis-free (DMF) rates for the entire cohort were 96.7, 80.6, 90.0, 100, and 88.7%, respectively (**Figure 3**). Although no significant difference was found, the LC and survival rates in patients with T4 disease were poorer (the 3-year OS, PFS, LC, and DMF rates being 95.7, 73.5, 86.9, and 84.0%) compared with T1-3 patients (the 3-year LC and survival rates were all 100%) (**Figure 4**).

Toxicities

The acute and late toxicities induced by PBRT are summarized in **Table 2**. Sixteen patients (42.1%) experienced 19 events of grade 2 acute toxicity, including mucositis, dermatitis, and xerostomia. Ten of the sixteen patients received PBT and CIRT boost treatment, CIRT only was performed in 4 patients and 2 patients only received PBT. No acute toxicities of grade 3 or above were observed.

Fifteen events of grade 1–2 late toxicity were observed including 9 patients received PBT and CIRT boost radiotherapy, 5 patients were treated with CIRT only and 1 with PBT only. The most common late toxicity was xerostomia. Other grade 1–2 toxicities included facial edema, facial numbness, vision impairment, epiphora, blepharoptosis, diplopia, and tinnitus. Only a small number of grade 3 toxicities occurred, including one event of xerostomia and one of vision impairment. The patient who developed grade 3 vision decreased at three

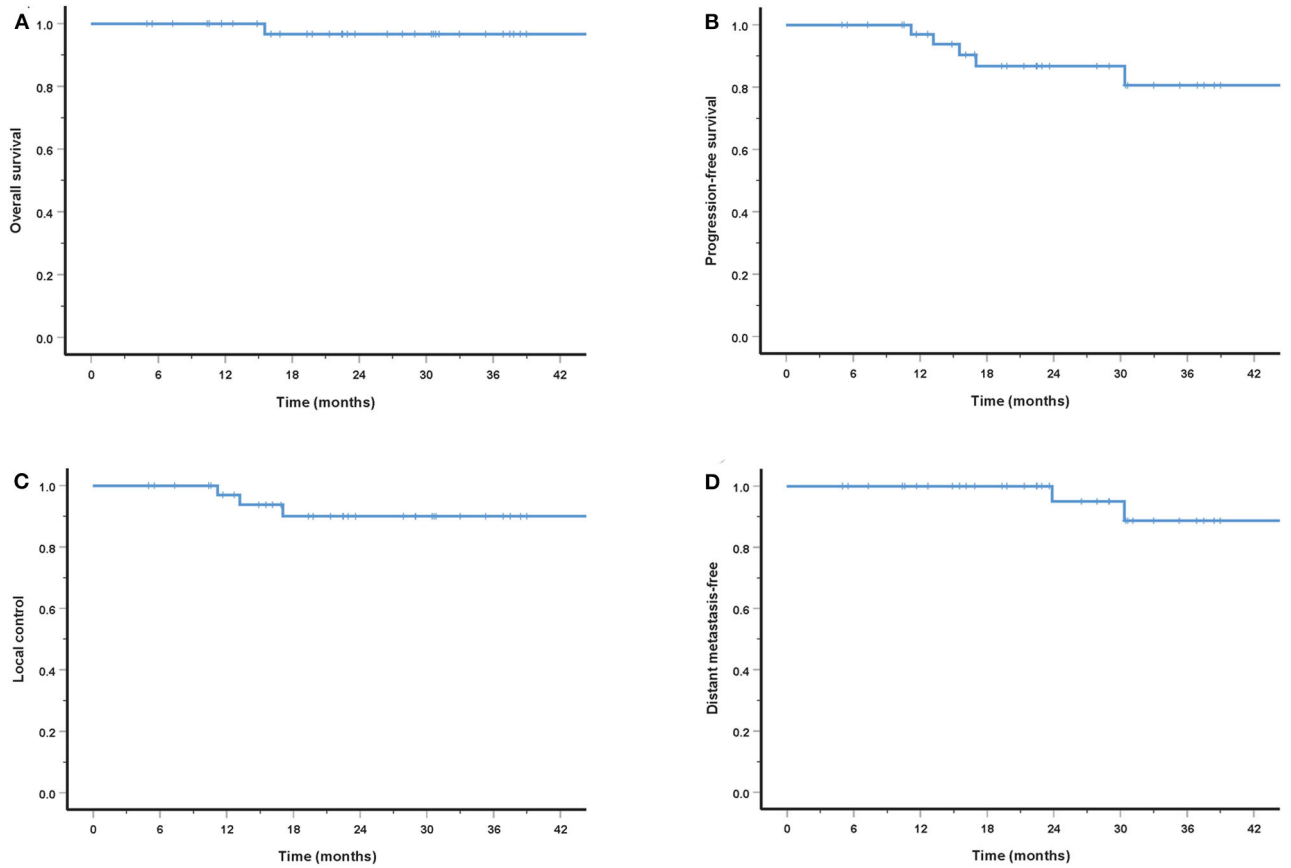

FIGURE 3 | Three-year survival rates for entire cohorts: OS **(A)**, PFS **(B)**, LC **(C)**, and DMF **(D)**.

months after the completion of CIRT re-irradiation. One patient died of hemorrhage (grade 5 toxicity associated with re-irradiation) 10 months after completing CIRT re-irradiation as salvage treatment.

DISCUSSION

The aim of our retrospective study was to describe the outcomes of SNACC patients treated with intensity-modulated PBRT. By examining a cohort of 38 SNACC patients, most of whom had T4 disease (76.3%) or locally recurrent disease after RT (26%), we found that PBT, CIRT, and a combination of the two appeared to be safe and effective. All but 1 patient were alive at a median follow-up of 27.2 months. The 3-year OS, PFS, LC, RC, and DMF rates of the cohort were 96.7, 80.6, 90.0, 100, and 88.7%, respectively. Additionally, no acute grade 3 or above toxicities were observed. Late toxicities of grade 3 or above were observed in 3 patients, including 1 patient who died from hemorrhage 10 months after completing CIRT re-irradiation as salvage treatment.

SNACC is a rare condition with poor prognosis that accounts for 10–25% of all head and neck ACC (11, 12). Given the complicated anatomy of the sinonasal region, gross tumor resection is difficult to achieve and can result in LC failure (13, 14). SNACC is a chemotherapy-resistant condition (15–22). Postoperative RT is usually used to improve LC and survival in these patients. The results of several retrospective studies have shown that, compared with surgery alone, the combination of RT and surgery not only decreases local failures, but also improves 5-year disease-specific survival (DSS) (4, 6). However, for patients with unresectable tumors, definitive radiotherapy is the only approach. As a result of it radioresistant nature (5), several recent researches reported an inferior 5-year LC of 42–56% in head and neck ACC (23, 24), with the 5-year DSS rate being only 37.3% for SNACC patients treated with RT alone (6).

Due to this radioresistance, PBRT, including neutron therapy, PBT, and CIRT, has been used to improve disease control rates. A prospective randomized phase-III trial comparing the LC rate of neutron and photon radiotherapy (13) found a 10-year LC rate of 56% in neutron therapy compared with 17% in conventional RT. Another retrospective study showed a significantly higher 5-year LC rate of 75% for the neutron therapy group compared with 32% in the photon therapy group (14). However, severe toxicities were more prevalent in the neutron therapy group (19%) than in the photon radiotherapy group (4%) (13, 14).

Due to the Bragg peak, PBT and CIRT can provide a more precise dose distribution, facilitating high-dose irradiation of tumor volume while sparing OARs. In a case series of 13 patients

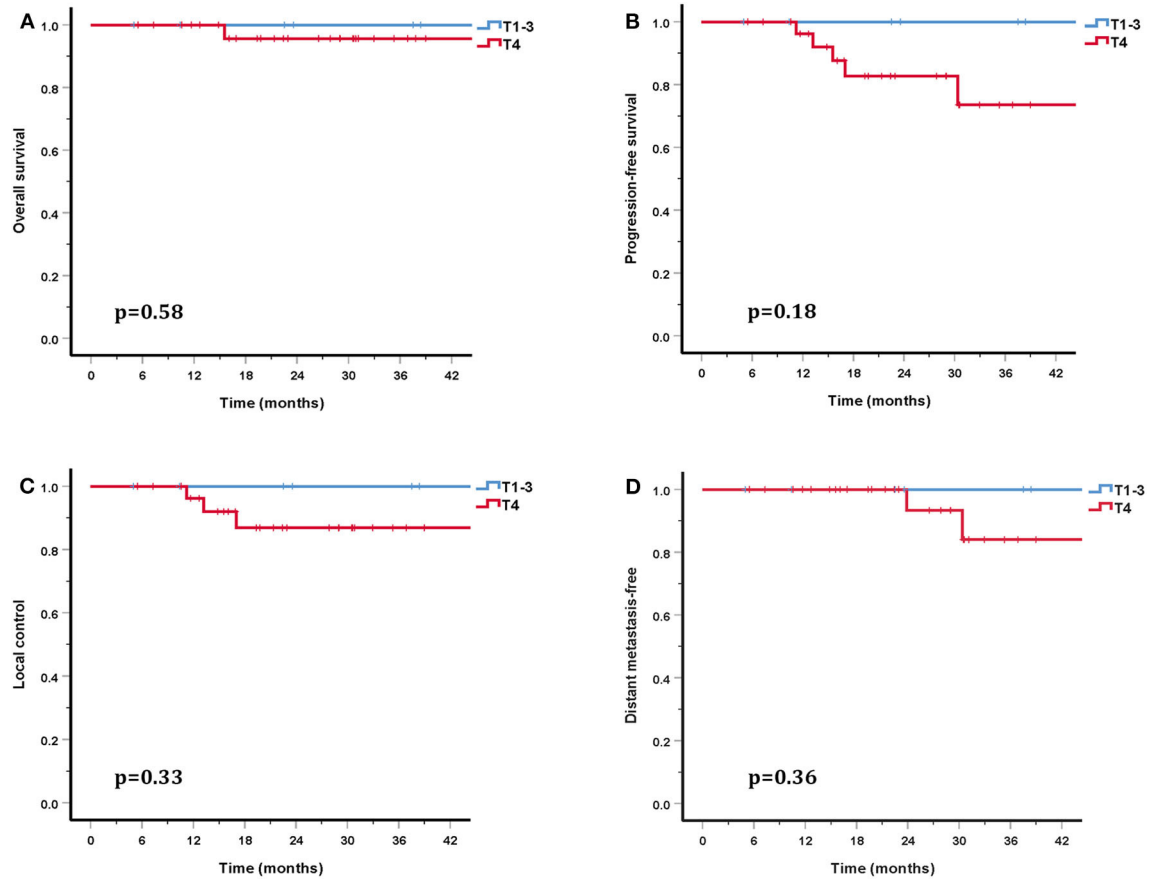

FIGURE 4 | Three-year survival rates for patients with T1-3 disease compared with T4 patients: OS **(A)**, PFS **(B)**, LC **(C)**, and DMF **(D)**.

TABLE 2 | Characteristics of acute and late toxicities.

	Acute toxicities		Late toxicities							
	Grade 2		Grade 1		Grade 2		Grade 3		Grade 5	
Type of adverse reaction	No	%	No	%	No	%	No	%	No	%
Dermatitis	1	2.6	0		0		0		0	
Mucositis	15	39.5	0		0		0		0	
Xerostomia	3	7.9	6	15.8	2	5.3	1	2.6	0	
Facial edema	0		1	2.6	0		0		0	
Decreased vision	0		1	2.6	0		1	2.6	0	
Epiphora	0		1	2.6	0		0		0	
Blepharoptosis	0		1	2.6	0		0		0	
Diplopia	0		1	2.6	0		0		0	
Tinnitus	0		1	2.6	0		0		0	
Facial numbness	0		0		1	2.6	0		0	
Hemorrhage	0		0		0		0		1	2.6

with locally advanced SNACC, Dautruche et al. retrospectively analyzed the survival of patients treated with PBT and/or tomotherapy. They reported 3-year OS, LC and DM free survival (DMFS) rates of 60, 48, and 60%, respectively (25). Recently, a retrospective study of postoperative PBT for head and neck ACC showed promising LC (26): 94% of patients achieved R0 or R1 resection with a median follow-up of 24.9 months. Only one patient developed in-field recurrence. Another study by

Pommier et al. analyzed the efficacy of PBT combined with photon radiotherapy in the treatment of 23 ACC patients with skull base invasion. They reported 5-year LC and OS rates of 93% and 77% (27). More recently, Linton et al. reported 2-year LC and OS rates of 92 and 82% in head and neck ACC patients treated with PBT (28). Although a higher LC rate was achieved in PBT, the incidence of radio-induced toxicities was still high. The incidence rates of severe acute and late toxicities were 6.3–26 and 4–13%, respectively (25–28).

In addition to PBT, CIRT is a high LET beam and has a higher RBE compared with proton and photon beams. In the COSMIC study, Jensen et al. investigated the efficacy and safety of IMRT combined with a CIRT boost for salivary malignancies. With a median follow-up of 42 months, the 3-year LC in ACC patients was 81.9% (29). In another study by the same researchers, Jensen et al. also compared the outcomes of IMRT and IMRT combined with a CIRT boost (30). This study included 95 inoperable or subtotal resection head and neck ACC patients. This study showed that the LC and OS rates were significantly higher in the CIRT boost group than in photon group (the 10-year LC and OS rates were 42.2 and 44.2% in the CIRT boost group and 32 and 19.6% in the IMRT alone group) (30). Another study included 309 head and neck ACC patients treated with IMRT and a CIRT boost, of whom 61% had T4 disease. The overall 3-year LC and OS rates were 83.7 and 88.9%, respectively (31). However, the 3-year LC and OS rates for T4 patients were 75.9–89.6% and 38.6–72.5%. This study also revealed that T classifications were significant prognostic factors for LC (31). More recently, a retrospective study that included 227 SNACC patients treated with IMRT combined with a CIRT boost reported 3-year LC and OS rates of 82 and 79% for patients who had received surgery before PBRT, and 79 and 64% for patients who did not receive surgery (32). This study also showed that patients with T4 disease had a significantly poorer LC rate (32). A retrospective study of CIRT alone with the largest number of head and neck ACC patients analyzed 289 eligible patients, including 122 with SNACC, reported 2-year OS and PFS rates of 94 and 68% (8). In this study, 41 patients (15%) had local recurrence. Both multivariate and univariate analysis suggested that a large GTV and T4 disease were associated with lower LC, OS, and PFS (8). In our study, 76.3% of patients suffered T4 disease and gross tumor was present in 84.2% patients. Although no significant difference was found, the 3-year LC and OS rates of patients with T4 disease (86.9 and 95.7%) were lower than that of T1-3 patients (LC and OS rates were both 100%). These observations were consistent with previous research. While there were many adverse prognostic factors present in these patients, our study still produced promising outcomes, the 3-year OS, PFS, LC, and DMF rates being 96.7, 80.6, 90.0, and 88.7%.

PBRT provides precise dose distribution to tumor volumes while sparing OARs. Studies report acute grade 2 toxicities, such as dermatitis, mucositis, and dysphagia occur in 27–62% of patients and the incidence rate of acute grade 3 dermatitis or mucositis was 6.3–26% after PBT (25–28). PBT-induced severe (grade 3 or 4) late toxicities (osteoradionecrosis, otologic, or ocular toxicities) occur in 4–13% of patients (27, 28). However, the incidence rate of brain injury induced by PBT in patients with skull base invasion is as high as 56.5%. Of these patients, 43.5% had a grade 3 brain injury (27). In a study using bimodal treatment (a combination of IMRT and CIRT), German researchers reported that the incidence rate of acute grade 3 toxicities, such as dermatitis, mucositis, dysphagia, or conjunctivitis, was between 4 and 42%, and severe late toxicities were reported in 2–17% of patients (29–32). The incidence rates of central neural system necrosis or cranial paralysis were reported at 2–6% (30, 31). In the above-mentioned study of CIRT alone for head and neck ACC treatment, Sulaiman et al. described acute grade 3 mucositis, grade 3 dermatitis, and late grade 3 or above toxicities (including osteoradionecrosis, visual impairment, brain injury, hemorrhage, and mucositis) occurring in 29, 3.8, and 15% of patients, respectively (8). In our study, no patients suffered acute toxicities of grade 3 or above. The incidence rates of grade 2 dermatitis, mucositis, and xerostomia were 2.6, 39.5, and 7.9%, respectively. Severe late toxicities occurred in three patients. One patient with orbital invasion who received CIRT re-irradiation developed grade 3 vision impairment. Another patient suffered grade 3 xerostomia. One patient with recurrent T4 maxillary sinus ACC developed grade 5 hemorrhage at 10 months after completing CIRT re-irradiation.

As head and neck ACC is insensitive to systemic therapy, distant metastasis remains a major problem; recent studies have found that the distant failure rate ranges between 30 and 55% (8, 25–32). Moreover, previous research has shown a significant linear correlation between distant metastasis and OS. In our cohort, the DM rate was 5.3%; however, this incidence rate may have been underestimated due to insufficient follow-up time. We also failed to find a correlation between DM and survival rates, which may be attributable to the short follow-up time and our small sample size. The latest ACCEPT trial found that the combination of cetuximab and IMRT with a CIRT boost was a feasible approach for head and neck ACC treatment. Long-term follow-up to verify the benefit in survivals is underway (33).

Two limitations of this study need to be discussed, the major one being its retrospective nature. However, due to the rarity of SNACC, this disease is predominantly investigated in retrospective studies, case reports, or single-center experiences. Secondly, we had tried to use COX regression model or competing risk model, but the sample size and number of events were too small for prognostic factor analyses. Additionally, as SNACC is a slow-growing tumor, the median follow-up time of 27.2 months was relatively short. Therefore, a longer follow-up time is needed.

CONCLUSION

Our results showed that PBRT is an effective and safe treatment option for SNACC. The 3-year OS, PFS, LC, RC, and DMC rates were 96.7, 80.6, 90.0, 100, and 88.7%, respectively. The toxicities related to PBRT were infrequent and mild. No severe acute toxicities were observed, but three patients developed severe late toxicities. Longer follow-up is needed to verify the long-term benefit of PBRT for patients with SNACC.

DATA AVAILABILITY STATEMENT

The raw data supporting the conclusions of this article will be made available by the authors, without undue reservation.

ETHICS STATEMENT

The studies involving human participants were reviewed and approved by institutional review board (IRB) of Shanghai Proton and Heavy Ion Center with a waiver of informed consent (IRB No. 200220EXP-02).

AUTHOR CONTRIBUTIONS

LK, JL, and WH: conception, design and final approval. WH, JH, QH, XQ, and JY: acquisition and assembly of data. WH, JH, and JG: date analysis and interpretation. WH, JH, LK, and JL: drafting or revising the article. LK: funding acquisition. All authors contributed to the article and approved the submitted version.

FUNDING

This study was supported by Science and Technology Commission of Shanghai Municipality (Project No. 19411951000).

REFERENCES

1. Amit M, Binenbaum Y, Sharma K, Ramer N, Ramer I, Agbetoba A, et al. Adenoid cystic carcinoma of the nasal cavity and paranasal sinuses: a meta-analysis. *J Neurol Surg B Skull Base*. (2013) 74:118–25. doi: 10.1055/s-0033-1347358
2. Lupinetti AD, Roberts DB, Williams MD, Kupferman ME, Rosenthal DI, Demonte F, et al. Sinonasal adenoid cystic carcinoma: the M. D Anderson Cancer Center experience. *Cancer*. (2007) 110:2726–31. doi: 10.1002/cncr.23096
3. Ellington CL, Goodman M, Kono SA, Grist W, Wadsworth T, Chen AY, et al. Adenoid cystic carcinoma of the head and neck: incidence and survival trends based on 1973-2007 surveillance, epidemiology, and end results data. *Cancer*. (2012) 118:4444–51. doi: 10.1002/cncr.27408
4. Chen AM, Bucci MK, Weinberg V, Garcia J, Quivey JM, Schechter NR, et al. Adenoid cystic carcinoma of the head and neck treated by surgery with or without postoperative radiation therapy: prognostic features of recurrence. *Int J Radiat Oncol Biol Phys*. (2006) 66:152–9. doi: 10.1016/j.ijrobp.2006.04.014
5. Stewart JG, Jackson AW, Chew MK. The role of radiotherapy in the management of malignant tumors of the salivary glands. *Am J Roentgenol Radium Ther Nucl Med*. (1968) 102:100–8. doi: 10.2214/ajr.102.1.100
6. Unsal AA, Chung SY, Zhou AH, Baredes S, Eloy JA. Sinonasal adenoid cystic carcinoma: a population-based analysis of 694 cases. *Int Forum Allergy Rhinol*. (2017) 7:312–20. doi: 10.1002/alr.21875
7. Durante M, Orecchia R, Loeffler JS. Charged-particle therapy in cancer: clinical uses and future perspectives. *Nat Rev Clin Oncol*. (2017) 14:483–95. doi: 10.1038/nrclinonc.2017.30
8. Sulaiman NS, Demizu Y, Koto M, Saitoh JI, Suefuji H, Tsuji H, et al. Multicenter study of carbon-ion radiation therapy for adenoid cystic carcinoma of the head and neck: subanalysis of the Japan Carbon-Ion Radiation Oncology Study Group (J-CROS) Study (1402 HN). *Int J Radiat Oncol Biol Phys*. (2018) 100:639–46. doi: 10.1016/j.ijrobp.2017.11.010
9. Emami B, Lyman J, Brown A, Coia L, Goitein M, Munzenrider JE, et al. Tolerance of normal tissue to therapeutic irradiation. *Int J Radiat Oncol Biol Phys*. (1991) 21:109–22. doi: 10.1016/0360-3016(91)90171-y
10. Koto M. Skull base and upper cervical spine tumors. In: Karasawa K, editor. *Carbon-Ion Radiotherapy*. Tokyo: Springer (2014). p. 155–61.
11. Rhee CS, Won TB, Lee CH, Min YG, Sung MW, Kim KH, et al. Adenoid cystic carcinoma of the sinonasal tract: treatment results. *Laryngoscope*. (2006) 116:982–6. doi: 10.1097/01.mlg.0000216900.03188.48
12. Sanghvi S, Patel NR, Patel CR, Kalyoussef E, Baredes S, Eloy JA. Sinonasal adenoid cystic carcinoma: comprehensive analysis of incidence and survival from 1973 to 2009. *Laryngoscope*. (2013) 123:1592–7. doi: 10.1002/lary.24085
13. Laramore GE, Krall JM, Griffin TW, Duncan W, Richter MP, Saroja KR, et al. Neutron versus photon irradiation for unresectable salivary gland tumors: final report of an RTOG-MRC randomized clinical trial. *Int J Radiat Oncol Biol Phys*. (1993) 27:235–40. doi: 10.1016/0360-3016(93)90233-l
14. Huber PE, Debus J, Latz D, Zierhut D, Bischof M, Wannenmacher M, et al. Radiotherapy for advanced adenoid cystic carcinoma: neutrons, photons or mixed beam? *Radiother Oncol*. (2001) 59:161–7. doi: 10.1016/s0167-8140(00)00273-5
15. Licitra L, Cavina R, Grandi C, Palma SD, Guzzo M, Demicheli R, et al. Cisplatin, doxorubicin and cyclophosphamide in advanced salivary gland carcinoma. A phase II trial of 22 patients. *Ann Oncol*. (1996) 7:640–2. doi: 10.1093/oxfordjournals.annonc.a010684
16. Hotte SJ, Winquist EW, Lamont E, MacKenzie M, Vokes E, Chen EX, et al. Imatinib mesylate in patients with adenoid cystic cancers of the salivary glands expressing c-kit: a Princess Margaret Hospital phase II consortium study. *J Clin Oncol*. (2005) 23:585–90. doi: 10.1200/JCO.2005.06.125
17. Gilbert J, Li Y, Pinto HA, Jennings T, Kies MS, Silverman P, et al. Phase II trial of taxol in salivary gland malignancies (E1394): a trial of the Eastern Cooperative Oncology Group. *Head Neck*. (2006) 28:197–204. doi: 10.1002/hed.20327
18. van Herpen CM, Locati LD, Buter J, Thomas J, Bogaerts J, Lacombe D, et al. Phase II study on gemcitabine in recurrent and/or metastatic adenoid cystic carcinoma of the head and neck (EORTC 24982). *Eur J Cancer*. (2008) 44:2542–5. doi: 10.1016/j.ejca.2008.08.014
19. Locati LD, Bossi P, Perrone F, Potepan P, Crippa F, Mariani L, et al. Cetuximab in recurrent and/or metastatic salivary gland carcinomas: A phase II study. *Oral Oncol*. (2009) 45:574–8. doi: 10.1016/j.oraloncology.2008.07.010
20. Laurie SA, Ho AL, Fury MG, Sherman E, Pfister DG. Systemic therapy in the management of metastatic or locally recurrent adenoid cystic carcinoma of the salivary glands: a systematic review. *Lancet Oncol*. (2011) 12:815–24. doi: 10.1016/S1470-2045(10)70245-X
21. Papaspyrou G, Hoch S, Rinaldo A, Rodrigo JP, Takes RP, van Herpen C, et al. Chemotherapy and targeted therapy in adenoid cystic carcinoma of the head and neck: a review. *Head Neck*. (2011) 33:905–11. doi: 10.1002/hed.21458
22. Jakob JA, Kies MS, Glisson BS, Kupferman ME, Liu DD, Lee JJ, et al. Phase II study of gefitinib in patients with advanced salivary gland cancers. *Head Neck*. (2015) 37:644–9. doi: 10.1002/hed.23647
23. Mendenhall WM, Morris CG, Amdur RJ, Werning JW, Hinerman RW, Villaret DB. Radiotherapy alone or combined with surgery for adenoid cystic carcinoma of the head and neck. *Head Neck*. (2004) 26:154–62. doi: 10.1002/hed.10380
24. Ali S, Palmer FL, Katabi N, Lee N, Shah JP, Patel SG, et al. Long-term local control rates of patients with adenoid cystic carcinoma of the head and neck managed by surgery and postoperative radiation. *Laryngoscope*. (2017) 127:2265–9. doi: 10.1002/lary.26565
25. Dautruche A, Bolle S, Feuvret L, Le Tourneau C, Jouffroy T, Goudjil F, et al. Three-year results after radiotherapy for locally advanced sinonasal adenoid cystic carcinoma, using highly conformational radiotherapy techniques proton therapy and/or Tomotherapy. *Cancer Radiother*. (2018) 22:411–6. doi: 10.1016/j.canrad.2017.11.015

26. Holliday E, Bhattasali O, Kies MS, Hanna E, Garden AS, Rosenthal DI, et al. Postoperative Intensity-Modulated Proton Therapy for Head and Neck Adenoid Cystic Carcinoma. *Int J Part Ther*. (2016) 2:533–43. doi: 10.14338/IJPT-15-00032.1
27. Pommier P, Liebsch NJ, Deschler DG, Lin DT, McIntyre JF, Barker FG II, et al. Proton beam radiation therapy for skull base adenoid cystic carcinoma. *Arch Otolaryngol Head Neck Surg*. (2006) 132:1242–9. doi: 10.1001/archotol.132.11.1242
28. Linton OR, Moore MG, Brigance JS, Summerlin DJ, McDonald MW. Proton therapy for head and neck adenoid cystic carcinoma: initial clinical outcomes. *Head Neck*. (2015) 37:117–24. doi: 10.1002/hed.23573
29. Jensen AD, Nikoghosyan AV, Lossner K, Haberer T, Jakel O, Munter MW, et al. COSMIC: A Regimen of Intensity Modulated Radiation Therapy Plus Dose-Escalated, Raster-Scanned Carbon Ion Boost for Malignant Salivary Gland Tumors: Results of the Prospective Phase 2 Trial. *Int J Radiat Oncol Biol Phys*. (2015) 93:37–46. doi: 10.1016/j.ijrobp.2015.05.013
30. Jensen AD, Nikoghosyan AV, Poulakis M, Hoss A, Haberer T, Jakel O, et al. Combined intensity-modulated radiotherapy plus raster-scanned carbon ion boost for advanced adenoid cystic carcinoma of the head and neck results in superior locoregional control and overall survival. *Cancer*. (2015) 121:3001–9. doi: 10.1002/cncr.29443
31. Jensen AD, Poulakis M, Nikoghosyan AV, Welzel T, Uhl M, Federspil PA, et al. High-LET radiotherapy for adenoid cystic carcinoma of the head and neck: 15 years' experience with raster-scanned carbon ion therapy. *Radiother Oncol*. (2016) 118:272–80. doi: 10.1016/j.radonc.2015.05.010
32. Akbaba S, Ahmed D, Mock A, Held T, Bahadir S, Lang K, et al. Treatment outcome of 227 patients with sinonasal adenoid cystic carcinoma (ACC) after intensity modulated radiotherapy and active raster-scanning carbon ion boost: a 10-year single-center experience. *Cancers*. (2019) 11:11. doi: 10.3390/cancers11111705
33. Adeberg S, Akbaba S, Lang K, Held T, Verma V, Nikoghosyan A, et al. The Phase 1/2 ACCEPT trial: concurrent cetuximab and intensity modulated radiation therapy with carbon ion boost for adenoid cystic carcinoma of the head and neck. *Int J Radiat Oncol Biol Phys*. (2020) 106:167–73. doi: 10.1016/j.ijrobp.2019.09.036

Conflict of Interest: The authors declare that the research was conducted in the absence of any commercial or financial relationships that could be construed as a potential conflict of interest.

Copyright © 2020 Hu, Hu, Huang, Gao, Yang, Qiu, Kong and Lu. This is an open-access article distributed under the terms of the Creative Commons Attribution License (CC BY). The use, distribution or reproduction in other forums is permitted, provided the original author(s) and the copyright owner(s) are credited and that the original publication in this journal is cited, in accordance with accepted academic practice. No use, distribution or reproduction is permitted which does not comply with these terms.

frontiers in Oncology

ORIGINAL RESEARCH
published: 19 November 2020
doi: 10.3389/fonc.2020.597702

Biological Guided Carbon-Ion Microporous Radiation to Tumor Hypoxia Area Triggers Robust Abscopal Effects as Open Field Radiation

Qingting Huang[1,2,3†], Yun Sun[3,4†], Weiwei Wang[3,5], Lien-Chun Lin[3,5], Yangle Huang[2], Jing Yang[1,3], Xiaodong Wu[3,5], Lin Kong[2,3] and Jiade Jay Lu[1,3*]*

[1] Department of Radiation Oncology, Shanghai Proton and Heavy Ion Center, Shanghai, China, [2] Department of Radiation Oncology, Shanghai Proton and Heavy Ion Center, Fudan University Cancer Hospital, Shanghai, China, [3] Shanghai Engineering Research Center of Proton and Heavy Ion Radiation Therapy, Shanghai, China, [4] Department of Research and Development, Shanghai Proton and Heavy Ion Center, Shanghai, China, [5] Department of Medical Physics, Shanghai Proton and Heavy Ion Center, Shanghai, China

Recently, a growing number of studies focus on partial tumor irradiation to induce the stronger non-target effects. However, the value of partial volume carbon ion radiotherapy (CIRT) targeting hypoxic region of a tumor under imaging guidance as well as its effect of inducing radiation induced abscopal effects (RIAEs) have not been well investigated. Herein, we developed a technique of carbon ion microporous radiation (CI-MPR), guided by ^{18}F-FMISO PET/computerized tomography (CT), for partial volume radiation targeting the hypoxia area of a tumor and investigated its capability of inducing abscopal effects. Tumor-bearing mice were inoculated subcutaneously with breast cancer 4T1 cells into the flanks of both hind legs of mouse. Mice were assigned to three groups: group I: control group with no treatment; group II: carbon ion open field radiation (CI-OFR group) targeting the entire tumor; group III: partial volume carbon ion microporous radiation (CI-MPR group) targeting the hypoxia region. The tumors on the left hind legs of mice were irradiated with single fraction of 20 Gy of CIRT. Mice treated with CI-MPR or CI-OFR showed that significant growth delay on both the irradiated and unirradiated of tumor as compared to the control groups. Tumor regression of left tumor irradiated with CI-OFR was more prominent as compared to the tumor treated with CI-MPR, while the regression of the unirradiated tumor in both CI-MPR and CI-OFR group was similar. Biological-guided CIRT using the newly developed microporous technique targeting tumor hypoxia region could induce robust abscopal effects similar to CIRT covering the entire tumor.

Keywords: carbon ion, microporous radiation, hypoxia, ^{18}F-FMISO PET/computerized tomography, abscopal effect

OPEN ACCESS

Edited by:
Daniel Michael Trifiletti, Mayo Clinic Florida, United States

Reviewed by:
Kenji Hirata, Hokkaido University, Japan
John G. Eley, Vanderbilt University, United States

***Correspondence:**
Jiade Jay Lu
jiade.lu@sphic.org.cn
Lin Kong
lin.kong@sphic.org.cn

†These authors have contributed equally to this work

Specialty section:
This article was submitted to Radiation Oncology, a section of the journal Frontiers in Oncology

Received: *21 August 2020*
Accepted: *19 October 2020*
Published: *19 November 2020*

Citation:
Huang Q, Sun Y, Wang W, Lin L-C, Huang Y, Yang J, Wu X, Kong L and Lu JJ (2020) Biological Guided Carbon-Ion Microporous Radiation to Tumor Hypoxia Area Triggers Robust Abscopal Effects as Open Field Radiation. Front. Oncol. 10:597702. doi: 10.3389/fonc.2020.597702

INTRODUCTION

The therapeutic effects of ionizing radiation are often limited by the hypoxia of tumors (1–4). Hypoxia plays important role in radiation resistance, angiogenesis, and metastatic potential (5). Various strategies include the combined use of chemotherapy or agents that directly target the hypoxic cells to increase the radiosensitivity with radiotherapy. However, local failure due to insufficient response to combined treatment modality, remains a major mode of treatment failure (6–9).

Recently, the results of a growing number of *in vitro* and *in vivo* studies indicate that, in addition to the local therapeutic effects, radiation therapy may be in favor of changing the tumor microenvironments correlated with immunity and endothelial cells of the tumor micro-vasculatures, thereby inducing the non-target effects, such as radiation induced bystander effects and abscopal effects (RIAEs) (10–13). RIAEs are radiation induced effects in unirradiated tumors distant from irradiated target regresses. Both pre-clinical and clinical studies have confirmed the existence of abscopal effects and its potential antitumor effects (14–16). Furthermore, Tubin *et al.* demonstrated that the exposure of lung cancer cells to hypoxia and irradiation of hypoxic cells triggered significant RIAEs (17). Additionally, the hypothesis of targeting the hypoxic area of the tumor with a high dose photon-based radiation in attempts to induce an intentional RIAEs in oligometastatic patients was tested (18–20), indicating that the hypoxic area in tumor may be a critical factor contributing to RIAEs from radiation. Massaccesi *et al.* also adopted the technique of high single-dose partial irradiation targeting the hypoxic tumor segment for patients with recurrent bulky lesions, and demonstrated anti-tumor efficacy in their initial clinical results (21). However, the mechanisms through which irradiation exerts its immune modulation effects, are not well clarified.

Based on these preliminary investigations, a growing number of studies focus on partial tumor irradiation with high-dose hypofractionation or single high dose schedule, with an aim to potentially increase the therapeutic efficacy for bulky tumors (14, 15). Of all types of ionizing radiation beams, carbon ion beams are featured with Bragg peak as it has higher linear energy transfer (LET) and relative biological effectiveness (RBE), compared to those of photon and proton (22). Ionization radiation beams of higher LET have been shown to induce more complex DNA damage, despite reportedly more effective in eradicating tumor cells under hypoxic environment, as compared to those with lower LET (23–27). Theoretically, the physical and biological advantages of carbon ion radiation therapy (CIRT) make it more appropriate in the management of bulky or radio-resistant tumors (28–30). Results of pre-clinical or retrospective studies have confirmed its advantages in tumor proliferation and metastasis over photon (31–33). Nevertheless, the value of partial volume CIRT targeting hypoxic region(s) of a tumor under imaging guidance, as well as its effect of inducing RIAEs, have not been well investigated.

^{18}F-Fluoromisonidazole (^{18}F-FMISO) as hypoxia PET imaging probe has commonly been applied for hypoxic imaging in clinic, and will occur redox reactions under the action of xanthine oxidase and stably combine with some cellular components, thereby reflecting the degree of hypoxia in solid tumors (34, 35). Herein, we developed a type of microporous radiation technique of CIRT (CI-MPR), guided by ^{18}F-FMISO PET/computerized tomography (CT), for partial volume radiation targeting the hypoxia area of a tumor and investigated its capability of inducing abscopal effects. This study provides the basis for further investigations for exploring the underlying mechanisms of immune modulating effect induced by CIRT.

MATERIAL AND METHODS

Cell Line

The mammary carcinoma cell line 4T1 (closely mimic stage IV human breast cancer) was obtained from the American Type Culture Collection (ATCC). The cells were cultured in Dulbecco modified Eagle medium (DMEM) with 10% fetal bovine serum (FBS) at 37°C in a humidified atmosphere of 5% CO2.

Animal Experiments

All animal experimental protocols and procedures were approved by the ethics committee of the SPHIC. Four-to-five-week-old and female BALB/c mice were purchased from Shanghai SLAC Laboratory Animal Company and required to acclimate for a week before experiment. The mice were maintained in the specific pathogen free (SPF) environment.

For experiments in which tumor-bearing mice were used, mice were inoculated subcutaneously with $1*10^6$ 4T1 cells into the flanks of both hind legs of mouse for initiating tumor. Tumors were allowed to grow to an area of 7*7 mm before irradiation and systematized within 10% differences in the intra- and inter-tumor volumes. Tumor volume was calculated with the following formula: $L \times W^2 \times 0.52$ (L was the longest diameter and W was orthogonal to L). The volume was measured every other day after radiation until tumor size reached 10% of the mouse's body weight. Tumor volume at each time point (Vt) was normalized to the initial volume (V0), and the fold change in tumor volume was calculated.

^{18}F-Fluoromisonidazole Micro-PET/Computerized Tomography Imaging and Quantitative Analysis

^{18}F-FMISO was produced using a modified Explora FDG4 module (Siemens) at SPHIC. For evaluation of the hypoxia status of tumors, micro-PET/CT (Inveon Siemens) scanning was performed on the day before irradiation treatment with an injection of 5.55 MBq (150 μCi) of ^{18}F-FMISO through the tail vein (**Figure 1**). ^{18}F-FMISO was injected 4 h before the scan (36). Isoflurane was utilized 10 minutes before the scan, and mice were kept under anesthesia during the period of scan. The images were reconstructed with a three dimensional ordered-subset expectation maximization (OSEM3D)/maximum algorithm. The region of interest (ROI) was manually delineated to cover the entire tumor on fused images for data analysis. A similar circular ROI was drawn on the muscle of the opposite hind leg of

the mouse on fused images. In order to evaluate the uptake of ^{18}F-FMISO in tumors, the maximum standardized uptake value (SUVmax) was calculated by measuring the maximal concentration of radioactivity in ROI. The tumor tissue SUVmax (T), the contralateral normal muscle SUVmax (N), and the ratio of the two values (T/N) were calculated.

Treatment Planning and Delivery of Carbon Ion Radiotherapy

Mice were assigned to three groups based on randomized experimental designs (37): group I: control group with no treatment; group II: CIRT with open field (CI-OFR group) targeting the whole tumor; group III: partial volume carbon ion microporous radiation (CI-MPR group) targeting hypoxia region. Each group had eight mice. The tumors on left hind legs of mice were irradiated using partial volume CI-MPR or CI-OFT using 20 Gy (physical dose) in a single fraction.

Mice were anesthetized and immobilized on poly(methyl methacrylate) (PMMA) plates. An EBT3 film was attached on plates, opposite to mice side, so that the mice positioning could be monitored by checking the film response after irradiation (**Supplementary Figure 1A**). Then the mouse was placed on a box chamber, where two hind legs of the mouse were perpendicular to the beam axis. To secure precise irradiation of the tumor hypoxia area, we developed a microporous radiation system using a block with a pore in the center (**Supplementary Figure 1B**). The rectangular block 1 with a hole in the center made of aluminum was manufactured for the CI-MPR group. The dimensions of the block were 70.0 mm * 70.0 mm * 20.0 mm, and diameter of hole was 1.5 mm in the center (**Supplementary Figure 1B**). Tuned carbon-ion beams penetrate the target with a relative dose of 35%. The dose profile presented in **Figure 2A** shows that the off-axis distance of the point radiation was 2 mm (full width at half maximum, FWHM). We named this technique carbon ion microporous radiation (CI-MPR). Another block 2 with a gap for the open-field irradiation group, was positioned as close as possible to the mouse. The dimension of the block 2 for open-field radiation group was 120.0 mm * 80.0 mm * 20.0 mm, and the left gap (40.0 mm * 30.0 mm) was left to expose the irradiation targets (**Supplementary Figure 1C**). The dose profile of the open field carbon-ion radiation (CI-OFR) used in the study was shown in **Figure 2C**, and the off-axis distance was 30 mm (FWHM). A horizontal beam was used to protrude through the hole or gap of the block and was adjusted to the isocenter of tumor of the left hind leg by the longitudinal and sagittal laser (see **Supplementary Figures 1B, C**).

CIRT treatment plans were generated in the Syngo (Version 13B, Siemens, Erlangen, Germany) treatment planning system (TPS). The modulated carbon-ion treatment plan had a circular field with a lateral diameter of 20.0 mm. The planned modulation width was 17.0 mm, the planned beam range was 20.0 mm. The prescribed dose to the spread-out Bragg-peak (SOBP) was 20 Gy (physical dose). The output factor of block 1 was calculated with the beam model, and dose profiles of CI-MPR and CI-OFR group were shown in **Figures 2A, C**. Since the plan was designed

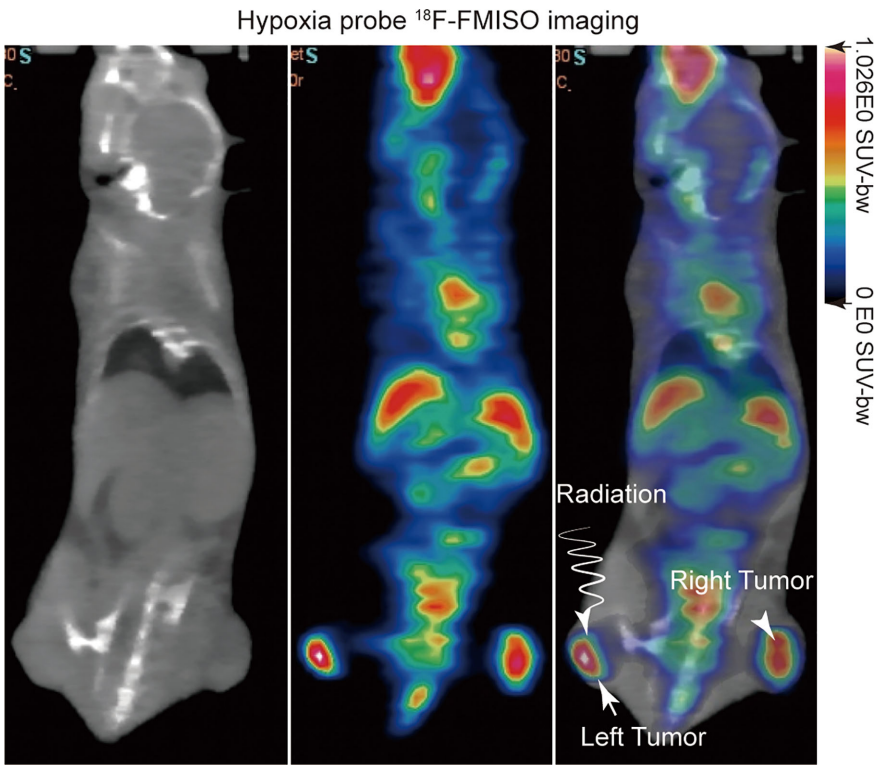

FIGURE 1 | ^{18}F-FMISO PET/computerized tomography (CT) imaging was performed before irradiation treatment for evaluating the hypoxia status of tumors.

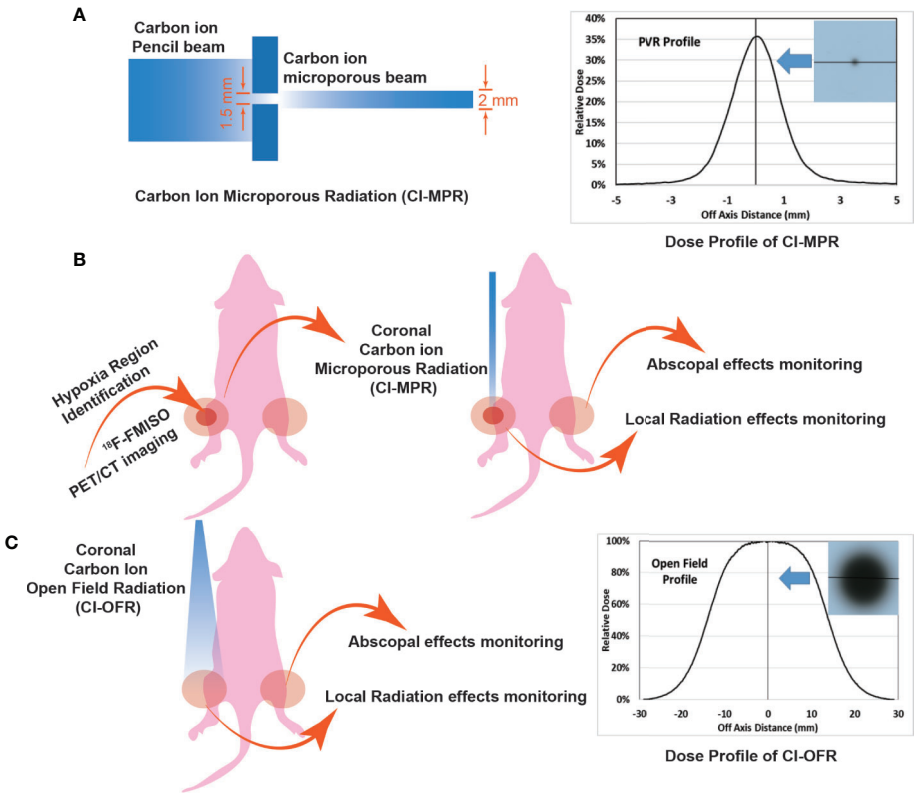

FIGURE 2 | Mouse irradiation and dose profile. **(A, B)** The radiation area and dose profile of carbon ion microporous radiation (CI-MPR) group. **(C)** The radiation area and dose profile of carbon ion open field radiation (CI-OFR) group.

to treat superficial targets, a PMMA range shifter was used to better the superficial dose distribution. The energies of the carbon beams used were from 116.48 to 141.7 MeV/u, with the corresponding dose averaged LET between 350.07 and 368.82 KeV/μm within the targets.

Statistical Analysis

The fold change differences of tumor volume on irradiated and unirradiated tumors during the period of observation and on day 15 between the control group and the other two groups were analyzed by two-way ANOVA and two-tailed unpaired Student's t test, respectively. P values of <0.05 were considered statistically significant.

RESULTS

^{18}F-FMISO Micro-PET/Computerized Tomography Imaging

To visualize the tumor hypoxia area, the positron emitted probe ^{18}F-FMISO was injected intravenously into a mouse *via* tail vein with a dose of 150 μCi. ^{18}F-FMISO PET/CT imaging was performed on tumor-bearing mice before radiation treatment. Typical images are shown in **Figure 1**. The probes were mainly distributed in the center of the tumor, which depicts the hypoxic area of the tumor clearly in the left and right hind leg of mice, with a T/N value of 1.4.

Carbon-Ion Microporous Radiation

To secure precise irradiation of the tumor hypoxia area, we developed a microporous radiation system called carbon ion microporous radiation (CI-MPR) using a block with a pore in the center with a diameter of 1.5 mm (**Supplementary Figure 1B**). To further protect the area from unnecessary irradiation, we maximized the block size to cover entire body of mouse except for the CIRT field (**Supplementary Figures 1B, C**).

Moreover, to further maintain radiation accuracy, a piece of EBT3 film was attached on plates, opposite to where the mouse is located, so that the positioning of the mice could be verified by the film response after irradiation. **Figure 3A** showed that the reaction on EBT3 film occurred only in the irradiated area in a case of CI-OFR and CI-MPR group. The outline of irradiated tumor and the left leg could be clearly seen in the CI-OFR group, while in the CI-MPR group, one vertex after irradiation on the EBT3 film, indicating that our radiation technology is feasible and reliable for both CI-MPR and CI-OFR.

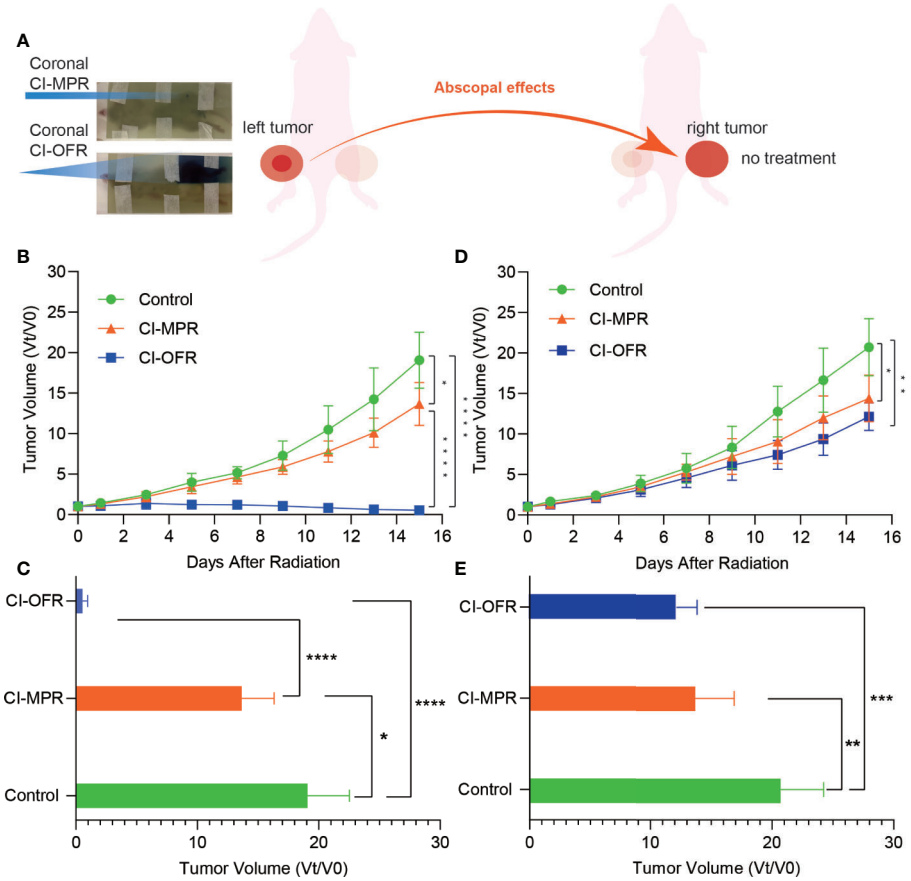

FIGURE 3 | The response after irradiation on EBT3 film and evaluation of tumor volume change of the irradiated and unirradiated tumors. **(A)** The response and one vertex of irradiation could be noted in carbon ion open field radiation (CI-OFR) and carbon ion microporous radiation (CI-MPR) group on the EBT3 film, respectively. **(B)** Tumor volume change on left side (irradiated) during the observation, and p <0.05 and 0.0001 are indicated by * and ****. **(C)** Tumor volume change on right side (unirradiated) during observation, and p <0.05 and 0.01 are indicated by * and **. **(D)** Quantitative analysis of irradiated tumor (left side) volume change on day 15. **(E)** Quantitative analysis of unirradiated tumor (right side) volume change on day 15. Each bar represents the standard error, and p <0.05, 0.01, 0.001, 0.0001 are indicated by *, **, ***, ****.

In Vivo Abscopal Effects After Carbon Ion Microporous Radiation and Carbon Ion Open Field Radiation

To compare the antitumor immune response to both CI-MPR and CI-OFR for primary and distant tumors, we first established an animal tumor model on both hind legs. When the tumor grew to approximately 7mm x 7mm, the tumor on the left hind leg was irradiated by CI-MPR or CI-OFR. The process of CIRT was shown in **Figure 2**.

The growth of the irradiated tumor (on the left hind leg) and the unirradiated tumor (on the right hind leg), as well as the fold changes of the tumor volumes during the observation and on day 15, were shown in **Figure 3**.

Tumors on both legs of the mice in the control group showed rapid growth as compared to the mice treated with CI-MPR or CI-OFR. Mice treated with CI-MPR or CI-OFR showed that significant growth delay on both the left side (irradiated) and right side (unirradiated) of tumor as compared to the control groups, indicating the direct and abscopal anti-tumor effects of carbon ion beams. Tumor regression of left-sided tumor irradiated with CI-OFR was more prominent as compared to the tumor treated with CI-MPR, and the fold change of the tumor volumes on day 15 in CI-MPR was 25.3 times that of CI-OFR group ($P<0.05$), demonstrating CI-OFR provided higher local radiation effects than CI-MPR. However, regression of the unirradiated tumor on the right side in both CI-MPR and CI-OFR group was similar, and the fold change of the tumor volumes on day 15 in CI-MPR was 1.1 times that of CI-OFR group ($P>0.05$), indicating that CI-MPR provided similar abscopal effects as CI-OFR. This phenomenon demonstrated that microporous CIRT with a diameter of 1.5 mm targeting the hypoxic area could achieve similar abscopal effects as open field irradiation.

DISCUSSION

This present study evaluated the anti-tumor effects triggered by carbon ion microporous radiation targeting hypoxic area with a

single high dose on murine tumor model as compared to the conventional open-field tumor technique. The hypoxic area was visualized by ^{18}F-FMISO Micro-PET/CT imaging, and the feasibility of the microporous irradiation technique was verified by the EBT3 film and an *in vivo* tumor model. Our study revealed two major new observations: CIRT could induce prominent abscopal effects *in vivo*, and more interestingly, CIRT using our microporous radiation technology could induce abscopal effects similar to CIRT open-field.

To the best of our knowledge, we presented the first *in vivo* evidence of anti-tumor effect of carbon ion microporous irradiation targeting tumor hypoxic area and explored its potential significance, with similar results reported in photon (17, 18, 38). Tubin *et al*. demonstrated that irradiation for hypoxic tumor cells induced higher RIAE compared to the normoxic cells in their preclinical research. Tubin *et al*. and Massaccesi *et al*. also adopted a radiation technique targeting the hypoxic segment of the tumor exclusively with single high dose as palliative treatment in oligometastatic cases or patients with previously irradiated recurrent bulky solid lesions. The researchers observed regression of the irradiated lesions as well as metastatic lesions (unirradiated) after treatment, thereby proving the anti-tumor effect and its validity through this strategy. The authors speculated that targeting the hypoxic region with ionizing radiation may release certain abscopal signals to activate the immune system in comparison with the normoxic region, thus triggering regression of irradiated and unirradiated tumor. As carbon ion beams possess higher RBE and induce more complex DNA damage (70% in the form of double bond break) as compared to photon (23), results of preclinical study have shown that carbon ion beams are more effective than photon beams in eradicating hypoxic tumor cells (28). Our study clearly demonstrated clear growth delays of irradiated and unirradiated tumor after CI-MRP targeting the hypoxic area, and we postulate that CIRT targeting hypoxic region of a tumor may lead to RIAEs in a different manner compared to the photon. However, the differences in the magnitude and mechanism between CIRT and photon beam radiation are awaiting to be investigated.

In the clinical setting, the prescribed dose of the conventional open-field RT for bulky tumors is frequently limited by the surrounding organs at risk. Partial volume tumor irradiation, such as GRID or Lattice, has been shown to evoke anti-tumor immune response and is constantly being applied for improving the therapeutic effect as well as side effects (13, 15, 39). In a clinical investigation, Tubin *et al*. compared the therapeutic effect of a stereotactic body radiotherapy group targeting partial tumor hypoxic segment (SBRT-PATHY) and a conventional palliative radiation group targeting the entire volume tumor for the unresectable stage IIIB/IV bulky non-small cell lung cancer (NSCLC) to similar doses. Interestingly, the control of both the irradiated bulky tumor and distant tumor (unirradiated) were significantly improved in the SBRT-PATHY groups, as compared to those in the palliatively irradiated group ($P<0.05$) (20). In our study, we observed that the response of the partially irradiated tumor targeting hypoxia in the CI-MPR group was not as significant as the open-field group. The underlying reason of the different observation described by Tublin *et al*. may be a result of, at least in part, the limited irradiated volume in our study which did not cover the entire hypoxic region of the tumor. Additionally, sufficient signaling mediating bystander effect to the unirradiated normoxic region could not be established (13). However, the similar abscopal effects in both the microporous and open-field group demonstrated in our study indicated that carbon ion targeting the hypoxic region, despite its small volume, is sufficient to generate RIAE in the same magnitude. As hypoxic areas are usually located near the center of the tumors, precision radiation therapy using particle beams targeting hypoxic area, even at a very high dose, usually does not result in unnecessary irradiation to the adjacent OARs, thereby substantially improving its therapeutic ratio.

As this is the first reported study on the partial volume particle beam radiation targeting hypoxic region using carbon ion beam, the observations of our study need to be investigated in other tumor models for its generality and specificity. Additionally, investigations that explore the differences in the magnitude between carbon-ion, proton, and photon beams are necessary. At the Shanghai Proton and Heavy Ion Center (SPHIC), studies using various ionizing beam types to explore the local and abscopal effects of hypoxia-targeting partial volume microporous radiation have been initiated using mouse models of glioma, lung cancer, and sarcoma.

Previous studies about RIAEs, induced by partial volume radiation with photon, demonstrated that partial volume irradiation may retain tumor infiltrating lymphocytes in unirradiated areas of the tumor, which can promote stronger anti-tumor responses (40). Additionally, it is suggested that the abscopal effect of partial volume radiation could be mediated by the immunogenic cell death (ICD) and immunogenic modulation (IM) (14). Immunogenic modulation (IM) triggered by radiation contains the upregulation of release of tumor associated antigen (TAAs), the expression of major histocompatibility complex I molecules (MHC-I), the activation of T cells effectively, and the secretion of chemokine and cytokine, thereby altering the tumor microenvironment (TME) and enhancing the anti-tumor immune system function (41). With ongoing investigations at SPHIC, we expect to further illustrate the mechanisms through which partial volume microporous irradiation with carbon ion exerts its immune modulation effect.

Our study demonstrated that biological-guided CIRT using the newly developed microporous technology, targeting tumor hypoxia region only without encompassing the entire tumor volume, could induce robust abscopal effects similar to CIRT covering the entire tumor. The underlying mechanism requires further investigations using animal modes before translating to clinical application.

DATA AVAILABILITY STATEMENT

The raw data supporting the conclusions of this article will be made available by the authors, without undue reservation.

ETHICS STATEMENT

The animal study was reviewed and approved by Shanghai Proton and Heavy Ion Center Institutional Animal Care and Use Committee.

AUTHOR CONTRIBUTIONS

JL, LK, XW, QH, and YS conceived the study and thoroughly revised the manuscript. QH, WW, LL, YH, and JY acquired and analyzed the data. QH, YS, and JL wrote the manuscript. All authors contributed to the article and approved the submitted version.

FUNDING

This work was mainly supported by the National Key Research and Development Program of China (no. 2018YFC0115700), the Science and Technology Commission of Shanghai Municipality (no.18XD1423000), the Program of Shanghai Technology Research Leader (no.19XD1432900) and the Natural Science Foundation Project of Shanghai Science and Technology Innovation Action Plan (no.20ZR1453400). All funding sources should be provided, including grant numbers if applicable. Please ensure to add all necessary funding information, as after publication this is no longer possible.

ACKNOWLEDGMENTS

We are grateful to Wenhui Lu for her help in the language editing and proofreading of this manuscript.

SUPPLEMENTARY MATERIAL

The Supplementary Material for this article can be found online at: https://www.frontiersin.org/articles/10.3389/fonc.2020.597702/full#supplementary-material

SUPPLEMENTARY FIGURE 1 | Mouse positioning and irradiation device. **(A)** Mice were anesthetized and immobilized on PMMA plates. An EBT3 film piece was attached on plates, opposite to mice side, so that the mice positioning could be monitored by checking the film response after irradiation. **(B)** The dimension of the block 1 for CI-MPR group. **(C)** The dimension of the block 2 for CI-OFR group, and the left gap was left to expose the irradiation targets.

REFERENCES

1. Swinson DE, Jones JL, Richardson D, Wykoff C, Turley H, Pastorek J, et al. Carbonic anhydrase IX expression, a novel surrogate marker of tumor hypoxia, is associated with a poor prognosis in non-small-cell lung cancer. *J Clin Oncol* (2003) 21(3):473–82. doi: 10.1200/JCO.2003.11.132
2. Li Y, Zhang W, Li S, Tu C. Prognosis value of Hypoxia-inducible factor-1alpha expression in patients with bone and soft tissue sarcoma: a meta-analysis. *Springerplus* (2016) 5(1):1370. doi: 10.1186/s40064-016-3064-x
3. Harrison L, Blackwell K. Hypoxia and anemia: factors in decreased sensitivity to radiation therapy and chemotherapy? *Oncologist* (2004) 9(Suppl 5):31–40. doi: 10.1634/theoncologist.9-90005-31
4. Horsman MR, Overgaard J. The impact of hypoxia and its modification of the outcome of radiotherapy. *J Radiat Res* (2016) 57(Suppl 1):i90–i8. doi: 10.1093/jrr/rrw007
5. Jing X, Yang F, Shao C, Wei K, Xie M, Shen H, et al. Role of hypoxia in cancer therapy by regulating the tumor microenvironment. *Mol Cancer* (2019) 18 (1):157. doi: 10.1186/s12943-019-1089-9
6. Wardman P. Chemical radiosensitizers for use in radiotherapy. *Clin Oncol (R Coll Radiol)* (2007) 19(6):397–417. doi: 10.1016/j.clon.2007.03.010
7. Linam J, Yang LX. Recent developments in radiosensitization. *Anticancer Res* (2015) 35(5):2479–85.
8. Dobrowsky W, Huigol NG, Jayatilake RS, Kizilbash NI, Okkan S, Kagiya VT, et al. AK-2123 (Sanazol) as a radiation sensitizer in the treatment of stage III cervical cancer: results of an IAEA multicentre randomised trial. *Radiother Oncol* (2007) 82(1):24–9. doi: 10.1016/j.radonc.2006.11.007
9. Salem A, Asselin MC, Reymen B, Jackson A, Lambin P, West CML, et al. Targeting Hypoxia to Improve Non-Small Cell Lung Cancer Outcome. *J Natl Cancer Inst* (2018) 110(1):djx160. doi: 10.1093/jnci/djx160
10. Asur R, Butterworth KT, Penagaricano JA, Prise KM, Griffin RJ. High dose bystander effects in spatially fractionated radiation therapy. *Cancer Lett* (2015) 356(1):52–7. doi: 10.1016/j.canlet.2013.10.032
11. Song CW, Lee YJ, Griffin RJ, Park I, Koonce NA, Hui S, et al. Indirect Tumor Cell Death After High-Dose Hypofractionated Irradiation: Implications for Stereotactic Body Radiation Therapy and Stereotactic Radiation Surgery. *Int J Radiat Oncol Biol Phys* (2015) 93(1):166–72. doi: 10.1016/j.ijrobp.2015.05.016
12. Nolan MW, Gieger TL, Karakashian AA, Nikolova-Karakashian MN, Posner LP, Roback DM, et al. Outcomes of Spatially Fractionated Radiotherapy (GRID) for Bulky Soft Tissue Sarcomas in a Large Animal Model. *Technol Cancer Res Treat* (2017) 16(3):357–65. doi: 10.1177/1533034617690980
13. Kanagavelu S, Gupta S, Wu X, Philip S, Wattenberg MM, Hodge JW, et al. In vivo effects of lattice radiation therapy on local and distant lung cancer: potential role of immunomodulation. *Radiat Res* (2014) 182(2):149–62. doi: 10.1667/RR3819.1
14. Markovsky E, Budhu S, Samstein RM, Li H, Russell J, Zhang Z, et al. An Antitumor Immune Response Is Evoked by Partial-Volume Single-Dose Radiation in 2 Murine Models. *Int J Radiat Oncol Biol Phys* (2019) 103 (3):697–708. doi: 10.1016/j.ijrobp.2018.10.009
15. Schultke E, Balosso J, Breslin T, Cavaletti G, Djonov V, Esteve F, et al. Microbeam radiation therapy - grid therapy and beyond: a clinical perspective. *Br J Radiol* (2017) 90(1078):20170073. doi: 10.1259/bjr.20170073
16. Amendola BE, Perez NC, Wu X, Amendola MA, Qureshi IZ. Safety and Efficacy of Lattice Radiotherapy in Voluminous Non-small Cell Lung Cancer. *Cureus* (2019) 11(3):e4263. doi: 10.7759/cureus.4263
17. Tubin S, Ahmed MM, Gupta S. Radiation and hypoxia-induced non-targeted effects in normoxic and hypoxic conditions in human lung cancer cells. *Int J Radiat Biol* (2018) 94(3):199–211. doi: 10.1080/09553002.2018.1422085
18. Tubin S, Raunik W. Hunting for abscopal and bystander effects: clinical exploitation of non-targeted effects induced by partial high-single-dose irradiation of the hypoxic tumour segment in oligometastatic patients. *Acta Oncol* (2017) 56(10):1333–9. doi: 10.1080/0284186X.2017.1346385
19. Tubin S, Popper HH, Brcic L. Novel stereotactic body radiation therapy (SBRT)-based partial tumor irradiation targeting hypoxic segment of bulky tumors (SBRT-PATHY): improvement of the radiotherapy outcome by exploiting the bystander and abscopal effects. *Radiat Oncol* (2019) 14(1):21. doi: 10.1186/s13014-019-1227-y
20. Tubin S, Khan MK, Salerno G, Mourad WF, Yan W, Jeremic B. Mono-institutional phase 2 study of innovative Stereotactic Body RadioTherapy targeting PArtial Tumor HYpoxic (SBRT-PATHY) clonogenic cells in unresectable bulky non-small cell lung cancer: profound non-targeted effects by sparing peri-tumoral immune microenvironment. *Radiat Oncol* (2019) 14(1):212. doi: 10.1186/s13014-019-1410-1
21. Dagoglu N, Karaman S, Caglar HB, Oral EN. Abscopal Effect of Radiotherapy in the Immunotherapy Era: Systematic Review of Reported Cases. *Cureus* (2019) 11(2):e4103. doi: 10.7759/cureus.4103

22. Jiang GL. Particle therapy for cancers: a new weapon in radiation therapy. *Front Med* (2012) 6(2):165–72. doi: 10.1007/s11684-012-0196-4
23. Dokic I, Mairani A, Niklas M, Zimmermann F, Chaudhri N, Krunic D, et al. Next generation multi-scale biophysical characterization of high precision cancer particle radiotherapy using clinical proton, helium-, carbon- and oxygen ion beams. *Oncotarget* (2016) 7(35):56676–89. doi: 10.18632/oncotarget.10996
24. Klein C, Dokic I, Mairani A, Mein S, Brons S, Haring P, et al. Overcoming hypoxia-induced tumor radioresistance in non-small cell lung cancer by targeting DNA-dependent protein kinase in combination with carbon ion irradiation. *Radiat Oncol* (2017) 12(1):208. doi: 10.1186/s13014-017-0939-0
25. Valable S, Gerault AN, Lambert G, Leblond MM, Anfray C, Toutain J, et al. Impact of Hypoxia on Carbon Ion Therapy in Glioblastoma Cells: Modulation by LET and Hypoxia-Dependent Genes. *Cancers (Basel)* (2020) 12(8):2019. doi: 10.3390/cancers12082019
26. Furusawa Y, Fukutsu K, Aoki M, Itsukaichi H, Eguchi-Kasai K, Ohara H, et al. Inactivation of aerobic and hypoxic cells from three different cell lines by accelerated (3)He-, (12)C- and (20)Ne-ion beams. *Radiat Res* (2000) 154 (5):485–96. doi: 10.1667/0033-7587(2000)154[0485:ioaahc]2.0.co;2
27. Tinganelli W, Ma NY, Von Neubeck C, Maier A, Schicker C, Kraft-Weyrather W, et al. Influence of acute hypoxia and radiation quality on cell survival. *J Radiat Res* (2013) 54(Suppl 1):i23–30. doi: 10.1093/jrr/rrt065
28. Zhang W, Tanaka M, Sugimoto Y, Takigawa T, Ozaki T. Carbon-ion radiotherapy of spinal osteosarcoma with long-term follow. *Eur Spine J* (2016) 25 Suppl 1:113–7. doi: 10.1007/s00586-015-4202-9
29. Calipel A, Lux AL, Guerin S, Lefaix JL, Laurent C, Bernaudin M, et al. Differential Radiosensitivity of Uveal Melanoma Cell Lines After X-rays or Carbon Ions Radiation. *Invest Ophthalmol Vis Sci* (2015) 56(5):3085–94. doi: 10.1167/iovs.14-15930
30. Yang J, Gao J, Qiu X, Hu J, Hu W, Wu X, et al. Intensity-Modulated Proton and Carbon-Ion Radiation Therapy in the Management of Head and Neck Sarcomas. *Cancer Med* (2019) 8(10):4574–86. doi: 10.1002/cam4.2319
31. Hu J, Bao C, Gao J, Guan X, Hu W, Yang J, et al. Salvage treatment using carbon ion radiation in patients with locoregionally recurrent nasopharyngeal carcinoma: Initial results. *Cancer* (2018) 124(11):2427–37. doi: 10.1002/cncr.31318
32. Ogata T, Teshima T, Kagawa K, Hishikawa Y, Takahashi Y, Kawaguchi A, et al. Particle irradiation suppresses metastatic potential of cancer cells. *Cancer Res* (2005) 65(1):113–20.
33. Akino Y, Teshima T, Kihara A, Kodera-Suzumoto Y, Inaoka M, Higashiyama S, et al. Carbon-ion beam irradiation effectively suppresses migration and invasion of human non-small-cell lung cancer cells. *Int J Radiat Oncol Biol Phys* (2009) 75 (2):475–81. doi: 10.1016/j.ijrobp.2008.12.090
34. Hirata K, Yamaguchi S, Shiga T, Kuge Y, Tamaki N. The Roles of Hypoxia Imaging Using (18)F-Fluoromisonidazole Positron Emission Tomography in Glioma Treatment. *J Clin Med* (2019) 8(8):1088. doi: 10.3390/jcm8081088
35. Crispin-Ortuzar M, Apte A, Grkovski M, Oh JH, Lee NY, Schoder H, et al. Predicting hypoxia status using a combination of contrast-enhanced computed tomography and [(18)F]-Fluorodeoxyglucose positron emission tomography radiomics features. *Radiother Oncol* (2018) 127(1):36–42. doi: 10.1016/j.radonc.2017.11.025
36. Kobayashi K, Manabe O, Hirata K, Yamaguchi S, Kobayashi H, Terasaka S, et al. Influence of the scan time point when assessing hypoxia in (18)F-fluoromisonidazole PET: 2 vs. 4 h. *Eur J Nucl Med Mol Imaging* (2020) 47 (8):1833–42. doi: 10.1007/s00259-019-04626-8
37. Festing MF. Randomized block experimental designs can increase the power and reproducibility of laboratory animal experiments. *ILAR J* (2014) 55 (3):472–6. doi: 10.1093/ilar/ilu045
38. Draganov PV, Wang AY, Othman MO, Fukami N. AGA Institute Clinical Practice Update: Endoscopic Submucosal Dissection in the United States. *Clin Gastroenterol Hepatol* (2019) 17(1):16–25 e1. doi: 10.1016/j.cgh.2018.07.041
39. Penagaricano JA, Griffin R, Corry P, Moros E, Yan Y, Ratanatharathorn V. Spatially fractionated (GRID) therapy for large and bulky tumors. *J Ark Med Soc* (2009) 105(11):263–5.
40. Billena C, Khan AJ. A Current Review of Spatial Fractionation: Back to the Future? *Int J Radiat Oncol Biol Phys* (2019) 104(1):177–87. doi: 10.1016/j.ijrobp.2019.01.073
41. Rodriguez-Ruiz ME, Vanpouille-Box C, Melero I, Formenti SC, Demaria S. Immunological Mechanisms Responsible for Radiation-Induced Abscopal Effect. *Trends Immunol* (2018) 39(8):644–55. doi: 10.1016/j.it.2018.06.001

Conflict of Interest: The authors declare that the research was conducted in the absence of any commercial or financial relationships that could be construed as a potential conflict of interest.

Copyright © 2020 Huang, Sun, Wang, Lin, Huang, Yang, Wu, Kong and Lu. This is an open-access article distributed under the terms of the Creative Commons Attribution License (CC BY). The use, distribution or reproduction in other forums is permitted, provided the original author(s) and the copyright owner(s) are credited and that the original publication in this journal is cited, in accordance with accepted academic practice. No use, distribution or reproduction is permitted which does not comply with these terms.

frontiers in Oncology

ORIGINAL RESEARCH
published: 21 January 2021
doi: 10.3389/fonc.2020.540096

Long-Term Outcomes and Prognostic Analysis of Computed Tomography-Guided Radioactive ^{125}I Seed Implantation for Locally Recurrent Rectal Cancer After External Beam Radiotherapy or Surgery

Hao Wang[1†], Lu Wang[1†], Yuliang Jiang[1], Zhe Ji[1], Fuxin Guo[1], Ping Jiang[1], Xuemin Li[1], Yi Chen[1], Haitao Sun[1], Jinghong Fan[1], Gang Du[2] and Junjie Wang[1]*

[1] Department of Radiation Oncology, Peking University Third Hospital, Beijing, China, [2] Department of Radiation Oncology, Bayannur Hospital, Bayannur, China

Background: Management of locally recurrent rectal cancer (LRRC) after surgery or external beam radiotherapy (EBRT) remains a clinical challenge, given the limited treatment options and unsatisfactory outcomes. This study aimed to assess long-term outcomes of computed tomography (CT)-guided radioactive ^{125}I seed implantation in patients with LRRC and associated prognostic factors.

Methods: A total of 101 patients with LRRC treated with CT-guided ^{125}I seed implantation from October 2003 to April 2019 were retrospectively studied. Treatment procedures involved preoperative planning design, ^{125}I seed implantation, and postoperative dose evaluation. We evaluated the therapeutic efficacy, adverse effects, local control (LC) time, and overall survival (OS) time.

Results: All the patients had previously undergone surgery or EBRT. The median age of patients was 59 (range, 31–81) years old. The median follow-up time was 20.5 (range, 0.89–125.8) months. The median LC and OS time were 10 (95% confidence interval (CI): 8.5–11.5) and 20.8 (95% CI: 18.7–22.9) months, respectively. The 1-, 2-, and 5-year LC rates were 44.2%, 20.7%, and 18.4%, respectively. The 1-, 2-, and 5-year OS rates were 73%, 31.4%, and 5%, respectively. Univariate analysis of LC suggested that when short-time tumor response achieved partial response (PR) or complete response (CR), or D_{90}>129 Gy, or GTV ≤ 50 cm^3, the LC significantly prolonged (P=0.044, 0.041, and <0.001, respectively). The multivariate analysis of LC indicated that the short-time tumor response was an independent factor influencing LC time (P<0.001). Besides, 8.9% (9/101)

OPEN ACCESS

Edited by:
Daniel Michael Trifiletti, Mayo Clinic Florida, United States

Reviewed by:
Ananth Ravi, Independent Researcher, Toronto, Canada
Toms Vengaloor Thomas, University of Mississippi Medical Center, United States

***Correspondence:**
Junjie Wang
junjiewang_edu@sina.cn

†These authors have contributed equally to this work and share first authorship

Specialty section:
This article was submitted to Radiation Oncology, a section of the journal Frontiers in Oncology

Received: *03 March 2020*
Accepted: *04 December 2020*
Published: *21 January 2021*

Citation:
Wang H, Wang L, Jiang Y, Ji Z, Guo F, Jiang P, Li X, Chen Y, Sun H, Fan J, Du G and Wang J (2021) Long-Term Outcomes and Prognostic Analysis of Computed Tomography-Guided Radioactive ^{125}I Seed Implantation for Locally Recurrent Rectal Cancer After External Beam Radiotherapy or Surgery. Front. Oncol. 10:540096. doi: 10.3389/fonc.2020.540096

of the patients had adverse effects (≥grade 3): radiation-induced skin reaction (4/101), radiation-induced urinary reaction (1/101), fistula (2/101), and intestinal obstruction (2/101). The cumulative irradiation dose and the activity of a single seed were significantly correlated with adverse effects ≥grade 3 (P=0.047 and 0.035, respectively).

Conclusion: CT-guided ^{125}I seed implantation is a safe and effective salvage treatment for LRRC patients who previously underwent EBRT or surgery. D_{90} and GTV significantly influenced prognosis of such patients.

Keywords: locally recurrent rectal cancer, ^{125}I seed implantation, dosimetry, prognosis, adverse effects

INTRODUCTION

Locally recurrent rectal cancer (LRRC) refers to the recurrence, progression, or development of new sites within the pelvis after previous standard treatment for rectal cancer (1). Although preoperative chemoradiotherapy followed by total mesorectal excision (TME) significantly decreased the local recurrence rate, local recurrence has been reported in 5–11% of patients (2). Prognosis in LRRC patients is poor, with a median survival time of 10 months without treatment (3), and a reported 5-year survival rate of 10% (4). The majority of patients have severe symptoms such as pain, hematochezia, and fistula.

Surgery is an effective option and radical (R_0) resection is an independent prognostic factor. Because the tumor typically shows extensive involvement in the pelvis, less than one-sixth of patients are eligible for R_0 resection (5). The benefits of reirradiation include possible palliation by decreased steroid use, improvement in neurological symptoms, and extension of progression-free survival (PFS) and overall survival (OS) in some patients. Nevertheless, considering previous irradiation to the normal tissue, sufficient doses can hardly be delivered to the recurrent tumor in the pelvis (6). Furthermore, locally recurrent tumors are mostly located in the previously irradiated field, making it more challengeable for patients to undergo reirradiation (7). In addition, reirradiation with conventional radiation therapy confers a high rate of grade 3 adverse effects and late toxicities.

Nevertheless, ^{125}I seed implantation can overcome the above-mentioned limitations. The dose of ^{125}I seed is inversely proportional to the square of the distance, indicating that the dose is remarkably reduced surrounding the tumor. Interstitial implantation of ^{125}I seeds delivers a high dose of radiation (140–180 Gy) to the tumor and spares surrounding normal tissues. In addition, ^{125}I seed provides a slow continuous release of radiation that allows repair of sublethal damage and reoxygenation of hypoxic areas in the late-responding tissues. Therefore, radioactive ^{125}I seed implantation might be a promising choice for the treatment of malignant tumors owing to its curative effect, minimal surgical trauma, and tolerable complications. The present study aimed to evaluate the efficacy and safety of computed tomography (CT)-guided ^{125}I seed implantation for LRRC patients who underwent external beam radiotherapy (EBRT) or surgery, in addition to analysis of some prognostic factors.

PATIENTS AND METHODS

Patients

This retrospective study collected the data of 101 patients with LRRC who were treated with CT-guided ^{125}I seed implantation from October 2003 to April 2019. The study protocol was approved by the Ethics Committee of our hospital. All patients signed the written informed consent. The inclusion criteria were as follows: (1) patients with LRRC who were pathologically diagnosed; (2) extraluminal pelvic recurrence, without distal metastasis or with controllable oligometastasis; (3) tumor size < 7cm; (4) recurrence after surgery or EBRT, or refusal of surgery or EBRT; (5) life expectancy≥3 months. The patients' median age was 59 (range, 31–81) years old. After tumor recurrence, all the patients received chemotherapy before seed implantation. And 17 (16.8%) patients received second-line or further chemotherapy. All the patients had received curative surgery or EBRT previously. Except for one case, 100 patients underwent surgery. Among all patients, 12 patients had no history of undergoing irradiation, 74 patients received one course of EBRT, and 14 patients received two courses of EBRT. The median cumulative dose in the pelvis was 50 (range, 30–130) Gy. All the patients had received chemotherapy previously. Demographic and clinical data of patients are listed in **Table 1**.

CT-Guided ^{125}I Seed Implantation

Supine or prone position was chosen according to the tumor location. All the patients underwent contrast-enhanced CT scan with a slice thickness of 5 mm, one week before the implantation. CT data were transmitted to the brachytherapy treatment planning system (BTPS) (KLSIRPS-3D) which was provided by the Beijing University of Aeronautics and Astronautics and Beijing Astro Technology Co., Ltd. The radiation oncologists delineated the gross target volume (GTV) and organs at risk (OARs). Planned target volume (PTV) was defined as an extension of 5–10 mm from GTV. The optimal access for implantation (site, direction, and depth), prescription dose, number of seeds, single-seed activity, and seed distribution were designed.

Spinal anesthesia was induced in all patients. Under CT guidance, the needles were inserted into the planned site and arranged in parallel 5–10 mm apart. Then, the ^{125}I seeds (6711_1985, Shanghai GMS Pharmaceutical Co., Ltd.) were implanted using a Mick seed implantation gun (Mick Radio-

TABLE 1 | Clinical details and patient demographics.

Characteristics	Value
Sex, n (%)	
Male	70 (69.3%)
Female	31 (30.7%)
Age (in years), range (median)	31-81 (59)
Histopathology	
Adenocarcinoma	100
Squamous carcinoma	1
Metastasis	
No metastasis, n (%)	82 (81.2%)
Distal metastasis, n (%)	19 (18.8%)
Lung	10 (10%)
Liver	7 (7%)
Prostate	1 (1%)
Axillary lymph nodes	1 (1%)
Previous surgery	
None	1
Once	86
Twice	13
Three times	1
Cumulative dose in the pelvis, EQD_2 (Gy)	
<50	18
50-100	66
≥100	6
Unknown	11
Number of RT sessions	
0	12
1	74
2	14
3	1
GTV, mean ± SD (ml)	70.0 ± 45.3
Time from radiotherapy to seed implantation, (in months), range (median)	0.1–68.1 (17.0)

EQD_2, equivalent dose in 2 Gy per fraction radiotherapy; RT, radiotherapy; GTV, gross tumor volume; SD, standard deviation.

Nuclear Inc., Mount Vernon, NY, USA), by maintaining 1 cm between two seeds. After finishing seeds implantation, another CT scan was performed to verify the distribution of the seeds, and to calculate the dosimetric parameters (**Figure 1**). The postoperative parameters included: D_{90} (dose delivered to 90% of target volume), D_{100} (dose delivered to 100% of target volume), V_{100} (percentage of the target volume that was covered by 100% of the prescription dose), V_{150} (percentage of the target volume that was covered by 150% of the prescription dose), HI (homogeneity index), CI (conformal index), and EI (external index).

Follow-Up

The patients were followed-up every 3 months by the radiation oncologists. The examinations included routine blood test, blood chemistry, tumor markers, magnetic resonance imaging (MRI) of pelvis, CT of the abdomen, and chest radiography. Positron emission tomography-CT (PET-CT) was employed when there were signs of metastasis. The local response was evaluated three months after ^{125}I seed implantation by Response Evaluation Criteria in Solid Tumors (RECIST) version 1.1 (8). Complete response (CR) was defined as disappearance of all target lesions; partial response (PR) was defined as at least a 30% decrease in the diameters of the target lesion; progressive disease (PD) was defined as at least a 20% increase in the diameters of the target lesion; and stable disease (SD) was between PR and PD. The numeric rating scale (NRS) was used to assess the pain level. Adverse effects were evaluated according to the toxicity criteria of the Radiation Therapy Oncology Group (RTOG). Local control (LC) was defined as lack of tumor progression of the implanted volume.

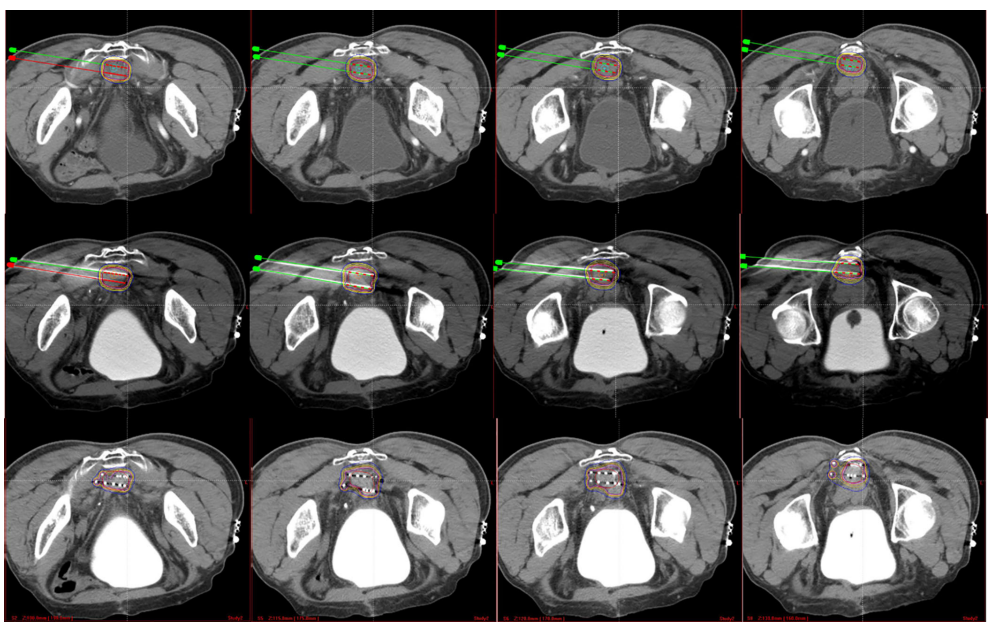

FIGURE 1 | The first line presents the preoperative plan. The second line presents the intraoperative plan. The third line presents the postoperative plan.

Statistical Analysis

All statistical analyses were carried out by SPSS 18.0 software (IBM, Armonk, NY, USA). LC and OS rates were calculated by plotting Kaplan–Meier curves. The log-rank test was employed for univariate analysis, and Cox proportional hazards regression model was used for multivariate analysis. The Chi-square test and Fisher's exact test were undertaken to analyze factors correlated with adverse effects. The two-tailed P<0.05 was considered statistically significant. The curves were plotted with GraphPad Prism 5.0 software (GraphPad Software Inc., San Diego, CA, USA).

RESULTS

Parameters of the Implantation

The volume of GTV was 6.5–234.8 (median, 66.9) cm^3. The activity of a single radioactive seed was 0.4–0.8 (median, 0.66) mCi. The number of seeds was 6–137 (median, 70). The postoperative parameters included D_{90} (110.7 ± 33.7) Gy, D_{100} (46.8 ± 24.4) Gy, V_{100} (68.9 ± 36.4) %, V_{150} (56.8 ± 17.5) %, HI (0.34 ± 0.14), CI (0.91 ± 0.55), and EI (0.79 ± 1.6).

Efficacy and Adverse Effects

The follow-up time was 0.89–125.8 (median, 20.5) months. The local response included 23 cases of CR, 35 cases of PR, 33 cases of SD, and 10 cases of PD. The objective response rate (ORR) was 57.4% (58/101). Adverse effects occurred in 14 (13.9%) patients, including 21 cases. Besides, 12 (57.1%) of the cases showed grades 1–2 adverse effects, including neuropathy (n=1, 4.8%), radiation-induced skin reaction (n=4, 19%), and radiation-induced urinary reaction (n=7, 33.3%). Additionally, 9 (42.9%) cases had adverse effects with ≥grade 3, including radiation-induced urinary reaction (n=1, 4.8%), fistula (n=2, 9.5%), intestinal obstruction (n=2, 9.5%), and radiation-induced skin reaction (n=4, 19.1%). Concerning implantation-related complications, seed migration was observed in two patients during the follow-up, and one patient developed needle-tract implantation metastases. No correlation was found between D_{90} (D_{90} ≤ 129 Gy vs. D_{90}>129 Gy) and adverse effects ≥grade 3 (P=0.160) (**Table 2**). The cumulative irradiation dose (≤100 Gy vs. >100 Gy) and the activity of a single seed (≤0.68 mCi vs. >0.68 mCi) were significantly correlated with adverse effects ≥grade 3 (P=0.047 and 0.035, respectively). The rates of adverse effects (grade ≥3) for cumulative dose ≤100 Gy and >100 Gy were 5.9% and 40%, respectively, and the rates of adverse effects (grade ≥3) for the activity of a single seed ≤0.68 mCi and >0.68 mCi were 3.4% and 16.3%, respectively.

Local Control

The median LC time was 10 (95% confidence interval (CI): 8.5–11.5) months. The 1-, 2-, and 5-year LC rates were 44.2%, 20.7%, and 18.4%, respectively. The univariate analysis of LC showed that D_{90} (≤129 Gy vs. >129 Gy), GTV (≤50 cm^3 vs. >50 cm^3), and short-time tumor response (CR+PR vs. SD+PD) significantly influenced LC time (P=0.044, 0.041, and <0.001, respectively) (**Table 3**). Besides, a prolonged trend was shown in LC when V_{100}>91% (P=0.053) (**Figure 2**). The 1-year LC rate for V_{100} ≤ 91% and V_{100}>91% was 42.1% and 62.5%, respectively. Multivariate analysis of these factors influencing LC time indicated that short-time tumor response was an independent factor of LC time (hazard ratio [HR] = 0.072; 95% CI=0.034–0.153; P<0.001). The LC of CR and PR was superior to that of SD and PD. The median LC time for (CR+PR) and (SD+PD) was 16.0 and 6.0 months, respectively.

Overall Survival

The median OS time was 20.8 (95% CI: 18.7–22.9) months. The 1-, 2-, and 5-year OS rates were 73%, 31.4%, and 5%, respectively. In the current research, 93 patients died at the end of the follow-up. Of these, 20 patients died of local recurrence, 54 died of metastasis, seven died of non-tumor causes, and 12 died of unknown causes. For the univariate analysis, only the short-time tumor response was significantly correlated with OS time (P=0.017). The median OS time for (CR+PR) and (SD+PD) was 22.0 and 14.8 months, respectively.

TABLE 2 | Analysis of factors associated with adverse effects.

Factors	Adverse effects		Total (n)	P
	Grade 0–2	≥Grade 3		
D_{90} (Gy)				
≤129	63 (94.0%)	4 (6.0%)	67	0.160
>129	29 (85.3%)	5 (14.7%)	34	
Total (n)	92	9	101	
Cumulative dose in the pelvis, EQD_2 (Gy)				
≤100	80 (94.1%)	5 (5.9%)	85	0.047
>100	3 (60.0%)	2 (40.0%)	5	
Total (n)	83	7	101	
Activity of a single seed (mCi)				
≤0.68	56 (96.6%)	2 (3.4%)	58	0.035
>0.68	36 (83.7%)	7 (16.3%)	43	
Total (n)	92	9	101	

D_{90}, dose that covers 90% target volume; EQD_2, equivalent dose in 2 Gy per fraction radiotherapy.

TABLE 3 | Univariate and multivariate analysis of factors influencing local control.

Factors		n	Median (months)	Univariate analysis	Multivariate analysis		
				P	HR	95% CI	P
Age (in years)	≤40	8	12	0.668			
	41-65	63	10				
	>66	30	10				
D_{90}	≤129 Gy	67	8	0.044			
	>129 Gy	34	13				
V_{100}	≤91%	89	10	0.053			
	>91%	12	–				
Activity of a single seed	≤0.68 mCi	58	10				
	>0.68 mCi	43	10	0.587			
GTV	≤50 cm3	38	13	0.041			
	>50 cm3	63	8				
Cumulative dose in the pelvis (EQD_2)	≤100Gy	85	10	0.765			
	>100Gy	5	12				
Tumor response	CR+PR	58	16	<0.001	0.072	0.034–0.153	<0.001
	SD+PD	43	6				

HR, hazard ratio; CI, confidence interval; D_{90}, dose that covers 90% target volume; V_{100}, percentage of the target volume that was covered by 100% of the prescription dose; GTV, gross tumor volume; EQD_2, equivalent dose in 2 Gy per fraction radiotherapy; CR, complete response; PR, partial response; SD, stable disease; PD, progressive disease.

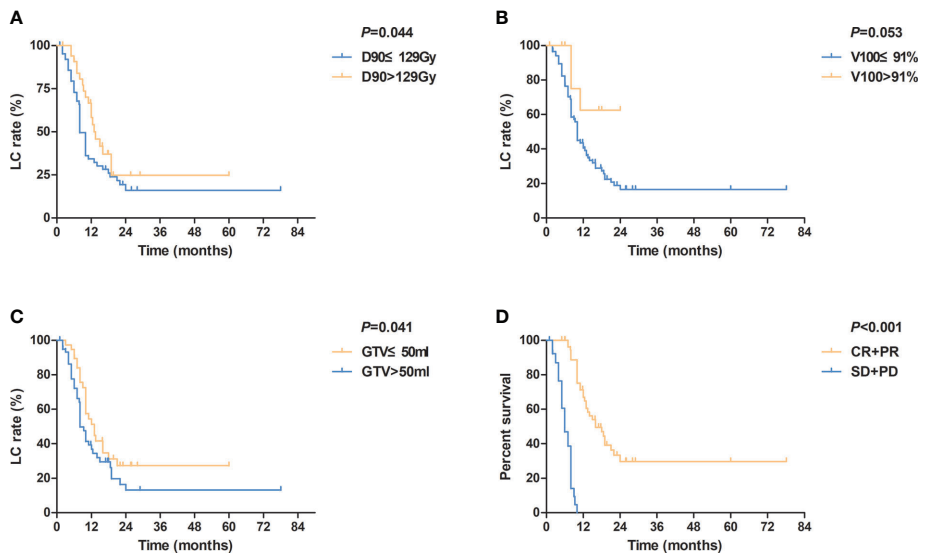

FIGURE 2 | Kaplan-Meier curves for local control according to **(A)** different values of D_{90} (≤ 129Gy vs. >129Gy); **(B)** different values of V_{100} (≤ 91% vs. >91%); **(C)** different values of GTV (≤ 50 ml vs. >50 ml); **(D)** different tumor responses (CR+PR vs. SD+PD). D_{90}, dose that covers 90% target volume; V_{100}, percentage of the target volume that was covered by 100% of the prescription dose; GTV, gross tumor volume; CR, complete response; PR, partial response; SD, stable disease; PD, progressive disease.

DISCUSSION

Numerous therapeutic modalities have been used for patients with LRRC, including surgery, EBRT, intraoperative radiotherapy (IORT), high-dose-rate (HDR) brachytherapy, chemotherapy, etc. Previously irradiated patients were found less sensitive to chemotherapy than those who did not receive pelvic radiotherapy (6, 9). Furthermore, chemotherapy alone is not effective for controlling pelvic recurrence. It was reported that the 5-year survival rate for R_0 resection ranged from 43% to 60% (10). However, only a limited number of patients were eligible for R_0 resection. LRRC typically presents with extensive involvement of the tumor in the pelvis, making it a great challenge to perform resection. Moreover, distorted anatomical structures and tissue fibrosis from previous irradiation increase the difficulty in surgery (6, 11). Besides, extensive resection is typically followed by high morbidity and mortality risks (10).

Several scholars have pointed out that re-irradiation is a reasonable option for patients with LRRC who have undergone EBRT previously. Besides, it could relieve symptoms to some extent (11–13). A systematic review reported 375 patients with LRRC who were reirradiated. Reirradiation was mostly

administered using hyperfractionated or 1.8 Gy once-daily chemoradiotherapy. Median survival time was 39–60 months for resected patients and 12–16 months for palliative patients. The symptomatic relief rate was 82%–100% (12). Nevertheless, it is challenging to deliver a definitive dose to the tumor lesions considering history of irradiation to the normal pelvic tissue (6). Late toxicity rates were high. Recently, with the advances of cutting-edge technologies, a more precise radiotherapy technique, namely stereotactic ablative radiotherapy (SABR), was used to treat LRRC. Murray et al. (14) performed a systematic review regarding the use of SABR for the reirradiation of recurrent malignant disease within the pelvis, to guide the clinical implementation of this technique, and demonstrated that for previously irradiated patients with recurrent pelvic disease, SABR re-irradiation could be a feasible intervention for those who otherwise have limited options. Dagoglu et al. (15) reported the outcomes of a series of patients with pelvic recurrences from colorectal cancer reirradiated with SBRT. They employed Cyberknife Robotic Stereotactic Radiosurgery system with fiducial based real time tracking, and noted that one patient had small bowel perforation and required surgery (grade IV), two patients had symptomatic neuropathy (grade III), and one patient developed hydronephrosis from ureteric fibrosis requiring a stent (grade III).

IORT refers to the direct irradiation of the tumor surgically. A number of scholars have used IORT alone in the treatment of patients with history of undergoing irradiation. However, their results were not satisfactory. The LC and OS rates of IORT alone were significantly lower than those of IORT combined with EBRT (13, 16, 17). Besides, a significant increase was observed in the rate of complications related to the wound and neuropathy.

Several studies reported HDR brachytherapy for the management of LRRC. HDR intraluminal brachytherapy plays a great therapeutic role in the treatment of intraluminal tumor recurrence. And HDR interstitial brachytherapy has also shown an impressive therapeutic efficacy. Sakurai et al. (18) reported that LC was achieved in 7 of 18 patients with LRRC at a median follow-up time of 14.4 months. Morimoto et al. (19) studied 9 patients, and it was demonstrated that the 8-year OS, LC, and PFS rates were 56%, 44%, and 33%, respectively. Three patients had grade 3 adverse effects. Nevertheless, it should be noted that the tumor location of these patients could be reached by a needle applicator through the perineum. Lateral or presacral recurrence was contraindicated for HDR brachytherapy, which, however, could be managed with ^{125}I seed implantation.

Recurrent tumor after EBRT or surgery is typically associated with a poor blood supply. Permanent implantation of ^{125}I seeds has significant advantages in killing hypoxic tumor cells by consistently radiating low-dose rays. Furthermore, it also has the major advantages of delivering a high dose of irradiation to the tumor with a very sharp fall-off outside the implanted volume. For patients who are not eligible candidates for reirradiation, surgery or HDR interstitial brachytherapy, ^{125}I seed implantation might be an alternative treatment option.

The results of the current research were comparable to those reported previously related to application of ^{125}I seed implantation for LRRC. In our study, the median LC time was 10 months, and the median OS time was 20.8 months. The first report related to application of brachytherapy for LRRC included 30 patients (20). The seeds were implanted after radical or debulking surgical resection. The LC rate was 37.5% for gross residual disease and 66% for microscopic residual disease. The tumors in 64% (18/30) of patients were still under control at the last follow-up. No mortality was observed, and the morbidity rate was low. Martinez et al. (21) reported 29 patients with recurrent colorectal cancer in the pelvis or the paraaortic lymph nodes treated with intraoperative ^{125}I seed implantation. The implanted volume received a median minimal peripheral dose of 140 Gy to total decay. The 1-, 2-, and 4-year LC rates were 38%, 17%, and 17%, (median, 11 months), respectively. The 1-, 2-, and 4-year OS rates were 70%, 35%, and 21%, (median, 18 months), respectively. Overall, 45% (13/29) of patients experienced 15 adverse events. Image-guided percutaneous ^{125}I seed implantation which was minimally invasive has gradually become the mainstream treatment approach. In Wang et al.'s study (22), 15 patients with LRRC received ^{125}I or ^{103}Pd seed implantation under CT guidance. The median minimal peripheral dose was 150 Gy. The median follow-up, LC, and OS time were 8, 7, and 9 months, respectively. Only one patient had a grade 4 toxic event. Wang et al. (23) reported 20 patients with LRRC who were treated with CT-guided ^{125}I seed implantation. The median peripheral dose was 120 Gy. CR or PR was achieved in 75% of patients. The median survival time was 18.8 months. The 1- and 2-year survival rates were 75% and 25%, respectively. Nevertheless, none of the above-mentioned studies analyzed optimal parameters and factors related to adverse effects. The optimal dosimetric parameters for ^{125}I seed implantation are still elusive except for prostate cancer. In prostate cancer, the prognosis of patients with $D_{90}\geq140$ Gy was significantly greater than those with $D_{90}<140$ Gy. The outcomes of patients with $V_{100}\geq90\%$ were also markedly superior than those with $V_{100}<90\%$ (24–26). Similarly, for LRRC, the present study revealed that patients with $D_{90}>129$ Gy achieved a notably longer LC time than those with $D_{90} \leq 129$ Gy. The median LC time for $D_{90}>129$ Gy and $D_{90} \leq 129$ Gy was 8 and 13 months, respectively. Moreover, a trend of prolonged LC time was observed in patients with $V_{100}>91\%$. The 1-year LC rate for $V_{100} \leq 91\%$ and $V_{100}>91\%$ was 42.1% and 62.5%, respectively.

Regarding adverse effects, a meta-analysis of irradiation for LRRC showed that the rates of adverse effects (≥grade 3) for acute and late complications were 11.7% and 25.2%, respectively (12). Bhangu et al. (27) summarized surgical outcomes of 22 studies on LRRC and revealed that the overall rate of complications was 51%. In the current research, the overall rate of adverse effects was 13.9% (14/101), and 8.9% (9/101) of patients had ≥grade 3 adverse effects. The complication rates reported in our study were relatively lower than those reported in studies that used other treatment modalities. Cumulative irradiation dose (≤100 Gy vs. >100 Gy) and the activity of a single seed (≤0.68 mCi vs. >0.68 mCi) were found to be correlated with adverse effects (≥grade 3). We considered that the adverse effects in 2 patients with cumulative irradiation

dose >100 Gy might be attributed to the late complications of previous high-dose irradiation. When low-activity seeds are used, the influence of a single seed on dosimetry is reduced, leading to a better dose homogeneity. The misplacement of a single seed would cause less damage to surrounding normal tissue. Sloboda et al. (28) reported that a range of 0.4–0.6 mCi per seed was optimal to cover the target volume and spare the urethra in prostate cancer. However, in the present study, the activity of a single seed had no effect on either LC or OS.

There are a number of limitations in this study. First, considering the short half-life of ^{125}I seed, all the dosimetric parameters were postoperative parameters which were calculated immediately after ^{125}I seed implantation, with assumption of complete dose delivery. According to the physical characteristic of ^{125}I seed, 65% of prescription dose was delivered in 3 months and 90% was delivered in about 6 months. All the patients were still alive 3 months after ^{125}I seed implantation except for one patient who died of pulmonary infection one month after the implantation. Moreover, the majority of patients were still alive 6 months after ^{125}I seed implantation. Thus, it could be concluded that the postoperative dosimetry was nearly close to the delivered dosimetry. Nevertheless, there may still exist some minor errors that require further investigation. Second, the treatment modalities used for LRRC patients before ^{125}I seed implantation were not consistent (e.g., some patients did not receive irradiation), which might influence patients' sensitivity to ^{125}I seed implantation and clinical outcomes. In addition, treatment modalities used for LRRC patients after ^{125}I seed implantation were not consistent as well. A number of patients received postoperative chemotherapy, while others poorly tolerated, which might lead to the low efficiency of ^{125}I seed implantation on OS. Third, it was sometimes difficult to indicate whether the adverse effects were caused by ^{125}I seed implantation, tumor progression, or previous high-dose irradiation. In such cases, we attributed the adverse effects to ^{125}I seed implantation, which might lead to an overestimation of the rates of adverse effects. Last but not the least, this was a single-center retrospective study with small sample size.

In conclusion, CT-guided ^{125}I seed implantation is a safe, effective, and minimally invasive treatment for LRRC patients with mild adverse effects. This treatment does not require patients to have a high physical strength and is not limited by previous irradiation dose. Patients with LRRC after previous EBRT with limited treatment options are especially proper candidates for ^{125}I seed implantation. Nevertheless, multicenter studies with a larger sample size and prospective design are needed to further investigate the effects of ^{125}I seed implantation on LRRC patients.

DATA AVAILABILITY STATEMENT

The datasets generated for this study are available on request to the corresponding author.

ETHICS STATEMENT

The studies involving human participants were reviewed and approved by the Institutional Review Boards of Peking University Third Hospital (IRB00006761). The patients/participants provided their written informed consent to participate in this study.

AUTHOR CONTRIBUTIONS

LW, HW, HS, and GD were responsible for the collection of the clinical data. LW and HW drafted the manuscript. JW was in charge of verifying the patients' implantation plan and directing the writing. YJ, ZJ, FG, PJ, XL, YC, and JF were responsible for the supplement and refinement of the clinical data and collectively carried out the implantation plan. HS was responsible for the design and production of radioactive seed implantation plan. All authors read and approved the final manuscript. LW and HW contributed equally to the article and are co-first authors of the article. All authors contributed to the article and approved the submitted version.

ACKNOWLEDGMENTS

We thank all our supporting colleagues in the Department of Radiation Oncology, Peking University Third Hospital.

REFERENCES

1. Beyond TMEC. Consensus statement on the multidisciplinary management of patients with recurrent and primary rectal cancer beyond total mesorectal excision planes. *Br J Surg* (2013) 100(8):1009–14. doi: 10.1002/bjs.9192
2. van Gijn W, Marijnen CA, Nagtegaal ID, Kranenbarg EM, Putter H, Wiggers T, et al. Preoperative radiotherapy combined with total mesorectal excision for resectable rectal cancer: 12-year follow-up of the multicentre, randomised controlled TME trial. *Lancet Oncol* (2011) 12:575–82. doi: 10.1016/S1470-2045(11)70097-3
3. Rasanen M, Carpelan-Holmstrom M, Mustonen H, Renkonen-Sinisalo L, Lepistö A. Pattern of rectal cancer recurrence after curative surgery. *Int J Color Dis* (2015) 30(6):775–85. doi: 10.1007/s00384-015-2182-1
4. Guyot F, Faivre J, Manfredi S, Meny B, Bonithon-Kopp C, Bouvier AM. Time trends in the treatment and survival of recurrences from colorectal cancer. *Ann Oncol* (2005) 16:756–61. doi: 10.1093/annonc/mdi151
5. Westberg K, Palmer G, Hjern F, Nordenvall C, Johansson H, Holm T, et al. Population-based study of factors predicting treatment intention in patients with locally recurrent rectal cancer. *Br J Surg* (2017) 104:1866–73. doi: 10.1002/bjs.10645
6. Hildebrandt B, Wust P, Drager J, Lüdemann L, Sreenivasa G, Tullius SG, et al. Regional pelvic hyperthermia as an adjunct to chemotherapy (oxaliplatin, folinic acid, 5-fluorouracil) in pre-irradiated patients with locally recurrent rectal cancer: a pilot study. *Int J Hyperthermia* (2004) 20(4):359–69. doi: 10.1080/02656730310001645010
7. Yu T-K, Bhosale PR, Crane CH, Iyer RB, Skibber JM, Rodriguez-Bigas MA, et al. Patterns of locoregional recurrence after surgery and radiotherapy or

chemoradiation for rectal cancer. *Int J Radiat Oncol Biol Phys* (2008) 71:1175–80. doi: 10.1016/j.ijrobp.2007.11.018
8. Eisenhauer EA, Therasse P, Bogaerts J, Schwartz LH, Sargent D, Ford R, et al. New response evaluation criteria in solid tumours: revised RECIST guideline (version 1.1). *Eur J Cancer* (2009) 45(2):228–47. doi: 10.1016/j.ejca.2008.10.026
9. Alberda WJ, Haberkorn BC, Morshuis WG, Oudendijk JF, Nuyttens JJ, Burger JW, et al. Response to chemotherapy in patients with recurrent rectal cancer in previously irradiated area. *Int J Colorectal Dis* (2015) 30 (8):1075–80. doi: 10.1007/s00384-015-2270-2
10. Hagemans JAW, van Rees JM, Alberda WJ, Rothbarth J, Nuyttens JJME, van Meerten E, et al. Locally recurrent rectal cancer; long-term outcome of curative surgical and non-surgical treatment of 447 consecutive patients in a tertiary referral centre. *Eur J Surg Oncol* (2020) 46(3):448–54. doi: 10.1016/j.ejso.2019.10.037
11. Lee J, Kim CY, Koom WS, Rim CH. Practical effectiveness of re-irradiation with or without surgery for locoregional recurrence of rectal cancer: A meta-analysis and systematic review. *Radiother Oncol* (2019) 140:10–9. doi: 10.1016/j.radonc.2019.05.021
12. Guren MG, Undseth C, Rekstad BL, Brændengen M, Dueland S, Spindler KL, et al. Reirradiation of locally recurrent rectal cancer: a systematic review. *Radiother Oncol* (2014) 113(2):151–7. doi: 10.1016/j.radonc.2014.11.021
13. Chung SY, Koom WS, Keum KC, Chang JS, Shin SJ, Ahn JB, et al. Treatment Outcomes of Re-irradiation in Locoregionally Recurrent Rectal Cancer and Clinical Significance of Proper Patient Selection. *Front Oncol* (2019) 9:529. doi: 10.3389/fonc.2019.00529
14. Murray LJ, Lilley J, Hawkins MA, Henry AM, Dickinson P, Sebag-Montefiore D. Pelvic re-irradiation using stereotactic ablative radiotherapy (SABR): A systematic review. *Radiother Oncol* (2017) 125(2):213–22. doi: 10.1016/j.radonc.2017.09.030
15. Dagoglu N, Mahadevan A, Nedea E, Poylin V, Nagle D. Stereotactic body radiotherapy (SBRT) reirradiation for pelvic recurrence from colorectal cancer. *J Surg Oncol* (2015) 111(4):478–82. doi: 10.1002/jso.23858
16. Susko M, Lee J, Salama J, Thomas S, Uronis H, Hsu D, et al. The Use of Re-irradiation in Locally Recurrent, Non-metastatic Rectal Cancer. *Ann Surg Oncol* (2016) 23(11):3609–15. doi: 10.1245/s10434-016-5250-z
17. Marzi S, Saracino B, Petrongari MG, Arcangeli S, Gomellini S, Arcangeli G, et al. Modeling ofalpha/beta for late rectal toxicity from a randomized phase II study: conventional versus hypofractionated scheme for localized prostate cancer. *J Exp Clin Cancer Res* (2009) 28:117. doi: 10.1186/1756-9966-28-117
18. Sakurai H, Mitsuhashi N, Harashima K, Muramatsu H, Ishikawa H, Kitamoto Y, et al. CT-fluoroscopy guided interstitial brachytherapy with image-based treatment planning for unresectable locally recurrent rectal carcinoma. *Brachytherapy* (2004) 3:222–30. doi: 10.1016/j.brachy.2004.09.007
19. Morimoto M, Isohashi F, Yoshioka Y, Suzuki O, Seo Y, Ogata T, et al. Salvage high-dose-rate interstitial brachytherapy for locally recurrent rectal cancer: long-term follow-up results. *Int J Clin Oncol* (2014) 19(2):312–8. doi: 10.1007/s10147-013-0567-0
20. Goes RN, Beart RW Jr, Simons AJ, Gunderson LL, Grado G, Streeter O. Use of brachytherapy in management of locally recurrent rectal cancer. *Dis Colon Rectum* (1997) 40:1177–9. doi: 10.1007/BF02055163
21. Martinez-Monge R, Naq S, Martin EW. 125Iodine brachytherapy for colorectal adenocarcinoma recurrent in the pelvis and paraortics. *Int J Radiat Oncal Biol Phys* (1998) 42:545–50. doi: 10.1016/S0360-3016(98)00269-7
22. Wang JJ, Yuan HS, Li JN, Jiang YL, Tian SQ, Yang RJ. CT-guided radioactive seed implantation for recurrent rectal carcinoma after multiple therapy. *Med Oncol* (2010) 27(2):421–9. doi: 10.1007/s12032-009-9227-7
23. Wang ZM, Lu J, Liu L, Liu T, Chen K, Liu F, et al. Clinical application of CT-guided 125I seed interstitial implantation for local recurrent rectal carcinoma. *Radiat Oncol* (2011) 6:138. doi: 10.1186/1748-717X-6-138
24. Keyes M, Morris WJ, Spadinger I, Araujo C, Cheung A, Chng N, et al. Radiation oncology and medical physicists quality assurance in British Columbia Cancer Agency Provincial Prostate Brachytherapy Program. *Brachytherapy* (2013) 12(4):343–55. doi: 10.1016/j.brachy.2012.03.006
25. Zapatero A, Garcia-Vicente F, Martin de Vidales C, Cruz Conde A, Ibáñez Y, Fernández I, et al. Long-term results after high-dose radiotherapy and adjuvant hormones in prostate cancer: how curable is high-risk disease? *Int J Radiat Oncol Biol Phys* (2011) 81(5):1279–85. doi: 10.1016/j.ijrobp.2010.07.1975
26. Stock RG, Stone NN, Tabert A, Iannuzzi C, DeWyngaert JK. A dose-response study for I-125 prostate implantation. *Int J Radiat Oncol Biol Phys* (1998) 41 (1):101–8. doi: 10.1016/S0360-3016(98)00006-6
27. Bhangu A, Ali SM, Darzi A, Brown G, Tekkis P. Metaanalysis of survival based on resection margin status following surgery for recurrent rectal cancer. *Color Dis* (2012) 14(12):1457–66. doi: 10.1111/j.1463-1318.2012.03005.x
28. Sloboda RS, Pedersen JE, Halperin R. Is there a preferred strength for regularly spaced 125I seeds in inverse-planned prostate implants? *Int J Radiat Oncol Biol Phys* (2003) 55(1):234–44. doi: 10.1016/S0360-3016(02)04123-8

Conflict of Interest: The authors declare that the research was conducted in the absence of any commercial or financial relationships that could be construed as a potential conflict of interest.

Copyright © 2021 Wang, Wang, Jiang, Ji, Guo, Jiang, Li, Chen, Sun, Fan, Du and Wang. This is an open-access article distributed under the terms of the Creative Commons Attribution License (CC BY). The use, distribution or reproduction in other forums is permitted, provided the original author(s) and the copyright owner(s) are credited and that the original publication in this journal is cited, in accordance with accepted academic practice. No use, distribution or reproduction is permitted which does not comply with these terms.

frontiers in Oncology

PERSPECTIVE
published: 22 February 2021
doi: 10.3389/fonc.2021.624786

The Emerging Potential of Multi-Ion Radiotherapy

Daniel K. Ebner[1], Steven J. Frank[2], Taku Inaniwa[1], Shigeru Yamada[1] and Toshiyuki Shirai[1]*

[1] National Institute of Radiological Science (NIRS), National Institutes of Quantum and Radiological Science and Technology (QST), Chiba, Japan, [2] Division of Radiation Oncology, The University of Texas MD Anderson Cancer Center, Houston, TX, United States

Research into high linear energy transfer (LET) radiotherapy now spans over half a century, beginning with helium and deuteron treatment in 1952 and today ranging from fast neutrons to carbon-ions. Owing to pioneering work initially in the United States and thereafter in Germany and Japan, increasing focus is on the carbon-ion beam: 12 centers are in operation, with five under construction and three in planning. While the carbon-ion beam has demonstrated unique and promising suitability in laboratory and clinical trials toward the hypofractionated treatment of hypoxic and/or radioresistant cancer, substantial developmental potential remains. Perhaps most notable is the ability to paint LET in a tumor, theoretically better focusing damage delivery within the most resistant areas. However, the technique may be limited in practice by the physical properties of the beams themselves. A heavy-ion synchrotron may provide irradiation with multiple heavy-ions: carbon, helium, and oxygen are prime candidates. Each ion varies in LET distribution, and so a methodology combining the use of multiple ions into a uniform LET distribution within a tumor may allow for even greater treatment potential in radioresistant cancer.

Keywords: heavy-ion radiotherapy, carbon-ion radiotherapy, helium-ion irradiation, radiation therapy, multi-ion radiotherapy

OPEN ACCESS

Edited by:
Timothy Dean Malouff, Mayo Clinic Florida, United States

Reviewed by:
Kevin Prise, Queen's University Belfast, United Kingdom
Tatsuya Ohno, Gunma University, Japan

****Correspondence:***
Daniel K. Ebner
daniel_ebner@alumni.brown.edu

Specialty section:
This article was submitted to Radiation Oncology, a section of the journal Frontiers in Oncology

Received: *01 November 2020*
Accepted: *04 January 2021*
Published: *22 February 2021*

Citation:
Ebner DK, Frank SJ, Inaniwa T, Yamada S and Shirai T (2021) The Emerging Potential of Multi-Ion Radiotherapy. Front. Oncol. 11:624786. doi: 10.3389/fonc.2021.624786

INTRODUCTION

Seventy years have passed since Lawrence and Tobias first employed helium and deuteron particle beams in human patients, beginning the clinical study of charged particle radiotherapy (CPT), or hadrontherapy (1, 2). Their results built off the pioneering experience of Stone and colleagues, who treated 226 patients with neutrons from 1936 to 1938, with efforts only abridged by World War II (3, 4). As research resumed following the war, and a deeper understanding of radiobiology and the role of linear energy transfer (LET) developed, Catterall and colleagues began neutron radiotherapy treatment at Hammersmith Hospital in London in 1965.

While neutron radiotherapy exhibits high-LET, its conventional dose distribution limited the beam due to inherent toxicity unmitigated by fractionation (5). CPT was viewed as a viable alternative, combining high-LET with the Bragg peak, a physical characteristic of ion radiotherapy in which dose is deposited at an inverse of particle energy (6). This combination of physical and radiobiological advantages over conventional radiotherapy leads to an enhancement of the therapeutic ratio (7), with areas of higher LET experiencing higher relative biological effect

(RBE); that is, an equal physical dose of CPT will have a resultant increased effect compared with conventional radiotherapy.

This expanded interest localized at the Lawrence Berkeley National Laboratory (LBNL). Following commissioning of the Bevalac in 1971, evaluation of fast neutron, proton, and negative pions, as well as helium, carbon, neon, nitrogen, silicon, and argon-ion beams began (3, 8). Each ion expresses high-LET regions within the particle travel path: the resultant distribution of LET varies between particles, as does the theorized physical dose distribution advantage. High-LET regions range from extreme distal in proton (9) to increasingly proximal with increase in atomic size (6). Each ion demonstrated benefits and limitations, with helium employed for improved dose localization and heavier-ions to amplify biological effect (10). Though initial work was promising, research ceased when the Bevalac and Bevatron were decommissioned in 1993 (8).

MODERN PARTICLE THERAPY

The advantages of particle radiotherapy are not without cost: the initial capital expense of particle centers is prohibitive and cost-benefit ratio remains a topic of considerable discussion (11–15). Moreover, in comparison with the relatively uniform ionization provided by conventional radiotherapy, with each ion comes varying considerations of intrabeam LET distributions, range uncertainty, lateral scattering, and distal fragmentation (16), as well as accurate dose deposition modeling along the beam path within varying tissues (17), and, finally, the combination of these factors into a treatment algorithm capable of providing a uniform biological effect within the treatment target. These latter elements, critically important for successful delivery of patient care, complicated the translation of photon doses into ion-beam treatment and informed the use of dose escalation clinical trials for determination of target and ceiling doses for histological sites (6).

Particle monotherapy has dominated discussion to date, and debate today continues: is there an ideal particle for treatment, and particularly for cost effective treatment? (18). When the Heavy Ion Medical Accelerator in Chiba (HIMAC) was constructed at the National Institute of Radiological Science (NIRS, Japan) in the early 1990s, prior experience at the Bevalac as well as previous usage of neutron at NIRS led to the selection of carbon-ions as the best ion for treatment, balancing considerations of particle size, center cost, and the perceived similarity of the RBE of the carbon-ion in its Bragg Peak to prior studies with neutron (6, 19).

Carbon-ion radiotherapy (CIRT) has remained under development for 30 years at the HIMAC, as well as at the German Society for Heavy Ion Research (Gesellschaft für Schwerionenforschung, GSI) and later Heidelberg Ion Beam Therapy Center (HIT), with significant physical, radiobiological, and clinical outcomes reported (6, 7). Clinical trials with CIRT have demonstrated enhanced kill effect in target tumors while simultaneously sparing normal tissue, with promising implications for reductions in secondary cancer incidence (20). The effect of the high-LET beam on traditionally radioresistant cancer has demonstrated unique promise, including in recurrent rectal cancer (21, 22), pancreas (23–25), glioma (26, 27), sarcoma (28–30), head-and-neck (31, 32), and others (7), with notable radiobiological effects seen in tissue *versus* conventional irradiation (33–35).

Nonetheless, CIRT can still result in imperfect local control, be this due to insufficient dose, uniquely radioresistant areas of the tumor [ranging from hypoxic regions (36) to isolated highly resistant stem-like cells (37)], or imperfect modeling of dose delivery (38). Other ions have demonstrated differing physical advantages, particularly with regard to variations in LET and physical dose distribution. After promising results at the LBNL, helium-ion radiotherapy has resurged through ongoing clinical translation at Heidelberg. Helium offers a decreased lateral scatter effect *versus* proton (39), with less fragmentation tail dose *versus* carbon. Kopp and colleagues have demonstrated single field setups with helium with an $RBE_{50\%}$ of 1.56 *versus* 2.16 for carbon in glioma, and 1.44 *vs.* 1.99 in ACC; this comes, however, with significantly lowered $LET_{50\%}$ (14.66 *vs.* 73.00 keV/micrometer in glioma and 13.39 *vs.* 64.92 in ACC). The authors concluded that combining the two would provide for more stable LET_d and RBE distributions *versus* monotherapy with either beam (40). Meanwhile, the United States has principally pursued proton irradiation with forays into LET optimization (NCT03750513), but has to date been unable to leverage the potential benefits of heavy-ion high-LET radiation in patient care.

LET AND RBE

The ability to sterilize a tumor is influenced both by physical dose delivered as well as the inherent LET of the beam path as it passes through the tumor. Heterogeneity of underlying tissue and the oxygen concentration within that tissue complicate the translation of target dose to cell-killing effect yet further, amplified by a current inability to study *in vivo* cell-level differences (41). Notably, the oxygen enhancement ratio, that is the particular radiation needed to result in equivalent treatment in the presence or absence of oxygen, is lower in particle therapy than with photon and generally increases with LET and decreases with atomic mass; this informs the apparent increased efficacy of heavy-ion radiotherapy in hypoxic conditions (19). To facilitate comparative utility between carbon-ion and photon irradiation, the RBE of a physical dose within a target was modeled: the Kanai model is experimentally derived and similar to the original models utilized at the Bevalac, defining RBE based on 10% survival of human salivary gland tumor cells under aerobic conditions (42). The microdosimetric kinetic model and local effect model were alternatively developed, the former for scanning CIRT in Japan and tuned to the Kanai model (43), while the latter was developed for European centers based on a biophysical modeling approach (44). Variations between the models have complicated regimen comparability between world centers (38).

Bassler and colleagues have demonstrated that even with equivalent dose distributions, substantially different LET distributions may be seen owing to LET dilution through secondary low-LET fragments generated through inflight nuclear reactions with increasing depth (45). The result is an equivalent dose delivered with variabilities in RBE. Clinically, this uncertainty has been effectively circumvented through dose escalation trials, tailoring dose delivered to levels of unacceptable toxicity. These phase I/II clinical trials have enabled the safe delivery of significantly ablative doses of CIRT (6), but with poor selectivity for delivering enhanced RBE to target regions within a tumor. LET/kill-painting is one method to bridge the gap between dose prescribed and cell kill-effect delivered: by optimizing and/or making uniform the high-LET region of CPT, oxygen effect may be minimized, thereby improving the uniformity of cell kill effect delivered (41). Moreover, low-LET regions of the beam could be preferentially relocated to healthy tissue, in theory further reducing healthy tissue toxicity (46). LET-weighted doses have effectively been demonstrated in proton radiotherapy (47).

The clinical relationship between LET distribution within a tumor and tumor control has been explored in CIRT. Hagiwara and colleagues studied the influence of dose-averaged LET on CIRT-irradiated pancreatic tumor control in 2020 (48), retrospectively evaluating 18 patients treated with 55.2 Gy (RBE) CIRT at a median of 22 months. Four infield central local recurrences were noted. While dose was uniform throughout the tumor, LET was lower within the central compartment of the target volume, owing to how particle paths were overlapped to generate a spread out Bragg peak. Notably, local control was improved in those patients with higher minimum dose-averaged LET within the gross tumor volume (GTV), independent of the minimal dose and D98 delivered (48). Improved dose-averaged LET within the GTV may thereby improve local control, though the ability to fully control the LET within the tumor target may be limited by the LET distribution inherent to the carbon-ion beam, and the tumor's relationship to nearby radiosensitive organs.

Okonogi and colleagues similarly considered uterine cancer, focusing on whether LET was correlative with late rectal toxicity rate (49). In evaluating 132 patients with CIRT-treated uterine carcinoma and greater than 6 months of follow-up, nine were noted to have grade 3 or 4 late rectal complications. Regression analysis demonstrated an association with rectal D_{2cc}, but not with dose-averaged LET nor physical dose. This echoes similar studies in proton that have demonstrated that LET and physical dose alone are poor correlative measures, and rather that the RBE-weighted dose is critical (50–52).

Seeking adequate base dose with strategically deployed high-LET irradiation led to initial combination studies, specifically modern CIRT-boost treatments (45) (p). Boost treatments typically combine CIRT or the lower-LET proton beam with intensity-modulated [photon] radiation therapy (IMRT), tomotherapy, or other forms of conventional radiotherapy (26, 53–59). Schulz-Ertner and colleagues in 2005 deployed carbon-boosted photon on adenoid cystic carcinoma to achieve three times the locoregional control of photon at 4 years (60). Another trial is investigating CIRT-boost for image-guided brachytherapy in locally advanced cervical cancer (61). Others have aimed to combine CIRT with proton, such as in one phase I/III trial on glioblastoma at the Shanghai Proton and Heavy Ion Center (62). Principally, the majority of modern high-LET clinical treatment has employed CIRT alone (6), and without LET optimization.

In seeking optimized LET within target tissues, Bassler and colleagues originated the concept of LET painting, building off the pioneering photon dose-painting concept by Ling et al. (63), and have evaluated multiple heavy-ions. For instance, LET-painting with carbon-ions allowed hypoxic subvolume control to a limit of 0.5 cm^3; oxygen-ions, by comparison, could be extended to 2 cm^3, and were further extendable with dose escalation (46). However, higher-LET oxygen-ion radiotherapy may cause increased normal tissue damage (41); no single ion has emerged as optimized for dose distribution, oxygen enhancement ratio (OER), nor overall translatability to hypoxic/radioresistant tumor kill effect.

Multi-ion radiotherapy (MIRT) theoretically provides for the benefits of each ion to be synergistically deployed in treatment. While intensity-modulated and LET-painted CIRT alone may achieve a high dose-optimized LET within a majority of tumor targets, the beam's utility is limited by its inherent physical LET distribution. As such, incorporating the varying LET distributions of other heavy-ions into a dose-LET-optimized composite treatment plan may allow for new treatment options for patients with complex cancers. Lower-LET beams such as helium may offer improved margin dosage where tumors lie close to normoxic, healthy tissues, while higher-LET irradiation can be layered into hypoxic, radioresistant regions. Adaptive treatment planning would involve optimizing across multiple ions so as to achieve ideal cell-killing effect in the target tumor.

This is an easy vision to articulate, but decades in the making; innumerable challenges remain prior to trial development.

ONGOING DEVELOPMENT OF MIRT

CIRT treatment at the NIRS-QST today combines pencil-beam raster (re)scanning (64–66), a phase-controlled 3D scanning irradiation system (67), motion management incorporating fast rescanning with respiratory gating (64, 68), and a superconducting gantry (69), enabling the conformal painting of heavy-ions voxel-by-voxel through a target and in theory the employment of combination dose- and LET-based treatment plans with LET/kill-painting of tumor tissue. Within this system, NIRS-QST plans to deploy helium, carbon, oxygen, and neon-ions for MIRT (70). Optimization of ion source insertion, and the rapid changing of sources, is critical for clinical throughput in a MIRT facility. This will use a single electron cyclotron resonance ion source (ECR-IS) with fast gas-switching operation. Particles are electron-stripped and then accelerated within a synchrotron, with beam purity assured due to mass separation owing to variation in mass-to-charge ratios. As helium-ions bear an equivalent ratio, Mizushima and

colleagues developed a method to ensure beam purity prior to treatment using an ionization chamber and Faraday cup, with a contamination rate less than 1% (70).

In 2016, Inaniwa and colleagues introduced a method to deliver two or more ion species in one treatment session, termed intensity modulated composite particle therapy (IMPACT) (71). By employing proton, helium, carbon, and oxygen ions, they were able to delineate valid prescribed LET ranges within a water phantom in opposing and orthogonal geometries. They further demonstrated the optimization method in a simulated prostate case, incorporating all four above ions. They were able to adjust the prostate, planning target volume, and rectum LETs to 80 keV/μm, 50 keV/μm, and below 30 keVμm, respectively, while maintaining dose in the PTV to a uniform 2 Gy. This served as proof of concept for the IMPACT system to dose and LET-average multiple ions within the treatment planning system at the NIRS. A demonstration of this system in pancreatic cancer may be seen in **Figure 1**, demonstrating the CIRT dose and LET distributions (**Figures 1A, B**), and the equivalent LET distribution using the IMPACT system (**Figure 1C**), with increased LET to 100 in the center field and decrease of OER from 2.8 to approximately 1.5. However, the IMPACT system at that time did not describe biological effect, and the authors noted that further development was required prior to beginning clinical trialing.

Inaniwa et al. additionally explored the nuclear interactions of particles within patients, adapting and validating the previously described planar integrated dose distribution measured in water (PID) correction method for scanned CIRT for treatment plans involving helium-, carbon-, oxygen-, and neon-ion beams (72). They similarly verified the stochastic microdosimetric kinetic model following previous work to optimize computational time and memory space, and verified the model within two cell irradiation experimental models, HSGc-C5 and MIA PaCa-2, which have notably different radiation sensitivities, for hypofractionated MIRT (73). This enables treatment planning of hypofractionated MIRT within treatment systems utilizing the MK model, principally centers in Japan.

At GSI, Scifoni et al. in 2013 developed an initial method for including OER in ion beam treatment planning (74, 75). Following the work by Tinganelli and colleagues of LET-mediated kill painting (41), Sokol et al. extended the methodology to incorporate multiple ions and voxel-by-voxel target oxygenation data. Utilizing this plan with helium and oxygen ion beams, mean brainstem dose was reduced by 3–5% for helium and 10–12% for oxygen, respectively, with full biological optimization. Dosimetric validation of these particle species (76), validation of Monte Carlo modeling FLUKA code (77), and experimental validation of the resultant treatment planning tool against dosimetric measurements in water, have similarly been performed (78).

Kopp and colleagues followed with the "PaRticle thErapy using single and Combined Ion optimization StratEgies" (PRECISE) treatment planning system, allowing for delivery of single field multi-ion particle therapy treatments (40). They validated these plans across three patient cases, as well as in a murine glioma cell line, generating a highly uniform physical dose while reducing high dose averaged LET gradients in comparison with CIRT monotherapy. They found that biophysical stability in the target volume was similar to protons, while normal tissue dose was similar or improved *versus* helium dose planning, with < 1% deviation from the planned target RBE value.

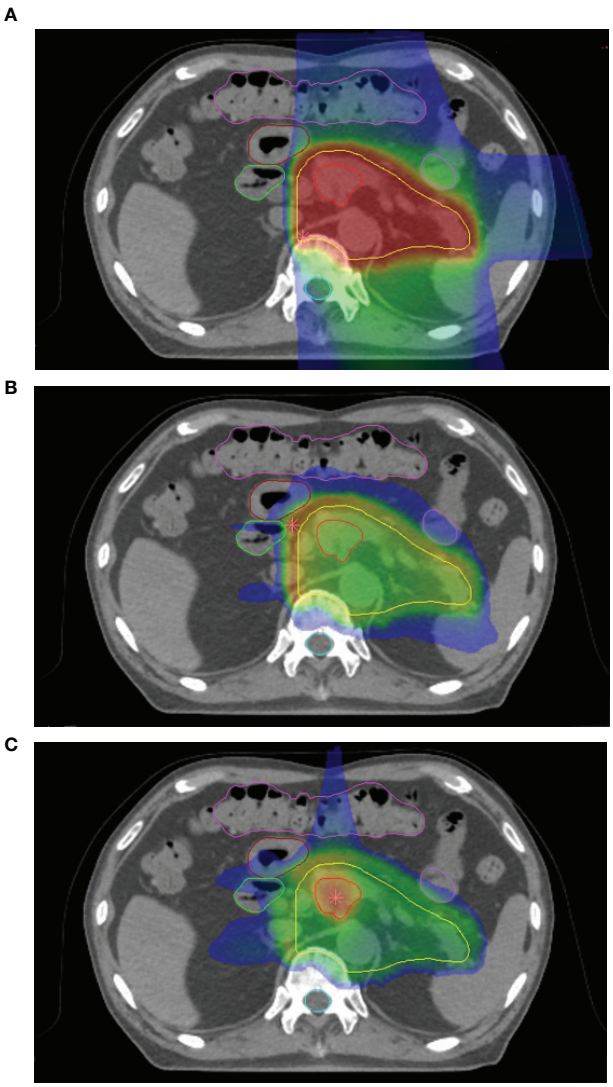

FIGURE 1 | **(A)** Dose distribution of carbon-ion radiotherapy (CIRT) for a case of pancreatic cancer. **(B)** Linear energy transfer (LET) distribution of the same case. Note overlying LET distribution near organs-at-risk. **(C)** The LET of the same case combining helium, carbon, and oxygen-ion treatments using the intensity modulated composite particle therapy (IMPACT) system.

CHALLENGES, FUTURE DIRECTIONS, AND CONCLUSIONS

Significant considerations are required for the possible translation of these initial developments within MIRT to

clinical treatment. Incorporation of lighter ions to reduce damage to target-adjacent normal tissues may risk underdosing relative single-beam irradiation. Careful multi-angle dose simulation, modeling, and validation is required. Center treatment throughput will require consideration: the NIRS has developed a system capable of source switching in under one minute, with ongoing development to reduce source switching to < 5 s. Treatment times could thereby only be limited by patient repositioning. Further details regarding a multi-ion clinical treatment system at the NIRS-QST are forthcoming.

Notably, dose-averaged LET is a macroscopic quantity, and may poorly approximate the physical reactions occurring at a cellular level (79). LET and RBE do not form a linear relationship, with track structure and microdosimetry potentially allowing an outsized increase in RBE with increases in LET (80, 81). Consequently, the translation of physical dose to a uniform cell-killing biological effect is model-dependent. Biological effects in varying tissues unique to any given ion may be as-yet unknown, and translation of physical dose and LET-optimized distributions to kill effect will require significant development.

To date, both the MKM and LEM models assume a normal oxygen pressure. As the key treatment targets for MIRT are focused on radioresistant and hypoxic tumors, evaluation of tissue oxygen conditions and resultant biological effects will be needed (82). Moreover, variation in biophysical models between ions (38, 83) requires reconciliation, including means by which to evaluate clinical uncertainty during treatment planning. As current dose plan arrangements encounter difficulty in intermodal translation (38), careful planning with MIRT is required so as not to exacerbate these issues during initial clinical trials. Further consideration of what range of LET provides the ideal clinical effect is also needed (84). Similarly, biological differences inherent to dose rate are currently being explored (i.e., FLASH); current biophysical modeling assumes a normal dose rate, and variations in treatment effect between dose rates may also influence future CPT and MIRT treatment. Developments within these areas of study will deserve careful note.

An external, international assessment of CIRT at NIRS was conducted in 2015, noting the significant promise of CIRT and recommending key consideration for methodologies improving patient throughput while reducing cost (7). These thoughts similarly inform efforts to translate MIRT from bench to bedside. Concerns regarding secondary cancer development with ion therapy remain, though a propensity score-weighted analysis comparing CIRT, conventional radiotherapy, and surgery for localized prostate cancer found a lower risk of subsequent primary cancer following CIRT *vs*. photon irradiation (20). Further verification will be needed as novel ion therapies are employed in treatment.

Particle irradiation has been studied for 70 years. Today, as the United States endeavors to construct its first heavy-ion capable facility and centers in Europe and Asia continue development of heavy-ion, multi-ion radiotherapy appears technically feasible for future treatment of radioresistant and hypoxic cancers. Robust international collaboration will be critical to produce dose modeling consensus, build upon the common borders of radiobiology and particle physics, and ensure access of the global population to novel treatments within radiation oncology. Significant technological and radiobiological progress has been made toward realizing initial trials for multi-ion radiotherapy, but more remains.

DATA AVAILABILITY STATEMENT

The original contributions presented in the study are included in the article/supplementary material. Further inquiries can be directed to the corresponding author.

AUTHOR CONTRIBUTIONS

DE: manuscript conception, writing, preparation TI: preparation. editing, review, figure preparation. DE, SF, SY and TS: conception, preparation, editing, review. All authors contributed to the article and approved the submitted version.

FUNDING

Supported in part by Cancer Center Support (Core) Grant P30 CA016672 (PI, PWT Pisters) from the National Cancer Institute, National Institutes of Health, to The University of Texas MD Anderson Cancer Center.

REFERENCES

1. Tobias CA, Anger HO, Lawrence JH. Radiological use of high energy deuterons and alpha particles. *Am J Roentgenol Radium Ther Nucl Med* (1952) 67(1):1.
2. Blakely EA. The 20th Gray lecture 2019: health and heavy ions. *Br J Radiol* (2020) 93(1115):20200172. doi: 10.1259/bjr.20200172
3. Curtis SB. The New Particles and Their Application in Medicine.In: *Advances in Radiation Protection and Dosimetry in Medicine*. NewYork: Springer (1980). p. 5–25. doi: 10.1007/978-1-4757-1715-0_2
4. Halperin EC. Particle therapy and treatment of cancer. *Lancet Oncol* (2006) 7 (8):676–85. doi: 10.1016/S1470-2045(06)70795-1
5. Bewley DK, Field SB, Morgan RL, Page BC, Parnell CJ. The response of pig skin to fractionated treatments with fast neutrons and X rays. *Br J Radiol* (1967) 40(478):765–70. doi: 10.1259/0007-1285-40-478-765
6. Tsujii H, Kamada T, Shirai T, Noda K, Tsuji H, Karasawa K. (eds). *Carbon-Ion Radiotherapy*. Japan: Springer (2014), Published online. doi: 10.1007/978-4-431-54457-9
7. Kamada T, Tsujii H, Blakely EA, Debus J, De Neve W, Durante M, et al. Carbon ion radiotherapy in Japan: an assessment of 20 years of clinical experience. *Lancet Oncol* (2015) 16(2):e93–e100. doi: 10.1016/S1470-2045(14)70412-7
8. Castro JR, Quivey JM, Lyman JT, Chen GT, Phillips TL, Tobias CA. Radiotherapy with heavy charged particles at Lawrence Berkeley Laboratory. *J Can Assoc Radiol* (1980) 31(1):30.

9. Saager M, Peschke P, Brons S, Debus J, Karger CP. Determination of the proton RBE in the rat spinal cord: Is there an increase towards the end of the spread-out Bragg peak? *Radiother Oncol* (2018) 128(1):115–20. doi: 10.1016/j.radonc.2018.03.002
10. Castro JR. *Progress report on heavy particle clinical radiotherapy trial at LawrenceBerkeley Laboratory July 1975-July 1979*. Berkeley, CA: Lawrence Berkeley Laboratory (1979), Published online. doi: 10.2172/5774694
11. Bekelman JE, Hahn SM. The Body of Evidence for Advanced Technology in RadiationOncology. *JNCI J Natl Cancer Inst* (2013) 105(1): 6–7.
12. Mobaraki A, Ohno T, Yamada S, Sakurai H, Nakano T. Cost-effectiveness of carbon ion radiation therapy for locally recurrent rectal cancer. *Cancer Sci* (2010) 101(8):1834–9. doi: 10.1111/j.1349-7006.2010.01604.x
13. Jäkel O, Land B, Combs SE, Schulz-Ertner D, Debus J. On the cost-effectiveness of carbon ion radiation therapy for skull base chordoma. *Radiother Oncol* (2007) 83(2):133–8. doi: 10.1016/j.radonc.2007.03.010
14. Ohno T, Kanai T, Yamada S, Yusa K, Tashiro M, Shimada H, et al. Carbon ion radiotherapy at the Gunma University Heavy Ion Medical Center: new facility set-up. *Cancers* (2011) 3(4):4046–60. doi: 10.3390/cancers3044046
15. Peeters A, Grutters JP, Pijls-Johannesma M, Reimoser S, De Ruysscher D, Severens JL, et al. How costly is particle therapy? Cost analysis of external beam radiotherapy with carbon-ions, protons and photons. *Radiother Oncol* (2010) 95(1):45–53. doi: 10.1016/j.radonc.2009.12.002
16. Amaldi U, Kraft G. Radiotherapy with beams of carbon ions. *Rep Prog Phys* (2005) 68(8):1861. doi: 10.1088/0034-4885/68/8/R04
17. Loeffler JS, Durante M. Charged particle therapy—optimization, challenges and future directions. *Nat Rev Clin Oncol* (2013) 10(7):411–24. doi: 10.1038/nrclinonc.2013.79
18. Beltran C, Amos RA, Rong Y. We are ready for clinical implementation of Carbon Ion Radiotherapy in the United States. *J Appl Clin Med Phys* (2020) 21 (12):6–9. doi: 10.1002/acm2.13133
19. Mohamad O, Makishima H, Kamada T. Evolution of carbon ion radiotherapy at the National Institute of Radiological Sciences in Japan. *Cancers* (2018) 10 (3):66. doi: 10.3390/cancers10030066
20. Mohamad O, Tabuchi T, Nitta Y, Nomoto A, Sato S, Kasuya G, et al. Risk of subsequent primary cancers after carbon ion radiotherapy, photon radiotherapy, or surgery for localised prostate cancer: a propensity score-weighted, retrospective, cohort study. *Lancet Oncol* (2019) 20(5):674–85. doi: 10.1016/S1470-2045(18)30931-8
21. Yamada S, Kamada T, Ebner DK, Shinoto M, Terashima K, Isozaki Y, et al. Carbon-ion radiation therapy for pelvic recurrence of rectal cancer. *Int J Radiat Oncol Biol Phys* (2016) 96(1):93–101. doi: 10.1016/j.ijrobp.2016.04.022
22. Shinoto M, Yamada S, Okamoto M, Shioyama Y, Ohno T, Nakano T, et al. Carbon-ion radiotherapy for locally recurrent rectal cancer: Japan carbon-ion radiation oncology study group (J-CROS) study 1404 rectum. *Radiother Oncol* (2019) 132:236–40. doi: 10.1016/j.radonc.2018.10.007
23. Ebner DK, Shinoto M, Kawashiro S, Isozaki Y, Kamada T, Yamada S. Phase 1/2 trial of preoperative short-course carbon-ion radiation therapy for patients with resectable pancreatic cancer. *Int J Radiat Oncol Biol Phys* (2017) 99(2): S144. doi: 10.1016/j.ijrobp.2017.06.334
24. Shinoto M, Yamada S, Yasuda S, Imada H, Shioyama Y, Honda H, et al. Phase 1 trial of preoperative, short-course carbon-ion radiotherapy for patients with resectable pancreatic cancer. *Cancer* (2013) 119(1):45–51. doi: 10.1002/cncr.27723
25. Kawashiro S, Yamada S, Okamoto M, Ohno T, Nakano T, Shinoto M, et al. Multi-institutional study of carbon-ion radiotherapy for locally advanced pancreatic cancer: Japan carbon-ion radiation oncology study group (J-CROS) study 1403 pancreas. *Int J Radiat Oncol Biol Phys* (2018) 101 (5):1212–21. doi: 10.1016/j.ijrobp.2018.04.057
26. Malouff TD, Peterson JL, Mahajan A, Trifiletti DM. Carbon ion radiotherapy in the treatment of gliomas: A review. *J Neurooncol* (2019) 145(2):191–9. doi: 10.1007/s11060-019-03303-y
27. Chiblak S, Tang Z, Lemke D, Knoll M, Dokic I, Warta R, et al. Carbon irradiation overcomes glioma radioresistance by eradicatingstem cells and forming an antiangiogenic and immunopermissive niche. *JCIInsight* (2019) 4 (2):e123837. doi: 10.1172/jci.insight.123837
28. Imai R, Kamada T, Araki N, Knoll M, Dokic I, Warta R, et al. Carbon ion radiotherapy for unresectable localized axial soft tissue sarcoma. *Cancer Med* (2018) 7(9):4308–14. doi: 10.1002/cam4.1679
29. Takenaka S, Araki N, Outani H, Hamada KI, Yoshikawa H, Kamada T, et al. Complication rate, functional outcomes, and risk factors associated with carbon ion radiotherapy for patients with unresectable pelvic bone sarcoma. *Cancer* (2020) 126(18):4188–96. doi: 10.1002/cncr.33082
30. Imai R, Kamada T, Araki N. Clinical efficacy of carbon ion radiotherapy for unresectable chondrosarcomas. *Anticancer Res* (2017) 37(12):6959–64. doi: 10.21873/anticanres.12162
31. Koto M, Demizu Y, Saitoh J, et al. Multicenter Study of Carbon-Ion Radiation Therapy for Mucosal Melanoma of the Head and Neck: Subanalysis of the Japan Carbon-Ion Radiation Oncology Study Group (J-CROS) Study (1402 HN). *Int J Radiat Oncol Biol Phys* (2017) 97(5):1054–60. doi: 10.1016/j.ijrobp.2016.12.028
32. Sulaiman NS, Demizu Y, Koto M, et al. Multicenter Study of Carbon-Ion Radiation Therapy for Adenoid Cystic Carcinoma of the Head and Neck: Subanalysis of the Japan Carbon-Ion Radiation Oncology Study Group (J-CROS) Study (1402 HN). *Int J Radiat Oncol Biol Phys* (2018) 100(3):639–46. doi: 10.1016/j.ijrobp.2017.11.010
33. Sato K, Nitta N, Aoki I, Imai T, Shimokawa T. Repeated photon and C-ion irradiations in vivo have different impact on alteration of tumor characteristics. *Sci Rep* (2018) 8(1):1–12. doi: 10.1038/s41598-018-19422-x
34. Sato K, Shimokawa T, Imai T. Radioresistance acquisition after repeated irradiation Acquisition of Radioresistance in Cancer Cells Following Repeated Photon or Particle Irradiation. *Front Oncol* (2019) 9:1213. doi: 10.3389/fonc.2019.01213
35. Schlaff CD, Krauze A, Belard A, O'Connell JJ, Camphausen KA. Bringing the heavy: carbon ion therapy in the radiobiological and clinical context. *Radiat Oncol* (2014) 9(1):88. doi: 10.1186/1748-717X-9-88
36. Valable S, Gérault AN, Lambert G, Leblond M, Anfray C, Toutain J, et al. Impact of Hypoxia on Carbon Ion Therapy in Glioblastoma Cells: Modulation by LET and Hypoxia-Dependent Genes. *Cancers* (2020) 12(8):2019. doi: 10.3390/cancers12082019
37. Oonishi K, Cui X, Hirakawa H, Fujimori A, Kamijo T, Yamada S, et al. Different effects of carbon ion beams and X-rays on clonogenic survival and DNA repair in human pancreatic cancer stem-like cells. *Radiother Oncol* (2012) 105(2):258–65. doi: 10.1016/j.radonc.2012.08.009
38. Fossati P, Matsufuji N, Kamada T, Karger CP. Radiobiological issues in prospective carbon ion therapy trials. *Med Phys* (2018) 45(11):e1096–110. doi: 10.1002/mp.12506
39. Knäusl B, Fuchs H, Dieckmann K, Georg D. Can particle beam therapy be improved using helium ions? – a planning study focusing on pediatric patients. *Acta Oncol* (2016) 55(6):751–9. doi: 10.3109/0284186X.2015.1125016
40. Kopp B, Mein S, Dokic I, Harrabi S, Böhlen TT, Haberer T, et al. Development and Validation of Single Field Multi-Ion Particle Therapy Treatments. *Int J Radiat Oncol Biol Phys* (2020) 106(1):194–205. doi: 10.1016/j.ijrobp.2019.10.008
41. Tinganelli W, Durante M, Hirayama R, Krämer M, Maier A, Kraft-Weyrather W, et al. Kill-painting of hypoxic tumours in charged particle therapy. *Sci Rep* (2015) 5(1):17016. doi: 10.1038/srep17016
42. Kanai T, Endo M, Minohara S, Miyahara N, Koyama-ito H, Tomura H, et al. Biophysical characteristics of HIMAC clinical irradiation system for heavy-ion radiation therapy. *Int J Radiat Oncol Biol Phys* (1999) 44(1):201–10. doi: 10.1016/S0360-3016(98)00544-6
43. Inaniwa T, Kanematsu N, Matsufuji N, Kanai T, Shirai T, Noda K, et al. Reformulation of a clinical-dose system for carbon-ion radiotherapy treatment planning at the National Institute of Radiological Sciences, Japan. *Phys Med Biol* (2015) 60(8):3271. doi: 10.1088/0031-9155/60/8/3271
44. Friedrich T, Durante M, Scholz M. *The local effect model-principles and applications. Health Risks ExtraterrEnviron*. (2013), Published online. Available at: https://three.jsc.nasa.gov/archive/.
45. Bassler N, Jäkel O, Søndergaard CS, Petersen JB. Dose- and LET-painting with particle therapy. *Acta Oncol* (2010) 49(7):1170–6. doi: 10.3109/0284186X.2010.510640
46. Bassler N, Toftegaard J, Lühr A, Sørensen BS, Scifoni E, Krämer M, et al. LET-painting increases tumour control probability in hypoxic tumours. *Acta Oncol* (2014) 53(1):25–32. doi: 10.3109/0284186X.2013.832835
47. McMahon SJ, Paganetti H, Prise KM. LET-weighted doses effectively reduce biological variability in proton radiotherapy planning. *Phys Med Biol* (2018) 63(22):225009. doi: 10.1088/1361-6560/aae8a5

48. Hagiwara Y, Bhattacharyya T, Matsufuji N, Isozaki Y, Takiyama H, Nemoto K, et al. Influence of dose-averaged linear energy transfer on tumour control after carbon-ion radiation therapy for pancreatic cancer. *Clin Transl Radiat Oncol* (2019) 21:19–24. doi: 10.1016/j.ctro.2019.11.002
49. Okonogi N, Matsumoto S, Fukahori M, Furuichi W, Inaniwa T, Matsufuji N, et al. Dose-averaged linear energy transfer per se does not correlate withlate rectal complications in carbon-ion radiotherapy. *Radiother Oncol* (2020) 153:272–8. doi: 10.1016/j.radonc.2020.08.029
50. Giantsoudi D, Sethi RV, Yeap BY, Eaton BR, Ebb DH, Caruso PA, et al. Incidence of CNS injury for a cohort of 111 patients treated with proton therapy for medulloblastoma: LET and RBE associations for areas of injury. *Int J Radiat Oncol Biol Phys* (2016) 95(1):287–96. doi: 10.1016/j.ijrobp.2015.09.015
51. Wang C-C, McNamara AL, Shin J, Schuemann J, Grassberger C, Taghian AG, et al. End-of-range Radiobiological Effect on Rib Fractures in Patients Receiving Proton Therapy for Breast Cancer. *Int J Radiat Oncol BiolPhys* (2020) 107(3): 449–54. doi: 10.1016/j.ijrobp.2020.03.012
52. Peeler CR, Mirkovic D, Titt U, et al. Clinical evidence of variable proton biological effectiveness in pediatric patients treated for ependymoma. *Radiother Oncol* (2016) 121(3):395–401. doi: 10.1016/j.radonc.2016.11.001
53. Jensen AD, Nikoghosyan A, Hinke A, Debus J, Münter MW. Combined treatment of adenoid cystic carcinoma with cetuximab and IMRT plus C12 heavy ion boost: ACCEPT [ACC, Erbitux® and particle therapy]. *BMC Cancer* (2011) 11(1):70. doi: 10.1186/1471-2407-11-70
54. Jensen AD, Krauss J, Potthoff K, Desta A, Habl G, Mavtratzas A, et al. Phase II study of induction chemotherapy with TPF followed by radioimmunotherapy with Cetuximab and intensity-modulated radiotherapy (IMRT) in combination with a carbon ion boost for locally advanced tumours of the oro-, hypopharynx and larynx-TPF-C-HIT. *BMC Cancer* (2011) 11(1):1–11. doi: 10.1186/1471-2407-11-182
55. Marvaso G, Jereczek-Fossa BA, Vischioni B, Ciardo D, Giandini T, Hasegawa A, et al. Phase II multi-institutional clinical trial on a new mixed beam RT scheme of IMRT on pelvis combined with a carbon ion boost for high-risk prostate cancer patients. *Tumori J* (2017) 103(3):314–8. doi: 10.5301/tj.5000587
56. Adeberg S, Windisch P, Ehret F, Baur M, Akbaba S, Held T, et al. Intensity Modulated Radiotherapy (IMRT) With Carbon Ion Boost in the Multimodal Treatment of Salivary Duct Carcinoma. *Front Oncol* (2019) 9:1420. doi: 10.3389/fonc.2019.01420
57. Akbaba S, Ahmed D, Mock A, Held T, Bahadir S, Lang K, et al. Treatment Outcome of 227 Patients with Sinonasal Adenoid Cystic Carcinoma (ACC) after Intensity Modulated Radiotherapy and Active Raster-Scanning Carbon Ion Boost: A 10-Year Single-Center Experience. *Cancers* (2019) 11(11):1705. doi: 10.3390/cancers11111705
58. Lang K, Baur M, Akbaba S, Held T, Kargus S, Bougatf N, et al. Intensity modulated radiotherapy (IMRT)+ carbon ion boost for adenoid cystic carcinoma of the minor salivary glands in the oral cavity. *Cancers* (2018) 10 (12):488. doi: 10.3390/cancers10120488
59. Kraus KM, Pfaffenberger A, Jäkel O, Debus J, Sterzing F. Evaluation of Dosimetric Robustness of Carbon Ion Boost Therapy for Anal Carcinoma. *Int J Part Ther* (2016) 3(3):382–91. doi: 10.14338/IJPT-16-00028.1
60. Schulz-Ertner D, Nikoghosyan A, Didinger B, Münter M, Jäkel O, Karger CP, et al. Therapy strategies for locally advanced adenoid cystic carcinomas using modern radiation therapy techniques. *Cancer* (2005) 104(2):338–44. doi: 10.1002/cncr.21158
61. Ohno T, Noda S, Murata K, Yoshimoto T, Okonogi N, Ando K, et al. Phase I study of carbon ion radiotherapy and image-guided brachytherapy for locally advanced cervical cancer. *Cancers* (2018) 10(9):338. doi: 10.3390/cancers10090338
62. Kong L, Gao J, Hu J, Lu R, Yang J, Qiu X, et al. Carbon ion radiotherapy boost in the treatment of glioblastoma: a randomized phase I/III clinical trial. *Cancer Commun* (2019) 39(1):5. doi: 10.1186/s40880-019-0351-2
63. Ling CC, Humm J, Larson S, Amols H, Fuks Z, Leibel S, et al. Towards multidimensional radiotherapy (MD-CRT): biological imaging and biological conformality. *Int J Radiat Oncol Biol Phys* (2000) 47(3):551–60. doi: 10.1016/s0360-3016(00)00467-3
64. Mori S, Zenklusen S, Inaniwa T, Furukawa T, Imada H, Shirai T, et al. Conformity and robustness of gated rescanned carbon ion pencil beam scanning of liver tumors at NIRS. *Radiother Oncol* (2014) 111(3):431–6. doi: 10.1016/j.radonc.2014.03.009
65. Furukawa T, Inaniwa T, Sato S, Shirai T, Takei Y, Takeshita E, et al. Performance of the NIRS fast scanning system for heavy-ion radiotherapy. *Med Phys* (2010) 37(11):5672–82. doi: 10.1118/1.3501313
66. Mizushima K, Furukawa T, Iwata Y, Shirai T, Takei Y, Takeshita E, et al. Performance of the HIMAC beam control system using multiple-energy synchrotron operation. *Nucl Instrum Methods Phys Res Sect B Beam Interact Mater At* (2017) 406:347–51. doi: 10.1016/j.nimb.2017.03.051
67. Mori S, Furukawa T, Inaniwa T, Zenklusen S, Nakao M, Shirai T, et al. Systematic evaluation of four-dimensional hybrid depth scanning for carbon-ion lung therapy. *Med Phys* (2013) 40(3):031720. doi: 10.1118/1.4792295
68. Ebner DK, Tsuji H, Yasuda S, Yamamoto N, Mori S, Kamada T. Respiration-gated fast-rescanning carbon-ion radiotherapy. *Jpn J Clin Oncol* (2017) 47 (1):80–3. doi: 10.1093/jjco/hyw144
69. Bhattacharyya T, Koto M, Ikawa H, Hayashi K, Hagiwara Y, Makishima H, et al. First prospective feasibility study of carbon-ion radiotherapy using compact superconducting rotating gantry. *Br J Radiol* (2019) 92 (1103):20190370. doi: 10.1259/bjr.20190370
70. Mizushima K, Iwata Y, Muramatsu M, Lee SH, Shirai T. Experimental study on monitoring system of clinical beam purity in multiple-ion beam operation for heavy-ion radiotherapy. *Rev Sci Instrum* (2020) 91(2):023309. doi: 10.1063/1.5127537
71. Inaniwa T, Kanematsu N, Noda K, Kamada T. Treatment planning of intensity modulated composite particle therapy with dose and linear energy transfer optimization. *Phys Med Biol* (2017) 62(12):5180. doi: 10.1088/1361-6560/aa68d7
72. Inaniwa T, Lee SH, Mizushima K, Sakata D, Iwata Y, Kanematsu N, et al. Nuclear-interaction correction for patient dose calculations in treatment planning of helium-, carbon-, oxygen-, and neon-ion beams. *Phys Med Biol* (2020) 65(2):025004. doi: 10.1088/1361-6560/ab5fee
73. Inaniwa T, Suzuki M, Lee SH, Mizushima K, Iwata Y, Kanematsu N, et al. Experimental validation of stochastic microdosimetric kinetic model for multi-ion therapy treatment planning with helium-, carbon-, oxygen-, and neon-ion beams. *Phys Med Biol* (2020) 65(4):045005. doi: 10.1088/1361-6560/ab6eba
74. Sokol O, Krämer M, Hild S, Durante M, Scifoni E. Kill painting of hypoxic tumors with multiple ion beams. *Phys Med Biol* (2019) 64(4):045008. doi: 10.1088/1361-6560/aafe40
75. Scifoni E, Tinganelli W, Weyrather WK, Durante M, Maier A, Krämer M. Including oxygen enhancement ratio in ion beam treatment planning: model implementation and experimental verification. *Phys Med Biol* (2013) 58 (11):3871–95. doi: 10.1088/0031-9155/58/11/3871
76. Tessonnier T, Mairani A, Brons S, Haberer T, Debus J, Parodi K. Experimental dosimetric comparison of 1H, 4He, 12C and 16O scanned ion beams. *Phys Med Biol* (2017) 62(10):3958–82. doi: 10.1088/1361-6560/aa6516
77. Battistoni G, Bauer J, Boehlen TT, Cerutti F, Chin MPW, Dos Santos Augusto R, et al. The FLUKA Code: An Accurate Simulation Tool for Particle Therapy. *Front Oncol* (2016). doi: 10.3389/fonc.2016.00116
78. Tessonnier T, Böhlen TT, Ceruti F, Ferrari A, Sala P, Brons S, et al. Dosimetric verification in water of a Monte Carlo treatment planning tool for proton, helium, carbon and oxygen ion beams at the Heidelberg Ion Beam Therapy Center. *Phys Med Biol* (2017) 62(16):6579–94. doi: 10.1088/1361-6560/aa7be4
79. Friedrich T, Durante M, Scholz M. Particle species dependence of cell survival RBE: Evident and not negligible. *Acta Oncol Stockh Swed* (2013) 52(3):589–603. doi: 10.3109/0284186X.2013.767984
80. Guan F, Peeler C, Bronk L, Geng C, Taleei R, Randeniya S, et al. Analysis of the track- and dose-averaged LET and LET spectra in proton therapy using the geant4 Monte Carlo code. *Med Phys* (2015) 42(11):6234–47. doi: 10.1118/1.4932217
81. Inaniwa T, Furukawa T, Kase Y, Matsufuji N, Toshito T, Matsumoto Y, et al. Treatment planning for a scanned carbon beam with a modified microdosimetric kinetic model. *Phys Med Biol* (2010) 55(22):6721–37. doi: 10.1088/0031-9155/55/22/008

82. Bopp C, Hirayama R, Inaniwa T, Kitagawa A, Matsufuji N, Noda K. Adaptation of the microdosimetric kinetic model to hypoxia. *Phys Med Biol* (2016) 61(21):7586–99. doi: 10.1088/0031-9155/61/21/7586
83. Mein S, Dokic I, Klein C, Tessonnier T, Böhlen TT, Magro G, et al. Biophysical modeling and experimental validation of relative biological effectiveness (RBE) for 4He ion beam therapy. *Radiat Oncol* (2019) 14(1):123. doi: 10.1186/s13014-019-1295-z
84. Brahme A. Accurate description of the cell survival and biological effect at low and high doses and LET's. *J Radiat Res (Tokyo)* (2011) 52(4):389–407. doi: 10.1269/jrr.10129

Conflict of Interest: The authors declare that the research was conducted in the absence of any commercial or financial relationships that could be construed as a potential conflict of interest.

Copyright © 2021 Ebner, Frank, Inaniwa, Yamada and Shirai. This is an open-access article distributed under the terms of the Creative Commons Attribution License (CC BY). The use, distribution or reproduction in other forums is permitted, provided the original author(s) and the copyright owner(s) are credited and that the original publication in this journal is cited, in accordance with accepted academic practice. No use, distribution or reproduction is permitted which does not comply with these terms.

frontiers in Oncology

REVIEW
published: 26 February 2021
doi: 10.3389/fonc.2021.601820

Boron Neutron Capture Therapy: A Review of Clinical Applications

Timothy D. Malouff[1], Danushka S. Seneviratne[1], Daniel K. Ebner[2], William C. Stross[1], Mark R. Waddle[1], Daniel M. Trifiletti[1] and Sunil Krishnan[1]*

[1] Department of Radiation Oncology, Mayo Clinic, Jacksonville, FL, United States, [2] Warren Alpert Medical School, Brown University, Providence, RI, United States

Boron neutron capture therapy (BNCT) is an emerging treatment modality aimed at improving the therapeutic ratio for traditionally difficult to treat tumors. BNCT utilizes boronated agents to preferentially deliver boron-10 to tumors, which, after undergoing irradiation with neutrons, yields litihium-7 and an alpha particle. The alpha particle has a short range, therefore preferentially affecting tumor tissues while sparing more distal normal tissues. To date, BNCT has been studied clinically in a variety of disease sites, including glioblastoma multiforme, meningioma, head and neck cancers, lung cancers, breast cancers, hepatocellular carcinoma, sarcomas, cutaneous malignancies, extramammary Paget's disease, recurrent cancers, pediatric cancers, and metastatic disease. We aim to provide an up-to-date and comprehensive review of the studies of each of these disease sites, as well as a review on the challenges facing adoption of BNCT.

Keywords: boron neutron capture, fast neutrons, particles, radiation, boron neutron capture therapy (BNCT)

OPEN ACCESS

Edited by:
Minesh P. Mehta, Baptist Health South Florida, United States

Reviewed by:
Elvira V. Grigorieva, Institute of Molecular Biology and Biophysics (RAS), Russia
Martin Tom, Baptist Hospital of Miami, United States

****Correspondence:***
Timothy D. Malouff
malouff.timothy@mayo.edu

Specialty section:
This article was submitted to Radiation Oncology, a section of the journal Frontiers in Oncology

Received: *01 September 2020*
Accepted: *27 January 2021*
Published: *26 February 2021*

Citation:
Malouff TD, Seneviratne DS, Ebner DK, Stross WC, Waddle MR, Trifiletti DM and Krishnan S (2021) Boron Neutron Capture Therapy: A Review of Clinical Applications. Front. Oncol. 11:601820. doi: 10.3389/fonc.2021.601820

INTRODUCTION

Increasing the therapeutic ratio is one of the most significant challenges of modern clinical oncology. To this end, there has been significant interest in targeted therapies, with the goal of selectively treating tumor cells while sparing normal tissues. Boron neutron capture therapy (BNCT) is an emerging treatment modality aimed at improving the therapeutic ratio for traditionally difficult to treat tumors. BNCT was first proposed by Gordon Locher in 1936, who suggested that, if boron were able to be concentrated in the tumor and then exposed to thermal neutrons, the tumor would selectively receive a higher dose compared to normal tissues (1).

Treatment with BNCT is based on the nuclear capture and fission following the irradiation of nonradioactive boron-10 with low thermal neutrons (<0.025 eV), which leads to the production of an alpha particle and a recoiling lithium-7 ($^{10}B_5 + {}^1n_{0(th)} \rightarrow [{}^{11}B_5]^* \rightarrow {}^4He_2\ (\alpha) + {}^7Li_3 + 2.38$ MeV). Alpha particles are a form of high linear energy transfer (LET) particles that deposit their energy over <10 μm, approximately the diameter of one cell (**Figure 1**) (1–3).

The most challenging aspect of successful treatment with BNCT is the delivery of boronated compounds to the tumor while avoiding significant uptake in normal tissues. The general requirements for successful boron delivery agents includes high tumor uptake, low normal tissue uptake, rapid clearance from tissue after treatment, and low toxicity (3). Boron delivery has been achieved typically with two agents: sodium borocaptate (BSH) and boronophenylalanine (BPA), with the latter complexed with fructose to form the more soluble BPA-F (2). The most efficacious

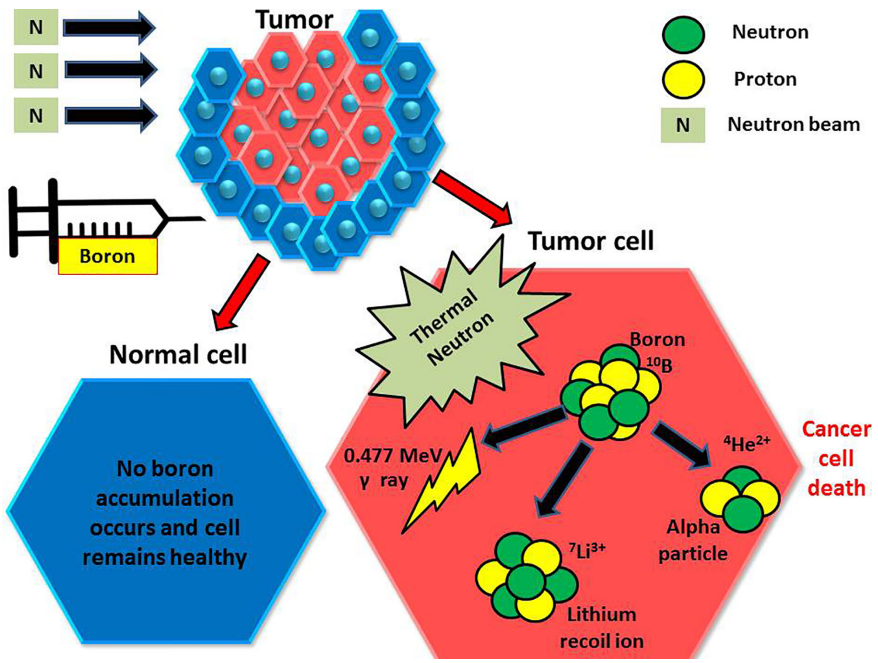

FIGURE 1 | Injected boron compounds are preferentially found in tumor cells, which are then irradiated with thermal neutrons. The boron then undergoes a reaction, giving an alpha particle and an inert lithium ion. The alpha particle then damages the tumor cell with a finite range.

boronated compound remains unclear, and trials have been variable as to which compound is given. The reader is referred to the text *Neutron Capture Therapy: Principles and Applications* for a more in-depth review of the technical aspects of treatment with BNCT (2).

In this review, our aim is to provide a comprehensive and updated summary of the current clinical literature for patients treated with BNCT. An overview of the largest studies is provided in **Table 1**.

GLIOBLASTOMA MULTIFORME

Glioblastoma multiforme is one of the most challenging malignancies to treat, with a median survival of approximately 14 months despite maximum resection, radiation, and adjuvant chemotherapy (16). Due to this, BNCT has been proposed as a treatment option in the upfront and recurrent settings. Further, boron has been shown to possess direct tumoricidal activity and many can cross the blood-brain barrier (17). Interestingly, prolonged infusion of 6 h with BPA-F was found to have a survival advantage compared to 2 h infusions with similar toxicity (18).

Miyatake et al. reported on their experience treating 167 cases of malignant brain tumors and high grade meningiomas treated with BNCT from 2002 to 2014. In the recurrent setting, BPA was administered over a 2 h period at a dose of 200 mg/kg/h prior and 100 mg/kg/h during neutron irradiation. Epithermal neutrons were given, with a dose was chosen to keep the peak brain dose below 12.0 Gy equivalent. The median survival time for BNCT with BPA for recurrent GBM was 10.8 months and that for BNCT with BPA and BSH for newly diagnosed GBM was 15.6 months without an x-ray boost and 23.5 months with an x-ray boost. The biggest drawbacks to BNCT were radiation necrosis and symptomatic pseudoprogression (8). BNCT showed the most prominent survival benefit in recursive partitioning analysis (RPA) classes 3 and 7 (19).

In a series by Kawabata et al. seven patients received BNCT intraoperatively (sulfhydryl borane dose of 5 g/body) and eight patients received external beam BNCT (p-dihydroxyboryl-phenylalanine dose of 250 mg/kg) with epithermal neutrons as part for the treatment of newly diagnosed glioblastoma using sulfhydryl borane as the boron carrier. External beam BNCT was combined with photon therapy to a dose of 30 Gy in 15 fractions or 30.6 Gy in 17 fractions. The median time to progression for all patients was 11.9 months, with no difference between intraoperative (12.0 months) and external beam (11.9 months). The 2-year OS was 53.3%. Four patients developed grade 2 orbital edema, and one patient in the intraoperative arm developed grade 4 post-epileptic brain edema (20, 21).

Thirty patients with glioblastoma were treated between 2001 and 2003 (the pre-temozolomide era) with BNCT in Sweden. BPA-F at a high dose (900 mg/kg) was given as the boron carrier, with epithermal neutron irradiation 2 h after the infusion. The median OS was 14.2 months and the time to progression was 5.8 months. Seven patients experienced seizures, five experienced thromboembolic events, and eight had grades 1–3 skin toxicity. Quality of life was found to progressively deteriorate after BNCT (6).

In the United States, Chadha et al. reported on patients treated at Brookhaven National Laboratory in the mid-1990s designed to

TABLE 1 | Summary of studies using BNCT by disease site.

Study	Number of patients	Boron carrier	Outcomes
Glioblastoma Multiforme			
Chanana et al. (4)	38	BPA-F	Median OS: 13 months Median time to progression: 31.6 months
Henriksson et al. (5)	30	BPA-F	Median OS: 14.2 months Median time to progression: 5.8 months
Kawabata et al. (6)	11	Combination BPA/BSH with EBRT	Median OS: 23.5 months
Kageji et al. (7)	23	BSH	Median survival: 19.5 months 5 year OS: 9.1%
Miyatake et al. (8)	167	BPA	Median OS: 10.8 months (recurrent) Median OS: 15.6 months (newly diagnosed)
Head and Neck (Definitive)			
Kankaanranta et al. (9)	30	BPA-F	Response rate: 76% Median PFS: 7.5 months 2 year OS: 30%
Head and Neck (Recurrent)			
Kato et al. (10)	26	BPA alone or BPA and BSH	Median survival: 13.6 months
Suzuki et al. (11)	62	BPA alone or BPA and BSH	Median survival: 10.1 months Response rate: 58% 2 year OS: 24.2%
Koivunoro et al. (12)	79	BPA-F	Complete response rate: 36% 2 year LRPFS 38% 2 year OS 21%
Wang et al. (13); Wang et al. (14)	23	BPA-F	2 year locoregional control: 28% 2 year OS: 47%
Cutaneous Melanoma			
Menendez et al. (15)	7	BPA	Response rate: 69%

BNCT, boron neutron capture therapy; BPA, boronophenylalanine; BSH, sodium borocaptate; EBRT, external beam radiation therapy; LRPFS, locoregional progression free survival; OS, overall survival; PFS, progression free survival.

test the feasibility of single fraction BNCT with an epithermal neutron beam (22). In the past, when thermal neutron beams were used, patients underwent a craniotomy to allow the thermal beam to irradiate the tumor. Also, in this study, they performed a meticulous biodistribution analysis with tumor, blood, scalp, and normal brain (whenever possible) collected at the time of a second debulking craniotomy and noted that tumor concentration was about 3.5 times that in blood, scalp concentration was about 1.5 times that in blood, and normal brain concentration was less than that in blood. BNCT was performed about 4 weeks after the surgery with a repeat dose of BPA-F and the prescription dose was based on normal brain tolerance with normal brain boron concentration assumed to be that of blood to account for brain endothelial dose. The median OS, albeit in just 10 patients, was 13.5 months at a time when the OS in cooperative group trials was 9.7 months. A total of 38 patients with glioblastoma were treated with BPA-fructose at a dose of 250 or 290 mg/kg as part of the phase I/II dose-escalation study. The median time to tumor progression was 31.6 weeks, with a median survival of 13.0 months. There were no grade 3 or 4 toxicities (4).

Kageji et al. reported on 23 newly diagnosed GBM patients treated with BNCT and without additional chemotherapy. 100 mg/kg BSH was given and patients underwent craniotomy for direct delivery of thermal neutrons to the tumor. The median survival was 19.5 months, with 2- and 5-year survivals of 31.8% and 9.1%, respectively. Toxicity was not reported (7, 23). Of note, five patients treated with BNCT survived more than 3 years after diagnosis (24). Notably, there are long term survivors treated with BNCT for high grade gliomas. In one series from 1994, of the 120 patients treated with BNCT for brain tumors, there were nine patients who had survivals of more than 10 years (25).

In the setting of recurrent disease, a phase I study by Kankaanranta et al. investigated the use of L-BPA-fructose in increasing doses ranging from 290 mg/kg to 450 mg/kg for patients with glioblastoma or anaplastic astrocytoma that progressed more than 6 months after surgery and external beam radiation therapy. The median survival following BNCT was 7 months. Four of the six patients at the 450 mg/kg dose level experienced grade 3 adverse effects, the most frequent being seizures. On subset analysis, patients who received >290 mg/kg L-BPA-fructose or those who received >34 Gy weighted dose to their planning target volumes had better outcomes than those who received 290 mg/kg L-BPA-fructose or ≤34 Gy weighted dose to their PTVs, respectively. The authors concluded that L-BPA-fructose at a dose of 400 mg/kg as a 2-h infusion is reasonable for recurrent gliomas (26). Aiyama et al. reported on a 54-year-old male with recurrent GBM and a 64-year-old female with atypical meningioma treated with BNC T in Japan. In the two cases, the only adverse event was grade 2 conjunctivitis, and the authors concluded that BNCT is effective and safe as palliative therapy for malignant brain tumors (27). Okazaki et al. reported on a 22-year-old patient with GBM who developed a total of three recurrences. BNCT was delivered using a dose of 100 mg/kg BSH. The patient survived for 9 years following BNCT, but ultimately developed carcinomatous encephalomyelopathy (28).

Given the increased use of protons, there has been interest in combining proton radiotherapy with BNCT. Patients receiving BNCT with proton therapy showed a better survival than those receiving radiation and temozolomide in a small study, although this was not statistically significant (29). Further research is needed to determine if there is a benefit to combination proton therapy and BNCT.

One of the concerns of BNCT in the setting of malignant gliomas is the high rates of symptomatic pseudoprogression and radionecrosis (30). In one series, 11 out of 52 malignant glioma

and three out of 13 malignant meningioma patients developed increases in edema following BNCT at 3 months (31). Due to the rates of radionecrosis following BNCT, researchers in Japan developed a pilot study for BNCT using BPA in combination with bevacizumab. Bevacizumab was started 2–6 weeks after BNCT and was given in 10 mg/kg doses biweekly. From 2013 to 2014, seven patients were treated with BNCT and bevacizumab. Median OS and PFS were 15.1 months and 5.4 months, respectively. There was one death due to uncontrolled edema after bevacizumab was interrupted due to meningitis. No radionecrosis was seen through December 2017, and the authors concluded that bevacizumab treatments prevented radionecrosis with prolonged OS and acceptable toxicity (32). Moreover, bevacizumab at a dose of 5 mg/kg was shown to improve symptomatic pseudoprogression in two patients treated with BNCT for recurrent gliomas. The authors concluded that BNCT in combination with bevacizumab may prolong survival (33).

In support of this, Miyatake et al. reported on four patients with recurrent malignant gliomas treated in Osaka, Japan with BNCT and bevacizumab. Of the three patients with RPA class 3, the survival time after BNCT was 14, 16.5, and over 23 months. The patient with an RPA class of 4 survived over 26 months. The authors concluded that BNCT with bevacizumab improved symptoms of symptomatic pseudoprogression or radionecrosis and prolonged survival (34).

Histopathological studies were performed on eight patients treated with BNCT for GBM either at the time of salvage surgery or autopsy. Tissue studies demonstrated residual tumor cells in four patients. The authors concluded that a dose of 68 Gy to the GTV and 44 Gy to the CTV was needed for histopathologic cure (35). In one interesting case of a patient with gliosarcoma previously treated with BNCT, only the sarcomatous component recurred 6 months post-BNCT (36). Radiographically, 50% of patients had cerebral changes within the first year of treatment, with atrophy affecting 42% of patients analyzed as part of the EORTC 11961 trial (37).

There are several current trials investigating the use of BNCT in high grade gliomas. In Japan, 21 patients with newly diagnosed glioblastoma were treated with combination BPA and BSH. Protocol 1 investigated 10 patients treated with BNCT alone with Protocol 2 investigating 11 patients receiving external beam radiation therapy. The median survival time was 15.6 months for all patients, and 23.5 months for Protocol 2. The 2-year overall survival was 25% (1, 6, 20). A phase II clinical trial (OSAKA-TRIBRAIN0902, NCT00974987) was designed based on that study and completed accrual in 2018. The Tsukuba BNCT trial is a phase II study evaluating combined photon irradiation with concurrent temozolomide combined with BNCT using 250 mg/kg BPA (38).

MENINGIOMA

Miyatake et al. described seven cases of malignant meningiomas, including three anaplastic meningiomas, two papillary meningiomas, one atypical meningioma, and one sarcoma transformed from a meningioma, treated with BNCT. 18F-BPA PET was applied before BNCT in six patients and one underwent methionine-PET. Two of the three anaplastic meningiomas showed a complete response, and all six patients analyzed showing radiographic improvement (39). Stenstam et al. described two patients treated with BNCT using BPA-fructose (900 mg/kg body weight) for recurrent meningeal tumors following surgery, radiation, and salvage surgery and concluded that BNCT is a potentially effective modality for malignant intracranial meningeal tumors (40).

Similarly, the median survival times after BNCT with BPA for high grade meningiomas recurrent after or refractory to treatment was 14.1 months from BNCT treatment in the study by Kawabata et al. In this study, BPA was administered prior to neutron irradiation (200 mg/kg/h) and during neutron irradiation (100 mg/kg/h). The duration was determined to not exceed the dose of 15 Gy-Eq to the normal brain (7, 41). Of 20 patients who underwent 28 BNCT treatments following at least one prior course of external beam radiation therapy or stereotactic radiosurgery, at least three patients had pseudoprogression, with five patients experiencing symptomatic radiation necrosis (41).

A retrospective review from the Osaka Medical College Hospital and the Kyoto University Research Reactor Institute investigated 31 patients treated with BNCT for recurrent high grade meningiomas, including seven skull base meningiomas. PET scans revealed a 3.8 times higher boron accumulation in the meningiomas compared to normal brain, with a mean maximum absorbed dose of 67.2 Gy-Eq. All lesions showed decrease in size, and the median survival of skull base meningiomas following BNCT was 24.6 months (42).

Tamura et al. reported on a 25-year-old patient with a recurrent malignant meningioma who underwent two resections and three courses of Gamma Knife radiosurgery without adequate control. She received 5 g BSH IV for 1 h approximately 13 h before radiation, and 500 mg/kg BPA before receiving epithermal neutrons. The minimum tumor dose was estimated to be 39.7 Gy-Eq. She regained the ability to ambulate within 1 week after the first treatment of BNCT and showed decrease in size of the tumor at 26 weeks (43).

A pathology study of a 70-year-old who died from systemic metastasis from anaplastic meningioma showed significantly lower proliferative activity of the meningioma recurrence compared to an untreated metastatic liver lesion and untreated meningioma. The study supports the early effect of BNCT on anaplastic meningiomas, with treatment effect seen as early as 2.5 months after treatment (44). Other pathology studies showed that radiation-induced focal venular fibrinoid necrosis and multifocal demyelination may occur after high doses of BNCT to neuroparenchyma (45).

DEFINITIVE TREATMENT FOR HEAD AND NECK CANCERS

Although the majority of clinical trials regarding BNCT use in head and neck malignancies investigated it in the recurrent setting, BNCT has been used for definitive therapy as well.

Single fraction BNCT using BPA-F at a dose of 400 mg/kg with epithermal neutrons using two circular 14 cm diameter beams with irradiation times of 15.3 min and 16.5 min has been used successfully for the treatment of unresectable, undifferentiated sinonasal carcinoma. The authors reported that although the patient recurred 6 months post-treatment, his quality of life improved following treatment and primary side effect experienced was mucositis (46). Kimura et al. reported on a 78-year-old patient with a papillary cystadenocarcinoma of the upper lip treated with BNCT using 500 mg/kg BPA as the boron carrier in two fractions with a total dose 63.4 Gy-Eq at the tumor peak. The tumor decreased by 86% at 5-month follow up, although the patient experienced acute extensive erosion (47).

Recently, Kankaanranta et al. reported on a 53-year-old woman successfully treated with BNCT for a large head and neck cancer in the definitive setting. The patient presented with a 7.4 cm intranasal mass and was treated with 400 mg/kg L-BPA-fructose followed by IMRT to a dose of 44 Gy following resolution of acute BNCT induced mucositis. Intravenous cetuximab and cisplatin were given concurrently with IMRT. The patient experienced grade 3 mucositis, alopecia, fatigue, and xerophthalmia. The patient achieved a complete response and had no evidence of disease at 6 month follow-up (48). The authors concluded that BNCT is a reasonable treatment with moderate toxicity in the setting of first line therapy for head and neck cancers.

Kankaanranta et al. reported on a prospective, phase I/II trial of 30 patients treated for inoperable, locally advanced head and neck cancer with BNCT between December 2003 and September 2008 in Finland (NCT00114790). Of the 30 patients, 29 had carcinomas as the primary histology, with one patient diagnosed with a sarcoma. Patients were treated with surgery and radiation therapy to a median dose of 60 Gy, with 33% of patients receiving concurrent chemotherapy. BNCT was administered in two fractions with 400 mg/kg L-BPA-fructose with neutrons given from two portals with a median beam time of 18.6 min. Of the 29 evaluable patients, there was a 76% response rate. The median PFS was 7.5 months, with a 2-year OS and PFS of 30% and 20%, respectively. Acute grade 3 mucositis and oral pain were noted in 54% of patients, with fatigue in 32% of patients. Three patients developed grade 3 osteoradionecrosis and one patient developed grade 4 soft tissue necrosis. Twenty percent of patients developed late grade 3 xerostomia (9).

Fatal carotid blowout remains a concern following BNCT for head and neck cancers, with one study by Aihara et al. reporting carotid blowout syndrome in two out of 33 patients treated with BNCT, developing between 1 and 3 months after BNCT (49).

RECURRENT HEAD AND NECK CANCERS

Kato et al. reported on the first six patients treated for recurrent head and neck cancers with BNCT, using combination BPA (250 mg/kg) and BSH (5 g) with epithermal neutron irradiation with a fluence ranging from 1.3 to 2.7. An improvement in quality of life was seen in five patients given the reduction in tumor volume (50). Suzuki et al. retrospectively reviewed the records of patients treated for locally recurrent or unresectable head and neck cancers treated with BNCT between 2001 and 2007 at Kyoto University. BPA alone or BPA and BSH were used as the boron compounds. For the 62 patients treated, the median follow up was 18.7 months, the median survival was 10.1 months, the overall response rate was 58% at 6 months, and the 2-year OS was 24.2%. Hyperamylasemia was the most common acute grade 3 or 4 toxicity (38.6%), followed by mucositis (9.7%) and pain (9.7%). Two patients had fatal carotid hemorrhage, and one patient died due to malnutrition (11). In another retrospective study, 79 patients with inoperable, locally recurrent squamous cell carcinoma of the head and neck were treated with BNCT in Finland between 2003 and 2012. Ninety-five percent of patients had previously received radiation to a median dose of 66 Gy. L-BPA-fructose was used at a dose of 350–400 mg/kg, with neutron irradiation lasting a median of 42 min. Thirty-nine patients received BNCT twice, while 40 patients received one fraction due to a variety of reasons, such as distant disease or medical comorbidities. Four of this patient cohort, 68% showed some response, with a 36% complete response rate. Patients treated twice with BNCT showed improved response compared to those who were treated once. With a median follow-up of 7.8 years, the 2-year locoregional progression free survival was 38% and 2-year OS was 21%. A minimum GTV dose of 18 Gy was associated with the best survival, suggesting that minimum tumor dose is predictive of survival (12).

Based on 26 patients treated with recurrent head and neck malignancies in Osaka, Japan since 2001, Kato et al. found an overall response rate of 85%, with improvement in quality of life. Combination BSH and BPA, or BPA alone (250 or 500 mg/kg) were used. The mean survival following treatment was 13.6 months. Transient mucositis and alopecia were the most common adverse effects, with three patients developing osteomyelitis and one suffering from brain necrosis. The authors conclude that BNCT is a new and promising technique (10). Another study reviewed 12 patients with inoperable, recurred, locally advanced head and neck cancers. L-BPA-F was given at a dose of 400 mg/kg followed by neutron irradiation, with the median time from the first field of 18.1 min and time of irradiation from the second field of 17.5 min. Eighty-three percent of patients had a response to BNCT; with 33% of patients without recurrence at a median follow up of 1.0 months. Two patients had grade 3 toxicity: one patient experienced xerostomia and one experienced dysphagia (51). Aihara et al. reported on 10 patients treated with recurrent squamous cell carcinoma and seven patients with recurrent and three newly diagnosed head and neck non-squamous cell carcinoma treated between 2003 and 2007 in Japan. Of these, 11 patients showed a complete response, with a total response of 90%. There were no severe acute or late toxicities (52).

In Finland, six patients with locally recurrent laryngeal squamous cell carcinoma and three patients with persistent laryngeal cancer were treated with BNCT from 2006 to 2012. L-BPA-F at a dose of 400 mg/kg was administered over 2 h. Of the eight patients analyzed, there were two complete responses

and four partial responses. Five patients developed early large grade 3 toxicity and 38% developed late grade 3 toxicity. The most common acute and late toxicities were stomatitis and mucositis. The median time to progression was 6.6 months (53).

Haginomori et al. reported on the first case of a 42-year-old patient treated for extensive squamous cell carcinoma of the temporal bone that recurred after initial chemotherapy, surgery, and radiation therapy. The patient underwent planned fractionated BNCT with BPA with two treatments given 1 month apart. The total radiation dose to the deepest point of the tumor was approximately 36.9 Gy-Eq. At 6 months after the first treatment, there was no evidence of residual tumor (1, 54).

In recurrent salivary gland cancers, a 48-year-old patient with recurrent submandibular gland malignancy undergoing 18F-BPA PET before BNCT showed complete regression after therapy (55). Aihara et al. reported on two patients with recurrent salivary gland cancer and three patients with newly diagnosed T4 salivary gland cancers treated with BNCT between 2003 and 2007. All patients achieved a complete response within 6 months. The median survival was 32 months, with two patients with distant metastatic disease. There were no severe grade 3 or high toxicity (56).

BNCT has also been used successfully in treating nodal recurrences. Four patients were enrolled at Osaka Medical College evaluating the use of BNCT for regional nodal recurrence of oral cavity cancers. All patients showed a partial response, with one patient having a marked improvement in quality of life, following administration of 500 mg/kg BPA. The neutron dose was determined by delivering 10–15 Gy-Eq to the oral mucosa (57). Of six patients treated at the same institution for recurrent oral cancer, three remained alive with improvement in quality of life. Five patients had decrease in pain (58), suggesting that BNCT may be beneficial for palliation.

Using the Tsing-Hua Open Pool Reactor (THOR) at the National Tsing-Hua University in Hsin-Chu, researchers initially enrolled 17 patients with 23 recurrent head and neck tumors between 2010 and 2013 in a phase I/II trial investigating BNCT for recurrent head and neck cancers. A fructose complex of L-BPA was used. Patients were then treated to a prescription dose of 20 Gy-Eq to cover 80% of the gross tumor using a single field and were treated in two fractions at 28-day intervals. With a median follow up of 19.9 months, 15 patients received both fractions, and six had a complete response. Nine patients reported improved quality of life, with low-grade oral mucositis, radiation dermatitis, and alopecia as the most common acute toxicities. One patient developed grade 4 acute laryngeal edema and carotid hemorrhage, and two patients developed late grade 3 cranial neuropathy. The 2-year overall survival was 47% (13, 14, 59). The 2-year locoregional control rate was 28%, and a second trial using image-guided IMRT was initiated in 2014 to improve local control. In this second protocol, IMRT was initiated 28 days after one administration of BNCT. Of the seven patients treated with this protocol, three had a complete response with a 1-year OS of 56%. Toxicity was similar to the first trial, with one patient developing grade 4 oral bleeding and another developing grade 4 dyspnea due to facial edema (14). Using nine patients with recurrent head and neck cancer from THOR, Lee et al. analyzed the dose distributions between BNCT alone and BNCT with IMRT. BNCT with IMRT had GTV conformity and improved homogeneity compared to BNCT monotherapy (60).

Eight patients underwent BNCT with IV BPA and seven patients were treated with intra-arterial BPA for recurrent head and neck malignancies. Efficacy was similar, and the authors determined that intra-arterial BPA is a viable delivery system for BNCT (61).

LUNG CANCERS

BNCT has been proposed for diffuse, non-resectable lung tumors (62), as well as for inoperable malignant pleural mesothelioma (63–65). Suzuki et al. reported on two patients with diffuse pleural tumors, one with malignant pleural mesothelioma and one with malignant short spindle cell tumor, treated with BNCT with BPA-F to a dose of 250 or 500 mg/kg. The tumors either were stable or regressed at 6-month follow up with no grade 3 or higher acute or late toxicities (63). The feasibility of treating shallow lung tumors with BNCT was confirmed in one study, although the role of BNCT in treating deeper tumors remains unknown (66).

BREAST CANCERS

There have been few studies to date investigating the use of BNCT in breast malignancies, although BNCT may have a role as a potential option for treating HER2 overexpressing breast cancers based on promising pre-clinical data. Immunoliposomes, such as those labeled with trastuzumab, have been proposed to act as a boron carrier and can selectively target HER2 overexpressing cells (67). Further, dosimetric analyses have shown the possibility of BNCT for locally recurrent breast cancer (68). Collectively, these studies suggest a benefit of BNCT for breast cancers, but further clinical studies are needed.

HEPATOCELLULAR CARCINOMA

Suzuki et al. reported on the first patient treated for multiple hepatocellular carcinomas in Japan. The patient had Child-Pugh grade B cirrhosis, and irradiation was confined to the right lobe. BPA (250 mg/kg) and BSA (1 g/body) were used as boron carriers. The peak dose to the right lobe of the liver was 4.9 Gy-Eq, and the mean dose was 2.7 Gy-Eq. At 1 month, the tumors treated with BNCT remained stable, although there was progression of disease after 3.5 months (69).

Yangie et al. performed a pilot study using selective intra-arterial infusion to deliver a BSH containing water-in-oil-in-water emulsion to a left liver lobe lesion in a 63-year-old man with hepatocellular carcinoma. Irradiation time was set to limit

the maximum dose to the liver of 5.0 Gy-Eq. The patient was considered to have stable disease on initial follow-up imaging, although he later developed multiple nodules in the left lobe of the liver as well as lung metastatic disease. The patient died from pneumonia 7 months after BNCT (70).

SARCOMAS

Osteosarcoma has been shown to be effectively and safely treated with BNCT. BNCT has also been used successfully in the treatment of osteosarcoma of the temporomandibular joint, with no evidence of recurrence after approximately 2 years (71). Futamura et al. reported on a 54-year-old female effectively treated for a recurrent radiation-induced osteosarcoma in the left occipital skull by BNCT. 500 mg/kg of BPA was administered. Although she was unable to ambulate at diagnosis, she regained the ability to ambulate without aid approximately 3 weeks following BNCT. The treatment was well tolerated, with the patient experiencing alopecia as the only reported toxicity (72).

Malignant peripheral nerve sheath tumors (MPNSTs) are a rare soft tissue malignancy with a poor prognosis despite surgical resection. Animal models using L-BPA showed efficacy of BNCT for MPNST (73), and a 70-year-old woman were treated for a MPNST in the right supraclavicular fossa with an initial response and no evidence of recurrence at 2 years (74). Animal models were promising for clear cell carcinoma (75).

CUTANEOUS MELANOMA

Patients diagnosed with melanoma often have poor prognoses despite optimal treatments. Due to this, Gonzalez et al. reported on a case of a 54-year-old women treated for cutaneous melanoma as part of the initial 30 patient cohort treated with BNCT. BPA-F to a dose of 14 g/m2 over 90 min was used with an estimated treatment time of 903 monitor units to keep the normal maximum skin dose below 16.5 RBEGy. Of the 25 skin nodules, 21 were in complete response 8 weeks following treatment with grade 1 acute skin reaction as the primary toxicity (76).

Further, Menendez et al. reported on seven patients treated with BNCT for cutaneous melanoma with multiple skin metastases in the extremities in Argentina between 2003 and 2007. All patients received 14 mg/m2 of BPA. The overall response rate was 69%, with a 30% grade 3 toxicity rate (ulceration) (15). Two patients enrolled in the trial were studied using dynamic infrared imaging, which registers the temperature evolution of normal skin and tumor. Researchers found the main erythematous reaction occurred between the second and 5th week after irradiation (77).

Most recently, the Third Xiangya Hospital of Central South University in Changsha China recently developed a protocol for treating malignant melanoma using BNCT, with a goal of accrual of 30 patients (NCT02759536). The authors report on the first patient treated for a left foot lesion in August 2014. In this study, BPA-F complex was used with 350 mg/kg infused into the patient over 90 min. Using the Monte Carlo N Particle Transport Code 6 program, the estimated dose was determined, and the patient was treated with two fields in a total of 20 min. The patient experienced only mild dandruff `1 week following irradiation, although this progressed to grade 2 dermatitis at 4 weeks. There were no significant lab value findings. Biopsy performed at 9 months post-BNCT and PET scan 24 months post-BNCT showed no evidence of disease (78). BNCT may also be used in controlling in-transit and lymph node metastasis from cutaneous melanoma (79).

EXTRAMAMMARY PAGET'S DISEASE

Due to the morbidity associated with wide local excision of extramammary Paget's disease of the genitals, Makino et al. reported on the first two cases of extramammary Paget's disease of the genitals treated with BNCT. Both patients were over the age of 70. At 12 months after treatment, both cases had a complete response with no evidence of recurrence or metastatic disease (1, 80).

Kyoto University treated one patient with vulvar melanoma and three with genital extramammary Paget's disease between 2005 and 2014. ^{10}B-enriched L-BPA was used as the boron delivery source to a dose of 200 mg/kg over 3 h (rate of 80 mg/kg/h for the first 2 h and 40 mg/kg/h for the last hour). Patients were irradiated in the last hour of the infusion. All four patients had a complete response in 6 months, with two patients developing grade 2 erosions, one patient developing grade 2 dysuria, and one patient developing grade 1 mucositis (81).

METASTATIC DISEASE

Although currently limited to translational studies and case reports, BNCT will likely be used in the setting of metastatic disease. The EORTC 11001 protocol is a translational phase I trial with the goal to measure the uptake of two boronated compounds in tissues and the blood. BSH and BPA are administered prior to surgical resection of hepatic metastasis, with no patients experiencing toxicity from the boron carriers. BSH was not a suitable carrier, as the liver concentration was higher than in the metastasis. BPA may be used for extracorporeal irradiation of the liver with BNCT (82), which has previously been used in a small series of two patients (83). The study was also performed for head and neck cancer patients, and found that BPA and BSH might allow effective treatment in squamous cell carcinoma (84). The study was repeated in thyroid cancer (85).

Interestingly, a proof of principle study using rats treated with BNCT showed that BNCT is capable of inducing the abscopal effect in rats inoculated with colon cancer cells (86). Further studies are needed to evaluate the immunogenicity of BNCT.

Clinically, BNCT has been shown to lead to suppression of tumor growth for 2 months in a 72-year-old man treated with recurrent gastric cancer and a left cervical node lesion (1, 87).

PEDIATRICS

BNCT has also shown benefit in children with malignant brain tumors. In one series, 23 patients under the age of 15 treated with BNCT were included. Four patients were under the age of 3. Three patients had glioblastomas, six patients with anaplastic astrocytomas, seven patients with PNET tumors, six patients with pontine gliomas, and one patient with anaplastic ependymoma. Four of the six anaplastic astrocytoma and the anaplastic ependymoma patients had no evidence of recurrence. The patients with GBM and PNET tumors died of disseminated tumor without local recurrence. The pontine glioma patients died of tumor regrowth. The authors concluded that BNCT can be used in children (88).

Zhang et al. analyzed the secondary malignancy risk in pediatric patients treated with BNCT for brain tumors in China. When comparing neutron beam geometries, the authors concluded that the lifetime attributable risk of secondary malignancy was lower with posterior-to-anterior arrangement compared to right-lateral and top-to-bottom. Younger patients and female patients also had higher risks of secondary malignancy (89). In Japan, only 1 out of 180 patients treated for malignant brain tumors since 1968 developed multiple radiation-induced meningiomas in the treatment field (90).

DISCUSSION

BNCT represents a promising treatment modality, with data suggesting the safety and efficacy of treatment in patients with advanced tumors. Caution should be taken when interpreting the data from BNCT. The studies exhibit a high degree of heterogeneity in inclusion criteria, boronated compounds used, times for infusion, and neutron dose given, which creates difficulty in comparing studies even within the same disease site. Additionally, there are no current studies investigating the outcomes of BNCT compared to other standards of care, which limit interpretation of the results. Well-designed phase II/III studies are needed to define the efficacy and safety of BNCT in a variety of tumor types.

Although initial results with BNCT are promising, toxicity rates remains relatively high. Further research into developing more selective boronated compounds is needed to improve the therapeutic ratio of treatment and decrease potential toxicity. In the era of immunotherapy and targeted agents, ^{10}B can conceivably be conjugated to these agents to increase selectivity, an area of needed research. Alternatively, BNCT may be coupled with immunotherapy to achieve optimum synergy between immune activation by the high LET attributes of BNCT and immunotherapy that maintains lymphocytes in an activated state.

Another barrier to adoption of BNCT is the high cost of developing and maintaining a BNCT treatment center. Currently, there are no centers in the United States treating with BNCT. Nakagawa et al. estimated that a BNCT facility in Japan costs approximately 1200 million Yen (approximately $11.4 million) to construct with an annual personnel cost of 113 million Yen (approximately $1 million) (91). The substantial initial startup costs are a barrier to developing a BNCT center in the United States, especially with a lack of studies investigating the cost effectiveness of BNCT compared to other modalities.

Another potential area of research is using non-boronated compounds, which, while offering similar mechanisms as BNCT, may have improved treatment effects or mitigation of BNCT limitations. ^{157}Gadolinium in particular has generated considerable interest, in no small part due to its role as a contrast agent in MRI and notable high uptake in (brain) tumor cells, where the large magnetic moment of the Gd3+ ion may be detected (92–96). Unlike ^{10}B, which releases both high LET He and Li ions, the $^{157}Gd(n,\gamma)^{158}Gd$ capture reaction generates gamma rays, x-rays, and internal conversion, Auger, and Coster-Kronig electrons. These electrons are similarly high-LET with limited range, concentrating damage within a diameter of approximately one cell and effectively generating double strand breaks. This offers unique potential if a highly localizing gadolinium-based agent can be achieved. However, the presence of gamma and x-rays broadens the dose delivery region, and may somewhat limit selectivity (94). In comparison with boronated compounds, the wider irradiation range may offer improved treatment of nearby cells undergoing limited deposition, forming a spectrum of utility amongst boronated and gadolinium-based agents. As such, treatment efforts hinge on the development of gadolinium-based compounds, of which many have been developed and assayed (94), though deployment within *in vivo* models has been limited. Early results were promising, such as Tokumitsu and colleagues' deployment of chitosan nanoparticles in 1999, finding significant suppression in a B16F10 murine melanoma model (95). Uniquely, combination agents have been introduced: a gadolinium/boron agent, bound to low-density lipoproteins (LDL), has demonstrated preliminary success in MRI-monitorable detection and treatment success both in-vitro and in a murine model (93).

CONCLUSIONS

Boron neutron capture therapy represents an emerging targeted therapy with promising results and acceptable toxicity in early clinical studies. Further prospective research is necessary to define the role of BNCT in clinical practice.

AUTHOR CONTRIBUTIONS

TM, DT, and SK were responsible for the concept of the manuscript. All authors contributed to the article and approved the submitted version.

REFERENCES

1. Nedunchezhian K, Aswath N, Thiruppathy M, Thirugnanamurthy S. Boron Neutron Capture Therapy - A Literature Review. *J Clin Diagn Res* (2016) 10 (12):Ze01–ze4. doi: 10.7860/jcdr/2016/19890.9024
2. Sauerwein W, Wittig A, Moss R, Nakagawa K. *Neutron Capture Therapy: Principles and Applications*. London: Springer Heidelberg New York Dordrecht (2012).
3. Barth RF, Zhang Z, Liu T. A realistic appraisal of boron neutron capture therapy as a cancer treatment modality. *Cancer Commun (Lond)* (2018) 38 (1):36. doi: 10.1186/s40880-018-0280-5
4. Chanana AD, Capala J, Chadha M, Coderre JA, Diaz AZ, Elowitz EH, et al. Boron neutron capture therapy for glioblastoma multiforme: interim results from the phase I/II dose-escalation studies. *Neurosurgery* (1999) 44(6):1182–92; discussion 92-3. doi: 10.1097/00006123-199906000-00013
5. Henriksson R, Capala J, Michanek A, Lindahl SA, Salford LG, Franzen L, et al. Boron neutron capture therapy (BNCT) for glioblastoma multiforme: a phase II study evaluating a prolonged high-dose of boronophenylalanine (BPA). *Radiother Oncol* (2008) 88(2):183–91. doi: 10.1016/j.radonc.2006.04.015
6. Kawabata S, Miyatake S, Nonoguchi N, Hiramatsu R, Iida K, Miyata S, et al. Survival benefit from boron neutron capture therapy for the newly diagnosed glioblastoma patients. *Appl Radiat Isot* (2009) 67(7-8 Suppl):S15–8. doi: 10.1016/j.apradiso.2009.03.015
7. Kageji T, Mizobuchi Y, Nagahiro S, Nakagawa Y, Kumada H. Clinical results of boron neutron capture therapy (BNCT) for glioblastoma. *Appl Radiat Isot* (2011) 69(12):1823–5. doi: 10.1016/j.apradiso.2011.05.029
8. Miyatake S, Kawabata S, Hiramatsu R, Kuroiwa T, Suzuki M, Kondo N, et al. Boron Neutron Capture Therapy for Malignant Brain Tumors. *Neurol Med Chir (Tokyo)* (2016) 56(7):361–71. doi: 10.2176/nmc.ra.2015-0297
9. Kankaanranta L, Seppala T, Koivunoro H, Saarilahti K, Atula T, Collan J, et al. Boron neutron capture therapy in the treatment of locally recurred head-and-neck cancer: final analysis of a phase I/II trial. *Int J Radiat Oncol Biol Phys* (2012) 82(1):e67–75. doi: 10.1016/j.ijrobp.2010.09.057
10. Kato I, Fujita Y, Maruhashi A, Kumada H, Ohmae M, Kirihata M, et al. Effectiveness of boron neutron capture therapy for recurrent head and neck malignancies. *Appl Radiat Isot* (2009) 67(7-8 Suppl):S37–42. doi: 10.1016/j.apradiso.2009.03.103
11. Suzuki M, Kato I, Aihara T, Hiratsuka J, Yoshimura K, Niimi M, et al. Boron neutron capture therapy outcomes for advanced or recurrent head and neck cancer. *J Radiat Res* (2014) 55(1):146–53. doi: 10.1093/jrr/rrt098
12. Koivunoro H, Kankaanranta L, Seppala T, Haapaniemi A, Makitie A, Joensuu H. Boron neutron capture therapy for locally recurrent head and neck squamous cell carcinoma: An analysis of dose response and survival. *Radiother Oncol* (2019) 137:153–8. doi: 10.1016/j.radonc.2019.04.033
13. Wang LW, Chen YW, Ho CY, Hsueh Liu YW, Chou FI, Liu YH, et al. Fractionated BNCT for locally recurrent head and neck cancer: experience from a phase I/II clinical trial at Tsing Hua Open-Pool Reactor. *Appl Radiat Isot* (2014) 88:23–7. doi: 10.1016/j.apradiso.2013.11.134
14. Wang LW, Liu YH, Chou FI, Jiang SH. Clinical trials for treating recurrent head and neck cancer with boron neutron capture therapy using the Tsing-Hua Open Pool Reactor. *Cancer Commun (Lond)* (2018) 38(1):37. doi: 10.1186/s40880-018-0295-y
15. Menendez PR, Roth BM, Pereira MD, Casal MR, Gonzalez SJ, Feld DB, et al. BNCT for skin melanoma in extremities: updated Argentine clinical results. *Appl Radiat Isot* (2009) 67(7-8 Suppl):S50–3. doi: 10.1016/j.apradiso.2009.03.020
16. Stupp R, Mason WP, van den Bent MJ, Weller M, Fisher B, Taphoorn MJ, et al. Radiotherapy plus concomitant and adjuvant temozolomide for glioblastoma. *N Engl J Med* (2005) 352(10):987–96. doi: 10.1056/NEJMoa043330
17. Altinoz MA, Topcu G, Elmaci I. Boron's neurophysiological effects and tumoricidal activity on glioblastoma cells with implications for clinical treatment. *Int J Neurosci* (2019) 129(10):963–77. doi: 10.1080/00207454.2019.1595618
18. Skold K, HS B, Diaz AZ, Giusti V, Pellettieri L, Hopewell JW. Boron Neutron Capture Therapy for glioblastoma multiforme: advantage of prolonged infusion of BPA-f. *Acta Neurol Scand* (2010) 122(1):58–62. doi: 10.1111/j.1600-0404.2009.01267.x
19. Miyatake S, Kawabata S, Yokoyama K, Kuroiwa T, Michiue H, Sakurai Y, et al. Survival benefit of Boron neutron capture therapy for recurrent malignant gliomas. *J Neurooncol* (2009) 91(2):199–206. doi: 10.1007/s11060-008-9699-x
20. Yamamoto T, Nakai K, Kageji T, Kumada H, Endo K, Matsuda M, et al. Boron neutron capture therapy for newly diagnosed glioblastoma. *Radiother Oncol* (2009) 91(1):80–4. doi: 10.1016/j.radonc.2009.02.009
21. Yamamoto T, Nakai K, Tsurubuchi T, Matsuda M, Shirakawa M, Zaboronok A, et al. Boron neutron capture therapy for newly diagnosed glioblastoma: a pilot study in Tsukuba. *Appl Radiat Isot* (2009) 67(7-8 Suppl):S25–6. doi: 10.1016/j.apradiso.2009.03.011
22. Chadha M, Capala J, Coderre JA, Elowitz EH, Iwai J, Joel DD, et al. Boron neutron-capture therapy (BNCT) for glioblastoma multiforme (GBM) using the epithermal neutron beam at the Brookhaven National Laboratory. *Int J Radiat Oncol Biol Phys* (1998) 40(4):829–34. doi: 10.1016/s0360-3016(97)00891-2
23. Kageji T, Nagahiro S, Mizobuchi Y, Matsuzaki K, Nakagawa Y, Kumada H. Boron neutron capture therapy (BNCT) for newly-diagnosed glioblastoma: comparison of clinical results obtained with BNCT and conventional treatment. *J Med Invest* (2014) 61(3-4):254–63. doi: 10.2152/jmi.61.254
24. Kageji T, Mizobuchi Y, Nagahiro S, Nakagawa Y, Kumada H. Long-survivors of glioblatoma treated with boron neutron capture therapy (BNCT). *Appl Radiat Isot* (2011) 69(12):1800–2. doi: 10.1016/j.apradiso.2011.03.021
25. Hatanaka H, Nakagawa Y. Clinical results of long-surviving brain tumor patients who underwent boron neutron capture therapy. *Int J Radiat Oncol Biol Phys* (1994) 28(5):1061–6. doi: 10.1016/0360-3016(94)90479-0
26. Kankaanranta L, Seppala T, Koivunoro H, Valimaki P, Beule A, Collan J, et al. L-boronophenylalanine-mediated boron neutron capture therapy for malignant glioma progressing after external beam radiation therapy: a Phase I study. *Int J Radiat Oncol Biol Phys* (2011) 80(2):369–76. doi: 10.1016/j.ijrobp.2010.02.031
27. Aiyama H, Nakai K, Yamamoto T, Nariai T, Kumada H, Ishikawa E, et al. A clinical trial protocol for second line treatment of malignant brain tumors with BNCT at University of Tsukuba. *Appl Radiat Isot* (2011) 69(12):1819–22. doi: 10.1016/j.apradiso.2011.04.031
28. Okazaki T, Kageji T, Mizobuchi Y, Miyamoto T, Nagahiro S. Nine-year interval recurrence after treatment of boron neutron capture therapy in a patient with glioblastoma: a case report. *Appl Radiat Isot* (2014) 88:28–31. doi: 10.1016/j.apradiso.2013.12.029
29. Nakai K, Yamamoto T, Aiyama H, Takada T, Yoshida F, Kageji T, et al. Boron neutron capture therapy combined with fractionated photon irradiation for glioblastoma: a recursive partitioning analysis of BNCT patients. *Appl Radiat Isot* (2011) 69(12):1790–2. doi: 10.1016/j.apradiso.2011.03.049
30. Miyatake SI, Kawabata S, Hiramatsu R, Kuroiwa T, Suzuki M, Ono K. Boron Neutron Capture Therapy of Malignant Gliomas. *Prog Neurol Surg* (2018) 32:48–56. doi: 10.1159/000469679
31. Miyatake S, Kawabata S, Nonoguchi N, Yokoyama K, Kuroiwa T, Matsui H, et al. Pseudoprogression in boron neutron capture therapy for malignant gliomas and meningiomas. *Neuro Oncol* (2009) 11(4):430–6. doi: 10.1215/15228517-2008-107
32. Shiba H, Takeuchi K, Hiramatsu R, Furuse M, Nonoguchi N, Kawabata S, et al. Boron Neutron Capture Therapy Combined with Early Successive Bevacizumab Treatments for Recurrent Malignant Gliomas - A Pilot Study. *Neurol Med Chir (Tokyo)* (2018) 58(12):487–94. doi: 10.2176/nmc.oa.2018-0111
33. Miyatake S, Furuse M, Kawabata S, Maruyama T, Kumabe T, Kuroiwa T, et al. Bevacizumab treatment of symptomatic pseudoprogression after boron neutron capture therapy for recurrent malignant gliomas. Report of 2 cases. *Neuro Oncol* (2013) 15(6):650–5. doi: 10.1093/neuonc/not020
34. Miyatake S, Kawabata S, Hiramatsu R, Furuse M, Kuroiwa T, Suzuki M. Boron neutron capture therapy with bevacizumab may prolong the survival of recurrent malignant glioma patients: four cases. *Radiat Oncol* (2014) 9:6. doi: 10.1186/1748-717X-9-6
35. Kageji T, Mizobuchi Y, Nagahiro S, Nakagawa Y, Kumada H. Correlation between radiation dose and histopathological findings in patients with gliblastoma treated with boron neutron capture therapy (BNCT). *Appl Radiat Isot* (2014) 88:20–2. doi: 10.1016/j.apradiso.2013.12.014
36. Miyatake S, Kuwabara H, Kajimoto Y, Kawabata S, Yokoyama K, Doi A, et al. Preferential recurrence of a sarcomatous component of a gliosarcoma after boron neutron capture therapy: case report. *J Neurooncol* (2006) 76(2):143–7. doi: 10.1007/s11060-005-4174-4
37. Vos MJ, Turowski B, Zanella FE, Paquis P, Siefert A, Hideghety K, et al. Radiologic findings in patients treated with boron neutron capture therapy for glioblastoma multiforme within EORTC trial 11961. *Int J Radiat Oncol Biol Phys* (2005) 61(2):392–9. doi: 10.1016/j.ijrobp.2004.06.008

38. Yamamoto T, Nakai K, Nariai T, Kumada H, Okumura T, Mizumoto M, et al. The status of Tsukuba BNCT trial: BPA-based boron neutron capture therapy combined with X-ray irradiation. *Appl Radiat Isot* (2011) 69(12):1817–8. doi: 10.1016/j.apradiso.2011.02.013
39. Miyatake S, Tamura Y, Kawabata S, Iida K, Kuroiwa T, Ono K. Boron neutron capture therapy for malignant tumors related to meningiomas. *Neurosurgery* (2007) 61(1):82–90; discussion -1. doi: 10.1227/01.neu.0000279727.90650.24
40. Stenstam BH, Pellettieri L, Sorteberg W, Rezaei A, Skold K. BNCT for recurrent intracranial meningeal tumours - case reports. *Acta Neurol Scand* (2007) 115(4):243–7. doi: 10.1111/j.1600-0404.2006.00776.x
41. Kawabata S, Hiramatsu R, Kuroiwa T, Ono K, Miyatake S. Boron neutron capture therapy for recurrent high-grade meningiomas. *J Neurosurg* (2013) 119(4):837–44. doi: 10.3171/2013.5.JNS122204
42. Takeuchi K, Kawabata S, Hiramatsu R, Matsushita Y, Tanaka H, Sakurai Y, et al. Boron Neutron Capture Therapy for High-Grade Skull-Base Meningioma. *J Neurol Surg B Skull Base* (2018) 79(Suppl 4):S322–s7. doi: 10.1055/s-0038-1666837
43. Tamura Y, Miyatake S, Nonoguchi N, Miyata S, Yokoyama K, Doi A, et al. Boron neutron capture therapy for recurrent malignant meningioma. Case report. *J Neurosurg* (2006) 105(6):898–903. doi: 10.3171/jns.2006.105.6.898
44. Kawaji H, Miyatake S, Shinmura K, Kawabata S, Tokuyama T, Namba H. Effect of boron neutron capture therapy for recurrent anaplastic meningioma: an autopsy case report. *Brain Tumor Pathol* (2015) 32(1):61–5. doi: 10.1007/s10014-014-0189-x
45. Aziz T, Peress NS, Diaz A, Capala J, Chanana A. Postmortem neuropathological features secondary to boron neutron capture therapy for glioblastoma multiforme. *J Neuropathol Exp Neurol* (2000) 59(1):62–73. doi: 10.1093/jnen/59.1.62
46. Kouri M, Kankaanranta L, Seppala T, Tervo L, Rasilainen M, Minn H, et al. Undifferentiated sinonasal carcinoma may respond to single-fraction boron neutron capture therapy. *Radiother Oncol* (2004) 72(1):83–5. doi: 10.1016/j.radonc.2004.03.016
47. Kimura Y, Ariyoshi Y, Miyatake S, Shimahara M, Kawabata S, Ono K. Boron neutron capture therapy for papillary cystadenocarcinoma in the upper lip: a case report. *Int J Oral Maxillofac Surg* (2009) 38(3):293–5. doi: 10.1016/j.ijom.2008.12.010
48. Kankaanranta L, Saarilahti K, Makitie A, Valimaki P, Tenhunen M, Joensuu H. Boron neutron capture therapy (BNCT) followed by intensity modulated chemoradiotherapy as primary treatment of large head and neck cancer with intracranial involvement. *Radiother Oncol* (2011) 99(1):98–9. doi: 10.1016/j.radonc.2011.02.008
49. Aihara T, Hiratsuka J, Ishikawa H, Kumada H, Ohnishi K, Kamitani N, et al. Fatal carotid blowout syndrome after BNCT for head and neck cancers. *Appl Radiat Isot* (2015) 106:202–6. doi: 10.1016/j.apradiso.2015.08.007
50. Kato I, Ono K, Sakurai Y, Ohmae M, Maruhashi A, Imahori Y, et al. Effectiveness of BNCT for recurrent head and neck malignancies. *Appl Radiat Isot* (2004) 61(5):1069–73. doi: 10.1016/j.apradiso.2004.05.059
51. Kankaanranta L, Seppala T, Koivunoro H, Saarilahti K, Atula T, Collan J, et al. Boron neutron capture therapy in the treatment of locally recurred head and neck cancer. *Int J Radiat Oncol Biol Phys* (2007) 69(2):475–82. doi: 10.1016/j.ijrobp.2007.03.039
52. Aihara T, Morita N, Kamitani N, Kumada H, Ono K, Hiratsuka J, et al. BNCT for advanced or recurrent head and neck cancer. *Appl Radiat Isot* (2014) 88:12–5. doi: 10.1016/j.apradiso.2014.04.007
53. Haapaniemi A, Kankaanranta L, Saat R, Koivunoro H, Saarilahti K, Makitie A, et al. Boron Neutron Capture Therapy in the Treatment of Recurrent Laryngeal Cancer. *Int J Radiat Oncol Biol Phys* (2016) 95(1):404–10. doi: 10.1016/j.ijrobp.2015.11.010
54. Haginomori S, Miyatake S, Inui T, Araki M, Kawabata S, Takamaki A, et al. Planned fractionated boron neutron capture therapy using epithermal neutrons for a patient with recurrent squamous cell carcinoma in the temporal bone: a case report. *Head Neck* (2009) 31(3):412–8. doi: 10.1002/hed.20895
55. Aihara T, Hiratsuka J, Morita N, Uno M, Sakurai Y, Maruhashi A, et al. First clinical case of boron neutron capture therapy for head and neck malignancies using 18F-BPA PET. *Head Neck* (2006) 28(9):850–5. doi: 10.1002/hed.20418
56. Aihara T, Morita N, Kamitani N, Kumada H, Ono K, Hiratsuka J, et al. Boron neutron capture therapy for advanced salivary gland carcinoma in head and neck. *Int J Clin Oncol* (2014) 19(3):437–44. doi: 10.1007/s10147-013-0580-3
57. Ariyoshi Y, Miyatake S, Kimura Y, Shimahara T, Kawabata S, Nagata K, et al. Boron neuron capture therapy using epithermal neutrons for recurrent cancer in the oral cavity and cervical lymph node metastasis. *Oncol Rep* (2007) 18(4):861–6. doi: 10.3892/or.18.4.861
58. Kimura Y, Ariyoshi Y, Shimahara M, Miyatake S, Kawabata S, Ono K, et al. Boron neutron capture therapy for recurrent oral cancer and metastasis of cervical lymph node. *Appl Radiat Isot* (2009) 67(7-8 Suppl):S47–9. doi: 10.1016/j.apradiso.2009.03.019
59. Wang LW, Chen YW, Ho CY, Hsueh Liu YW, Chou FI, Liu YH, et al. Fractionated Boron Neutron Capture Therapy in Locally Recurrent Head and Neck Cancer: A Prospective Phase I/II Trial. *Int J Radiat Oncol Biol Phys* (2016) 95(1):396–403. doi: 10.1016/j.ijrobp.2016.02.028
60. Lee JC, Chuang KS, Hsueh Liu YW, Lin TY, Teng YC, Wang LW. A comparison of dose distributions in gross tumor volume between boron neutron capture therapy alone and combined boron neutron capture therapy plus intensity modulation radiation therapy for head and neck cancer. *PloS One* (2019) 14(4):e0210626. doi: 10.1371/journal.pone.0210626
61. Suzuki M, Sakurai Y, Nagata K, Kinashi Y, Masunaga S, Ono K, et al. Impact of intra-arterial administration of boron compounds on dose-volume histograms in boron neutron capture therapy for recurrent head-and-neck tumors. *Int J Radiat Oncol Biol Phys* (2006) 66(5):1523–7. doi: 10.1016/j.ijrobp.2006.07.1373
62. Trivillin VA, Garabalino MA, Colombo LL, Gonzalez SJ, Farias RO, Monti Hughes A, et al. Biodistribution of the boron carriers boronophenylalanine (BPA) and/or decahydrodecaborate (GB-10) for Boron Neutron Capture Therapy (BNCT) in an experimental model of lung metastases. *Appl Radiat Isot* (2014) 88:94–8. doi: 10.1016/j.apradiso.2013.11.115
63. Suzuki M, Endo K, Satoh H, Sakurai Y, Kumada H, Kimura H, et al. A novel concept of treatment of diffuse or multiple pleural tumors by boron neutron capture therapy (BNCT). *Radiother Oncol* (2008) 88(2):192–5. doi: 10.1016/j.radonc.2008.06.009
64. Suzuki M, Sakurai Y, Masunaga S, Kinashi Y, Nagata K, Maruhashi A, et al. A preliminary experimental study of boron neutron capture therapy for malignant tumors spreading in thoracic cavity. *Jpn J Clin Oncol* (2007) 37(4):245–9. doi: 10.1093/jjco/hym022
65. Suzuki M, Sakurai Y, Masunaga S, Kinashi Y, Nagata K, Maruhashi A, et al. Feasibility of boron neutron capture therapy (BNCT) for malignant pleural mesothelioma from a viewpoint of dose distribution analysis. *Int J Radiat Oncol Biol Phys* (2006) 66(5):1584–9. doi: 10.1016/j.ijrobp.2006.08.026
66. Farias RO, Bortolussi S, Menendez PR, Gonzalez SJ. Exploring Boron Neutron Capture Therapy for non-small cell lung cancer. *Phys Med* (2014) 30(8):888–97. doi: 10.1016/j.ejmp.2014.07.342
67. Gadan MA, Gonzalez SJ, Batalla M, Olivera MS, Policastro L, Sztejnberg ML. Application of BNCT to the treatment of HER2+ breast cancer recurrences: Research and developments in Argentina. *Appl Radiat Isot* (2015) 104:155–9. doi: 10.1016/j.apradiso.2015.07.006
68. Yanagie H, Kumada H, Sakurai Y, Nakamura T, Furuya Y, Sugiyama H, et al. Dosimetric evaluation of neutron capture therapy for local advanced breast cancer. *Appl Radiat Isot* (2009) 67(7-8 Suppl):S63–6. doi: 10.1016/j.apradiso.2009.03.110
69. Suzuki M, Sakurai Y, Hagiwara S, Masunaga S, Kinashi Y, Nagata K, et al. First attempt of boron neutron capture therapy (BNCT) for hepatocellular carcinoma. *Jpn J Clin Oncol* (2007) 37(5):376–81. doi: 10.1093/jjco/hym039
70. Yanagie H, Higashi S, Seguchi K, Ikushima I, Fujihara M, Nonaka Y, et al. Pilot clinical study of boron neutron capture therapy for recurrent hepatic cancer involving the intra-arterial injection of a (10)BSH-containing WOW emulsion. *Appl Radiat Isot* (2014) 88:32–7. doi: 10.1016/j.apradiso.2014.01.014
71. Uchiyama Y, Matsumoto K, Murakami S, Kanesaki T, Matsumoto A, Kishino M, et al. MRI in a case of osteosarcoma in the temporomandibular joint. *Dentomaxillofac Radiol* (2014) 43(2):20130280. doi: 10.1259/dmfr.20130280
72. Futamura G, Kawabata S, Siba H, Kuroiwa T, Suzuki M, Kondo N, et al. A case of radiation-induced osteosarcoma treated effectively by boron neutron capture therapy. *Radiat Oncol* (2014) 9:237. doi: 10.1186/s13014-014-0237-z
73. Fujimoto T, Andoh T, Sudo T, Fujita I, Fukase N, Takeuchi T, et al. Potential of boron neutron capture therapy (BNCT) for malignant peripheral nerve sheath tumors (MPNST). *Appl Radiat Isot* (2015) 106:220–5. doi: 10.1016/j.apradiso.2015.07.059

74. Inoue M, Lee CM, Ono K, Suzuki M, Tokunaga T, Sawa Y, et al. Clinical effectiveness of boron neutron capture therapy for a recurrent malignant peripheral nerve sheath tumor in the mediastinum. *J Thorac Oncol* (2010) 5 (12):2037–8. doi: 10.1097/JTO.0b013e3181f1cd86
75. Andoh T, Fujimoto T, Sudo T, Suzuki M, Sakurai Y, Sakuma T, et al. Boron neutron capture therapy as new treatment for clear cell sarcoma: trial on different animal model. *Appl Radiat Isot* (2014) 88:59–63. doi: 10.1016/j.apradiso.2013.12.007
76. Gonzalez SJ, Bonomi MR, Santa Cruz GA, Blaumann HR, Calzetta Larrieu OA, Menendez P, et al. First BNCT treatment of a skin melanoma in Argentina: dosimetric analysis and clinical outcome. *Appl Radiat Isot* (2004) 61(5):1101–5. doi: 10.1016/j.apradiso.2004.05.060
77. Santa Cruz GA, Gonzalez SJ, Bertotti J, Marin J. First application of dynamic infrared imaging in boron neutron capture therapy for cutaneous malignant melanoma. *Med Phys* (2009) 36(10):4519–29. doi: 10.1118/1.3218760
78. Yong Z, Song Z, Zhou Y, Liu T, Zhang Z, Zhao Y, et al. Boron neutron capture therapy for malignant melanoma: first clinical case report in China. *Chin J Cancer Res* (2016) 28(6):634–40. doi: 10.21147/j.issn.1000-9604.2016.06.10
79. Omori M, Fujiwara S, Shimizu H, Ikeda T, Bito T, Suzuki M, et al. Boron neutron capture therapy using reactor epithermal neutron beams could effectively control in-transit and lymph node metastases originating from a cutaneous malignant melanoma. *J Dermatol* (2018) 45(4):e90–e1. doi: 10.1111/1346-8138.14134
80. Makino E, Sasaoka S, Aihara T, Sakurai Y, Maruhashi A, Ono K, et al. The First Clinical Trial of Boron Neutron Capture Therapy Using 10B-para-boronophenylalanine for Treating Extramammary Paget's Disease. *Eur J Cancer* (1013) 2012) 48:S244–S5. doi: 10.1016/S0959-8049(12)71630-1
81. Hiratsuka J, Kamitani N, Tanaka R, Yoden E, Tokiya R, Suzuki M, et al. Boron neutron capture therapy for vulvar melanoma and genital extramammary Paget's disease with curative responses. *Cancer Commun (Lond)* (2018) 38 (1):38. doi: 10.1186/s40880-018-0297-9
82. Wittig A, Malago M, Collette L, Huiskamp R, Buhrmann S, Nievaart V, et al. Uptake of two 10B-compounds in liver metastases of colorectal adenocarcinoma for extracorporeal irradiation with boron neutron capture therapy (EORTC Trial 11001). *Int J Cancer* (2008) 122(5):1164–71. doi: 10.1002/ijc.23224
83. Zonta A, Pinelli T, Prati U, Roveda L, Ferrari C, Clerici AM, et al. Extra-corporeal liver BNCT for the treatment of diffuse metastases: what was learned and what is still to be learned. *Appl Radiat Isot* (2009) 67(7-8 Suppl):S67–75. doi: 10.1016/j.apradiso.2009.03.087
84. Wittig A, Collette L, Appelman K, Buhrmann S, Jackel MC, Jockel KH, et al. EORTC trial 11001: distribution of two 10B-compounds in patients with squamous cell carcinoma of head and neck, a translational research/phase 1 trial. *J Cell Mol Med* (2009) 13(8B):1653–65. doi: 10.1111/j.1582-4934.2009.00856.x
85. Wittig A, Collette L, Moss R, Sauerwein WA. Early clinical trial concept for boron neutron capture therapy: a critical assessment of the EORTC trial 11001. *Appl Radiat Isot* (2009) 67(7-8 Suppl):S59–62. doi: 10.1016/j.apradiso.2009.03.012
86. Trivillin VA, Pozzi ECC, Colombo LL, Thorp SI, Garabalino MA, Monti Hughes A, et al. Abscopal effect of boron neutron capture therapy (BNCT): proof of principle in an experimental model of colon cancer. *Radiat Environ Biophys* (2017) 56(4):365–75. doi: 10.1007/s00411-017-0704-7
87. Yanagie H, Higashi S, Seguchi K, Ikushima I, Oyama K, Nonaka Y, et al. Pilot clinical study of boron neutron capture therapy for recurrent hepatic cancer and gastric cancer. In: *the international congress on neutron capture therapy*. Tsukuba, Japan (2012).
88. Nakagawa Y, Kageji T, Mizobuchi Y, Kumada H, Nakagawa Y. Clinical results of BNCT for malignant brain tumors in children. *Appl Radiat Isot* (2009) 67 (7-8 Suppl):S27–30. doi: 10.1016/j.apradiso.2009.03.090
89. Zhang X, Geng C, Tang X, Bortolussi S, Shu D, Gong C, et al. Assessment of long-term risks of secondary cancer in paediatric patients with brain tumours after boron neutron capture therapy. *J Radiol Prot* (2019) 39(3):838–53. doi: 10.1088/1361-6498/ab29a3
90. Kageji T, Sogabe S, Mizobichi Y, Nakajima K, Shinji N, Nakagawa Y. Radiation-induced meningiomas after BNCT in patients with malignant glioma. *Appl Radiat Isot* (2015) 106:256–9. doi: 10.1016/j.apradiso.2015.06.004
91. Nakagawa Y, Yoshihara H, Kageji T, Matsuoka R, Nakagawa Y. Cost analysis of radiotherapy, carbon ion therapy, proton therapy and BNCT in Japan. *Appl Radiat Isot* (2009) 67(7-8 Suppl):S80–3. doi: 10.1016/j.apradiso.2009.03.055
92. Lee GH, Chang Y, Kim T-J. 7 - Thermal neutron capture therapy (NCT). In: GH Lee, Y Chang, T-J Kim, editors. *Ultrasmall Lanthanide Oxide Nanoparticles for Biomedical Imaging and Therapy*. Waltham, MA: Woodhead Publishing (2014). p. 97–102.
93. Geninatti-Crich S, Alberti D, Szabo I, Deagostino A, Toppino A, Barge A, et al. MRI-guided neutron capture therapy by use of a dual gadolinium/boron agent targeted at tumour cells through upregulated low-density lipoprotein transporters. *Chemistry* (2011) 17(30):8479–86. doi: 10.1002/chem.201003741
94. Cerullo N, Bufalino D, Daquino G. Progress in the use of gadolinium for NCT. *Appl Radiat Isot* (2009) 67(7-8 Suppl):S157–60. doi: 10.1016/j.apradiso.2009.03.109
95. Tokumitsu H, Hiratsuka J, Sakurai Y, Kobayashi T, Ichikawa H, Fukumori Y. Gadolinium neutron-capture therapy using novel gadopentetic acid-chitosan complex nanoparticles: in vivo growth suppression of experimental melanoma solid tumor. *Cancer Lett* (2000) 150(2):177–82. doi: 10.1016/s0304-3835(99)00388-2
96. Jung KH, Park JA, Kim JY, Kim MH, Oh S, Kim HK, et al. Image-Guided Neutron Capture Therapy Using the Gd-DO3A-BTA Complex as a New Combinatorial Treatment Approach. *Contrast Media Mol Imaging* (2018) 2018:3727109. doi: 10.1155/2018/3727109

Conflict of Interest: DT has received clinical trial funding from Novocure and publishing fees from Springer.

The remaining authors declare that the research was conducted in the absence of any commercial or financial relationships that could be construed as a potential conflict of interest.

Copyright © 2021 Malouff, Seneviratne, Ebner, Stross, Waddle, Trifiletti and Krishnan. This is an open-access article distributed under the terms of the Creative Commons Attribution License (CC BY). The use, distribution or reproduction in other forums is permitted, provided the original author(s) and the copyright owner(s) are credited and that the original publication in this journal is cited, in accordance with accepted academic practice. No use, distribution or reproduction is permitted which does not comply with these terms.

frontiers in Oncology

ORIGINAL RESEARCH
published: 02 March 2021
doi: 10.3389/fonc.2020.601620

Effect of Carbon Ion Radiation Induces Bystander Effect on Metastasis of A549 Cells and Metabonomic Correlation Analysis

Zhen Yang[1†], Qiuning Zhang[2,3†], Hongtao Luo[2], Lihua Shao[3], Ruifeng Liu[2], Yarong Kong[2], Xueshan Zhao[4], Yichao Geng[4], Chengcheng Li[4] and Xiaohu Wang[1,2,3,4]*

[1] The Basic Medical College of Lanzhou University, Lanzhou, China, [2] Institute of Modern Physics, Chinese Academy of Sciences, Lanzhou, China, [3] Department of Oncology, Lanzhou Heavy Ion Hospital, Lanzhou, China, [4] Department of Oncology, The First School of Clinical Medicine, Lanzhou University, Lanzhou, China

OPEN ACCESS

Edited by:
Daniel Michael Trifiletti, Mayo Clinic Florida, United States

Reviewed by:
Christopher Paul Cifarelli, West Virginia University Hospitals, United States
Narongchai Autsavapromporn, Chiang Mai University, Thailand
Ianik Plante, KBRwyle, United States

***Correspondence:**
Xiaohu Wang
xhwang@impcas.ac.cn

[†]These authors have contributed equally to this work

Specialty section:
This article was submitted to Radiation Oncology, a section of the journal Frontiers in Oncology

Received: *01 September 2020*
Accepted: *31 December 2020*
Published: *02 March 2021*

Citation:
Yang Z, Zhang Q, Luo H, Shao L, Liu R, Kong Y, Zhao X, Geng Y, Li C and Wang X (2021) Effect of Carbon Ion Radiation Induces Bystander Effect on Metastasis of A549 Cells and Metabonomic Correlation Analysis. Front. Oncol. 10:601620. doi: 10.3389/fonc.2020.601620

Objective: To analyze the effect of carbon ion ($^{12}C^{6+}$) radiation may induce bystander effect on A549 cell metastasis and metabonomics.

Methods: A549 cell was irradiated with carbon ion to establish the clone survival model and the transwell matrix assay was applied to measure the effect of carbon ion on cell viability, migration, and invasion, respectively. Normal human embryonic lung fibroblasts (WI-38) were irradiated with carbon ions of 0 and 2 Gy and then transferred to A549 cell co-culture medium for 24 h. The migration and invasion of A549 cells were detected by the Transwell chamber. The analysis of metabonomic information in transfer medium by liquid phase mass spectrometry (LC-MS), The differential molecules were obtained by principal pomponent analysis (PCA) and the target proteins of significant differences ($p = 1.7 \times 10^{-3}$) obtained by combining with the STICH database. KEGG pathway was used to analyze the enrichment of the target protein pathway.

Results: Compared with 0 Gy, the colony formation, migration, and invasion of A549 cells were significantly inhibited by carbon ion 2 and 4 Gy irradiation, while the inhibitory effect was not significant after 1 Gy irradiation. Compared with 0 Gy, the culture medium 24 h after carbon ion 2 Gy irradiation significantly inhibited the metastasis of tumor cells ($p = 0.03$). LC-MS analysis showed that 23 differential metabolites were obtained in the cell culture medium 24 h after carbon ion 0 and 2 Gy irradiation (9 up-regulated and 14 down-regulated). Among them, two were up-regulated and two down-regulated ($p = 2.9 \times 10^{-3}$). 41 target proteins were corresponding to these four differential molecules. Through the analysis of the KEGG signal pathway, it was found that these target molecules were mainly enriched in purine metabolism, tyrosine metabolism, cysteine and methionine metabolism, peroxisome, and carbon metabolism. Neuroactive ligand-receptor interaction, calcium signaling pathway, arachidonic acid metabolism, and Fc epsilon RI signaling pathway.

Conclusion: The bystander effect induced by 2 Gy carbon ion radiation inhibits the metastasis of tumor cells, which indicates that carbon ions may change the metabolites of irradiated cells, so that it may indirectly affect the metabolism of tumor cell growth microenvironment, thus inhibiting the metastasis of malignant tumor cells.

Keywords: carbon ions, metastasis, radiation-induced bystander effect, liquid phase mass spectrometry, metabonomics

INTRODUCTION

In 2018, there were 18.1 million new cases of cancer worldwide, of which the incidence of lung cancer was 11.6% and the mortality rate was 18.4% (1). However, the metastasis of lung cancer is a major cause of treatment failure (2). Carbon ions with high LET rays ($^{12}C^{6+}$) can inhibit the metastasis of tumor cells by their advantages in physics and biology (3, 4). Radiation induces bystander effect (RIBE) refers to the plethora of biological phenomena occurring in non-irradiated cells as a result of signal transmission from an irradiated cell (5). The study of proton targeting cancer cells and unirradiated normal fibroblasts also found an induced bi-directional bystander effect, and RIBE was detected *in vitro*, 3D tissues and mouse models (6).Growing evidence show that bystander responses can be regulated by four mechanisms-(i) gap junction intercellular communication (ii) communication of soluble factors released by irradiated cells or organs (iii) clastogenic factors and exosomes (7, 8).

Recently, it has been found that reactive oxygen species (ROS) (9), superoxide dismutase (SOD), nitric oxide (NO) (10), cyclooxygenase 2 (COX2), CD95 ligand (Fals), transforming growth factor-β1 (TGFβ1), and tumor necrosis factor-α(TNF-α) (11) play an important roles in RIBE. Among all these factors, some are soluble factors (TGFβ1 and TNF-α), some are exosome released factors (Fals), others are common factors of both (ROS, SOD, NO, and COX2), are very similar effect to RIBE. The maximum molecular weight allowed to pass through the pores of gap junctional intercellular communication (GJIC) is 1,000 to 1,500 Da, which allows ions, small molecular metabolites and second messengers to communicate directly between cells. The molecular weight of soluble factors is between 1,000 and 10,000 kDa. Molecules smaller than 1,000 Da are selected as the main metabolic factors in this study, so they belong to clastogenic factors and exosomes-mediated bystander effect factors (12). At the same time, the GJIC also plays an interesting role in RIBE (13). After GJIC inhibition, the fractionated doses of proton radiation-induced less DNA damage than single-dose radiation in the secondary bystander effects (14). The mechanism of the radiation-induced bystander effect, whether involving cell-cell contact or mediated by soluble factors, is not clear, is likely to be complex, and involves multiple pathways (15). At present, there are two main research reports—(i) For cells in direct contact, bystander signaling can occur through GJIC. Gap junctions are multimeric protein channels between cells that allow transmission of signaling molecules. Key ions and metabolites that are known to be transmitted through GJIC include ions such as Ca^{2+}, nucleotides, peptides and other secondary messengers (16). (ii) Its mechanism that radiation exposure can result in the release of soluble (clastogenic) factors or exosomes into the microenvironment that are capable of inducing chromosome damage in cultured cells, thus changing the biological characteristics of unirradiated cells. Among them, the studies on cytokine signal transduction and production of reactive oxygen species and nitrogen species are relatively clear (17).

Although there are many reports about RIBE research, only a few studies about the relationship of carbon ion bystander effects (CIBE) and malignant tumor cell metastasis. It has been found that glutamate involved in tumorigenesis, and glutamate concentration plays a key role in the invasion and migration of pancreatic cancer cells (18). Understanding radiation-induced signaling pathways is essential for developing new strategies in both cancer radiotherapy and the prevention of radiation carcinogenesis (19). Therefore, in our study, we used metabonomics techniques were used to analyze the metabolic molecules of carbon ion-induced fine radiation bystander effects, meanwhile we combined with bioinformatics methods to screen differential metabolites and possibly target molecules to explain the effect and potential effects of carbon ion radiation bystander effects on non-small cell lung cancer (NSCLC) cell metastasis.

MATERIALS AND METHODS

Cell Culture

Human lung adenocarcinoma cell line A549 and normal human embryonic fibroblasts WI-38 cells were purchased from the American Type Culture Collection (ATCC). The cells were maintained in RPMI1640 medium supplemented with 10% (v/v) fetal bovine serum (FBS), 100 U/ml penicillin and 100 mg/ml streptomycin (Life Technologies) in a humidified atmosphere of 5% (v/v) CO_2 and 95% (v/v) air at 37°C. Every other day, the medium was changed, and cells in the logarithmic growth phase (1×10^7 cells were harvested at 70% confluence) were used in the experiments.

Irradiation Condition

Heavy ions were obtained from the carbon ion ($^{12}C^{6+}$) beam of the Deep Therapy Terminal, Institute of Modern Physics, Chinese Academy of Sciences (HIRFL-CSR) (Ray parameters: energy of 100 MeV, the dose rate of 1 Gy/min, broadened Bragg peak of 5 mm, radiation field of 5 cm × 5 cm), for cell irradiation. Irradiation doses were 0, 1, 2, and 4 Gy. The experiment was repeated four times.

Medium Transfer Protocol

Exponentially growing cells were irradiated with carbon ion, and then incubated in fresh medium to allow for the release of soluble

bystander factors. After carbon ion treatment (counted as 0 h), irradiation conditioned medium was harvested at the time points of 24 h, respectively. These irradiation conditioned medium were filtered through 0.22-μm filter (Millpore, USA) to remove any floating cells and cellular debris. These irradiation conditioned medium were used to culture the nonirradiated cells (bystander cells). For the controls in all experiments, the irradiation conditioned medium were collected from a parallel culture that had not been irradiated.

Colony Formation Assay

Cells in logarithmic growth were detached with 0.25% trypsin and then triturated into single cells and centrifuged. The number of cells was counted with a counting board. A549 cells were inoculated separately in a six-well plate after being resuspended in culture medium containing 10% FBS: 0 Gy group: 400 cells/well, 1 Gy group: 800 cells/well, 2 Gy group: 1,000 cells/well, and 4 Gy group, 4,000 cells/well. Three replicate wells were used for each group. After overnight inoculation, the cells were exposed to 0, 1, 2, and 4 Gy carbon ion rays and cultured in a cell incubator for 13 days. When the cell colonies were visible to the naked eye, approximately 50 cells were counted under the microscope, and the experiment was terminated. Next, the cells were fixed with 4% polyformaldehyde (500 μl) for 15 min, stained with a crystal violet solution (500 μl) for 15 min, and observed. Plating efficiency (PE) = colony number/inoculation number × 100%, and survival fraction (SF) = colony rate in the experimental group/colony rate in the control group × 100%. The cell dose survival curve was generated using the formula SF=e^(−(αD + βD^2)) and GraphPad Prism 6 software. The experiment was repeated three times.

Cell Counting kit-8 (CCK-8) Assay

A549 cells grown in wells were detached with trypsin and resuspended in a small amount of culture medium, and the cells were then counted. Next, 100 μl (approximately 10,000 cells) of cell suspension was added to each well of a 96-well plate. Six replicate wells were used for each group, and the culture plate was placed in an incubator for pre-culture for 24 h (37°C, 5% CO_2) to allow the cells to adhere. The cells were exposed to carbon ion radiation when the cells reached 50% to 60% confluence. Cell proliferation was detected at 24, 48, and 72 h after irradiation. Each well was incubated with 10 μl CCK-8 solution for 2 h. The optical density (OD) value of each well was detected by a microplate reader (450 nm). The experiment was repeated three times.

Detection of A549 Metastasis by Direct and Indirect Effects of Carbon Ion Irradiation

The A549 cells were irradiated with different doses of carbon ions, and then Transwell was used to detect migration and invasion. Migration and invasion of A549 were detected by transwell chamber after carbon ion irradiation. The Transwell assay for the ability of invasion was performed as the following protocol: the polycarbonate membranes with an 8-μm pore (Corning, USA) were placed on 24-well Transwell plates (Corning, USA), The lower side of the filter was precoated with 10μg/mL collagen type I-C (Millpore, USA). After incubation for 3 h, the number of cells that had migrated to the lower side was counted in five independent fields. These experiments were repeated a minimum of four times. The Transwell assay for the ability of migration was performed as the following protocol: Millpore filters with 8-lm pores (Millpore, USA) were precoated with 100 ml of 0.1 μg/ml Matrigel (BD, USA). After incubation for 24 h, the number of cells that had invaded to the lower side through the pores was counted in five independent fields. In both assays, FBS was used as a chemoattractant. These experiments were repeated a minimum of four times. The irradiated cells were prepared by trypsin digestion and cells (3×10^4) were resuspended in medium RPMI 1640 containing 1% (v/v) FBS and added to the top chamber. A culture medium containing 5% (v/v) FBS was then added to the bottom chamber. Meanwhile, for determining the influence of conditioned medium on the metastasis of bystander cells, medium of unirradiated cells in Transwells chamber was replaced with irradiation conditioned mediumn collected nonirradiated cells. For the controls in experiments, the irradiation conditioned mediumn were collected from a parallel culture that had not been irradiated. Other experimental conditions are the same as those for the detection of radiation-induced direct effects. Cell motility/migration was measured as the number of cells migrated from a defined area of the uncoated microfilter through micropores in the given time, 24 h. The cells that migrated to the lower surface of the membrane were fixed with methanol for 10 min and stained with 0.5% (w/v) crystal violet (BD Biosciences) for 30 min.

Metabonomics Analysis of RIBE Factors

After WI-38 cells were irradiated by carbon ion 2 Gy, the culture medium was collected at 24 h, and the differential factors in the culture medium were detected by LC-MS.LC-TOFMS (Agilent,1290 Infinity LC, 6530 UHD, and Accurate-Mass Q-TOF/MS) was used for the metabonomic profiling of all samples in the study. The profiling procedure (sample preparation, metabolite separation and detection, metabonomic data preprocessing, metabolite annotation, and statistical analysis for biomarker identification) was performed following our previously published protocols with minor modifications. The separation column was a C18 column (Agilent, 100 mm × 2.1 mm, 1.8 μm). The chromatographic separation conditions are as follows: column temperature 40 °C, flow rate 0.4 ml/min; mobile phase A: water + 0.1% formic acid, B: acetonitrile + 0.1% formic acid; according to a certain gradient elution procedure. The injection volume is 4ul and the temperature of the automatic injector is 4°C.

Data Analysis and Statistics

Mean values of control and treated samples were compared using one-way analysis of variance (ANOVA) where $P < 0.05$ was considered to be statistically significant. All annotated metabolites from GC-TOFMS data sets were combined and exported to SIMCA-P+ 13.0 (Umetrics AB, Umea, Sweden) and R 3.6.1 for multivariate statistical analysis. Partial least

squares discriminant analysis (OPLS-DA) and orthogonal partial least squares-discriminant analysis (OPLS-DA) was performed to discriminate between carbon 2 and 0 Gy. Initially, an exploratory multivariate analysis was applied to log2-transformed ratios scaled to unit variance. The multiple test problem was addressed by calculating the false discovery rate (FDR) using the Benjamini and Hochberg method.

RESULTS

Carbon Ion Beams Inhibited Cell Colony Formation and Cell Proliferation

We also evaluated the effect of carbon ion beams on the colony formation ability of A549 cells. The results confirmed that the colony formation ability was significantly lower in cells treated with 1, 2, and 4 Gy than in cells treated with 0 Gy (**Figure 1A**). There was a positive correlation between the clone inhibition rate and the carbon ion irradiation dose. The survival of A549 cell lines decreased after 1 Gy irradiation, but there was no significant difference (**Figure 1B**). However, after 2 and 4 Gy irradiation, cell survival decreased significantly ($p = 0.02$). The plating effiency of each group is 24.5, 8.75, 1.90, and 2.04%. The CCK-8 assay results revealed different growth changes after 24, 48, and 72 h. After 1 Gy irradiation, A549 cell proliferation was significantly inhibited at 24 h, and this inhibition increased in a dose-dependent manner. With the extension of time after irradiation, the ability of cell proliferation was gradually restored (**Figure 1C**).

Effect of Carbon Ion on Metastasis of A549 Cells

The results of the cell Transwell chamber assay revealed that carbon ion rays inhibited cell migration and invasion compared with the control group (**Figure 2A**). Carbon ions at 2 and 4 Gy significantly inhibited the migration and invasion of A549 cells ($p = 0.01$) (**Figure 2B**). The migration and invasion abilities of A549 cells were decreased in 1 Gy group with respect to the 0 Gy group, but it was not significantly different ($p = 0.07$).

Migration and Invasion of A549 Cells After Culture Medium Transfer

According to the direct effect results obtained above, we chose 24 h after carbon ion 2 Gy irradiation as the dose and time for the study of bystander effects. The results of Transwell showed that the migration of A549 cells was significantly inhibited by the culture medium irradiated by carbon ion 2 Gy compared with that of 0 Gy (**Figures 3A, B**), and the migration of A549 cells was significantly inhibited by the culture medium irradiated by carbon ion 2 Gy ($p = 0.03$) (**Figure 3C**). Compared with 0 Gy (**Figures 3D, E**), the culture medium irradiated by 2 Gy carbon ions for 24 h could significantly inhibit the invasion of A549 cells ($p = 0.05$) (**Figure 3F**).

Liquid Chromatography Coupled to Mass Spectrometry (LC-MS) Detection and Principal Component Analysis (PCA)

In this study, the mass spectrometer uses both positive and negative ion modes for quality detection, and the response value in the positive ion mode is generally low, and the fragment ion information is lacking, so the negative ion mode is finally selected for analysis. Total ion chromatography of 0 and 2 Gy was obtained by ultra-high-performance liquid chromatography coupled to quadruple time-of flight mass spectrometer (UPLC/Q-TOF/MS) analysis (**Figure 4**). The reproducibility and stability of the instrument were preliminarily examined. A total of 361 metabolites were structurally identified from the LC-MS

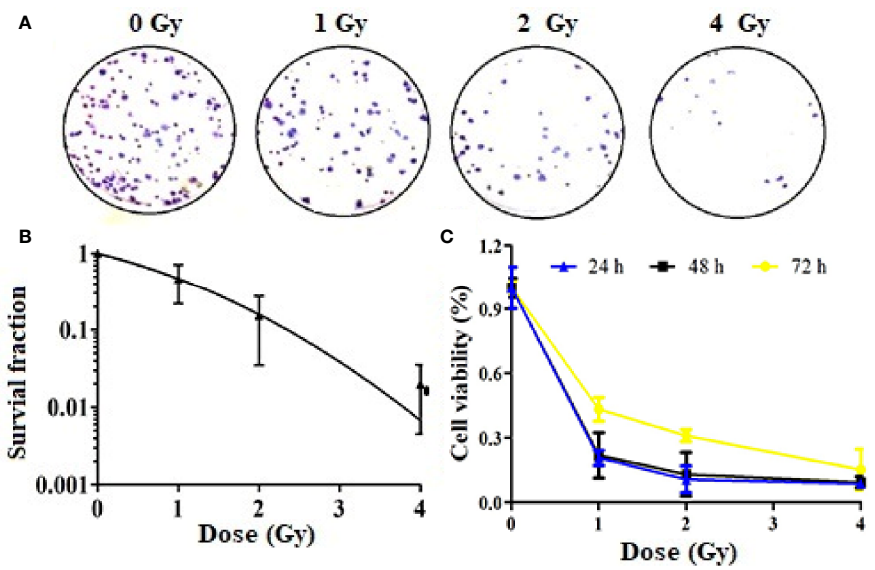

FIGURE 1 | Inhibition of Colony formation and proliferation of A549 cells by carbon ions [**(A)** colony formation, **(B)** survival fraction, **(C)** inhibition of cell viability].

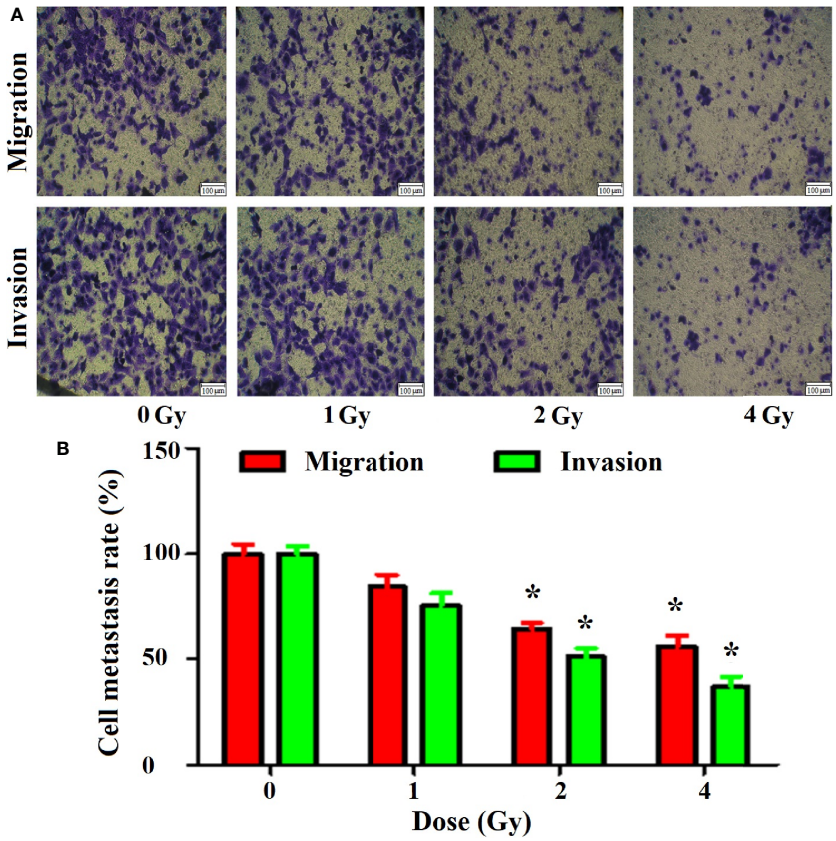

FIGURE 2 | Inhibition of migration and invasion of A549 cells by carbon ions [**(A)** migration and invasive staining, **(B)** metastasis difference analysis] *$p < 0.05$.

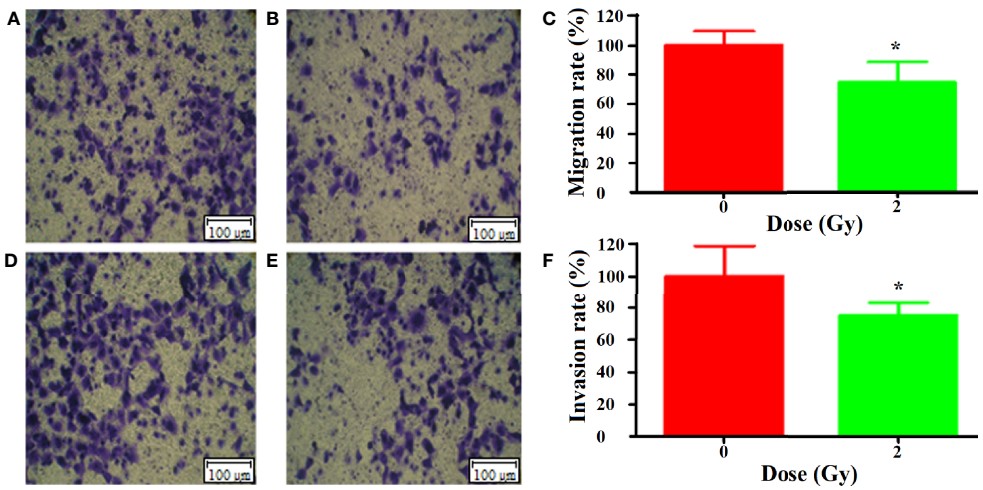

FIGURE 3 | Bystander effect of carbon ion ($^{12}C^{6+}$) 2 Gy irradiation on metastasis of A549 cells [**(A)** 0 Gy migration, **(B)** 2 Gy migration, **(C)** mobility difference analysis; **(D)** 0 Gy invasion, **(E)** 2 Gy invasion, **(F)** analysis of the difference of invasion rate]. *$p < 0.05$.

data based on spectral matching against a reference database. Of the 361 metabolites, 162 metabolites were distributed in 0 Gy group and 176 in 2 Gy group. The molecular characterization is completed through the online database (http://metlin.scripps.edu/) (comparing the exact molecular weight mass of mass spectrometry).To analyze the different molecules between the two groups, the data obtained were unsupervised by PCA and PLS-DA. The scoring graph of the first principal component ($t[1]$) direction and the second principal component ($t[2]$) direction are shown in Fig. 5A. The results showed that the metabolic components of the two groups were separated well, indicating that different doses of carbon ion radiation could significantly change the metabolites.

Analysis and Screening of Metabolites

In **Figure 5A** we show Principal Component Analysis (PCA) of the carbon ion irradiation along with the control group. The negative mode of PLS-DA shows that the current PLS-DA model (R2X = 0.813, R2Y = 0.984, Q2 = 0.965) is very reliable (**Figure 5B**), which is suitable for explaining the metabolic differences between the two groups and finding the differences in expressed metabolites between the two groups. The supervised OPLS-DA method was further used to model and analyze the differential metabolites (**Figure 5C**). The results showed that one principal component and one orthogonal component were obtained in negative mode (R2X = 0.887, R2Y = 0.965, Q2 = 0.863). Significantly altered irradiation metabolites with the variable importance in the projection (VIP) threshold (VIP > 1) in the above-mentioned OPLS-DA model, as well as the Mann-Whitney U test ($p < 0.05$), were selected differentially expressed molecular induced by radiation. The cross-validation Q2 (cum) in the PLS-DA model was 0.965 (**Figure 5D**). Heatmap analysis of these differential proteins corresponding to volcano plot. It could be observed that there were 162 and 176 important differentially expressed metabolites in the 0 Gy group and 2 Gy group, respectively. Among these differential metabolites those differential co-expression metabolites in top 23 VIP value were collected (**Table 1**).

Target and Network Prediction of Differential Molecules and Analysis of KEGG Pathway

Of the 384 metabolites, 185 metabolites were normally distributed in 0 Gy group and 199 in 2 Gy group. Combined with fold change value, the expression changes of differential molecules were analyzed (**Figures 6A, B**). The results of co-expression analysis shows that 23 differential molecules were identified, nine molecules were up-regulated, and 14 were down-regulated (**Table 1**). Further analysis showed that the expression of 14 metabolites such as Betain, Creatinine, Xanthine, Sphinganine, Talopyranose, Ketodeoxycholic acid and Pyroglutamic acid decreased after 2 Gy irradiation (**Figure 6C**). The expression of nine metabolic molecules such as Pipecolic acid, Leukotriene C4, Ribose, Niacin, Homophenylalanine, and Serotonine was up-regulated (**Figure 6B**). A total of 41 potential target proteins of four significant differences molecules (Betain and Creatinine, Pipecolic acid, and Leukotriene C4) were obtained from the STITCH database (**Figure 7**). Through KEGG pathway enrichment analysis, we discovered the top 20 significantly metabolism regulated KEGG

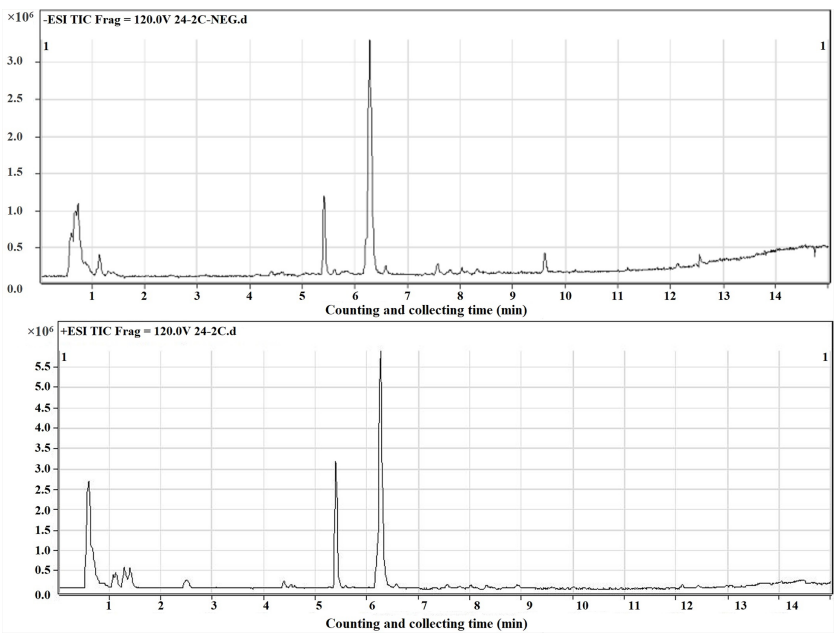

FIGURE 4 | Total ion current chromatogram of carbon ion 2 Gy irradiated sample.

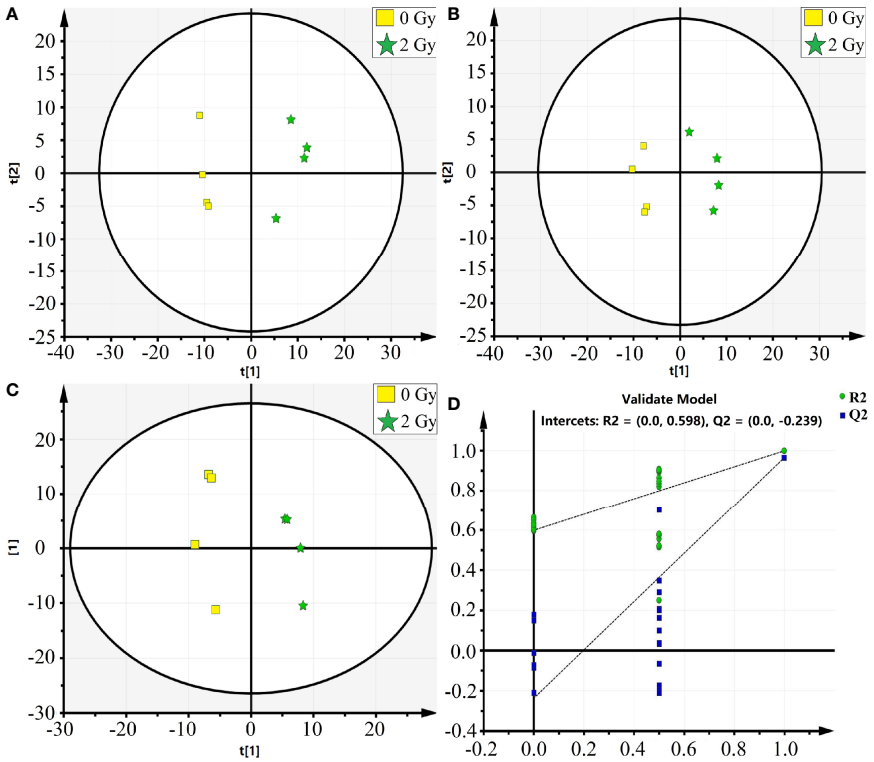

FIGURE 5 | The PCA and OPLS-DA analysis on the differential metabolic molecules after carbon Ion irradiation [**(A)** PCA analysis, **(B)** PAS-DA analysis, **(C)** OPLS-DA analysis, **(D)** PLS-DA score plot, in which the abscissa represents similarity with the original model, the ordinate represents R2Y and Q2 values].

TABLE 1 | Differential carbon ion irradiaton induced metabolites between 2 and 0 Gy controls in the Learning Group.

Name	Mass	VIP	T-test	Fold change*
Pipecolic acid	129.079	1.433	0.000	10.341
Methylglutaric acid	146.058	1.212	0.001	1.548
Leukotriene C4	625.293	1.007	0.000	3.512
Ribose	150.053	1.057	0.002	1.105
Betaine	117.107	1.360	0.000	−0.791
PS(21:0)	567.348	1.259	0.009	0.634
Niacin	123.032	1.279	0.007	0.507
Homophenylalanine	179.095	1.035	0.002	0.286
Serotonine	176.095	1.365	0.012	0.129
Aminoadipic acid	161.069	1.627	0.040	−0.190
Indoleacrylic acid	187.064	1.307	0.042	−0.201
Isoleucine/Leucine	131.095	1.205	0.018	−0.216
Benzoic acid	122.037	1.477	0.019	−0.279
Valine/Norvaline	117.079	1.341	0.003	−0.343
Ketodeoxycholic acid	390.278	1.138	0.003	−0.369
Pyroglutamic acid	129.043	1.318	0.003	−0.450
Talopyranose	180.201	1.240	0.001	−1.57
Sphinganine	301.299	1.443	0.001	−0.529
PC(16:0)	495.333	1.512	0.004	−0.746
Creatinine	113.059	1.512	0.000	−0.794
Xanthine	152.033	1.453	0.010	−0.639
Glycocholic acid	465.318	1.160	0.002	0.004
Phenylacetic acid	136.128	1.114	0.012	−0.348

**The fold change (FC) was calculated by the average value of 2 Gy group to that of control group. FC with a value larger than 0.0 indicates a significantly higher level of the carbon irradiation induced metabolite in 2 Gy while a FC value lower than 0.0 indicates a lower level compared to 0 Gy controls. Student t test was used for statistical comparisons.*

pathways (**Figure 8**). it was found that 20 target proteins of the two down-regulated differential molecules, Betain and Creatinine were mainly enriched in the Purine metabolism, Tyrosine metabolism, Cysteine, and methionine metabolism, Peroxisome, and Carbon metabolism pathway (**Figure 8A**). The 21 target proteins of two up-regulated differential molecules of Pipecolic acid and Leukotriene C4 were mainly enriched in Neuroactive ligand-receptor interaction, Calcium signaling pathway, Arachidonic acid metabolismand Fc epsilon RI signaling pathway (**Figure 8B**).

DISCUSSION

The main aim of this study was to assess the global metabonomics and metastasis changes in A549 cell line after carbon ion radiation. Ionizing radiation is defined as a radiation which has sufficient energy to ionize biological molecules. Carbon ion therapy is more advantageous than conventional radiotherapy because of the protection of normal tissues adjacent to the tumor during dose-escalation therapy (20). In this study, we first investigated the direct effects of carbon ions on A549 cells, and carbon ion radiation caused changes in the colony formation and proliferation of A549 cells. We observed that the colony formation rate of A549 cells irradiated with carbon ion rays was significantly lower, and the

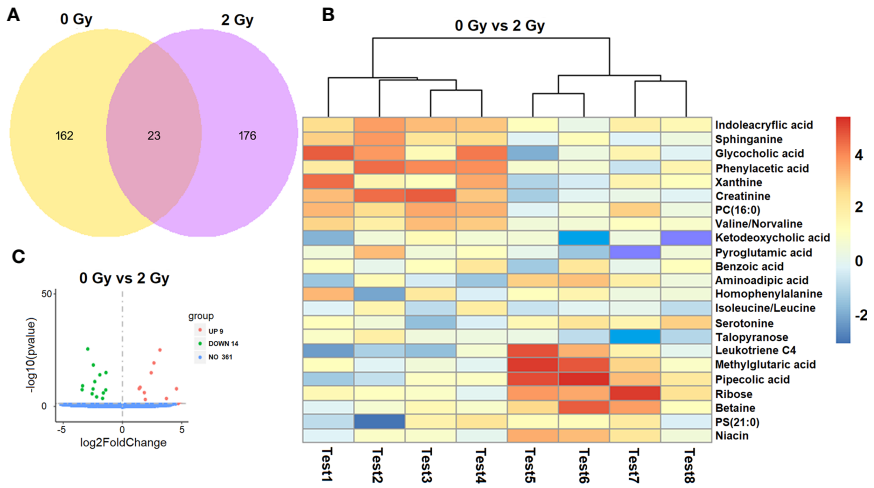

FIGURE 6 | Screening analysis of a differential molecules after different doses of carbon ion irradiation [**(A)** Venn diagram of co-expression molecule, **(B)** expression changes of differential molecules in two groups. **(C)** screening of differential molecules].

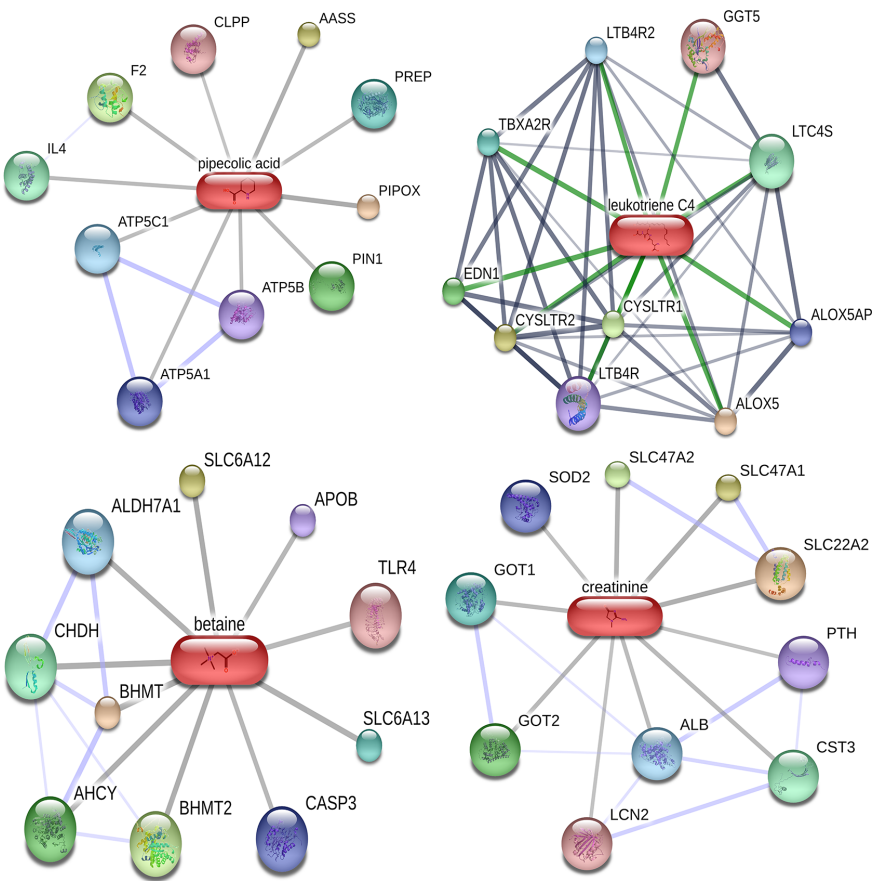

FIGURE 7 | Target molecular network diagram for predicting four significantly different metabolites in Cytoscape.

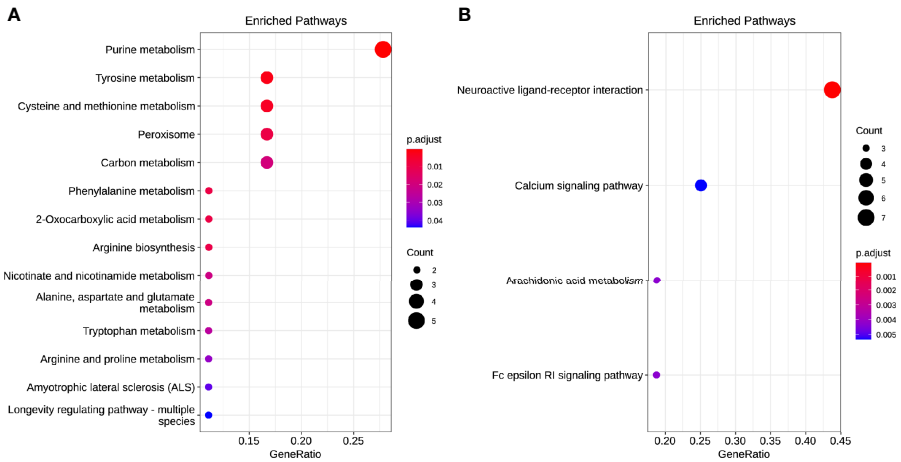

FIGURE 8 | The enrichment model of target molecules in the KEGG pathway [**(A)** downregulated and **(B)** up-regulated].

colony formation rate and survival fraction of A549 cells were significantly lower after irradiation at each dose (1, 2, and 4 Gy) compared with 0 Gy, especially this change was most pronounced at 4 Gy. Carbon ions could inhibit the proliferation of A549 cells, and the activity of A549 cells was the lowest at 24 h after irradiation, as we previously observed in esophageal cancer (21). Secondly, we studied the effect of carbon ion irradiation on the metastasis of A549 cells, and analyzed the migration and invasion of A549 cells after carbon ion irradiation. We observed that carbon ion 2 and 4 Gy significantly inhibited the migration and invasion of A549 cells 24 h after irradiation compared with 0 Gy. Different LET rays can inhibit the migration and invasion of tumor cells (22), with a dependent relationship between the inhibitory ability and irradiation dose (23). At the same time, the indirect effect of carbon ion irradiation on A549 cells was studied. The culture medium collected 24 h after 2 Gy carbon ion irradiation on human normal cells (WI-38) was transferred to A549 cells by the method reported by (13, 24), and the metastasis changes of A549 cells were observed again. The co-culture method was used to study the bystander effect induced by iron ion irradiation in AG01522 cells and its relationship with time (25). It was found that the medium of A549 cells after carbon ion radiation was used as a medium, thus changing the biology of non-irradiated cells. Carbon ions induce upsurge in bystander cell death in lung carcinoma cells, but manifest Type II bystander effects in hepatoma cells (26). It is possible that the primary bystander cells themselves are capable of producing secondary bystander signals to their neighboring cells and creating the radiation-induced Type II bystander effect.

In this study, we found that carbon ion radiation changed the metabolite secretion of irradiated cells, thus affecting the biological behavior of unirradiated cells. Generally, X-rays promote migration and invasiveness under normoxic conditions, and carbon ions can significantly reduce migration (27) and invasion of tumor cells *in vitro* and vivo (23, 28). Further, we used metabonomic analysis to confirm that the culture medium collected from carbon ion irradiated WI-38 cells is related to the decrease of metastatic potential of A549 cells. Compared with untreated cells, the biological process of culture medium related to tumor metastasis after carbon ion irradiation. It had shown that fractionated doses of protons caused less DNA damage in the secondary bystander WI-38 cells compared to a single radiation dose, where the means differ by 20%. This may also be due to the involvement of primary bystander cells releasing secreted diffusible factors into shared growth media (14).Our studies have shown that carbon ions of 2 Gy can induce up-regulation of metabolites in irradiated cells, such as pipemidic acid, leukotriene C4, ribose, niacin, homophenylalanine, and 5-hydroxytryptamine. Exosomes are closely related to lipids, lipid transporters and lipid metabolic enzymes. Radiation-induced up-regulation of cytokine and death ligand secretion by glioblastoma cells established the conditions for radiation-induced bystander response of NSC that was mediated mostly soluble factors released in the media by cancer cells (29). Cholesterol, phospholipids and sphingomyelin are the key substances for the formation of exocrine phospholipid bilayers. Exocrine induces the biosynthesis of leukotriene (LTs). Leukotriene is an effective pro-inflammatory lipid intermediary. Neutral sphingomyelinase overexpressed in exosomes can catalyze the production of ceramide and lead to neuronal apoptosis (30). The results of this study showed that the medium of WI-38 cells 24 h after irradiation with 2 Gy of carbon ions significantly inhibited the migration and invasion of A549 cells, which may be that carbon ion radiation bystander changed the metabolic pattern of A549 cells, thereby inhibiting tumor metastasis. We hypothesize that metabolites induced after carbon ion radiation alter the microenvironment of non-irradiated cells (energy changes, small molecule expression, etc.), which affects the biological behavior of

tumor cells. Previous studies implicated in irradiated WI-38 and irradiated A549 cells demonstrated metabolic interference between irradiated and non-irradiated cells (31).

Metabolic conversion is one of the markers of cancer (32). Therefore, our study clearly showed that carbon ions can change the metabolic factors of tumor, and these metabolic factors regulate the characteristics of tumor by changing the metabolic mode of tumor to act on targeted molecules. Many reports have demonstrated the involvement of piperidic acid and its derivatives can be used as inhibitors of matrix metalloproteinases (33) and related transferases for the synthesis of anti-tumor drugs. In order to maintain the dynamic balance of the microenvironment, these cancer cells secrete more lactic acid, thus reducing the pH value in the tumor microenvironment and enhancing the metastatic potential of these cancer cells (34). Furthermore, we demonstrated that CIRE induced changes in glycolysis, cyanoamino acid, and citric acid metabolic pathways. Studies have found that the Warburg effect not only gives the energy needed for the growth of cancer cells, but also promotes the process of metastasis (35). The Warburg effect is a metabolic phenomenon in cancer cells, where even in the presence of adequate oxygen, there is high glycolytic activity (aerobic glycolysis) and lactate production. Our results show that CIBE can significantly inhibit the metastasis of A549 cells, so it can be speculated that carbon ion radiation can reduce the energy metabolism of cancer cells. We speculated that Betaine may inhibit tumor glucose metabolism and play an anti-tumor effect. At the same time, Betaine has significant difference in the metabolism of liver cancer, so it can be used as an excellent and potential diagnostic index (36). Our analysis founds that the differential metabolites induced by carbon ion radiation interact with other molecules (IL4, TLR4, SOD2, SLC22A2, etc.) to regulate the metastasis of A549 cells. Carbon ions not only directly act on tumor cells and change the phenotype of tumor cells, but also affect the phenotype of non-irradiated cells near irradiated cells. This may be attributed to the activation of multiple signal transduction pathways in bystander cells. It has been shown that indicate that heavy ions inactivate clonogenic potential of bystander cells, and that the time course of the response to heavy ions differs between irradiated and bystander cells (37).

These metabolisms allow the tumor microenvironment to be under acidic conditions that can inhibit the migration and invasion of tumor cells by dependent on the p53 and Caspase 3 pathways for necrosis and apoptosis (38). We have found that down-regulated molecule (betaine and creatinine) is mainly involved in Purine metabolism, Tyrosine metabolism, Cysteine and methionine metabolism, Peroxisome and Carbon metabolism pathway. Of these molecules we know, arachidonic acid has immunomodulatory and anticancer effects (39). Glucose reprogramming and glutamine metabolism not only provide the factors needed for tumor cell growth, but also reduce the pressure on the tumor microenvironment through redox reactions (40). The inhibition degree of these irreversible catabolic enzymes is highly related to tumor invasiveness, and can independently predict clinical outcomes (41). Up-regulation of molecular (Pipecolic acid and Leukotriene C4) is mainly involved in Neuroactive ligand-receptor interaction, Calcium signaling pathway, Arachidonic acid metabolism and Fc epsilon RI signaling pathway. Researcher have previously shown that RIBE responses differ among patients. Among which, it is found that Pyruvate, Lactic acid, Arginine and Glutamic acid decreased significantly, Tryptophan metabolism up-regulated, Histamine and Glutamate metabolic pathway, Tricarboxylic acid cycle and intestinal flora metabolic were disorders in colorectal cancer (42). Furthermore, there is an evidence that Serine, Glycine and one-carbon metabolism are involved in the synthesis of proteins, nucleotides and phospholipids, and related enzymes regulate the proliferation and metastasis of hepatocellular carcinoma (43). As we mentioned above, multiple signaling pathways involving metabolic molecules that cause CIBE are associated with patient inflammation, immune response and lung cancer risk prediction as well as other diseases. Calcium signaling pathway and inflammasome are closely related to immune response (44). The observations that immune prognostic biomarkers in the microenvironment are involved in Neuroactive ligand-receptor interaction pathway in osteosarcoma (45), and that pathway and gated ion channel activity are associated with the risk of lung cancer (46). Given these results, when taken together, the CIBE signals transit either through ICM milieu, may be dependent on cell type and radiation quality.

CONCLUSION

Through this study, we prove the potential value of metabonomics after carbon ion radiation. The bystander effects induced by carbon ion radiation may change the non-irradiated tumor microenvironment, thus increasing or decreasing the corresponding metabolites. These metabolites can act on targeted molecules and finally show the ability of collective complex signal regulatory network to act on the metastasis and invasion of malignant tumor cells. The further study of radiation bystander effect and malignant tumor metastasis and its mechanism is expected to provide a scientific basis for the optimization of clinical tumor radiotherapy and radiation protection. A better understanding of the cellular and molecular mechanisms of the bystander phenomenon, together with evidence of their occurrence *in vivo*, will allow us to formulate a more accurate model in assessing the health effects of low doses of high LET radiation.

DATA AVAILABILITY STATEMENT

The raw data supporting the conclusions of this article will be made available by the authors, without undue reservation.

AUTHOR CONTRIBUTIONS

Conception and design: ZY, XW, and QZ. Administrative support: XW, HL, and QZ. Experiment operation: HL, ZY, LS,

YK, RL, XZ, YG, and CL. Data analysis and interpretation: HL, QZ, ZY, and LS. Manuscript writing: all authors. Final approval of manuscript: all authors. All authors contributed to the article and approved the submitted version.

FUNDING

The article were supported by the Lanzhou Innovation and Entrepreneurship Talent Project (award number: 2017-RC-23/2020-RC-113) and the Science and Technology Plan Project of Chengguan District, Lanzhou (award number: no. 2020-2-2-5).

SUPPLEMENTARY MATERIAL

The Supplementary Material for this article can be found online at: https://www.frontiersin.org/articles/10.3389/fonc.2020.601620/full#supplementary-material

REFERENCES

1. Bray F, Ferlay J, Soerjomataram I, Siegel RL, Torre LA, Jemal A. Global cancer statistics 2018: GLOBOCAN estimates of incidence and mortality worldwide for 36 cancers in 185 countries. *CA Cancer J Clin* (2018) 68(6):394–24. doi: 10.3322/caac.21492
2. Sperduto PW, Yang TJ, Beal K, Pan H, Mehta MP. Estimating Survival in Patients With Lung Cancer and Brain Metastases: An Update of the Graded Prognostic Assessment for Lung Cancer Using Molecular Markers (Lung-molGPA). *JAMA Oncol* (2017) 3(6):827–31. doi: 10.1001/jamaoncol.2016.3834
3. Feng Z, Li C, Zheng Q, Mao W, Li T, Xing L, et al. Heavy-ion beam irradiation inhibits invasion of tongue squamous cell carcinoma Tca8113 cells. *Oncol Lett* (2019) 18(4):4092–99. doi: 10.3892/ol.2019.10761
4. Suetens A, Konings K, Moreels M, Quintens R, Verslegers M, Soors E, et al. Higher Initial DNA Damage and Persistent Cell Cycle Arrest after Carbon Ion Irradiation Compared to X-irradiation in Prostate and Colon Cancer Cells. *Front Oncol* (2016) 6:87. doi: 10.3389/fonc.2016.00087
5. Wang H, Yu KN, Hou J, Liu Q, Han W. Radiation-induced bystander effect: early process and rapid assessment. *Cancer Lett* (2015) 356(1):137–44. doi: 10.1016/j.canlet.2013.09.031
6. Kobayashi A, Tengku Ahmad TAF, Autsavapromporn N, Oikawa M, Homma-Takeda S, Furusawa Y, et al. Enhanced DNA double-strand break repair of microbeam targeted A549 lung carcinoma cells by adjacent WI38 normal lung fibroblast cells via bi-directional signaling. *Mutat Res* (2017) 803-805:1–8. doi: 10.1016/j.mrfmmm.2017.06.006
7. Klammer H, Mladenov E, Li F, Iliakis GJCL. Bystander effects as manifestation of intercellular communication of DNA damage and of the cellular oxidative status. *Cancer Lett* (2015) 356(1):58–71. doi: 10.1016/j.canlet.2013.12.017
8. Ariyoshi K, Miura T, Kasai K, Fujishima Y, Nakata A, Yoshida MJER. Radiation-Induced Bystander Effect is Mediated by Mitochondrial DNA in Exosome-Like Vesicles. *Sci Rep* (2019) 9:9103. doi: 10.1038/s41598-019-45669-z
9. Heeran AB, Berrigan HP, O'Sullivan J. The Radiation-Induced Bystander Effect (RIBE) and its Connections with the Hallmarks of Cancer. *Radiat Res* (2019) 192(6):668–79. doi: 10.1667/RR15489.1
10. He M, Dong C, Konishi T, Tu W, Liu W, Shiomi N, et al. Differential effects of p53 on bystander phenotypes induced by gamma ray and high LET heavy ion radiation. *Life Sci Space Res (Amst)* (2014) 1:53–9. doi: 10.1016/j.lssr.2014.02.003
11. Wozny AS, Vares G, Alphonse G, Lauret A, Monini C, Magne N, et al. ROS Production and Distribution: A New Paradigm to Explain the Differential Effects of X-ray and Carbon Ion Irradiation on Cancer Stem Cell Migration and Invasion. *Cancers (Basel)* (2019) 11(4):468. doi: 10.3390/cancers11040468
12. Prise KM, O'Sullivan JM. Radiation-induced bystander signalling in cancer therapy. *Nat Rev Cancer* (2009) 9(5):351–60. doi: 10.1038/nrc2603
13. Kobayashi A, Autsavapromporn N, Ahmad T, Oikawa M, Homma-Takeda S, Furusawa Y, et al. Bystander Wi-38 Cells Modulate DNA Double-Strand Break Repair in Microbeam-Targeted A549 Cells through Gap Junction Intercellular Communication. *Radiat Prot Dosimetry* (2019) 183(1-2):142–46. doi: 10.1093/rpd/ncy249
14. Autsavapromporn N, Liu C, Kobayashi A, Ahmad T, Oikawa M, Dukaew N, et al. Emerging Role of Secondary Bystander Effects Induced by Fractionated Proton Microbeam Radiation. *Radiat Res* (2019) 191(2):211–16. doi: 10.1667/RR15155.1
15. Zhou H, Ivanov VN, Gillespie J, Geard CR, Amundson SA, Brenner DJ, et al. Mechanism of radiation-induced bystander effect: role of the cyclooxygenase-2 signaling pathway. *Proc Natl Acad Sci U S A* (2005) 102(41):14641–46. doi: 10.1073/pnas.0505473102
16. Herve JC, Bourmeyster N, Sarrouilhe D, Duffy HS. Gap junctional complexes: from partners to functions. *Prog Biophys Mol Biol* (2007) 94(1-2):29–65. doi: 10.1016/j.pbiomolbio.2007.03.010
17. Jabbari N, Karimipour M, Khaksar M, Akbariazar E, Heidarzadeh M, Mojarad B, et al. Tumor-derived extracellular vesicles: insights into bystander effects of exosomes after irradiation. *Lasers Med Sci* (2020) 35(3):531–45. doi: 10.1007/s10103-019-02880-8
18. Xie G, Lu L, Qiu Y, Ni Q, Zhang W, Gao YT, et al. Plasma metabolite biomarkers for the detection of pancreatic cancer. *J Proteome Res* (2015) 14 (2):1195–02. doi: 10.1021/pr501135f
19. Dong C, Tu W, He M, Fu J, Kobayashi A, Konishi T, et al. Role of Endoplasmic Reticulum and Mitochondrion in Proton Microbeam Radiation-Induced Bystander Effect. *Radiat Res* (2020) 193(1):63–72. doi: 10.1667/RR15469.1
20. Mohamad O, Yamada S, Durante M. Clinical Indications for Carbon Ion Radiotherapy. *Clin Oncol (R Coll Radiol)* (2018) 30(5):317–29. doi: 10.1016/j.clon.2018.01.006
21. Luo H, Yang Z, Zhang Q, Shao L, Wei S, Liu R, et al. Carbon ion therapy inhibits esophageal squamous cell carcinoma metastasis by up-regulating STAT3 through the JAK2/STAT3 signaling pathway. *Front Public Health* (2020) 8:579705. doi: 10.3389/fpubh.2020.579705
22. Tong L, Yu KN, Bao L, Wu W, Wang H, Han W. Low concentration of exogenous carbon monoxide protects mammalian cells against proliferation induced by radiation-induced bystander effect. *Mutat Res* (2014) 759:9–15. doi: 10.1016/j.mrfmmm.2013.11.006
23. Ogata T, Teshima T, Inaoka M, Minami K, Tsuchiya T, Isono M, et al. Carbon ion irradiation suppresses metastatic potential of human non-small cell lung cancer A549 cells through the phosphatidylinositol-3-kinase/Akt signaling pathway. *J Radiat Res* (2011) 52(3):374–79. doi: 10.1269/jrr.10102
24. Song J, Wang W, Wang Y, Qin Y, Wang Y, Zhou J, et al. Epithelial-mesenchymal transition markers screened in a cell-based model and validated in lung adenocarcinoma. *BMC Cancer* (2019) 19(1):680. doi: 10.1186/s12885-019-5885-9
25. Yang H, Anzenberg V, Held KD. The time dependence of bystander responses induced by iron-ion radiation in normal human skin fibroblasts. *Radiat Res* (2007) 168(3):292–98. doi: 10.1667/RR0864.1
26. Mukherjee S, Chakraborty A. Radiation-induced bystander phenomenon: insight and implications in radiotherapy. *Int J Radiat Biol* (2019) 95 (3):243–63. doi: 10.1080/09553002.2019.1547440
27. Moncharmont C, Guy JB, Wozny AS, Gilormini M, Battiston-Montagne P, Ardail D, et al. Carbon ion irradiation withstands cancer stem cells' migration/invasion process in Head and Neck Squamous Cell Carcinoma (HNSCC). *Oncotarget* (2016) 7(30):47738–49. doi: 10.18632/oncotarget.10281
28. Rief H, Chaudhri N, Tonndorf-Martini E, Bruckner T, Rieken S, Bostel T, et al. Intensity-modulated radiotherapy versus proton radiotherapy versus carbon ion radiotherapy for spinal bone metastases: a treatment planning study. *J Appl Clin Med Phys* (2015) 16(6):186–94. doi: 10.1120/jacmp.v16i6.5618

29. Ivanov VN, Hei TK. Radiation-induced glioblastoma signaling cascade regulates viability, apoptosis and differentiation of neural stem cells (NSC). *Apoptosis* (2014) 19(12):1736–54. doi: 10.1007/s10495-014-1040-x
30. Wang W, Zhu N, Yan T, Shi YN, Chen J, Zhang CJ, et al. The crosstalk: exosomes and lipid metabolism. *Cell Commun Signal* (2020) 18(1):119. doi: 10.1186/s12964-020-00581-2
31. Desai S, Kobayashi A, Konishi T, Oikawa M, Pandey BN. Damaging and protective bystander cross-talk between human lung cancer and normal cells after proton microbeam irradiation. *Mutat Res* (2014) 763-764:39–44. doi: 10.1016/j.mrfmmm.2014.03.004
32. Kulcenty K, Piotrowski I, Rucinski M, Wroblewska JP, Jopek K, Murawa D, et al. Surgical Wound Fluids from Patients with Breast Cancer Reveal Similarities in the Biological Response Induced by Intraoperative Radiation Therapy and the Radiation-Induced Bystander Effect-Transcriptomic Approach. *Int J Mol Sci* (2020) 21(3):1159. doi: 10.3390/ijms21031159
33. Zhang J, Zhang P, Liu X, Fang K, Lin G. Synthesis and biological evaluation of (R)-N-(diarylmethylthio/sulfinyl)ethyl/propyl-piperidine-3-carboxylic acid hydrochlorides as novel GABA uptake inhibitors. *Bioorg Med Chem Lett* (2007) 17(13):3769–73. doi: 10.1016/j.bmcl.2007.04.010
34. Estrella V, Chen T, Lloyd M, Wojtkowiak J, Cornnell HH, Ibrahim-Hashim A, et al. Acidity generated by the tumor microenvironment drives local invasion. *Cancer Res* (2013) 73(5):1524–35. doi: 10.1158/0008-5472.CAN-12-2796
35. Lu J, Tan M, Cai Q. The Warburg effect in tumor progression: mitochondrial oxidative metabolism as an anti-metastasis mechanism. *Cancer Lett* (2015) 356(2 Pt A):156–64. doi: 10.1016/j.canlet.2014.04.001
36. Huang Q, Tan Y, Yin P, Ye G, Gao P, Lu X, et al. Metabolic characterization of hepatocellular carcinoma using nontargeted tissue metabolomics. *Cancer Res* (2013) 73(16):4992–02. doi: 10.1158/0008-5472.CAN-13-0308
37. Hamada N, Ni M, Funayama T, Sakashita T, Kobayashi Y. Temporally distinct response of irradiated normal human fibroblasts and their bystander cells to energetic heavy ions. *Mutat Res* (2008) 639(1-2):35–44. doi: 10.1016/j.mrfmmm.2007.11.001
38. Gatenby RA, Gillies RJ. A microenvironmental model of carcinogenesis. *Nat Rev Cancer* (2008) 8(1):56–61. doi: 10.1038/nrc2255
39. Konings K, Vandevoorde C, Baselet B, Baatout S, Moreels M. Combination Therapy With Charged Particles and Molecular Targeting: A Promising Avenue to Overcome Radioresistance. *Front Oncol* (2020) 10:128. doi: 10.3389/fonc.2020.00128
40. Yue M, Jiang J, Gao P, Liu H, Qing G. Oncogenic MYC Activates a Feedforward Regulatory Loop Promoting Essential Amino Acid Metabolism and Tumorigenesis. *Cell Rep* (2017) 21(13):3819–32. doi: 10.1016/j.celrep.2017.12.002
41. Ericksen RE, Lim SL, McDonnell E, Shuen WH, Vadiveloo M, White PJ, et al. Loss of BCAA Catabolism during Carcinogenesis Enhances mTORC1 Activity and Promotes Tumor Development and Progression. *Cell Metab* (2019) 29(5):1151–65 e6. doi: 10.1016/j.cmet.2018.12.020
42. Tan B, Qiu Y, Zou X, Chen T, Xie G, Cheng Y, et al. Metabonomics identifies serum metabolite markers of colorectal cancer. *J Proteome Res* (2013) 12 (6):3000–09. doi: 10.1021/pr400337b
43. Li AM, Ye J. Reprogramming of serine, glycine and one-carbon metabolism in cancer. *Biochim Biophys Acta Mol Basis Dis* (2020) 1866(10):165841. doi: 10.1016/j.bbadis.2020.165841
44. Kito H. Calcium signaling and inflammasome. *Nihon Yakurigaku Zasshi* (2016) 148(1):57. doi: 10.1254/fpj.148.57
45. Hong W, Yuan H, Gu Y, Liu M, Ji Y, Huang Z, et al. Immune-related prognosis biomarkers associated with osteosarcoma microenvironment. *Cancer Cell Int* (2020) 20:83. doi: 10.1186/s12935-020-1165-7
46. Ji X, Bosse Y, Landi MT, Gui J, Xiao X, Qian D, et al. Identification of susceptibility pathways for the role of chromosome 15q25.1 in modifying lung cancer risk. *Nat Commun* (2018) 9(1):3221. doi: 10.1038/s41467-018-05074-y

Conflict of Interest: The authors declare that the research was conducted in the absence of any commercial or financial relationships that could be construed as a potential conflict of interest.

Copyright © 2021 Yang, Zhang, Luo, Shao, Liu, Kong, Zhao, Geng, Li and Wang. This is an open-access article distributed under the terms of the Creative Commons Attribution License (CC BY). The use, distribution or reproduction in other forums is permitted, provided the original author(s) and the copyright owner(s) are credited and that the original publication in this journal is cited, in accordance with accepted academic practice. No use, distribution or reproduction is permitted which does not comply with these terms.

frontiers in Oncology

ORIGINAL RESEARCH
published: 15 March 2021
doi: 10.3389/fonc.2021.621394

In Vivo 3-D Dose Verification Using PET/CT Images After Carbon-Ion Radiation Therapy

Lining Sun[1,2], *Weigang Hu*[1,2]*, *Songtao Lai*[1,2], *Leijun Shi*[3] and *Junchao Chen*[1,2]

[1] Department of Radiation Oncology, Fudan University Shanghai Cancer Center, Shanghai, China, [2] Department of Oncology, Shanghai Medical College, Fudan University, Shanghai, China, [3] Department of Nuclear Medicine, Shanghai Proton and Heavy Ion Center, Shanghai, China

Objective: To investigate the usefulness of positron emission tomography (PET) images obtained after carbon-ion irradiation for dose verification in carbon-ion radiotherapy.

Methods and Materials: An anthropomorphic head phantom was used in this study. Three cubes with volumes of 1, 4, and 10 ml were contoured as targets in the phantom CT through a treatment planning system. Treatment plans with six prescriptions from 2.5 to 10 Gy (2.5, 3, 5, 6, 8, and 10 Gy effective dose) were designed and delivered by 90° fixed carbon-ion beams, respectively. After irradiation of the phantom, a PET/CT scan was performed to fuse the treatment-planning CT image with the PET/CT image. The relationship between target volume and the standard uptake value (SUV) in PET/CT was evaluated for corresponding plan prescription. The MIM Maestro software was used for the image fusion and data analysis.

Results: SUV in the target had an approximate linear relationship with the effective dose. The same effective dose could generate a roughly equal SUV for different target volumes ($p < 0.05$).

Conclusions: It is feasible to verify the actual 3-D dose distribution of carbon-ion radiotherapy by the approach in this study.

Keywords: carbon ion, radiation therapy, positron emission tomography, standard uptake value, dose verification

OPEN ACCESS

Edited by:
Timothy Dean Malouff,
Mayo Clinic Florida, United States

Reviewed by:
Yuanzeng Min,
University of Science and Technology of China, China
Xudong Xue,
Hubei Cancer Hospital, China

***Correspondence:**
Weigang Hu
jackhuwg@gmail.com

Specialty section:
This article was submitted to Radiation Oncology, a section of the journal Frontiers in Oncology

Received: *26 October 2020*
Accepted: *26 January 2021*
Published: *15 March 2021*

Citation:
Sun L, Hu W, Lai S, Shi L and Chen J (2021) In Vivo 3-D Dose Verification Using PET/CT Images After Carbon-Ion Radiation Therapy. Front. Oncol. 11:621394. doi: 10.3389/fonc.2021.621394

INTRODUCTION

Radiation therapy is one of the primary methods in cancer treatment. To improve treatment outcomes, high accuracy of radiotherapy technology is emphasized. For ion-beam radiotherapy, particle therapy–positron emission tomography (PT-PET) is becoming popular for treatment verification. Although there are a number of radiation dose-verification methods, none can be used directly in 3-D patient dose verification. PT-PET is currently the only clinically applied method for *in vivo* verification. This study proposes an approach using PET/CT images and standard uptake value (SUV) after carbon-ion radiotherapy for *in vivo* 3-D dose verification. During carbon-ion

Abbreviations: PET, Positron Emission Tomography; SUV, Standard Uptake Value; TPS, Treatment Planning System; GyE, Gray Effective; 3D-OSEM, three-dimensional maximum expected ordered subset; FWHM, Full Width at Half Maximum; CTV, Clinical Target Volume; SNR, Signal to Noise Ratio; DVH, Dose Volume Histogram.

irradiation, ^{11}C (half-life $T_{1/2} \approx 20$ min) is formed in nuclear interactions between the ions and the tissue mainly within the range of the carbon-ion Bragg peak. Distribution and radioactivity of this positron emitter can be detected *via* PET/CT shortly after therapy, which indicates the distribution of dose deposited by carbon ions. The carbon-ion dose distribution should correspond to the prescription in the treatment plan. To achieve a goal of 3-D dose verification, the relationship between the dose prescribed in the target volume and SUV values on corresponding images from a PET/CT scan was analyzed quantitatively.

MATERIALS AND METHODS

Materials and Experiment Device

A Rando head phantom (The Phantom Laboratory, Salem, NY) was used in this study, and a SIEMENS Definition AS 64 CT simulator was used to acquire the planning image of the phantom. All the phantom plans were created by the Syngo VIA Version 12 particle Treatment Planning System. A SIEMENS Biograph mCT system was used for PET/CT scan (**Figure 1**). The phantom was scanned with a PET/CT scanning scope of 60.5 cm (transverse) by 21.6 cm (axial) with a 3-D maximum expected ordered subset (3-D-OSEM) image reconstruction algorithm, point dispersion function, and line time algorithm.

Principle and Method

During the carbon-ion irradiation, positron emitters are formed on the beam path *via* nuclear fragmentation reactions, which can be acquired with a PET/CT scanner. A relatively low β^+ activity of 1.6k Bq cm^{-3} is formed per gray of therapeutic dose in the tissue under the carbon-ion irradiation.

For heavier ions (such as ^{16}O), the fragmentation reaction can happen on both the incident particles (projectile fragmentation) and target nuclei (target fragmentation) (1–3). Then target dose distribution calculated by the treatment planning system (TPS) and the positron activity distribution of the target region in actual irradiation are compared to find out the relationship between them to decide whether it is feasible to do the PET-based target dose verification for carbon-ion radiotherapy.

CT Immobilization and Irradiation Planning

The Alfa-cradle foam was used to fix the Rando head phantom. The markers placed on the surface of the phantom defined the original zero point of the CT scanning axis. In addition, the accuracy of the irradiation field size was known in this study. There were no other possible motions of the phantom.

The clinical head tumor CT scanning protocol was applied for this study (axial supine position, 512*512 pixel dimension, slice thickness 1.5 mm, tube voltage 120 kVp and 300 mAs current). After scanning, all CT images were imported to the TPS for the virtual target contouring. Some cubes (virtual CTV) were created to represent different clinical target volumes for chordoma patients in the TPS. Volumes of the cubes were 10, 4, and 1 ml. A single 90° fixed carbon-ion beam was delivered for each virtual CTV and effective fraction doses were from 2.5 to 10 Gy (2.5, 3, 5, 6, 8, and 10 Gy), respectively.

Eighteen groups of different target volume and dose combinations (6*3) were created to generate virtual treatment plans. Clinical treatment parameters (full width at half maximum (FWHM) = 3.0 mm, ripple filter level = 3.0 mm, and dose calculation grid = 2.0 mm) were applied in this study to

FIGURE 1 | Diagram of carbon-ion virtual target irradiation experimental plan.

do the planning optimization. In the single-beam optimization mode, the optimum solution was chosen as the virtual treatment plan after at least 50 iterations.

A dose-volume histogram (DVH) was created for each treatment plan. In the DVH, a 100% prescription dose completely covered more than 95% of the virtual target volume for nine groups of tests.

Phantom Study

The Rando head phantom was used to simulate a clinical patient treatment workflow on the IONTRIS facility. In total, 18 beam plans that had various target volumes and different target doses were created. Before each plan delivery, the accuracy of the phantom setup was verified by the integrated orthogonal X-ray image system. The tolerance of setup deviation was ±1 mm in each direction. The time of plan delivery was recorded to calculate decay time of radioactive elements (**Table 1**). All carbon-ion beams were raster scanning pencil beams with an energy range from 174.5 to 248.6 MeV.

TABLE 1 | Time list of beam-on time and phantom transit time of every delivery (unit: min).

Single Fraction Dose (Gy)	Target volume	Real "beam on" time (T_{irr})	Phantom transit time (Δt)	PET/CTScanning time (T_{PET})
2.5 Gy	CTV-1 ml	1:20	5:15	30:00:00
3 Gy	CTV-1 ml	1:25	5:20	30:00:00
5 Gy	CTV-1 ml	1:36	4:40	30:00:00
6 Gy	CTV-1 ml	1:38	4:58	30:00:00
8 Gy	CTV-1 ml	1:58	4:56	30:00:00
10 Gy	CTV-1 ml	2:10	4:52	30:00:00
2.5 Gy	CTV-4 ml	1:43	5:22	30:00:00
3 Gy	CTV-4 ml	1:50	5:30	30:00:00
5 Gy	CTV-4 ml	1:55	5:19	30:00:00
6 Gy	CTV-4 ml	2:01	5:22	30:00:00
8 Gy	CTV-4 ml	2:03	5:16	30:00:00
10 Gy	CTV-4 ml	2:10	5:12	30:00:00
2.5 Gy	CTV-10 ml	2:33	5:23	30:00:00
3 Gy	CTV-10 ml	1:50	5:30	30:00:00
5 Gy	CTV-10 ml	2:41	5:18	30:00:00
6 Gy	CTV-10 ml	2:01	5:22	30:00:00
8 Gy	CTV-10 ml	2:50	5:02	30:00:00
10 Gy	CTV-10 ml	3:00	5:42	30:00:00

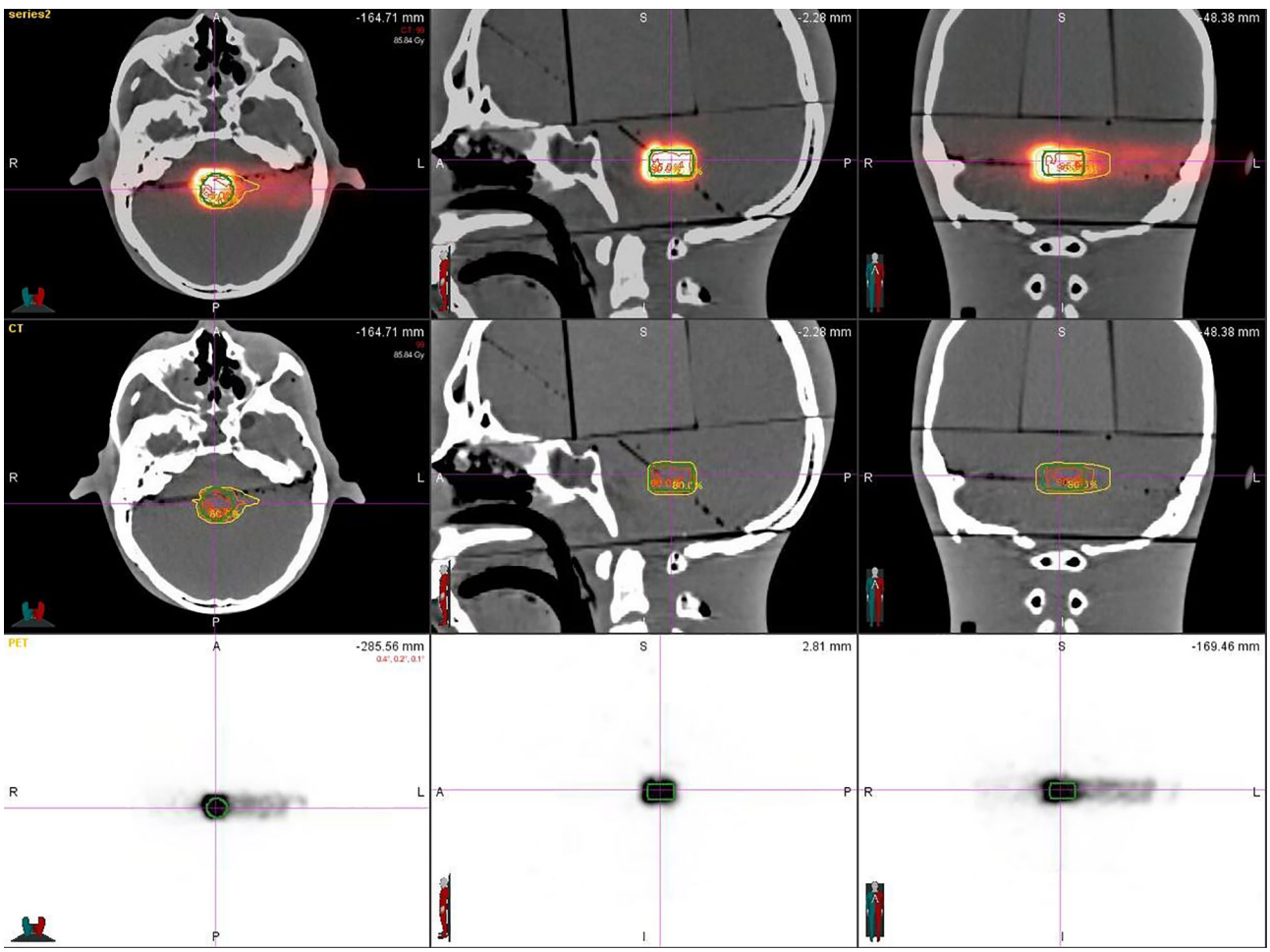

FIGURE 2 | Rando head phantom PET/CT scanning.

PET/CT Scan After Carbon-Ion Beam Irradiation

After plan delivery, the head phantom was quickly transferred to the PET/CT room within 6 min, which was much shorter than the half-life of the ^{11}C ($t_{1/2}$ = 20.38 min), to get PET/CT images with high signal-to-noise ratio (SNR). After the scanning setup, we referred to the routine diagnosis SUV value of the PET/CT image obtained by the 18 FDG radiopharmaceutical using the parameters of the pretest: the virtual body weight is 50 Kg, the virtual radioactive drug injection, the decay time parameter is fine-tuned according to each delivery, and every substudy total scanning time is 30 min. That means, when the scanning is finished, the signal, including a half-life time of the activated substance (^{11}C) produced by the carbon-ion irradiation in the phantom, was fully collected. Eighteen sets of PET/CT verification images were acquired (**Figure 2**).

Processing of Image Registration

Eighteen groups of DICOM studies were imported to the MIM Maestro software version 6.5.9 as the reference data for image registration, including CT images, virtual clinical target contours, and the relative effective plan doses. Eighteen sets of PET/CT verification images were also imported. To ensure the accuracy of image registration, we used a rigid registration workflow. After automatic registration by MIM Maestro, slight manual adjustment was done (**Figure 3**).

These experimental data were processed by a linear fitting method after obtaining them for each different volume and dose group. The correlation between these data was also analyzed.

The data statistics function module of the MIM software was used to calculate SUV for each virtual CTV to find out the maximum, minimum, mean, and total SUV of the corresponding target volume. To compare the differences in the same set obtained with the same relative dose to different volume targets, the SPSS statistical analysis software Version 22 was used to perform rigid alignment on the fusion images of each group. The maximum, minimum, and mean SUV data were also processed by this software. The difference of SUV data between variant target volumes was analyzed by independent sample *t* test.

RESULTS

Experimental Research Data Analysis

The virtual CTV was registered to the corresponding structure of the PET/CT image for statistical analysis. We get the following results listed in **Table 2**:

TABLE 2 | SUV of each target volume under different carbon-ion irradiation doses.

Single Fraction Dose	Target Volume	Max SUV	Mean SUV	Min SUV	Total SUV
2.5 Gy	CTV-1ml	5.91	2.67	1.5	80.32
3 Gy	CTV-1ml	7.18	3.24	1.82	97.59
5 Gy	CTV-1ml	16.92	10.17	2.69	307.38
6 Gy	CTV-1ml	17.23	10.71	4.37	371.93
8 Gy	CTV-1ml	31.51	22.6	9.86	684.42
10 Gy	CTV-1ml	35.53	23.39	9.42	706.97
2.5Gy	CTV-4ml	6.49	3.54	1.56	426.27
3 Gy	CTV-4ml	7.72	4.21	1.86	507.26
5Gy	CTV-4ml	17.08	11	2.87	1315.56
6 Gy	CTV-4ml	17.76	11.37	4.27	1369.61
8Gy	CTV-4ml	36.38	24.19	11.03	2812.43
10 Gy	CTV-4ml	38.43	26.40	12.34	3223.12
2.5Gy	CTV-10ml	6.83	3.45	1.31	1069.95
3 Gy	CTV-10ml	7.99	4.04	1.53	1251.84
5Gy	CTV-10ml	16.09	9.8	2.55	3010.65
6 Gy	CTV-10ml	18.38	10.90	3.53	3379.97
8Gy	CTV-10ml	35.88	20.73	9.23	6438.01
10 Gy	CTV-10ml	37.01	22.05	10.25	6773.96

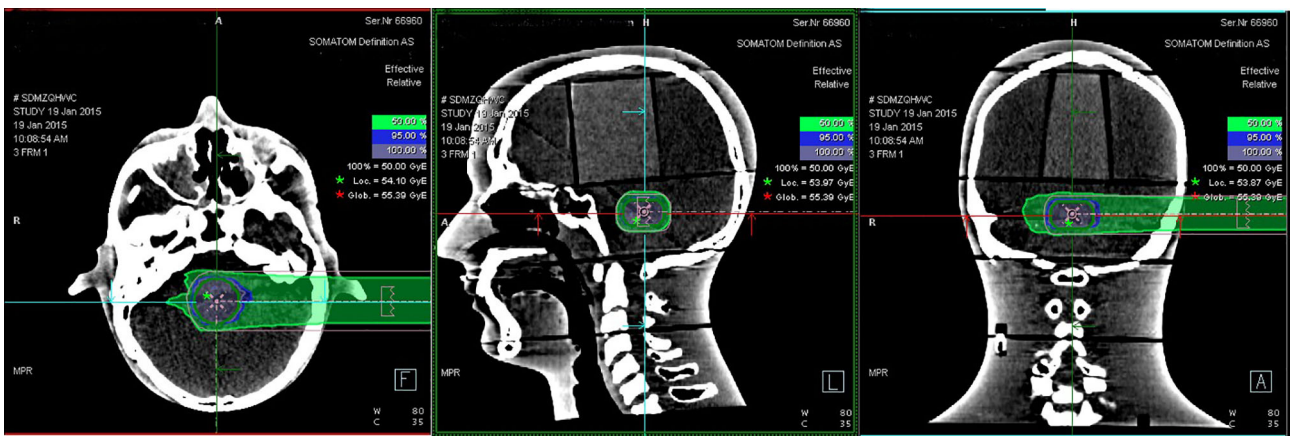

FIGURE 3 | Example of rigid registration fusion for planned CT and PET/CT image.

In the experimental data, the maximum, minimum, average, and total SUV values of three groups of different target sites were measured after different doses of carbon-ion irradiation, the results were showed on the **Figures 4–6**. The SPSS statistical analysis software version 22 was used to perform rigid alignment on the fusion images of each group and the R^2 value of each group was calculated.

For R^2 comparison, the results are as follows:

The six sets of histograms show SUV of single fraction doses from 10 to 2.5 Gy for different target volumes. It can be found

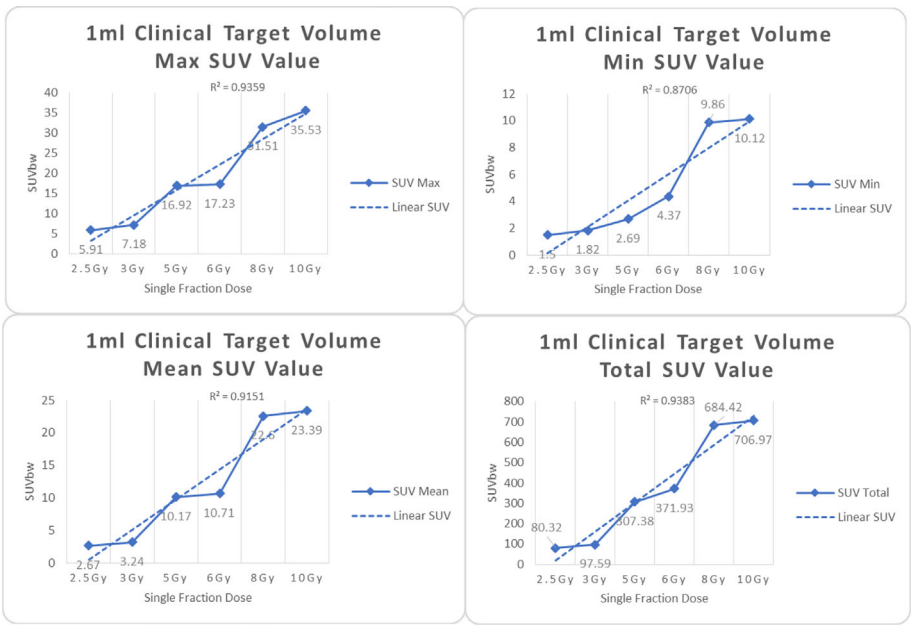

FIGURE 4 | Maximum, minimum, average, and total SUV of 1 ml clinical volume for different target doses.

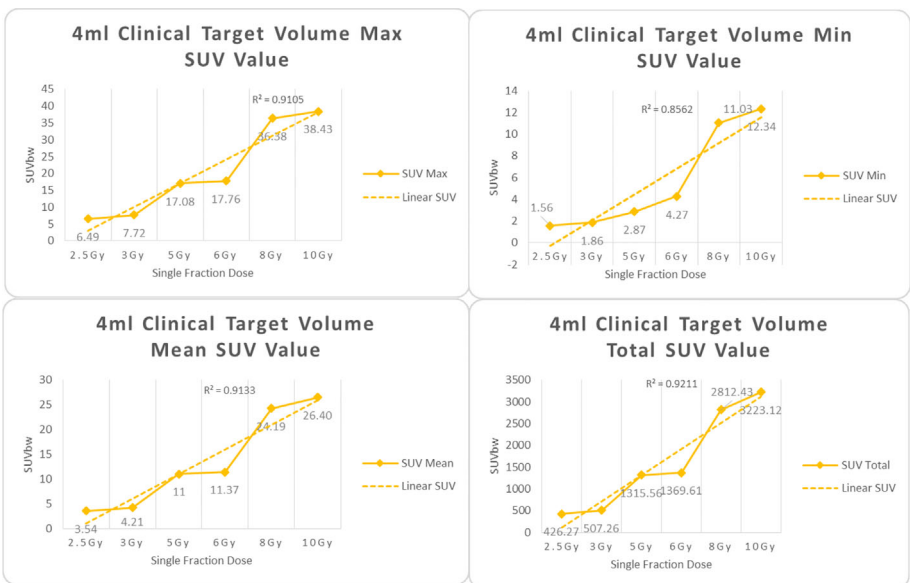

FIGURE 5 | Maximum, minimum, average, and overall SUV of 4 ml clinical volume for different target doses.

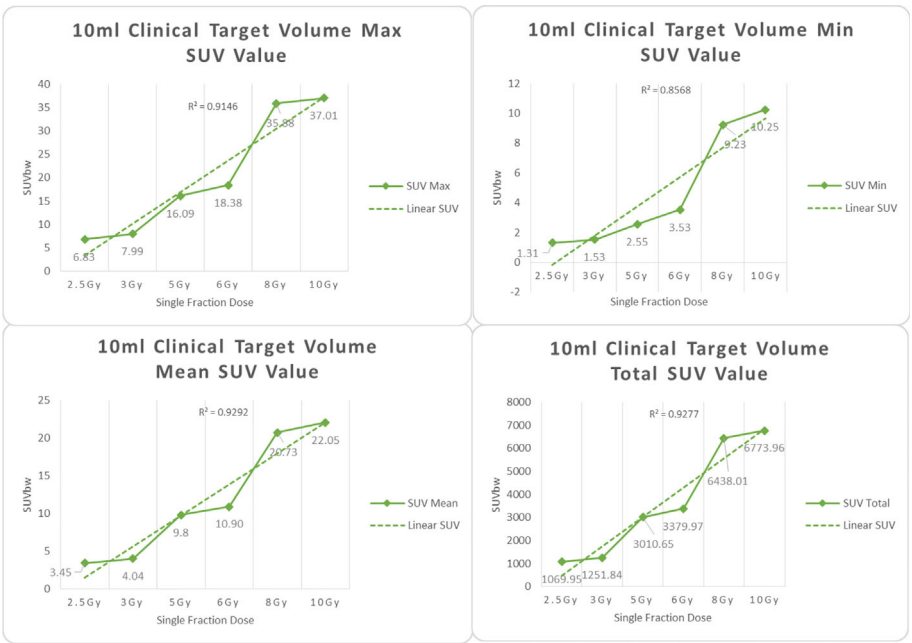

FIGURE 6 | Maximum, minimum, average, and overall SUV of 10 ml clinical volume for different target doses.

that the maximum, minimum, or mean SUV for the different target volumes with same single fraction dose do not have statistically significant differences ($P > 0.05$).

From **Figures 7–12** and **Table 3**, we can see that, for different delivered doses, R^2 values were approximately equal to 1 for maximum, minimum, and average SUV within the same target volume. This means, for various doses in different target volumes, the ion-induced SUV can have an interdeducible linear relationship with the target volumes. The SUV on PET/CT image could be quantitatively used for dose verification.

From **Table 3** and these six histograms for different volume target area carbon-ion irradiation, corresponding to different irradiation doses, the same volume target area shows the maximum, minimum, and average SUV numerical fit R^2 values

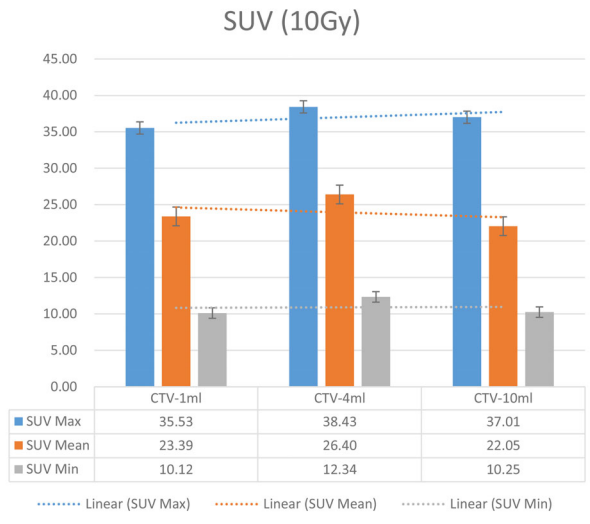

FIGURE 7 | SUV comparison of different target volumes after 10 Gy single fraction dose irradiation.

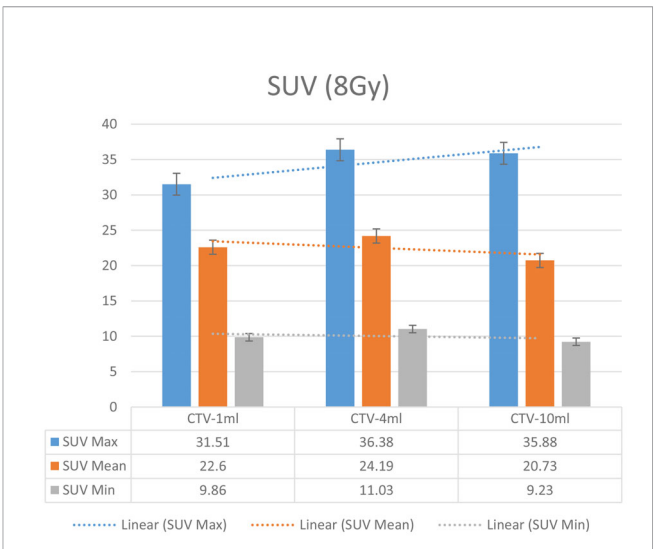

FIGURE 8 | SUV comparison of different target volumes after 8 Gy single fraction dose irradiation.

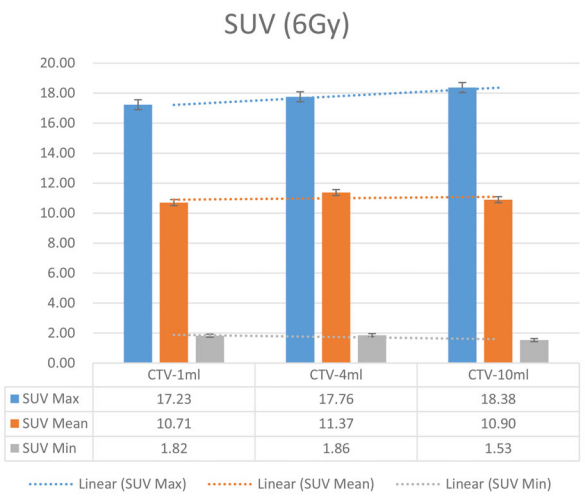

FIGURE 9 | SUV comparison of different target volumes after 6 Gy single fraction dose irradiation.

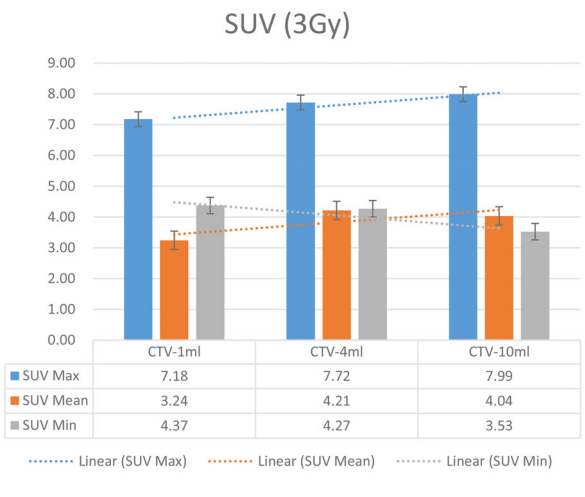

FIGURE 11 | SUV comparison of different target volumes after 3 Gy single fraction dose irradiation.

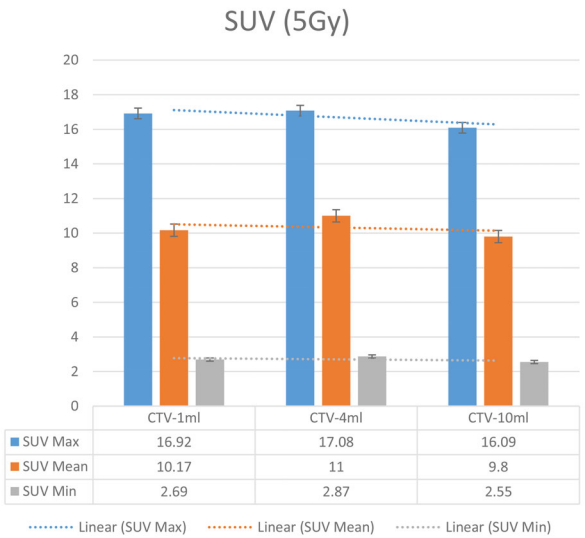

FIGURE 10 | SUV comparison of different target volumes after 5 Gy single fraction dose irradiation.

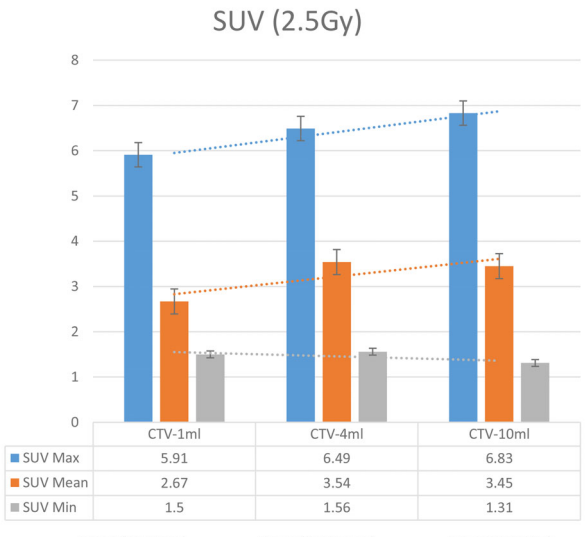

FIGURE 12 | SUV comparison of different target volumes after 2.5 Gy single fraction dose irradiation.

similar to 1, that is, different from the irradiation dose for each group of different target volumes of radiation, the target volume generated by the SUV value between the existence of a deductible linear relationship, corresponds to the same volume of the target area due to carbon ions. The gamma photon dose value generated by the beam irradiation induction can be quantified as the SUV value exhibited by the volume in the PET/CT scan image and can be taken from the target SUV in the verification image under certain conditions Dose value can be extended to the use of the target SUV of the accuracy of the dose to verify.

On the other hand, to compare the differences in the same set obtained with the same relative dose to different volume targets, the maximum, minimum, and mean SUV data were also processed by this software. The difference of SUV data between variant target volumes was analyzed by independent sample *t* test.

TABLE 3 | SUV R^2 values for different target volumes.

Target Volume	SUV Max R^2	SUV Mean R^2	SUV Min R^2	SUV Total R^2
CTV-1 ml	0.9359	0.9151	0.8706	0.9383
CTV-4 ml	0.9105	0.9133	0.8562	0.9211
CTV-10 ml	0.9146	0.9292	0.8568	0.9277

TABLE 4 | Comparison of SUV values for different target volumes that received the same irradiation dose of 10 Gy.

Irradiation dose of virtual target	CTV-1 ml vs CTV-4 ml	CTV-1 ml vs CTV-10 ml	CTV-4 ml vs CTV-10 ml
10 Gy	$P = 0.787$	$P = 0.873$	$P = 0.644$

TABLE 5 | Comparison of SUV values for different target volumes that received same irradiation dose of 8 Gy.

Irradiation dose of virtual target	CTV-1 ml vs CTV-4 ml	CTV-1 ml vs CTV-10 ml	CTV-4 ml vs CTV-10 ml
8 Gy	$P = 0.755$	$P = 0.975$	$P = 0.754$

TABLE 6 | Comparison of SUV values for different target volumes that received the same irradiation dose 6 of Gy.

Irradiation dose of virtual target	CTV-1 ml vs CTV-4 ml	CTV-1 ml vs CTV-10 ml	CTV-4 ml vs CTV-10 ml
6 Gy	$P = 0.748$	$P = 0.964$	$P = 0.832$

TABLE 7 | Comparison of SUV values for different target volumes that received the same irradiation dose 5 Gy.

Irradiation dose of virtual target	CTV-1 ml vs CTV-4 ml	CTV-1 ml vs CTV-10 ml	CTV-4 ml vs CTV-10 ml
5 Gy	$P = 0.863$	$P = 0.958$	$P = 0.819$

TABLE 8 | Comparison of SUV values for different target volumes that received the same irradiation dose of 3 Gy.

Irradiation dose of virtual target	CTV-1 ml vs CTV-4 ml	CTV-1 ml vs CTV-10 ml	CTV-4 ml vs CTV-10 ml
3 Gy	$P = 0.315$	$P = 0.476$	$P = 0.971$

TABLE 9 | Comparison of SUV values for different target volumes that received the same irradiation dose of 2.5 Gy.

Irradiation dose of virtual target	CTV-1 ml vs CTV-4 ml	CTV-1 ml vs CTV-10 ml	CTV-1 ml vs CTV-10 ml
2.5 Gy	$P = 0.443$	$P = 0.489$	$P = 0.993$

It can be explicitly seen from **Tables 4–9** that, for the same dose irradiated, SUV in virtual CTV with different volumes were not significantly different ($P > 0.05$). The maximum, minimum, and mean SUV values presented on different target volumes were very close to each other.

DISCUSSION

In the PET/CT scan process, the facility control system could use a specialized series of algorithms to correct the persistent decay data of the radioactive substance (^{11}C, etc.) in the image reconstruction and acquirement to ensure that the image data processing procedure is correct within the time of one half-life of the radioactive isotope (4–7).

However, if the PET/CT scan start time is much later or more than one half-life of the radioactive isotope after radiotherapy delivery, the SNR of the positron signal would become much lower, and the background noise of the obtained image data would increase heavily. This leads to a degradation of usefulness of the image. Radionuclides formed during carbon-ion irradiation are very unstable and continue to β^+ decay. Even if the energy of the β^+ released by ^{11}C isotope decay is only 1.0 MeV, this factor should be taken into account if the high image quality is required. In addition, it is necessary to consider the distance of the path of the positrons before annihilation, which would impact the resolution of the PET image.

Compared with the phantom, different tissues in the human body could change the range of SUV on PET/CT images. When the carbon-ion beam is delivered to the human body, the elemental composition of the various tissues on the beam path affect the number of positrons. For example, when the beam goes through the body cavity or low-density part of lung tissue, the corresponding amount of positrons is reduced, which can affect the measured SUV of these relevant regions.

Cyclic metabolism of organisms would also change the distribution of positrons in the body (8, 9). In this study, dose verification experiments on PET/CT images were performed on the Rando phantom without any blood circulation or various tissue motions. However, in living organisms, if the time interval of carbon-ion radiotherapy and PET/CT image scanning is long enough, the nuclide in the irradiated tissue will not only decay by the physical properties, but also be transported to other parts to participate in biological tissue metabolic activity (10–12). This process includes a number of possible blood or tissue fluids circulation, biological tissues within a variety of molecules associated with carbon-ion irradiation generated by a variety of radioactive isotope capture, microcirculation flow, and so on (13–15). Metabolism in the biological tissue also affects the distribution accuracy of these β^+ positrons, changes the PET/CT imaging quality, and reduces the accuracy of target dose verification. The biological washout must be corrected in real patients because it can affect the activity distribution significantly. For an accurate simulation, it is important to consider the biological washout of β^+ emitters due to vital functions. Mathematical expressions for washout

have mainly been determined by using radioactive beams of ^{10}C and ^{11}C ions, both β^+ emitters, to enhance the counting statistics in the irradiated area (16–18). Still, the question of how the choice of autoactivating or nonautoactivating projectile influences the washout coefficients has been unsolved (19). Therefore, if the target dose verification based on the PET/CT image is carried out in the organisms, the possible impact of precision caused by the metabolic process of β^+ positrons in organisms must be noted.

CONCLUSION

Accurate dose verification is an important prerequisite for the safe and effective implementation of radiation therapy. PET/CT after carbon-ion radiotherapy for clinical dose verification has been demonstrated to be a feasible method. Due to the limited experimental conditions, there is some further work needed to be carried out. More data should be collected in the future to find the exact relationship between the positron distribution and prescribed dose distribution.

DATA AVAILABILITY STATEMENT

The original contributions presented in the study are included in the article/supplementary material. Further inquiries can be directed to the corresponding author.

AUTHOR CONTRIBUTIONS

LSun contributed the central idea, analyzed most of the data, and wrote the initial draft of the paper. The remaining authors contributed to refining the ideas, carrying out additional analyses, and finalizing this paper. All authors contributed to the article and approved the submitted version.

ACKNOWLEDGMENTS

Thanks for the support of the department of radiation physics and nuclear medicine in Shanghai Proton and Heavy Ion Center.

REFERENCES

1. Hishikawa Y, Kagawa K, Murakami M, Sasaki H, Akagi T, Abe M. Usefulness of positron-emission tomographic images after proton therapy. *Int J Radiat Oncol Biol Phys* (2002) 53:1388–91. doi: 10.1016/S0360-3016(02)02887-0
2. Parodi K, Enghardt W, Haberer T. In-beam PET measurements of b +-radioactivity induced by proton beams. *Phys Med Biol* (2002) 47:21–36. doi: 10.1088/0031-9155/47/1/302
3. Litzenberg DW, Roberts DA, Lee MY, Pham K, Vander Molen AM, Ronningen R, et al. On-line monitoring of radiotherapy beams: Experimental results with proton beams. *Med Phys* (1999) 26:992–1006. doi: 10.1118/1.598491
4. Ammar C, Frey K, Bauer J, Melzig C, Chiblak S, Debus J, et al. Comparing the biological washout of beta(+)-activity induced in mice brain after C-12-ion and proton irradiation. *Phys Med Biol* (2014) 59.23:7229–44. doi: 10.1088/0031-9155/59/23/7229
5. Parodi K, Polf JC. In vivo range verification in particle therapy. *Med Phys* (2018) 45(11):e1036–50. doi: 10.1002/mp.12960
6. Kurz C, Bauer J, Unholtz D, Richter D, Herfarth K, Debus J, et al. Initial clinical evaluation of PET-based ion beam therapy monitoring under consideration of organ motion. *Med Phys* (2016) 43(2):975–82. doi: 10.1118/1.4940356
7. Nischwitz SP, Bauer J, Welzel T, Rief H, Jäkel O, Debus J, et al. Clinical implementation and range evaluation of in vivo PET dosimetry for particle irradiation in patients with primary glioma. *Radiother Oncol* (2015) 115 (2):179–85. doi: 10.1016/j.radonc.2015.03.022
8. Antonuk LE. Electronic portal imaging devices: a review and historical perspective of contemporary technologies and research. *Phys Med Biol* (2002) 47(6):R31. doi: 10.1088/0031-9155/47/6/201
9. Nutting C, Dearnaley DP, Webb S. Intensity modulated radiation therapy: a clinical review. *Br J Radiol* (2000) 73(869):459–69. doi: 10.1259/bjr.73.869.10884741
10. Bauer J, Unholtz D, Sommerer F, Kurz C, Haberer T, Debus J, et al. Implementation and initial clinical experience of offline PET/CT-based verification of scanned carbon ion treatment. *Radiother Oncol* (2013) 107 (2):218–26. doi: 10.1016/j.radonc.2013.02.018
11. Zhu X, Espana S, Daartz J, Liebsch N, Ouyang J, Paganetti H, et al. Monitoring proton radiation therapy with in room PET imaging. *Phys Med Biol* (2011) 56:4041–57. doi: 10.1088/0031-9155/56/13/019
12. Attanasi F, Knopf A, Parodi K, Paganetti H, Bortfeld T, Rosso V, et al. Extension and validation of an analytical model for in-vivo PET verification of proton therapy–a phantom and clinical study. *Phys Med Biol* (2011) 56:5079–98. doi: 10.1088/0031-9155/56/16/001
13. Nishio T, Miyatake A, Inoue K, Gomi-Miyagishi T, Kohno R, Kameoka S, et al. Experimental verification of proton beam monitoring in a human body by use of activity image of positron-emitting nuclei generated by nuclear fragmentation reaction. *Radiol Phys Technol* (2008) 1:44–54. doi: 10.1007/s12194-007-0008-8
14. Parodi K, Paganetti H, Shih H, Fischman AJ, Knopf A, Bortfeld T, et al. Patient study on in-vivo verification of beam delivery and range using PET/CT imaging after proton therapy. *Int J Radiat Oncol Biol Phys* (2007) 68:920–34. doi: 10.1016/j.ijrobp.2007.01.063
15. Parodi K, Paganetti H, Cascio E, Flanz JB, Bonab AA, Alpert NM, et al. PET/CT imaging for treatment verification after proton therapy: a study with plastic phantoms and metallic implants. *Med Phys* (2007) 34:419–35. doi: 10.1118/1.2401042
16. Nishio T, Ogino T, Nomura K, Uchida H. Dose–volume delivery guided proton therapy using beam on-line PET system. *Med Phys* (2006) 33:4190–7. doi: 10.1118/1.2361079
17. Iseki Y, Mizuno H, Futami Y, Tomitanie T, Kanaif T, Kanazawa M, et al. Positron camera for range verification of heavy-ion radiotherapy. *Nucl Instrum Methods Phys Res A* (2003) 515(3):840–9. doi: 10.1016/j.nima.2003.07.005
18. Mizuno H, Tomitani T, Kanazawa M, Kitagawa A, Pawelke J, Iseki Y, et al. Washout measurement of radioisotope implanted by radioactive beams in the rabbit. *Phys Med Biol* (2003) 48(15):2269. doi: 10.1088/0031-9155/48/15/302
19. Kraan AC. Range Verification Methods in Particle Therapy: Underlying Physics and Monte Carlo Modeling. *Front Oncol* (2015) 5:150. doi: 10.3389/fonc.2015.00150

Conflict of Interest: The authors declare that the research was conducted in the absence of any commercial or financial relationships that could be construed as a potential conflict of interest.

Copyright © 2021 Sun, Hu, Lai, Shi and Chen. This is an open-access article distributed under the terms of the Creative Commons Attribution License (CC BY). The use, distribution or reproduction in other forums is permitted, provided the original author(s) and the copyright owner(s) are credited and that the original publication in this journal is cited, in accordance with accepted academic practice. No use, distribution or reproduction is permitted which does not comply with these terms.

frontiers in Oncology

ORIGINAL RESEARCH
published: 19 March 2021
doi: 10.3389/fonc.2021.620388

A Modular System for Treating Moving Anatomical Targets With Scanned Ion Beams at Multiple Facilities: Pre-Clinical Testing for Quality and Safety of Beam Delivery

Michelle Lis[1,2], *Wayne Newhauser*[2,3]*, *Marco Donetti*[4], *Moritz Wolf*[1], *Timo Steinsberger*[1,5], *Athena Paz*[1], *Marco Durante*[1,5] *and Christian Graeff*[1]

[1] Biophysics, GSI Helmholtzzentrum für Schwerionenforschung GmbH, Darmstadt, Germany, [2] Department of Physics and Astronomy, Louisiana State University, Baton Rouge, LA, United States, [3] Department of Radiation Physics, Mary Bird Perkins Cancer Center, Baton Rouge, LA, United States, [4] Research and Development Department, Centro Nazionale di Androterapia Oncologia, Pavia, Italy, [5] Institute of Condensed Matter Physics, Technical University of Darmstadt, Darmstadt, Germany

OPEN ACCESS

Edited by:
Timothy Dean Malouff,
Mayo Clinic Florida, United States

Reviewed by:
Xuanfeng Ding,
William Beaumont Hospital, United States
Claudiu Porumb,
The Alfred Hospital, Australia

***Correspondence:**
Wayne Newhauser
newhauser@lsu.edu

Specialty section:
This article was submitted to Radiation Oncology, a section of the journal Frontiers in Oncology

Received: 22 October 2020
Accepted: 25 January 2021
Published: 19 March 2021

Citation:
Lis M, Newhauser W, Donetti M, Wolf M, Steinsberger T, Paz A, Durante M and Graeff C (2021) A Modular System for Treating Moving Anatomical Targets With Scanned Ion Beams at Multiple Facilities: Pre-Clinical Testing for Quality and Safety of Beam Delivery. Front. Oncol. 11:620388. doi: 10.3389/fonc.2021.620388

Background: Quality management and safety are integral to modern radiotherapy. New radiotherapy technologies require new consensus guidelines on quality and safety. Established analysis strategies, such as the failure modes and effects analysis (FMEA) and incident learning systems have been developed as tools to assess the safety of several types of radiation therapies. An extensive literature documents the widespread application of risk analysis methods to photon radiation therapy. Relatively little attention has been paid to performing risk analyses of nascent radiation therapy systems to treat moving tumors with scanned heavy ion beams. The purpose of this study was to apply a comprehensive safety analysis strategy to a motion-synchronized dose delivery system (M-DDS) for ion therapy.

Methods: We applied a risk analysis method to new treatment planning and treatment delivery processes with scanned heavy ion beams. The processes utilize a prototype, modular dose delivery system, currently undergoing preclinical testing, that provides new capabilities for treating moving anatomy. Each step in the treatment process was listed in a process map, potential errors for each step were identified and scored using the risk probability number in an FMEA, and the possible causes of each error were described in a fault tree analysis. Solutions were identified to mitigate the risk of these errors, including permanent corrective actions, periodic quality assurance (QA) tests, and patient specific QA (PSQA) tests. Each solution was tested experimentally.

Results: The analysis revealed 58 potential errors that could compromise beam delivery quality or safety. Each of the 14 binary (pass-or-fail) tests passed. Each of the nine QA and four PSQA tests were within anticipated clinical specifications. The modular M-DDS was modified accordingly, and was found to function at two centers.

Conclusion: We have applied a comprehensive risk analysis strategy to the M-DDS and shown that it is a clinically viable motion mitigation strategy. The described strategy can be utilized at any ion therapy center that operates with the modular M-DDS. The approach can also be adapted for use at other facilities and can be combined with existing safety analysis systems.

Keywords: 4D therapy, carbon ion therapy, failure modes and effects analysis, motion-mitigation, patient safety, quality assurance, motion-synchronized dose delivery

INTRODUCTION

Quality, safety, and radioprotection are integral parts of radiotherapy facilities (1). Radioprotection and area monitoring systems are designed to protect staff under the principles of justification, optimization and limitation (2). During regular operation, the critical safety operations of each accelerator are regulated by the main treatment control room and, for redundancy, by independent safety interlock systems (3). Medical systems used for radiotherapy, including accelerators, treatment control systems, and safety systems, typically take into account safety considerations during the design, construction, preclinical, and clinical phases. In addition, safety is considered in regulatory processes, e.g., in the USA, the 510k premarket clearance by the Food and Drug Administration (FDA) (21 C.F.R. § 807.81–807.97). Once in clinical use, exhaustive safety, and quality assurance testing must be periodically performed. Quality management has been an integral part of modern radiotherapy and is essential for safe and effective treatments. Organizations such as the American Association of Physicists in Medicine (AAPM), American College of Radiology (ACR), the American Society for Radiation Oncology (ASTRO), the International Atomic Energy Agency (IAEA), and the European Society for Radiology and Oncology (4) have established safety standards and guidelines (5). Radiotherapy device manufacturers and therapy centers typically agree upon test procedures as part of the acceptance testing process and guidelines are published for verifying the performance and safety of radiotherapy equipment during commissioning and periodic quality assurance testing (6–10). Beam commissioning and QA standards have been established for proton beams in the AAPM Task Group 224 report (11) and are being established for ion beam therapies through the PAR-13-371 National Cancer Institute (NCI) grant (12). As the complexity of modern treatment planning and delivery technologies, such as scanned ion beam therapy, has increased, additional consideration of safety is necessary. There is typically a lag between implementing modern therapies into the clinic and developing consensus safety guidelines for these therapies. The AAPM's Task Group 100 (TG-100) wrote a report (13) on an analysis methodology that aims to reduce this lag. The report is a framework to prospectively assess all aspects of workflow for possible critical safety errors in existing and new therapy methods (13, 14).

Broadly, the methods of safety analysis and risk mitigation are mature, rich, and generally applicable. Several major analysis strategies have been applied to clinical radiotherapy. For example, the AAPM and the Joint Commission on Accreditation of Healthcare Organizations (JCAHO) recommended the failure modes and effects analysis (FMEA), adapted from aviation safety to radiotherapy, as a general guidance for performing safety analyses (15). Additionally, guidelines have been developed by groups such as the "Accidental and unintended exposures in radiotherapy" (ACCIRAD) project of the European Commission (EC), the Radiation Oncology Incident Learning System (RO-ILS; ASTRO, Arlington, VA), which are based on pooled data on reported adverse events (16, 17). Many photon therapy clinics have adopted these methods (18, 19), while others have developed their own variations (20). However, knowledge of the safety of emerging radiation therapy technologies is inherently incomplete. Furthermore, emerging technologies have been identified as a common source of delivery errors (21). It is not yet clear how best to address the safety of emerging technologies, particularly for systems that treat moving tumors. It has been suggested that developing and simultaneously performing quality assurance during clinical trials of emerging technologies decreases safety errors (22). Prospective analyses, such as FMEA, could be a useful tool for emerging technologies (23), including conformal ion therapy for treating moving tumors (24). Though several motion handling strategies with ion beams exist (25–28), few of these motion handling strategies are integrated into their beam delivery systems (29). Relatively less is known about the safety risks of a modular motion-synchronized dose delivery system (M-DDS) for ion beam therapy (30), and no comprehensive assessment of the safety of a dose delivery system with integrated motion compensation has been reported in the scientific literature.

The purpose of this study was to apply an established method to analyze safety risks from a novel, modular, motion-synchronized dose delivery system for scanned ion beams. The system is in the late stages of preclinical development and testing. Here, we focused on the beam delivery process, identified motion-related errors, and implemented corresponding solutions. The performance of the M-DDS has been previously described by Lis et al. (2020). We developed and performed sample commissioning-style tests and quality assurance (QA) tests. These results provide information for subsequent clinical

safety assessments of a novel, modular motion-synchronized dose delivery system in development.

MATERIALS AND METHODS

This work describes a safety assessment of a dose delivery system (DDS) that is undergoing pre-clinical testing at two ion therapy centers. The M-DDS is an extended version of a clinical products used at the National Center for Oncological Hadrontherapy (CNAO) and MedAustron that have undergone full safety certification. The two most important extensions to the DDS were to make it portable and to allow for motion mitigation by synchronizing beam delivery to anatomical motion. The performance of the prototype motion-mitigation DDS was previously demonstrated, including preliminary tests such as the delivery of conformal, motion-synchronized beams (30). These results focused on proof of concept and the preliminary characterization of performance, but not safety. However, failures in the functionality of the M-DDS components could theoretically compromise patient safety. To minimize this risk, safety was integrated into each stage of development, in an effort to maintain the existing safety system for reintegration of the M-DDS into CNAO.

The assessment strategy described in this work applies an established methodology from AAPM Task Group 100 (13). This strategy is a prospective risk analysis method that has been widely used in the medical and other industries. With this strategy, we first defined each step of the treatment process, in detail, with a process map. We then identified possible errors that could occur at each step and quantified the effect on patient treatment with an FMEA. Finally, we identified the causes of errors with a fault tree analysis (FTA). After determining the potential safety risks, we developed and tested solutions for these errors (13).

The prospective risk analysis was performed on a DDS, with integrated capabilities for target motion compensation (30). For convenience, the general characteristics of the M-DDS are summarized here. The DDS was adapted from the DDS found at CNAO to function with the therapy research line (Cave M) at GSI Helmholtz Center for Heavy Ion Research (GSI). The DDS is composed of commercial field programmable gate arrays (FPGAs) (PXIe-1085; National Instruments, Austin, TX), which control each beam delivery component, including the scanning magnets, beam monitoring detectors, timing system, and interlock system. The DDS has been modified to synchronize the delivery of 4D-optimized plan libraries (24, 31) to detected target motion.

Motion mitigation features are integrated into the M-DDS. The first step of motion synchronized dose delivery is creating 4D treatment plan libraries from 4DCTs, where each plan in the library contains delivery information for a motion phase within the 4DCT. During beam delivery, a motion-monitoring device continuously monitors the tumor position, from which the M-DDS determines the current motion phase (32, 33). The delivery progresses in sequence until the tumor position has entered into another motion phase and delivery is redirected to the plan from the plan library that corresponds to the detected motion phase. Further information on the M-DDS is described by Lis et al. (30).

Good manufacturing practices were followed through the development of the M-DDS. Critical processes in the M-DDS were maintained from the clinical M-DDS design and all changes were evaluated experimentally in the clinical environment. The implemented software design choices were based on the existing software structure, so most uncovered sources of error were found to be related to unclear workflow and limitations to memory or signal speed. All changes and additions were documented. In the following sections, we describe a safety assessment strategy for the M-DDS. Additionally, we provide example safety and quality assurance tests for the M-DDS.

Process Steps

The first step of the prospective risk analysis was to identify the sub-processes that occur through the course of treatment with a process map. A process map is a visual representation of a process that demonstrates the flow of each step from start to end. We divided the process of treating a patient with scanned ion beams into 10 main stages, based on the guidelines proposed by the World Health Organization (34). In this study, we focused on six of these stages—planning, simulation, patient setup, treatment delivery, treatment verification, and monitoring—as these were the most relevant to treating moving targets. For each of these stages, we identified the sub-processes that occur at an ion beam therapy center (21), such as delivery of an iso-energy slice (IES) during the course of treatment. We then amended each stage to include any additional sub-processes when delivering motion-synchronized ion beams with the M-DDS, such as redirecting the plan delivery to compensate for detected motion. Modes of failure were then identified for each of these sub-processes.

Failure Modes and Effects Analysis

The FMEA assesses the likelihood and impact of failures from each step of a process. An FMEA was applied to each of the identified process steps and potential modes of failure at each step were described. Each of the failures were assigned a rank value on a numerical scale of 1 to 10 for each of three safety indices: the severity index (S) is the extent of harm of the failure on the patient, the occurrence index (O) is the likelihood that a cause will result in a failure, and the detection index (D) is the likelihood that a failure will not be detected. All three of these indices are estimated under the assumption that there was no safety check in place for that failure. The corresponding definitions for the rankings of each of these values are summarized in **Table 1**. This data has been adapted from the TG-100 (13). The failures were then ranked by calculating the risk priority numbers (RPN), which is the product of these three indices (RPN = S × O × D). RPN values of above 125 were considered high risk, and any S score above 5 was also considered high risk. One example error is the gradual drift of the scanning magnet throughout the course of delivering an IES. This could potentially cause limited toxicities or overdose, as the drift may be on the scale of a few mm, and would potentially occur for

TABLE 1 | Numerical scale used to assign rank values to Severity Index, Occurrence Index, and Detectability Index for each failure.

Rank value	Severity Index	Occurrence Index (mean time between failure)	Detectability Index
1	No effect on patient care	+ 4 years	Impossible to miss
2	Inconvenience or delay in care	2 years	"
3	"	1	Highly likely to notice
4	Minor dosimetric error	6 months	Easy to detect
5	"	1 month	Fairly easy to detect
6	Limited toxicity or overdose	2 weeks	Fairly difficult to detect
7	Potentially serious under- or overdose or toxicity	1 week	"
8	"	3 days	Nearly undetectable
9	Very serious under- or overdose or toxicity	1 day	"
10	Patient death	1 hour	Undetectable

These data have been adapted from the TG-100 report on failure modes and effects analysis (FMEA). For each case, a rank of 1 was considered harmless, and a rank of 10 was catastrophic. Chosen rank values were based on observed or estimated.

every delivery in the absence of position feedback. Such an error would be difficult to detect without monitoring. The resulting RPN would then be $6 \times 10 \times 7 = 420$. Selected FMEA indices were agreed on by a consensus group of experts, including the authors on this work.

Fault Tree Analysis

Causes of each identified failure were mapped out with a fault tree analysis (FTA). The FTA allows for visualizing potential points to perform quality management procedures and to minimize the propagation of errors (35). Each failure mode was traced back to its potential causes using a logic tree. Possible failure modes include user errors, such as selecting the wrong delivery setting or incorrect patient setup, software errors, equipment failures, and patient non-compliance. For the example of an error in delivery of an IES, the cause could be traced back to a faulty position feedback from the beamline monitors to correct the scanning magnet power supplies. Other causes of the error could also be postulated, including slow scan speeds and incorrect magnet calibration. Once causes for each failure were identified, methods to eliminate the cause or to detect the possibility of each failure were developed.

Solutions and Tests

After identifying the potential solutions for the safety risks, appropriate solutions were implemented and error-handling tests were designed and performed. Solutions for failure modes can be classified into several categories: permanent corrective actions, error states and interlocks, commissioning and quality assurance tests, and plan verifications. Permanent corrective actions are changes in the workflow of the planning or delivery software or user protocols in order to eliminate the possibility of that failure mode occurring. This can include implementing redundancies, such as redundant devices and communication protocols. Pass-fail tests were performed by simulating error states and checking that the delivery system entered an error state or triggered an interlock. Commissioning and QA tests are tests that verify that the system consistently works according to manufacturer specifications and within acceptable fault tolerances. Plan verification tests verify the accuracy of patient plans. For example, scan magnet position errors can be prevented in several redundant ways. Two position-monitoring chambers are used during delivery to monitor the accurate delivery of beam spots within an IES. Additionally, interlocks are in place in the case of failure of one of the monitoring or scanning magnets. Finally, daily QA is performed to confirm the functionality of the entire delivery system. Whenever possible, permanent corrective actions were implemented.

Description of Error Handling Tests

Error handling tests were created for each of the failures identified in the FTA. Pass-fail test cases were written for each of these failures. Corresponding software tests were then created that inject error scenarios into the delivery process to confirm that the DDS can respond to the respective error. In the case that an error-handling test failed, the underlying delivery software was modified to prevent the error from occurring. In other cases, an interlock was also implemented to trigger the interruption or termination of treatment in the presence of a motion synchronization error. The implemented interlocks were also tested by injecting error scenarios into the delivery process.

Daily, Weekly, and Annual QA

The performance of the accelerator and beam delivery components was characterized through a series of quality assurance measurements. While existing QA protocols (11) will confirm the functionality of most aspects of motion-synchronized dose delivery, additional tests must still be performed to ensure the performance of additional features, including the motion monitoring system and 4D plan library. QA tests were designed that prioritized a simple set up, are multi-purpose, are fast and use well-characterized phantoms. A QA concept was designed to test the safety and reproducibility of motion-deliveries. Where possible, the current clinical protocols at ion therapy centers, such as those used at CNAO (36) were extended to include motion scenarios. Each test was verified experimentally in a clinical setting at CNAO.

Daily QA tests were designed and performed for measuring field uniformity, beam spot positions, and beam reproducibility. Setups with water-equivalent plastics (RW3 slab phantom; PTW, Freiburg, Germany) and radiochromic films (EBT3 Gafchromic; International Specialty Products, Wayne, NJ) were selected, as their assembly time is fast and they are both well-characterized systems. The daily QA procedures found at CNAO were modified and applied to test the delivery quality of motion compensation with the M-DDS. This allowed faster delivery that was not dependent on additional custom-made software for analysis. The daily QA setup, a radiochromic film, mounted behind 2 cm of water-equivalent plastic, was mounted on top of a linear stage with programmable motion patterns (M-414.2PD; Physik Instrumente GmbH, Karlsruhe, Germany). Motion

amplitudes, detected from an optical laser distance sensor (OD100 – 35P840; SICK, Waldkirch, Germany), were converted into motion states (30). For each test, the clinical (non-moving) procedure was performed first, followed by the motion-compensation variant. For these beam deliveries, the linear stage moved with 20 mm amplitude sinusoidal or Lujan2 motion (37–40) while delivering a uniform square profile with eight surrounding spots. The purpose of each test and the measurement criteria are summarized in **Table 2**.

All films were calibrated in a series of steps. Before the QA tests, standard dosimetry was performed (44), and calibration films, composed of eight squares with fluences from 2×10^5 to 4×10^7 particles/mm, were acquired for each batch of films. The calibration plan was delivered with 280 MeV/u carbon ions to films placed behind 2 cm of water-equivalent plastic. After delivery, the QA films were scanned with a laser film scanner (VIDAR DosimetryPRO Advantage Red; VIDAR System Corporation, Herndon, VA, USA) in landscape orientation, using 16 bit sampling and a 300 dpi resolution. A batch-specific optical density correction was applied to each film by subtracting out the optical density of an unirradiated area of the film, using an image analysis software (ImageJ version 1.52a; National Institute of Health, Bethesda, MD). The calibration films were used to apply a calibration curve, converting optical density to particle intensities. Each film was cropped, aligned, and corrected for linear energy transfer (LET) quenching effects (43), by applying a relative efficiency (RE) correction curve as follows:

$$RE(LET) = \frac{D_{280MeV/u}(netOD)}{D_{abs}}$$

where $D_{280MeV/u}$(netOD) is the 280 MeV/u carbon ion dose needed to produce the measured, corrected optical density, and D_{abs} is the actual dose delivered with carbon ions to the film. After, calibration, the films were analyzed.

TABLE 2 | Description of the purpose and pass criteria for each quality assurance test.

Test type	Quantity tested	Pass criteria
Daily QA		
Field uniformity	Homogeneity index (41)	≥95%
Spot shape	FWHM in X and Y direction across scan field (11)	Symmetrical
Spot position	Distance to agreement (42)	< ± 1 mm
Motion-monitoring system functionality	Function test	Functioning
Weekly QA		
Beam monitor calibration reproducibility	Coefficient of variation (43)	<1%
Annual QA		
Dose distribution with homogeneous phantom	Percent error from expected dose (36)	<5%
Dose distribution with heterogeneous phantom	Percent error from expected dose (36)	<5%
QC		
Motion-monitoring system performance	Distance to agreement (42)	<0.1 mm

The uniformity was assessed through the homogeneity index (HI), which is defined as

$$HI = 100 - \frac{D_{max} - D_{min}}{D_p}$$

where D_{max} and D_{min} are the maximum and minimum measured absorbed dose, respectively, and D_p is the prescribed dose. The *HI* was measured in the center 70% of the target volume. *HI* values above 90% were considered clinically acceptable. Additionally, the beam spot position accuracy was assessed by measuring the relative distance between each pair of beam spots in 2D profiles of the films. The beam spot shape and distortion was measured by determining the FWHM in the horizontal and vertical directions. Beam reproducibility tests were performed by comparing the delivery results across several weeks with a coefficient of variation (45). Finally, the increases to QA delivery time were assessed by measuring the setup and delivery time for each test and estimating the increased time for QA, when performing motion-specific testing alongside the currently performed QA tests in each treatment room.

Equipment quality control (QC) is generally also performed daily to verify the functionality and accuracy of treatment equipment. To verify the performance accuracy of the motion-monitoring equipment (a linear stage and an optical distance (OD) laser) the linear stage was programmed to move in an increasing stepwise motion pattern. The measured OD laser signal was compared to the motion files for the linear stage.

Annual QA is a series of extensive tests to measure machine performance. Annual QA tests were performed to measure dose distributions with a 3D homogenous setup and a 3D inhomogeneous setup. First, 4DCTs of an heterogenous phantom (CIRS 062 electron density phantom; CIRS, Norfolk, VA, USA) and a water tank (MP3-P; PTW, Freiburg, Germany) were acquired. $60 \times 60 \times 60$ mm^3 cubes were delivered to 12 small-sized ionization chambers (PinPoint 3D ion chamber model T31015; PTW, Freiburg, Germany) in a water tank for both setups. For the 3D inhomogeneous setup, density compensation measurements were performed by the heterogeneous phantom mounted in front of the water tank. Both deliveries were performed without motion, and with motion compensation. Standard deviations for measured doses of < 5% were considered acceptable.

Patient Plan Verification

Plan verification, or patient specific quality assurance (PSQA), is performed to assure the accuracy of a treatment plan. Treatment planning and treatment delivery errors, unique to the motion mitigation system, can be discovered through PSQA testing. Errors may include selecting the wrong motion trajectories during planning or delivery, or planning with an unintended motion compensation strategy. If not detected, these errors could lead to severe dose degradations. Several plan verification methods were chosen to test the extent to which planning and delivery errors related to mitigating for respiratory motion can be detected. The chosen PSQA tests included patient verification protocols that are used in ion therapy clinics, including 1) 3D

dose measurements with small-sized ICs, 2) repeat 2D measurements at three depths with a 2D ionization chamber array detector (Octavius 1500 XDR; PTW, Freiburg, Germany), and 3) log file analysis. Additionally, 3D dose measurements were also performed with 4) a stack of radiochromic films (46). These measurements were analyzed with standard deviation calculations, gamma index analysis, and through the evaluation of dose volume histogram (DVH) metrics, respectively. To perform these measurements, the detector or film was placed into its respective holder, and the holder was mounted onto a linear stage. 4D-optimized patient plan libraries were delivered to each detector setup. The linear stage was programmed to move with trajectories derived from the patient 4DCTs. Other aspects of PSQA were also considered when designing each setup, including favoring simpler phantom setup processes and higher resolution of the recorded data.

3D dose measurements were performed by delivering patient plans to 12 small-sized ICs. These ICs were selected, as they are used in several clinical ion facilities for patient verification (47–49). The ICs were inserted into a custom removable holder, connected to a linear stage that generated the motion of the ICs (**Figure 1**). The linear stage was mounted on top of a water tank, similar to the commercially used water tank phantoms, and the water tank was filled with water. Each patient plan was delivered to this phantom, with the linear stage moving with the patient's breathing pattern. Each IC recorded a dose measurement and standard deviations were calculated from these doses. The chosen prescription dose was 6 Gy per fraction. Standard deviations of < 5% are typically considered acceptable.

2D dose measurements were performed by delivering the patient plan to a 2D ionization chamber array detector at three tumor depths. The chosen depths corresponded to the proximal end, middle, and distal end of the tumor depth. The appropriate thickness of water equivalent plastic (RW3; LAP GmbH, Lüneburg, Germany) was placed in front of the detector for each case (**Figure 2**). This setup was mounted on the linear stage to generate patient motion and a patient plan was delivered to the detector with and without motion. The delivery results were compared to the planned doses for each depth with the gamma index analysis (42), where a criterion of 3%/3 mm was used, with a dose threshold of 5% of the prescription dose. Pass rates of >90% for measurements made at all three depths were considered passing.

3D measurements with a stack of films were made to acquire higher resolution dose distributions. Seven 5" × 4" radiochromic films were slotted into an in-house built film holder phantom. The phantom was composed of a stack of 15 × 13 × 1 cm^3 polymethyl methacrylate (PMMA) plastic slabs, with slits for the films, as seen in the technical drawing in **Figure 3**. This setup was mounted on top of the linear stage, which generated periodic motion. Each film was numbered and labeled at the top right corner before delivery. Each patient plan was delivered to the film stacks, in the presence and absence of motion. After delivery, the films were processed as described in section above. Each film was then analyzed with the gamma index analysis. The average gamma index pass rates for each film stack were evaluated using an in-house developed research software for data analysis, ArrayParser, where each film was compared to the respective treatment plan at the appropriate tumor depth. Gamma index pass rates of above 90% were considered clinically acceptable.

Log file analysis has been used to decrease PSQA measurement time. The patient plan was delivered to the IC

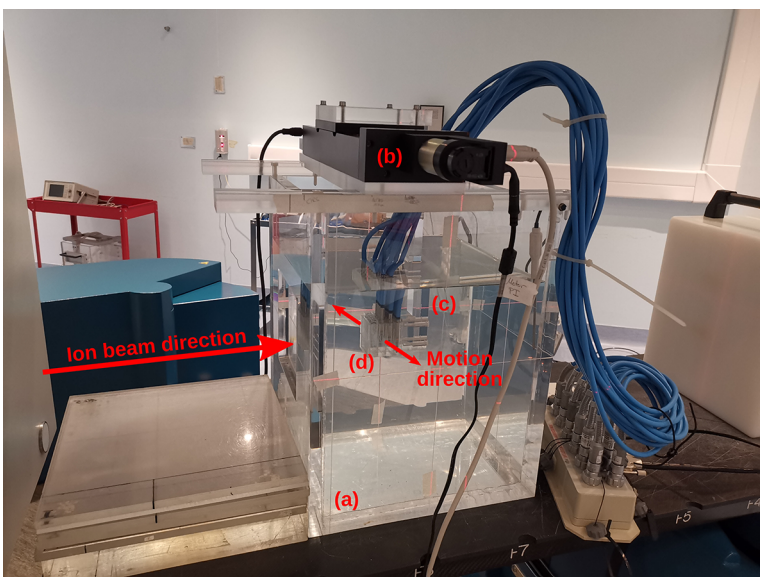

FIGURE 1 | Experimental setup for patient-specific quality assurance (PSQA) measurements with **(A)** a water tank and **(B)** a linear stage mounted on top. The linear stage is programmed to move a variety of attachments in periodic, respiratory-like motion patterns. Here, **(C)** a holder with **(D)** 12 small-sized ionization chambers (IC) inserted inside is attached. This IC holder aligns with the isocenter markings on the water tank phantom, which is filled with water.

FIGURE 2 | Schematic of the ionization chambers (IC) detector array setup. The IC array detector is placed inside of a 5 mm polymethylmethacrylate (PMMA) holder, mounted onto a linear stage. Water-equivalent plastic of thickness "d," corresponding to the distal, middle or proximal depths of a target, are then placed in front of the detector.

array detector and log files from the scanner magnets and nozzle detectors were used to reconstruct the delivered doses on the planning 4DCT, using TRiP4D (30). The motion signal from the linear stage was used directing plan delivery during motion-compensation. However, a simulated motion signal could also be used for these measurements. The dose reconstructions were then compared with planned dose distributions using the gamma index analysis to a criterion of 3%/3 mm, where > 90% pass rates were considered acceptable.

RESULTS

Process Map

A process map was created to map out the sub-processes of patient treatment at a typical ion therapy center. The processes for moving tumors are presented in **Figure 4**. This map consists of five main workflow steps, starting with patient imaging through the last fraction of treatment delivery. Patient-specific verification procedures were included as well. Several of these steps were critical to patient errors.

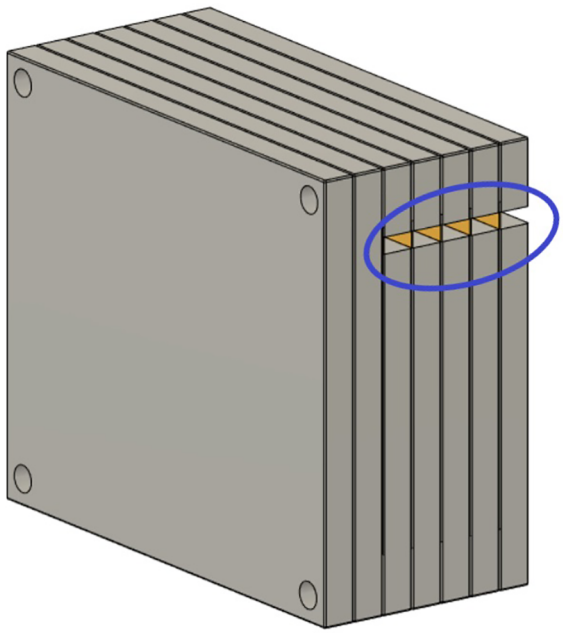

FIGURE 3 | Schematic of the film stack. The film stack contains up to nine slabs of polymethylmethacrylate (PMMA) with precisely machined slots for holding radiochromic films (5" × 4") as well as several slabs of additional PMMA to vary the delivery depth. The phantom measures 15 × 13 × 9 cm^3 when nine slabs are in place. The slabs are aligned and held together by plastic screws at each corner of the phantom. The lateral cutouts (blue circle) are used for easy access of the irradiated films (yellow) without the need to disassemble the film stack phantom.

Failure Modes and Effects Analysis

A systematic evaluation of the process map identified 58 failures. A subset of these failures is shown in **Table 3**, including the highest ranked failures during treatment delivery. Values for S, O, and D indices were estimated based on the metrics from

Table 1 and were used as a guide to determine the highest risks for conformal, motion-synchronized therapy. All failures with an RPN of 125 or greater and all failures with a severity > 5 were considered in this study. In total, 41% of failures were identified to be low risk (RPN = 1–75), 33% were found to be medium risk (RPN = 76–125) and 26% were found to be high risk (RPN > 125). The highest ranked failures, with an RPN score of 294 were caused by delivery errors due to patient movement and absolute changes to breathing position. Potential failures that are common to both static site and moving site treatments were not included in the analysis, such as miscommunications between physicians and technicians and certain treatment planning errors.

Fault Tree Analysis

Fault tree analysis was performed to identify sources for the potential errors identified in the FMEA. Solutions for each error in the FMEA were identified, implemented, and tested. A sample fault tree can be seen in **Figure 5** for the case of gating magnet failure. Identified causes of error included human error, such as

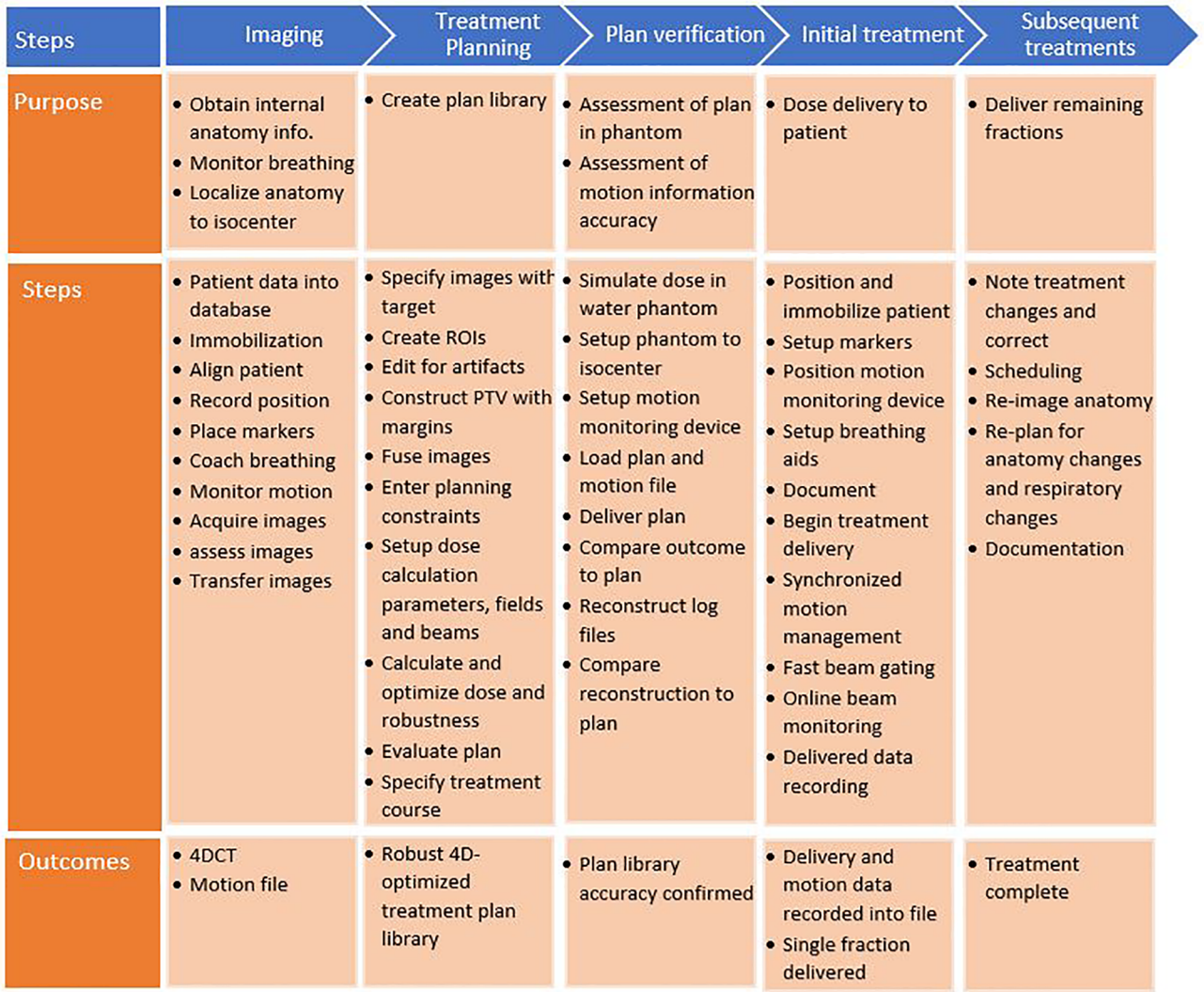

FIGURE 4 | Process map for motion-synchronized dose delivery as commonly found in ion therapy clinics. The treatment process is broken down into five categories: imaging, treatment planning, plan verification, initial treatment fraction, and subsequent treatments. Each step in these processes is described.

setting the treatment to the wrong delivery mode, machine errors, such as noise on the motion signal, and treatment errors, such as changes to the breathing patterns between image acquisition and treatment. Proposed solutions for these errors varied for each error type, and included disabling the option for gating when a 4D plan library is loaded, implementing a noise reduction filter on the motion signal, and using a monitoring method that compares planned to measured motion and gates delivery when out of range. Following implementation, the solutions to the identified errors were tested.

Safety Testing

Solutions were implemented to prevent the identified errors from occurring and each solution was tested. The implemented permanent corrective actions included noise filtering to smoothen the respiratory signal, automatic extraction and setting of the number of motion phases from the treatment plan library, and implementing a checkpoint to prevent the beginning of delivery until the motion-monitoring system is calibrated and sending a motion phase. Many errors were identified to be due to mistakes made by the user. Some examples include setting up the motion-monitoring system in an orientation other than what was used during planning image acquisition, and not accounting for changes to the tumor position, relative to isocenter (50). In these cases, the proposed solutions included performing a second check by another clinician or reimaging the patient periodically. Additionally, using a checklist to check the patient setup before treatment could reduce the incidence of user errors.

TABLE 3 | Summary of failure modes and effects analysis (FMEA) results for potential errors during patient therapy with motion-synchronized ion beams using a DDS with integrated motion compensation controls. Risk priority numbers (RPNs) of over 125 were considered high risk.

Failure mode	Severity	Occurrence	Detectability	RPN
Patient movement	7	6	7	294
Absolute change in breathing position	6	7	7	294
Patient alignment	7	5	6	210
No gating during sporadic movements	5	5	8	200
Gating window too large	6	8	4	192
Beam sweeping distance dose	3	8	9	192
Sending incorrect motion phase info	7	3	7	147
Error creating of slice files	7	3	7	147
Failure to gate	9	2	8	144
Position calibration incorrect	8	2	7	112
Changes to respiration pattern	7	8	2	112
Setup of motion management device to wrong position	9	2	6	108
Patient not re-imaged after anatomy change	7	3	5	105
Position feedback missing/not working	4	5	5	100
Determined wrong number of motion phases	6	2	5	90
Incorrect motion direction	9	2	5	90
Loading wrong treatment plan	4	2	10	80
Motion data recording stops	4	2	9	72
Failure to progress to next slice	6	2	5	60
Plan incomplete	6	2	5	60
Motion signal loss	9	2	3	54

Pass Fail Tests

A series of error handling tests were created to test each of the implemented solutions. These tests included pass-fail tests, where the expected results included either triggering a temporary interlock, aborting treatment, or entering the "setup error" state. The summary of pass-fail test results is listed in **Table 4**.

Daily, Monthly, Annual QA

QA tests were proposed for identifying errors in the functionality of the motion-synchronized delivery components. These tests are summarized in **Table 2**. QA setups were chosen that are available or are similar to those found in ion therapy centers. Delivered profiles were analyzed for uniformity, agreement with the treatment plan, and for beam reproducibility, the uniformity index, and gamma index analysis were chosen as analysis metrics.

Delivery uniformity with motion-compensation was determined by assessing a square profile for a single energy of 240 MeV/u, delivered with motion-compensation, to a radiochromic film. HI for the static and 10 phase compensation deliveries were 95.3 and 94.8%, respectively. The spot position accuracy was found to be within ± 0.5 mm from the expected position. The beam spot shape was determined through a measurement of the FWHM in the X- and Y-directions, where the X-direction was the direction of motion. For static deliveries, this was found to be 3.9 and 3.4 mm, respectively, and for the 10 phase deliveries, this was found to be 4.7 and 3.3 mm, respectively. The observed broadening of the beam in motion direction is an indication of the residual motion both within and between the motion phases, and spot size increases of up to ± 0.5 mm were tolerated.

The increased time to perform both static and motion compensation QA tests was measured and compared to static QA alone. For the current clinical QA procedures, setup and irradiation time was found to be 5 and 3 min, respectively, and for the motion compensation QA, the setup, and irradiation time was found to be 5 and 10 min, respectively. The estimated increase in QA-personnel time for a facility with three treatment rooms is 3 × 7 = 21 min, based on current QA methods and experience.

Annual QA tests included measuring 3D uniformity in a homogeneous and heterogeneous phantom. The static cube delivery measured a homogeneity of ± 1.2% and the motion compensated delivery measured a homogeneity of ± 3.5%. The static cube delivery of 10 Gy, through the heterogeneous phantom, measured a homogeneity of ± 2.1% and the motion compensated delivery measured a homogeneity of ± 2.3%.

The basic functions and accuracy of the motion-monitoring equipment were also determined. The measured motion was within ± 0.5 mm for all steps within the measurement range of −30 to 20 mm, as seen in **Figure 6A**. The agreement between the programmed linear stage positions and measured positions from the distance sensor are seen in **Figure 6B**, where the linear relationship indicates a high degree of measurement accuracy.

Patient Specific QA Results

Patient plan verification tests were performed to compare the measured accuracy of the delivered 4D plan libraries. Patient verification deliveries were found to be within clinical requirements; however, the measurement resolution varied for each approach. Results are summarized in **Table 5**. The small-sized IC measurements were found to be within ± 2.4 and ± 8.9% of the prescription dose for static deliveries and 10 phase motion compensation deliveries, respectively, where ± 5% is ideal, but due to residual motion, ± 10% was considered acceptable at this stage; however, higher precision may be necessary before clinical use. The measurements at three depths, with an ionization chamber array detector were assessed using the gamma index analysis. Pass rates (Pearson correlation score) for the static delivery were found to be 84.1% (0.9883), 100.0% (0.9947), and 99.4% (0.9983), for distal, middle, and proximal profiles, respectively. As only the distal measurement did not meet the pass criteria, log file analysis was performed to verify delivery quality. Pass rates (Pearson correlation score) for the motion-compensated delivery were found to be 91.6% (0.9901), 98.6% (0.9954), 90.9% (0.9971) for distal, middle and proximal profiles, respectively. The average gamma index pass rates for the film stacks were 92.4%, and 90.4% for conventional 4D optimized and robust 4D optimized deliveries, respectively. The average pass rate for the static delivery was 92.2%. The homogeneity for robustly optimized and conventionally optimized 10 phase motion compensated deliveries was 90.6% and 92.4%, respectively. Delivered dose data (DDD) log files were reconstructed and compared to planning simulations. The

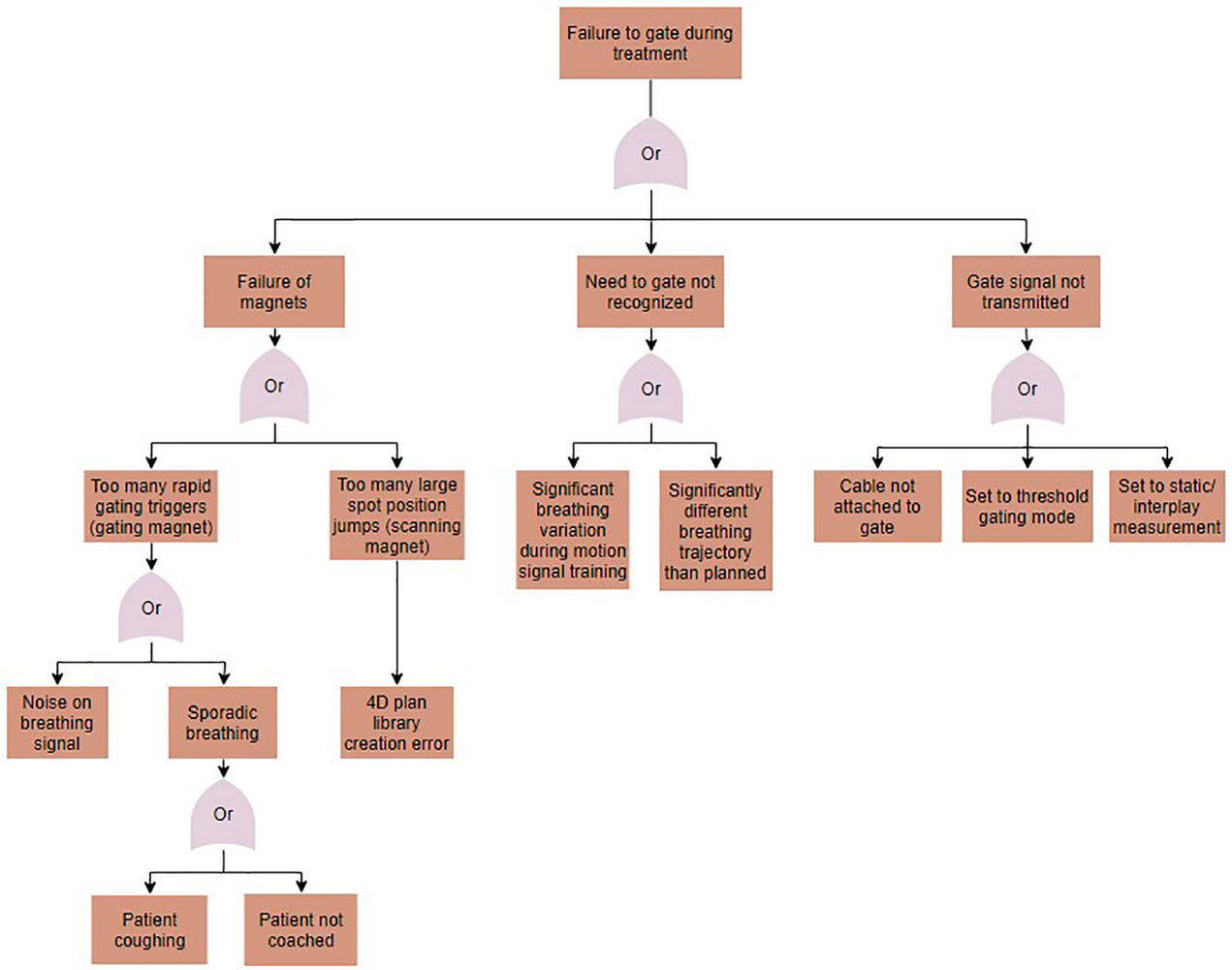

FIGURE 5 | A fault tree analysis for the case of gating failures during motion-synchronized dose deliveries.

gamma pass rates were found to be 99.4 and 96.0% for static and motion-compensated deliveries, respectively. The measured motion signals were used to reconstruct the delivered beam spot position. The comparability of the data for each setup was limited by the lack of direct correlation between analysis methods (51). The small-sized IC and film stack phantoms were found to have a relatively fast setup and execution. Due to the limited number of detectors, small-sized IC measurements provided less information in cases where results were nearly passing. In those cases, DDD dose reconstructions were necessary to determine the dose distributions. 2D dose measurements with the IC array detector took multiple times longer to deliver than the film stack and small-sized IC measurements, due to the multiple measurements at varying depths.

Each PSQA method was also assessed for the ability to detect motion-specific planning and setup errors. Errors in positioning and orientation of the motion-monitoring system were visible for all PSQA methods, but were least apparent in the film stack deliveries. Selection of the wrong number of motion phases were only visible in log file reconstruction and films, but had little impact on the delivery results. Delivering a few beam spots to the wrong positions, not delivering a few beam spots and using the wrong motion file during planning were both only visible in the log file reconstructions, but there were no measurable changes to the treatment delivery quality. Finally, selecting the incorrect motion compensation strategy was visible on film stack images and IC detector array measurements but was not immediately clear without log file reconstructions. Log file reconstructions were quicker than other methods, due to requiring no phantom setup time. Likewise, log file analysis, and to some extent, film analysis, did not require precise positioning. IC array detector measurements took nearly three times as long as small-sized IC measurements, but provided a higher number of measurement points. In both cases, measurement analysis programs are available to assess plan accuracy. Films require

additional time for digitizing and show a non-linear dose response. Calibrating the dose response of a film requires considerable effort before it can be used for QA measurements.

DISCUSSION

We have designed and tested a prospective risk analysis strategy for the motion-synchronized dose delivery system, developed for scanned ion beam therapy of moving targets. We created this strategy specifically to assess the safety of the motion mitigation portion of the DDS for its eventual use in the clinic. Additionally, we have implemented and tested solutions for possible errors related to motion mitigation. The major finding of this study is that we have identified the sources of and solutions to major errors with a comprehensive risk assessment strategy. We also obtained pre-clinical test results that suggest the clinical reliability in motion-synchronized dose delivery. The results of this study have determined that the proposed safety assessment tests can be utilized at ion therapy centers, which operate with the modular M-DDS.

The implication of this study is that the described comprehensive risk analysis strategy and proposed tests can serve as an example during initial safety, commissioning, and QA tests leading to implementation of the M-DDS into clinical use. This assessment is part of a larger effort to confirm and maintain the clinical safety of the M-DDS from the design stage through clinical implementation. The M-DDS has been implemented following good manufacturing practices, including testing at several stages and maintaining extensive documentation. The described preliminary safety tests suggest that the M-DDS is safe, reliable, and ready for additional tests, leading to eventually treating patients. Further, the proposed error tests and QA tests could be performed within clinically reasonable timeframes. The safety tests are not the final solution for commissioning and QA procedures within the clinic, but rather are an example of a general safety strategy for the M-DDS, which can be modified and extended to meet the specific needs of a particular clinic. Full acceptance testing and commissioning will be performed before re-implementing the modified DDS into the clinic.

This is the first implementation of a comprehensive, prospective safety assessment for pre-clinical testing of a motion-synchronized dose delivery system. The results of this study are coherent with the recommendations found in the TG-100 and other AAPM reports (2, 6, 11, 13, 52). All plan verification and QA tests were within clinical specifications. Log file analysis provided the additional benefit of recognizing individual beam spot errors and indicating other errors during treatment preparation that could otherwise be unnoticed and should be performed alone or along with regular plan verification.

TABLE 4 | Summary of pass-fail tests and results.

Error	Expected action	Result
Incorrect plan library structure		
Wrong number of beam spots in plan library	Setup error state	Passed
Missing motion information in plan header	"	"
Particle numbers below or above limitations	"	"
Plan library larger than size limitations	"	"
Beam delivery errors		
Motion signal lost	Beam aborted	"
Motion trajectory deviating from expected trajectory	Temporary gate	"
Scanning magnet failure	Interlock	"
Gating magnet failure	"	"
Delivery of a beam spot skipped	Treatment is halted	"
MMD file recording error	Treatment stops, errors message, and file dump	"
Treatment stops prematurely	Delivery data recorded	"
Motion calibration incomplete before delivery starts	Beam gate activated	"
Treatment setup errors		
Wrong motion compensation strategy selected	Set automatically from plan	"
Motion system not fully set up or not on	Delivery cannot start	"

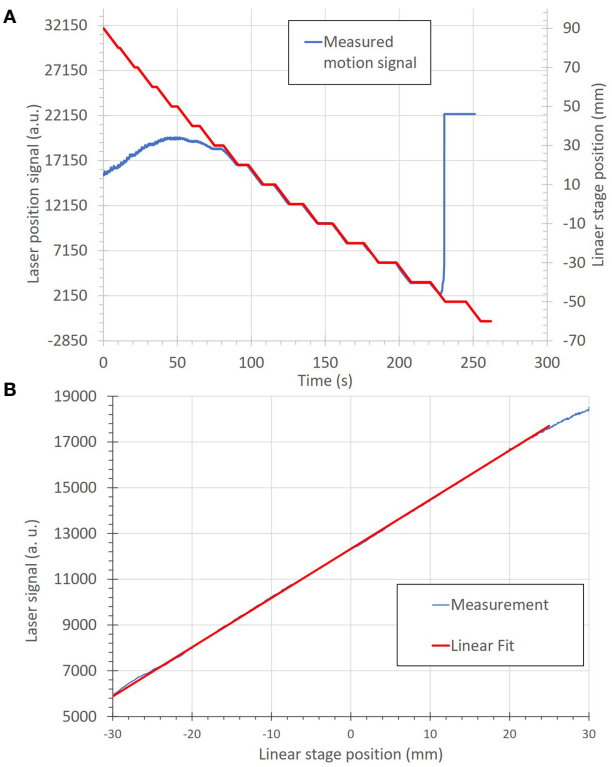

FIGURE 6 | **(A)** Correlation of motion position to the measured signal of the motion-monitoring device (an optical distance laser sensor) for a step-wise motion pattern. The motion positions, in mm, (red) are uploaded onto the linear stage as a motion file and used to move the linear stage. The motion-monitoring device then records the relative displacement (blue) as an analog signal. The left and right portions of the motion signal show where the motion-monitoring device is out of signal range. **(B)** A plot of position accuracy between the optical distance laser signal (in arbitrary units) and the linear stage position (in mm).

TABLE 5 | Summary of patient specific quality assurance results for four measurements.

QA test	Metric (pass criteria)		Static results	Motion mitigation results
Pinpoints	Dose deviation (± 5%)		± 2.4%	± 8.9%
Log files (planned to reconstructed)	Gamma index analysis (>90%)		99.4%	96.0%
Film stacks	Gamma index analysis (>90%)		92.4%	90.4%
IC detector to log file reconstructions	Gamma index analysis (>90%)	*Distal*	84.1% (0.9883)	91.6% (0.9901)
		Middle	100.0% (0.9947)	98.6% (0.9954)
		Proximal	99.4% (0.9983)	90.9% (0.9971)

These measurements included calculating 3D dose measurement agreement with 12 small-sized ionization chambers (IC), and calculating gamma index analysis pass rates for comparisons between log file reconstructions and treatment plans as well as IC array detector measurements. Acceptable criteria and analysis results are summarized.

Several studies have applied the safety assessment protocols presented in TG-100 to ion therapy (21, 53). To our knowledge, no studies have been performed to apply this approach to new technologies in ion therapy, including motion mitigation systems. Additionally, several studies have assessed the practicality of QA procedures. One study, by Hara et al. (54), describes a plan verification procedure for moving tumors. This strategy involves delivering patient plans to a 2D IC at three depths, and performing gamma analysis on each measurement. This study also concluded that this procedure is a beneficial QA procedure for moving tumors. Another study (55) described the process of plan verification with small-sized IC deliveries. The procedure and phantoms were modified in our study for motion compensation. Further, Matter et al. (56) investigated the capabilities of various plan verification procedures to ensure the integrity of treatment plans under a variety of planning errors. Of the measured errors, two cases were relevant considerations for motion-synchronized deliveries with the M-DDS: the "all spots shifted randomly" case, and the "increase in spot weights" case. In particular, residual motion within a motion phase can be as high as 1-2 mm, and is accounted for in planning margins. In contrast, small increases in spot weights may be possible when the beam is frequently gated or when there are frequent jumps in the scan position due to non-optimally created plans can result in non-trivial increases to the integral dose. As such, we conclude that log file analysis could provide a supplement to plan verification measurements. This study did not consider failures associated with using real-time imaging to monitor target motion. This is a vital part of motion-mitigation and will be investigated in future studies. Though a variety of imaging techniques and motion monitoring devices can be integrated with the M-DDS, additional risk analysis must be performed to identify and mitigate for failures associated with these devices.

Our study has several strengths. One is that this method is based on established methods (e.g., FMEA, FTA) that have been applied in clinics worldwide. It can be extended to any modular device with integrated motion mitigation strategies. Yet, it allows for identifying errors that may specifically occur when using motion synchronized delivery devices. Further, the strategy uses the official risk assessment proposed by the AAPM, can be applied to any motion-synchronized dose delivery implementation, and to any clinic that integrates the described M-DDS to their treatment systems. This strategy is a well-developed, well-known, and comprehensive risk analysis strategy. Though clinic-specific modifications will need to be made, the described approach can provide insight into potential complications, which could arise with the M-DDS. Finally, the presented quality assurance tests were designed with phantoms that are regularly found in proton and ion therapy clinics. These tests were performed at an ion therapy center (CNAO) under clinical conditions, with interlocks in place. QA and most PSQA tests were also performed at CNAO and GSI, except the film stack analysis, which was only performed at GSI.

One limitation of this study is that all safety procedures were tested with a predefined, 1D movement, generated by a motion-phantom. The motion patterns were well known and in complete agreement between the measured and actual motion. This is not a major limitation, as the delivery results with irregular motion will be characterized in future studies. Another limitation of this study is that no high-precision 3D dose distributions could be measured. 3D gels could potentially provide nearly instantaneous 3D dose distribution information. Gels produced by Maryanski et al. (57), which are readout with optical CT have recently been developed for 3D dosimetry of carbon ions. However, this strategy is still in the early stages of testing and has only been optimized for high doses for carbon ions. Another dosimeter for high precision 3D dose measurements would be measurements with a 2D IC array detector in a water tank phantom (58, 59). Though this strategy automatically provides high-resolution 3D dose information, this strategy requires delivering prohibitively long times for patient specific QA and assumes no phase dependence for motion-compensated deliveries; therefore, this method is better suited for beam commissioning. Another limitation of this study is that no independent dose calculations, such as Monte Carlo (MC) based dose calculations, were performed. However, this is not a major limitation, as MC dose calculations are typically time consuming; therefore, they are currently mainly performed to verify dose distributions when patient QA measurements do not pass. Additionally, the proposed patient verification methods are example solutions, and each clinic should select their appropriate plan verification method. Finally, MC performed at CNAO showed that MC simulations are sensitive to input conditions and simplifications to the MC models (60). Nevertheless, MC verification of patient plans has been growing in popularity and can serve as a powerful tool for independent dose calculation on well-characterized data sets.

The M-DDS is substantially complete and the current version has been transferred back to CNAO for use in the research room

there. Additional features are still in development that aim to handle irregular respiratory scenarios and other complications related to respiration; these will be completed before the M-DDS is implemented for clinical use. Additionally, interoperability with other centers and full compatibility to DICOM and I-HERO standards will be implemented, along with any necessary regulatory approvals for human use, followed by a full clinical commissioning. Before clinical use, the plan library structure must also be implemented into commercial treatment planning systems.

CONCLUSION

We have applied a comprehensive safety assessment strategy for the motion-synchronized portion of the dose delivery system. This work has shown that M-DDS is a clinically viable motion compensation strategy. The efficacy of possible QA procedures for motion-synchronized deliveries have been confirmed. Importantly, this strategy is specific to the motion-synchronized dose delivery system, but not to a specific clinic. Therefore, the presented methods can be adapted to other facilities using the M-DDS.

DATA AVAILABILITY STATEMENT

The original contributions presented in the study are included in the article/supplementary material. Further inquiries can be directed to the corresponding author.

AUTHOR CONTRIBUTIONS

ML and WN devised the topic of this work. CG and MDo devised the project. ML and MDo developed the M-DDS that is the device studied in this work. WN, CG, and MDu supervised this work. ML, MW, TS, and AP performed experiments, data gathering, and data analysis. ML wrote the manuscript with input from all of the authors. All authors contributed to the article and approved the submitted version.

FUNDING

This project has received funding from the European Union's Horizon 2020 research and innovation program under the Marie Sklodowska-Curie grant agreement No 675265, OMA—Optimization of Medical Accelerators.

ACKNOWLEDGMENTS

We would like to thank the medical physics staff at CNAO for their assistance in setting up dosimetry equipment, and the GSI workshop, for designing and building our detector holders and phantoms. We would also like to thank C Schuy for his feedback on designing beamtime experiments and for his work in preparing beamlines for experiments at GSI. Finally, we would like to thank C Hartmann-Sauter for his contributions to the development of Cave M at GSI. The research presented here is a result of a R&D project experiment SBIO at the beam line SIS-18 in the frame of FAIR Phase-0 supported by the GSI Helmholtzzentrum für Schwerionenforschung in Darmstadt (Germany).

REFERENCES

1. Purdie TG, Moseley DG, Bissonnette JP, Sharpe MB, Franks K, Bezjak A, et al. Respiration correlated cone-beam computed tomography and 4DCT for evaluating target motion in Stereotactic Lung Radiation Therapy. *Acta Oncol* (2006) 45(7):915–22. doi: 10.1080/02841860600907345
2. ICRU. ICRU Report 78: Prescribing, Recording and Reporting Proton-Beam Therapy. *J ICRU* (2007) 7(2):1–210. doi: 10.1093/jicru_ndm021
3. Nath R, Biggs PJ, Bova FJ, Ling CC, Purdy JA, van de Geijn J, et al. AAPM code of practice for radiotherapy accelerators: Report of AAPM Radiation Therapy Task Group No. 45. *Med Phys* (1994) 21(7):1093–121. doi: 10.1118/1.597398
4. Mestrovic A, Milette MP, Nichol A, Clark BG, Otto K. Direct aperture optimization for online adaptive radiation therapy. *Med Phys* (2007) 34 (5):1631–46. doi: 10.1118/1.2719364
5. International Electrotechnical Commission (IEC). *Guidelines for Radiotherapy Treatment Rooms Design*, Vol. 1997. (1997). Available at: https://global.ihs.com/doc_detail.cfm?document_name=IEC%2FTR%2061859&item_s_key=00257408#abstract-section.
6. Kutcher GJ, Coia L, Gillin M, Hanson WF, Leibel S, Morton RJ, et al. Comprehensive QA for radiation oncology: Report of AAPM Radiation Therapy Committee Task Group 40. *Med Phys* (1994) 21(4):581–618. doi: 10.1118/1.597316
7. Klein EE, Hanley J, Bayouth J, Yin F, Simon W, Dresser S, et al. Task Group 142 report: Quality assurance of medical acceleratorsa). *Med Phys* (2009) 36 (9Part1):4197–212. doi: 10.1118/1.3190392
8. Fraass B, Doppke K, Hunt M, Kutcher G, Starkschall G, Stern R, et al. American Association of Physicists in Medicine Radiation Therapy Committee Task Group 53: Quality assurance for clinical radiotherapy treatment planning. *Med Phys* (1998) 25(10):1773–829. doi: 10.1118/1.598373
9. Quality Assurance in Radiotherapy. (1998).
10. Guckenberger M, Andratschke N, Dieckmann K, Hoogeman MS, Hoyer M, Hurkmans C, et al. ESTRO ACROP consensus guideline on implementation and practice of stereotactic body radiotherapy for peripherally located early stage non-small cell lung cancer. *Radiother Oncol* (2017) 124(1):11–7. doi: 10.1016/j.radonc.2017.05.012
11. Arjomandy B, Taylor P, Ainsley C, Safai S, Sahoo N, Pankuch M, et al. AAPM task group 224: Comprehensive proton therapy machine quality assurance. *Med Phys* (2019) 46(8):e678–705. doi: 10.1002/mp.13622
12. National Institutes of Health. *PAR-13-371: Planning for a National Center for Particle Beam Radiation Therapy Research (P20). p20 Exploratory Grants 2013*, (2013) [cited 2020 06.10.2020]; Available at: https://grants.nih.gov/grants/guide/pa-files/PAR-13-371.html.
13. Huq MS, Fraass BA, Dunscombe PB, Gibbons JPJr, Ibbott GS, Mundt AJ, et al. The report of Task Group 100 of the AAPM: Application of risk analysis methods to radiation therapy quality management. *Med Phys* (2016) 43 (7):4209–62. doi: 10.1118/1.4947547
14. Ishikura S. Quality Assurance of Radiotherapy in Cancer Treatment: Toward Improvement of Patient Safety and Quality of Care. *Jpn J Clin Oncol* (2008) 38 (11):723–9. doi: 10.1093/jjco/hyn112
15. Fallon EF, Chadwick L, van der Putten W. Learning from Risk Assessment in Radiotherapy. In: *Digital Human Modeling*. Berlin, Heidelberg: Springer Berlin Heidelberg (2009).
16. Malicki J, Bly R, Bulot M, Godet J, Jahnen A, Krengli M, et al. Patient safety in external beam radiotherapy, results of the ACCIRAD project: Current status

of proactive risk assessment, reactive analysis of events, and reporting and learning systems in Europe. *Radiother Oncol* (2017) 123(1):29–36. doi: 10.1016/j.radonc.2017.02.016
17. Koo J, Shin DO, Lim YK, Park S, Rah JE, Hwang UJ, et al. Radiotherapy Risk Estimation Based on Expert Group Survey. *Front Phys* (2019) 7(118). doi: 10.3389/fphy.2019.00118
18. Veronese I, De Martin E, Martinotti AS, Fumagalli ML, Vite C, Redaelli I, et al. Multi-institutional application of Failure Mode and Effects Analysis (FMEA) to CyberKnife Stereotactic Body Radiation Therapy (SBRT). *Radiat Oncol (London England)* (2015) 10:132–2. doi: 10.1186/s13014-015-0438-0
19. Faught JT, Balter PA, Johnson JL, Kry SF, Court LE, Stingo FC, et al. An FMEA evaluation of intensity modulated radiation therapy dose delivery failures at tolerance criteria levels. *Med Phys* (2017) 44(11):5575–83. doi: 10.1002/mp.12551
20. Ralston A, Graham P, Poder J, Yuen J. The RABBIT risk-based approach to clinical implementation of new technology: SRS as a case study. *Tech Innov Patient Support Radiat Oncol* (2020) 14:51–60. doi: 10.1016/j.tipsro.2020.04.003
21. Cantone MC, Ciocca M, Dionisi F, Fossati P, Lorentini S, Krengli M, et al. Application of failure mode and effects analysis to treatment planning in scanned proton beam radiotherapy. *Radiat Oncol (London England)* (2013) 8:127–7. doi: 10.1186/1748-717X-8-127
22. Broggi S, Cantone MC, Chiara A, Muzio ND, Longobardi B, Mangili P, et al. Application of failure mode and effects analysis (FMEA) to pretreatment phases in tomotherapy. *J Appl Clin Med Phys* (2013) 14(5):265–77. doi: 10.1120/jacmp.v14i5.4329
23. Kim J, Miller B, Siddiqui MS, Movsas B, Glide-Hurst C. FMEA of MR-Only Treatment Planning in the Pelvis. *Adv Radiat Oncol* (2019) 4(1):168–76. doi: 10.1016/j.adro.2018.08.024
24. Graeff C. Motion mitigation in scanned ion beam therapy through 4D-optimization. *Phys Med* (2014) 30(5):570–7. doi: 10.1016/j.ejmp.2014.03.011
25. Dueck J, Knopf A, Lomax A, Albertini F, Persson GF, Josipovic M, et al. Robustness of the Voluntary Breath-Hold Approach for the Treatment of Peripheral Lung Tumors Using Hypofractionated Pencil Beam Scanning Proton Therapy. *Int J Radiat Oncol Biol Phys* (2016) 95(1):534–41. doi: 10.1016/j.ijrobp.2015.11.015
26. Grassberger C, Dowdell S, Sharp G, Paganetti H. Motion mitigation for lung cancer patients treated with active scanning proton therapy. *Med Phys* (2015) 42(5):2462–9. doi: 10.1118/1.4916662
27. Mori S, Knopf A-C, Umegaki K. Motion management in particle therapy. *Med Phys* (2018) 45(11):e994–e1010. doi: 10.1002/mp.12679
28. Fracchiolla F, Dionisi F, Giacomelli IHild S, Esposito PG. Implementation of proton therapy treatments with pencil beam scanning of targets with limited intrafraction motion. *Phys Med* (2019) 57:215–20. doi: 10.1016/j.ejmp.2019.01.007
29. Furukawa T, Inaniwa T, Sato S, Shirai T, Mori S, Takeshita E, et al. Moving target irradiation with fast rescanning and gating in particle therapy. *Med Phys* (2010) 37(9):4874–9. doi: 10.1118/1.3481512
30. Lis M, Donetti M, Newhauser W, Durante M, Wolf M, Graeff C, et al. A modular dose delivery system for treating moving targets with scanned ion beams: Performance and safety characteristics, and preliminary tests. *Phys Med* (2020) 76:307–16. doi: 10.1016/j.ejmp.2020.07.029
31. Wolf ME, Anderle K, Durante M, Graeff C. Robust treatment planning with 4D intensity modulated carbon ion therapy for multiple targets in stage IV non-small cell lung cancer. *Phys Med Biol* (2020). doi: 10.1088/1361-6560/aba1a3
32. Fattori G, Safai S, Carmona PF, Peroni M, Perrin R, Weber, et al. Monitoring of breathing motion in image-guided PBS proton therapy: comparative analysis of optical and electromagnetic technologies. *Radiat Oncol* (2017) 12 (1):63. doi: 10.1186/s13014-017-0797-9
33. Bertholet J, Knopf A, Eiben B, McClelland J, Grimwood A, Harris E, et al. Real-time intrafraction motion monitoring in external beam radiotherapy. *Phys Med Biol* (2019) 64(15):15TR01. doi: 10.1088/1361-6560/ab2ba8
34. The World Health Report 2008. Global Initiative on Radiation Safety in Healthcare Settings, in Technical Meeting Report. In: World Health Organization (2008).
35. Bloch HP, Geitner FK. Preface. In: FK Geitner, HP Bloch, editors. *Machinery Failure Analysis and Troubleshooting, 4th ed.* Oxford: Butterworth-Heinemann (2012). p. xv.
36. Mirandola A, Molinelli S, Vilches Freixas G, Mairani A, Gallio E, Panizza D, et al. Dosimetric commissioning and quality assurance of scanned ion beams at the Italian National Center for Oncological Hadrontherapy. *Med Phys* (2015) 42(9):5287–300. doi: 10.1118/1.4928397
37. Lujan AE, Balter JM, Ten Haken RK. A method for incorporating organ motion due to breathing into 3D dose calculations in the liver: Sensitivity to variations in motion. *Med Phys* (2003) 30(10):2643–9. doi: 10.1118/1.1609057
38. Yonai S, Arai C, Shimoyama K, Fournier-Bidoz N. Experimental Evaluation Of Dosimetric Characterization Of Gafchromic EBT3 And EBT-XD Films For Clinical Carbon Ion Beams. *Radiat Prot Dosimetry* (2018) 180(1-4):314–8. doi: 10.1093/rpd/ncy006
39. Spielberger B, Scholz M, Kramer M, Kraft G. Calculation of the x-ray film response to heavy charged particle irradiation. *Phys Med Biol* (2002) 47 (22):4107–20. doi: 10.1088/0031-9155/47/22/313
40. Castriconi R, Ciocca M, Mirandola A, Sini C, Broggi S, Schwarz M. Dose–response of EBT3 radiochromic films to proton and carbon ion clinical beams. *Phys Med Biol* (2016) 62(2):377–93. doi: 10.1088/1361-6560/aa5078
41. Kataria T, Sharma K, Subramani V, Karrthick KP, Bisht SS. Homogeneity Index: An objective tool for assessment of conformal radiation treatments. *J Med Phys* (2012) 37:207–13. doi: 10.4103/0971-6203.103606
42. Low DA, Harms WB, Mutic S, Purdy JA. A technique for the quantitative evaluation of dose distributions. *Med Phys* (1998) 25(5):656–61. doi: 10.1118/1.598248
43. Gambarini G, Bettega D, Camoni G, Barzon G, Bettinelli L, Giove D, et al. Development of a procedure for quenching-effect correction in images of absorbed dose from protons or carbon ions acquired with Gafchromic EBT3 films. *Radiat Phys Chem* (2019) 155:138–45. doi: 10.1016/j.radphyschem.2018.06.019
44. Karger CP, Jakel O, Palmans H, Kanai T. Dosimetry for ion beam radiotherapy. *Phys Med Biol* (2010) 55(21):R193–234. doi: 10.1088/0031-9155/55/21/R01
45. McKenzie EM, Balter PA, Stingo FC, Jones J, Followill DS, Kry SF. Reproducibility in patient-specific IMRT QA. *J Appl Clin Med Phys* (2014) 15(3):4741–1.
46. McCaw TJ, Micka JA, DeWerd LA, McCaw TJ, Micka JA, DeWerd LA. Development and characterization of a three-dimensional radiochromic film stack dosimeter for megavoltage photon beam dosimetry. *Med Phys* (2014) 41 (5):052104. doi: 10.1118/1.4871781
47. Henkner K, Winter M, Echner G, Ackermann B, Brons S, Horn J, et al. A motorized solid-state phantom for patient-specific dose verification in ion beam radiotherapy. *Phys Med Biol* (2015) 60:7151. doi: 10.1088/0031-9155/60/18/7151
48. Choi K, Mein SB, Kopp B, Magro G, Molinelli S, Ciocca M, et al. FRoG-A New Calculation Engine for Clinical Investigations with Proton and Carbon Ion Beams at CNAO. *Cancers (Basel)* (2018) 10(11). doi: 10.3390/cancers10110395
49. Karger CP, Jäkel O, Hartmann GH. A system for three-dimensional dosimetric verification of treatment plans in intensity-modulated radiotherapy with heavy ions. *Med Phys* (1999) 26(10):2125–32. doi: 10.1118/1.598728
50. Meschini G, Seregni M, Pella A, Ciocca M, Fossati P, Valvo F, et al. Evaluation of residual abdominal tumour motion in carbon ion gated treatments through respiratory motion modelling. *Phys Med* (2017) 34:28–37. doi: 10.1016/j.ejmp.2017.01.009
51. Zhen H, Nelms BE, Tomé WA. Moving from gamma passing rates to patient DVH-based QA metrics in pretreatment dose QA. *Med Phys* (2011) 38 (10):5477–89. doi: 10.1118/1.3633904
52. Bevins NB, Silosky MS, Badano A, Marsh RM, Flynn MJ, Walz-Flannigan AI, et al. Practical application of AAPM Report 270 in display quality assurance: A report of Task Group 270. *Med Phys* (2020). doi: 10.1002/mp.14227
53. Filippini R, Urschütz P. Risk management for a particle therapy accelerator *The MedAustron experience* (2018). 1879–86.
54. Hara Y, Furukawa T, Tansho R, Saraya Y, Mizushima K, Saotome N, et al. (2016). A Patient-Specific QA Procedure for Moving Target Irradiation in Scanned Ion Therapy, in: *IBIC2015 4th International Beam Instrumentation Conference*. 62–65
55. Arjomandy B, Sahoo N, Ding X, Gillin M. Use of a two-dimensional ionization chamber array for proton therapy beam quality assurance. *Med Phys* (2008) 35(9):3889–94. doi: 10.1118/1.2963990

56. Matter M, Nenoff L, Meier G, Weber DC, Lomax AJ, Albertini F, et al. Alternatives to patient specific verification measurements in proton therapy: a comparative experimental study with intentional errors. *Phys Med Biol* (2018) 63(20):205014. doi: 10.1088/1361-6560/aae2f4
57. Maryanski MJ, Gore JC, Kennan RP, Schulz RJ. NMR relaxation enhancement in gels polymerized and cross-linked by ionizing radiation: A new approach to 3D dosimetry by MRI. *Magn Reson Imaging* (1993) 11(2):253–8. doi: 10.1016/0730-725X(93)90030-H
58. Schuy C, Simeonov Y, Durante M, Zink K, Weber U. Technical note: Vendor-agnostic water phantom for 3D dosimetry of complex fields in particle therapy. *J Appl Clin Med Phys* (2020) 21:227–32. Accepted. doi: 10.1002/acm2.12996
59. Lin L, Kang M, Solberg T, Mertens T, Bäumer C, Ainsley L, et al. Use of a novel two-dimensional ionization chamber array for pencil beam scanning proton therapy beam quality assurance. *J Appl Clin Med Phys* (2015) 16:270. doi: 10.1120/jacmp.v16i3.5323
60. Lima TVM, Dosanjh M, Ferrari A, Molineli S, Ciocca M, Mairani A. Monte Carlo Calculations Supporting Patient Plan Verification in Proton Therapy. *Front Oncol* (2016) 6(62). doi: 10.3389/fonc.2016.00062

Conflict of Interest: The authors declare that the research was conducted in the absence of any commercial or financial relationships that could be construed as a potential conflict of interest.

Copyright © 2021 Lis, Newhauser, Donetti, Wolf, Steinsberger, Paz, Durante and Graeff. This is an open-access article distributed under the terms of the Creative Commons Attribution License (CC BY). The use, distribution or reproduction in other forums is permitted, provided the original author(s) and the copyright owner(s) are credited and that the original publication in this journal is cited, in accordance with accepted academic practice. No use, distribution or reproduction is permitted which does not comply with these terms.

frontiers in Oncology

MINI REVIEW
published: 12 April 2021
doi: 10.3389/fonc.2021.616831

The Particle Radiobiology of Multipotent Mesenchymal Stromal Cells: A Key to Mitigating Radiation-Induced Tissue Toxicities in Cancer Treatment and Beyond?

Alexander Rühle[1,2,3], *Anca-Ligia Grosu*[1,2] *and Nils H. Nicolay*[1,2,3]*

[1] Department of Radiation Oncology, University of Freiburg - Medical Center, Freiburg, Germany, [2] German Cancer Consortium (DKTK) Partner Site Freiburg, German Cancer Research Center (dkfz), Heidelberg, Germany, [3] Department of Molecular Radiation Oncology, German Cancer Research Center (dkfz), Heidelberg, Germany

OPEN ACCESS

Edited by:
Daniel Michael Trifiletti,
Mayo Clinic Florida, United States

Reviewed by:
Igor Maiborodin,
Institute of Chemical Biology and Fundamental Medicine (RAS), Russia
Umberto Galderisi,
University of Campania Luigi Vanvitelli, Italy

***Correspondence:**
Nils H. Nicolay
nils.nicolay@uniklinik-freiburg.de

Specialty section:
This article was submitted to Radiation Oncology, a section of the journal Frontiers in Oncology

Received: 13 October 2020
Accepted: 23 March 2021
Published: 12 April 2021

Citation:
Rühle A, Grosu A-L and Nicolay NH (2021) The Particle Radiobiology of Multipotent Mesenchymal Stromal Cells: A Key to Mitigating Radiation-Induced Tissue Toxicities in Cancer Treatment and Beyond? Front. Oncol. 11:616831. doi: 10.3389/fonc.2021.616831

Mesenchymal stromal cells (MSCs) comprise a heterogeneous population of multipotent stromal cells that have gained attention for the treatment of irradiation-induced normal tissue toxicities due to their regenerative abilities. As the vast majority of studies focused on the effects of MSCs for photon irradiation-induced toxicities, little is known about the regenerative abilities of MSCs for particle irradiation-induced tissue damage or the effects of particle irradiation on the stem cell characteristics of MSCs themselves. MSC-based therapies may help treat particle irradiation-related tissue lesions in the context of cancer radiotherapy. As the number of clinical proton therapy centers is increasing, there is a need to decidedly investigate MSC-based treatments for particle irradiation-induced sequelae. Furthermore, therapies with MSCs or MSC-derived exosomes may also become a useful tool for manned space exploration or after radiation accidents and nuclear terrorism. However, such treatments require an in-depth knowledge about the effects of particle radiation on MSCs and the effects of MSCs on particle radiation-injured tissues. Here, the existing body of evidence regarding the particle radiobiology of MSCs as well as regarding MSC-based treatments for some typical particle irradiation-induced toxicities is presented and critically discussed.

Keywords: stem cell therapy, normal tissue toxicities, radiotherapy, particle irradiation, mesenchymal stem cells, mesenchymal stromal cells, space irradiation, radiation accidents

INTRODUCTION

Mesenchymal stromal cells (MSCs) were first isolated from the human bone marrow by Friedenstein and colleagues in the late 1960s (1, 2), but have since been described in various other tissue types such as adipose and glandular tissues, brain and umbilical cord (3–6) and many other organs. As MSCs are a heterogeneous population that can only be characterized by combining

molecular and functional traits, the International Society for Cellular Therapy (ISCT) proposed minimal defining criteria for MSCs in order to enhance comparability between the various studies: MSCs are required to adhere to plastic surfaces, exhibit a pattern of positive and (absent) negative surface markers and possess the ability to differentiate along the adipogenic, osteogenic and chondrogenic lineages (7). Currently, MSC-based treatments hold approval for several indications including graft-versus-host disease, Crohn's-related enterocutaneous fistular disease, bone regeneration, osteoarthritis and cartilage repair (8–11). MSCs possess several characteristics that make them an attractive cell type for cell-based treatments: MSCs can be conveniently isolated and expanded; they are immune-privileged cells, therefore not requiring immunosuppression prior to application, and exhibit the ability to migrate to damaged tissues (12–15). Meta-analyses with more than 1000 patients showed the general safety of MSC-based treatments and did not reveal any severe adverse effects (16). As MSCs also home to tissues damaged by ionizing radiation, these cells came into focus as potential treatments for radiation-induced toxicities, for instance, radiation mucositis, pulmonary fibrosis and enteritis (17–20).

In the context of treating radiation-induced tissue injuries, the MESRIX trial provided a major step towards the routine usage of MSCs in radiation oncology. This randomized, placebo-controlled, double-blinded phase I/II study evaluated for the first time the efficacy of an MSC application for radiotherapy-induced tissue damage (21): Autologous adipose tissue-derived MSCs were transplanted into the submandibular salivary glands of patients with severe radiotherapy-related xerostomia at three or more years after treatment. Upon MSC administration, salivary flow rates were found significantly increased compared to the placebo group, and consistently, xerostomia symptoms decreased in MSC-treated but not in placebo-treated patients. Based on these encouraging results, a follow-up trial (NCT03874572) aims to validate these findings also for allogenic MSCs.

So far, most *in vitro* and *in vivo* studies have focused on the impact of photon irradiation on MSCs, and little is known about the particle radiobiology of these multipotent cells, which is a crucial step towards the usage of MSC-based therapies for particle radiation-associated tissue damage, e.g. after particle radiotherapy or during manned deep space flight (22–24).

MATERIAL AND METHODS

The databases PubMed, Google Scholar and Web of Science were screened for studies investigating the impact of MSC-based treatments for particle irradiation-induced toxicities as well as the influence of particle irradiation on MSCs by using the search terms *mesenchymal stem cells/mesenchymal stromal cells* in combination with *protons*, *proton radiotherapy*, *helium ions*, *alpha particles*, *carbon ions*, *carbon ion radiotherapy*, *oxygen ions*, *iron ions*, *heavy ions* and *heavy ion radiotherapy*, respectively.

APPLICATION OF MSCS FOR THE ATTENUATION OF TYPICAL TOXICITIES AFTER PARTICLE RADIATION

Particle Radiotherapy in Cancer Treatment

Currently, heavy ion radiotherapy most commonly employs ^{12}C carbon ions for patient treatment. Clinical feasibility and benefits of carbon ion radiotherapy have been studied in various malignancies such as intracranial tumors, head-and-neck cancers, lung cancer, gastrointestinal malignancies, prostate cancer, sarcomas, gynecological cancers and pediatric malignancies (25).

Head-and-Neck Tumors

Particle radiotherapy has been shown to be an effective treatment for salivary gland, nasopharyngeal and sinunasal carcinomas (25–29); however, bone- and mucosa-related toxicities are common, and no causative treatments have been licensed to date for these radiation-induced lesions.

Radiation-related mucositis is a common acute normal tissue toxicity and affects most patients receiving radiotherapy for head-and-neck malignancies. It considerably worsens patients' quality of life, increases the risk for malnutrition and infection and can therefore result in treatment interruptions that may in turn deteriorate oncological outcomes. The incidence of severe mucositis after proton irradiation for head-and-neck squamous cell carcinomas ranges between 40 and 79% (30). The impact of both bone marrow- and adipose tissue-derived MSCs on radiation-induced mucositis has been examined in several preclinical studies (19, 31–33). In the study of Maria and colleagues, MSCs significantly attenuated radiation-induced oral mucositis in mice, as evident by reduced ulcer duration and ulcer size, leading to increased weight as well as improved hydration and nutritional status (31). Osteoradionecrosis constitutes another rare but severe chronic toxicity after head-and-neck radiotherapy and is characterized by chronically exposed bone structures that fail to heal within 90 days after irradiation. In the head-and-neck region, osteoradionecrosis commonly affects the mandibular bone, and the incidence of mandibular osteoradionecrosis is reported to be less than 10% in most studies after intensity-modulated radiotherapy, although the variation of incidence in the literature is wide (34). The pathophysiology of osteoradionecrosis is complex and is driven by chronic inflammation, hypovascularity, hypoxia and hypocellularity (35). Treatment aims at alleviating symptoms and may comprise antibiotic treatment, surgical debridement, reconstructive surgery and hyperbaric oxygen; however, management of mandibular osteoradionecrosis remains a clinical challenge (36). Although the incidence of mandibular or maxillary osteoradionecrosis may be lower after carbon ion radiotherapy compared to photon radiotherapy, there are several case reports describing severe cases of osteoradionecrosis after carbon ion treatment (37, 38). In a retrospective analysis, 3 of 63 patients developed grade 3 osteoradionecrosis after carbon ion radiotherapy of head-and-neck malignancies (39). Stem-cell based treatments using MSCs obtained from the bone marrow,

adipose tissue or tonsils have been examined for osteoradionecrosis after photon irradiation in four *in vivo* studies and in two clinical case reports (40–46).

While it is conceivable that MSCs may exert their beneficial effects regarding immunomodulation and replacement of functional cells also after carbon ion irradiation, confirmative data for the treatment of particle radiation-induced mucositis and osteoradionecrosis are still lacking.

Prostate Cancer

In a *post-hoc* analysis including more than 1000 patients with prostate cancer receiving carbon ion radiotherapy within prospective phase II trials, the 10-year rates of moderate-to-severe gastrointestinal and genitourinary toxicities were found to be 1.7% and 11.7%, respectively (47). Analyses of the SEER database comparing photon and proton radiotherapy for prostate cancer observed an increased risk for rectal bleeding in patients treated with particle radiation (48). MSCs have been successfully investigated for radiation-induced proctitis, cystitis and fistulas. For instance, four patients received allogeneic bone marrow-derived MSCs for hemorrhagic radiation-induced fistulizing colitis after a radiation oncology accident at a public hospital in France, in which prostate cancer patients were overdosed by up to 30% (49). While two patients exhibited a significant response regarding pain and hemorrhage, another patient experienced a relapse after 6 months that was responsive to a second MSC administration. Considering these encouraging results, a prospective phase II trial is currently evaluating the impact of MSC-based treatments for late severe gastrointestinal complications such as proctitis and cystitis (PRISME trial, NCT02814864). However, similar to the other discussed late sequelae here, there are no studies available that exclusively investigate MSC-based therapies after proton or carbon ion radiotherapy.

MSC Administration as a Treatment Against Acute Radiation Syndrome

The acute radiation syndrome (ARS) represents a complex clinical situation, consisting of the hematopoietic syndrome, the gastrointestinal syndrome and (only clinically relevant for doses exceeding 10 Gy) the cerebrovascular syndrome (50). ARS regularly occurs after radiation exposure of the whole body with doses exceeding 0.5-1 Gy over a short time period. Currently, the standard of care for ARS consists of mainly symptomatic measures, e.g. intravenous hydration, antiemetic and analgesics medication, antibiotic treatment, blood transfusions, application of hematopoietic growth factors and rarely stem cell transplantation. Depending on the extent of medical interventions, the $LD_{50/60}$ (dose that kills 50% of the population within the first 60 days) ranges between 2.5 and 5 Gy. There are several scenarios in which a particle radiation-induced ARS may occur, e.g. during radiation accidents, nuclear terrorism or warfare and in deep space. The rising number of centers providing particle radiotherapy as well as the increasing usage of nuclear technology for medical purposes, industrial procedures and military functions emphasizes the importance of effective medical countermeasures to treat particle radiation-induced ARS.

Animal studies have shown beneficial effects of MSC-based treatments (including both bone marrow MSCs and MSC-derived exosomes) on the hematopoietic system in lethally irradiated mice (51–54). There are also several case reports showing both the feasibility and efficacy of MSC-based therapies for the treatment of tissue damage caused by radiation accidents (55–58). However, no studies have yet been reported that described the impact of MSC-based therapies on particle irradiation-induced ARS. MSCs from different tissues of origin (bone marrow and umbilical cord) have successfully been investigated for ARS treatment (51, 59). Besides its relevance for unintended radiation accidents, stem cell-based treatments including both MSCs and hematopoietic stem cells are discussed also in the case of nuclear terrorism (60). In this context, the United States Army Medical Research Institute of Chemical Defense (USAMRICD) has established production methods in order to have MSC-based treatments available for ARS (61).

RESPONSES OF MSCS TO PARTICLE RADIATION EXPOSURE

For photon radiotherapy, it has been demonstrated that MSCs from different tissues of origin (e.g. bone marrow, adipose tissue, umbilical cord) are relatively radioresistant and maintain their stem cell traits even after high radiation doses (23, 62, 63). A high anti-oxidative capacity, an effective DNA double-strand break repair, low levels of pro-apoptotic proteins (e.g. Bim and Puma) accompanied by high levels of anti-apoptotic proteins (e.g. Bcl-2 and Bcl-XL) have been reported to contribute to photon radioresistance of these multipotent stromal cells (64, 65). However, only limited data are available on the particle radiobiology of MSCs, and it remains unclear if the photon radioresistance can be extrapolated to radiation with protons or heavier particles. To date, proton radiation has not yet been systematically studied regarding the MSC radiobiology as it is believed to biologically resemble photon radiation. However, there are limited data available on the radiation effects of ^{12}C and heavier particles such as ^{56}Fe on MSCs.

Cellular Survival After Particle Irradiation

Work by our group demonstrated a relatively radioresistant phenotype of bone marrow-derived MSCs after ^{12}C particle radiation (**Table 1**). The relative biological effectiveness (RBE) calculated at 10% clonogenic survival in bone marrow-derived MSCs ranged between 2.0 and 3.1 compared to photon radiation, underpinning the known heterogeneity of MSCs (69). In line with a radioresistant phenotype after particle radiation, apoptosis rates in bone marrow-MSCs remained low even after exposure to 4 Gy of ^{12}C irradiation. However, no data are available for the influence of protracted courses of low-dose ^{12}C radiotherapy on MSCs that may be more relevant in the space environment and also during radiation exposure in the time of cancer treatment.

TABLE 1 | Summary of preclinical studies that investigated the effects of different types of particle irradiation on MSCs.

Authors and year	Reference	MSCs' species and tissue/Animal model	Particle type	Main findings
Almeida-Porada et al., 2018	(66)	Human bone marrow	Protons +^{56}Fe	• More pronounced deleterious effects after sequential proton and ^{56}Fe ion IR on both MSCs and HSCs than after exposure to either ion alone • Upregulation of cytokines involved in the maintenance of hematopoiesis and immune cell development after ^{56}Fe ion IR (but downregulation after proton IR) • Persistence of transcriptional changes induced by protons and ^{56}Fe ions over several passages in culture (in contrast to photons)
Alessio et al., 2017	(67)	Human bone marrow	α particles	• Reduction of S-phase cells after 0.04 Gy and 2 Gy α particle IR • Elevated apoptosis rates at 48 hours after 2 Gy α particle IR but not after photons • More residual DNA double-strand breaks at 48 hours after exposure to 2 Gy α particles compared to 2 Gy photons • Increased pATM activation after 2 Gy α particle IR than after 2 Gy photon IR
Kurpinski et al., 2009	(68)	Human bone marrow	^{56}Fe	• Pronounced G2/M phase arrest after 1 Gy^{56}Fe IR • Maintenance of osteogenic differentiation after 1 Gy^{56}Fe IR • Higher p53 activation after ^{56}Fe exposure compared to photons • More pronounced transcriptomic effects regarding DNA replication, DNA strand elongation and DNA binding/transferase activity for^{56}Fe than for photons
Nicolay et al., 2015	(69)	Human bone marrow	^{12}C	• RBE values of ^{12}C between 2.0 and 3.1 (at 10% clonogenic survival) • Maintenance of stem cell characteristics • Pronounced G2/M phase arrest after 4 Gy^{12}C IR • No increases in apoptosis after 4 Gy^{12}C IR • No residual DNA double-strand breaks after 4 Gy^{12}C IR • Strong phosphorylation of pATM at 2 hours after 4 Gy^{12}C IR but return to baseline levels after 24 hours

HSC, hematopoietic stem cell, IR, ionizing radiation, RBE, relative biological effectiveness.

The different biological effects between photon and ^{56}Fe irradiation on human bone marrow-MSCs have also been thoroughly characterized *in vitro* (68). While it was reported that neither photon nor ^{56}Fe ions impaired the osteogenic differentiation capability of MSCs, ^{56}Fe irradiation with 1 Gy resulted in a G2/M-phase arrest, which was more pronounced than after physically equivalent doses of photon irradiation. Microarray analyses showed that several genes playing a role in cell cycle progression including cyclin B1 and cyclin E2 were significantly downregulated after 0.1 Gy ^{56}Fe ions, while only a marginal response was observed after photon radiation. Additionally, a more pronounced activation of p53 was found after ^{56}Fe ion radiation than after photon treatment.

While these analyses were based on 2D systems, some groups also investigated the effects of particle irradiation on adipose-derived stem cells in 3D sphere cultures based on agar coating (70). Both after photon and carbon ion radiation, radiation sensitivity was higher in 2D culture than in 3D culture, which could to some extent be related to the development of radioprotective tissue hypoxia inside of the 3D spheres. In this regard, one should take into consideration that particle irradiation can partly overcome the radioresistance caused by tissue hypoxia (71).

Stem Cell Characteristics After Particle Irradiation

The influence of particle radiation on the defining stem cell characteristics has been investigated both for ^{12}C and ^{56}Fe ions. After ^{12}C irradiation, bone marrow-derived MSCs maintained their adhesive and cellular motility abilities independently of the MSC donor as well as their multi-lineage differentiation capability, which are all pre-requisites for the cells' regenerative effects (69). Kurpinski et al. could show that the osteogenic differentiation potential of human bone marrow-derived MSCs was maintained after exposure to 1 Gy ^{56}Fe ions. While undirected cellular motility as assessed by time-lapse microscopy remained unaffected after ^{12}C irradiation, directed migration towards particle-irradiated hematopoietic cells has not been examined so far. For lighter alpha particles, the preservation of MSC functions seems to depend on the dose, and only higher doses (2 Gy) have been shown to inhibit the stemness capacity of bone marrow MSCs (67).

DNA Damage Repair After Particle Irradiation

As particle irradiation induces clustered and more complex DNA lesions than photon irradiation, many cell lines have been found to exhibit increased numbers of initial and residual DNA lesions after physically equivalent doses of particle radiation (72–74). However, γH2AX foci analyses in human bone marrow-derived MSCs revealed an effective DNA double strand-break repair after 4 Gy ^{12}C irradiation as evident by low numbers of residual double strand-breaks and only temporary activation of the DNA double-strand break signaling pathways (69). This effective DNA double strand-break repair may also contribute to the reported low apoptosis rates after ^{12}C irradiation in this study (69). However, in the study of Alessio, residual γH2AX levels were significantly higher after 2 Gy alpha particle irradiation than after 2 Gy photon irradiation in bone marrow-isolated MSCs (67). In line with these findings, the authors also observed increased pATM expression at 48 hours after 2 Gy alpha particle irradiation when compared to baseline levels, which was not observed after 2 Gy photon irradiation. Lower alpha particle doses of 0.04 Gy were found to result in an upregulation of pATM at 1 hour after exposure and a

decline at later timepoints; additionally, there was no significant difference regarding the number of γH2AX-positive cells at 48 hours after 0.04 Gy alpha particle irradiation compared to unirradiated controls. In the study of Kurpinski and colleagues, pathway and network analyses of transcriptomic profiles revealed differential effects of ^{56}Fe and photons on DNA replication, DNA strand elongation and DNA binding/transferase activity of human bone marrow-MSCs with a more pronounced effect of ^{56}Fe ions on these pathways. Furthermore 1 Gy^{56}Fe ions resulted in a stronger activation of p53 than 1 Gy photons.

MSC-Based Treatment Concepts for Space Radiation-Induced Toxicities

Galactic cosmic rays (GCR) and solar cosmic radiation (SCR) constitute the main components of space irradiation. With an proportion of about 90%, protons form by far the largest component of both GCR and SCR, followed by helium ions (about 10%), electrons and heavier ions (75). Solar particle events (SPEs) as part of SCR, are unpredictable events that occur when protons are accelerated during a flare or during a coronal mass ejection. Besides highly energetic protons and helium ions, SPEs include heavier charged (HZE) particles such as carbon, oxygen and iron ions. Long-term missions to the Mars that may last more than 2 years harbor the risk for considerable radiation exposures, as the shielding provided by the Earth's magnetic field is absent. Therefore, the National Aeronautics and Space Administration (NASA) classifies the ARS caused by SPEs as a major obstacle to long-term manned space expeditions (76).

Besides higher doses encountered by SPEs, cumulative annual GCR particle doses inside a space craft amount to 176 ± 29 mGy based on measurements in the Mars Science Laboratory (77). *In vivo* data demonstrated that even low and protracted oxygen ion (^{16}O) radiation doses of 0.1 Gy impair hematopoiesis (78), and the effective proton dose to reduce the whole blood cell count (WBC) by half was shown to be approximately 1 Gy (79).

A major step towards the usage of MSCs for space irradiation-induced toxicities was performed recently by Huang and colleagues, who demonstrated the feasibility to grow human bone marrow-MSC aboard the International Space Station (ISS) (80). The MSCs' phenotype was observed unaltered during proliferation in space, and MSCs maintained their proliferative characteristics aboard ISS. Interestingly, space-expanded MSCs seem to exhibit pronounced immunosuppressive effects compared to MSCs grown on the Earth. At least in short-term space cultures, there were no signs for tumorigenic transformation and genomic instability in MSCs.

Recently, a Chinese study reported transcriptional changes of murine bone marrow cells after whole-body ^{12}C irradiation with 2 Gy (81), that would mimic the acute bone marrow exposure during a severe SPE. ^{12}C irradiation resulted in increased reactive oxygen species production, γH2AX foci and apoptosis levels in bone marrow cells. Significant alterations in genes belonging to the immune response, DNA damage repair, MAPK, TNF signaling and apoptosis pathways were observed in murine bone marrow cells after 2 Gy ^{12}C irradiation.

A high-quality study simulating the combined effects of GCR and SPE on the interaction between human bone marrow MSCs and hematopoietic progenitor cells was conducted by Almeida-Porada (66). Interestingly, ^{56}Fe ions upregulated many cytokines involved in hematopoiesis and immune cell development, whereas proton irradiation produced the opposite effect and downregulated key cytokines involved in these functions. Also very importantly, the transcriptional changes after proton and ^{56}Fe ion irradiation were long-lasting and persisted over several passages.

It is important to consider that low-dose irradiation (≤ 0.1 Gy) has shown to have significantly different effects on MSCs and adipose-derived stem cells than higher radiation doses (24, 82, 83). Low dose irradiation was found to enhance proliferation and to increase the secretion of stem-cell factor (SCF) and GM-CSF, which may favor hematopoiesis (83). In the study of Yang et al., the pro-survival effects of low-dose irradiation on human bone marrow MSCs were mediated *via* several proteins involved in cell cycle control such as Rb, cyclin E, CDK1, and CDC25B (83). Following these findings, there are considerations to use low-dose irradiation to support large scale expansion as well as therapeutic effects of MSCs (82, 84). Unfortunately, to the best of our knowledge, no studies have reported effects of low-dose particle irradiation, especially protons, on the proliferation rate of MSCs. Additionally, protracted low-dose irradiation over several weeks to mimic GCR are complicated by the difficulty to long-term culture MSCs due to premature senescence and therefore limited passage numbers (85). In the case of prolonged MSC culturing, which may be necessary to expand autologous MSC of astronauts prior to space missions, one should be aware that the DNA repair capacity is lowered leading to more spontaneous and radiation-induced micronuclei (86).

In the space environment, the more convenient way would be the usage of commercially available allogenic off-the-shelf MSCs. Due to the low immunogenicity and immune-privileged behavior, allogenic MSC treatments are generally feasible without prior immune suppression, as demonstrated in large clinical trials (10, 87). In this regard, effective shielding of these off-the-shelf MSCs would be desirable to avoid damage prior to application in a case of SPE.

CONCLUSION

In general, MSC-based therapies hold promise for the treatment of irradiation-induced toxicities such as mucositis, osteoradionecrosis, proctitis or cystitis as typical sequelae after radiotherapy in the head-and-neck or pelvic region, respectively. So far, preclinical and clinical research has been conducted focussing on the effects of MSCs on photon-induced toxicities, wherefore the role of MSCs as cell therapy for particle irradiation-related adverse reactions in cancer treatment remains to be elucidated. Furthermore, MSC-based therapies may be used after nuclear accidents or during future manned space missions, although the evidence is very limited. In summary, many further efforts are needed in the future to fully

examine the impact of particle irradiation on the regenerative abilities of MSCs and potential attenuating effects of MSCs on particle irradiation-induced normal tissue toxicities.

AUTHOR CONTRIBUTIONS

AR, A-LG, and NN wrote and revised this mini-review. All authors contributed to the article and approved the submitted version.

FUNDING

AR was supported by the IMM-PACT-Program for Clinician Scientists, Department of Medicine II, Medical Center – University of Freiburg and Faculty of Medicine, University of Freiburg, funded by the Deutsche Forschungsgemeinschaft (DFG, German Research Foundation) – 413517907. We thank the European Space Agency (ESA) for their financial support of the project "Human mesenchymal stem cells as potential mitigators of bone marrow toxicity caused by spaceradiation" within the CORA-IBER program.

REFERENCES

1. Friedenstein AJ, Petrakova KV, Kurolesova AI, Frolova GP. Heterotopic of bone marrow. Analysis of precursor cells for osteogenic and hematopoietic tissues. *Transplantation* (1968) 6(2):230–47. doi: 10.1097/00007890-196803000-00009
2. Friedenstein AJ, Deriglasova UF, Kulagina NN, Panasuk AF, Rudakowa SF, Luria EA, et al. Precursors for fibroblasts in different populations of hematopoietic cells as detected by the in vitro colony assay method. *Exp Hematol* (1974) 2(2):83–92.
3. Zuk PA, Zhu M, Ashjian P, De Ugarte DA, Huang JI, Mizuno H, et al. Human adipose tissue is a source of multipotent stem cells. *Mol Biol Cell* (2002) 13 (12):4279–95. doi: 10.1091/mbc.e02-02-0105
4. Bieback K, Kern S, Kluter H, Eichler H. Critical parameters for the isolation of mesenchymal stem cells from umbilical cord blood. *Stem Cells* (2004) 22 (4):625–34. doi: 10.1634/stemcells.22-4-625
5. Paul G, Özen I, Christophersen NS, Reinbothe T, Bengzon J, Visse E, et al. The adult human brain harbors multipotent perivascular mesenchymal stem cells. *PloS One* (2012) 7(4):e35577. doi: 10.1371/journal.pone.0035577
6. Rotter N, Oder J, Schlenke P, Lindner U, Böhrnsen F, Kramer J, et al. Isolation and characterization of adult stem cells from human salivary glands. *Stem Cells Dev* (2008) 17(3):509–18. doi: 10.1089/scd.2007.0180
7. Dominici M, Le Blanc K, Mueller I, Slaper-Cortenbach I, Marini F, Krause D, et al. Minimal criteria for defining multipotent mesenchymal stromal cells. The International Society for Cellular Therapy position statement. *Cytotherapy* (2006) 8(4):315–7. doi: 10.1080/14653240600855905
8. Godoy JAP, Paiva RMA, Souza AM, Kondo AT, Kutner JM, Okamoto OK. Clinical Translation of Mesenchymal Stromal Cell Therapy for Graft Versus Host Disease. *Front Cell Dev Biol* (2019) 7:255–. doi: 10.3389/fcell.2019.00255
9. Morata-Tarifa C, del Mar Macías-Sánchez M, Gutiérrez-Pizarraya A, Sanchez-Pernaute R. Mesenchymal stromal cells for the prophylaxis and treatment of graft-versus-host disease—a meta-analysis. *Stem Cell Res Ther* (2020) 11(1):1–12. doi: 10.1186/s13287-020-01592-z
10. Panes J, Garcia-Olmo D, Van Assche G, Colombel JF, Reinisch W, Baumgart DC, et al. Expanded allogeneic adipose-derived mesenchymal stem cells (Cx601) for complex perianal fistulas in Crohn's disease: a phase 3 randomised, double-blind controlled trial. *Lancet* (2016) 388(10051): 1281–90. doi: 10.1016/S0140-6736(16)31203-X
11. Jo CH, Lee YG, Shin WH, Kim H, Chai JW, Jeong EC, et al. Intra-articular injection of mesenchymal stem cells for the treatment of osteoarthritis of the knee: a proof-of-concept clinical trial. *Stem Cells* (2014) 32(5):1254–66. doi: 10.1002/stem.1634
12. Ruhle A, Lopez Perez R, Zou B, Grosu AL, Huber PE, Nicolay NH. The Therapeutic Potential of Mesenchymal Stromal Cells in the Treatment of Chemotherapy-Induced Tissue Damage. *Stem Cell Rev* (2019) 15(3):356–73. doi: 10.1007/s12015-019-09886-3
13. Li L, Jiang J. Regulatory factors of mesenchymal stem cell migration into injured tissues and their signal transduction mechanisms. *Front Med* (2011) 5 (1):33–9. doi: 10.1007/s11684-011-0114-1
14. Le Blanc K, Tammik C, Rosendahl K, Zetterberg E, Ringden O. HLA expression and immunologic properties of differentiated and undifferentiated mesenchymal stem cells. *Exp Hematol* (2003) 31(10):890–6. doi: 10.1016/S0301-472X(03) 00110-3
15. De Miguel MP, Fuentes-Julian S, Blazquez-Martinez A, Pascual CY, Aller MA, Arias J, et al. Immunosuppressive properties of mesenchymal stem cells: advances and applications. *Curr Mol Med* (2012) 12(5):574–91. doi: 10.2174/156652412800619950
16. Lalu MM, McIntyre L, Pugliese C, Fergusson D, Winston BW, Marshall JC, et al. Safety of cell therapy with mesenchymal stromal cells (SafeCell): a systematic review and meta-analysis of clinical trials. *PloS One* (2012) 7(10): e47559. doi: 10.1371/journal.pone.0047559
17. Nicolay NH, Lopez Perez R, Debus J, Huber PE. Mesenchymal stem cells - A new hope for radiotherapy-induced tissue damage? *Cancer Lett* (2015) 366 (2):133–40. doi: 10.1016/j.canlet.2015.06.012
18. Chang PY, Qu YQ, Wang J, Dong LH. The potential of mesenchymal stem cells in the management of radiation enteropathy. *Cell Death Dis* (2015) 6(8): e1840–e. doi: 10.1038/cddis.2015.189
19. Schmidt M, Haagen J, Noack R, Siegemund A, Gabriel P, Dorr W. Effects of bone marrow or mesenchymal stem cell transplantation on oral mucositis (mouse) induced by fractionated irradiation. *Strahlenther Onkol* (2014) 190 (4):399–404. doi: 10.1007/s00066-013-0510-3
20. Zanoni M, Cortesi M, Zamagni A, Tesei A. The Role of Mesenchymal Stem Cells in Radiation-Induced Lung Fibrosis. *Int J Mol Sci* (2019) 20(16). doi: 10.3390/ijms20163876
21. Gronhoj C, Jensen DH, Vester-Glowinski P, Jensen SB, Bardow A, Oliveri RS, et al. Safety and Efficacy of Mesenchymal Stem Cells for Radiation-Induced Xerostomia: A Randomized, Placebo-Controlled Phase 1/2 Trial (MESRIX). *Int J Radiat Oncol Biol Phys* (2018) 101(3):581–92. doi: 10.1016/j.ijrobp.2018.02.034
22. Ruhle A, Perez RL, Glowa C, Weber KJ, Ho AD, Debus J, et al. Cisplatin radiosensitizes radioresistant human mesenchymal stem cells. *Oncotarget* (2017) 8(50):87809–20. doi: 10.18632/oncotarget.21214
23. Chen MF, Lin CT, Chen WC, Yang CT, Chen CC, Liao SK, et al. The sensitivity of human mesenchymal stem cells to ionizing radiation. *Int J Radiat Oncol Biol Phys* (2006) 66(1):244–53. doi: 10.1016/j.ijrobp.2006.03.062
24. Liang X, So YH, Cui J, Ma K, Xu X, Zhao Y, et al. The Low-dose Ionizing Radiation Stimulates Cell Proliferation via Activation of the MAPK/ERK Pathway in Rat Cultured Mesenchymal Stem Cells. *J Radiat Res* (2011) 52 (3):380–6. doi: 10.1269/jrr.10121
25. Malouff TD, Mahajan A, Krishnan S, Beltran C, Seneviratne DS, Trifiletti DM. Carbon Ion Therapy: A Modern Review of an Emerging Technology. *Front Oncol* (2020) 10(82). doi: 10.3389/fonc.2020.00082
26. Akbaba S, Held T, Lang K, Forster T, Federspil P, Herfarth K, et al. Bimodal radiotherapy with active raster-scanning carbon ion radiotherapy and intensity-modulated radiotherapy in high-risk nasopharyngeal carcinoma results in excellent local control. *Cancers* (2019) 11(3):379. doi: 10.3390/cancers11030379
27. Akbaba S, Ahmed D, Lang K, Held T, Mattke M, Hoerner-Rieber J, et al. Results of a combination treatment with intensity modulated radiotherapy and active raster-scanning carbon ion boost for adenoid cystic carcinoma of the minor salivary glands of the nasopharynx. *Oral Oncol* (2019) 91:39–46. doi: 10.1016/j.oraloncology.2019.02.019
28. Jensen AD, Nikoghosyan AV, Lossner K, Haberer T, Jäkel O, Münter MW, et al. COSMIC: A Regimen of Intensity Modulated Radiation Therapy Plus Dose-Escalated, Raster-Scanned Carbon Ion Boost for Malignant Salivary Gland Tumors: Results of the Prospective Phase 2 Trial. *Int J Radiat Oncol Biol Phys* (2015) 93(1):37–46. doi: 10.1016/j.ijrobp.2015.05.013

29. Koto M, Hasegawa A, Takagi R, Sasahara G, Ikawa H, Mizoe J-e, et al. Feasibility of carbon ion radiotherapy for locally advanced sinonasal adenocarcinoma. *Radiother Oncol* (2014) 113(1):60–5. doi: 10.1016/j.radonc.2014.09.009
30. Beddok A, Vela A, Calugaru V, Tessonnier T, Kubes J, Dutheil P, et al. Proton therapy for head and neck squamous cell carcinomas: A review of the physical and clinical challenges. *Radiother Oncol* (2020) 147:30–9. doi: 10.1016/j.radonc.2020.03.006
31. Maria OM, Shalaby M, Syme A, Eliopoulos N, Muanza T. Adipose mesenchymal stromal cells minimize and repair radiation-induced oral mucositis. *Cytotherapy* (2016) 18(9):1129–45. doi: 10.1016/j.jcyt.2016.06.008
32. Elsaadany B, El Kholy S, El Rouby D, Rashed L, Shouman T. Effect of Transplantation of Bone Marrow Derived Mesenchymal Stem Cells and Platelets Rich Plasma on Experimental Model of Radiation Induced Oral Mucosal Injury in Albino Rats. *Int J Dent* (2017) 2017:8634540. doi: 10.1155/2017/8634540
33. Schmidt M, Piro-Hussong A, Siegemund A, Gabriel P, Dorr W. Modification of radiation-induced oral mucositis (mouse) by adult stem cell therapy: single-dose irradiation. *Radiat Environ Biophys* (2014) 53(4):629–34. doi: 10.1007/s00411-014-0552-7
34. Aarup-Kristensen S, Hansen CR, Forner L, Brink C, Eriksen JG, Johansen J. Osteoradionecrosis of the mandible after radiotherapy for head and neck cancer: risk factors and dose-volume correlations. *Acta Oncol* (2019) 58(10):1373–7. doi: 10.1080/0284186X.2019.1643037
35. Marx RE. Osteoradionecrosis: a new concept of its pathophysiology. *J Oral Maxillofac Surg* (1983) 41(5):283–8. doi: 10.1016/0278-2391(83)90294-X
36. Rice N, Polyzois I, Ekanayake K, Omer O, Stassen LF. The management of osteoradionecrosis of the jaws–a review. *Surgeon* (2015) 13(2):101–9. doi: 10.1016/j.surge.2014.07.003
37. Dell'Era V, Aluffi Valletti P, Garzaro G, Garzaro M. Maxillo-mandibular osteoradionecrosis following C-ion radiotherapy: Clinical notes and review of literature. *Eur J Inflamm* (2020) 18:2058739220934562. doi: 10.1177/2058739220934562
38. Oki M, Kanazaki A, Taniguchi H, Oki M, Kanazaki A, Taniguchi H. Osteoradionecrosis Following Carbon Ion Radiotherapy: Case History Report of a Soft Palate Defect. *Int J Prosthod* (2016) 29(5):448–50. doi: 10.11607/ijp.4836
39. Sasahara G, Koto M, Ikawa H, Hasegawa A, Takagi R, Okamoto Y, et al. Effects of the dose-volume relationship on and risk factors for maxillary osteoradionecrosis after carbon ion radiotherapy. *Radiat Oncol* (2014) 9(1):92. doi: 10.1186/1748-717X-9-92
40. Janus JR, Jackson RS, Lees KA, Voss SG, Wilson ZC, Remmes NB, et al. Human Adipose-Derived Mesenchymal Stem Cells for Osseous Rehabilitation of Induced Osteoradionecrosis: A Rodent Model. *Otolaryngol Head Neck Surg* (2017) 156(4):616–21. doi: 10.1177/0194599816688647
41. Park HS, Lee J, Kim JW, Kim HY, Jung SY, Lee SM, et al. Preventive effects of tonsil-derived mesenchymal stem cells on osteoradionecrosis in a rat model. *Head Neck* (2018) 40(3):526–35. doi: 10.1002/hed.25004
42. Jin IG, Kim JH, Wu HG, Kim SK, Park Y, Hwang SJ. Effect of bone marrow-derived stem cells and bone morphogenetic protein-2 on treatment of osteoradionecrosis in a rat model. *J Craniomaxillofac Surg* (2015) 43(8):1478–86. doi: 10.1016/j.jcms.2015.06.035
43. Xu J, Zheng Z, Fang D, Gao R, Liu Y, Fan Z, et al. Mesenchymal stromal cell-based treatment of jaw osteoradionecrosis in Swine. *Cell Transplant* (2012) 21(8):1679–86. doi: 10.3727/096368911X637434
44. Manimaran K, Sankaranarayanan S, Ravi VR, Elangovan S, Chandramohan M, Perumal SM. Treatment of osteoradionecrosis of mandible with bone marrow concentrate and with dental pulp stem cells. *Ann Maxillofac Surg* (2014) 4(2):189–92. doi: 10.4103/2231-0746.147130
45. Mendonça JJ, Juiz-Lopez P. Regenerative facial reconstruction of terminal stage osteoradionecrosis and other advanced craniofacial diseases with adult cultured stem and progenitor cells. *Plast Reconstr Surg* (2010) 126(5):1699–709. doi: 10.1097/PRS.0b013e3181f24164
46. Gundestrup AK, Lynggaard CD, Forner L, Heino TJ, Jakobsen KK, Fischer-Nielsen A, et al. Mesenchymal Stem Cell Therapy for Osteoradionecrosis of the Mandible: a Systematic Review of Preclinical and Human Studies. *Stem Cell Rev Rep* (2020) 16(6):1208–21. doi: 10.1007/s12015-020-10034-5
47. Kasuya G, Ishikawa H, Tsuji H, Haruyama Y, Kobashi G, Ebner DK, et al. Cancer-specific mortality of high-risk prostate cancer after carbon-ion radiotherapy plus long-term androgen deprivation therapy. *Cancer Sci* (2017) 108(12):2422–9. doi: 10.1111/cas.13402
48. Sheets NC, Goldin GH, Meyer AM, Wu Y, Chang Y, Stürmer T, et al. Intensity-modulated radiation therapy, proton therapy, or conformal radiation therapy and morbidity and disease control in localized prostate cancer. *Jama* (2012) 307(15):1611–20. doi: 10.1001/jama.2012.460
49. Tamarat R, Benderitter M. The Medical Follow-up of the Radiological Accident: Épinal 2006. *Radiat Res* (2019) 192(3):251–7. doi: 10.1667/RR15262.1
50. López M, Martín M. Medical management of the acute radiation syndrome. *Rep Pract Oncol Radiother* (2011) 16(4):138–46. doi: 10.1016/j.rpor.2011.05.001
51. Hu KX, Sun QY, Guo M, Ai HS. The radiation protection and therapy effects of mesenchymal stem cells in mice with acute radiation injury. *Br J Radiol* (2010) 83(985):52–8. doi: 10.1259/bjr/61042310
52. Lange C, Brunswig-Spickenheier B, Cappallo-Obermann H, Eggert K, Gehling UM, Rudolph C, et al. Radiation Rescue: Mesenchymal Stromal Cells Protect from Lethal Irradiation. *PloS One* (2011) 6(1):e14486. doi: 10.1371/journal.pone.0014486
53. Yang X, Balakrishnan I, Torok-Storb B, Pillai MM. Marrow Stromal Cell Infusion Rescues Hematopoiesis in Lethally Irradiated Mice despite Rapid Clearance after Infusion. *Adv Hematol* (2012) 2012:142530. doi: 10.1155/2012/142530
54. Alchinova I, Polyakova M, Yakovenko E, Medvedeva YS, Saburina I, Karganov MY. Effect of Extracellular Vesicles Formed by Multipotent Mesenchymal Stromal Cells on Irradiated Animals. *Bull Exp Biol Med* (2019) 166(4):574–9. doi: 10.1007/s10517-019-04394-3
55. Guo M, Dong Z, Qiao J, Yu C, Sun Q, Hu K, et al. Severe acute radiation syndrome: treatment of a lethally 60Co-source irradiated accident victim in China with HLA-mismatched peripheral blood stem cell transplantation and mesenchymal stem cells. *J Radiat Res* (2014) 55(2):205–9. doi: 10.1093/jrr/rrt102
56. Lataillade J, Doucet C, Bey E, Carsin H, Huet C, Clairand I, et al. New approach to radiation burn treatment by dosimetry-guided surgery combined with autologous mesenchymal stem cell therapy. *Regen Med* (2007) 2(5):785–94. doi: 10.2217/17460751.2.5.785
57. Chapel A, Francois S, Douay L, Benderitter M, Voswinkel J. New insights for pelvic radiation disease treatment: Multipotent stromal cell is a promise mainstay treatment for the restoration of abdominopelvic severe chronic damages induced by radiotherapy. *World J Stem Cells* (2013) 5(4):106–11. doi: 10.4252/wjsc.v5.i4.106
58. Chapel A, Francois S, Douay L, Benderitter M, Voswinkel J. Fifteen years of preclinical and clinical experiences about biotherapy treatment of lesions induced by accidental irradiation and radiotherapy. *World J Stem Cells* (2013) 5(3):68–72. doi: 10.4252/wjsc.v5.i3.68
59. Shim S, Lee SB, Lee J-g, Jang W-S, Lee S-J, Park S, et al. Mitigating effects of hUCB-MSCs on the hematopoietic syndrome resulting from total body irradiation. *Exp Hematol* (2013) 41(4):346–53.e2. doi: 10.1016/j.exphem.2013.01.002
60. Gale RP, Armitage JO. Are We Prepared for Nuclear Terrorism? *N Engl J Med* (2018) 378(13):1246–54. doi: 10.1056/NEJMsr1714289
61. Eaton EB Jr, Varney TR. Mesenchymal stem cell therapy for acute radiation syndrome: innovative medical approaches in military medicine. *Mil Med Res* (2015) 2:2. doi: 10.1186/s40779-014-0027-9
62. Nicolay NH, Sommer E, Lopez R, Wirkner U, Trinh T, Sisombath S, et al. Mesenchymal stem cells retain their defining stem cell characteristics after exposure to ionizing radiation. *Int J Radiat Oncol Biol Phys* (2013) 87(5):1171–8. doi: 10.1016/j.ijrobp.2013.09.003
63. Rühle A, Xia O, Perez RL, Trinh T, Richter W, Sarnowska A, et al. The Radiation Resistance of Human Multipotent Mesenchymal Stromal Cells Is Independent of Their Tissue of Origin. *Int J Radiat Oncol Biol Phys* (2018) 100(5):1259–69. doi: 10.1016/j.ijrobp.2018.01.015
64. Nicolay NH, Lopez Perez R, Saffrich R, Huber PE. Radio-resistant mesenchymal stem cells: mechanisms of resistance and potential implications for the clinic. *Oncotarget* (2015) 6(23):19366–80. doi: 10.18632/oncotarget.4358

65. Sugrue T, Brown JA, Lowndes NF, Ceredig R. Multiple facets of the DNA damage response contribute to the radioresistance of mouse mesenchymal stromal cell lines. *Stem Cells* (2013) 31(1):137–45. doi: 10.1002/stem.1222
66. Almeida-Porada G, Rodman C, Kuhlman B, Brudvik E, Moon J, George S, et al. Exposure of the Bone Marrow Microenvironment to Simulated Solar and Galactic Cosmic Radiation Induces Biological Bystander Effects on Human Hematopoiesis. *Stem Cells Dev* (2018) 27(18):1237–56. doi: 10.1089/scd.2018.0005
67. Alessio N, Esposito G, Galano G, De Rosa R, Anello P, Peluso G, et al. Irradiation of Mesenchymal Stromal Cells With Low and High Doses of Alpha Particles Induces Senescence and/or Apoptosis. *J Cell Biochem* (2017) 118 (9):2993–3002. doi: 10.1002/jcb.25961
68. Kurpinski K, Jang DJ, Bhattacharya S, Rydberg B, Chu J, So J, et al. Differential effects of x-rays and high-energy 56Fe ions on human mesenchymal stem cells. *Int J Radiat Oncol Biol Phys* (2009) 73(3):869–77. doi: 10.1016/j.ijrobp.2008.10.002
69. Nicolay NH, Liang Y, Lopez Perez R, Bostel T, Trinh T, Sisombath S, et al. Mesenchymal stem cells are resistant to carbon ion radiotherapy. *Oncotarget* (2015) 6(4):2076–87. doi: 10.18632/oncotarget.2857
70. Rong –Y, Dong -P, Xiong –Y, Gang -X, Xin –Z, Man –X, et al. Irradiation Response of Adipose-derived Stem Cells under Three-dimensional Culture Condition. *Biomed Environ Sci* (2015) 28(- 8):549. doi: 10.3967/bes2015.079
71. Durante M, Debus J. Heavy Charged Particles: Does Improved Precision and Higher Biological Effectiveness Translate to Better Outcome in Patients? *Semin Radiat Oncol* (2018) 28(2):160–7. doi: 10.1016/j.semradonc.2017.11.004
72. Lopez Perez R, Nicolay NH, Wolf JC, Frister M, Schmezer P, Weber KJ, et al. DNA damage response of clinical carbon ion versus photon radiation in human glioblastoma cells. *Radiother Oncol* (2019) 133:77–86. doi: 10.1016/j.radonc.2018.12.028
73. Walenta S, Mueller-Klieser W. Differential Superiority of Heavy Charged-Particle Irradiation to X-Rays: Studies on Biological Effectiveness and Side Effect Mechanisms in Multicellular Tumor and Normal Tissue Models. *Front Oncol* (2016) 6(30). doi: 10.3389/fonc.2016.00030
74. Hartfiel S, Häfner M, Perez RL, Rühle A, Trinh T, Debus J, et al. Differential response of esophageal cancer cells to particle irradiation. *Radiat Oncol* (2019) 14(1):119. doi: 10.1186/s13014-019-1326-9
75. Kennedy AR. Biological Effects of Space Radiation and Development of Effective Countermeasures. *Life Sci Space Res* (2014) 1:10–43. doi: 10.1016/j.lssr.2014.02.004
76. Chancellor JC, Scott GBI, Sutton JP. Space Radiation: The Number One Risk to Astronaut Health beyond Low Earth Orbit. *Life (Basel)* (2014) 4(3):491–510. doi: 10.3390/life4030491
77. Zeitlin C, Hassler DM, Cucinotta FA, Ehresmann B, Wimmer-Schweingruber RF, Brinza DE, et al. Measurements of Energetic Particle Radiation in Transit to Mars on the Mars Science Laboratory. *Science* (2013) 340(6136):1080–4. doi: 10.1126/science.1235989
78. Wang Y, Chang J, Li X, Pathak R, Sridharan V, Jones T, et al. Low doses of oxygen ion irradiation cause long-term damage to bone marrow hematopoietic progenitor and stem cells in mice. *PloS One* (2017) 12(12): e0189466. doi: 10.1371/journal.pone.0189466
79. Sanzari JK, Cengel KA, Wan XS, Rusek A, Kennedy AR. Acute Hematological Effects in Mice Exposed to the Expected Doses, Dose-rates, and Energies of Solar Particle Event-like Proton Radiation. *Life Sci Space Res* (2014) 2:86–91. doi: 10.1016/j.lssr.2014.01.003
80. Huang P, Russell AL, Lefavor R, Durand NC, James E, Harvey L, et al. Feasibility, potency, and safety of growing human mesenchymal stem cells in space for clinical application. *NPJ Microgravity* (2020) 6:16. doi: 10.1038/s41526-020-0106-z
81. Liu F, Wang Z, Li W, Wei Y. Transcriptional response of murine bone marrow cells to total-body carbon-ion irradiation. *Mutat Res Genet Toxicol Environ Mutagen* (2019) 839:49–58. doi: 10.1016/j.mrgentox.2019.01.014
82. Schröder A, Kriesen S, Hildebrandt G, Manda K. First Insights into the Effect of Low-Dose X-Ray Irradiation in Adipose-Derived Stem Cells. *Int J Mol Sci* (2019) 20(23):6075. doi: 10.3390/ijms20236075
83. Yang L, Liu Z, Chen C, Cong X, Li Z, Zhao S, et al. Low-dose radiation modulates human mesenchymal stem cell proliferation through regulating CDK and Rb. *Am J Transl Res* (2017) 9(4):1914–21.
84. Guo W-Y, Wang G-J, Wang P, Chen Q, Tan Y, Cai L. Acceleration of Diabetic Wound Healing by Low-Dose Radiation is Associated with Peripheral Mobilization of Bone Marrow Stem Cells. *Radiat Res* (2010) 174(4):467–79. doi: 10.1667/RR1980.1
85. Estrada JC, Torres Y, Benguría A, Dopazo A, Roche E, Carrera-Quintanar L, et al. Human mesenchymal stem cell-replicative senescence and oxidative stress are closely linked to aneuploidy. *Cell Death Dis* (2013) 4(6):e691–e. doi: 10.1038/cddis.2013.211
86. Hladik D, Höfig I, Oestreicher U, Beckers J, Matjanovski M, Bao X, et al. Long-term culture of mesenchymal stem cells impairs ATM-dependent recognition of DNA breaks and increases genetic instability. *Stem Cell Res Ther* (2019) 10(1):218. doi: 10.1186/s13287-019-1334-6
87. Vega A, Martín-Ferrero MA, Del Canto F, Alberca M, García V, Munar A, et al. Treatment of knee osteoarthritis with allogeneic bone marrow mesenchymal stem cells: a randomized controlled trial. *Transplantation* (2015) 99(8):1681–90. doi: 10.1097/TP.0000000000000678

Conflict of Interest: The authors declare that the research was conducted in the absence of any commercial or financial relationships that could be construed as a potential conflict of interest.

Copyright © 2021 Rühle, Grosu and Nicolay. This is an open-access article distributed under the terms of the Creative Commons Attribution License (CC BY). The use, distribution or reproduction in other forums is permitted, provided the original author(s) and the copyright owner(s) are credited and that the original publication in this journal is cited, in accordance with accepted academic practice. No use, distribution or reproduction is permitted which does not comply with these terms.

frontiers in Oncology

SYSTEMATIC REVIEW
published: 25 May 2021
doi: 10.3389/fonc.2021.620534

The Efficacy and Safety of Carbon Ion Radiotherapy for Meningiomas: A Systematic Review and Meta-Analysis

Jie-yun Li[1,2,3†], Jing-wen Li[2,3†], Yuan-chang Jin[4,5,6], Mei-xuan Li[1,2,3], Li-ping Guo[1,2,3], Zhi-tong Bing[5], Qiu-ning Zhang[5,6], Fei Bai[1,2,3,7], Xiao-hu Wang[4,5,6], Xiu-xia Li[1,2,3*] and Ke-hu Yang[1,2,3*]*

[1] Evidence-Based Medicine Center, School of Basic Medical Sciences, Lanzhou University, Lanzhou, China, [2] Health Technology Assessment Center of Lanzhou University, School of Public Health, Lanzhou University, Lanzhou, China, [3] Key Laboratory of Evidence Based Medicine and Knowledge Translation of Gansu Province, Lanzhou, China, [4] The First School of Clinical Medicine, Lanzhou University, Lanzhou, China, [5] Institute of Modern Physics, Chinese Academy of Sciences, Beijing, China, [6] Lanzhou Heavy Ions Hospital, Lanzhou, China, [7] National Health Commission Medical Management Center, Beijing, China

OPEN ACCESS

Edited by:
Daniel Michael Trifiletti,
Mayo Clinic Florida, United States

Reviewed by:
Timothy Dean Malouff,
Mayo Clinic Florida, United States
Wei Zhao,
Stanford University, United States

***Correspondence:**
Xiao-hu Wang
xhwanggansu@163.com
Xiu-xia Li
lixiuxia@lzu.edu.cn
Ke-hu Yang
kehuyangebm2006@126.com

[†]These authors have contributed equally to this work

Specialty section:
This article was submitted to Radiation Oncology, a section of the journal Frontiers in Oncology

Received: 23 October 2020
Accepted: 27 April 2021
Published: 25 May 2021

Citation:
Li J-y, Li J-w, Jin Y-c, Li M-x, Guo L-p, Bing Z-t, Zhang Q-n, Bai F, Wang X-h, Li X-x and Yang K-h (2021) The Efficacy and Safety of Carbon Ion Radiotherapy for Meningiomas: A Systematic Review and Meta-Analysis. Front. Oncol. 11:620534. doi: 10.3389/fonc.2021.620534

Objective: The purpose of this systematic review and meta-analysis is to evaluate the efficacy and safety of carbon ion radiotherapy (CI-RT) in improving meningioma by comparing photon and protons radiotherapy.

Methods: A comprehensive search for relevant studies published until March 17, 2021, was conducted in PubMed, the Cochrane Library, Chinese Biomedical Literature Database and EMBASE. Statistical analyses were performed with R 4.0.3.

Results: We identified 396 studies, of which 18 studies involving 985 participants were included. Except for one low quality study, the quality of the included studies was found to be either moderate or high quality. The analyses conducted according random effects model indicated that the 1-year overall survival rate (OS) of benign and non-benign meningiomas after the CI-RT treatment was 99% (95%CL=.91-1.00, I^2 = 0%). The overall average 5-year OS for meningiomas was 72% (95%CL=0.52-0.86, I^2 = 35%), not as effective as proton radiotherapy (PR-RT) 85% (95%CL=.72-.93, I^2 = 73, Q=4.17, *df*=2, *p*=.12). Additionally, 5-year OS of atypical meningiomas (81%) was found to be significantly higher than anaplastic meningiomas (52%). The 10-year OS after CI-RT of patients with mixed grade meningioma was 91% (95%CL=.75-.97, I^2 = 73%). The 15-year OS after CI-RT 87% (95%CL=.11-1.00) or PR-RT 87% (95%CL=.23-.99, I^2 = 79%) were the same (Q=0, *df*=1, *p*=.99). After undergoing CI-RT for 3 and 5 years, the LC for benign meningioma was 100% and 88%, respectively, while the 2-year LC of non-benign meningiomas (atypical/anaplastic) was 33%. Headache, sensory impairment, cognitive impairment, and hearing impairment were found to be the most common adverse reactions, with individual incidences of 19.4%, 23.7%, 9.1%, and 9.1%, respectively.

Conclusion: CI-RT is a rapidly developing technique that has been proven to be an effective treatment against meningioma. The efficacy and safety of CI-RT for meningiomas

were similar to those of PR-RT, better than photon radiotherapy (PH-RT). However, there is a need for more prospective trials in the future that can help provide more supportive evidence.

Keywords: carbon ion radiotherapy, proton therapy, meningiomas, systematic review, meta-analysis

INTRODUCTION

Meningiomas are typically slow-growing, well-defined benign tumors that original from arachnoid cells. Meningioma is the most common primary non-glioma tumor in adults, and accounts for 25% of primary brain tumors (1). The annual incidence rate of meningiomas is approximately 8.3 in 100,000 (2). The World Health Organization (WHO) classifies meningiomas into three different categories, including grade I (benign), grade II (atypical) and grade III (malignant or anaplastic) (3). Although most meningiomas are benign, meningiomas do often adjoin or infiltrate key neurovascular structures. Furthermore, their growth can cause neurocognitive impairment and significant deterioration of their quality of life. Meningiomas are mostly diagnosed among middle-aged and elderly patients, but can also occur in young patients (4, 5). The frequency of meningiomas increases with age, and women are twice as likely to be diagnosed as men (6).

Benign meningiomas, including convex meningiomas and easily accessible skull base meningiomas, account for approximately 90% of all meningiomas (3, 7). Neurosurgical resection is considered to be the first choice of treatment for tumors that are easier to resect. Furthermore, there is no high risk of treatment-related side effects post-resection. In addition to surgery, a variety of radiation therapy (RT) methods are often used to strengthen local control of the tumor, particularly when surgery alone does not seem to be enough. Atypical and anaplastic meningiomas are characterized by more aggressive growth patterns, both of them are relatively rare tumors and only account for 4.7% and 2.8% of all meningiomas, respectively (8). Compared to patients with benign meningioma, they tend to have higher local recurrence and lower survival rate (9). Although traditional RT has been conducted across many meningioma treatments, it has been shown to significantly improve local control and prolong survival. However, the effect of treatment is still not satisfactory, and most patients tend to have recurrence during follow-up. In 1997, the Department of Radiation Oncology at the University of Heidelberg Hospital provided carbon ion therapy in Gesellschaft für Schwerionenforschung (GSI), Darmstadt, Germany. Carbon ion therapy involves the use of active beam transmission through raster scanning technology to irradiated patients with different brain and skull base tumors (10–12). The study demonstrated that all patients had good tolerance to carbon ion therapy. The 1-year local control rate was found to be 94%, and no severe toxicity or local recurrence within the treatment volume was observed. The clinical effect and technical feasibility of the carbocation therapy were announced. Carbon ion radiotherapy (CI-RT) is characterized through its unique physical and biological properties that allow for a gradual increase of dose deposition through a steep gradient. As a result, high-dose local therapy can be applied, while normal structures are likely to survive. Furthermore, tumors near normal dangerous organs may be treated more effectively with higher doses (13, 14). Additionally, CI-RT has a higher local tumor control rate, as well as increasing relative biological effectiveness (RBE), which is defined as the ratio of ion dose to photon radiotherapy (PH-RT). RBE fluctuates with environmental factors (15). The increasing RBE offers further potential radiobiological advantages, such as reduced repair capacity, decreased cell-cycle dependence, and possibly, stronger immunological responses (16).

Application of CI-RT for treating meningiomas is a currently developing research field. In recent years, clinical trials of CI-RT for meningiomas have gradually increased and have been able to evaluate overall survival rate (OS), local control rate (LC), tumor volume and additional indicators of meningioma after CI-RT. Hence, a meta-analysis for this small but heterogeneous body of evidence is needed and may be useful for further advancing the application and knowledge within this field. The present systematic review and meta-analysis analyzed all available literature for evidence of efficacy and safety of CI-RT for the treatment of meningiomas by comparing PR-RT and PH-RT.

METHOD

The Cochrane Handbook for Systematic Reviews of Interventions and PRISMA Statement were used to guide the conduct and reporting of this review. A study search was done using four electronic databases, including PubMed, the Cochrane Library, Chinese Biomedical Study Database, and EMBASE (17). As a systematic review and meta-analysis, our study does not have ethical issues and therefore no need approval from institutional review board.

Inclusion and Exclusion Criteria

Studies were included if they matched the following criteria: (a) patients with meningioma had been diagnosed by histopathology (b) the clinical treatments were carbon-ion, photon, or protons radiotherapy; (c) reported data that can be used to calculate the effectiveness and/or adverse effects; (d) prospective or retrospective clinical trials.

Publications were excluded if they were (a) case reports; (b) letters, editorials, protocols, reviews; (c) duplicate publications; (d) cell and animal experimental studies; (e) lacking detailed data.

Data Sources and Search Strategy

A comprehensive search was conducted for relevant studies that were published in English or Chinese, databases including PubMed, the Cochrane Library, Chinese Biomedical Literature Database, and EMBASE on March 17, 2021. The search keywords including ("meningioma" OR "Meningiomas" OR "meningioma" OR "meningothelioma") AND ("ion" OR "proton" OR "photon"). Details on the search strategy have been provided in **Supplementary Material** (18). The reference lists of the studies were searched manually to identify additional studies (19). The Clinical Trials.gov website was also searched for studies that were registered as completed but not yet published.

Selection Criteria and Data Extraction

The titles and abstracts of studies identified in the databases were screened by two reviewers (J-WL and J-YL) independently with a standardized approach. We retrieved the full-text articles of all potentially eligible studies (20). We resolved any disagreements about research qualifications by discussing or consulting the third reviewer (Y-CJ or M-XL). A flow diagram of the systematic search and study selection process is shown in **Figure 1**.

Eligible studies were screened in their entirety and developed a data extraction form, and the information including authors and year of publication, publication type, type of treatment, sample size, WHO grade, total dose, duration of intervention and follow-up were recorded in an Excel spreadsheet. We pre-tested it on five studies and subsequently adapted the final version. If the inclusion criteria were met, the full-text of each study was coded by the first authors (J-YL and J-WL) using this template.

If there was any evidence for the use of the same sample in different publications, authors were contacted for clarification (21). If it was confirmed that two studies were based on the same data, we chose the study that reported the most comprehensive results (17). If a study conducted multiple interventions and targeted with different population, each intervention was considered as an independent report.

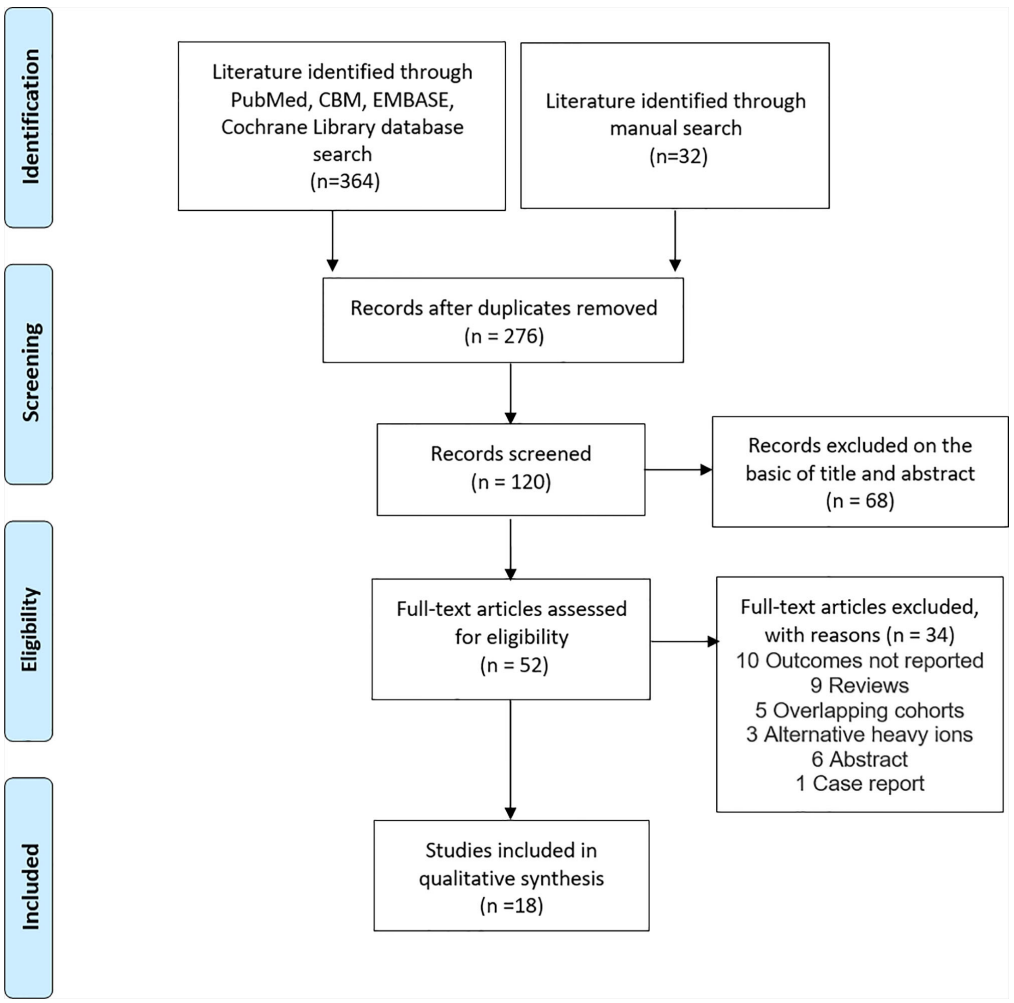

FIGURE 1 | PRISMA flowchart showing study selection.

Heterogeneity, Sensitivity, and Publication Bias

Based on the Cochrane Handbook Version 6.1.0, 2020, heterogeneity was assessed using Q-test to estimate the standard deviation of the true effect sizes (22). A significant Q-test indicates that effect sizes of primary studies do not belong to the same distribution of effect sizes. When performance qualification statistics $p \geq .05$, was considered no significant heterogeneity among the included studies (21). I^2 index is used to the estimated amount of variability in the true effect sizes, and the proportion of observed variability that can be explained by true heterogeneity. 25%, 50%, and 75% of I^2 index indicate low, moderate, and high degrees of heterogeneity, respectively.

"Leave-one-out" method is used in sensitivity analyses to check for outliers that potentially influence the results of the meta-analysis disproportionately (21). All analyses were performed repeatedly with each study removed once to detect whether overall results effect on a single study.

Publication bias means that statistically significant results are more likely to be published, while statistically insignificant results are less likely to be published. Therefore, these studies with no significant significance could be more likely to remain in the "file drawer" (23). Publication bias was assessed by three methods. Funnel plots illustrate the effect sizes of primary studies as a function of study precision. Asymmetry in plots can indicate publication bias (24). Egger's regression test yields a statistical verification of funnel plot asymmetry. If any bias could be assumed based on these analyses, we planned to apply the trim-and-fill procedure to estimate the unbiased overall effect (25).

Risk of Bias Assessment

In order to assess the quality of the case series, the authors (J-WL and J-YL) independently assessed bias using an evaluation scale that was developed by the Canadian Institute of Health Economics (IHE) (26). The authors evaluated the biases to create their own research list that meets the inclusion and exclusion criteria. The third author (Y-CJ) examined differences between the two lists. The difference was resolved through discussion between the three authors. The IHE case series methodology quality evaluation list is composed of a total of 20 setting items. Each of the items were assessed as "yes," "no," and "unclear." Trials that had more than 14 "yes" components were identified as having a moderate risk of bias (**Supplementary Table 1**).

Data Synthesis and Statistical Analysis

The fixed-effects model and the random-effects model are based on different assumptions. The results of meta-analysis using fixed-effect models are limited to specific populations (27). As the fact that the studies were conducted under different conditions (e.g., cancer grade, intervention, etc.) could indispensably cause differences among the results. Thus, in the synthesis of effect sizes during the present meta-analytical processes, analyses were conducted according to the random effects model. We computed proportion with 95% confidence intervals (95%CI) to estimate effect sizes for continuous outcomes. Besides, we use stratified analysis to explore subgroup analysis. The whole process of data analysis was performed in R 4.0.3. with the 'meta' package.

RESULT

Selection and Characteristics of Studies

Among the 396 studies that were related to ion, proton or photon radiotherapy were identified, 52 were selected for full-text review. Eventually, 18 studies were included in the meta-analysis (see **Figure 1**) (28–42). 12 studies reported OS (28–31, 35, 36, 38, 41–43), 17 studies reported LC rates (29–43), and nine studies reported toxic reactions (29, 31, 32, 34, 35, 38, 39, 41, 42). Eight studies about CI-RT were all from Heidelberg, Germany and were published between 2010 and 2018 (28, 30, 31, 36, 43–45). Among these studies, two prospective studies (28, 43), while the remaining six were retrospective studies (30, 31, 38, 44, 45). The number of patients that were included in each study ranged from 8 to 110, the follow-up ranged from 2 to 243 months. Eight studies about PR-RT were from four various countries, three of them from Switzerland (35, 41, 42), two from Sweden (32, 40), two from the United States (33, 37) and South Africa (39). The number of patients that were included in each study ranged from 13 to 170, the follow-up ranged from 32 to 207 months. Three studies were on photons or photons combined with protons. Two of them were from the United States (34, 36) and one from France (29). The number of patients included in each study ranged from 24 to 44, the follow-up ranged from 1 to 193 months. CI-RT was applied at a median dose of 18 Gy E, while PH-RT was applied at a dose of 50 to 50.4 Gy E and PR-RT was applied with a dose of 21.9 to 57.6 Gy E. In these studies, at least 433 patients were with benign meningioma (WHO grade I), while 138 patients were with atypical meningioma (WHO grade II), and 32 patients were with anaplastic meningioma (WHO grade III). Characteristics of these studies are shown in **Table 1**.

Risk of Bias

As shown in the **Supplemental Table 1**. Except for one low quality study (32), the quality of the included studies was found to be either moderate or high quality. All the assumptions, and objectives of included studies were described in detail, as well as the characteristics of the patients and interventions. All included studies used reasonable methods and statistical tests to measure relevant outcome indicators. Meanwhile, reported the duration of follow-up and the number of people lost to follow-up and the reasons. But it's worth noting that only 16 percent of all studies were multicenter. Inclusion and exclusion criteria were elaborated in 56.5% of the studies. Whether the inclusion of patients was continuous is unknown in 50% of the studies. 38.9% of the joint intervention measures were clearly described. 11.1% of the studies were prospective studies, and it was unclear of all included studies that whether or not to blind the outcome evaluator.

TABLE 1 | Characteristics of the study.

Study	Institute	Design	Patient (n)	Age(Median)	WHO GRADE(N)				Intervention	Radiation modality	Follow up (Month)	Overall survival	Local control	Toxicity Note
					I	II	III	Unknow						
Gudjonsson et al. (32)	Uppsala. Sweden	Retrospective cohort	19	52 (34–66)	15	/	/	4	Proton	24 Gy, 6 Gy fr	40 (12–115).	/	100% at 3-year	No toxicity. No additional cranial nerve dysfunctions have occurred during follow-up.
Hug et al. (34)	MGH, Boston MA.USA	Retrospective cohort	31	60 (33–85)	/	15	16	/	Photo or Proton+ Photon	62.5 (50.4-68.4) Gy/CGE	48	/	50% at 5 years for atypical, 19% at 8 years for malignant	One patient developed radiation necrosis. The investigators did not report when this occurred relative to treatment
Vernimmen et al. (39)	Tygerberg, South Africa	Retrospective cohort	23	45.6 (7.2–64.8)	23	/	/	/	Proton	54 Gy in 27 fr to 61.6 Gy in 16 fr	40(13–69)	/	88% at 5 years	1 patient developed short-term memory disturbance
Weber et al. (41)	PSI, Switzerland	Retrospective cohort	13	/	11	2	/	/	Proton	56 Gy (52.2–64 Gy)	34.1	84.6% at 3 years	100% at 3 years	Cumulative 3-year toxicity free survival
Boskos et al. (29)	CPO, Orsay, France	Retrospective cohort	24		/	19	5	/	Photo or Proton+ Photon	68(56–68)Gy/ CGE	48(1–87)	100% at 1-year 95.5% at 2-year 80.4% at 3-year 65.3% at 4-year 53.2% at 5-year 46.6% at 8-year	82.9% at 1-year 82.9% at 2-year 61.3% at 3-year 61.3% at 4-year 46.7% at 5-year 47.7% at 8-year	Most common possible complications induced are neuropathy, radiation necrosis, and insufficiency of the pituitary gland.
Combs 2010a (46)	Heidelberg Germany	Retrospective cohort	8	52	/	/	/	8	Carbon Ion Boost, Photons	Carbon ion, 18 Gy E; Photon, 50.4 Gy E	77(6–108)	75% at 5 years	86% at 5 years 72% at 7 years	/
Halasz et al. (33)	MGH, Boston MA.USA	Retrospective cohort	50	60 (33–85)	50	/	/	/	Proton	13 Gy (10–15.5) in 1 fr	32(6–133)	/	94% at 3 years	/
Adeberg et al. (28)	Heidelberg Germany	Prospective cohort	85	55	/	85		/	Proton and carbon ion boost	57.6 Gy E	73 (3–243)	81% and 53% at 5 years for atypical or anaplastic	/	/
Rieken et al. (38)	Heidelberg Germany	Retrospective cohort	7	42(7–77)	3	3	1	/	Proton and carbon ion boost	Carbon ion, 18 Gy E; Proton, 52.2–57.6 Gy E.	4.5	100%	100%	/
Slater et al. (37)	Loma Linda University Medical Center, USA	Retrospective cohort	47	54.2 (22–85)	/	/	/	47	Proton	59 Gy	74	/	99% at 5 years	13% of patients developed neurologic symptoms 6% of patient presented pan hypopituitarism
Weber et al. (42)	PSI, Switzerland	Retrospective cohort	39	48.3	/	/	/	39	Proton	56(52.2–64 Gy)	62	82% at 5 years	84.6% at 5 years	Cumulative 5-year Grade 3 late toxicity-free survival
Combs 2013a (43)	Heidelberg Germany	Retrospective cohort	107	48(1–85)	/	/	/	107	Proton and carbon ion boost	Carbon ion, 18 Gy E; Proton, 52.2 – 57.6 GyE.	12(2–39)	100% at 3 years	54% at 1 year 33% at 2 years	/
Combs 2013b (41)	Heidelberg Germany	Prospective cohort	70	55(27–83)	30	23	4	13	Carbon Ion Boost, Photons	Photon, 50 Gy E; carbon ion, 18 Gy E.	6(2–22)	100% at 1 years	100% at 1 years	/
Murray et al. (35)	PSI, Switzerland	Retrospective cohort	96	/	61	35		/	Proton	54(50.4–64 Gy)	56.9 (12.1-207.2)	92% and 80% at 5 years for benign or non-benign	95% and 69% at 5 years for benign or non-benign	5 years grade III Free survival=89.1%
Sanford et al. (36)	MGH, Boston MA.USA	Retrospective cohort	44	9-87	/	44	/	/	Proton+ Photon	55.8 Gy or 63.0 Gy	73 (3–193)	100% and 92% at 15 years for high and low dose	99% at 10 year 91% at 15 years	/
Vlachogiannis et al. (40)	Uppsala. Sweden	Retrospective cohort	170	54.2 (22–85)	170	/	/	/	Proton	21.9 (14–46 Gy)	84		93% at 5 year 85% at 10 years	/
El Shafie 2018a (30)	Heidelberg Germany	Retrospective cohort	110	53	60	7	1	42	Proton and carbon ion boost	Proton, 54 Gy E; Carbon ion 18Gy E.	46.8(34.3–61.7)	96.2% at 5 years 92% at 6 years	100% at 3years 96.6% at 5 years	/
El Shafie 2018b (31)	Heidelberg Germany	Retrospective cohort	42	54	10	25	6	1	Proton and carbon ion boost	Proton, 54 Gy E; Carbon ion 19Gy E.	49.7	89.6% at 1-year 71.4% at 2 years	71% at 1 year 56.5% at 2 years	No grade 4 or 5 toxicities were observed

Overall Survival *R*ate

Overall survival (OS) is one of the study's primary outcomes. The duration of survival is the time interval between an initial diagnosis (date of the neuropathology report) and date of death due to any cause. Patients that were not reported to be dead or lost to follow-up were censored at the date of the last follow-up examination. Among the studies related to the CI-RT, five studies (28, 30, 44, 45) reported the OS of patients with meningioma (**Figure 2**). The 1-year OS, no matter benign or non-benign meningiomas was 99% (95%CL=.91-1.00, I^2 = 0%). As shown in **Supplementary Figure 1** and **Table 2**, there was a significant difference among the three different treatments (Q=5.81, *df*=2, *p*=.04). The 3-year OS of CI-RT was 100% (95%CL=0.90-1) is better than that of PR-RT 85% (95% CL=0.55-0.96) and proton combined with photon radiotherapy 79% (95%CL=.59-.91). The overall average 5-year OS for meningiomas was 72% (95%CL=.52-.86, I^2 = 35%), not as effective as proton radiotherapy (PR-RT) 85% (95%CL=.72-.93, I^2 = 73, Q=4.17, *df*=2, *p*=.12) (**Supplementary Figure 2**). Additionally, 5-year OS of atypical meningiomas (81%) was found to be significantly higher than anaplastic meningiomas (52%). The 10-year OS after CI-RT of patients with mixed grade meningioma was 91% (95%CL=.75-0.97, I^2 = 73%). The 15-year OS after CI-RT 87% (95%CL=.11-1.00) or PR-RT 87% (95% CL=.23-.99, I^2 = 79%) were the same (Q=0, *df*=1, *p*=.99) (**Supplementary Figure 3**). The 1-year and 2-year survival rates of patients with recurrent intracranial meningiomas were 90% and 71%, respectively.

Sensitivity and Publication Bias

According to the "leave-one-out" strategy, the effect sizes estimated values of eight studies related to CI-RT from .74 to .87, indicated that there were no particularly prominent sensitivity issues in the included literature (**Supplementary Figure 4**). The shape of the funnel plots appeared symmetrical in the comparison model showed that most effect sizes seem

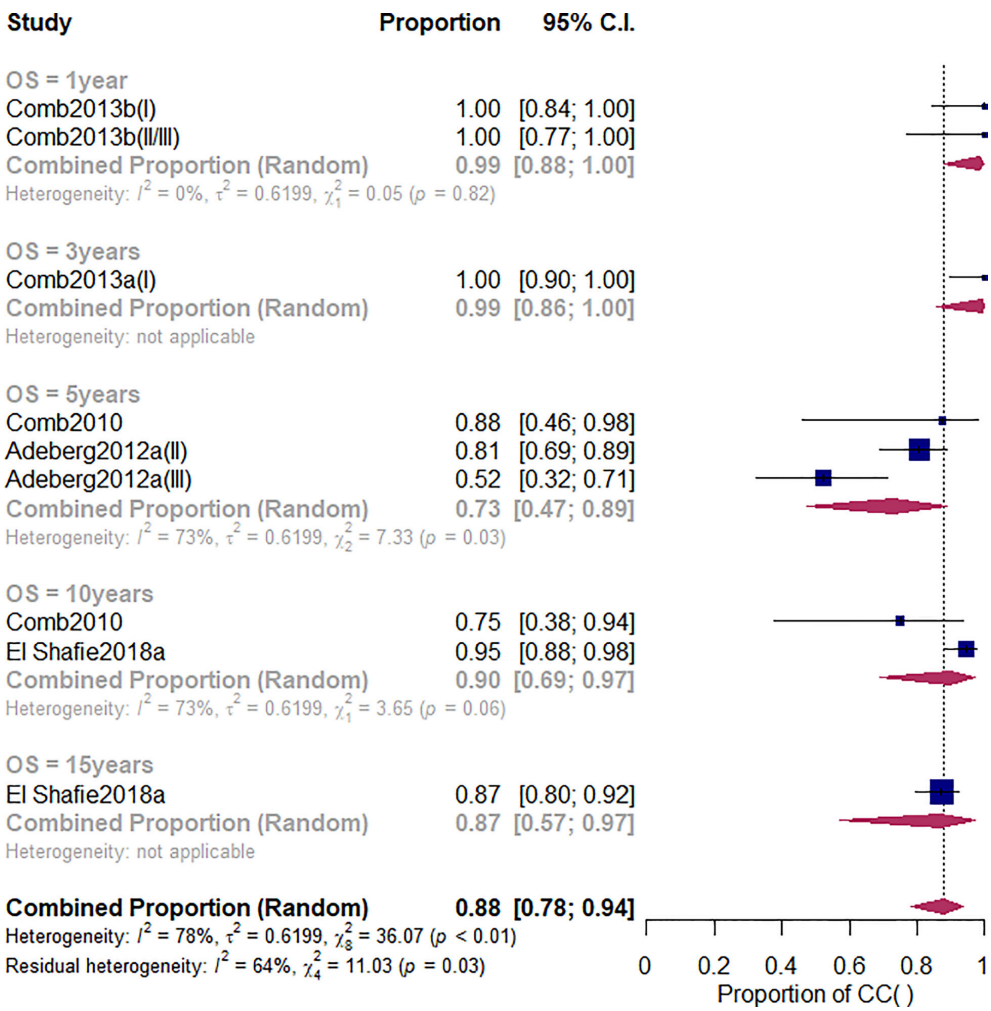

FIGURE 2 | The overall survival rate of meningioma initial diagnosis treated with CI-RT.

TABLE 2 | Outcomes with various treatment methods for meningioma.

	Intervention	K	Proportion	95%CI	I^2	Q	*df*	*p*
1-year OS	Proton+photon	1	98%	0.75–1	-	0.04	1	0.84
	Carbon+photon	2	99%	0.91–1	0%			
	Total	3	98%	0.92–1				
3-year OS	Proton+photon	1	79%	0.59–0.91	-	5.81	2	<.05
	Proton	1	85%	0.55–0.96	-			
	Carbon+photon	1	100%	0.90–1	-			
	Total	3	90%	0.65–0.98				
5-year OS	Proton+photon	1	54%	0.23–0.83	-	4.17	2	0.12
	Proton	3	85%	0.72–0.93	73%			
	Carbon+proton	3	72%	0.52–0.86	35%			
	Total	7	77%	0.66–0.85				
10-year OS	Carbon+photon	2	91%	0.75–0.97	73%	-	-	-
15-year OS	Proton+photon	2	87%	0.23–0.99	79%	0	1	0.99
	Carbon+proton	1	87%	0.11–1	-			
	Total	3	87%	0.36–0.99				
1-year LC	Proton+photon	1	83%	0.63–0.94	-	5.46	1	<.01
	Carbon+photon	1	53%	0.37–0.68	-			
	Total	2	69%	0.34–0.91				
2-year LC	Proton+photon	1	83%	0.63–0.94	-	12.48	1	<.01
	Carbon+photon	1	33%	0.20–0.50	-			
	Total	2	60%	0.14–0.94				
3-year LC	Proton+photon	1	62%	0.42–0.97		17.28	2	<.01
	Proton	2	94%	0.85–0.98	0%			
	Carbon+photon	1	99%	0.9–1				
	Total	4	83%	0.72–1				
5-year LC	Proton+photon	3	41%	0.21–0.65	0%	16.46	3	<.01
	Proton	7	89%	0.80–0.95	72%			
	Carbon+proton	1	88%	0.36–0.99	-			
	Total	11	79%	0.68–0.87				
8-year LC	Proton+photon	3	29%	0.14–0.51	53%	-	-	-
10-year LC	Proton+photon	1	98%	0.86–1	-	3.71	1	<.05
	Proton	1	85%	0.79–0.90	-			
	Total	2	93%	0.65–0.99				

to locate symmetrically upwards the graph, and scatter around both sides of the line. Egger's regression test did not show a publication bias (p=0.26). Besides, there was no obvious change in the results after the trim and -fill estimate (**Supplementary Figure 5**). Besides, as shown in **Supplementary Figure 6**, different study designs were not the potential source of heterogeneity.

Local Control Rate

As shown in **Figure 3**, after undergoing CI-RT for 3 and 5 years, the local control rate (LC) for benign meningioma was 100% and 88%, respectively, while the 2-year LC of non-benign meningiomas (atypical/anaplastic) was 33%. Compared with other treatments, the 3-year LC of CI-RT is better than PR-RT and proton combined with photon (99% *vs.* 94% *vs.* 62%,

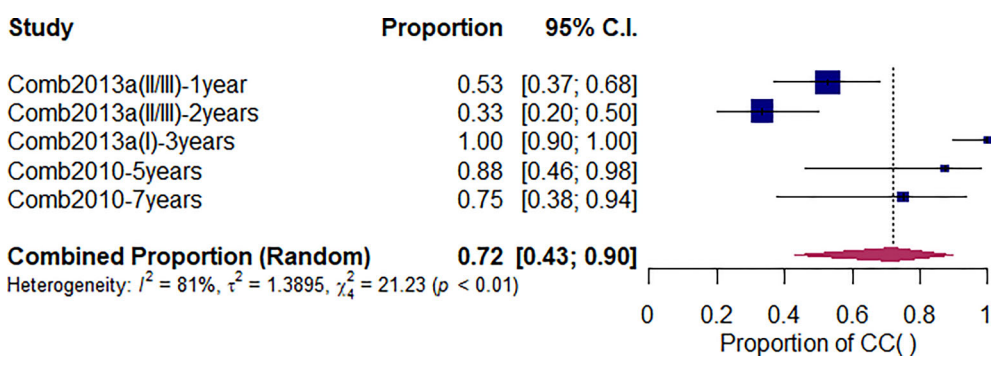

FIGURE 3 | The local control rate of meningioma initial diagnosis treated with CI-RT.

Q=17.28, df=2, p<.01) (**Supplementary Figure 5**). As shown in **Supplementary Figure 8** and **Table 2**, the 5-year LC of CI-RT combined with PR-RT was 88%(95%CL=.36-.99) same as the PR-RT 89% (95%CL=.80-.95, I^2 = 72), but significantly higher than PR-RT combined with PH-RT. 41% (95%CL=.21-.65, I^2 = 0, Q=16.46, *df*=3, *p*<.01)

Toxic and Side Effect

According to the General terminology Standard for adverse events (CTCAEv4.0), grade I and II side effects are classified as low-grade side reactions, while any symptoms of grade III or higher are classified as high-grade reactions (47). Overall, six studies have reported adverse reactions in patients with meningiomas that were treated with carbon ions. Five studies reported detailed data, among which one described only the symptoms and severity of adverse reactions (44), including alopecia, skin erythema, conjunctivitis, mucositis, dry mouth, headache, and nausea. As shown in **Table 3**, all side effects of CI-RT were grade I and grade II. Among them, focal alopecia, fatigue, skin stress and headache were the most common side effects of acute radiotherapy, with incidence rates of 19.5%, 15.3%, 10.5% and 10.1%, respectively. The results of the most common adverse reactions were almost the same proton and photon therapy, with incidence rates of 12%, 13%, 21% and 9%, respectively. With regards to the side effects of late radiotherapy, the most common adverse reactions were headache, sensory impairment, cognitive impairment, and hearing impairment, which had incidence rates of 19.4%, 23.7%, 9.1% and 9.1%, respectively.

DISCUSSION

Our study aims to investigate the efficacy and safety, as well as the influencing factor of CI-RT among meningiomas. The results indicated that the OS, LC, and the common toxic and side effect of CI-RT for meningiomas is similar to PR-RT, better than PH-RT.

According to EANO (European Association of Neuro-Oncology) guidelines (48), for WHO grade I meningiomas that were totally resected, the 10-year recurrence varies from 20% to 39% (49–51). The 5-year progression of WHO grade II meningiomas may be as high as 30% after gross total resection and 40% after subtotal resection (52, 53). For WHO grade III meningiomas, the 5-year progression-free survival ranged from 12% to 57%, even after resection and radiotherapy (54). With the development of science and technology, radiotherapy for meningioma has been proven to be a promising treatment option, which is more effective than conventional surgical excision (55). Previous studies have reported local control rates ranging from 66.5% for grade II meningiomas at 2 years follow-up to 81% at 5 years for high-grade meningiomas using precision photon therapy (9). Same as our results shown in **Table 2**, the 5-year LC reached 68% to 87%, and the 5-year OS increased to 66% to 85% after particle RT. Among them, carbon-ion beams and protons directly cleave double-stranded DNA at low concentrations of oxygen and emit lower doses of radiation to the surrounding healthy tissue, which results in improved therapeutic ratios when compared to photon (56). A review by Adeberg et al. (28) supported the efficacy and safety of proton and carbon ion therapy. Consistent with our results, either CI-RT or PR-RT produced a better comparable rate of LC compared with traditional photon therapy. However, a recent systematic review presented comparable rates of LC between photon and proton RT with regards to benign brain tumors. Due to the small sample sizes, the conclusions may not robust enough (57). CI-RT for meningioma is a novel treatment. The inherent physical characteristics of CI-RT provide a special dose distribution, according to the specific range shown by Bragg Peak. This has the advantages of accuracy and omits key intracranial tissues, which make it particularly suitable for the treatment of these tumors (56). A systematic review by *Coggins et al.* indicated that ion therapy represents a burgeoning field in the treatment of atypical and anaplastic meningiomas. Proton and carbon ion radiotherapy maintain comparable rates of local control to conventional photon therapy and allow for more targeted treatment plans that may limit excess radiation damage (9). Although the Hug *et al.* study did not specify the rate of OS, the LC rate after protons and photons treatment (62 Gy E) was 88% (34), which was slightly better than CI-RT combined proton therapy. Regardless of whether the meningiomas are primary or recurrent, our meta-analysis also indicated that the LC of meningioma in 3- and 5-year after PR-RT has similar rates with CI-RT, and significantly better than PH-RT.

Treatment optimization for patients with high-grade meningiomas is the main goal for a radiation oncologist. It is known, that, for long-term local tumor control, high doses of radiotherapy are required (28). Previous studies have demonstrated beneficial results for particle therapy among patients with meningiomas (9, 58). However, most studies have evaluated PR-RT in low-grade meningioma patients (9, 57).Regarding differences in grade of meningioma, we observed superior local control over longer intended times of follow-up for grade II meningiomas. This finding remains unsurprising given the nature of histologic grading. Compared with CI-RT, we observed higher LC with PR-RT, which had a mean LC of 59.62% over 5 years. In contrast, CI-RT failed to deliver comparable rates of local control in either grade II (50% at 34 months) or III (63% at 2 years) meningiomas. However, our finding may not represent a deficiency between the two modalities and may be a result of heterogenous populations or patient selection factors. There was a protocol for the MARCIE trial with a carbon ion boost in combination with postoperative photon radiotherapy for Simpson grade 4 and 5 atypical meningiomas patients (46), and more trials are expected to be published in the future to produce more convincing results.

Five studies (28, 30, 31, 44, 45) reported minimal or no acute high-grade toxicities. However, three studies did report similar findings with regards to late high-grade toxicities (30, 31, 43). Furthermore, a study by El Shafie *et al.* (31), which has the highest sample size across all studies in our review, supports these results. This finding is highly significant as it corroborates the

TABLE 3 | Acute and late treatment-related toxicity.

Intervention	Reason	Acute treatment-related toxicity < 6 months		Rate (%)	Late treatment-related toxicity > 6 months		Rate (%)
		CTCAE(I-II)	CTCAE (III OR higher)		CTCAE(I-II)	CTCAE (III OR higher)	
Carbon+ proton/photon	Focal alopecia	117	0	19.5	2	0	0.9
	Fatigue	92	0	15.3	19	1	8.6
	Skin irritation	63	0	10.5	4	0	1.8
	Headache	61	0	10.1	45	0	19.4
	Nausea	42	1	7.2	8	0	3.4
	Localized pain	26	0	4.3	12	0	5.2
	Sensory deficits	72	0	12	55	0	23.7
	Lymphedema	9	0	1.5	6	0	2.6
	Xerostomia	6	0	0.9	6	1	3.2
	Mucositis	2	3	0.8	1	0	0.4
	Radio necrosis	1	0	0.2	0	3	1.3
	Cognitive dysfunction	16	0	2.7	21	0	9.1
	Hair loss	40	1	6.8	9	0	3.9
	Hearing impairment	16	1	2.8	21	0	9.1
	Dizziness	17	0	2.8	7	0	3
	Seizures	9	0	1.5	10	0	4
	Change in character	1	0	0.2	0	0	0
	Lacrimation of eyes	0	1	0.2	0	0	0
	Acute hemorrhage	0	0	0	1	0	0.4
	Slight visual impairment	4	0	0.7	0	0	0
	Total	594	7	100	227	5	100
Proton	Seizure	17	0	29.7	0	0	0
	Skin toxicity	26	0	45.1	0	0	0
	Optic neuropathy	4	0	6.8	1	0	16.7
	Dry eye	6	0	10.3	1	0	16.7
	Hypogonadism	3	0	5.2	2	0	33.3
	Asymptomatic hypothyroidism	2	0	3	2	0	33.3
	Total	58	0	100	6	0	100
Proton+photon	Vision loss	3	0	2	3	4	5.6
	Visual field deficit	1	0	1	6	0	4.8
	Diplopia	2	0	1	3	1	3.2
	Exophthalmos	1	0	1	2	0	2.5
	Conjunctivitis	3	0	2	0	0	0
	Eye, other	7		2	5	0	4
	Hearing loss	3	0	2	8	2	7.5
	Tinnitus	1	0	1	5	0	4
	Olfactory alteration	2	0	1	2	0	1.6
	Gustation alteration	4	0	2	1	0	0.8
	Dysphasia	0	0	0	1	0	0.8
	Neuromotor deficit	0	1	1	0	2	1.6
	Weakness	0	1	1	3	0	2.4
	Facial numbness	3	0	2	5	0	4
	Facial weakness	4	0	2	6	0	2.4
	Ataxia	1	0	1	5	0	4
	Seizure	2	0	1	0	0	0
	Fall	0	0	0	3	0	2.4
	Dysarthria	0	0	0	1	0	0.8
	Headache	11	0	9	8	0	6.4
	Nausea	17	0	12	0	0	0
	Dizziness	2	0	1	1	0	0.8
	Vertigo	5	0	2	2	0	2.4
	Syncope	1	0	1	0	0	0
	Depression	3	0	3	1	0	0.8
	Neuralog deficit	4	0	2	12	1	10.4
	Endocrine deficit	1	0	1	16	1	13.6
	Osteoporosis	0	0	0	1	0	0.8
	Cerebral edema	0	0	0	0	2	2.4
	Brain atrophy	0	0	0	1	0	0.8
	Skin changes	34	0	21	2	0	2.4
	Alopecia	18	0	12	2	0	2.4
	Fatigue	21	1	13	7	0	4.4
	Total	154	3	100	112	13	100

commonly held view that CI-RT has reduced side effects compared to conventional PH-RT (59). Most articles reported headaches and sensory impairment as the predominant adverse effect among patients, which is expected. The lack of late high-grade toxicities remains particularly promising as it affirms the hypothesis that CI-RT limits extraneous radiation to normal brain tissue (60, 61). These results are promising in confirming the belief that ion RT predisposes patients to marginal side effects.

Although this systematic review and meta-analysis has been proven to be an effective treatment against meningioma, our outcomes need to be treated with caution due to several significant limitations. Firstly, the number of studies included in this meta-analysis was not much many that some subgroup analyses could only be combined with two or three studies. As there is an obvious correlation between the study quality and results, this problem needs to be taken seriously. Secondly, all CI-RT studies were found to be from the same country, and heterogeneity among the studies was obvious. Hence, the bias of results could not be ruled out. Thirdly, many studies did not classify benign and non-benign meningiomas, which may confuse the conclusions. Although CI-RT is a novel clinical treatment, as it becomes more common and affordable, additional prospective studies with larger sample sizes will be necessary to quantify efficacy.

CONCLUSIONS

CI-RT is a rapidly developing technique that has been proven to be an effective treatment against meningioma. The efficacy and safety of CI-RT for meningiomas is similar to PR-RT, better than PH-RT. However, there is a need for more prospective trials in order to quantify the efficacy of ion beam RT compared to conventional therapies and to provide meaningful comparisons of local control rates and survival rates among patients undergoing alternative interventions.

DATA AVAILABILITY STATEMENT

The original contributions presented in the study are included in the article/**Supplementary Material**, further inquiries can be directed to the corresponding authors.

AUTHOR CONTRIBUTIONS

Conception and design: K-HY, X-HW, and X-XL. Search and collection of data: J-YL, J-WL, M-XL. Data analysis and interpretation: L-PG, Z-TB, and FB. Manuscript writing: J-YL, J-WL, and Y-CJ. All authors contributed to the article and approved the submitted version.

FUNDING

Supported by the National Social Science Fund of China (no. 19ZDA142); Key Laboratory of Evidence Based Medicine and Knowledge Translation Foundation of Gansu Province (no. GSEBMKT-2020KF01).

SUPPLEMENTARY MATERIAL

The Supplementary Material for this article can be found online at: https://www.frontiersin.org/articles/10.3389/fonc.2021.620534/full#supplementary-material

REFERENCES

1. Whittle IR, Smith C, Navoo P, Collie D. Meningiomas. *Lancet (London England)* (2004) 363(9420):1535–43. doi: 10.1016/S0140-6736(04)16153-9
2. Ostrom QT, Gittleman H, Xu J, Kromer C, Wolinsky Y, Kruchko C, et al. CBTRUS Statistical Report: Primary Brain and Other Central Nervous System Tumors Diagnosed in the United States in 2009-2013. *Neuro-Oncology*. (2016) 18(suppl_5):v1–75. doi: 10.1093/neuonc/now207
3. Buttrick S, Shah AH, Komotar RJ, Ivan ME. Management of Atypical and Anaplastic Meningiomas. *Neurosurgery Clinics North America* (2016) 27 (2):239–47. doi: 10.1016/j.nec.2015.11.003
4. Chacko G. Meningiomas: A Continuum of Progress in Risk-Stratification. *Neurol India* (2018) 66(1):161–2. doi: 10.4103/0028-3886.222841
5. Harter PN, Braun Y, Plate KH. Classification of Meningiomas-Advances and Controversies. *Chin Clin Oncol* (2017) 6(Suppl 1):S2. doi: 10.21037/cco.2017.05.02
6. Wang N, Osswald M. Meningiomas: Overview and New Directions in Therapy. *Semin Neurology* (2018) 38(1):112–20. doi: 10.1055/s-0038-1636502
7. Bourhaleb F, Marchetto F, Attili A, Pitta G, Cirio R, Donetti M, et al. A Treatment Planning Code for Inverse Planning and 3D Optimization in Hadrontherapy. *Comput Biol Med* (2008) 38(9):990–9. doi: 10.1016/j.compbiomed.2008.07.005
8. Roland Goldbrunner GM, Preusser M, Jenkinson MD, Sallabanda K, Houdart E, von Deimling A, et al. EANO Guidelines for the Diagnosis and Treatment of Meningiomas. *Lancet Oncol* (2016) 17:e383–91. doi: 10.1016/S1470-2045(16)30321-7
9. Coggins WS, Pham NK, Nguyen AV, Branch DW, Guillet JY, Korst G, et al. A Systematic Review of Ion Radiotherapy in Maintaining Local Control Regarding Atypical and Anaplastic Meningiomas. *World Neurosurgery* (2019) 132:282–91. doi: 10.1016/j.wneu.2019.08.149
10. Debus J, Haberer T, Schulz-Ertner D, Jakel O, Wenz F, Enghardt W, et al. [Carbon Ion Irradiation of Skull Base Tumors At GSI. First Clinical Results and Future Perspectives]. *Clin Oncol (R Coll Radiol)* (2000) 12(2):71–2. doi: 10.1007/s001740050113
11. Gademann G, Hartmann GH, Kraft G, Lorenz WJ, Wannenmacher M. The Medical Heavy Ion Therapy Project At the Gesellschaft Fur Schwerionenforschung Facility in Darmstadt. *Basic Life Sci* (1990) 54:249–58. doi: 10.1007/1978-1001-4684-5802-1002_1019
12. Kraft-Weyrather W, Bohl J, Elsaesser T, Schulz-Ertner D, Debus J, Combs SE. Radiobiological Evaluation and Correlation With the Local Effect Model (Lem) of Carbon Ion Radiation Therapy and Temozolomide in Glioblastoma Cell Lines. *Int J Radiat Oncol Biol Phys* (2008) 72(1):126–37. doi: 10.1016/j.ijrobp.2008.06.530
13. Fujii Y, Kato TA, Ueno A, Kubota N, Fujimori A, Okayasu R. Ascorbic Acid Gives Different Protective Effects in Human Cells Exposed to X-Rays and Heavy Ions. *Am J Clin Oncol* (2010) 33(6):646–9. doi: 10.1097/COC.1090b1013e3181cdf1090fe
14. Gong L, Jin X, Li Q, Liu J, An L. Heavy Ion Beams Induce Survivin Expression in Human Hepatoma SMMC-7721 Cells More Effectively Than X-Rays. *J Radiat Res* (2007) 48(5):377–83. doi: 10.1269/jrr.07029

15. Adeberg S, Jensen A, Akbaba S, Katayama S, Verma V, Bernhardt D, et al. The Phase I/II ACCEPT Trial: Cetuximab and IMRT With Carbon Ion Boost for Adenoid Cystic Carcinoma. *Radiotherapy Oncol* (2019) 132:90. doi: 10.1016/S0167-8140(19)30335-4
16. Kamada T, Tsujii H, Blakely EA, Debus J, De Neve W, Durante M, et al. Carbon Ion Radiotherapy in Japan: An Assessment of 20 Years of Clinical Experience. *Lancet Oncol* (2015) 16(2):e93–e100. doi: 10.1016/S1470-2045(14)70412-7
17. Xiu-xia L, Ya Z, Yao-long C, Ke-hu Y, Zong-jiu Z. The Reporting Characteristics and Methodological Quality of Cochrane Reviews About Health Policy Research. *Health Policy* (2015) 119(4):503–10. doi: 10.1016/j.healthpol.2014.09.002
18. Wang X, Chen Y, Yao L, Chen Y, Yao L, Zhou Q, Wu Q, Estill J, et al. Reporting of Declarations and Conflicts of Interest in WHO Guidelines Can Be Further Improved. *J Clin Epidemiol* (2018) 98:1–8. doi: 10.1016/j.jclinepi.2017.12.021
19. Ge L, Tian JH, Li YN, Pan JX, Li G, Wei D, et al. Association Between Prospective Registration and Overall Reporting and Methodological Quality of Systematic Reviews: A Meta-Epidemiological Study. *J Clin Epidemiol* (2018) 93:45–55. doi: 10.1016/j.jclinepi.2017.10.012
20. Yang K. Evidence-Based Social Science: The Origin, Development and Prospects. *Libr Inf* (2018) 03):1–10.
21. Higgins JP, Thompson SG. Quantifying Heterogeneity in a Meta-Analysis. *Stat Med* (2002) 21(11):1539–58. doi: 10.1002/sim.1186
22. Flemyng E, Dwan K, Moore TH, Page MJ, Higgins JP. Risk of Bias 2 in Cochrane Reviews: A Phased Approach for the Introduction of New Methodology. *Cochrane Database Systematic Rev* (2020) 10:Ed000148. doi: 10.1002/14651858.ED000148
23. Rosenthal R. The "File Drawer Problem" and Tolerance for Null Results. *psychol Bulletin* (1979) 86(3):638–41. doi: 10.1037/0033-2909.86.3.638
24. Page MJ, Sterne JAC, Higgins JPT, Egger M. Investigating and Dealing With Publication Bias and Other Reporting Biases in Meta-Analyses of Health Research: A Review. *Res Synthesis Methods* (2020)12(2):248–59. doi: 10.1002/jrsm.1468
25. Duval S, Tweedie R. Trim and Fill: A Simple Funnel-Plot-Based Method of Testing and Adjusting for Publication Bias in Meta-Analysis. *Biometrics.* (2000) 56(2):455–63. doi: 10.1111/j.0006-341X.2000.00455.x
26. Wang Xiaoqin CY, Qingyuan Q, Yang K. Interpretation of Methodological Quality Assessment Tools for Case Series Research. *Chin J Evidence-Based Pediatr* 10(5). doi:10.3969/j.issn.1673-5501.2015.05.012
27. Yan P, Yao L, Li H, Zhang M, Xun Y, Li M, et al. The Methodological Quality of Robotic Surgical Meta-Analyses Needed to Be Improved: A Cross-Sectional Study. *J Clin Epidemiol* (2019) 109:20–9. doi: 10.1016/j.jclinepi.2018.12.013
28. Adeberg S, Hartmann C, Welzel T, Rieken S, Habermehl D, von Deimling A, et al. Long-Term Outcome After Radiotherapy in Patients With Atypical and Malignant Meningiomas–Clinical Results in 85 Patients Treated in a Single Institution Leading to Optimized Guidelines for Early Radiation Therapy. *Int J Radiat Oncol Biol Phys* (2012) 83(3):859–64. doi: 10.1016/j.ijrobp.2011.08.010
29. Boskos C, Feuvret L, Noel G, Habrand JL, Pommier P, Alapetite C, et al. Combined Proton and Photon Conformal Radiotherapy for Intracranial Atypical and Malignant Meningioma. *Int J Radiat Oncol Biol Phys* (2009) 75(2):399–406. doi: 10.1016/j.ijrobp.2008.10.053
30. El Shafie RA, Czech M, Kessel KA, Habermehl D, Weber D, Rieken S, et al. Evaluation of Particle Radiotherapy for the Re-Irradiation of Recurrent Intracranial Meningioma. *Radiat Oncol* (2018) 13(1):86. doi: 10.1186/s13014-018-1026-x
31. El Shafie RA, Czech M, Kessel KA, Habermehl D, Weber D, Rieken S, et al. Clinical Outcome After Particle Therapy for Meningiomas of the Skull Base: Toxicity and Local Control in Patients Treated With Active Rasterscanning. *Radiat Oncol* (2018) 13(1):86. doi: 10.1186/s13014-018-1002-5
32. Gudjonsson O, Blomquist E, Nyberg G, Pellettieri L, Montelius A, Grusell E, et al. Stereotactic Irradiation of Skull Base Meningiomas With High Energy Protons. *Acta Neurochirurgica* (1999) 141(9):933–40. doi: 10.1007/s007010050399
33. Halasz LM, Bussière MR, Dennis ER, Niemierko A, Chapman PH, Loeffler JS, et al. Proton Stereotactic Radiosurgery for the Treatment of Benign Meningiomas. *Int J Radiat Oncol Biol Phys* (2011) 81(5):1428–35. doi: 10.1016/j.ijrobp.2010.07.1991
34. Hug EB, Devries A, Thornton AF, Munzenride JE, Pardo FS, Hedley-Whyte ET, et al. Management of Atypical and Malignant Meningiomas: Role of High-Dose, 3D-Conformal Radiation Therapy. *J Neuro-Oncology* (2000) 48(2):151–60. doi: 10.1023/a:1006434124794
35. Murray FR, Snider JW, Bolsi A, Lomax AJ, Walser M, Kliebsch U, et al. Long-Term Clinical Outcomes of Pencil Beam Scanning Proton Therapy for Benign and Non-Benign Intracranial Meningiomas. *Int J Radiat Oncol Biol Phys* (2017) 99(5):1190–8. doi: 10.1016/j.ijrobp.2017.08.005
36. Sanford NN, Yeap BY, Larvie M, Daartz J, Munzenrider JE, Liebsch NJ, et al. Prospective, Randomized Study of Radiation Dose Escalation With Combined Proton-Photon Therapy for Benign Meningiomas. *Int J Radiat Oncol Biol Phys* (2017) 99(4):787–96. doi: 10.1016/j.ijrobp.2017.07.008
37. Slater JD, Loredo LN, Chung A, Bush DA, Patyal B, Johnson WD, et al. Fractionated Proton Radiotherapy for Benign Cavernous Sinus Meningiomas. *Int J Radiat Oncol Biol Phys* (2012) 83(5):e633–7. doi: 10.1016/j.ijrobp.2012.01.079
38. Stefan Rieken DH, Haberer T, Jaekel O, Debus J, Comb SE. Proton and Carbon Ion Radiotherapy for Primary Brain Tumors Delivered With Active Raster Scanning At the Heidelberg Ion Therapy Center (HIT): Early Treatment Results and Study Concepts. *Radiat Oncol* (2012) 99(4):787–96. doi: 10.1186/1748-717X-7-41
39. Vernimmen FJ, Harris JK, Wilson JA, Melvill R, Smit BJ, Slabbert JP. Stereotactic Proton Beam Therapy of Skull Base Meningiomas. *Int J Radiat Oncol Biol Phys* (2001) 49(1):99–105. doi: 10.1016/S0360-3016(00)01457-7
40. Vlachogiannis P, Gudjonsson O, Montelius A, Grusell E, Isacsson U, Nilsson K, et al. Hypofractionated High-Energy Proton-Beam Irradiation is an Alternative Treatment for WHO Grade I Meningiomas. *Acta neurochirurgica* (2017) 159(12):2391–400. doi: 10.1007/s00701-017-3352-4
41. Weber DC, Lomax AJ, Rutz HP, Stadelmann O, Egger E, Timmermann B, et al. Spot-Scanning Proton Radiation Therapy for Recurrent, Residual or Untreated Intracranial Meningiomas. *Radiother Oncol* (2004) 71(3):251–8. doi: 10.1016/j.radonc.2004.02.011
42. Weber DC, Schneider R, Goitein G, Koch T, Ares C, Geismar JH, et al. Spot Scanning-Based Proton Therapy for Intracranial Meningioma: Long-Term Results From the Paul Scherrer Institute. *Int J Radiat Oncol Biol Phys* (2012) 83(3):865–71. doi: 10.1016/j.ijrobp.2011.08.027
43. Combs SE, Welzel T, Habermehl D, Rieken S, Dittmar JO, Kessel K, et al. Prospective Evaluation of Early Treatment Outcome in Patients With Meningiomas Treated With Particle Therapy Based on Target Volume Definition With MRI and 68Ga-DOTATOC-PET. *Acta Oncol* (2013) 52(3):514–20. doi: 10.3109/0284186X.2013.762996
44. Combs SE, Hartmann C, Nikoghosyan A, Jäkel O, Karger CP, Haberer T, et al. Carbon Ion Radiation Therapy for High-Risk Meningiomas. *Radiotherapy Oncol J Eur Soc Ther Radiol Oncol* (2010) 95(1):54–9. doi: 10.1016/j.radonc.2009.12.029
45. Combs SE, Kessel K, Habermehl D, Haberer T, Jäkel O, Debus J. Proton and Carbon Ion Radiotherapy for Primary Brain Tumors and Tumors of the Skull Base. *Acta Oncol (Stockholm Sweden)* (2013) 52(7):1504–9. doi: 10.3109/0284186X.2013.818255
46. Combs SE, Edler L, Burkholder I, Rieken S, Habermehl D, Jäkel O, et al. Treatment of Patients With Atypical Meningiomas Simpson Grade 4 and 5 With a Carbon Ion Boost in Combination With Postoperative Photon Radiotherapy: The MARCIE Trial. *BMC Cancer* (2010) 10:615. doi: 10.1186/1471-2407-10-615
47. Freites-Martinez A, Santana N, Arias-Santiago S, Viera A. Using the CommonTerminology Criteria for Adverse Events (CTCAE - Version 5.0) to Evaluate the Severity of Adverse Events of Anticancer Therapies. *Actas Dermosifiliogr* (2021) 112(1):90–2. doi: 10.1016/j.ad.2019.05.009.
48. Goldbrunner R, Minniti G, Preusser M, Jenkinson MD, Sallabanda K, Houdart E, et al. EANO Guidelines for the Diagnosis and Treatment of Meningiomas. *Lancet Oncol* (2016) 17(9):e383–391. doi: 10.1016/S1470-2045(16)30321-7
49. Mirimanoff RO, Dosoretz DE, Linggood RM, Ojemann RG, Martuza RL. Meningioma: Analysis of Recurrence and Progression Following Neurosurgical Resection. *J Neurosurgery* (1985) 62(1):18–24. doi: 10.3171/jns.1985.62.1.0018
50. Shay JW, Homma N, Zhou R, Naseer MI, Chaudhary AG, Al-Qahtani M, et al. Abstracts From the 3rd International Genomic Medicine Conference (3rd

IGMC 2015) : Jeddah, Kingdom of Saudi Arabia. 30 November - 3 December 2015. *BMC Genomics* (2016) 17 Suppl 6(Suppl 6):487.
51. Soyuer S, Chang EL, Selek U, Shi W, Maor MH, DeMonte F. Radiotherapy After Surgery for Benign Cerebral Meningioma. *Radiother Oncol* (2004) 71 (1):85–90. doi: 10.1016/j.radonc.2004.01.006
52. Aghi MK, Carter BS, Cosgrove GR, Ojemann RG, Amin-Hanjani S, Martuza RL, et al. Long-Term Recurrence Rates of Atypical Meningiomas After Gross Total Resection With or Without Postoperative Adjuvant Radiation. *Neurosurgery* (2009) 64(1):56–60; discussion 60. doi: 10.1227/01.NEU.0000330399.55586.63
53. Hammouche S, Clark S, Wong AH, Eldridge P, Farah JO. Long-Term Survival Analysis of Atypical Meningiomas: Survival Rates, Prognostic Factors, Operative and Radiotherapy Treatment. *Acta Neurochirurgica* (2014) 156 (8):1475–81. doi: 10.1007/s00701-014-2156-z
54. Sughrue ME, Sanai N, Shangari G, Parsa AT, Berger MS, McDermott MW. Outcome and Survival Following Primary and Repeat Surgery for World Health Organization Grade III Meningiomas. *J Neurosurgery* (2010) 113 (2):202–9. doi: 10.3171/2010.1.JNS091114
55. Adeberg S, Harrabi SB, Verma V, Bernhardt D, Grau N, Debus J, et al. Treatment of Meningioma and Glioma With Protons and Carbon Ions. *Radiat Oncol* (2017) 12(1):193. doi: 10.1186/s13014-017-0924-7
56. Li C, Zhang Q, Li Z, Feng S, Luo H, Liu R, et al. Efficacy and Safety of Carbon-Ion Radiotherapy for the Malignant Melanoma: A Systematic Review. *Cancer Med* (2020) 9(15):5293–305. doi: 10.1002/cam4.3134
57. Lesueur P, Calugaru V, Nauraye C, Stefan D, Cao K, Emery E, et al. Proton Therapy for Treatment of Intracranial Benign Tumors in Adults: A Systematic Review. *Cancer Treat Rev* (2019) 72:56–64. doi: 10.1016/j.ctrv.2018.11.004
58. Seidensaal K, Harrabi SB, Uhl M, Debus J. Re-Irradiation With Protons or Heavy Ions With Focus on Head and Neck, Skull Base and Brain Malignancies. *Br J Radiology* (2020) 93(1107):20190516. doi: 10.1259/bjr.20190516
59. Ma T, Weier E, Nguyen T, Huang YC. Carbonising Radiation Therapy: is Carbon Ion Radiation Therapy the Way for the Future? *J Med Radiat Sci* (2019) 66:105–6. doi: 10.1002/jmrs.1-324
60. Habl G, Uhl M, Katayama S, Kessel KA, Hatiboglu G, Hadaschik B, et al. Acute Toxicity and Quality of Life in Patients With Prostate Cancer Treated With Protons or Carbon Ions in a Prospective Randomized Phase II Study–the IPI Trial. *Int J Radiat Oncology Biology Physics* (2016) 95(1):435–43. doi: 10.1016/j.ijrobp.2016.02.025
61. Laine AM, Pompos A, Timmerman R, Jiang S, Story MD, Pistenmaa D, et al. The Role of Hypofractionated Radiation Therapy With Photons, Protons, and Heavy Ions for Treating Extracranial Lesions. *Front In Oncol* (2016) 5:1–14. doi: 10.3389/fonc.2015.00302

Conflict of Interest: The authors declare that the research was conducted in the absence of any commercial or financial relationships that could be construed as a potential conflict of interest.

Copyright © 2021 Li, Li, Jin, Li, Guo, Bing, Zhang, Bai, Wang, Li and Yang. This is an open-access article distributed under the terms of the Creative Commons Attribution License (CC BY). The use, distribution or reproduction in other forums is permitted, provided the original author(s) and the copyright owner(s) are credited and that the original publication in this journal is cited, in accordance with accepted academic practice. No use, distribution or reproduction is permitted which does not comply with these terms.

frontiers in Oncology

ORIGINAL RESEARCH
published: 10 June 2021
doi: 10.3389/fonc.2021.601784

Monitoring Carbon Ion Beams Transverse Position Detecting Charged Secondary Fragments: Results From Patient Treatment Performed at CNAO

Marco Toppi[1,2], Guido Baroni[3], Giuseppe Battistoni[4], Maria Giuseppina Bisogni[5,6], Piergiorgio Cerello[7], Mario Ciocca[8], Patrizia De Maria[9], Micol De Simoni[10,11], Marco Donetti[8], Yunsheng Dong[4,12], Alessia Embriaco[13], Veronica Ferrero[7], Elisa Fiorina[7,8], Marta Fischetti[1,11], Gaia Franciosini[10,13], Aafke Christine Kraan[6], Carmela Luongo[13,14], Etesam Malekzadeh[8], Marco Magi[1], Carlo Mancini-Terracciano[10,11], Michela Marafini[11,15], Ilaria Mattei[4], Enrico Mazzoni[6], Riccardo Mirabelli[10,11,15], Alfredo Mirandola[8], Matteo Morrocchi[5,6], Silvia Muraro[4], Vincenzo Patera[1,11,15], Francesco Pennazio[7], Angelo Schiavi[1,11], Adalberto Sciubba[1,2,15], Elena Solfaroli-Camillocci[9,10,11], Giancarlo Sportelli[5,6], Sara Tampellini[8], Giacomo Traini[11,15], Serena Marta Valle[4], Barbara Vischioni[8], Viviana Vitolo[8] and Alessio Sarti[1,11,15]*

[1] Dipartimento di Scienze di Base e Applicate per l'Ingegneria, Sapienza Università di Roma, Rome, Italy, [2] INFN Laboratori Nazionali di Frascati, Frascati, Italy, [3] Dipartimento di Elettronica Informazione e Bioingegneria, Politecnico di Milano, Milano, Italy, [4] INFN Section of Milan, Milan, Italy, [5] Dipartimento di Fisica "E. Fermi", Università di Pisa, Pisa, Italy, [6] INFN Sezione di Pisa, Pisa, Italy, [7] INFN Sezione di Torino, Turin, Italy, [8] CNAO Centro Nazionale di Adroterapia Oncologica, Pavia, Italy, [9] Scuola di Specializzazione in Fisica Medica, Sapienza Università di Roma, Roma, Italy, [10] Dipartimento di Fisica, Sapienza Università di Roma, Rome, Italy, [11] INFN Section of Rome 1, Rome, Italy, [12] Dipartimento di Fisica, Università degli studi di Milano, Milan, Italy, [13] INFN Sezione di Pavia, Pavia, Italy, [14] Dipartimento di Chimica e Chimica Industriale, Università di Pisa, Pisa, Italy, [15] CREF - Museo Storico della Fisica e Centro Studi e Ricerche E.Fermi, Rome, Italy

Particle therapy in which deep seated tumours are treated using ^{12}C ions (Carbon Ions RadioTherapy or CIRT) exploits the high conformity in the dose release, the high relative biological effectiveness and low oxygen enhancement ratio of such projectiles. The advantages of CIRT are driving a rapid increase in the number of centres that are trying to implement such technique. To fully profit from the ballistic precision achievable in delivering the dose to the target volume an online range verification system would be needed, but currently missing. The ^{12}C ions beams range could only be monitored by looking at the secondary radiation emitted by the primary beam interaction with the patient tissues and no technical solution capable of the needed precision has been adopted in the clinical centres yet. The detection of charged secondary fragments, mainly protons, emitted by the patient is a promising approach, and is currently being explored in clinical trials at CNAO. Charged particles are easy to detect and can be back-tracked to the emission point with high efficiency in an almost background-free environment. These fragments are the product of projectiles fragmentation, and are hence mainly produced along the beam path inside the patient. This experimental signature can be used to

OPEN ACCESS

Edited by:
Timothy Dean Malouff,
Mayo Clinic Florida,
United States

Reviewed by:
Dalong Pang,
Georgetown University,
United States
Tomohiro Yamashita,
Kobe University, Japan

***Correspondence:**
Giacomo Traini
giacomo.traini@roma1.infn.it

Specialty section:
This article was submitted to Radiation Oncology, a section of the journal Frontiers in Oncology

Received: 01 September 2020
Accepted: 11 May 2021
Published: 10 June 2021

Citation:
Toppi M, Baroni G, Battistoni G, Bisogni MG, Cerello P, Ciocca M, De Maria P, De Simoni M, Donetti M, Dong Y, Embriaco A, Ferrero V, Fiorina E, Fischetti M, Franciosini G, Kraan AC, Luongo C, Malekzadeh E, Magi M, Mancini-Terracciano C, Marafini M, Mattei I, Mazzoni E, Mirabelli R, Mirandola A, Morrocchi M, Muraro S, Patera V, Pennazio F, Schiavi A, Sciubba A, Solfaroli-Camillocci E, Sportelli G, Tampellini S, Traini G, Valle SM, Vischioni B, Vitolo V and Sarti A (2021) Monitoring Carbon Ion Beams Transverse Position Detecting Charged Secondary Fragments: Results From Patient Treatment Performed at CNAO. Front. Oncol. 11:601784. doi: 10.3389/fonc.2021.601784

monitor the beam position in the plane orthogonal to its flight direction, providing an online feedback to the beam transverse position monitor chambers used in the clinical centres. This information could be used to cross-check, validate and calibrate, whenever needed, the information provided by the ion chambers already implemented in most clinical centres as beam control detectors. In this paper we study the feasibility of such strategy in the clinical routine, analysing the data collected during the clinical trial performed at the CNAO facility on patients treated using ^{12}C ions and monitored using the Dose Profiler (DP) detector developed within the INSIDE project. On the basis of the data collected monitoring three patients, the technique potential and limitations will be discussed.

Keywords: particle therapy, carbon ions, online monitoring, charged particles, fibre detectors

INTRODUCTION

Carbon ion beams in Particle Therapy (PT) are used to achieve a high dose conformation to the target volume in combination with a high Relative Biological Effectiveness (RBE) (1). According to the Particle Therapy Co-operative group (PTCOG), thirteen ^{12}C ions beam facilities located in Italy, Austria, Germany, China and Japan are currently in operation (2), and five are under construction. At present, a wide spectrum of pathologies located in several districts is eligible for carbon ion therapy. The reader is addressed to (3) for an updated review of the diseases treatable with carbon ions and the corresponding clinical outcome.

Despite the physical and biological advantages of carbon ion therapy, its intrinsic accuracy in targeting the treatment volume is not yet fully exploited. In the current clinical work-flow, most of the QA procedures are performed before the treatment, then all the arising inter-fraction effects as patient mis-alignment or morphological changes, which translate in an effective range difference with respect to the planning, have to be taken into account at the planning stage. A typical approach is the use of safety margins after defining the Clinical Target Volume (CTV) and safe irradiation strategies that avoid the potential exposure of organs at risk to unwanted dose (4, 5).

Great efforts have been made to develop a technique capable of giving a real time feedback on the dose conformity to the target volume. Such systems are typically based on the detection of secondary radiations as prompt-gammas (6), annihilation photons produced by the beam-induced β^+ activation (7, 8), or charged fragments (9, 10).

The Dose Profiler (DP) has been designed and built to be operated at CNAO as an *in vivo* verification system of the carbon ion treatments (11). It exploits charged secondary fragments, mainly protons, that are detected and tracked by means of eight planes of plastic scintillating fibers. The DP is a part of a bi-modal system, developed within the INSIDE collaboration (12) and installed in the CNAO treatment room n.1, including also a PET scanner used to measure the beam-induced β^+ activity. In 2019 a clinical trial started with the aim of evaluating the system capability to detect the morphological changes occurred in the patient during the several session of a full treatment delivery. The results obtained monitoring the first three patients can be found in Fischetti et al. (13), where the authors discuss the case of a patient for which internal morphological changes were detected by comparing the fragments spatial emission maps measured in different treatment fractions. In this manuscript, instead, we focus on a completely different matter: the possibility to exploit the secondary fragments produced during the treatment to monitor the beam position at the entrance point in the patient body. Such monitoring will be complementary to the techniques that are already routinely implemented in clinical centres to control the beam delivery and that are usually implemented using ionization chambers positioned at the end of the accelerator nozzle just before the beam exit window (14).

A CIRT treatment is composed of many irradiation by single Pencil Beams (PBs), with own scheduled direction, energy (i.e range) and fluency. Presently the transverse beam position of each PB is generally verified on-line by *ad hoc* devices [i.e. ionization chambers (15)] placed before the beam exit window. However, as stated in (16), a robust monitoring strategy independent of the diagnostics embedded in the nozzle could be of great interest, in particular in the frame of adaptive radio therapy using image guidance.

In CIRT, protons and neutrons are the most abundant products of the incoming beam fragmentation occurring inside the patient tissues (17) and a significant fraction of the protons produced at large angles with respect to the beam direction has enough kinetic energy to escape from the patient, as reported in several measurements (9, 18–20). In (16) a method based on the detection of such charged secondary fragments has been proposed, and its performance has been evaluated on an anthropomorphic phantom for different energies of the carbon ion beam. In this work we propose a monitoring technology, alternative to the ones currently implemented in the clinical centres using ionization chambers, based on charged fragments detection, and we evaluate its feasibility in the clinical practice analysing the data collected monitoring three patients enrolled in the INSIDE clinical trial.

The obtained results and the technique performance and limitations are reported and discussed hereafter.

MATERIAL AND METHODS

Unlike neutral radiation, secondary charged particles can be easily detected and back-tracked with high efficiency and with

little background. The measured fragments emission yield is anti-correlated with the production depth, since the kinetic energy of fragments decreases with the increasing path travelled inside the patient.

Fragments that have the kinetic energy needed to exit from the patient are mainly products of the projectile fragmentation, as the products of target fragmentation have, in average, lower kinetic energies and are not able to exit from the body to be detected. In this latter case the products have kinetic energy of few MeV and can not escape from the patient, while projectiles fragments mainly keep the beam velocity and direction, causing the characteristic dose tail beyond the Bragg peak. The same arguments applies to the products of re-interactions of fragments inside the patient body (tertiary fragments): such fragments can be produced (especially in the case of neutrons) far away from the primary interaction of the beam with the patient along the path towards the target volume, but their contribution becomes to be significant only in the distal region where the direct production from the fragmentation drops. In the entrance channel, however, the fragments are mainly produced directly by the fragmentation of the projectile and for that reason their production vertexes have to lie in a truncated cone whose circular section, at different depths inside the patient body, has a radius that is a convolution of the beam spot size and the effect of the multiple scattering interactions undergone by the primary beam. The fragments produced at large angle (60°-90° with respect to the incoming beam direction) are mainly protons, with a low contamination of deuteron and tritons (less than 10%) and most of them are generated directly from the primary projectile fragmentation (21). When back-tracking those reconstructed fragments, towards their production region inside the patient, and performs the projection of the reconstructed tracks in the plane orthogonal to the beam direction, one thus expects an accumulation along the beam incoming direction with the aforementioned experimental uncertainty, as shown in **Figure 1**.

In this work, we therefore propose to evaluate the beam transverse position as the accumulation point in the plane orthogonal to the beam direction of the fragments-related tracks reconstructed by a tracking detector.

The method has been tested analysing the data collected monitoring three patients treated with carbon ions at CNAO. The data collection occurred in the context of the clinical trial at CNAO (22), as described in *Clinical Trial and Data Taking Conditions*, in which a test of the performance of the INSIDE system was carried out.

To evaluate the monitoring precision achievable on the incoming beam position, fragments coming from each PB were reconstructed, and their position in the transverse plane was compared to the nominal one provided by the Dose Delivery System (DDS). In the following, the details about the patient treatment and the tracking detector used for the monitoring are quickly summarized. The full procedure used to measure the beam position in the transverse plane is described in detail afterwards.

The Dose Profiler

The DP [whose detailed description and performance can be found elsewhere (11)] is made of 8 scintillating fibers planes (each fiber has a square cross-section with 500 μm side) and has been carefully optimized to detect and reconstruct the charged fragments exiting from the patient. More than 3,000 Silicon Photo-multipliers (each one of 1 mm^2 active area) are used to collect the scintillation light from pairs of fibres in each plane and reconstruct the 3D path traversed by the fragments inside the detector active volume. The DAQ system, capable of collecting the signals from all the SiPMs and providing a self-triggering acquisition mode, was optimized to minimize the detector dead time (measured using the data collected during the patient monitoring and equal to ~5 μs per event), allowing to sustain the fragment detection rate (O ~ 100 kHz) reached in a typical treatment at CNAO. A per track back-pointing resolution of 5–7 mm, depending on the fragment energy and angle inside the detector, has been measured with the device placed at 50 cm from a point-like target in a pre-trial characterisation data-taking campaign. The fiber planes and the read-out electronics are embedded in a light-tight box held by a movable cart (shown in **Figure 2**) that also support a PET scanner formed by two planar LYSO detectors, used to measure the beam-induced β^+ activation. The cart is inserted and hooked in the operation

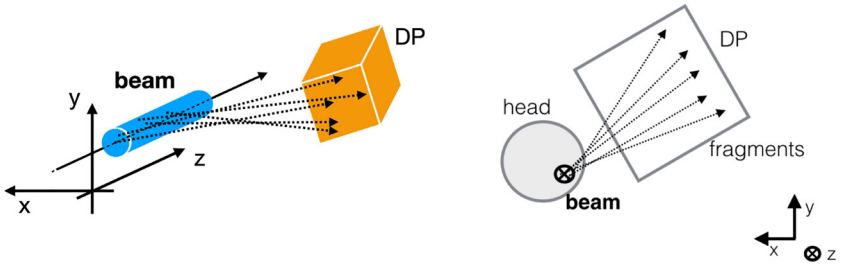

FIGURE 1 | Sketch of the experimental setup. On the left a 3D sketch is showing the measurement principle: the production point of the fragments (dashed lines) detected by the DP are all located around the transverse beam position, within the beam lateral size (cyan cylinder). On the right the 2D projection is shown from the perspective in which the beam (black bold cross) is orthogonal to the picture. The rationale of the strategy proposed in the manuscript can be observed: in the plane orthogonal to the beam direction, the tracks intersections can be used to identify the beam incoming direction in the x,y plane.

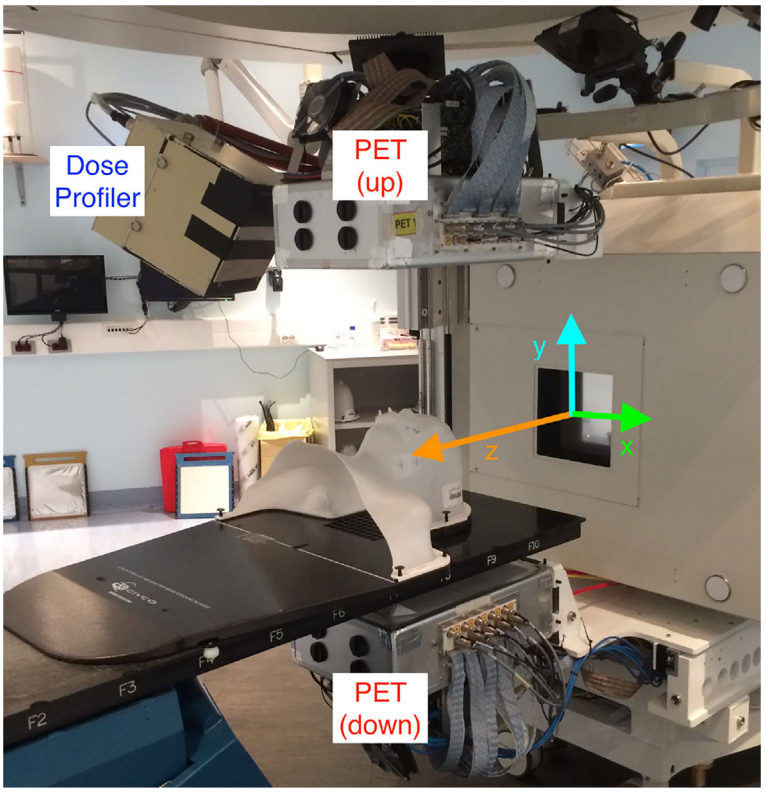

FIGURE 2 | View of the INSIDE cart holding the DP and the PET heads installed in the CNAO treatment room 1. A patient mask is attached to the bed to show the patient position with respect to the DP during a treatment. The reference frame used to present the DP measurements is over-imposed (the *z*-axis, in orange, is along the incoming beam direction).

position just before the treatment start, and it is moved back to a rest position located in a room side once the treatment is finished.

During its operation the DP is located at ~50 cm from the room isocenter, forming an angle respectively of 60° with respect to the beam direction (z) in the xz plane, and of 30° in the yz plane. A precise measurement of the DP position with respect to the treatment room isocenter has been obtained by means of a laser survey system. It was found that the cart anchoring system allows for a highly reproducible positioning when removing and inserting the cart ensuring an accuracy of this procedure below 1 mm, as evaluated in the system commissioning phase.

Clinical Trial and Data Taking Conditions

The INSIDE Clinical trial (22) has started in September 2019 at CNAO with the purpose of evaluating the carbon ion treatments inter-fraction monitoring capability of the DP. Ten patients, affected by pathologies involving the head-neck district, have been selected and monitored during the whole period of the therapy administration (3–4 weeks, typically four fractions per week). The clinical study was performed in accordance with all the relevant guidelines and running regulations on clinical trials and was approved by the referral ethics committee "CNAO" with the code CNAO-OSSINSIDE-02-18 on July 31, 2019; the informed consent was obtained from all the adult participants enrolled. No information or images that could lead to identification of the participant are present in this work.

We have analyzed the data of three patients affected by an Adenoid Cystic Carcinoma (ACC) of salivary glands, monitored during the clinical trial and already examined in Fischetti et al. (13) with the names PZA, PZB, and PZC. While the reader can found the full treatment plans description in the cited manuscript, the number of monitored treatment fraction, the number of delivered PB, the number of ions per PB as well as the beam energies foreseen by each plan are reported in **Table 1**. A Range Shifter (RS, a solid water 3 cm thick layer positioned between the beam exit window and the patient along the beam path) was used when delivering the treatment of all the considered patients.

Transverse Position Assessment

The fragments position measurement starts from the signal registration performed for each triggered event. The fragments crossing the DP produce light in the scintillating fibers, which is detected by the SiPMs to build a 3D track inside the detector local reference frame using the Hough transform (23) applied to each detected 'hit'. The track parameters are hence evaluated with a linear fit, as described in details in Traini et al. (11). The

laser survey results are finally used to transform the track parameters in the global reference frame of the treatment room. While performing this change of reference frame the systematic uncertainty due to the DP positioning accuracy (at the level of 1 mm) is assumed to be negligible as the contribution from the limited statistics and multiple scattering on the final results are significantly larger. The high incoming fragment rate (more than 100 kHz in some of the slices that have to be treated with high energy and high number of ions) resulted in a significant fraction of events (~ 10%) with a track multiplicity larger than 1. Such events have been rejected to avoid the additional contribution to the position measurement uncertainty. Starting from the fully reconstructed sample, the tracks projections in the plane (xy), orthogonal to the beam direction, are computed. With such information, a 2D histogram representing the track density $\rho_{\mathrm{Track}}(x,y)$ in the transverse plane is built for each PB using the measured emission points along the beam path inside the patient of all the reconstructed tracks. A binning of 3 ×3 mm^2, comparable with the CNAO carbon ion beam spot size (24), has been chosen. According to the MC simulation of the full treatment, performed with the FLUKA software (25, 26) and described in (13), the average angular deflection of the escaped fragments provoked by the multiple scattering is of the order of 60 mrad. For this reason the track density distributions do not present an evident peak for PBs with a low number of reconstructed tracks. We decided then to apply to each histogram a filter to avoid that the statistical fluctuations could result in a bias affecting the peak measured position. Different filters have been investigated: Gaussian, Median and Average based algorithms were applied to the 2D distribution and the measured PB positions have been compared with the nominal ones provided by the DDS. Among the different available filters we selected the Gaussian one, as it provided an unbiased result for all the data analysed. Different resolutions were tested, and the best results have been obtained smoothing the picture applying a 2D Gaussian filter with a σ_f of 1.0 cm.

An example of the track density histogram before and after the smoothing is shown in **Figure 3** respectively in the Left and Right panels. The observed stretched shape, asymmetrical in the vertical and horizontal axis, is due to the relative positioning of the DP with respect to the beam incoming direction. Since the DP is place at 60° with respect to the treatment room z axis, in the x,z plane, the resolution that can be obtained on the x position of the PCA is worse when compared to the one achievable along the vertical axis. This geometrical effect results in the shape that can be observed in **Figure 3**. A 2D elliptical Gaussian function was used to fit the data when estimating the distribution maximum value and measuring the PB position (x_{meas},y_{meas}).

RESULTS

To evaluate the precision and the accuracy of the method outlined in the previous section, for each PB the measured position (evaluated as the accumulation point position identified as explained in Section *Transverse Position Assessment* and shown in **Figure 3**) has been compared with

TABLE 1 | Details of the treatment plans delivered to the patients considered in this paper.

Patient ID	PZA	PZB	PZC
n. monitored fractions	6	10	6
n. PB	~ 37k	~ 7k	~ 33k
n. ions per PB	10^4 - $8{\cdot}10^5$	10^4 - $1.5{\cdot}10^5$	10^4 - $7{\cdot}10^5$
kinetic energies	126–297 MeV/u	153–269 MeV/u	126–278 MeV/u

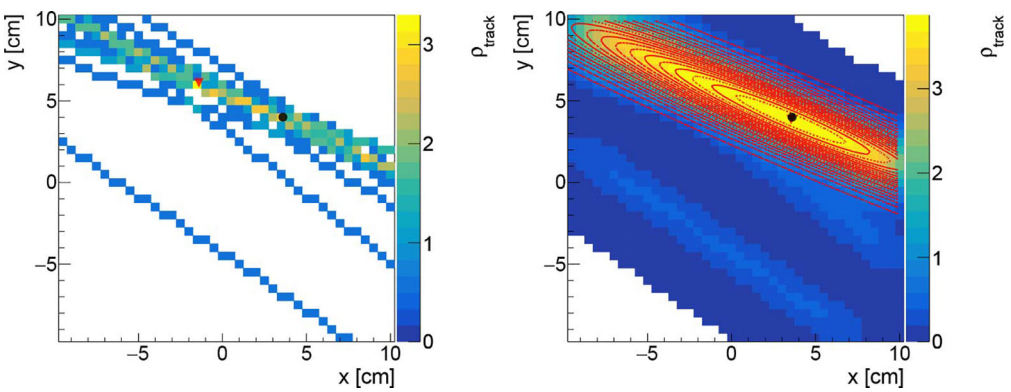

FIGURE 3 | Left: Track density histogram for a PB with 17 reconstructed tracks (no filter applied). Right: the same figure is drawn applying a Gaussian filter with σ_f equal to 1.0 cm. Both figures are obtained with a binning of 3 mm in both axis. The black (circle) and the red (triangle) markers represents respectively the nominal beam position, and the reconstructed one. The 2D Gaussian fit is super-imposed (red curves).

the nominal one provided by the DDS (27), which unambiguously identifies the position of each PB in each treatment fraction. All the reconstructed tracks have a well defined DDS identifier and can be associated to a given PB. When considering the overall track sample, ~50–70% of the detected particles (depending on the patient positioning) are produced when the beam interacts with the range shifter, while the remaining ones are produced by the interaction with the patient. Despite that the former ones could be certainly used for the transverse position assessment, they have been excluded from this analysis in order to investigate the worst case scenario in which the treatment is performed without the RS and the fragments are emitted only by the patient. Applying such selection, the average number of reconstructed tracks per PB is ~7, ~14 and ~15 respectively for PZA, PZB and PZC, as can be observed in **Figure 4** where the distributions of the number of tracks measured in the first treatments fraction are shown as an example.

The distributions of the differences $\Delta x = x_{meas} - x_{nom}$ and $\Delta y = y_{meas} - y_{nom}$ of the reconstructed PB positions using the algorithms outlined here-before (x_{meas},y_{meas}) with respect to the nominal PB ones (x_{nom},y_{nom}) as coming from the raster file are shown in **Figure 5** for the first fraction of PZC.The histograms have been populated selecting only the PBs with a number of reconstructed tracks coming from the patient larger than 5 (~ 80% of the total number of PBs in the treatment fraction).

Both distributions show a Gaussian core (solid, red line) with a slightly asymmetrical tail (parametrized with a further Gaussian function with different central value shown as a dotted red line), due to the fact that the DP orientation is not orthogonal to the beam line, as described in section *The Dose Profiler*. The cores have respectively σ_x ~ 1.4 cm and σ_y ~ 1.1 cm along the x and y axes, while the fraction of the events associated to the tail is ~20%. The mean of the distributions is found to be consistent with zero (within a 1 mm bias that has a negligible

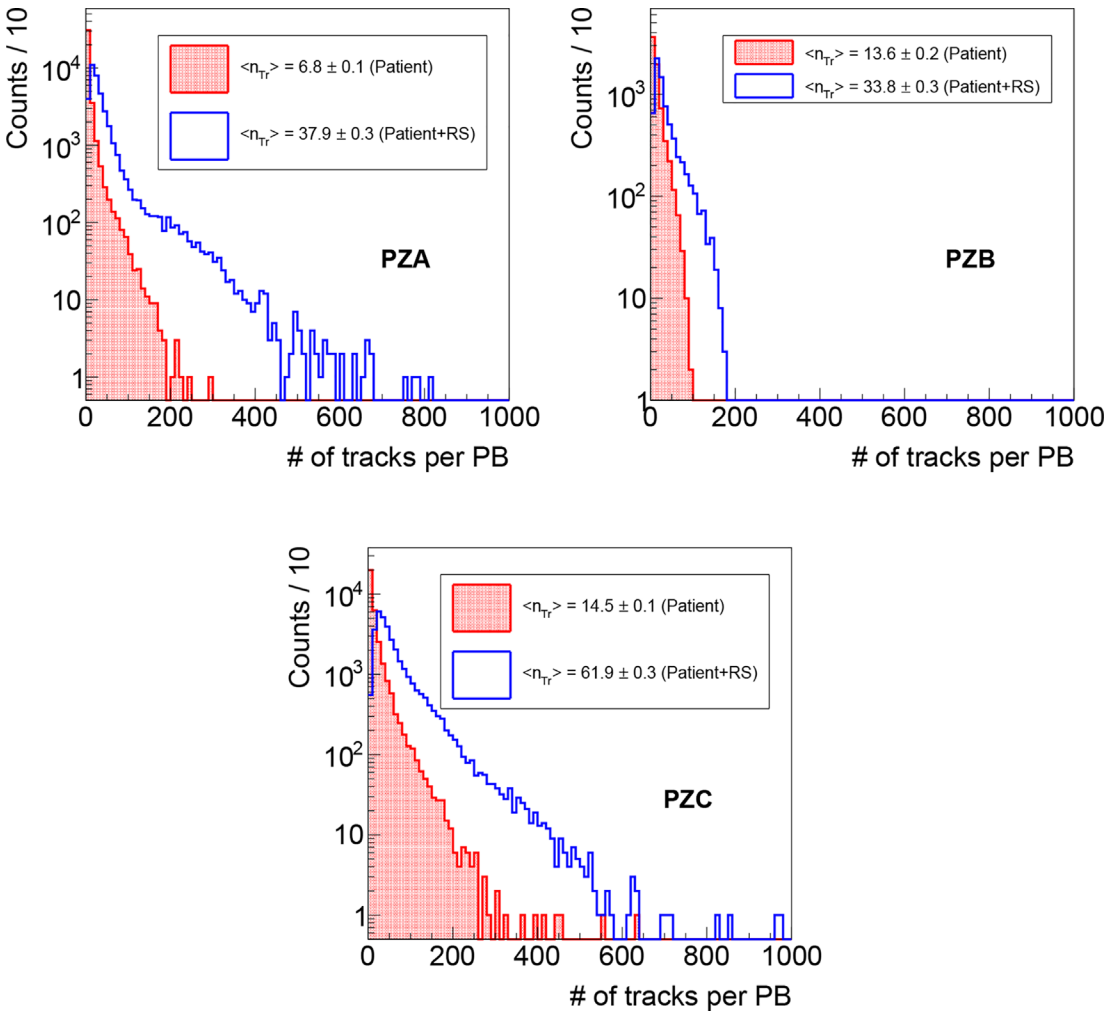

FIGURE 4 | Distributions of the number of reconstructed tracks per PB as measured during the first fraction monitoring for PZA, PZB and PZC, obtained respectively selecting the fragments produced only in the patient (red line, dotted area), and that ones produced also in the RS (blue line, empty area).

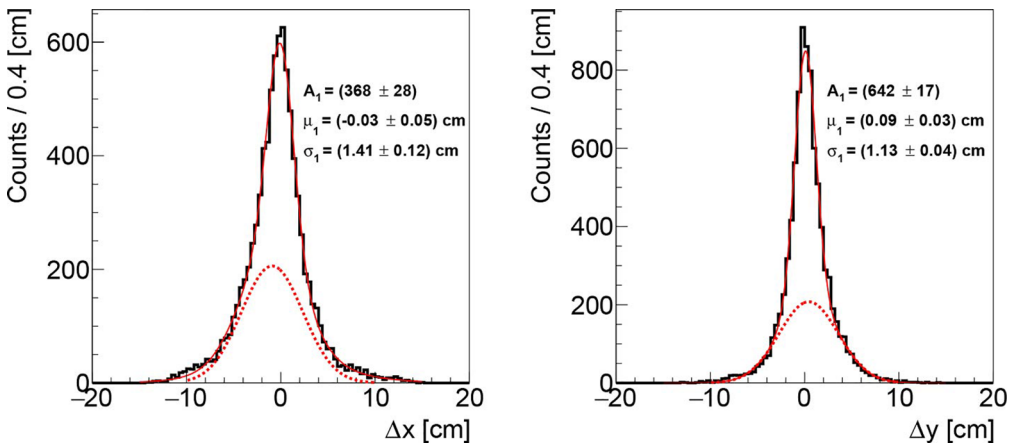

FIGURE 5 | Distributions of the differences between the measured and the actual beam transverse position, respectively in the x (left) and y (right) axis, obtainded analysing the data acquired during the first fraction of PZC. The solid, red line represents the overall fit function while the dotted, red line highlights the tail contribution.

impact on the results), confirming that the technique is able to follow the PB scanning without introducing a systematic uncertainty that has to be accounted for. Finally, the obtained results are not significantly affected by little variations of the filtering parameter σ_f (see section *Transverse Position Assessment*), as σ_x, σ_y vary of ±0.1 cm when using a σ_f between 0.8 and 1.2 cm.

Similar resolution have been obtained also for PZA and PZB. The results are very stable against the different treatment fractions, as summarized in **Table 2**, where the mean value $<\sigma_x>$, $<\sigma_x>$ and the corresponding standard deviations $S_{\sigma_x}, S_{\sigma_y}$, of the Gaussian core sigmas are reported for the three patients.

The measured resolutions shown in **Table 2** are significantly larger than the PBs spatial separation (2 mm) limiting the single PB monitoring capability of the DP. However, as stated in section *Transverse Position Assessment*, the accuracy on the transverse position is expected to be strongly slice and position dependent, as the number of reconstructed tracks per PB is highly affected by both the initial beam kinetic energy and by the amount of material that fragments have to cross to exit from the patient.

To study the potential of the technique assuming that the detector technology could be changed, the dependence of the obtained resolution on the beam energy and the collectable statistic has been studied using the data collected in the first fraction of PZC. In such analysis also the fragments produced in the RS have been included. The resolution dependence on the beam energy can be clearly observed in **Figure 6**. The observed behaviour is due to the larger number of fragments emitted when delivering PB with higher energies.

The dependence on the collectable statistics is shown in **Figure 7** where the x and y position resolutions are shown as a function of the number of collected tracks per PB. The resolution scales as expected, following the $p_0/\sqrt{N}$ trend which is over-imposed on both plots to guide the eye.

Concerning the DP monitoring capabilities in a real case scenario, an average number of tracks per PB $<n_{Tr}>$ between 5 and 15 and between 35 and 60 is observed respectively when selecting only the particles produced within the patient and when considering also the ones produced in the RS, as shown in **Figure 4**.

DISCUSSION

In this manuscript we explored, in the frame of CIRT technology, the online monitoring capabilities of the beam transverse position using a charged fragments detector. The real case of three patients treated for an ACC was used to collect the data and evaluate the performance in a clinical scenario. The reported results suggest that the accuracy of such technique is mainly limited by two factors:

- the multiple scattering suffered by the fragments travelling within the patient from their production point towards the detector, which add an unavoidable resolution term to the measurement of the accumulation point of the reconstructed tracks;

TABLE 2 | Mean values $<\sigma_x>$, $<\sigma_x>$ and standard deviations $S_{\sigma_x}, s_{\sigma_y}$ of the resolutions obtained in the different treatment fraction for PZA, PZB and PZC.

Patient ID	PZA	PZB	PZC
n. monitored fractions	6	10	6
$<\sigma_x>$	(1.55 ± 0.02) cm	(1.58 ± 0.03) cm	(1.41 ± 0.02) cm
$<\sigma_y>$	(1.08 ± 0.02) cm	(1.09 ± 0.02) cm	(1.17 ± 0.02) cm
S_{σ_x}	0.05 cm	0.08 cm	0.04 cm
S_{σ_y}	0.03 cm	0.06 cm	0.05 cm

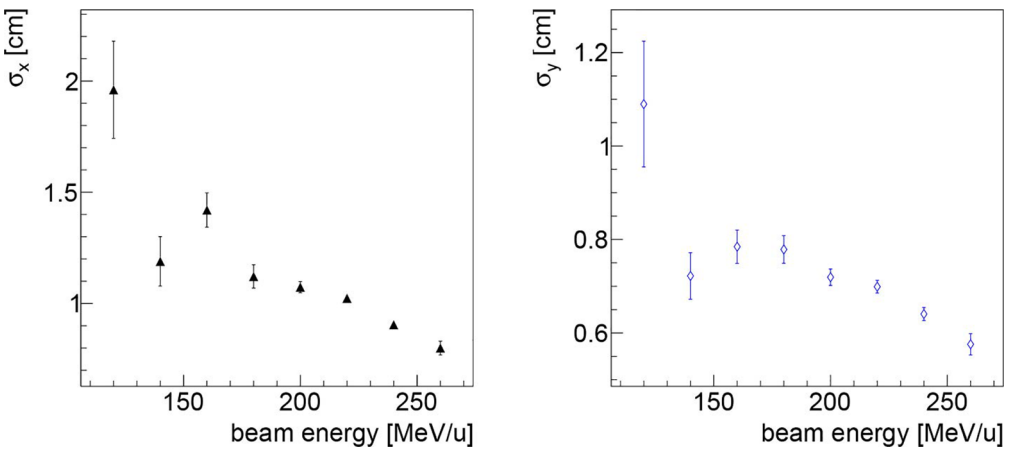

FIGURE 6 | Resolution on the beam transverse position as a function of the beam energy along the x (left) and y (right) directions, obtained analysing the data collected in first fraction of PZC. As expected, the higher is the beam energy, the better is the resolution, as expected since there is a larger number of emitted fragments that are capable of escaping from the patient.

- the number of particles detected per PB. The number of reconstructed tracks per PB is, on average, few tens, with a strong dependency on the patient treatment details and on the energy of the incoming projectiles. In order to improve the resolution, strategies to increase the number of detectable fragments have to be defined and implemented.

Figure 7 shows that the resolution decreases, in the range up to 300 tracks per PB, as $1/\sqrt{N}$, and we can therefore use the observed behaviour to predict the expected resolution for larger number of tracks. To reach a resolution comparable with the lateral PB distance (2 mm), a number of tracks per PB >500 would be needed according to the $1/\sqrt{N}$ scaling and the DP absolute positioning in the room reference frame would need to be known with a better precision (smaller than the current uncertainty of: 1 mm). In that case an absolute position resolution measurement, performed online, could be used to provide a valuable independent feedback to the DDS and to the treatment QA software. With lower number of tracks the resolution degrades and only the average position of close PB will be accessible.

The number of fragments that can be detected by the dose profiler while monitoring a CIRT treatment is limited by the detector dead time (: 5 μs at the measured DAQ rates (~ 60-70 kHz in average with peaks above 100 kHz). While the presence of RS can significantly boost the number of detectable fragments, we have shown that very few PBs could match the >500 requirement even if these additional tracks are considered.

We estimate that reducing the detector dead time, the detectable fragments could be easily doubled. To reach the required precision,

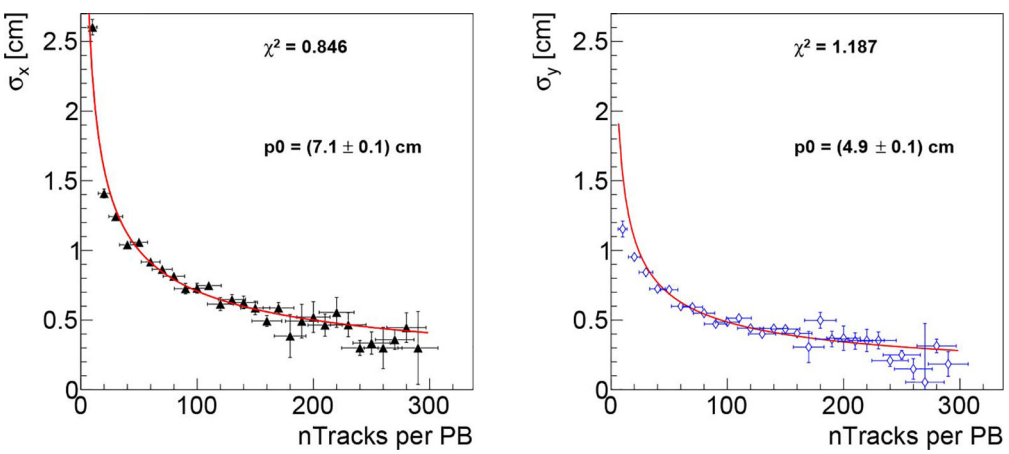

FIGURE 7 | Beam transverse position resolution as a function of the number of reconstructed tracks per PB, respectively for the x (left) and y (right) directions, obtained analysing the data collected in first fraction of PZC. As expected, the resolution scales proportionally to $p_0/\sqrt{N}$, the trend is superimposed on the figures in red to guide the eye.

we are still missing a factor ~ 15 (worst case scenario) and ~4 (if all available tracks coming either from the patient or from the RS can be used) in statistics: a possible solution might be to enlarge the detector acceptance (increasing the active volume or putting the detector closer to the patient) or to reduce the tilt angle with respect to the beam line, at the expense of some additional distortion effect when back-projecting the tracks.

These changes might not be easy to implement in the current setup of the INSIDE system. Thus, to confirm the capability of the proposed technique of monitoring of the transverse beam position in carbon ions treatments with a resolution comparable or lower the lateral PB spatial separation, as suggested by the data trend, an adequate technological solution capable of overcoming the current DP limitations will be needed.

DATA AVAILABILITY STATEMENT

The raw data supporting the conclusions of this article will be made available by the authors, without undue reservation.

ETHICS STATEMENT

The studies involving human participants were reviewed and approved by CNAO (code:CNAO-OSSINSIDE-02-18). The patients/participants provided their written informed consent to participate in this study.

AUTHOR CONTRIBUTIONS

GT, MT, and ASar wrote the main manuscript text and prepared the figures. GBat, GBis, PC, MS, YD, AE, VF, EF, AK, EM, MMor, SM, FP, GT, SV, and ASar took active part in acquiring the data during the INSIDE clinical trial. GBar, MC, MD, CL, MMag, EMaz, AM, GS, ST, BV, and VV played a decisive role in setting up the INSIDE cart, the INSIDE infrastructure and starting and selecting the patients for the clinical trial. MS, IM, MMar, VP, ASar, ASci, ASch, and GT have proposed the idea of the Dose Profiler detector, supervised the detector operation and the data taking. PM, MS, MF, GF, VP, ASar, ASci, ASch, GT, and MT implemented and performed the data analysis. All authors contributed to the article and approved the submitted version.

ACKNOWLEDGMENTS

We would like to thank all the staff of the CNAO centre, and in particular M. Pullia and G. Venchi, for their support during the clinical trial operations, system commissioning and monitoring preparations.

REFERENCES

1. Karger CP, Peschke P. RBE and Related Modeling in Carbon-Ion Therapy. *Phys Med Biol* (2017) 63:01TR02. doi: 10.1088/1361-6560/aa9102
2. Particle Therapy Co-Operative Group. (2020). Dataset.
3. Malouff TD, Mahajan A, Krishnan S, Beltran C, Seneviratne DS. Trifiletti DM.Carbon Ion Therapy: A Modern Review of an Emerging Technology. *Front Oncol* (2020) 10:82. doi: 10.3389/fonc.2020.00082
4. Vogin G, Wambersie A, Koto M, Ohno T, Uhl M, Fossati P, et al. A Step Towards International Prospective Trials in Carbon Ion Radiotherapy: Investigation of Factors Influencing Dose Distribution in the Facilities in Operation Based on a Case of Skull Base Chordoma. *Radiat Oncol* (2019) 14:24. doi: 10.1186/s13014-019-1224-1
5. Fattori G, Riboldi M, Scifoni E, Krämer M, Pella A, Durante M, et al. Dosimetric Effects of Residual Uncertainties in Carbon Ion Treatment of Head Chordoma. *Radiother Oncol* (2014) 113:66–71. doi: 10.1016/j.radonc.2014.08.001
6. Krimmer J, Dauvergne D, Létang J, Testa E. Prompt-Gamma Monitoring in Hadrontherapy: A Review. *Nucl Instrum Methods Phys Res Sect A: Accel Spectrometers Detectors Associated Equip* (2018) 878:58–73. doi: 10.1016/j.nima.2017.07.063
7. Pennazio F, Battistoni G, Bisogni MG, Camarlinghi N, Ferrari A, Ferrero V, et al. Carbon Ions Beam Therapy Monitoring With the INSIDE in-Beam PET. *Phys Med Biol* (2018) 63:145018. doi: 10.1088/1361-6560/aacab8
8. Parodi K. On- and Off-Line Monitoring of Ion Beam Treatment. *Nucl Instrum Methods Phys Res Sect A: Accel Spectrometers Detectors Associated Equip* (2016) 809:113–119. doi: 10.1016/j.nima.2015.06.056
9. Rucinski A, Battistoni G, Collamati F, Lucia ED, Faccini R, Fralliciardi PM, et al. Secondary Radiation Measurements for Particle Therapy Applications: Charged Particles Produced by 4He and 12C Ion Beams in a PMMA Target At Large Angle. *Phys Med Biol* (2018) 63:055018. doi: 10.1088/1361-6560/aaa36a
10. Traini G, Battistoni G, Bollella A, Collamati F, Lucia ED, Faccini R, et al. Design of a New Tracking Device for on-Line Beam Range Monitor in Carbon Therapy. *Physica Med* (2017) 34:18–27. doi: 10.1016/j.ejmp.2017.01.004
11. Traini G, Mattei I, Battistoni G, Bisogni M, Simoni MD, Dong Y, et al. Review and Performance of the Dose Profiler, a Particle Therapy Treatments Online Monitor. *Physica Med* (2019) 65:84–93. doi: 10.1016/j.ejmp.2019.07.010
12. Ferrero V, Fiorina E, Morrocchi M, Pennazio F, Baroni G, Battistoni G, et al. Online Proton Therapy Monitoring: Clinical Test of a Silicon-Photodetector-Based in-Beam Pet. *Sci Rep* (2018) 8:4100. doi: 10.1038/s41598-018-22325-6
13. Fischetti M, Baroni G, Battistoni G, Bisogni G, Cerello P, Ciocca M, et al. Inter-Fractional Monitoring of ^{12}C Ions Treatments: Results From a Clinical Trial At the CNAO Facility. *Sci Rep* (2020) 10:20735. doi: 10.1038/s41598-020-77843-z
14. Patera V, Sarti A. Recent Advances in Detector Technologies for Particle Therapy Beam Monitoring and Dosimetry. *IEEE Trans Radiat Plasma Med Sci* (2020) 4:133–46. doi: 10.1109/TRPMS.2019.2951848
15. Giordanengo S, Donetti M, Garella M, Marchetto F, Alampi G, Ansarinejad A, et al. Design and Characterization of the Beam Monitor Detectors of the Italian National Center of Oncological Hadron-Therapy (Cnao). *Nucl Instrum Methods Phys Res Sect A: Accel Spectrometers Detectors Associated Equip* (2013) 698:202–207. doi: 10.1016/j.nima.2012.10.004
16. Félix-Bautista R, Gehrke T, Ghesquière-Diérickx L, Reimold M, Amato C, Turecek D, et al. Experimental Verification of a non-Invasive Method to Monitor the Lateral Pencil Beam Position in an Anthropomorphic Phantom for Carbon-Ion Radiotherapy. *Phys Med Biol* (2019) 64:175019. doi: 10.1088/1361-6560/ab2ca3
17. Durante M, Paganetti H. Nuclear Physics in Particle Therapy: A Review. *Rep Prog Phys* (2016) 79:96702. doi: 10.1088/0034-4885/79/9/096702
18. Haettner E, Iwase H, Krämer M, Kraft G, Schardt D. Experimental Study of Nuclear Fragmentation of 200 and 400 MeV/u12c Ions in Water for Applications in Particle Therapy. *Phys Med Biol* (2013) 58:8265–79. doi: 10.1088/0031-9155/58/23/8265
19. Gunzert-Marx K, Iwase H, Schardt D, Simon RS. Secondary Beam Fragments Produced by 200 MeV u-112c Ions in Water and Their Dose Contributions in Carbon Ion Radiotherapy. *New J Phys* (2008) 10:75003. doi: 10.1088/1367-2630/10/7/075003
20. Piersanti L, Bellini F, Bini F, Collamati F, Lucia ED, Durante M, et al. Measurement of Charged Particle Yields From PMMA Irradiated by a 220 Mev/U12cbeam. *Phys Med Biol* (2014) 59:1857–72. doi: 10.1088/0031-9155/59/7/1857

21. Muraro S, Battistoni G, Collamati F, De Lucia E, Faccini R, Ferroni F, et al. Monitoring of Hadrontherapy Treatments by Means of Charged Particle Detection. *Front Oncol* (2016) 6:177. doi: 10.3389/fonc.2016.00177
22. CNAO. *Clinicaltrials.Gov Identifier* (2019). Available at: https://clinicaltrials.gov/ct2/show/NCT03662373?term=NCT03662373&draw=1&rank=1.
23. Duda RO, Hart PE. Use of the Hough Transformation to Detect Lines and Curves in Pictures. *Commun ACM* (1972) 15:11–5. doi: 10.1145/361237.361242
24. Mirandola A, Molinelli S, Vilches Freixas G, Mairani A, Gallio E, Panizza D, et al. Dosimetric Commissioning and Quality Assurance of Scanned Ion Beams At the Italian National Center for Oncological Hadrontherapy. *Med Phys* (2015) 42:5287–300. doi: 10.1118/1.4928397
25. Ferrari A, Sala PR, Fasso A, Ranft J. *Fluka: A Multi-Particle Transport Code (Program Version 2005). CERN-2005-010, Slac-R-773, Infn-Tc-05-11*. CERN Yellow Reports: Monographs (2005). Report number: CERN-2005-010, SLAC-R-773, INFN-TC-05-11, CERN-2005-10.
26. Battistoni G, Bauer J, Boehlen TT, Cerutti F, Chin MPW, Dos Santos Augusto R, et al. The FLUKA Code: An Accurate Simulation Tool for Particle Therapy. *Front Oncol* (2016) 6:116. doi: 10.3389/fonc.2016.00116
27. Giordanengo S, Garella MA, Marchetto F, Bourhaleb F, Ciocca M, Mirandola A, et al. The Cnao Dose Delivery System for Modulated Scanning Ion Beam Radiotherapy. *Med Phys* (2015) 42:263–75. doi: 10.1118/1.4903276

Conflict of Interest: The authors declare that the research was conducted in the absence of any commercial or financial relationships that could be construed as a potential conflict of interest.

Copyright © 2021 Toppi, Baroni, Battistoni, Bisogni, Cerello, Ciocca, De Maria, De Simoni, Donetti, Dong, Embriaco, Ferrero, Fiorina, Fischetti, Franciosini, Kraan, Luongo, Malekzadeh, Magi, Mancini-Terracciano, Marafini, Mattei, Mazzoni, Mirabelli, Mirandola, Morrocchi, Muraro, Patera, Pennazio, Schiavi, Sciubba, Solfaroli-Camillocci, Sportelli, Tampellini, Traini, Valle, Vischioni, Vitolo and Sarti. This is an open-access article distributed under the terms of the Creative Commons Attribution License (CC BY). The use, distribution or reproduction in other forums is permitted, provided the original author(s) and the copyright owner(s) are credited and that the original publication in this journal is cited, in accordance with accepted academic practice. No use, distribution or reproduction is permitted which does not comply with these terms.

Advantages of publishing in Frontiers

OPEN ACCESS
Articles are free to read for greatest visibility and readership

FAST PUBLICATION
Around 90 days from submission to decision

HIGH QUALITY PEER-REVIEW
Rigorous, collaborative, and constructive peer-review

TRANSPARENT PEER-REVIEW
Editors and reviewers acknowledged by name on published articles

Frontiers
Avenue du Tribunal-Fédéral 34
1005 Lausanne | Switzerland

Visit us: www.frontiersin.org
Contact us: frontiersin.org/about/contact

REPRODUCIBILITY OF RESEARCH
Support open data and methods to enhance research reproducibility

DIGITAL PUBLISHING
Articles designed for optimal readership across devices

FOLLOW US
@frontiersin

IMPACT METRICS
Advanced article metrics track visibility across digital media

EXTENSIVE PROMOTION
Marketing and promotion of impactful research

LOOP RESEARCH NETWORK
Our network increases your article's readership